PROCEEDINGS

Eight International Symposium on SPRAYED CONCRETE

- Modern Use of Wet Mix Sprayed Concrete for Underground Support

Trondheim, Norway, 11.- 14. June 2018

www.sprayedconcrete.no

ITA-AITES

norsk betongforening

Tekna

8TH INTERNATIONAL SYMPOSIUM ON

SPRAYED CONCRETE

MODERN USE OF
WET MIX SPRAYED CONCRETE FOR
UNDERGROUND SUPPORT

TRONDHEIM, NORWAY 11. – 14. June 2018

Edited by
Thomas Beck
Synnøve A. Myren
Siri Engen

8th International Symposium on - SPRAYED CONCRETE
- Modern Use of Wet Mix Sprayed Concrete for Underground Support
Trondheim, Norway, 11. – 14. June 2018

ORGANIZING COMMITTEE

- **Mrs Synnøve A. Myren (Chair)**
  Norwegian Public Roads Administration
- **Mrs. Siri Engen**
  Tekna / Norwegian Concrete Association
- **Dr. Christine Hauck**
  Veidekke Entreprenør AS
- **Mr. Jan Erik Hetlebakke**
  Entreprenørservice A/S
- **Mr. Brede Nermoen**
  Bane NOR
- **Mr. Ove Ugelstad**
  AF Gruppen AS
- **Mr. Ola Woldmo**
  Normet Norway
- **Mr. Arnstein Aarset**
  Norwegian Geotechnical Institute

SCIENTIFIC COMMITTEE

- **Mr. Thomas Beck (Chair)**
  Normet Norway
- **Dr. Stefan Bernard**
  TSE P/L, Australia
- **Dr. Øyvind Bjøntegaard**
  Norwegian Public Roads Administration, Norway
- **Mr. Eystein Grimstad**
  Norway
- **Chief scientist / Professor II Eivind Grøv**
  SINTEF Byggforsk / NTNU, Norway
- **Dr. Christine J. Hauck**
  Veidekke Entreprenør AS, Norway
- **Professor Jonas Holmgren**
  KTH, Sweden
- **Dr. Karl Gunnar Holter**
  Norwegian Geotechnical Institute, Norway
- **Professor Marc Jolin**
  Laval University, Canada
- **Professor Wolfgang Kusterle**
  OTH, Germany
- **Dr. Benedikt Lindlar**
  Sika Services AG, Switzerland
- **Mr. Roar Myrdal**
  Normet International, Switzerland
- **Dr. Veit Reinstadler**
  Mapei S.p.S, Austria
- **Mr. Benoit de Rivaz**
  Bekaert Maccaferri Underground Solutions, Belgium
- **Mr. Alun Thomas**
  Minova, UK

- Professor Kyong-Ku Yun
Kangwon National University, Korea

SECRETARY

Mrs. Siri Engen (siri.engen@tekna.no)
The Norwegian Society of Graduate Technical and Scientific Professionals – Tekna /
Norwegian Concrete Association

SPONSORED BY

ITA-AITES International Tunnelling and Underground Space Association
Norwegian Tunnelling Society
Norwegian Group for Rock Mechanics
The Norwegian Society of Chartered Technical and Scientific Professionals - Tekna
Norwegian Concrete Association

ISBN: 978-82-8208-060-6

CONTENTS

Invited speakers:
"Highway to Hell"
Gullikstad, J., Norway 7

Experience with Wet Sprayed Concrete the last Twety Years and Expectations for the Future
Ugelstad, O., Hetlebakke, J-E., Kristiansen, B., Norway 8

Design and Construction of a Shallow Cover Tunnel Junction using Sprayed Concrete, Sydney Australia
Aitchison, B., Oliveira, D., Backhouse, D., Netterfield, R., Australia 9

Laboratory investigation of steel fibre reinforced sprayed concrete using a computed tomography method
Ansell, A., Nordström, E., Guarin, A., Sweden 24

Optimisation of Plant Employed to Install Permanent Shotcrete Lining using Open Gripper TBMs
Ashcroft, B., Peach, G., Norway 39

Encapsulation Quality of Reinforcement: From Laboratory Tests to Structural Design Guidelines
Basso Trujillo, P., Jolin, M., Canada 54

Sprayed Concrete used as Avalanche Securing of Road in the Open Day during Freezing Conditions
Beck, T., Brusletto, K., Norway 69

Metakaolin as a Binder for Free Lime in Sprayed Concrete
Bézard, D., Otten, G., Switzerland 78

Instant and Delayed Mechanical Behavior of Sprayed Concrete used on Andra's URL: Towards an Understanding of the Links between Formulation, Implementation and In Situ Properties
Bhewa, Y., Rougelot, T., Zghondi, J., Burlion, N., France 84

Quality Control of Fibre Reinforced Sprayed Concrete: Norwegian Requirements and Experiences from Laboratory Studies and Tunnel Projects
Bjøntegaard, Ø., Myren, S., Beck, T. Norway 97

Sustainability and the Responsible Disposal of Contaminated Waste
Crehan, D., Eide, S., Vlietstra, D., Norway 108

Specifying and Testing Fibre Reinforced Spray Concrete: Advances and Challenges
de Rivaz, B., Belgium 116

A New Approach for Fibre Reinforced Shotcrete under Dynamic Loading
Gagnon, A., Jolin, M., Canada 129

From Lab Scale Spraying to Real Scale Shotcreting and Back to the Lab
Galan, I., Briendl, L., Röck, R., Steindl, F., Juhart, J., Mittermayr, F., Austria, Kusterle, W., Thumann, M., Germany 139

Adhesion Test with Anchor Bolts - Methodology for Shotcrete Adhesion Tension on Rock inside Mining Tunnels
Guajardo, J.I., Jarufe, J.A., Alegria, W., Garcia, S., Munoz, C.P., Chile 154

Durability of Sprayed Concrete for Rock Support - A tale from the Tunnels
Hagelia, P., Norway 167

Utilization of Modern IoT Systems in Sprayed Concrete Processes
Hauki, M, Switzerland, Beck, T., Norway 183

A 20 Year History of Stress and Strain in a Shotcrete Primary Lining
Jones, B.D., UK 201

TamCrete SSL (Structural Spray-on Liner)
Kleven, O-B., Switzerland 223

Correlation between Trials of Polymer Fibers Shotcrete (SRF): Fiber Content in Fresh Mixture, Energy Absorption and Barcelona Test
Madrid, C.A., Garcia, S.E., Rodriguez, F.B., Parada, C.F., Chile 226

Ultra Fast Rapid Hardening Sprayed Concrete
Mills, P., Tadolini, S., Thomas, A., UK & Denmark 233

Sprayed Concrete without Portland Cement
Myrdal, R., Switzerland, Tong, S., Taiwan 244

The Ban of Polymer Fibre in FRSC in Norwegian Road Tunnels
Myren, S., Hagelia, P., Bjøntegaard, Ø., Norway 252

Shotcrete Quality Control for the New M5 Tunnel, Sydney Australia
Oliveira, D.A.F., Aitchison, B.W., Gowans, A., Andersen, G., Australia 256

MiniBars TM – A new Durable Composite Mineral Macro Fiber for Shotcrete, Meeting the Energy Absorption Criteria for the Industry
Sandbakk S., Miller, L., Standal, P.C., Norway 267

Modelling Aspects to Predict Failure of a Bolt-Anchored Fibre Reinforced Shotcrete Lining
Sjölander, A., Hellgren, R., Ansell , A., Sweden 278

The Design Philosophy for Permanent Sprayed Concrete Linings
Thomas, A., Denmark, Dimmock, R., UK 293

Pumpability of Wet Mix Sprayed Concrete with Reduced Clinker Content
Thumann, M., Kusterle, W., Germany 308

Applications of Cellular Sprayed Concrete at Tunnel Portals
Yun, K-K., Han, S-Y., Lee, K-R., Kim, Y-G., S.Korea 320

The Importance of Rheology on Shotcrete Performance
Yurdakul, E., Rieder, K-A., USA 330

Monitoring and Behaviour of an Instrumented Thick Sprayed Concrete Lining Excavated in the Callovo Oxfordian Claystone at the Meuse Haute-Marne Underground Research Laboratory (URL) - Andra, France
Zghondi, J., Armand, G., France 341

Sprayed Concrete 11.-14. June 2018

Abstract for Jørund Gullikstad, Nye Veier – Wednesday 13. June

HIGHWAY TO HELL

- 106 km of new E6 through Trøndelag in mid Norway

Nye Veier AS is a public company founded in 2015 by the Norwegian Authorities, with the task to execute 530 km of national road, with overall and cost-effective focus to achieve more national road per invested public money.

In Trøndelag 106 km of road shall be executed, split in two sections on each side of the city of Trondheim:

- E6 North (42 km) from Ranheim to Åsen
- E6 South (64 km) from Melhus to Ulsberg

The presentation of the new main road through Trøndelag will include the following main tasks:

- Description of the total project
- Measures to increase the economic benefits for the society
    - Road optimisations and cost reductions
    - 4-lane highway and increased speed to reduce travel time
- Tender method: Best Value Procurement
- Execution model: Early contractor involvement and integrated collaboration
- Focus on the 40 km of tunnels being part of the project
    - 32 km of new tunnels
    - 8 km of existing tunnels to be rehabilitated

ABSTRACT

EXPERIENCE WITH WET SPRAYED CONCRETE LAST TWENTY YEARS AND EXPECTATIONS FOR THE FUTURE

Authors:
Ove Ugelstad, AF Anlegg, Norway
Jan-Erik Hetlebakke, Entreprenørservice, Norway
Bernt Kristiansen, AF Anlegg, Norway

Wet sprayed concrete has been used in Norway at least 50 years as rock support.
During the 90s it was developed a new accelerator called "alkali-free accelerator" (AFA). The AFA gave a good early strength. What has happened after millennium?

New requirements to the environment have given a lot of different binders with pozzolanes instead of and in addition to portland clinker. The aggregates are not only nature sand from rivers, but often crushed rock.

What is the experience with wet sprayed concrete last 20 years with new materials, binders and aggregates and what is the expectations for the future?

DESIGN AND CONSTRUCTION OF A SHALLOW COVER TUNNEL JUNCTION USING SPRAYED CONCRETE, SYDNEY AUSTRALIA

B. Aitchison[1], D. Oliveira[2], D. Backhouse[3] and R. Netterfield[4]
E-mail: [1]brodie.aitchison@aurecongroup.com

Abstract: *A unique solution was developed to provide construction access to the WestConnex New M5 Tunnels at Kingsgrove, Australia. The access junction involves the development of an intersection between a 10 metre span adit and a 16.5 metre span motorway tunnel at shallow depth below Wolli Creek. Adaptation to geotechnical uncertainty was a key consideration in the design with a meandering palaeochannel running through the construction site, shaft and tunnels. The selected design involved the construction of a sprayed concrete lined adit which was developed into a large span low cover sprayed concrete lined intersection with an effective span of approximately 19 metres. Optimisations to the tunnel geometry were required to promote arching of the soil and rock and to maintain compressive stresses in the tunnel lining. At locations gantry pile footings are supported by the sprayed concrete lining to facilitate removal of materials and machinery from the tunnels. Geotechnical and structural 3D finite element analysis was undertaken to assess the complex interactions of the junction including the design of the permanent primary lining and a permanent secondary lining for water resisting treatment. Composite lining interactions were considered between the primary and secondary linings for a sprayed membrane and sheet membrane waterproofing options.*

1 Introduction

WestConnex is a 33-kilometre underground motorway currently being constructed in Sydney's Inner West (Figure 1). The New M5 is one of the three stages of WestConnex and comprises of approximately 10-kilometres of dual underground motorway from Kingsgrove to St Peters. Early access to construct the tunnels on the New M5 was a key focus for the design and construction teams. At the Kingsgrove tunnelling site access to the shallow cover tunnels is provided by a shaft and adit from a small industrial site adjacent Wolli Creek and the existing M5 East Motorway.

Geotechnical uncertainly and shallow overburden ultimately led to the development of a sprayed concrete junction. This was aided by developments in recent years on the application of permanent sprayed concrete tunnel linings. Advancements in 3D design analysis tools allowed a greater understanding of the lining actions during the stages of construction.

Figure 1 WestConnex motorway

2 Geology and Site Investigations

The WestConnex tunnel is located within the Sydney Basin which is comprised of Permian and Triassic sedimentary rocks. The tunnel alignment intersects two main formations, the Ashfield Shale and Hawkesbury Sandstone. Geotechnical investigations revealed that the construction site is intersected by a palaeochannel associated with Wolli Creek which was converted from a natural creek to a concrete lined channel in the early 1940's (Figure 2).

Borehole logs indicated that the base of the alluvial channel has been infilled with loose sands, soft to stiff alluvial clays and residual clayey sands overlying the rock head. Due to the nature of the sandstone, the incision of Wolli Creek channel was inferred to have left several buried shelves/cliffs along the base of the channel which will locally reduce the thickness of rock in the tunnel crown over a relatively short distance before cover is regained. The preferential weathering and development of Wolli Creek alignment could also indicate the presence of the geological feature (joint swarm, faulting, dykes) that has not been intersected by the project investigations.

Limited geotechnical investigations had been conducted in the site compound where the shaft and adit were constructed due to access constraints. Given the uncertainty in the top of rock level discussed above only limited confidence could be gained from the boreholes. A subsequent geophysical investigation using Multi-Channel Analysis of Seimic Waves (MASW) was conducted to improve the understanding in the rock level. Results from the analysis indicated a varying rock head across the site dipping to the north-east.

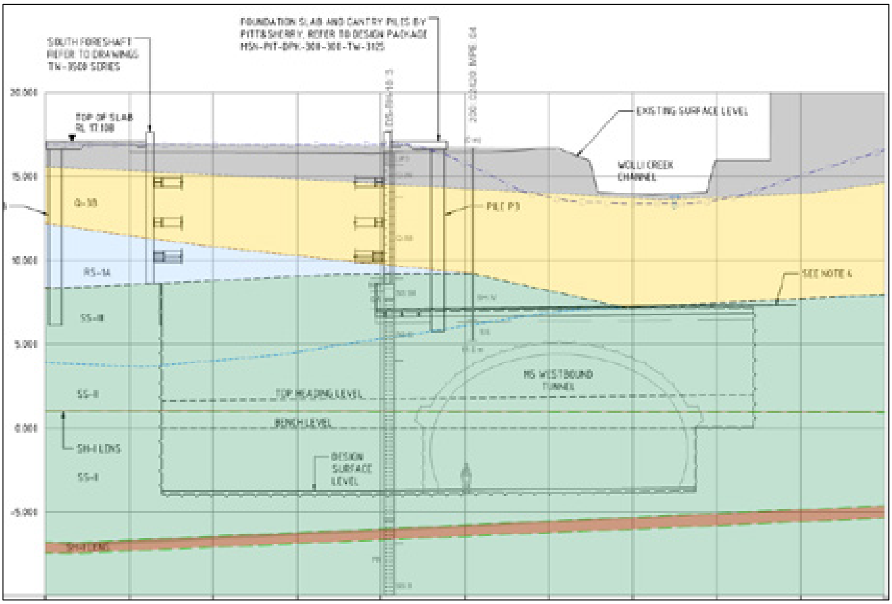

Figure 2 Inferred geotechnical cross section through shaft and adit during design

3 Concept / Background

The final design for the adit is a product of managing geotechnical uncertainty and project constraints:

3.1 Alignment

The tunnel alignment passes very close to the construction site boundary and directly adjacent the shaft location (Figure 3). A solution to simplify construction access was to alter the tunnel alignment to pass directly beneath the construction site and shaft such that the tunnels could be developed from the shaft invert, however, this was not feasible due to the additional cross passage length and subsequent changes to the fire and life safety design and alignment constraints at the portals. The vertical alignment of the tunnels was fixed by a maximum 4% road grade exiting the portals and constrained by a nearby pedestrian underpass which the motorway needed to pass over. The shaft location was also restricted by existing 3rd party authority services and contaminated ground. The shaft and adit option therefore remained as the preferred option to provide access to the 16.5 m span mainline tunnel.

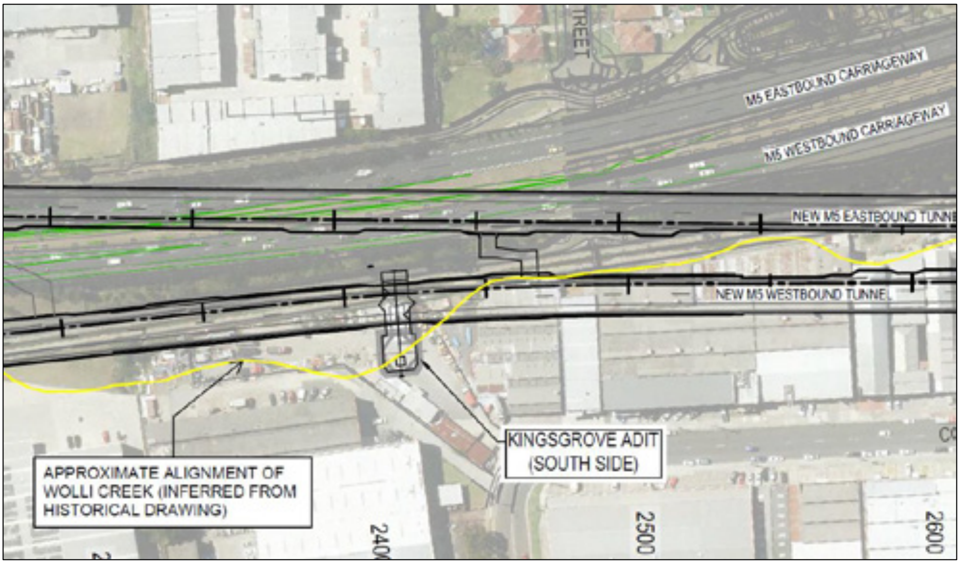

Figure 3 Tunnel alignment

3.2 Construction methods

The adit and mainline tunnels were constructed utilising roadheaders with the initial section of adit developed using a 14-tonne excavator fitted with a hydraulic hammer. The adit excavation was completed using a Mitsui S220 roadheader which was replaced by a Mitsui S300 machine for development of the mainline tunnels. The working limits of the machines (Maximum cutting heights, cutting profiles, angles and machine movements) set the geometrical constraints for the adit.

3.3 Geology and development of the tunnel profile

Geotechnical investigations uncovered varying rock head levels with up to 3.0 m difference in the top of rock between two boreholes separated by only 8.0 m. Although there was uncertainty in the top of rock level, the boreholes did reveal limited weathering profile with the site underlaid by slightly weathered to fresh Hawkesbury Sandstone. This created somewhat favourable conditions by having competent rock to foot a sprayed concrete tunnel lining on.

By capitalising on the underlying Hawkesbury Sandstone a unique mushroom shaped adit profile was developed using a top-down construction sequence. The initial heading drive was pre-supported with ø139 mm fully grouted canopy tubes and lined with a reinforced sprayed concrete lining. The sprayed concrete lining was founded on sandstone abutments with subsequent bench and invert excavation. The heading profile was heavily arched to promote ground arching and to minimise bending and maximise axial compression within the lining. The breakout location for the mainline tunnel excavation also needed to be considered to provide sufficient space and capacity to redistribute stresses within the sprayed concrete lining.

4 Primary Lining Design

4.1 Geotechnical analysis

The primary support for the adit consisted of heading excavation pre-supported by 26 m long ø139 mm grouted canopy tubes. The primary lining consisted of a 350 mm thick reinforced steel fibre sprayed concrete lining. Development of the mainline tunnels commenced via a split heading from the adit with a 300 mm thick steel fibre sprayed concrete lining reinforced with P130-20-30 lattice girders at 1.25 m centres.

The construction sequence, ground movements and primary lining design was assessed using 3D Finite Element Analysis (FEA) software. Geotechnical FEA software Plaxis 3D was employed to assess the proposed excavation sequence and ground-structure interaction including tunnel convergence and surface settlement. The structural design of the primary lining shell was performed using Strand7. The model staging is described in Figure 4.

Stage	Description	
1	Initial stage (no excavation, initialise in-situ stress, solve to equilibrium, reset displacements)	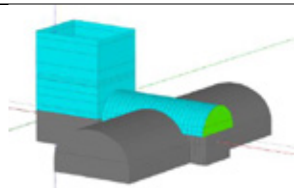
2	Install shaft support (sheet piling) and excavate	
3	Continue excavation of shaft to the adit heading level	
4	Excavate and support the adit heading in cycles.	
5	Excavate and support mainline tunnel heading 1 in cycles. Terminate 20 m east of the adit.	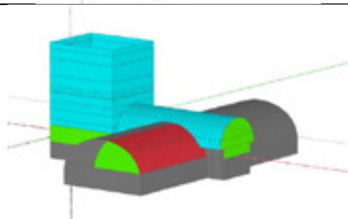
6	Excavate and support mainline tunnel heading 2 in cycles. Terminate 20 m west adit	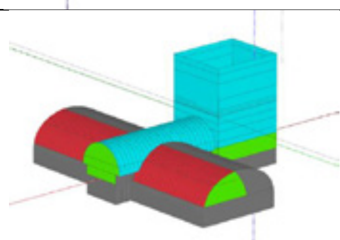

7	Excavate and support mainline tunnel heading 3 in cycles. Terminate 20 m east adit	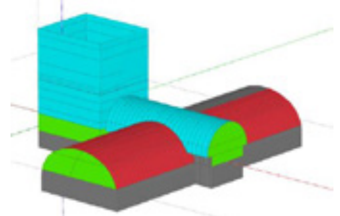
8	Excavate and support mainline tunnel heading 3 in cycles. Terminate 20 m west adit	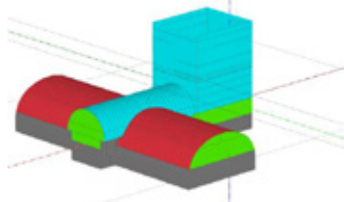
9	Excavate and support the adit invert in cycles.	
10	Excavate and support the mainline tunnel bench in cycles	

Figure 4 Plaxis 3D model staging

Staged material properties were adopted for the sequenced model. The build-up of shotcrete thickness was modelled including the strength gain by-virtue of elastic modulus. An elastic modulus of 10 GPa was used for early age shotcrete, 15 GPa for intermediate age and 32 GPa for 28-day strength shotcrete. The effect of shrinkage in the shotcrete was not modelled; the shotcrete lining is quite thick and shrinkage was not expected to be significant. In addition, in a lining analysis with high axial compression, ignoring shrinkage is a conservative assumption.

The geotechnical units were modelled with elasto-plastic elements with Mohr-Coulomb properties derived from the ground investigation.

4.2 Structural analysis

The staged construction sequence of the primary lining was modelled using the *Stages* function in Strand7. The design of the primary lining was conducted for short and long-term load cases. Short-term load cases considered the primary lining during the construction period prior to the installation of the secondary lining. Long-term load cases accounted for load sharing between the primary and secondary linings and creep of the sprayed concrete lining.

Loads considered on the primary lining included self-weight, ground load, construction loads (ventilation ducts, cabling and services) and surface surcharge. The tunnels were designed as drained therefore groundwater pressures on the primary lining were managed using weep holes and exposed rock faces.

The interaction between the tunnel lining and surrounding ground was modelled using springs after Duddeck and Erdmann [1]. The spring stiffness was assessed based on the expected ground type. The frictional effects between the extrados of the primary lining and the surrounding rock was considered by tangential shear springs.

Structural design actions (bending moments, axial forces, shear forces and displacements) were analysed from the models. The development of tensile forces above the mainline tunnel breakout zones was a focal point of the design (Figure 5). The staged modelling approach highlighted the development of the tensile forces as portions of the adit lining were demolished. Assumptions regarding the connection between the adit lining and the mainline tunnel lining affected the magnitude of forces developed. The assumption of a fixed connection between the two linings generated unmanageable connection forces. The joint between the adit lining and mainline tunnel lining was treated as a zero-moment connection. Compression forces between the linings could be transferred without bending moments. This assumption leads to the development of a controlled hinge / crack between the two sprayed concrete shells. The opening tensile forces were managed by the inclusion of horizontal reinforcement above the mainline tunnel openings.

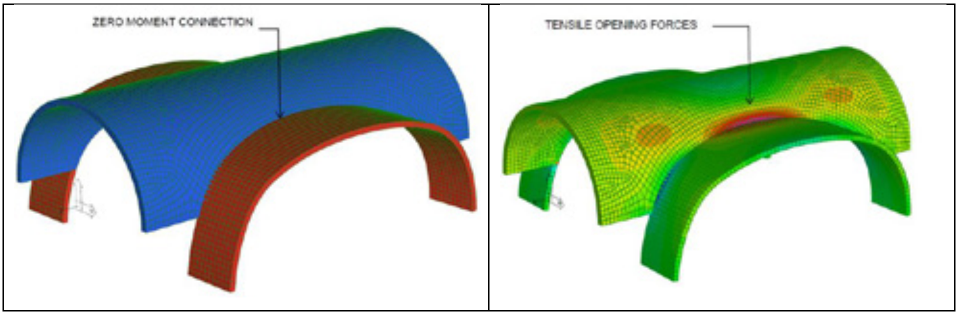

Figure 5 Tensile forces above mainline tunnel breakout zones

A late addition during the design phase was the loading from ø750 mm gantry crane piles designed by a temporary works sub-consultant. The toe level from one gantry pile clashed with the adit heading and resulted in the pile cage needing to be suspended (Figure 6). The design of end bearing gantry piles indicates the limited rock cover and thickness of alluvium above the tunnels.

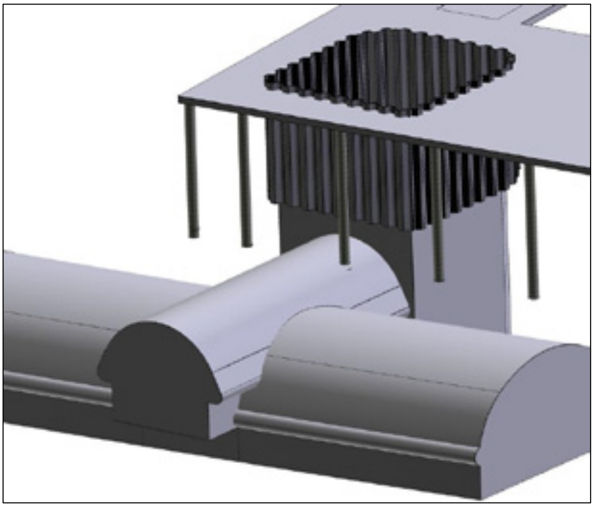

Figure 6 Isometric view showing gantry piles

Because of the pile loading, the first section of the adit lining was strengthened by 200UC52 steel sets to support the 280 kN pile toe load. During construction a 110-tonne crawler crane was used for spoil removal and a 250 tonne mobile crane was used to remove equipment until the initial section of adit had been constructed and reached a minimum 30 MPa compressive strength.

5 Secondary Lining Design

5.1 Water resisting design

The WestConnex New M5 Tunnel is a drained tunnel and employs a Water Resisting Strategy for managing groundwater ingress through the tunnel roof. The strategy treats groundwater ingress according to inflow rate and geological structures which have the potential to be water bearing features. Because the Kingsgrove tunnels are located at shallow depth beneath Wolli Creek, the tunnels required a mandatory waterproofing membrane and secondary lining. Two membrane options exist under the project Water Resisting Strategy; A double bonded sprayed membrane option and a traditional sheet membrane option. The secondary lining design needed to be compatible with both membrane options.

5.2 Composite lining design approach

The composite lining approach considers that although reinforcement elements embedded in the primary shotcrete lining may compromise the long-term durability of the primary lining, the lining does not completely deteriorate and maintains the ability to carry load.

Over time, after the completion of construction, a portion of the ground load which is supported by the primary lining may be transferred to the secondary lining due to deterioration of the primary support which contains embedded reinforcement and lattice girders. Additionally, the modulus of the primary lining will reduce over time causing relaxation and loading of the secondary lining. This deterioration and relaxation of the primary lining causes loading of the secondary lining (i.e. load sharing).

The degree of load sharing between the primary and secondary lining is complex and depends on a range of factors, the main of which are:

- Relative stiffness between the primary and secondary linings including the timing of loading of the primary and secondary linings
- Bond between the primary and secondary lining (e.g. unbonded or bonded)
- Ground conditions such as rock strength and stiffness
- Tunnel shape
- In-situ stress conditions
- Effects of concrete creep under sustained load
- Durability of the primary lining

5.2.1 Composite lining approach 1 – sheet or spray membrane

Traditionally the most common composite lining approach is to account for some load sharing between the primary and secondary linings (Figure 7). The amount of load sharing depends on a range of factors (Key factors listed above) but is typically between 15 and 50% [2,3]. For example, a higher share of load could be expected where a double bonded spray applied membrane is used and lower share of load where a unbonded sheet membrane is used, however, the author notes that the load sharing mechanisms are complex and the assumption of a bonded condition may lead to significantly lower loads carried by the secondary lining with an increased risk of cracking of the secondary lining due to higher bending stresses as highlighted by Su [4].

It should be highlighted that the degree of load sharing be assessed on a case-by-case basis considering the in-situ ground conditions. For example, a tunnel in soft ground (clay) exhibits a change between short-term and long-term behaviour which changes the ground load. Additionally, ground water pressures in clay can re-establish slowly over time.

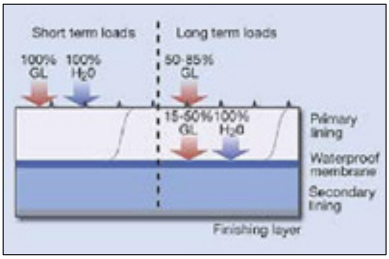

Figure 7 Typical composite lining (partial composite with no shear or adhesive bond) [2]

5.2.2 Composite lining approach 2 – double bonded spray applied membrane

Recent developments in composite lining design on tunnel projects such as London's Crossrail have examined the primary and secondary lining as a true composite material which is bonded by the spray applied membrane. This can only be performed where there is a bond between the primary and secondary lining such as a double bonded spray applied membrane (Figure 8).

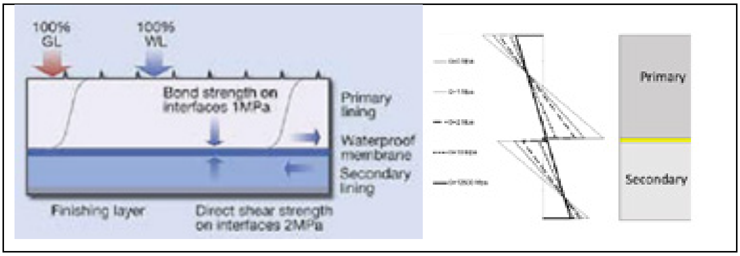

Figure 8 Left) Typical fully composite lining (shear and adhesive bond) [2], Right) Stress diagram for varying shear modulus [6]

The findings of recent studies [5,6,7,8] do however highlight shortfalls in the availability and reliability of long-term data for spray applied membranes, current industry standards and applicability of design codes to composite lining design. Further research, testing and development of applicable design standards are required before the composite action depicted in Figure 8 can become an industry standard and adopted on major transport projects such as WestConnex. Some of the issues which require addressing:

- Although the spray applied membrane contributes negligible stiffness to the overall lining system the composite action of the primary and secondary lining increases the lining stiffness which causes higher bending moments in the lining.
- Since the shear stiffness of the spray applied membrane is relied upon in the long-term case, effects of creep and aging need to be understood.
- The design of a composite tunnel linings raises issues in the non-linear analysis and code compliance.

- Depending on the bonding assumption, the groundwater may either be considered to act on the composite primary and secondary lining or the secondary lining only.
- A composite lining which relies upon bond between the primary and secondary lining tends to cause the primary lining to be more heavily loaded that the secondary lining. This increases the risk of cracking of the secondary lining.
- Experience has shown that the spray applied membrane can be difficult to apply when there is running ground water and that the membrane can debond/blister if there is a prolonged period between spraying or casting the secondary lining.

For these reasons the traditional composite lining approach (#1) was adopted for the design which allows for some load sharing between the primary and secondary lining, the degree of which depends upon if a PVC sheet or spray applied membrane is used. The approach was considered acceptable as it reduces the overall lining thickness compared to double shell lining approach, uses industry standard and best practice which has been proven on similar tunnel projects.

To quantify the amount of load sharing between the primary and secondary lining a 2D sensitivity study was performed. The results of the assessment show that between 10% and 60% load sharing between the primary and secondary loading can be expected considering either a PVC sheet membrane or double bonded spray membrane. When a PVC water resisting membrane is used between the primary and secondary linings, an unbonded analysis shows that there may be between 10-15% load sharing for the situation analysed. In the case of a bonded analysis which is relevant to a double bonded spray applied membrane between the primary and secondary linings, the results show between 50 and 60% load sharing between the primary and secondary lining.

The finding of the study shows a reasonable agreement with industry standard and loading conditions adopted on other similar tunnel projects and recent research [2,3,9]. Typically, 15-70% sharing of load between the primary and secondary lining is considered reasonable.

The secondary lining design was performed considering a higher percentage of long-term load sharing (50%) with checks conducted for 10% long-term load sharing also.

5.3 Structural analysis

The design of the secondary lining was performed using 3D finite element analysis software Strand7. Because of the complex geometry and time available the secondary lining was modelled in isolation without the primary lining shell. The structural analysis of tunnel linings is well documented [1,10] including established industry standards and will therefore not be discussed in this paper. The proceeding section will discuss the fire design approach for the secondary lining.

The secondary sprayed concrete lining was designed to withstand the standard 4-hour fire curve (Cellulosic ISO 834 as per AS1530.4 [11]) and 2-hour hydrocarbon fire curve (Eurocode 1: EN1991 1-2 [12]) (Figure 9).

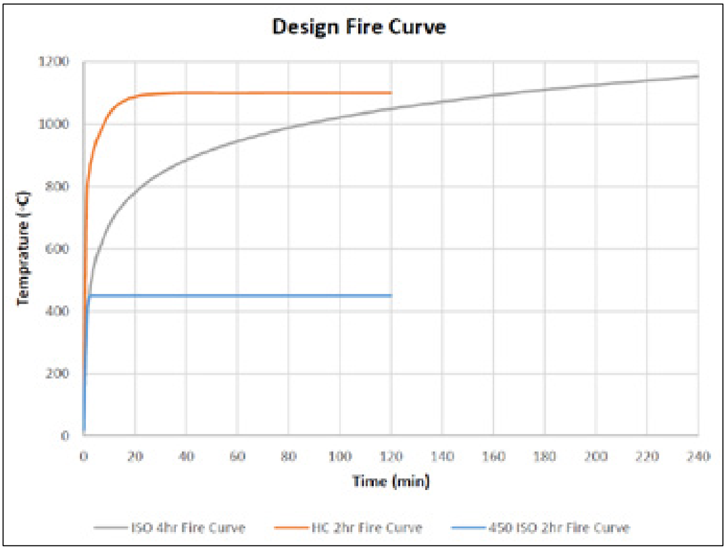

Figure 9 Design fire curves

To derive the thermal and mechanical properties of the sprayed concrete lining a two-dimensional FEA was performed for the project using Strand7 (Table 1). The transient heat solver was used to assess the non-linear temperature profile within the concrete section at various time increments. The thermal actions for the temperature analysis of concrete structures exposed to fire followed BS EN 1991-1-2:2002 [12], and BS EN 1992-1-2:2004 [14].

Table 1 Equivalent thermal and mechanical properties

Fire case	Equivalent elastic modulus (MPa)	Equivalent thickness (mm)	Equivalent width (mm)	Equivalent node temp. (°C/m)	Equivalent temp. gradient (°C/m)	Heat affected zone (mm)
2-hr HC	20,100	211	1305	44	496	35
4-hr ISO	14,800	203	1353	82	220	55

To provide enhanced thermal resistance the secondary lining was specified to contain micro polypropylene (PP) fibres. The addition of micro PP fibres mitigates the risk of explosive spalling of the sprayed concrete lining under fire loading by expanding at a different rate compared to the concrete matrix, creating small openings between the cement paste matrix and the fibres. These openings relieve some of the vapour pressure that builds up in the pores of the concrete. At approximately 170 °C the fibres melt and above 360 °C evaporate [13]. The evaporation of the fibres provides voids which further relieve vapour pressures and help prevent concrete spalling.

To assess the requirement for explosive spalling a project study [13] was undertaken examining the results of fire testing completed on projects such as London's Crossrail Project, North West Rail Link in Sydney and the Clem7, Airport Link and Legacy Way Tunnels in Brisbane. The objective of the study was to limit the spalling depth to 25 mm under the 4-hour ISO fire curve. Statistical analysis of the data showed that the addition of 1 kg/m^3 of PP micro fibres would limit the average spalling depth to 25 mm with a 99.99% confidence interval. The level of spalling resistance provided by the inclusion of 1 kg/m^3 of PP fibres was evident after the completion of independent fire testing undertaken at CSIRO's laboratory (Figure 10).

Specimen A: Steel fibre mix without PP fibre: Spalling depth: max 170 mm

Specimen B: Steel fibre mix with 1 kg/m^3 PP fibre: Spalling depth: 0-1 mm

Figure 10 Left: Specimen containing no PP fibres after 120 min test following 4-hr ISO curve; Right: Specimen containing PP fibres after 120 min test following 2-hr HC curve

The structural assessment of the shotcrete lining was performed following the principles outlined in BS EN 1992 1-2:2004 [14]. The structural design for fire is considered as an extreme event with the objective to confirm structural stability. Therefore, load factors of 1.0 are applied and the member capacity determined using a reduction factor of 1.0. Hinges are gradually introduced into the model to simulate the cracked concrete lining until structural capacity is satisfied.

6 Construction Overview To-Date

6.1 Primary lining

The sprayed concrete mix adopted for the primary lining was a 180 mm slump steel fibre reinforced mix with a 28-day compressive strength of 40 MPa. A fibre dosage of 35 kg/m^3 was adopted to achieve the minimum 3.0 MPa flexural strength CMOD4 in beam tests. The mix design was in accordance with standard practice for Australian Civil/Tunnel applications. Additional reactivity testing was completed to verify the compatibility of the accelerators proposed for use with the hydration control additives and superplasticisers.

In the heading excavation cycle a minimum 2.5 MPa concrete strength was required prior personnel entry. Prior to advance the tunnel lining was required to have a minimum strength of 8 MPa. Tamshot 80AF alkali-free accelerator was used with a dosage rate of 6% to achieve a shotcrete strength of 8 MPa in 13 hrs. To reduce time waiting for strength gain this was optimised during the construction phase to 6 MPa based on tunnel convergence data and geotechnical information gained from the drilling of canopy tubes and face mapping records. A summary of the measured strength gain is provided in Table 2.

The sprayed concrete mix design was constrained to the mix design that would be used project wide for permanent primary sprayed concrete. The mix design was based on a 25% fly ash as supplementary cementitious due to durability requirements. This significantly limited the ability to target early age strength and had implications for accelerator reactivity.

The competing target strengths of 6 MPa for advance and 30 MPa for crane loading presented a challenge of optimisation of accelerator dosage. Significant site testing was conducted to assess the interaction of hydration control and accelerator additives from different suppliers. The hydration control was proven to have a slightly detrimental effect on early age strength however was retained in the mix due to the positive effect on the strength gain to 30MPa target and overall shotcrete quality.

Site trials for sprayed concrete mix design also included trials comparing the performance of a specialised accelerator that is typically better suited to handle blended cements, Normet 110AF [15]. The results of this indicated significantly faster strength gain in the 0-2.5MPa range with a corresponding reduction in 7 day and 28 day strength. Accelerator dosage of 80AF was assessed to be suitable to achieve specification requirements in the range of 4%-8%. On site testing confirmed that a dosage of 6% minimised cycle time loss during excavation and maximised the 7-day strength gain for the target 30 MPa requirement.

Table 2 Shotcrete strength gain

Age	Compressive strength (MPa)
6 hours	2.5 MPa
11 hours	6 MPa
13 hours	8 MPa
1 day	12 MPa
3 days	18 MPa
7 days	28 MPa
28 days	49 MPa

6.2 Instrumentation and monitoring

Instrumentation and monitoring installed during the construction phase consisted of automated surface settlement monitoring, borehole extensometers, convergence prisms and groundwater monitoring.

Current observations of surface settlement show that approximately 13 mm of settlement has occurred. During the design phase up to 24 mm of surface settlement was predicted which comprised approximately 14 mm caused by tunnel convergence and up to 10 mm by from ground water draw down. The effects of consolidation settlement occurring from groundwater draw down are expected to occur over the medium to long-term (months to years).

A borehole extensometer installed directly above the adit shows that the measured movements agree reasonably well with the predicted movements from the design phase (Figure 11). The amber trigger level shown in Figure 11 is set slightly before the predicted design value.

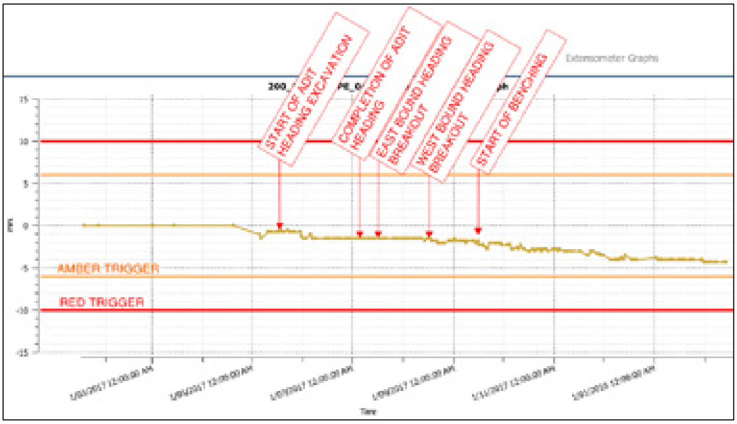

Figure 11 Extensometer readings

Convergence monitoring arrays attached to the tunnel lining showed high horizontal movements characteristic of the Hawkesbury Sandstone. The high horizontal stresses contained within the Hawkesbury Sandstone are well documented [16,17,18,19], the major horizontal stress can be up to 4 times higher than minor vertical stress, although, during the design phase high horizontal stresses were not predicted at such shallow depths (7 m cover) particularly considering the crown of the tunnel was predicted to be partially excavated in alluvium. The incision of Wolli Creek which had eroded through the upper layers of rock leaving buried sandstone cliffs creating the variable rock head levels encountered in the geotechnical investigations was considered to have relieved some of the stresses in the rock mass.

Up to 14 mm of lateral movement was recorded which confined the tunnel lining and causing only 5 mm vertical crown sag at some locations. At the beginning of the adit where the shotcrete lining was strengthened by steel sets, 10 mm of crown heave was recorded. A similar phenomenon was also observed on the South West Rail Link Underpass in South-West Sydney [20]. The invert and sidewalls of the tunnel were founded in the Minchinbury Sandstone of the Wianamatta Group. The sprayed concrete lining containing steel sets was squeezed as the stresses were relieved from the Sandstone causing up to 24 mm of heave.

At the time of writing this paper, benching in the adit area has been completed and preparations have commenced for waterproofing and secondary shotcrete trials.

7 Summary and Conclusions

The final design of the Kingsgrove construction access adit was driven by managing geotechnical risks and project constraints. The main geotechnical risks included the construction of a large intersection at shallow depth beneath 3rd party assets (Existing M5 motorway and Wolli Creek) and uncertainty in the rock head level caused by the presence of an incised creek channel and associated palaeochannel. Project constraints included constructing the tunnels from a small industrial property with fixed shaft and tunnel alignments and the ability to provide sufficient space to excavate the tunnels. Development of the design involved consideration to roadheader excavation profiles, bolting arm clearances and articulated dump truck clearances.

The design of the primary sprayed concrete lining was driven by the shallow overburden conditions. The tunnel profile was heavily arched to promote ground arching and to maximise compression within the shotcrete lining. The intersection between the two arched profiles of the adit and mainline tunnels created high tensile stresses above the openings which required conventional steel reinforcement.

The design of the secondary sprayed concrete lining followed a traditional composite lining approach where by load sharing between the primary and secondary linings is considered. Uncertainty in long term bond performance of sprayed waterproof membranes and lack of standards and guidelines regarding composite lining design methods resulted in the true composite lining approach, as shown in Figure 8, not being adopted for the design.

Fire testing conducted for the project confirmed the significant benefits that the addition of micro PP fibres provide for the fire performance and spalling resistance of sprayed concrete linings. Almost no spalling was observed in concrete mixes containing micro PP fibres which were exposed to thermal conditions matching the 2-hour HC curve. The marked improvement in fire resistance from the addition of micro PP fibres is outweighed by the comparatively small increase in cost per cubic metre of sprayed concrete (approx. \$15/m^3).

A close relationship between the design and construction teams allowed an observational approach to be adopted for the tunnels. Geotechnical records obtained from the installation canopy tubes, face mapping and geotechnical probing combined with the instrumentation and monitoring records allowed for the design to be verified. Optimisations were made to the design during construction including refinement of the minimum concrete strengths required prior to advance from 8.0 MPa to 6.0 MPa and the change from a split heading excavation sequence to full heading excavation sequence for the development of the mainline tunnels from the adit.

Automated surface settlement monitoring has recorded up to 13 mm of settlement above the adit to date. This is expected to increase by approximately 10 mm due to consolidation settlement caused by groundwater draw down. It is anticipated that this will to occur over the medium to long term. The settlement impacts on 3rd party infrastructure such as Wolli Creek remain on track and are predicted to be well below the maximum acceptable limits of 40 mm settlement and 1 in 250 angular distortion.

8 References

[1] Duddeck, H., and Erdmann, J. (1985). On structural design models for tunnels in soft soil. Tunnelling and Underground Space, 9 (5-6), 246-259.

[2] Thomas, A.H., Pickett, A.P. (2013). Where Are We Now with Sprayed Concrete Lining in Tunnels?. Tunnelling Journal, 44-53.

[3] Sun, Y., McRae, M., and Greunen, J.V. (2013). Load Sharing in Two-pass Lining Systems for NATM Tunnels. Rapid Excavation and Tunneling Conference 2013 Proceedings, 1178-1192.

[4/5] Su, J., Uhrin, M. (2016). Primary-Secondary Lining Interactions for Composite Sprayed Concrete Lined Tunnels Using Sprayed Waterproofing Membrane. World Tunnel Congress 2016, San Francisco, CA, United States.

[6] Jäger, J. (2016). Structural Design of Composite Shell Linings. World Tunnel Congress 2016, San Francisco, CA, United States.

[7] Su, J., Bloodworth, A., and Haig, B. (2013). Experimental Investigation into the Interface Properties of Composite Concrete Lined Structures. Proceedings of the World

Tunnel Congress 2013, Underground. The Way to the Future. Abingdon, GB, CRC Press, 1518–1525.

[8] Clement, F., and Holter, K.G. (2016). Experiences With Spray Applied Waterproofing Membranes. Proceedings of the World Tunnel Congress 2016, San Francisco, ITA-AITES.

[9] Thomas, A. (2009). Sprayed Concrete Lined Tunnels. Applied Geotechnics Volume 2, Taylor and Francis, Abingdon.

[10] BTS/ICE (2004). Tunnel Lining Design Guide, Thomas Telford, London.

[11] Standards Australia (2014). AS 1530.4-2014 Methods for fire tests on building materials, components and structures. Part 4: Fire-resistance test of elements of construction, Standards Australia, Sydney, NSW, Australia.

[12] BSI (2002). Eurocode 1: Actions on structures Part 1-2: General actions – Actions on structures exposed to fire, BS EN 1991-1-2:2002, British Standards Institution, London.

[13] McMillen Jacobs Associates. (2016). WestConnex M4 East, Fire Study: Spalling Protection Using Propylene Fibres, Rev C.

[14] BSI (2004). Eurocode 2: Design of Concrete Structures Part 1-2: General rules – Structural fire design, BS EN 1992-1-2: 2004, British Standards Institution, London.

[15] Rispin, M, Kleven, OB, Dimmock, R & Myrdal, R 2017, 'Shotcrete: early strength and re-entry revisited – practices and technology', in M Hudyma & Y Potvin (eds), *Proceedings of the First International Conference on Underground Mining Technology*, Australian Centre for Geomechanics, Perth, pp. 55-70.

[16] Enever, J. R. (1999). Near surface in-situ stress and its counterpart at depth in the Sydney metropolitan area. Australian Geomechanics, 65-76.

[17] Pells, P. K. N. (2004). Substance and mass properties for the design of engineering structures in the Hawkesbury Sandstone. Australian Geomechanics, 39, 1-21.

[18] McQueen, L.B. (2004). In situ rock stress and its effect in tunnels and deep excavation in Sydney. Australian Geomechanics, 39(3).

[19] Bertuzzi., R. (2014). Sydney sandstone and shale parameters for tunnel design. Australian Geomechanics, Vol. 49(1).

[20] Clarke, S.J., Walker, C.S. (2014). Deformation Mechanisms of the South West Rail Link Underpass beneath the Hume Highway, 15th Australasian Tunnelling Conference 2014, Sydney, NSW, Australia

LABORATORY INVESTIGATION OF STEEL FIBRE REINFORCED SPRAYED CONCRETE USING A COMPUTED TOMOGRAPHY METHOD

Anders Ansell
KTH Royal Institute of Technology, Stockholm, Sweden
anders.ansell@byv.kth.se

Erik Nordström
KTH Royal Institute of Technology and
Sweco Energuide, Hydro Power & Dams, Stockholm, Sweden
erik.nordstrom@byv.kth.se

Alvaro Guarin
KTH Royal Institute of Technology, Stockholm, Sweden
alvaro.guarin@abe.kth.se

ABSTRACT

A laboratory method for investigation of cored samples of steel fibre reinforced sprayed concrete (shotcrete) is described. A pilot study on computed tomography (CT) has been conducted, with focus on how the technique can be used for non-destructive testing where the cores remain intact after scanning and evaluation. The CT method require advanced integrated equipment for X-ray scanning and image detection, together with a computerized visualization system that can reproduce a three-dimensional virtual, transparent model of the studied object. The method is well suited to describe orientation and distribution of steel fibres within the concrete. Interfaces between rock-concrete and concrete-concrete, between layers of different sequences of spraying, can also be identified. The results from the CT investigations can be presented as qualitative data that in 3D shows locations of steel fibres, aggregates, etc., and also as quantitative data showing relative distributions of cement paste, aggregates, steel fibres and voids, which is here demonstrated by a selection of examples. The method is well suited for practical analysis of sprayed concrete in situ specimens and it is recommended that it is established as a standard method for special inspections and performance evaluation of rock support in tunnels and subspace structures.

INTRODUCTION

The ability to optimize the composition of sprayed concrete (shotcrete) for use in efficient tunnelling and rock construction depends on knowledge of the material properties, its structure and distribution of aggregates, air voids and steel or synthetic fibres if added. For rock engineering and tunnelling, more cost-effective, sustainable and safe tunnels and subspace structures would then be the result. The most common investigation methods for the interior of in situ samples of standard cast or sprayed specimens are today slicing or sawing followed by microscopy. This is time consuming and also prevent further investigations since the specimens are destroyed. Computed tomography (CT), which is an advanced method based on X-ray scanning and image detection, now provides new possibilities. Integrated systems with equipment for computerized visualization can reproduce three-dimensional (3D) virtual, transparent models of the studied objects. The results from tomography investigations can be analysed and presented in the forms of qualitative and quantitative results for the test specimens. The quantitative data that can be calculated for a concrete specimen at a macro or meso scale are typically distributions of cement paste, aggregates, steel fibres, voids and air pores within the studied volume. Of particular interest is to study steel fibre reinforced concrete, cast and sprayed, and how the fibres are orientated inside the concrete and also how they work in shrinkage, tensile stressing and cracking [1]. As young concrete hardens, its strength and bond to the fibres increases, which affects the cracking process [2]. The boundary layers between different materials, such as rock and concrete, are of great interest, see e.g. [3] and [4]. Through samples taken in situ it will also be possible to continuously monitor any degradation of the material, for example by corrosion in steel fibre reinforcement, see e.g. [5]. A laboratory pilot study [6] has been carried out at the KTH Civil and Architectural Engineering laboratory to describe the possibilities and limitations of the technique and also the procedures for an examination. Examples demonstrate how the method can be implemented for examination of standard size cast concrete cylinders and drilled core samples of cast and sprayed concrete, with a focus on finding practical routines for investigations to obtain the qualitative and quantitative data. The included literature review of previous research in the area shows very little published work focusing on analyses of laboratory samples of normal size and of in situ cores drilled directly out of existing structures. There is little or no previous research attempts on adapting the technique for use with sprayed concrete specimens. This paper summarizes, demonstrates and comments the result of the pilot study [6], with focus on the possibilities of conducting investigation of sprayed concrete in situ samples of the type used in civil engineering rock work and tunnel construction. A shorter summary with comments on the pilot study is also given in [7].

X-RAY COMPUTED TOMOGRAPHY

X-ray computed tomography (CT) is a digital technique for visualizing the interior of solid objects down to microscopic detail level. Medical X-ray CT systems are e.g. used for acquiring images of bones and soft tissues. Further advancement of the medical CT technique have today also led to the development of industrial CT systems. High-resolution industrial X-ray CT differs from conventional medical CT-scanning in its ability to utilize higher energy X-rays. This increase in penetrative power makes it possible to detect details as small as a few tens of micrometres in size, also in high density materials. In the following, a brief summary of the CT technique is given. For a more detailed description see e.g. [8], on which part of the summary is based.

Industrial tomography systems

Industrial X-ray CT systems are today used for studies of materials within geo-sciences, engineering and manufacturing. The ability of the X-rays to differentiate materials depends on their respective linear attenuation coefficients, which basically is proportional to the material density. The volume studied is described by constant thickness slices, series of stacked CT images represented by volume elements (voxels), and not two-dimensional picture elements (pixels). The quality of the scanned pictures depend on the noise level, the slice thickness, the low and high contrast resolutions, which in turn depend on the X-ray source, detectors used and the geometry of the scanned material specimen. The variables that determine how effective an X-ray source will be for a particular task are size of the focal spot, the spectrum of the X-ray energies generated and the X-ray intensity. The energy spectrum defines the penetrative ability of the X-rays, as well as their expected relative attenuation as they pass through materials of different density. Higher-energy X-rays penetrate more effectively than lower-energy ones, but are less sensitive to changes in material density and composition. The X-ray intensity directly affects the signal-to-noise ratio and thus the image clarity. The scanning configuration refers to the source-object-detector distances and the resolution of the scanned object is magnified by minimizing the source-object distance and maximizing the object-detector distance. The main sample preparation prior to a CT scanning is to position the object inside the field of view and secure it against displacement during the scan. The full scan field for CT is a cylinder and therefore, when possible, it is advantageous to have a cylindrical sample geometry – see Figure 1.

Computed tomography system

The X-ray CT system used in the pilot study is stationed at the laboratory of the KTH Department of Civil and Architectural Engineering in Stockholm. It is of the type NSI X5000 [10], an advanced system integrating computerized visualization and image detection with equipment for X-ray scanning, see Figure 2. The system is controlled from a workstation with software for CT calibration, 3D real time visualization and numerical analysis tools. There are 225 kV and 450 kV X-ray tubes within an adjacent radiation-shielded enclosure. These have focal spot sizes of 5 µm and 400 µm, respectively, and there is also an integrated high-resolution digital detector with 200 µm pixel pitch (Figure 3b). Data with voxel sizes down to 5 µm can thus be obtained, depending on e.g. specimen size and the tube used. An MTS Uniaxial Test System for up to 100 kN force and 150 mm displacement is mounted in the enclosure and it is also possible to use a small climate chamber for testing temperatures from -20ºC to +80ºC.

Investigation procedure

The first step of the investigation of a test sample is to place this on the rotating turntable between the X-ray source and the detector. X-rays are then sent through the sample while the table undergoes a full rotation at constant speed. The resulting digital three-dimensional image will consist of a "stack" of horizontal 2D images with equal thickness that together defines the 3D volume. Each 2D CT image is thus composed by 3D elements, i.e. voxels. Details on the complete procedure of sample preparation, calibration, data acquisition and reconstruction are e.g. found in [8], but are here in the following briefly summarized.

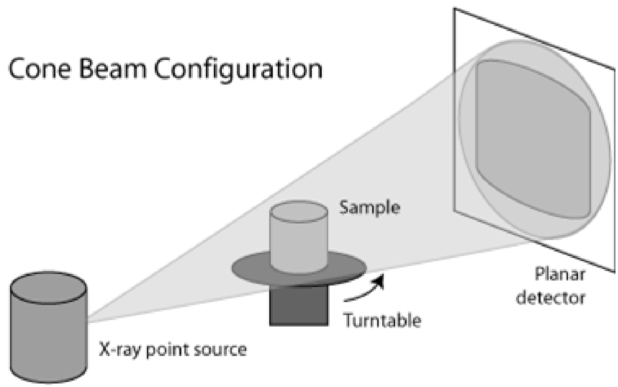

Figure 1: X-ray scanning of a rotating, circular test sample [9].

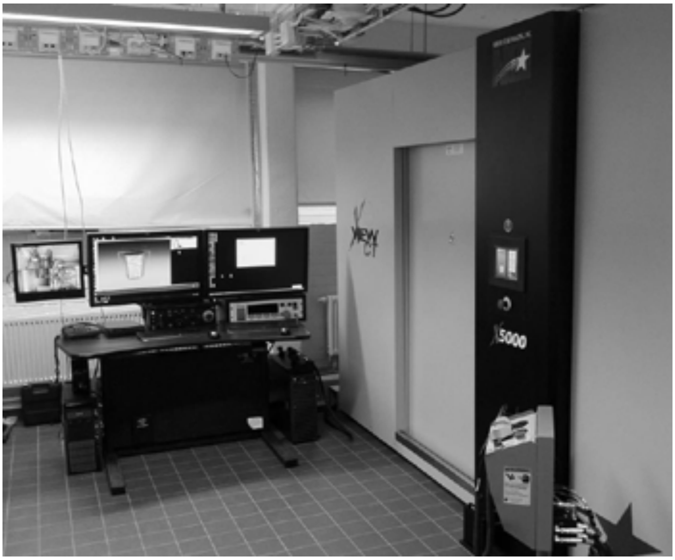

Figure 2: X-ray CT system at KTH Department of Civil and Architectural Engineering.

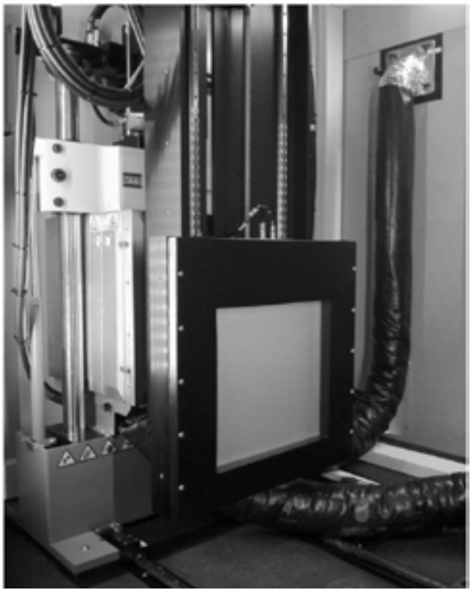

Figure 3a: Detector with 200m pixel pitch.

Figure 3b: X-ray sources, 225kV and 450kV.

Calibration is necessary to establish the characteristics of the X-ray signal as read by the detectors under scanning conditions, and to reduce geometrical uncertainties. The principal variables in collection of CT data are the numberof views and the signal acquisition time per view. The number of views used ranges from 600 to 3600 or more, each representing a rotational interval equal to 3608 divided by the total number of views. Each line of this raw data contains a single set of detector readings for a view, and time progresses from top to bottom. In this so-called sinogram is every single point in the scanned object corresponding to a sinusoidal curve. Reconstruction is the mathematical process of converting sinograms into 2D slice images. The most often used technique is filtered back-projection. During this reconstruction, the raw intensity data in the sinograms are converted to CT numbers that have a range determined by the computer system. Industrial CT systems are sometimes calibrated so that air has a value of 0, water of 1000, and aluminium of 2700, so that the CT number corresponds roughly to the density [11]. These values are then coupled to the grayscale in the image files created by the system. A complete analysis of a tested sample also requires subsequent post-processing in which the images are interpreted and information extracted with additional numerical calculations carried out using a general numerical procedure. A typical workflow for post-processing includes the four main steps; image de-noising and correction, materials segmentation, quantitative analysis and volume meshing. The correction procedure is demonstrated for a sample of asphalt concrete in Figure 4, which shows the gradual transformation from the original CT image via a corrected image with enhanced contrast and more clearly identifiable borders to a segmented picture with sharp borders between identified materials. In this final image, the material with the highest attenuation coefficient, i.e. for concrete the aggregate, will be bright grey, the material with the lowest attenuation coefficient, i.e. air voids, will be dark (here black) while the cement paste will be shown in darker grey that falls between these limits. Steel fibres would appear as bright light ("white") lines or dots, depending on their orientation.

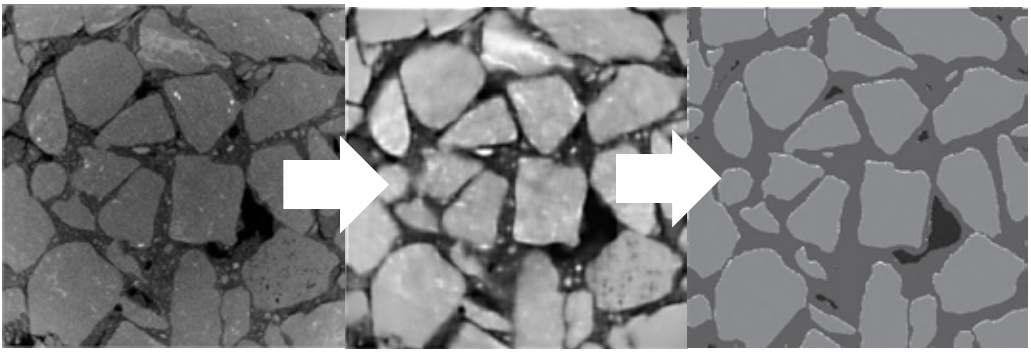

Figure 4: Correction of a CT image. From left to right: original image, corrected and de-noised image, identified pre-defined material types. From [12].

IN SITU AND LABORATORY CASES

Computed tomography has previously been used mostly for studies of microstructures in materials other than concrete and cement pastes, see e.g. the compilation by Sharma et al. [13]. Early examples of computer tomography performed on concrete are e.g. [14] and [15]. The pilot study summarized here investigates the possibilities and limitations of the technology as an investigation method for especially young and old sprayed concrete in tunnels. The focus is on methods of full-size cylinders cast of concrete with steel fibre content or test cores taken in the field or from laboratory beams. Important for the practical use of the method is that concrete with full size aggregates can be investigated and not only small specimens of cement paste. No previous documented tomography investigations of sprayed concrete specimens has been found, but there are some interesting studies on e.g. steel fibre concrete.

Previous investigations

Most studies on concrete and cement paste in which computed tomography is used focus on the structure and properties of the porous system, see e.g. [16] and [17]. A study in which in situ samples are examined with regard to clogging of the porous system is presented in [18]. Concrete cores with a diameter of 100 mm from outdoor parking spaces show significantly lower porosities for older concrete. Interesting are also an investigation of concrete taken from a 40 year old water channel, [19]. Computed tomography was used to determine the degree of seasonal frost degradation and cracking in 75 mm diameter test cores. The effect of fibre corrosion in connection with tensile testing has also been investigated, see [20]. First, short-term tensile loads and then long-term load during ongoing corrosion attacks where applied. The first damage was noted after about 5 weeks and after 44 weeks of exposure, samples with steel fibres showed multiple cracks while samples that also contained PVA fibres remained un-cracked. An interesting study on fibre content, distribution and orientation in steel fibre reinforced concrete is presented in [21]. The CT scanned specimens were 600 mm long beams of a concrete type containing 78 kg/m^3, 36 mm long steel fibres and aggregate in fractions up to 16 mm. The beams were first exposed to three-point bending, after which 100 mm of the centre sections were scanned. The orientation of shorter steel fibres in concrete has been investigated, for samples taken from fibre reinforced concrete floors, [22]. The directions of the fibres were assessed based on a 3D skeleton image derived from the tomography results. The compilation showed that the fibres are mostly horizontally oriented near the centre of the slabs but more vertically close to the edges where the casting moulds have had an impact. More details and further relevant projects are summarized in [6]. The X-ray CT equipment at KTH Civil and Architectural Engineering was first used to investigate the internal structure of asphalt concrete, [12] and [23]. Results from these investigations are shown here as examples of the type of presentation of material data that also are relevant for full size samples of sprayed and cast concrete. The characterization of the internal structure of the asphalt concrete was designed to determine parameters for aggregate orientation, distribution and geometry as well as interaction in the contact zones between stones, binders and air pores. Examples on visualized 3D results are given in Figure 5, where the pore structure and aggregate configurations within an asphalt concrete cube are shown. These illustrations have been post-processed using a CAD program. The cubes were later further analysed using a finite element program for stress state analysis of the cooling asphalt material, [12].

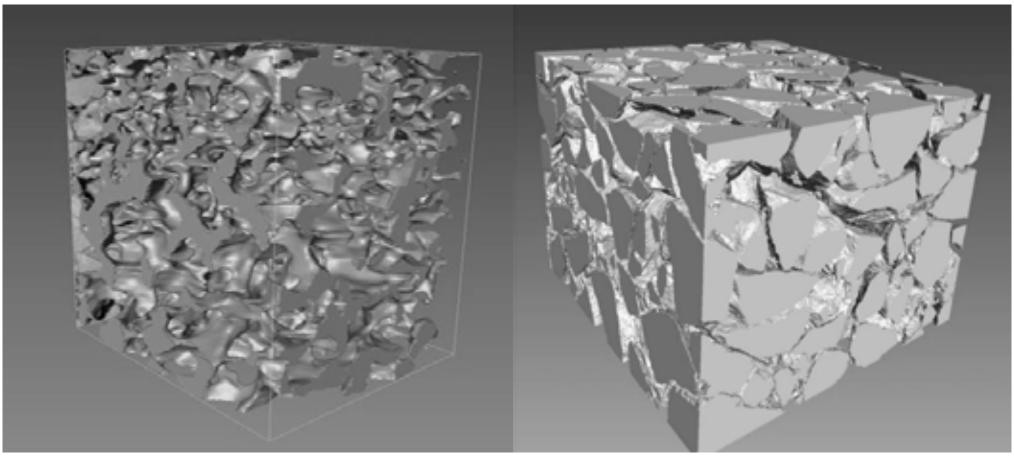

Figure 5: Pores (left) and aggregates (right) within an asphalt concrete cube. From [23].

Long time field exposure

A Swedish project with long-term field exposure of cracked steel fibre reinforced sprayed concrete have now been going on for 18 years, [5] and [24]. More than 300 sprayed concrete beams have been exposed in situ at three different sites; submerged in a river, along a motorway and inside a tunnel, see Figure 6. The goal is to define time to initiation and rate of corrosion, to investigate relevant parameters on the corrosion process and to study the long-term residual strength capacity with respect to ongoing corrosion. Thus far, it has been concluded that the durability against corrosion of the steel fibre reinforcement is good, especially in concrete specimens without cracks. The time for initiation depend on the crack widths but these have only a limited influence on the corrosion rate. It has also been found that due to the larger cathode area, longer fibres will corrode faster. As part of the pilot study here summarized, CT investigations of samples from the beams submerged in river water were investigated, see [6]. As will be demonstrated by a following example it was possible to detect degradation at the ends of cores taken from the test beams. The possibility to use tomography investigation to evaluate the status of the aging test samples will be further evaluated within the project.

Figure 6: Steel fibre reinforced test beams mounted in traffic tunnel. From [24].

In situ samples

The ability to investigate in situ core samples is of particular interest because the interaction between temperature, humidity, spray technology and the quality of the rock surfaces has a direct impact on the sprayed concrete quality. For young and hardening sprayed concrete it is of particular interest to study steel fibre content and orientation of these and the concrete homogeneity with respect to aggregate distribution and the presence of pores and possible cavities. For older concrete, the effect of freezing and penetrating water can be studied. The nature of the bonding interface is also of interest, between rock-concrete and between different layers of concrete. From cores containing both concrete and rock, the bond interface can be identified and studied. It is usually complicated to investigate the microstructure in the transition zone between rock and sprayed concrete, e.g. with scanning electron microscopes, see e.g. [3] and [4]. Even though there are a number of established test methods for estimating the bond strength between sprayed concrete and rock, there are relatively few detailed studies of how the properties of the boundary layer affect that strength. It is known that the structure and texture of the rock surface affects the bond strength between rock and shotcrete, see e.g. the summary in [4]. Mechanical bond-test results often shows a variation in failure types, from pure tensile concrete failures to complete bond failures and combinations of the two. As shown by the examples presented in the following, it is possible to use this type of CT results to study the interface topography and how the cement paste fills out and penetrate irregularities in the rock. This technique can thus contribute to and be an important part of analyses of the mechanisms that governs the bond between rock and sprayed concrete, together with microscopy and mechanical testing.

EXAMPLES

In the following, examples of results from CT analyses of cast and sprayed concrete cylinders are shown. These are laboratory cylinders, cores taken from cast concrete beams and in situ cores. All tests specimens are of concrete qualities and compositions that are either sprayed or would be sprayable. In all examples are steel fibres included. Detailed description of test specimens, system settings during tomography investigation, etc. are given in the pilot study research report [6].

Cast laboratory samples

The first example in Figure 7 show a cast concrete cylinder, 220 mm high and with 100 mm diameter. The volume is made up from 1982 slices, each 0.111 mm thick. The lighter colour represents a higher density in the material, whereas darker colour show lower densities. To distinguish between the four main components of the concrete, i.e. aggregate, cement paste, air pores and steel fibres, the colour scale (or grayscale) corresponding to the materials densities are defined so that the steel fibres are the brightest (white) points while the very dark areas are voids, cracks or air pores. The intermediate grey areas consist of aggregates (lighter grey) and cement paste (darker grey), which here also contains the minimum aggregate fractions since these are difficult to distinguish due to dissolution. The left sub-figure shows the outer surface of the cylinder, where some steel fibres appear clearly, and in the centre figure the steel fraction only, where the orientation of the fibres is clearly visible. The third sub-figure shows a vertical cut across the CT-generated 3D volume. Figure 8 shows diagrams on how the fractions of the three sub-materials (including void/air) vary along the cylinder. Here, it is clear that the steel fibres are unevenly distributed with a variation within 31-78 kg/m^3 in the cylinder. The figure also shows two of the 1982 sections included in the representation.

Cracked laboratory sample

Figure 9 shows a cast cylinder of the same type as in the previous example, but which has been cracked in an MTS test machine before the CT investigation. The purpose was to study a crack in an otherwise still intact steel fibre reinforced concrete volume. A local impression after the applied load is visible in the photo to the left. The crack propagation through the cylinder is shown in the centre sub-figure where an oblique section cuts through the cylinder. There and in the right sub-figure, the crack width decreases downwards in the cylinder where the fibre content is higher. The main crack is also shown in Figure 10, where the blow-up figure shows steel fibres that bridge the crack and corresponding measured crack widths.

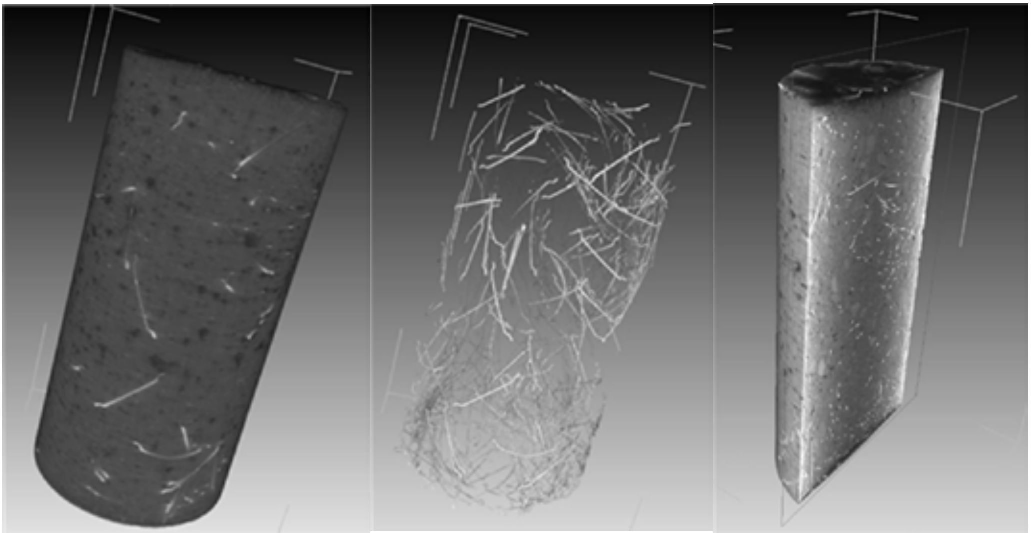

Figure 7: Three-dimensional presentation of CT-scanned concrete cylinder. Exterior surface, steel fibres and a vertical centre-cut. From [6].

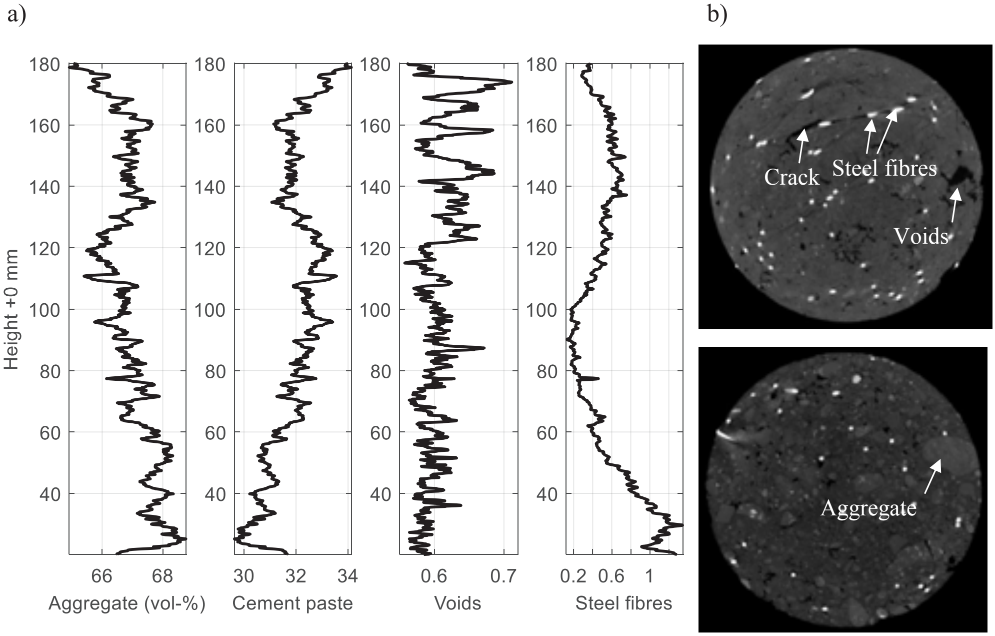

Figure 8: Distribution of aggregates, cement paste, voids and steel fibres along a 160 mm length of a CT-scanned concrete cylinder. From [6].

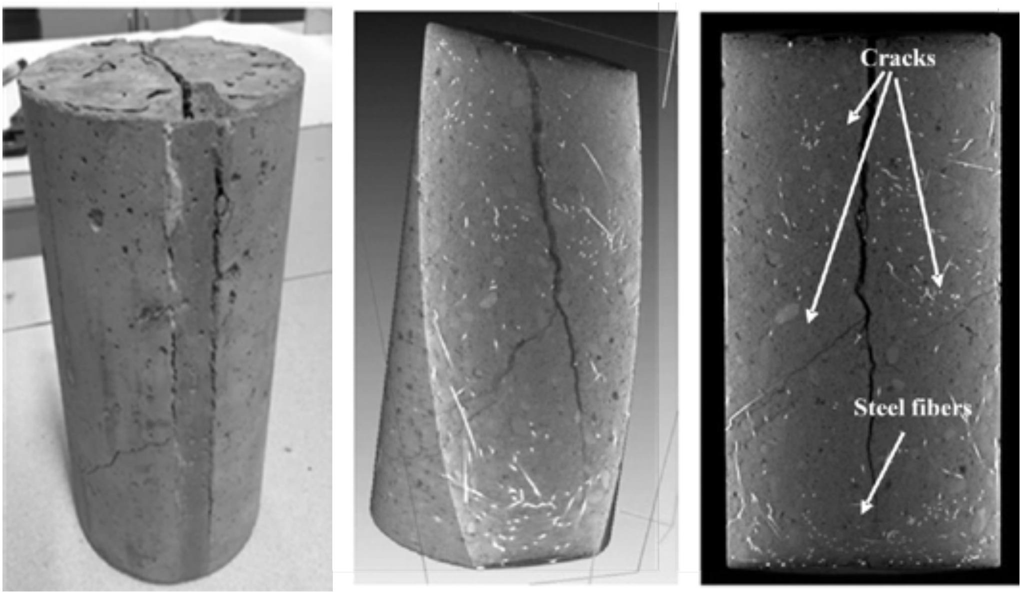

Figure 9: Cracked 200 mm long, 100 mm diameter concrete cylinder, with diagonal and vertical cuts through the CT-generated volume. From [6].

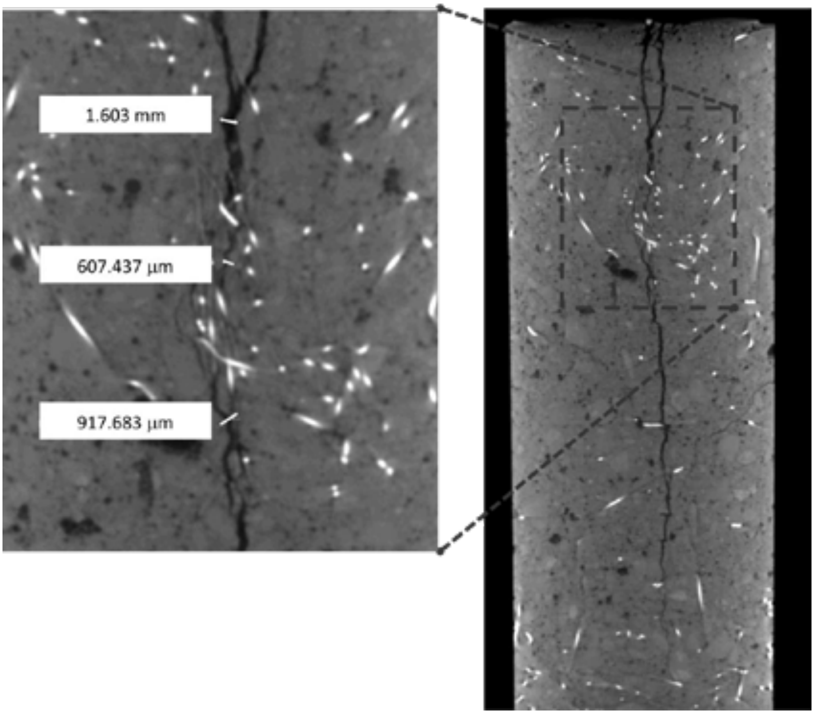

Figure 10: Cracks and bridging steel fibres in cracked concrete cylinder. From [6].

Core from sprayed beam

An example of a drilled out core from a laboratory tested sprayed concrete beam is shown in Figure 11. The specimen come from the long-term observation project and was exposed to flowing freshwater [24], after which the cylinders were cored for examination in the laboratory. The cylinder is 125 mm long, of which the upper 50 mm has been immersed in water, and with a diameter of 50 mm. To the left is a photo and to the right 3D CT images of the specimen exterior and the steel fibres only, with a fibre orientation that is highly variable. The variation of the concrete composition within the volume is given in Figure 12. Here it can be seen that the fibre concentration is somewhat higher towards mid-height of the core and that there are significantly small aggregate contents towards the ends of the core and loss of fibres towards the top.

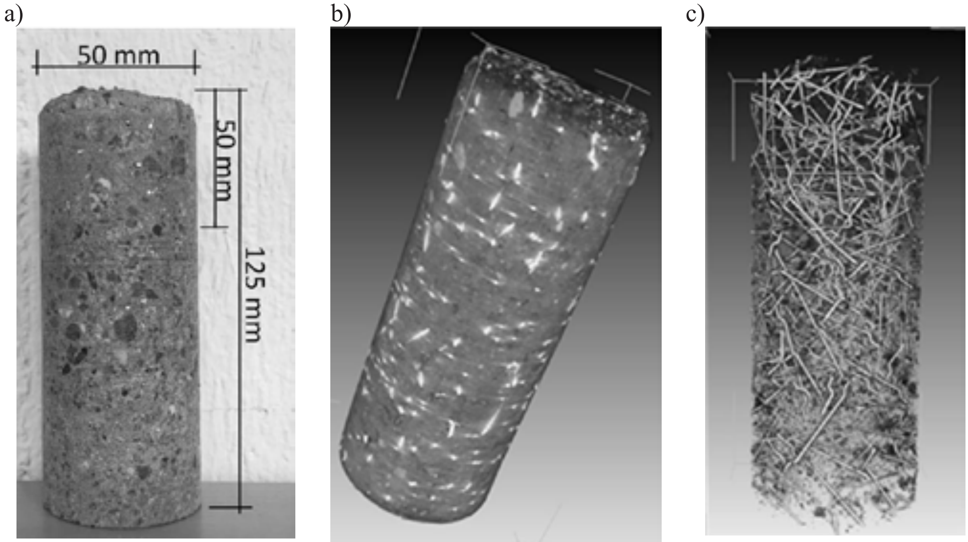

Figure 11: Shotcrete core from a laboratory test beam (a), CT image of its outer cylinder surface (b) and of the steel fibre configuration only (c). From [6].

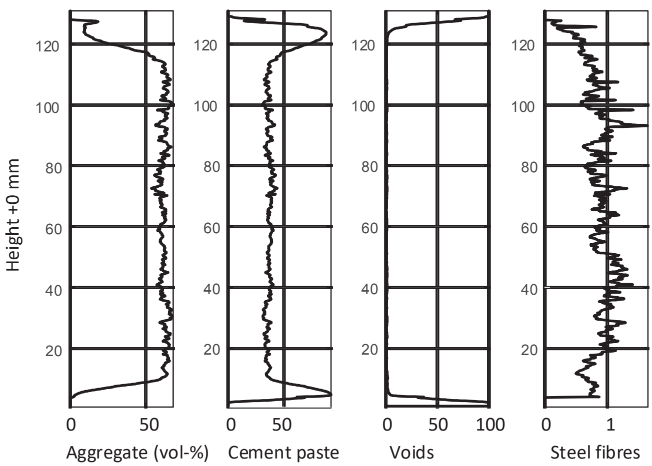

Figure 12: Variation in concrete composition over the 125 mm long concrete core. From [6].

a) b)

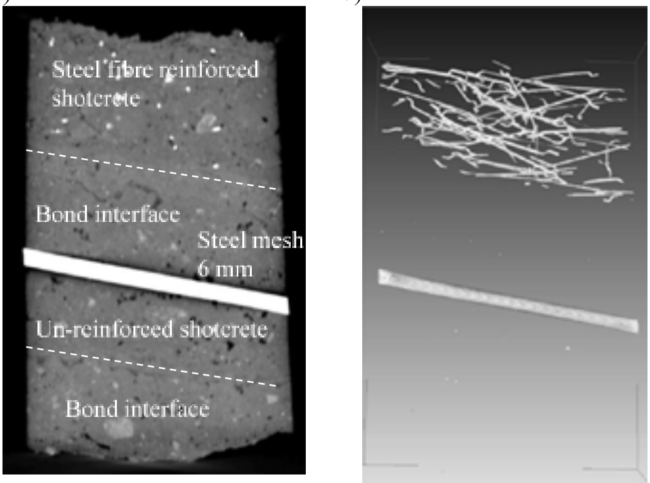

Figure 13: CT image of an in situ core with three layers of sprayed concrete (a) and steel fibre and mesh configuration (b). From [6].

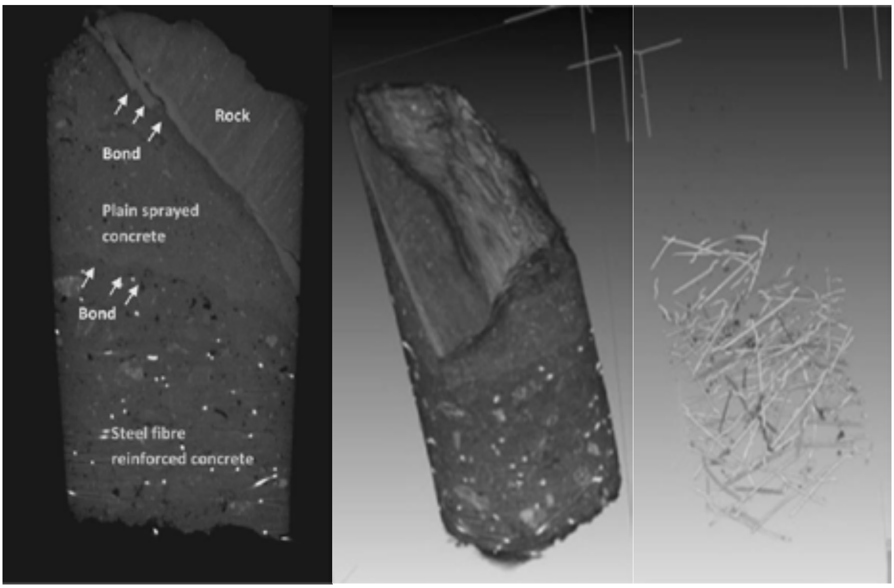

Figure 14: CT image of an in situ core with two layers of sprayed concrete and a section of rock. The steel fibres are shown in the right sub-figure. From [6].

In situ cores

The forth example is shown in Figure 13, a core drilled through a three-layer sprayed concrete lining. Two bond interfaces are here clearly seen, between a lower un-reinforced layer and an intermediate layer with steel mesh reinforcement, and between the latter and a thinner layer with steel fibre reinforced concrete. Most likely, the lower layer was first sprayed and on top of this was then the steel mesh mounted. This was later over-sprayed and then also covered by a layer of steel fibre reinforced concrete. The core show no remains of fractured rock at the inner surface and it can thus be assumed that there was tensile concrete failure, or possibly a pure bond failure, during the extraction of the core. Only the steel material is shown in the 3D figure (b), with sections of the reinforcing mesh and fibres. The concrete is anisotropic with a significant reinforcing effect in the surface plane, since the fibre orientation here coincides with the tunnel surface direction. A further, and last example also shows an in-situ core, but here containing two layers, with fibre reinforced and plain concrete sprayed on an inclined rock surface that also is part of the core, see Figure 14. In the left sub-figure the interfaces appear clearly and there is also a visible crack in the rock. In the two 3D images, the outer structure of the core is shown and also the content of steel fibres present in the outer part of the core. The fibre orientation are here more isotropic than in the previously shown core, see Figure 13 for comparison.

CONCLUSIONS

The pilot study [6] here summarized shows that the method of computed tomography (CT) is suitable for practical analysis of in situ sprayed concrete specimens. The examples presented demonstrate that the technology and equipment has great potential as an investigation method of full size sprayed specimens. It will be possible, by regular testing and analysis, to follow degradation of concrete materials in situ and also to optimize concrete materials for rock construction through laboratory investigations. The results from the CT investigations can be analysed and presented as quantitative data showing distributions of cement paste, aggregates, steel fibres and voids, and as qualitative data that shows 3D locations of fibres, aggregates, etc. It is recommended that the method is established as a standard method for non-destructive testing of sprayed concrete cores taken in situ, as an advanced tool to be used in special inspections and performance evaluations. The further development of the method depends on the possibilities to compare analysis results from various types of concrete and environments. It is therefore recommended that an open database with results from major construction projects is started, based on CT test data grouped in a standardised way to facilitate comparisons.

ACKNOWLEDGEMENT

The presented project was supported by BeFo, The Rock Engineering Research Foundation, which is hereby gratefully acknowledged. The authors also thank Dr. Lamis Ahmed at KTH for contributing to the pilot study and Research Engineer Per-Erik Thorsell at Vattenfall AB for providing test samples for the analyses.

REFERENCES

1. Lagerblad, B., Fjällberg, B., Westerholm, M. *Shrinkage of shotcrete - modification of concrete mix* (In Swedish: *Sprutbetongs krympning – modifiering av betongsammansättning*), Report 86, SveBeFo, Stockholm, 2007.

2. Ansell, A., Holmgren, J. *Shrinkage of shotcrete - addition of fibers for crack distribution* (In Swedish: *Sprutbetongs krympning - fiberinblandning för bättre sprickfördelning*), Report 87, SveBeFo, Stockholm, 2007.

3. Bryne, L.E, Lagerblad, B. "Texture and bond at the interfacial zone between rock and sprayed concrete", *Proceedings of fib Symposium - Concrete Structures for Sustainable Community*, Stockholm, 2012.

4. Bryne, L.E. *Time dependent material properties of shotcrete*. Doctoral Thesis, KTH Concrete Structures, Stockholm, 2014.

5. Nordström, E. *Durability of sprayed concrete – Steel fibre corrosion in cracks*, Doctoral Thesis, Luleå University of Technology, Luleå, 2005.

6. Ansell, A., Ahmed, L., Guarin, A. *Computed tomography as investigation method for young and old, sprayed and cast concrete for tunnels*, BeFo report 165, Stockholm, 2017.

7. Ansell, A., Ahmed, L., Guarin, A. "Computed tomography as investigation method for steel fibre reinforced tunnel shotcrete", Proceedings of the *XXIII Nordic Concrete Research Symposium*, Aalborg, 2017.

8. Ketcham, R.A., Carlson, W.D. "Acquisition, optimization and interpretation of X-ray computed tomographic imagery: applications to the geosciences", *Computers & Geosciences*, 27, 381-400 (2001).

9. Ketcham, R.A. *X-ray computed tomography* (*CT*), University of Texas at Austin, http://serc.carleton.edu/research_education/geochemsheets/techniques/CT.html (2016).

10. *X5000 system*, North Star Imaging Inc., http://4nsi.com/systems/x5000/ (2016).

11. Johns, R.A., Steude, J.S., Castanier, L.M., Roberts, P.V. "Non-destructive measurements of fracture aperture in crystalline rock cores using X-ray computed tomography", *Journal of Geophysics Research*, 98, 1889–1900 (1993).

12. Onifade, I. *Internal structure characterization of asphalt concrete using X-Ray computed tomography*, Master Thesis, KTH Civil and Architectural Engineering, Stockholm, 2013.

13. Sharma, R., Ren, W., McDonald, S.A., Yang, Z. "Micro mechanisms of concrete failure under cyclic compression: X-ray tomographic in-situ observations", c *9th International Conference on Fracture Mechanics of Concrete and Concrete Structures*, FraMCoS-9, Berkeley, 2016.

14. Heiskainen, K.A., Rhim, H.C., Monteiro, P.J.M. "Computer simulations of limited angle tomography of reinforced concrete", *Cement and Concrete Research*, 21, 625-634 (1991).

15. Desrues, J. "X-Ray CT for geomaterials soils, concrete, rocks", Proceedings of the *International Workshop on X-Ray CT for Geomaterials*, Kumamoto, 2003.

16. Lu, S., Landis, E.N., Keane, D.T. "X-ray microtomographic studies of pore structure and permeability in Portland cement concrete", *Materials and Structures*, 36, 11-20 (2006).

17. Diamond, S., Landis, E.N. “Microstructural features of a mortar as seen by computed tomography”, *Materials & Structures*, 40, 989-993 (2007).

18. Manahiloh, K.N., Muhunthan, B., Kayhanian, M, Gebremariam, S.Y. “X-Ray computed tomography and non-destructive evaluation of clogging in porous concrete field samples”, *Journal of Materials in Civil Engineering*, 24, 1103-1109, (2012).

19. Suzuki, T., Aoki, M., Ohtsu, M. “Damage identification of cracked concrete by X-Ray computed tomography method”, Proceedings of the *7th International Conference on Fracture Mechanics of Concrete and Concrete Structures*, FraMCoS-7, Seoul, 2010.

20. Nguyen, W., Hernández-Cruz, D., Celik, K., Duncan, J.F., Monteiro, P.J.M, Ostertag, C.P. “In-situ tensile and corrosion damage characterization of fiber-reinforced cementitious composites using X-ray micro-computed tomography”, Proceedings of the *9th International Conference on Fracture Mechanics of Concrete and Concrete Structures*, FraMCoS-9, Berkeley, 2016.

21. Fuentes, R., Geiker, M.R., Stang, H. “Characterisation of fibre content, distribution and orientation to predict fibre reinforced concrete behaviour”, *Nordic Concrete Research*, 52, 1–22 (2015)

22. Suuronen, J.P., Kallonen, A., Eik, M., Puttonen, J., Serimaa, R., Herrmann, H. “Analysis of short fibres orientation in steel fibre-reinforced concrete (SFRC) by X-ray tomography”, *Journal of Materials Science*, 48, 1358–1367 (2013).

23. Guarin, A., Jelagin, D., Kringos, N., Birgisson, B. *X-ray computed tomography with tension/compression system with climate control*. Report RILEM TC on Mechanism of Cracking and Debonding - TG3 - State of the Art, 2012.

24. Nordström, E. *Evaluation after 17 years with field exposures of cracked steel fibre reinforced shotcrete*, BeFo report 153, Stockholm, 2016.

OPTIMISATION OF PLANT EMPLOYED TO INSTALL PERMANENT SHOTCRETE LINING USING OPEN GRIPPER TBMs

Bruce G Ashcroft
Multiconsult Norge AS, Norway
bra@multiconsult.no

Gary R Peach
Multiconsult Norge AS, Norway
garypeach@heraldix.com

SUMMARY

Twin 8.5 m diameter, approximately 10 km long parallel headrace tunnels under overburdens of up to 1 870 m with high horizontal stresses were excavated for a hydroelectric project located in north-eastern Pakistan using two open gripper Tunnel Boring Machines (TBMs).

This paper presents an assessment of the plant used to apply the permanent shotcrete (sprayed concrete) lining for the headrace tunnels excavated by the TBMs. The shotcrete operation was observed over a period of four months, during which time extensive data was collected on the final shotcrete application. Most of the shotcrete in the TBM tunnels was applied as the permanent lining about 65 m behind the cutterhead and is referred to as the 'L2 shotcrete'.

The assessment found that in terms of the plant, a different layout of pumps to that which was originally installed on the TBMs was required. This was necessary to better capitalise on the operational ranges of different pumps employed for installing different sections of the lining.

INTRODUCTION

General

The hydroelectric project is located in the Muzaffarabad district of Azad Jammu & Kashmir (AJK), in northeastern Pakistan. Geographically, the area consists of rugged terrain between 500 m and 3200 m in elevation within the Himalayan foothill zone known as the Sub-Himalayan Range.

The project is a run-of-river one, employing 28.6 km long headrace and 3.6 km long tailrace tunnels to cut off a major loop in the river system, transferring the waters of the Neelum River into the Jhelum River, for a total head gain of 420 m (Figure 1). The headrace tunnels comprise both single (31%) and twin (69%) tunnels, while the tailrace tunnel consists of a single tunnel. Design capacity of the waterway system is 283 m^3/s.

The project will have an installed capacity of 969 MW, generated by four Francis-type turbines located in an underground powerhouse.

When construction commenced in 2008, all tunnels were to be excavated using conventional drill & blast techniques. However, after excavation began, it soon became apparent that with the equipment being employed, a 13.5 km long section of the headrace twin tunnels overlain by high terrain that precludes construction of additional access adits, would take too long to excavate.

Consequently, the construction contract was amended to allow the operation of two 8.5 m diameter open gripper hard rock TBMs to excavate approximately 10 km of the twin headrace tunnels (Figure 1). The open gripper design was selected to give the most flexibility for the expected conditions – possible squeezing ground given the relatively weak rock mass and overburdens up to 1 870 m, and the potential for rockbursts in the stronger beds. Excavation of the TBM tunnels started in January 2013 in the left tunnel (viewed looking downstream), and a month later in the right tunnel. During the assessment which this paper describes, the TBM in the left tunnel was ahead of the TBM in the right tunnel by distances of approximately 100 m to 350 m. The TBMs in the left and right tunnels are hereon referred to as the 'Leading TBM' and 'Trailing TBM' respectively. Excavation was completed in the left tunnel in October 2016 and in the right tunnel in April 2017.

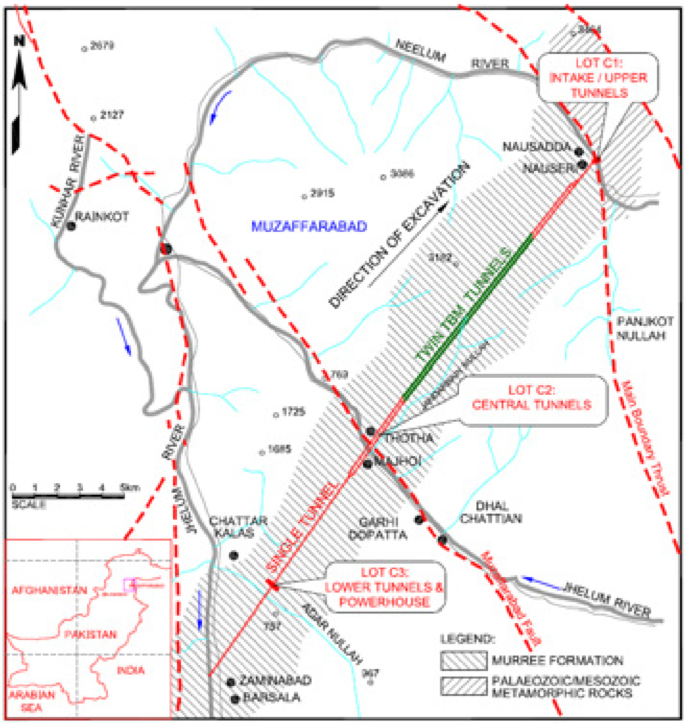

Figure 1: Project layout showing TBM Twin tunnels (in green), major faults (dashed) and simplified alignment geology

Objective of Assessment

This paper outlines both the successful investigation into assessing the effectiveness and efficiency of the plant employed for the application of L2 shotcrete and the recommendations made for improvements to the plant and logistics.

SHOTCRETE APPLICATION

Overview

Shotcrete was applied at the following three zones on the TBMs:

- L1 zone
- L2 zone
- Invert zone

Initial support was applied at the 'L1 zone' just behind the TBM shield, primarily to secure any loose rock and limit the convergence of the rock mass. Initial support typically consisted of rock bolts and mesh, although shotcrete was also used in poorer quality rock masses. Shotcrete was installed systematically at the 'L2 zone' and formed the upper 260° of the permanent lining of the tunnel. The invert shotcrete was sprayed systematically between the L1 and L2 zones and formed the lower 100° of the permanent lining of the tunnel. Figure 2 shows a typical schematic of an open gripper TBM.

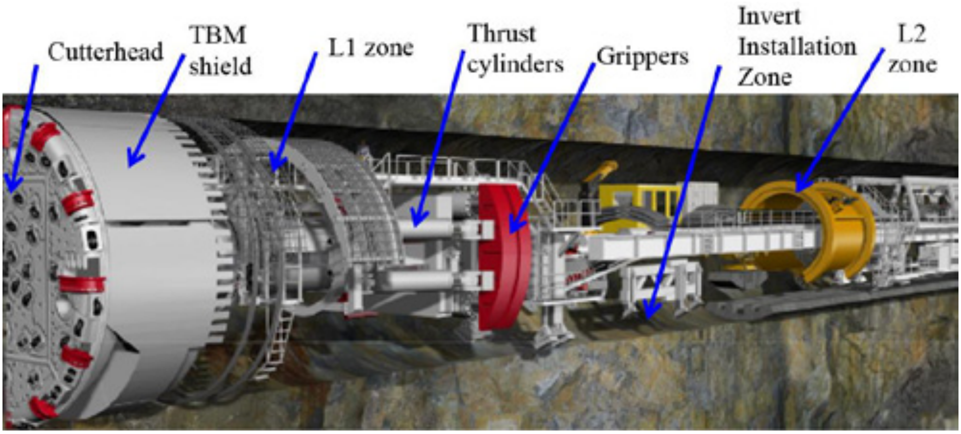

Figure 2: Schematic of gripper TBM (indicative only) (Courtesy of Herrenknecht)

L2 Shotcrete Zone

The L2 zone was located 65 m behind the cutterhead. The system consisted of two spray robots mounted on lifting beams, one on the left and one on the right hand side (Figure 3). The lifting beams moved radially, perpendicular to the direction of the tunnel. Each lifting beam could cover the 135° on its own side as well as overlapping by 45° past the crown to the other side if need be. A spray robot was mounted on each lifting beam and moved longitudinally in the direction of the tunnel. The overall maximum coverage of the L2 zone system was 270° of the tunnel circumference. The spray robot was outside of a cylindrical shield that protected workers and equipment and allowed unhindered access to the front of the TBM from the upper deck of the TBM. It also deflected shotcrete rebound and fall-out to the tunnel invert.

In the longitudinal direction, the spray robots could travel 7 m along the lifting beams. The cylindrical shield itself could move 3 m independently of the TBM it was mounted on. This gave a total reach of 10 m. Shotcrete was sprayed systematically at the L2 zone over the initial support installed at the L1 zone. The thickness of the shotcrete sprayed at the L2 zone typically varied between 125 mm and 250 mm and was dependent upon the quality of the rock mass.

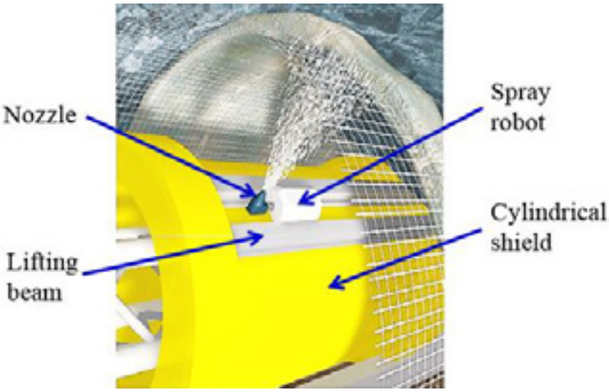

Figure 3: Shotcrete application at L2 zone [1]

Stages of Shotcrete Application at the L2 Zone

The flow chart in Figure 4 shows the different stages of shotcrete transport and application.

Batching Plant → Underground TBM Assembly Chamber → Pumps (TBM) → L2 zone (TBM)

Figure 4: Stages of shotcrete application

The shotcrete was first mixed at the TBM Batching Plant. It was then loaded into concrete mixer trucks and driven from the Batching Plant to the Assembly Chamber and up a ramp. A locomotive was then manoeuvred into position on the tracks so that a shotcrete transit car could be positioned directly beneath the point of discharge of the truck. The shotcrete was then discharged from the truck into the shotcrete transit car. The locomotive was then driven from the Assembly Chamber to the TBM while the shotcrete was agitated in the shotcrete transit car. Upon arrival at the TBM the shotcrete transit car was lifted from the locomotive and positioned above one of the shotcrete pumps on the TBM. When ready the contents of the shotcrete transit car were discharged and the shotcrete was pumped to the L2 zone where it is applied as the final lining.

The shotcrete transit cars were manufactured by Maschinen Stahlbau Dresden (MSD). They had a dead weight of 3.8 tonnes and a load capacity of 6 m^3, and were typically filled with 5 m^3 of shotcrete. Shotcrete transit cars at the L2 zone are shown in Figure 5.

Figure 5: Shotcrete transit cars in use

Pump Types

At the time of the assessment, there were two types of shotcrete piston pump employed on the TBMs to deliver shotcrete to the L2 zone, 20 m^3/hour capacity pumps and 25 m^3/hour capacity pumps. Both pumps had a maximum working pressure of 70 bar (7 MPa).

Concrete piston pumps operate on the same principle as a twin cylinder reciprocating engine. One cylinder draws concrete from the hopper on the return stroke and another pushes it on the forward stroke into the line. Pistons in both cylinders operate in opposite directions, so there is uninterrupted flow and constant pressure on the concrete in the line. The pistons were driven by a hydraulic pump. [2]

The pre-excavation grouting pumps used at the L1 zone were single plunger type pumps with a maximum capacity of 7.5 m^3/hour. These pumps had a maximum working pressure of 50 bar (5 MPa). Assessment of the pre-excavation grouting pumps is outside the scope of this paper.

Initially Installed Layout of Pumps

A schematic of the initially installed pump arrangement is shown in Figure 6.

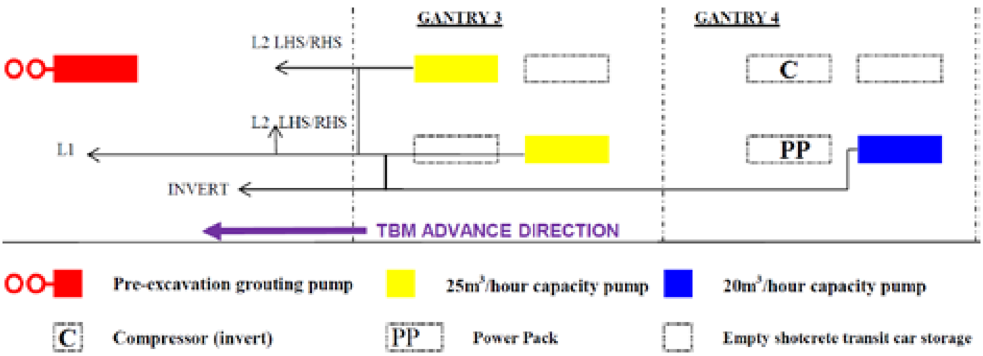

Figure 6: Initially installed pump arrangement

SHIFT REPORTING

Pumping Statistics

The parameters recorded during the shift reporting are outlined in Table 1.

Table 1: Parameters recorded during the assessment

Volume of shotcrete pumped	This is the volume of shotcrete from any particular shotcrete transit car applied at the L2 zone
Rate of pumping	This is the volume of shotcrete pumped divided by the duration of the discharge and is given in m^3/hour
Number of strokes per hour	This is the rate of pump strokes per hour, based on the rate of pumping
Piston speed	The piston speed is calculated from the number of piston strokes in one hour and the length of the piston
Stoppage duration	This is the duration of stoppages experienced while applying shotcrete from that particular transit car

Stoppages

This refers to any interruption in the application of shotcrete that occurs during the discharge of a shotcrete car. A differentiation has been made between blockages and disruptions for the analysis of the results, since the blockages are mainly related to the pumps while disruptions are due to other factors. Table 2 outlines the categories of stoppages:

Table 2: Categories of stoppages recorded during the assessment

Blockages	*A. Solid Pipe*	Blockages in the solid pipe between the pump and the flexible hose
	B. Flexible hose	Blockages in the flexible hose between the solid pipe and the robot
	C. Nozzle/ Manipulator	Blockages at the nozzle or along the length of the lifting spray beam
	D. Accelerator	Blockages in the pipe supplying accelerator to the nozzle
Disruptions	*E. Other/unspecified (not related to pumps)*	• Changing over from one spray robot to the other • Power cut • Repairing existing rock support before shotcreting • Issues with the air compressor

RESULTS FROM SHIFT REPORTING

Pumping Statistics

Volume of shotcrete pumped

The volume of applied shotcrete observed for each TBM and pump is shown in Table 3.

Table 3: Volume of shotcrete observed for each TBM and pump

	Volume of shotcrete applied (m^3)	Number of shifts observed	Average volume applied per shift (m^3/shift)
All shifts (total)	344.3	26	13.2
Trailing TBM	214.8	17	12.6
Leading TBM	129.5	9	14.4
20 m^3/hour capacity pump	70.3	6	11.7
25 m^3/hour capacity pump	274.1	20	13.7

Rate of pumping

The results for the rate of pumping of shotcrete are shown in Table 4 and Figure 7.

Table 4: Rate of pumping of shotcrete for each TBM and pump

	Minimum rate of pumping (m^3/hour)	Maximum rate of pumping (m^3/hour)	Average rate of pumping (m^3/hour)
All shifts - average	2.8	12.6	8.6
Trailing TBM	6.0	12.6	9.2
Leading TBM	2.8	12.5	7.9
20 m^3/hour capacity pump	7.1	10.7	8.8
25 m^3/hour capacity pump	2.8	12.6	8.6

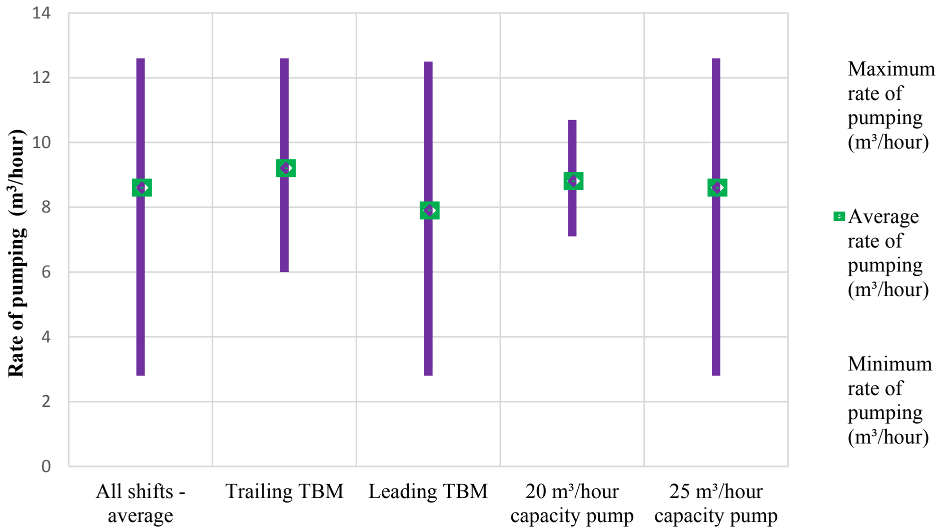

Figure 7: Minimum, maximum and average pumping rates for each TBM and pump

The 20 m^3/hour and 25 m^3/hour capacity pumps operated at an average efficiency of 44% and 34% respectively. This is shown in the Figure 8.

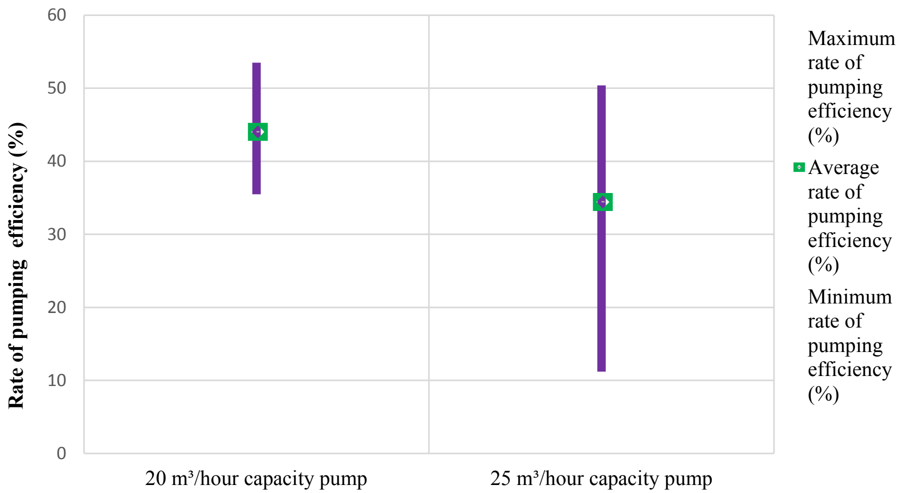

Figure 8: Minimum, maximum and average pumping efficiency rates for different pumps

Figure 8 shows that the 20 m^3/hour capacity pump operated within a much more steady range of pumping efficiency than the 25 m^3/hour capacity pump. The former had a range of 18.3% between the maximum and minimum values while the latter had a range of 39.2% between these values.

The large range of pumping efficiencies for the 25 m^3/hour capacity pumps meant that they were not working at a steady rate. This made it more difficult to predict the duration required to pump the contents of a transit car of shotcrete and hence limited the ability to plan shotcrete deliveries and logistics effectively. The 20 m^3/hour capacity pumps worked within a much smaller range of pumping efficiency, allowing for better planning of shotcrete deliveries.

Number of strokes per hour

The results for the number of pump strokes per hour are shown in Table 5.

Table 5: Number of pumps strokes per hour for each pump

	Minimum number of pump strokes per hour (strokes/hour)	Maximum number of pump strokes per hour (strokes/hour)	Average number of pump strokes per hour (strokes/hour)
20 m^3/hour capacity pump	630	960	790
25 m^3/hour capacity pump	120	890	375

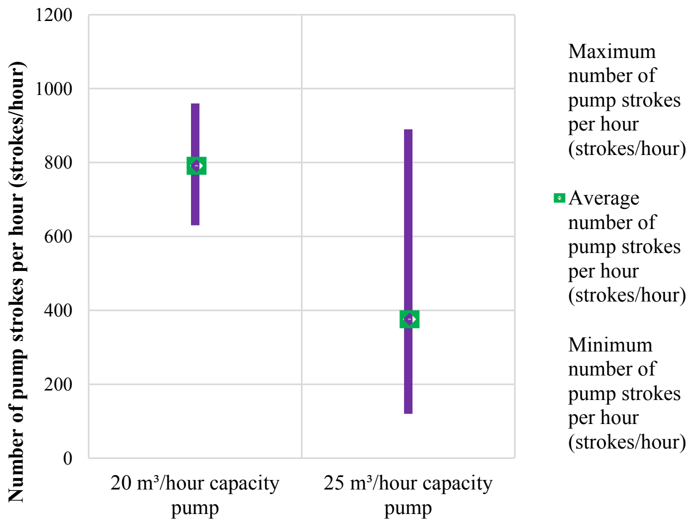

Figure 9: Minimum, maximum and average pump strokes per hour for each pump

Piston speed

The results for the pump piston speed are shown in Table 6.

Table 6: Pump piston speed for each pump

	Minimum pump piston speed (m/s)	Maximum pump piston speed (m/s)	Average pump piston speed (m/s)
20 m^3/hour capacity pump	0.12	0.19	0.15
25 m^3/hour capacity pump	0.03	0.25	0.10

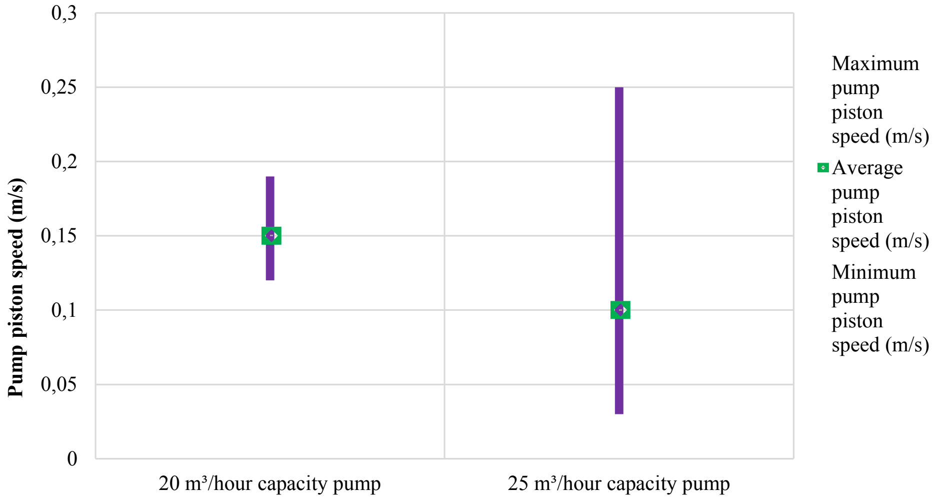

Figure 10: Minimum, maximum and average pump piston speeds for each pump

Stoppages Statistics

Duration of pumping and stoppages

The results for the average duration of pumping and stoppages recorded during the assessment are shown in Table 7.

Table 7: Average duration of pumping and stoppages for each TBM and pump as percentage of shotcrete discharge cycle

	Average duration of pumping (%)	Average duration of stoppages (%)
Average	72.9	27.1
Trailing TBM	76.3	23.7
Leading TBM	68.5	31.5
20 m^3/hour capacity pump	75.2	24.8
25 m^3/hour capacity pump	72.3	27.7

Figure 11 shows that there is little variation in the average duration of stoppages with respect to TBM and pump type. The following general observations were made:

- The trailing TBM experienced slightly fewer stoppages than the leading TBM.
- The 20 m^3/hour capacity pump experienced slightly fewer stoppages than the 25 m^3/hour capacity pump.

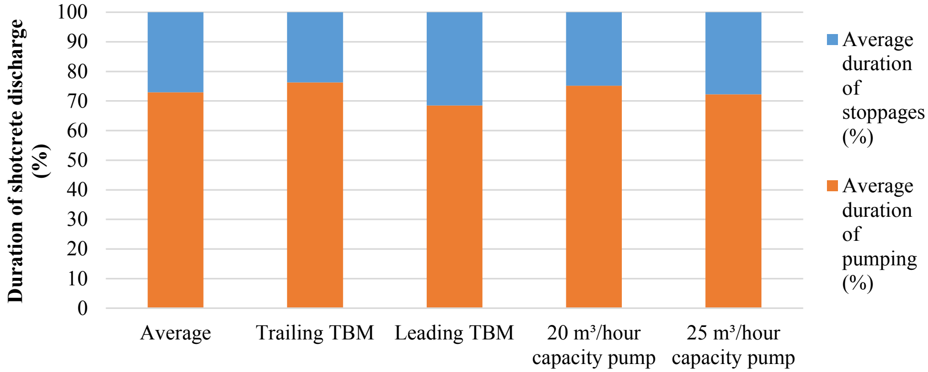

Figure 11: Average duration of pumping and stoppages for each TBM and pump

The results for the average duration of various stoppages are shown in Table 8 and summarised in Figure 12.

Table 8: Average duration of stoppages for each TBM and pump as percentage of shotcrete discharge cycle

	Average duration of pumping (%)	A. Solid Pipe blockage (%)	B. Flexible Hose blockage (%)	C. Nozzle blockage (%)	D. Accelerator blockage (%)	E. Disruptions (%)
Average	72.9	2.3	8.1	7.9	1.8	7.1
Trailing TBM	76.3	4.0	6.6	1.1	3.2	8.7
Leading TBM	68.5	0	9.9	16.5	0	5.1
20 m^3/hour capacity pump	75.2	0.8	13.6	0	0	10.4
25 m^3/hour capacity pump	72.3	2.6	6.8	9.8	2.2	6.3

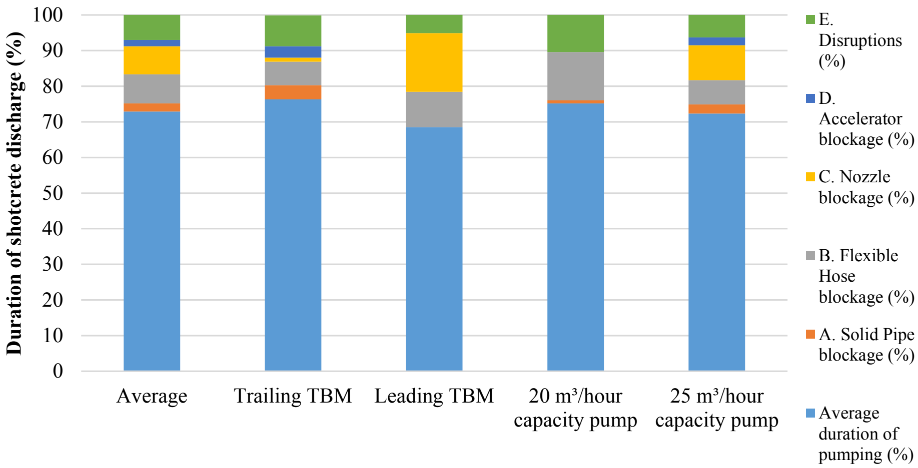

Figure 12: Duration of pumping and stoppages for each TBM and pump

Analysis of duration of stoppages

The results for the analysis of the duration of stoppages are shown in Table 9 and summarised in Figure 13.

Table 9: Duration of stoppages for each TBM and pump type as percentage of stoppage time

	A. Solid Pipe blockage (%)	B. Flexible Hose blockage (%)	C. Nozzle blockage (%)	D. Accelerator blockage (%)	**Blockages (A-D) (%)**	**E. Disruptions (%)**
Average	8.3	29.8	29.0	6.6	**73.8**	**26.2**
Trailing TBM	17.0	28.0	4.8	13.5	**63.3**	**36.7**
Leading TBM	0.0	31.6	52.3	0.0	**83.9**	**16.1**
20 m^3/hour pump	3.2	54.8	0.0	0.0	**58.0**	**42.0**
25 m^3/hour capacity pump	9.4	24.5	35.2	8.1	**77.2**	**22.8**

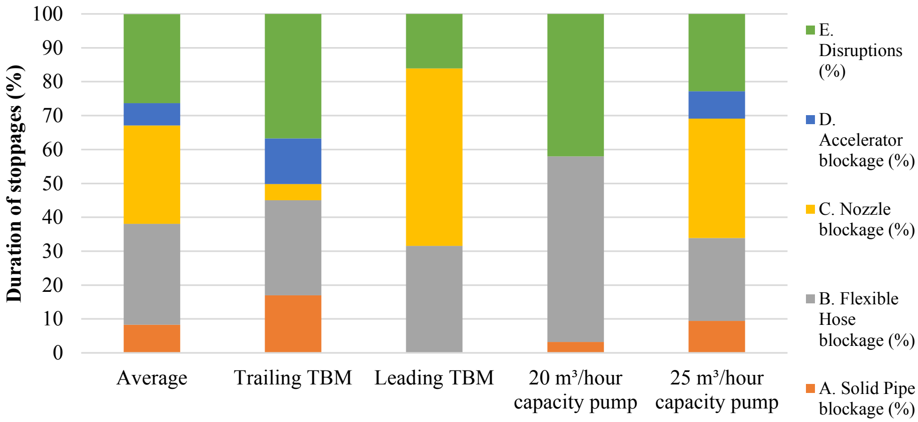

Figure 13: Duration of stoppages for each TBM and pump

The following general observations were made:

- On average, the most common blockage was in the flexible hose, followed by the nozzle (these contributed to 29.8% and 29.0% of the blockages respectively).
- The 20 m^3/hour capacity pump did not experience any nozzle or accelerator pump blockages.
- More than half of the 20 m^3/hour capacity pump stoppages were caused by flexible hose blockages.

As mentioned previously, it is important to distinguish between blockages and disruptions. On average, blockages accounted for 73.8% of the stoppages although this number is as high as 83.9% for the leading TBM and as low as 58% for the 20 m^3/hour capacity pump.

The 20 m^3/hour capacity pump experienced a higher proportion of disruptions than the 25 m^3/hour capacity pump and therefore a lower proportion of blockages. The disruptions were not related to the pumps, they were caused by other factors, such as changing over from one robot to another or repairing existing rock support before applying shotcrete. Therefore the rate of pumping for the 20 m^3/hour capacity pump could be further enhanced by improving the management of logistics, and thereby reducing these disruptions.

Rate of Pumping and Age When Shotcrete Discharge Started

Figure 14 shows the rate of pumping (not including any stoppages) against the age of the shotcrete when discharge was commenced at the L2 zone. Figure 15 shows the average total time of discharge (including stoppages) against the age of the shotcrete when discharge was started at the L2 zone.

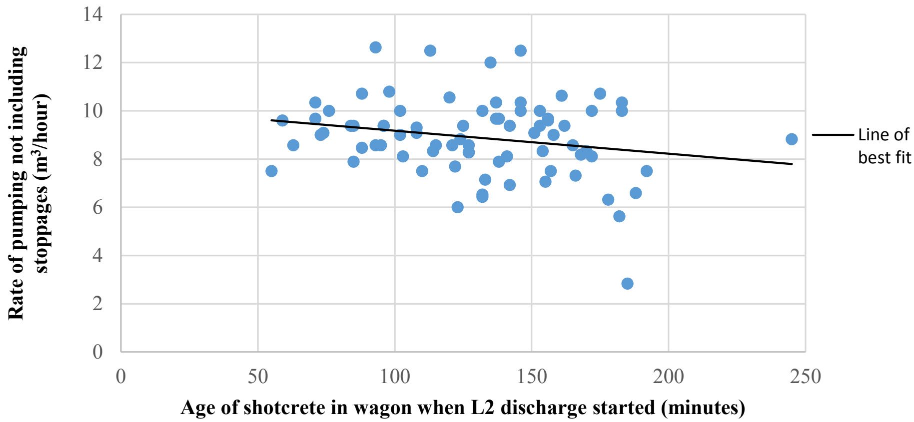

Figure 14: Rate of pumping (not including any stoppages) against the age of the shotcrete when discharge was started at the L2 zone

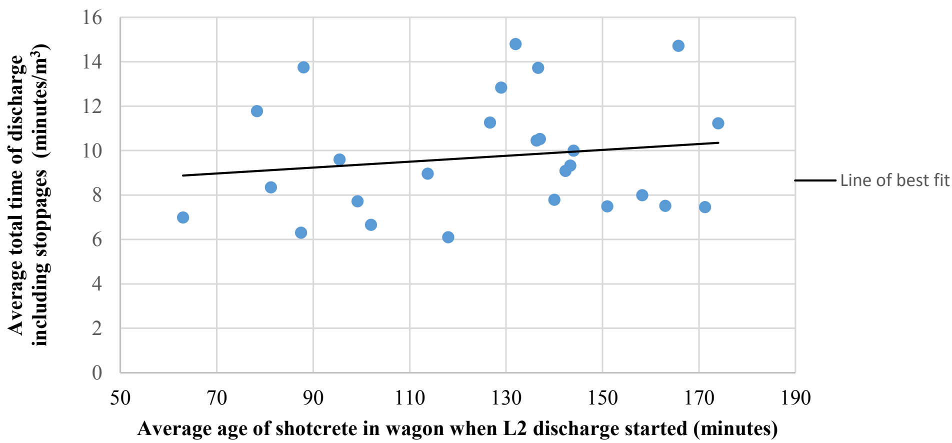

Figure 15: Average total time of discharge (including stoppages) against the age of the shotcrete when discharge was started at the L2 zone (higher values signify lower efficiency)

These results show a trend of a slightly reduced rate of pumping with increased shotcrete age when shotcrete discharge started at the L2 zone. It also shows that the shotcrete took slightly longer to pump, (more minutes per cubic metre) as the average age of the shotcrete in the wagon discharged at L2 increased.

CONCLUSIONS AND RECOMMENDATIONS

The following recommendations were made and implemented for the shotcrete plant:

- 20 m^3/hour capacity pumps rather than 25 m^3/hour capacity pumps should be used for the application of shotcrete at the L2 zone as they have a narrower operational range, allowing for better planning of shotcrete deliveries.
- 20 m^3/hour capacity pumps should be used for application of shotcrete at the L2 zone as they experience fewer stoppages and blockages than the 25 m^3/hour capacity pumps.
- 25 m^3/hour capacity pumps are preferred for the application of invert shotcrete because the invert offers a less challenging working environment than the L2 zone, given that it is larger in area (typically 10 m in length sprayed in one shift) and drop out of the shotcrete is not possible because gravity acts to stabilise the freshly-applied layer. This environment was therefore more forgiving of the larger operational range and more frequent blockages that the 25 m^3/hour capacity pumps experienced.
- The recommended pump layout is shown in Figure 16.

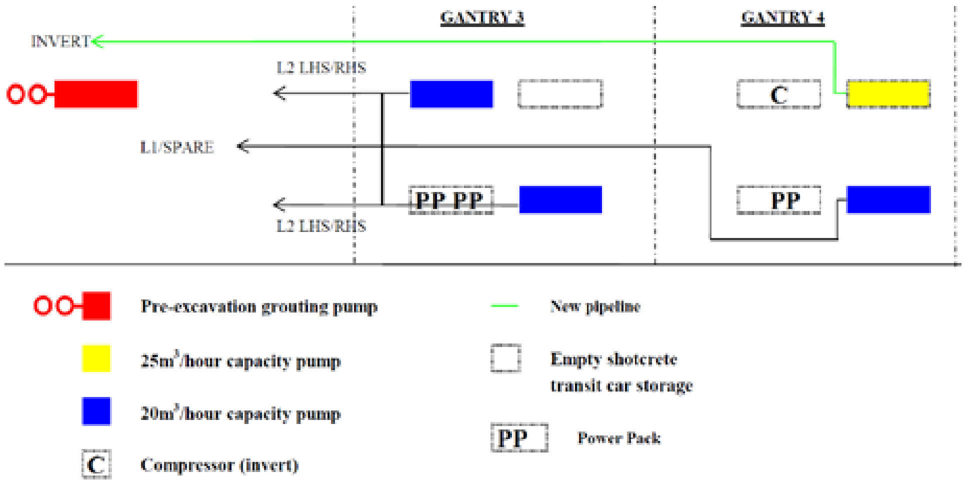

Figure 16: Recommended pump layout

- It was recommended that logistics were managed to both minimise the age of the shotcrete when discharged at the L2 zone as well as implement trials to extend the life of the shotcrete using retarder.

REFERENCES

1. *Jehle, C. Roof Support and Ground Control Equipment. Herrenknecht. 2011.*
2. *Riseer B. Using Concrete Pumps for Shotcreting, Concrete Construction. 1995.*

8th INTERNATIONAL SYMPOSIUM ON SPRAYED CONCRETE – Modern Use of Wet Mix Sprayed Concrete for Underground Support
– Trondheim, Norway, 11. – 14. June 2018

ENCAPSULATION QUALITY OF REINFORCEMENT: FROM LABORATORY TESTS TO STRUCTURAL DESIGN GUIDELINES

Pasquale Basso Trujillo, *Ph.D. candidate*
Marc Jolin, *Ph.D., Professor*
Department of Civil and Water Engineering, Université Laval, Canada
pasquale.basso-trujillo.1@ulaval.ca; marc.jolin@gci.ulaval.ca

SUMMARY

For many years, a particular concern among engineers has been the possible creation of imperfections behind reinforcing bars when shotcrete is inappropriately applied and how their presence affect the behavior of structural elements. However, despite the serious effect imperfections behind the reinforcement might cause, only few research studies have been completed on the subject. To this day, engineers are limited to codes that do not have specific guidelines regarding the design of *reinforced shotcrete* elements. Moreover, the current guidelines for the evaluation of the encasement quality of reinforcing bars are based on empirical data. For these reasons, the aim of this paper is to review a comprehensive research (on-going) that was undertaken as part of a doctoral program to 1) enhance the current evaluation methods used to assess the encasement quality of sprayed bars and 2) propose modification factors for the *development length* equation when shotcrete is used. Initially, a brief historical review of the past encasement quality evaluation methods and the development of the current modification factors for the *development length* equation (accounting for other phenomena such as bleeding, and the size and coating of bars) will be discussed. Thereafter, a detailed review of the experimental program, which included "pull-out" and ASTM A944-10 "beam-end" specimens, and a description of the analytical methods used to derive modification factors will be presented. Also, the range of applicability of the developed modification factors will be discussed based on the results of a FE model of the "beam-end" specimen. Finally, the situations in which the aforementioned modification factors can be used and how to apply them will be reviewed.

INTRODUCTION

The use of sprayed concrete has become a viable and practical alternative in comparison with cast-in-place (CIP) concrete to build complete reinforced concrete elements. Indeed, improved mixtures developed over the past few years have considerably helped to reduce the amount of rebound whilst increasing the possible buildup thickness of shotcrete [1-4]. In addition, the equipment has also evolved considerably [5] allowing the optimization of the entire spraying procedure. However, imperfections such as voids or entrapped aggregates could be created behind the reinforcement if, among others, the experience of nozzle operators is not adequate, if the elements present heavily congested zones of reinforcement, or if the job site conditions make it difficult to spray the concrete. In *wet-mix* shotcrete, imperfections could be created mainly if the dosage of set-accelerating admixtures is excessive whereas in *dry-mix* shotcrete they are mainly created by the inadequate experience nozzlemen (refer to Fig. 1a and 1b). Unfortunately, the issue has not been properly addressed and reliable guidelines for the design and the evaluation of shotcrete structures whenever imperfections at the bar-concrete interface are expected have not been established.

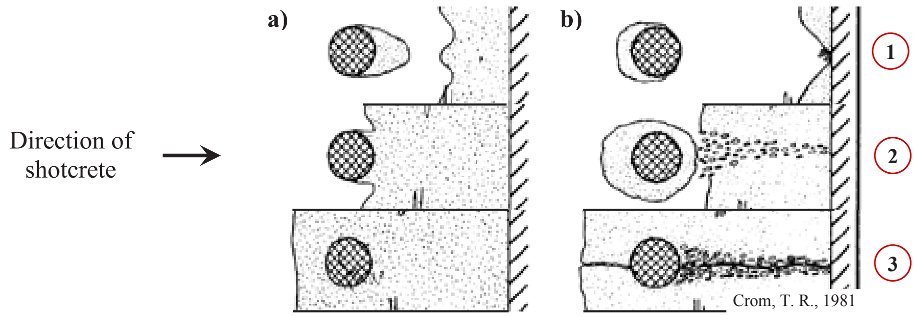

Figure 1 – (a) correct and (b) incorrect shotcrete placement method resulting in voids

In the past years, the first official attempt came with the introduction of the *core-grading system* in the American Concrete Institute's (ACI) document "*506.2-95: Specification for shotcrete*" [6] in which the imperfections behind reinforcing bars were visually graded from 1 (perfect encapsulation) to 5 (poorest encapsulation). Nonetheless, despite the effort, the reliability of the *core-grading system* was widely questioned [7-9] and it has even led some engineers to make unsupported design decisions [10]. Consequently, the *core-grading system* was removed in the 2013 version of the document (ACI 506.2-13) [11] and was recently replaced (up to a certain level) by the ACI's technical note "*506.6T-17 Visual shotcrete core quality evaluation technote*" [12] in which the size of the imperfections (if any) is reported as a percentage of the bars' perimeter. Still, the adopted percentage limits in the "*506.6T-17"* technote defining different qualities of encapsulation (from "very good" to "poor") were established based on experience and not on the actual bond strength performance of reinforcing bars with varying encapsulation qualities.

In that regard, an alternative (and perhaps a more advantageous way to deal with possible imperfections behind reinforcing bars) is to use modification factors for the *development length* (ℓ_d) equation of reinforcing bars in tension, as expressed by Eq. 1a and 1b (in SI units) according to the ACI 318-14 design code [13]. These modification factors could be based on the expected inadequately encased perimeter of the bars, i.e. the *un-bonded perimeter* (*u.p.*). Making use of the factors during the design phase of shotcrete structures would allow the evaluation of cores taken from pre-construction panels[1] (or even actual structures if needed) to be less severe since preventive actions would have been taken during the design phase.

$$\ell_d = \frac{1}{1.1}\frac{f_y}{\lambda\sqrt{f'_c}}\frac{\psi_t\psi_e\psi_s}{\left(\frac{c_b+K_{tr}}{d_b}\right)}d_b \qquad (1a)$$

[1]Pre-construction panels are replicas of the actual members of the structure that are sprayed, cored and evaluated in complex projects to verify if the mixture, equipment, and the crew can guarantee the quality of shotcrete.

Where:

$$K_{tr} = \frac{40A_{tr}}{sn} \tag{1b}$$

And the restrictions expressed in Eq. 2a, 2b, 2c and 2d must be respected.

$$\ell_d \geq 300 \text{ mm} \tag{2a}$$

$$\psi_t \psi_e \leq 1.7 \tag{2b}$$

$$(c_b + K_{tr}) / d_b \leq 2.5 \tag{2c}$$

$$f'_c \leq 69 \text{ MPa} \tag{2d}$$

Eq. 1a incorporates modification factors (ψ_t, ψ_e, and ψ_s) which were added by ACI Committee 318 to the original equation proposed by Orangun et al. [14]. The "top-bar" factor (ψ_t) [15-17] accounts for the adverse effect on bond of bleeding water accumulating under the reinforcing bars, the "bar coating" factor (ψ_e) [18, 19] accounts for the adverse effect on bond of epoxy or zinc bar coatings and lastly, the "bar size" factor (ψ_s) [13] acknowledges the more favorable bond performance of small size bars. Historically, modification factors have been established by computing *bond performance ratios* between "control" bond specimens ("beam-end", "beam-splice", "development length" or other specimen) and those accounting for the variable under study. For such purpose, the ultimate loads, the ultimate slips or the loads at a given slip have been used. However, since the adverse effect on bond of inadequately encased bars (as it may occur in shotcrete) is not explicitly accounted in Eq. 1a, a comprehensive doctoral program was undertaken to overcome the shortcoming of the current design and evaluation procedures. Thus, the aim of this paper is to review the procedure of such investigation [20-24] that led to establish a set of modification factors for the ℓ_d equation when shotcrete structures are designed and the recommendations proposed to enhance the bar encasement evaluation methods when imperfections can be expected to be created behind bars.

GLOBAL METHODOLOGY

The complete procedure of the investigation, shown in Fig. 2, included an experimental, analytical, and a Finite Element (FE) modeling phase in order to achieve the objectives of the investigation. During the experimental phase, "pull-out" specimens (built with shotcrete and cast-in-place concrete -CIP-) and "beam-end" (built only with CIP concrete) specimens were tested. The "pull-out" specimens were only used for screening purposes as their stress field is representative of only a few real-life situations. In contrast, the "beam-end" specimen was used for the actual proposal of modification factors since their stress field is representative most reinforced concrete members (both the bar and the concrete are placed in tension) [25].

In order to obtain different qualities of reinforcing bar encapsulation, the shotcrete "pull-out" specimens were built using the *dry-mix* process so that the nozzlemen could intentionally create imperfections by changing the *consistency* of the mixture. The "beam-end" specimens were not built using shotcrete because an early attempt showed that imperfections were created in other reinforced parts of the specimen; the solution was to use silicone inserts encased with CIP shotcrete mixture to recreate actual shotcrete voids. The main advantage of using *artificial voids* was that they allowed to obtain precise bond strength values whilst testing a reduced amount of experimental specimens. Then, to account for the inherent size variability of shotcrete voids (the *un-bonded perimeter*) along the reinforcement, principles of *possibility theory* were applied and ultimately *bond performance ratios* (similar to those used to establish the current modification factors for ℓ_d) were computed. The Finite Element (FE) model, of the "beam-end" specimen only, served to establish reasonable limits for the use of the proposed modification factors based on the ultimate load (linked to the *un-bonded perimeter* of voids) and the type of failure of specimens (i.e. a change from a *splitting* to a *pull-out* failure mode).

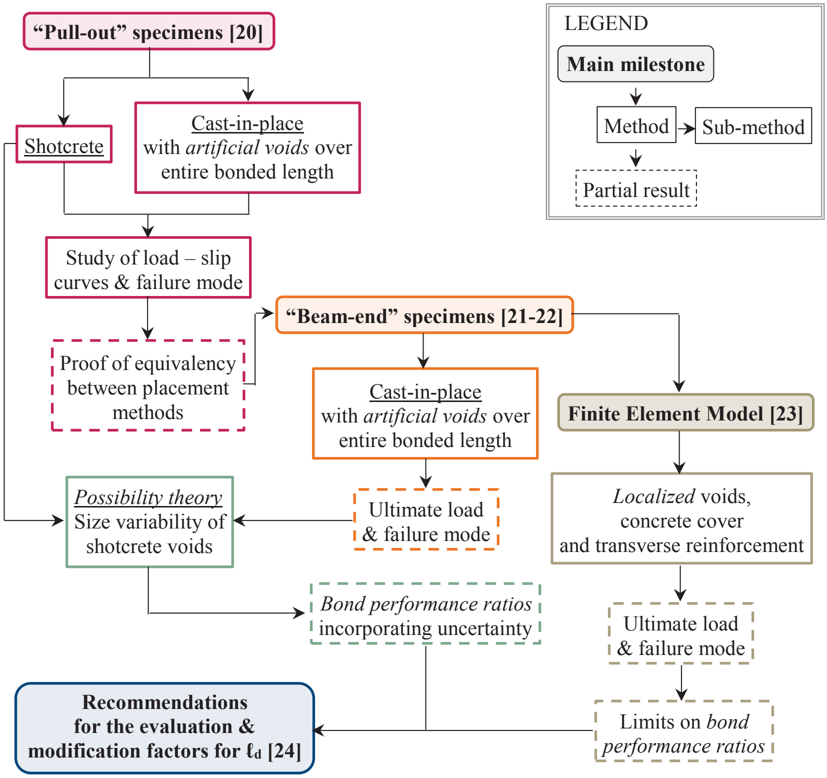

Figure 2 - Global methodology of the investigation

EXPERIMENTAL METHODS

Bond specimens

The "pull-out" specimen consisted of 150 x 150 x 285 mm prisms cut from wooden rectangular panels; the same molds were used for either sprayed (refer to Fig. 3) or CIP specimens. A single 16.0 mm nominal diameter (d_b) test bar concentric with the longitudinal axis of the prism and a 40 mm ($2.5d_b$) bonded length were used. The specimens were tested by pulling the bar vertically whilst the top of the specimens was retained with a 322 MTS testing frame at 1.0

mm/min displacement control. The displacement of the bar was measured with two linear position sensors with return spring attached to the test bar at the *loaded* end.

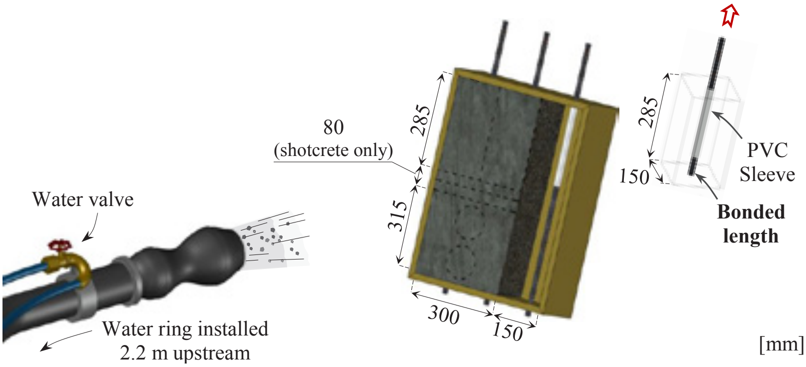

Figure 3 – “Pull-out” specimens [20]

The remaining concrete in the panels was cored to measure the mechanical and durable properties of the concrete and only in the case of shotcrete specimens, two concrete plates were cut to obtain five values of the *un-bonded perimeter* as the one shown in Fig. 4a. In CIP specimens, the *un-bonded perimeters* that were studied corresponded to 0, 10, 20 and 30% of the bar’s d_b as shown in Fig. 4b and only a single value was measured at the bottom of the specimens.

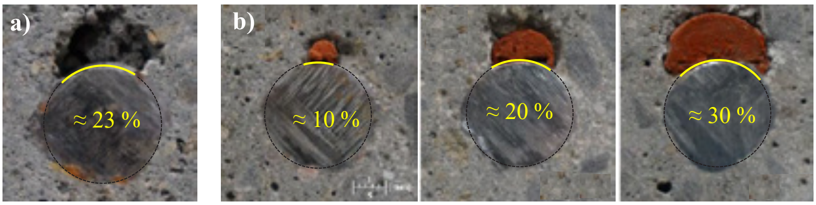

Figure 4 – (a) *u.p.* of shotcrete specimen and (b) of CIP specimens with *artificial voids* [20]

The “beam-end” specimens, as shown in Fig. 5, were built in accordance to the ASTM A944-10 standard [26] and consisted of 210 x 600 x 450 prisms with a test bar passing through a PVC sleeve at the *loaded* end and through a second sleeve at the *un-loaded* end. The sleeves served to control the bonded length of the test bar whilst avoiding a conical concrete failure at the *loaded* end. Test bars of 15.9 and 19.1 mm d_b were used and the bonded length was set to 100 and 120 mm for each bar size respectively (6.3d_b); the concrete cover above the test bars was set to 2.5d_b. Moreover, the specimens incorporated flexural bars and stirrups to assure an adequate behavior in flexure and in shear and transversal PVC sleeves were placed in between the stirrups to facilitate moving the specimen. The specimens were tested by pulling the test bar whilst retaining the specimen with a *compression reaction plate* (simulating the internal compressive force in flexural members) and with a *tie-down plate* (simulating the shear gradient of an infinitesimal section in a flexural member) using a 311 MTS testing frame at 0.5 mm/min displacement control. A similar shotcrete mixture (either sprayed or CIP) was used for both types of specimens. However, in the case of the “beam-end” specimens, a water-reducer was used to avoid as much as possible an additional bond strength reduction due to possible bleeding water accumulating under the test bar. Moreover, the same *un-bonded perimeters* shown in Fig. 4b were studied.

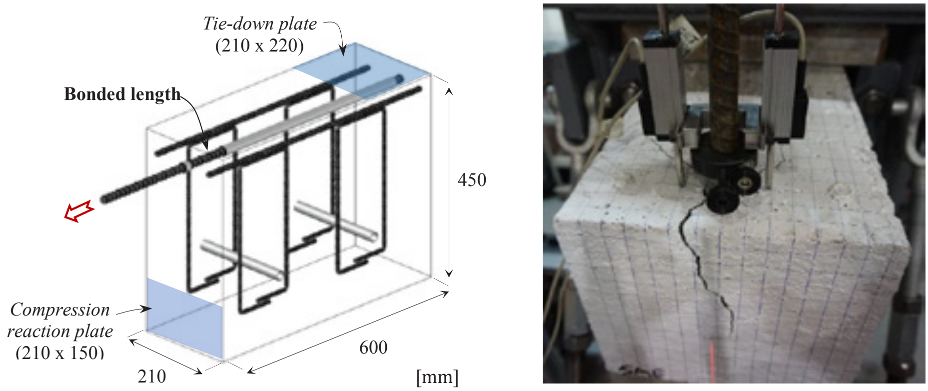

Figure 5 – “Beam-end” specimens

Partial results and discussion

The results of CIP “pull-out” specimens with *artificial voids* were extremely valuable in depicting tendencies, especially with regard of the *un-bonded perimeter* threshold beyond which the load was considerably reduced in comparison with perfectly encapsulated bars; the results suggested the threshold to be around a 20% *u.p.* The same value was supported by results obtained with shotcrete “pull-out” specimens despite the results were harder to interpret because of the size variability of shotcrete voids. Nonetheless, it was found that only the absolute ultimate load values obtained with CIP specimens were equivalent to the ones obtained with shotcrete specimens (based on a statistical hypothesis testing comparison). Indeed, the slope of the load-slip curves of shotcrete specimens always resulted higher than those of CIP specimens because of the better-compacted mixture around the bar as a consequence of the velocity at which the mixture is sprayed.

For such reasons, the ultimate load (normalized to the cross-section of the test bars, or P_{max}/A_b) obtained with the “beam-end” specimens was chosen for the creation of modification factors for the *development length* equation (refer to Eq. 1a). However, one of the challenges that needed to be addressed at that moment concerned the inclusion of the size variability of the voids found in actual shotcrete elements. Since only *artificial voids* with “crisp” (precise) sizes had been tested using the “beam-end” specimens, a simple ratio computed between the average ultimate loads would imply that 50% of the time, the ratio (if used as a modification factor for ℓ_d) would be insufficient to guarantee the same bond performance as perfectly encapsulated bars. Such issue did not seem to be crucial when the current modification factors (ψ_t, ψ_e, and ψ_s) were developed because the parameters (i.e. the position, size and coating thickness of the bars) are well-known before the concrete is placed. In shotcrete, voids may be created over the entire length of the bonded length or only in localized areas. In addition, wherever they are present, their *un-bonded perimeters (u.p.*) may vary from as low as 10% up to 60% away from the mean *u.p.* as revealed from the measurements in “pull-out” specimens [20]. The approach to solve this issue included computing *bond performance ratios* using the ultimate loads of the "beam-end" specimens to which the size variability of the voids was added using principles of *possibility theory*.

ANALYTICAL METHODS

Possibility theory

Possibility theory [27, 28] refers to an approach to model the epistemic uncertainty (lack of knowledge) of a phenomenon or variable. With this theory, the uncertainty of a variable (x) is defined using a *possibility function* ($\pi(x)$) which varies from 1 to 0. When $\pi(x) = 1$ it is considered that the value of x is "unsurprising" or the "closest to the *true*" value and when $\pi(x) = 0$ its value is not considered as possible. The concept can be extrapolated to two variables (x, y) as shown in Fig. 6 for the *un-bonded perimeter* (*u.p.*) and the normalized ultimate load (P_{max}/A_b) to which the range of uncertainty can be specified based on experience. In the present study, the uncertainty (*i*) associated to the *u.p.* was randomly assigned to each single "crisp" CIP result in between $i = \pm 10$ to $\pm 60\%$ in line with the variability observed with "pull-out" specimens. Moreover, a fixed $i = \pm 2\%$ was added to the P_{max}/A_b. The distribution function between $\pi = 1$ and 0, which in this case was chosen as linear, defines the set of values that are plausible from those that are less plausible (the projection of values obtained for a given horizontal cut of the pyramid in Fig. 6). As such, each pyramid represents a *pseudo-shotcrete* result built with CIP specimens having *artificial voids*. Such types of values have been normally called *fuzzy* numbers (and represented with a tilde over them) since they do not incorporate random but epistemic uncertainty. In many areas of civil engineering, this approach has already been successfully applied to, among others, model the variability of cable tension measurements in bridges [29] and model the variability of grades assigned to structural elements to assess their physical condition [30].

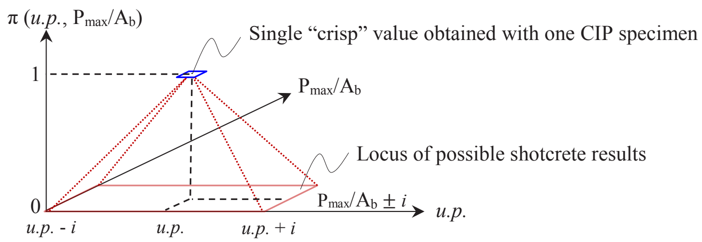

Figure 6 – Possibilistic representation of "crisp" values

Plotting all of the *pseudo-shotcrete* values, as shown in Fig. 7, makes it possible to depict a tendency of the bond strength reduction as the *u.p.* increases whilst incorporating the uncertainty linked to the size of actual shotcrete voids. Thus, the tendency can be used to compute *bond performance ratios* that can eventually be used as modification factors for the ℓ_d equation (refer to Eq. 1a) if voids are expected to appear in shotcrete structures. Tracing tendencies using *fuzzy* data can be accomplished using *fuzzy* regression techniques in which the imprecision is linked to the observations and not on the model as it is the case of classic regression techniques. The *fuzzy* model that was used in Fig. 7 was the one proposed by Hong et al. [31] as expressed in Eq. 3.

$$\tilde{Y} = \tilde{A}_0 \oplus (\tilde{A}_1 \otimes \tilde{X}) \oplus (\tilde{A}_2 \otimes \tilde{X}^2) \quad (3)$$

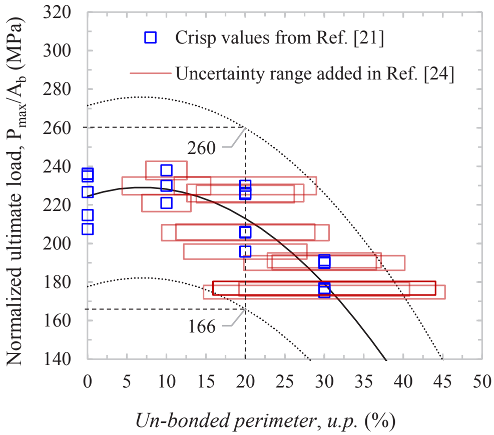

Figure 7 – Polynomial regression using *fuzzy* input-output values

As can be seen, the fuzzy polynomial model considers outputs, inputs, and regression coefficients to be *fuzzy* numbers (all represented with a tilde over them). Accordingly, the tendency lines are linked to a *possibility function* in the same manner as *fuzzy* numbers meaning that the central line corresponds to the "closest to the *true*" tendency and values that fall beyond the outer bounds are considered as impossible outcomes. The model links the uncertainty of a normalized ultimate load resulting from the presence of an *u.p.* "close to" a certain value. For a 20% *u.p.* for instance, the normalized ultimate load of *pseudo-shotcrete* values might vary from 166 and 260 MPa (with its "closest to the *true*" value being 213 MPa) because in reality the void might vary in size from one section to another (not to mention the normal variation of the concrete properties from one specimen to another). Although no shotcrete specimens were tested to verify the model's accuracy, a similar model built with the results of "pull-out" specimens proved to properly encompass the ultimate loads of most shotcrete specimens [24].

Bond performance ratios

The polynomial model developed previously can be used to compute *bond performance ratios* (BPR), as defined by Eq. 4, representing the bond performance of test bars with voids relative to the bond performance of perfectly encapsulated test bars. Moreover, since they are computed using arithmetic operations rules on *fuzzy* numbers, the result is also a *fuzzy* number [27].

$$\mathrm{BPR} = \frac{\tilde{Y}(\mathrm{u.p.}\ = 0\%)}{\tilde{Y}(\mathrm{u.p.}\ > 0\%)} \quad (4)$$

Based on Eq. 4, the BPR for the 20% *u.p.* was calculated and is presented in Fig. 8. In that case, the "closest to the *true*" value represents a BPR of 1.1 but this does not mean that higher values should not be considered. However, the challenge resides in selecting the most appropriate value for a specific job and doing so based on a possibility representation may not be the easiest way to do it.

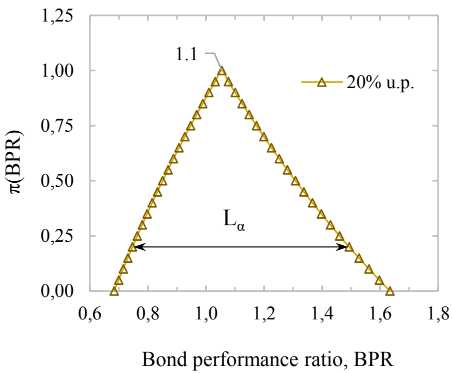

Figure 8 – *fuzzy* BPR for a 20% *u.p.*

Alternatively, the information contained in a *fuzzy* number can be transformed to a probabilistic representation which is perhaps a more comfortable way for most engineers to deal with uncertainty and make decisions. Here, the *possibility – probability* transformation method proposed by Dubois et al. [32] (and described in detail by Aven el al. [33] using numerous examples) expressed by Eq. 5 was used to obtain the probability density function of the BPR (Pro(BPR)) and thereafter the cumulative probability function.

$$\mathrm{Pro(BPR)} = \int_{\pi=0}^{\pi=1} \frac{d\alpha}{|L_\alpha|} \tag{5}$$

Where:

L_α = the length of the interval at a given *possibility function* value between 1 and 0.

The transformation method conservatively chooses a single probability distribution with the highest uncertainty possible and ensures consistency to the extent that there is no violation of the formal rules connecting possibility and probability (interval-valued probabilities to point-valued ones). In reality, the procedure enables us to compute the probability that a bar with a given *u.p.*(over its entire bonded length) will perform as a bar having a perfect encapsulation for a given BPR. The cumulative probability of equal performance for bars having a 20% *u.p.* is presented in Table 1 based on BPR's from 1.0 to 1.5.

Table 1 – Cumulative probability of equal bond performance for a 20% *u.p.*

Bond performance ratio, BPR	**1.0**	**1.1**	**1.2**	**1.3**	**1.4**	**1.5**
Cumulative probability	35 %	72 %	87 %	93 %	98 %	100 %

The cumulative probability, albeit based on subjective data, has a more meaningful value for *decision-makers*. In this particular case, if a modification factor of 1.0 was to be used with the ℓ_d equation, the designer needs be confident that voids would not appear regularly when considering, among others, the congestion of reinforcement, the experience of the spraying crew, the extent of the quality control campaign or even the experience of both if the structure is to be built in a different location from where the structure was designed. In such instances, it may seem a safe option to use a factor of 1.1 and reduce the risk by 72%/35% = 2 whilst having a good absolute probability of equal performance (72 %). Higher factors can be used according to the engineers' judgment using Table 1 based on the importance of the structure for instance but actual recommendations regarding this area are out of the scope of the investigation. The actions taken during the design phase in regard of the ℓ_d equation can be verified during the inspection of cores taken from pre-construction panels; the acceptance or the specification of corrective actions could be determined based on the modification factors used and the size and frequency of the voids observed.

FE MODEL OF THE "BEAM-END" SPECIMEN

Geometry and modeling technique

A "rib-scale" representation of the "beam-end" specimen using a 15.9 mm d_b test bar was modeled using *Abaqus 6.13* [34] as shown in Fig. 9. The concrete was defined using the *Concrete Damage Plasticity* (CDP) constitutive law and the steel was defined as an elastic perfectly-plastic material. For simplicity, the ribs were modeled normal to the longitudinal axis of the bar and the interaction between the test bar and the concrete was defined through a general contact algorithm. The adhesion component of the bond mechanism was defined with a "zero-thickness" cohesive law that was assigned in the normal and in the tangential direction of the interface. The friction component was defined with a Coulomb friction law in the tangential direction and a "hard" pressure-overclosure relationship which allowed separation in the normal direction. The mechanical component of the bond mechanism was guaranteed by ribs of the bar. Thereafter, the different sections of the bar-concrete interface were progressively placed on a *contact/stick*, a *contact/slip* or a *separation* state as the load was applied.

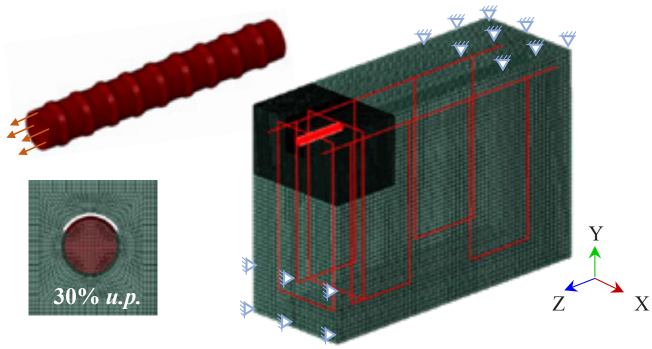

Figure 9 – FE model of the "beam-end" specimen

The concrete and the test bar elements were modeled using 8-node linear brick elements with a one-point integration scheme (C3D8R) and a *relaxed stiffness* hourglass control method. The flexural bars and the stirrups were modeled using 2-node linear truss elements (T3D2) and were embedded in the concrete assuming perfect bond. The imperfections were modeled by removing the concrete elements around the test bar needed to uncover its ribs as shown in Fig. 9. The translational degrees of freedom of the nodes covering the same area of the *compression reaction plate* and the *tie-down plate* were restrained in the Z and in the Y direction respectively. Moreover, the load was uniformly applied on the test bar by imposing a "smooth" displacement function. The model was conceptualized as a dynamic problem and was solved using *Abaqus*/explicit. Thus, the ratio between the kinetic (E_K) and the internal energy (E_I) of the whole model needed to be kept below 5% to minimize as much as possible inertia effects. For this purpose, the time period in which the load was applied was set to 10 times the lowest fundamental period of vibration (T_n) of the specimen which resulted in $10T_n = 0.02$ s. Once the model was calibrated, the parameters that were studied included *localized* voids (voids covering only a partial part of the bonded length of test bars), the concrete cover, the presence of transversal reinforcement over the test bars (see Fig. 9) and *un-bonded perimeters* of 40%.

Limits on *bond performance ratios* (BPR)

Over a first phase, the strategy was to gradually reduce the length of the void over the bonded length of the test bar to determine at what point the behavior became similar to a perfectly encapsulated bar. In the case of a 20% *u.p.* for instance, it was found that only voids covering the majority of the bonded length would be important enough to consider the use of a BPR. In practical terms, this means that the structural integrity of an element would not be compromised if a modification factor of 1.0 was used in conjunction with the ℓ_d equation and voids "close to" 20% *u.p.* were observed, even frequently, in cores from pre-construction panels. However, if voids of such size were observed in every core, the sagacious use of a 1.1 modification factor (at least) during the design phase would guarantee a reasonable bond performance of the bars and whilst reassuring inspectors and owners that no corrective measures are needed.

Over a second phase, the contribution of the confinement over the test bar was studied to detect and set limits based on the failure mode change of the specimens. For this purpose, the concrete cover was increased from $2.5d_b$ to $5.0d_b$ and transverse reinforcing spaced at 50 mm were placed over the bonded length. Consider the case of a $2.5d_b$ concrete cover as shown in Fig. 10. As can be seen, a change from concrete *splitting* to a *pull-out* failure occurs as the *u.p.* increases from 30 to 40%; this was also suggested in Ref. [21] based on experimental results. Therefore, it would be then unsafe to accept *un-bonded perimeters* larger than 30% as the elements might behave in a brittle manner. In any case, the creation of such sizes of voids would usually imply a considerable increase of rebound. It is presumed (as some results are still to come) that increasing the concrete cover would result in a reduction of the acceptable *u.p.* as a *pull-out* failure might develop earlier. The idea is to include restrictions of this type when the complete set of BPRs (as developed earlier) would be used. Such restrictions would be equivalent to the one expressed by Eq. 2c which was set to avoid a *pull-out* failure as the amount of transverse reinforcement and concrete cover increases.

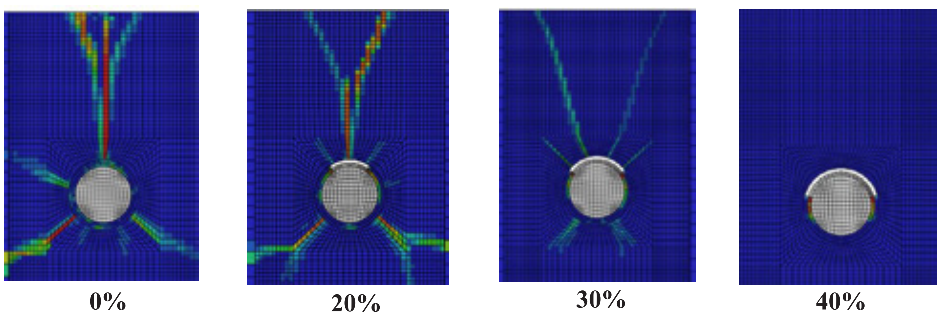

Figure 10 – Cracking pattern at the front surface of the "beam-end" FE model

CONCLUSION: IMPLICATIONS FOR DESIGN AND EVALUATION

A comprehensive research program was undertaken with the objective to enhance the current evaluation methods used to assess the encasement quality of reinforcing bars and to propose modification factors for the *development length* equation specified by North American design codes when shotcrete is used. This was accomplished by designing an extensive experimental, analytical, and a Finite Element (FE) modeling phases. The bond strength and the failure mode of specimens were analyzed based on different sizes of voids, concrete covers and the presence of transverse reinforcement. Then, by applying principles of *possibility theory* in combination with the results of the FE model, the way to create *bond performance ratios* for shotcrete structures was demonstrated and example limits for their adequate use were set.

The proposed method is intended to give structural engineers a set of modification factors for the ℓ_d equation so shotcrete can be explicitly considered during the design phase of structural elements and avoid costly corrective measures for the structure if voids are foreseeable. Imperfections behind reinforcing bars can result, among others, from the excessive congestion of reinforcement, the insufficient experience of the spraying crew or the use of excessive set-accelerating admixtures. The informed selection of modification factors will significantly increase the confidence level by which pre-construction panel evaluators accept a certain level of imperfections to be present behind reinforcing bars. Reassuringly, preliminary results show that the current evaluation method (ACI “506.6T-17” technical note), albeit established based on empirical evidence, is on the right track as its qualitative grades essentially capture what it should and should not be acceptable in practice.

ACKNOWLEDGEMENTS

The authors are grateful to the Concrete Infrastructure Research Center (CRIB) of Québec, the Natural Sciences and Engineering Research Council of Canada (NSERC), King Packaged Materials and Co., the Canadian Council of Independent Laboratories (CCIL), The American Shotcrete Association (ASA) and the Québec and East Ontario Chapter of the American Concrete Institute (ACI) for their financial support. Furthermore, special thanks are extended to Jean-Daniel Lemay and Mathieu Thomassin-Mailhot (research engineers), to René Malo (expert laboratory technician) and to Pierre-André Tremblay and Alain Melançon (laboratory technicians) for their outstanding work during casting and testing operations.

LIST OF SYMBOLS FOR THE ℓ_d EQUATION

f_y = specified yield strength of reinforcing bars
λ = lightweight concrete modification factor
f'_c = specified compressive strength of concrete
c_b = lesser of a) the distance from the center of a bar to the nearest concrete surface or b) one-half of the center-to-center spacing of the bars being developed.
K_{tr} = transverse reinforcement index
d_b = nominal diameter of the bar
A_{tr} = total cross-sectional area of all transverse reinforcement within spacing s that crosses the potential plane of splitting through the reinforcement being developed
s = center-to-center spacing of transverse reinforcement
n = number of bars being developed or lap spliced along the plane of splitting

REFERENCES

1. ACI Committee 506, "506R-16 Guide to shotcrete," American Concrete Institute, 2016, 52 p.

2. Fily-Paré, I., Jolin, M., "The use of recycled glass in shotcrete," Shotcrete Magazine, V. 15, No. 4, 2013, pp. 14-16.

3. Gagnon, A., Fily-Paré, I., Jolin, M., "Rethinking shotcrete mixture design through sustainable ingredients," Shotcrete Magazine, V. 18, No. 4, 2016, pp. 28-31.

4. Lemay, J.-D., Jolin, M., Gagné, R., " Ultra-rapid strength development in dry-mix shotcrete for ultra rapid support in challenging mining conditions," Shotcrete Magazine, V. 16, No. 4, 2014, pp. 14-19.

5. Bridger, P., "The history of shotcrete equipment - Dry mix shotcrete - the first shotcrete," Shotcrete Magazine, V. 19, No. 4, 2017, pp. 34-37.

6. ACI Committee 506, "506.2-95 Specification for shotcrete," American Concrete Institute, 1995, 8 p.

7. Warner, J., "Understanding shotcrete - Structural applications," Concrete International, V. 17, No. 10, 1995, pp. 55-61.

8. Warner, J., "Bond strength of reinforcing bars in reinforced shotcrete - Discussion by James Warner," ACI Materials Journal, 1998, pp. 196-197.

9. Concrete Construction Staff, "Shotcrete core grading: Is it working?," Concrete Construction Magazine, V. 45, 2000, 2 p.

10. Fischer, M., Hofmann, M., "Reinforced shotcrete with bar diameters up to 32 mm," Crossrail learning legacy, 2015, 13 p.

11. ACI Committee 506, "506.2-13 Specification for shotcrete," American Concrete Institute, 2014, 12 p.

12. ACI Committee 506, "506.6T-17 Visual shotcrete core quality evaluation technote", American Concrete Institute, 2017, 4 p.

13. ACI Committee 318, "318-14 Building code requirements for structural concrete and commentary," American Concrete Institute, 2014, 520 p.

14. Orangun, C. O., Jirsa, J. O., Breen, J. E., "The strength of anchor bars: A revaluation of the test data on development length and splices," The University of Texas, 1975, 78 p.

15. Clark, A. P., "Comparative bond efficiency of deformed concrete reinforcing bars," Journal of Research, of the National Bureau of Standards, V. 37, 1946, pp. 399-407.

16. Jirsa, J. O., Breen, J. E., "Influence of Casting Position and shear on Development and Splice Length - Design Recommendations," The University of Texas, 1981, 45 p.

17. Jeanty, P. R., Mitchell, D., Mirza, M. S., "Investigation of 'top bar' effects in beams," ACI Structural Journal, V. 85, No. 3, 1988, pp. 251-257.

18. Johnston, D. W., Zia, P., "Bond characteristics of epoxy-coated reinforcing bars," North Carolina State University, 1982, 163 p.

19. Treece, R. A., Jirsa J. O., "Bond strength of epoxy-coated reinforcing bars," ACI Materials Journal, V. 86, No. 2, 1989, pp. 167-174.

20. Basso Trujillo, P., Jolin, M., Massicotte, B., Bissonnette, B., "Bond strength of reinforcing bars encased with shotcrete," Construction and Building Materials, V. 169, 2018, pp. 678-688.

21. Basso Trujillo, P., Jolin, M., Massicotte, B., Bissonnette, B., "Bond strength of reinforcing bars with varying encapsulation qualities," ACI Structural Journal, 2018 (in press).

22. Basso Trujillo, P., Malo, R., Jolin, M., "Alternative set-up apparatus to test ASTM A944-10 beam-end specimens," Journal of Testing and Evaluation, 2018 (in press).

23. Basso Trujillo, P., Lagier, F., Jolin, M., Massicotte, B., Bissonnette, B., "Finite element modeling of beam-end specimens with different qualities of reinforcing bar encapsulation," Materials and Structures, 2018 (to be submitted).

24. Basso Trujillo, P., Jolin, M., Massicotte, B., Bissonnette, B., "Shotcrete modification factors for the development length equation using possibility theory," ACI Structural Journal, 2018 (to be submitted).

25. ACI Committee 408, "408R-03 Bond and development of straight reinforcing bars in tension," American Concrete Institute, 2003, 49 p.

26. ASTM, "A944-10 Standard test method for comparing bond strength of steel reinforcing bars to concrete using beam-end specimens," American Society of Testing and Materials, 2015, 4 p.

27. Klir, G. J., Yuan, B., "Fuzzy sets and fuzzy logic - Theory and applications," Prentice Hall, 1995, 574 p.

28. Zadeh, L. A., "Fuzzy sets as a basis for a theory of possibility," Fuzzy Sets and Systems, V. 1, No. 1, 1978, pp. 3-28.

29. Kaneyoshi, M., Tanaka, H., Kamei, M., Furuta, H., "New system identification technique using fuzzy regression analysis," First international symposium on uncertainty modeling and analysis, 1990, pp. 528-533.

30. Tee, A. B., Bowman, M. D., Sinha K. C., "A fuzzy mathematical approach for bridge condition evaluation," Civil Engineering Systems, V. 5, No. 1, 1988, pp. 17-24.

31. Hong, D. H., Do H. Y., "Fuzzy polynomial regression analysis using shape preserving operation," Journal of Computational & Applied Mathematics, V. 8, No. 3, 2001 pp. 645-656.

32. Dubois, D., Prade, H., Sandri, S., "On possibility/probability transformations," Fuzzy Logic: State of the Art, 1993, pp. 103-112.

33. Aven, T., Baraldi, P., Flage, R., Zio, E., "Uncertainty in risk assessment - The representation and treatment of uncertainties by probabilistic and non-probabilistic methods," 2014, 186 p.

34. Dassault systems, "ABAQUS Theory Manual V. 6.11," 2011, 1172 p.

8th International Symposium on Sprayed Concrete – Modern Use of Wet Mix Srayed Concrete for Underground Support – Trondheim, Norway, 11. – 14. June 2018

Sprayed Concrete used as Avalanche Securing of road in the open day during Freezing Conditions

Thomas Beck
Normet Norway AS, Slomarka 57, 2100 Skarnes, Norway. thomas.beck@normet.com

Knut Brusletto
Contexo AS, Hvervenmoveien 49, 3511 Hønefoss, Norway. knut@contexo.no

ABSTRACT

In the project of avalanche securing road 13 between Odda and Lofthus on the west-coast of Norway, sprayed concrete has been used in huge amounts in combination with self-drilling anchoring bolts in the open day. The amount of sprayed concrete was originally estimated to be 1 000 m3, but has exceeded 10 000 m3. Since the spraying operation has been carried out continuously through the year, there has been spraying operation at days with temperatures below freezing point. Discussions if the sprayed concrete could freeze to damage have led to lab-tests to verify that sprayed concrete which is sprayed with alkali free accelerator does not freeze to damage. Specially designed spraying equipment has been developed for this specific project in order to increase the range of the nozzle in the partly high rock walls to be secured.

PROJECT DESCRIPTION

Highway 13 along the fjord "Sørfjorden" has partly steep mountain sides adjoined to the road. In order to increase safety and reduce the risk of avalanche of rock and soil mass onto the road, Public Roads Administration (PRA) in Norway started the project of securing 2650 meters of the road. Project started in January 2016 and is going to be finalized in June 2018.

The road will be given an increased width, and main securing method is soil nailing, where combination of steel fiber reinforced sprayed concrete is used in combination with self-drilling anchors.

Figure 1: Overview of some of the project area.

Figure 2: Soil nailing as main securing method.

The contractor, Contexo, used a specially designed spraying machine for having a large range in the spraying in the quite high rock and soil walls in the open day. A Volvo excavator was re-built and a trailer connected to the back of the Volvo carries the compressor, concrete pump and accelerator dosage system. See pictures 3 and 4.

Figure 3: Volvo excavator, rebuilt as spraying machine.

Figure 4: Long range spraying machine.

Figure 5: Well suitable range for working in the open day.

BACKGROUND/RISK DEFINITION

Challenges with frost and concrete spraying are mainly present in Arctic areas and in areas north in Europe, North-America and Russia. In Norway, Norwegian Concrete Association's Publication no. 7 (NB7) [1] is stating that spraying have to be carried out onto a rock surface with temperature of minimum +2 °C. The exception is spraying in permafrost rock and zones which have been mechanically stabilized with frost. The risk is reduced or no adhesion and bonding between sprayed concrete and rock surface.

In general, frost and temperatures below 0 °C is seen as a threat to concrete, as water inside air pores and capillary system inside the concrete is in risk of freezing before the concrete hydrates and consumes most of the water. When water freezes, the water volume expands with 9 % by volume and can therefore be leading to expanding processes inside the concrete.

A photo showing frost exposed concrete on ground in a parking place can be seen below.

For ordinary cast concrete air entrain agents, which converts the natural air bubbles in matrix to smaller micro air bubbles, is used to prevent frost erosion. The surface tension of water is so strong that water cannot manage to fill a micro air bubble completely. In this way, the micro air voids are not completely saturated with water and when the water freezes there is air space for the frozen water to expand into.

Figure 6: Ordinary cast concrete on ground in a parking place. This concrete is probably not designed with air entraing agent to obtain micro air.

In sprayed concrete, micro air from air entraining agents are not commonly used for making frost durable concrete. Micro air is sometimes used in sprayed concrete, but then for achieving improved pump-ability and to reduce cement and improve economy in mix design.

Studies of tunnels with older sprayed concrete, done by PRA [2], has not revealed any durability challenges due to frost. Some older tunnels showed reduced adhesion between sprayed concrete and rock in zones of permanent water leakage. Modern sprayed concrete with more durable mix design (lower w/c-ratio and use of pozzolans) indicated improved performance.

In the actual project ~11 000 m3 of sprayed concrete have been sprayed in open day, during all four seasons, and therefore in temperature conditions below 0 °C. All the sprayed concrete is installed in the open day and will therefore be exposed to water and frost in the coming years.

There were discussions during the first winter if frost could harm the freshly sprayed concrete. Reduced bonding was not seen as a challenge due to the use of self-drilling anchors, which bond the fiber reinforced sprayed concrete to the rock.

For ordinary cast concrete, there is a general rule that the concrete should be protected against frost, until it has reached a compressive strength of 5 MPa. Theory is that once reaching 5 MPa, the hydration of cement has come so far that the water consumption from the chemical reactions between cement and water has lowered the water content in pores and capillary system in concrete to a low enough level.

LAB EXPERIMENTS

In order to verify if frost can damage sprayed concrete within the first hours, a lab experiment was designed.

Sprayed concrete was mixed in lab, with the following raw materials:

- OPC
- Microsilica
- Natural sand 0-8 mm
- Water
- Superplasticizer
- Alkali free accelerator

All raw materials were stored in refrigerator over-night in order to obtain a temperature of +5 °C. Mortar prism molds were kept in freezer over-night to obtain a temperature of -10 °C.

Two mix designs were made, both with water/binder-ratio of 0.45.

One of the samples was added alkali free accelerator, and the other one had no accelerator. With +5 °C in all raw materials, it is easier to mix 5 % alkali free accelerator into the concrete without achieving stiffening at once. Because of the low temperature in the fresh concrete it was possible to cast the concrete, even with 5 % alkali free accelerator, in the mold.

Both samples, with and without accelerator, were put into a freezer containing -10 °C immediately after casting in mold.

RESULTS

After 24 hours, both samples were taken out from freezer and surfaces were inspected. See picture below.

Figure 7: Reference without alkali-free accelerator above, and sample with alkali-free accelerator below.

There is an obvious visible difference in surfaces of the two samples. In the reference, there are ice crystals along the whole surface. In the sample containing alkali-free accelerator, no ice crystals can be detected.

The only difference of these two samples is the addition of 5 % alkali free accelerator.

SOLUTION

What mechanism is making up the huge difference of surface after 24 hours at -10 °C? The answer lies in the chemical composition of the alkali-free accelerator. Alkali-free accelerators are made from various chemicals, but the chemical which is most present is aluminum sulfate, $Al_2(SO_4)_3$. Aluminium sulfate lead to immediate formation of ettringite crystals in the cement paste [3].

Ettringite formula: $(CaO)_3(Al_2O_3)(CaSO_4)_3$ x $\underline{32\ H_2O}$

The underlined last part, indicates that etteringite is a crystal material containing so-called crystal water, which is basically water "trapped" inside the crystalline material.

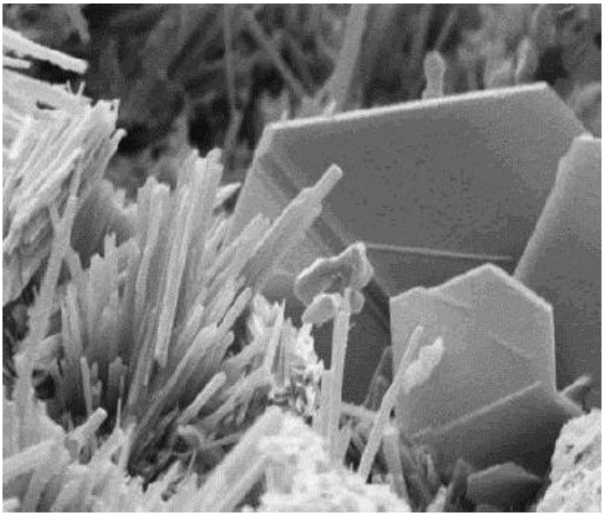
Figure 8 [4]: Scanning Electron Microscope picture of fractured hardened cement paste, showing plates of Calcium Hydroxide and needles of ettringite (micron scale).

Ettringite leads to a rapid stiffening and water consumption. Even though the strength development of the sprayed concrete with alkali-free accelerator is not achieving high early strength, due to temperature below freezing point, it still doesn’t freeze to damage.

CONCLUSION

Spraying concrete using alkali-free accelerator during temperatures below freezing point is not causing frost damage to the final sprayed concrete product. This is mainly due the chemical composition of alkali-free accelerator and the following formation of large amounts of ettringite crystals in the cement paste.

The etteringite is consuming large amounts of water, making the remaining part of free water in the concrete so small that frost damage can-not occur.

Spraying concrete with alkali-free accelerator below freezing point will likely cause low adhesion between concrete and rock surface, caused by potential ice and frost layer on rock surface. In this specific project this is not a problem, because the fiber reinforced sprayed concrete was connected to rock mass through self-drilling anchors, as soil nailing.

REFERENCES

1. Norwegian Concrete Association, Publication no. 7 Sprayed Concrete for Rock Support, Aug 2011.
2. Statens vegvesen, Vegdirektoratet-report: “Riktig bruk av sprøytebetong i vegtunneler – Frostsoner – Sluttrapport C», Oct 1997.
3. Myrdal, Roar: Chemical Reflections on Accelerators for Sprayed Concrete, Past, Present and Future Challenges, Proceedings 6^{th} International Symposium on Sprayed Concrete, Tromsø, Norway 12 – 15 Sep 2011.
4. Wikipedia: Searched the phrase: “Ettringite”.

METAKAOLIN AS A BINDER FOR FREE LIME IN SPRAYED CONCRETE

Denis Bézard
Newchem AG, Switzerland
bezard@newchem.org

Gilbert Otten
Newchem AG, Switzerland
sales@newchem.org

From the supplementary cementitious materials only metakaolin is produced in larger quantities on purpose. Due to different calcination methods and kaolin qualities from different sources many different types can be generated. This allows the production of defined materials that may suit many purposes in the mortar and concrete industry. The material is based on natural kaolin available in many locations around the globe.

Metakaolins react with available free lime to bind it to new CSH, CAH and CASH phases that develop a higher mechanical strength. Through the platelet structure they also partly act as reinforcement for the cement matrix.

Using the right metakaolin it is possible to improve the early mechanical strength of shotcrete and reduce the amount of free lime that will lead to sintering in the effluent of tunnels. Due to its thixotropic effect the addition of metakaolin will also reduce the rebound of shotcrete applications.

By giving concrete a finer pore structure, the durability of concrete will be extended, and the effect of possible chemical attacks reduced.

BASICS

Concretes and mortars using Ordinary Portland Cement have the problem that cement clinker is producing about 15 to 32% of hydrated lime in the hydration process.

This hydrated lime is water soluble and can migrate through the material to the surface. There it can generate efflorescence and sintering in contact with the CO_2 of the air, producing calcium carbonate deposits. In tunneling these deposits can fill the drainage pipes.

With time the drainage may get clogged and the water is unable to flow of. As a result, the pressure in the system increases and can lead to damage in the tunnel. The cleaning of the pipes is the major costs in tunnel maintenance [1]. Any reduction in sintering should therefore reduce the maintenance costs strongly and keep it to a minimum.

Figure 1: PP drainage pipe with precipitations, Picture: M. Testor, BEG

SOLUTION

Pozzolanic materials can bind the hydrated lime developed by the OPC and produce more cementitious binders as CSH, CAH and CASH. The most reactive pozzolanic material is metakaolin reacting along the chemical equation:

$$CH + A/S\ (Metakaolin) + H = CSH + CAH + CASH$$

If the reaction between the free lime and the type of metakaolin is fast enough, a major part of the soluble lime is transformed to an insoluble binder thereby reducing the leaching and sintering to a minimum.

ANALYSIS

One way to prove the higher density of the cement matrix produced using metakaolin, is to look to the diffusion of chloride.

The most accepted test to measure the chlorine diffusion is the NT BUILD 492 Nordtest method. In this test methods chloride diffusion coefficient are defined as:

Chloride penetration resistance	Dcl [m2 / s]
Very good	$Dcl < 2 \times 10^{-12}$
Good	$2 \times 10^{-12} > Dcl < 8 \times 10^{-12}$
Medium	$8 \times 10^{-12} > Dcl < 16 \times 10^{-12}$
Poor	$Dcl > 16 \times 10^{-12}$

Table 1: chloride diffusion coefficient depending on OPC replacement by metakaolin

Designation of concrete	M 1	M 2	M 3
Short description of the mixture	Concrete without Metaver	Concrete with 8% Metaver	Concrete with 12% Metaver
Medium compressive strength after 28 days (N/mm^2)	74.4	88.0	91.4
Medium chloride diffusion coefficient ($\times 10^{-12}$ m^2/s)	9.61	2.53	**1.37**

As can be easily seen the penetration resistance of the concrete improves from "medium" to "good" and "very good". This is because the pore diameter is reduced by the higher amount of cementitious binder formed [2].

To prove that this reaction works well we can have a look at the mechanical strength of a 10% OPC replacement of a typical metakaolin in a EN 196-1 test:

Table 2: typical mechanical values of a 10 % OPC replacement by metakaolin

Tests according to EN 196:	**1 / 7 and 28 days**	
w/b = 0,5	**1**	**5**
Standard sand %	75	75
CEM I 42,5 R Holcim Romania (%)	25	**22,5**
Metakaolin O	0	**2,5**
Total	100	100
FLEXURE - 1 days (N/mm^2)	**3,97**	**2,74**
COMPRESION - 1 days (N/mm^2)	**13,03**	**9,00**
FLEXURE - 7 days (N/mm^2)	**7,87**	**8,19**
COMPRESION - 7 days (N/mm^2)	**35.37**	**39,06**
FLEXURE - 28 days (N/mm^2)	**9,23**	**10,99**
COMPRESION - 28 days (N/mm^2)	**41,16**	**53,93**
K-Factor	1	**1,3102527**

These mechanical improvements can also reduce shrinkage, creep and thixotropy. The denser structure will give acid and sulphate resistance, reduce chlorine migration and the aluminium content will reduce the alkali silica reaction [2].

TEST METHODS

To define the total lime binding capacity of a pozzolanic material there is the modified Chapelle methods that defines the maximal amount of $Ca(OH)_2$ that can be bound by 1.000 mg of pozzolan. For metakaolin the values are normally between 1.000 and 1.400 mg. Similar values can also be obtained by slower materials as microsilica and slag.

The big difference is how fast these materials react as unreacted $Ca(OH)_2$ will invariably be leached out and transform to $CaCO_3$ when in contact to CO_2. We therefore developed a method to measure the reactivity of pozzolanic materials with hydrated lime adding some potassium sulphate to accelerate the reaction. This alkali addition is similar to the alkali of the cement. The mix is:

Pozzolan (metakaolin, fly ash, microsilica)	375,0 g
K_2SO_4 (water free)	7,5 g
Hydrate of white lime (CL 90)	125,0 g

Water w/b-ratio 0,5 - 1,3 (to get a slump of 150 $\pm$ 2 mm)

First put the water to the Hobart mixer than add the premixed powder and start mixing process for 30 s at speed I, then 30 s at speed II, then stop for 30 s to remove adhering material from the wall and continue mixing for 90 s at grade II.

Test the slump of the mixture on the slump table (Hägermann, 15 strokes). Repeat the test procedure with different levels of water additions until a slump of 150 mm is reached.

After obtaining the right slump pour the wet mix into a Vicat ring and start the setting test procedure with a testing step every 15 or 30 minutes, depending on reactivity.

The usual reaction time with metakaolin lies between 2 and 15 hours, fly ash 15 to 30 hours and microsilica even slower.

METAKAOLIN IN SHOTCRETE

To test the leaching behaviour a test given by the Austrian code of practice “Festlegung des Reduzierten Versinterungspotentials” (Determination of the Reduced Potential for Precipitations) is used [3].

According to test performed at the University of Applied Sciences, Regensburg, Germany [4] the Ca-Release of shotcrete usually used with more than 400 kg/m³ lies around 1 kg/ton. In Austria several tunnels have already been sprayed with reduced cement content to achieve values of 0,7 kg/m³ at sufficient strength development.

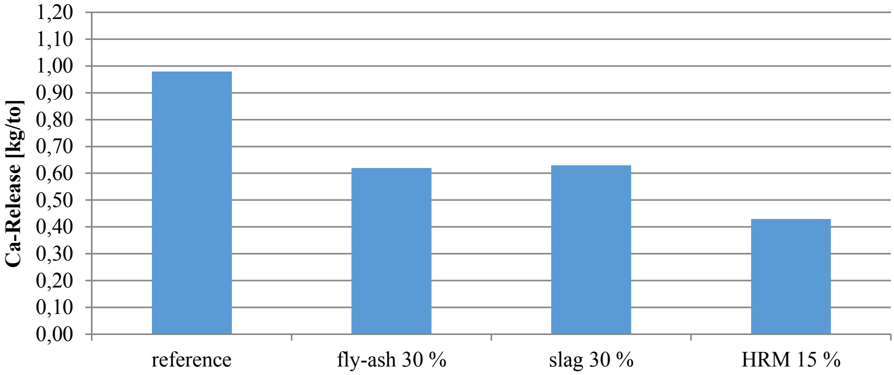

Figure 2: Ca-Release from mortars with different binder compositions after 56 days

As can be seen from these results the Ca- Release can be strongly reduced by using pozzolanic or latent-hydraulic materials. Using slow pozzolanic materials it is necessary to add high quantities of replacement to get a decent reduction in total release. For HRM (highly reactive metakaolin) a 15% replacement already leads to a higher reduction in Ca-Release because of fast lime capture.

Nevertheless, under wet conditions slower pozzolanic additives can in a later stage bind the smaller amounts released in time but the major amount of hydrated lime released in the early cement reaction will not be bound and remain in the effluent.

Analysing the rebound in practical shotcrete tests a reduction of 25% could be obtained. This is slightly lower then with the use of microsilica.

CONCLUSION

The use of HRM high reactivity metakaolin in shotcrete reduces strongly the precipitation of $Ca(CO)_3$ that usually comes with the formation of free lime in the reaction of Portland Cement. Through the fast binding of hydrated lime, the concentration can be kept low and leaching reduced.

This reduction in precipitations reduces the costs for the clearing of the water evacuation pipes in tunnels.

It also reduces the efflorescence of sprayed concrete in visible applications and repair works.

Because of its denser structure the concrete produced with HRM will be more resistant to chemical attack and have a longer life time.

Reduction in chloride migration will reduce the chloride attack on rebars and prolong life cycles of reinforced structures.

LITERATUR

[1] Pichler W.; Wagner H.; Insam R.; "Sprayed Concrete with reduced precipitation potential – Practical experiences from major construction sites in Austria", 11th Shotcrete Conference, 29.-30.01.2015 Alpbach, Austria 2015

[2] Güneyisi, E., Gesoğlu, M. & Mermerdaş, K. "Improving strength, drying shrinkage, and pore structure of concrete using metakaolin", Mater Struct (2008) 41: 937. https://doi.org/10.1617/s11527-007-9296-z

[3] Österreichische Bautechnik Vereinigung: Festlegung des Redizuierten Versinterungspotentials (Determination of the Reduced potential for Precipitatons). Merkblatt. Wien (0/2012)

[4] Thumann M.; Hartmaier M.; Saxer A.; Kusterle W.: "Potential f or Precipitations – Lab Tests and Sprayed Mortar Tests for the Reduction of Calcium Leaching", 11th Shotcrete Conference, 29.-30.01.2015 Alpbach, Austria 2015

INSTANT AND DELAYED MECHANICAL BEHAVIOUR OF SPRAYED CONCRETE USED ON ANDRA'S URL: TOWARDS AN UNDERSTANDING OF THE LINKS BETWEEN FORMULATION, IMPLENTATION AND IN SITU PROPERTIES

Yasir Bhewa*, Thomas Rougelot*, Jad Zghondi**, Nicolas Burlion*
* LaMcube, University of Lille, CNRS FRE 3723, Cité Scientifique F-59650 Villeneuve d'Ascq, France
** ANDRA, Meuse/Haute-Marne Underground Research Laboratory 55290 Bure, France
yasir.bhewa@polytech-lille.fr

ABSTRACT

In the framework of the ongoing experimental program at the URL (underground research Laboratory) of Andra (French National Radioactive Waste Management Agency), sprayed concrete is mainly used for the primary support of different experimental drift.

The aim of this study is to experimentally investigate the evolutions of the basic mechanical properties of sprayed concrete with respect to time (1, 7, 14, 28 and 90 days), specially at early age. The experiments are carried out with cylindrical samples (37mm in diameter) produced on the real site and cored in the same direction as the projection (parallel direction) and in a perpendicular direction. So far, compressive tests have been performed and analysed to obtain information about the mechanical properties of sprayed concrete: compressive strength, Young's modulus and Poisson's ratio. Ultrasonic measurements have also been realized to get additional data on its mechanical behaviour and its evolution in time.

The obtained results demonstrate that samples extracted in the perpendicular direction (to the projection) have better basis mechanical properties than those extracted in parallel direction in function of time. Perpendicular specimens have better compressive strength and a higher Young's modulus value than parallel ones and this was also proved with the ultrasonic measurement results. The difference is about 10%: the setup procedure has an impact on the properties and should be carefully analysed in the future mechanical tests such as shrinkage and creep.

1. INTRODUCTION

Sprayed concrete is often used in underground construction. It could be used for different kind of retaining structures in Cigéo project (Industrial Center for Geological Disposal). It is therefore crucial to know, understand and model the behaviour in the short and long terms of such specific material to guarantee the provisional or long term stability of the facility.

Until now the knowledge of this very particular material is still fragmented. The relationships between formulation, implementation and short- or long-term in situ mechanical characteristics of the material are often poorly known. Few basic scientific studies have attempted to make the link [1-2]. In addition to this, the study of deferred behaviours is very incomplete and the link between material and structure, particularly in terms of convergence of the surrounding argillite, the effect of shrinkage and creep, adhesion properties or long-term permeability remain quite challenging.

The purpose of this global study is therefore to propose an engineering model that can be used for the dimension of the shotcrete structures. This model will take in account the evolution of basic mechanical properties such as Young's modulus, Poisson's ratio, resistance parameters such as adhesion and compression with respect to time from young age (since three hours after the projection of shotcrete) up to the lifetime of the construction.

In this paper, we are going to focus on the evolutions of the basic mechanical properties of sprayed concrete with respect to time that are mentioned above. In addition, the knowledge of the mechanical behaviour is restricted to the properties of the material in the same direction as the projection (parallel direction) [1-2]. No study has been performed in the perpendicular direction but the shotcrete setup could imply anisotropy of the properties. An experimental campaign was therefore carried out with samples that were cored in a parallel and in a perpendicular direction as shown in figure 1 below.

2. EXPERIMENTAL PROGRAM

2.1 Shotcrete composition

The sprayed concrete used and tested in all experimental tests is a concrete which is issued from real manufacturing on site at the URL of Andra. The method used for the projection is the wet shotcrete spraying.

The composition of the sprayed concrete used for the experimental tests is as follows:

- Non-alkaline high performance liquid accelerator for wet shotcrete with high mechanical resistance at young age with a ratio of accelerator/cement of 0.06
- Hydration stabilizer for sprayed concrete
- Polypropylene reinforcing fibers for shotcrete with a dosage of not more than 6 kg/m^3
- Water/cement ratio of 0.5
- Dry mix of cement for wet projection in an aggressive environment (Exposure classes according to EN 206-1: XS1, XA2, XD2, XF2):
    1. 400 kg/m^3 of cement CEM I 52.5 N
    2. Granularity: 0/8 mm (recommended by AFTES [3])
    3. Weight of dry mix: 1800 kg (for 1 m^3 of concrete)

The slump class of the concrete is S2 and has a characteristic compressive cylinder strength of about 30 MPa at 28 days.

2.2 Sample preparation

First of all, the sprayed concrete is projected in crates of dimension 45 cm x 45 cm x 12 cm depth. The figure 2 below illustrates the layout that has been put in place during concrete spraying. The crates were fixed on the template with a fixing system so that they do not move during the projection and that will also serve to ensure the inclination of 10° with the vertical plane as recommended by ASQUAPRO [4-5].

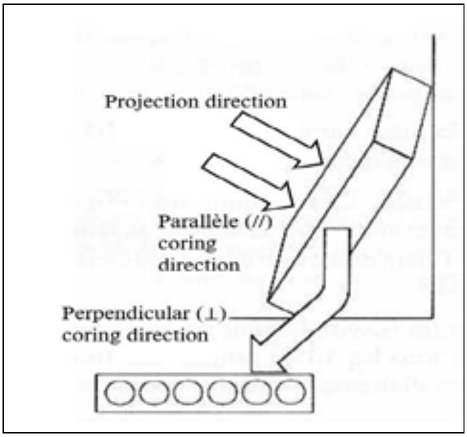

Figure 1: Parallel and perpendicular cored samples

Once the concrete sprayed, the samples are cored parallel and perpendicular to the direction of projection as shown in the figure 1. The cored samples are cylindrical with a diameter of 37 mm (about 4-5 times the maximum diameter of the aggregates which can be regarded as representative of the material) and a height of 74 mm and all tests afterwards were realized with this geometry. Both coring and sawing were carried out under water, so it could be assumed that no desiccation occurred during sample preparation. Coring form crates is performed between 3 and 6 hours, 7, 14, 28 and 90 days after the projection to study the effect of the maturation with respect to time.

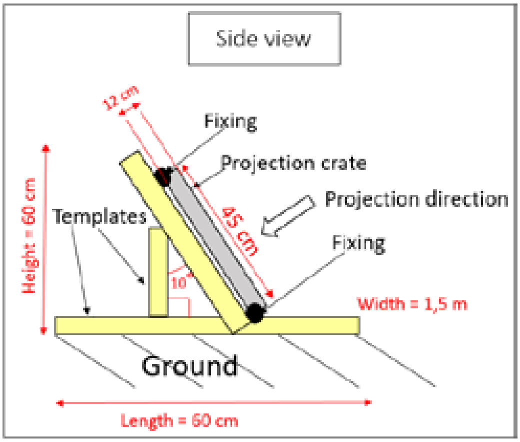

Figure 2: Crates fixing system

3. DISCUSSIONS OF TESTS RESULTS

3.1 Compression strength

3.1.1 Experimental procedure

In order to ensure that the experimental results can be statistically considered representative, a minimum of three samples were tested for each time sequences. The experimental tests were performed with an *ENERPAC®* 10T hydraulic press to obtain the compressive strength. The use of this relatively small equipment is explained by the need to perform compression tests as close as possible to the projection site.

3.1.2 Tests results

The mean compressive strength (Rc) values of the wet sprayed concrete 3-6 hours after the projection for samples cored in the parallel and perpendicular to the projection direction is 3.8 MPa and 4.5 MPa respectively. The averages were calculated on the basis of 3 specimens cored in each direction of projection that were produced on site at the URL of Andra. Afterwards the remaining tests were carried out in our laboratory and with 6 to 12 specimens in each direction for each maturity date.

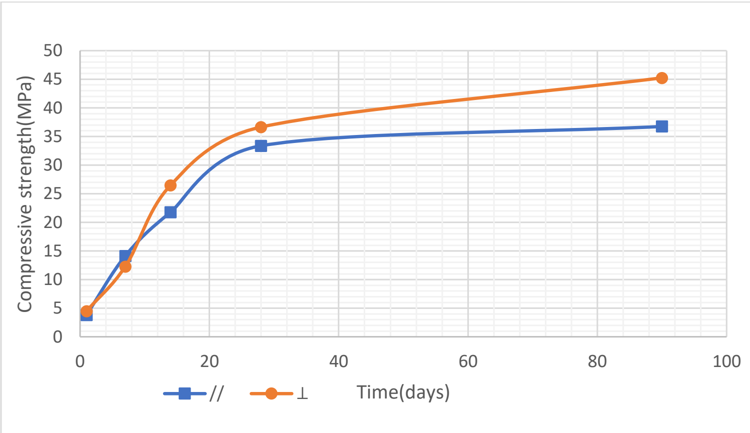

Figure 3: Evolution of compressive strength with time

The average compressive strength (figure 3) at 28 days is equal to 33.4 MPa with a variation of 29.2 to 36.4 MPa in the parallel coring direction and 36.6 MPa with a variation of 31.3 to 39.9 MPa in the perpendicular coring direction. The values obtained are greater than the current requirements and the dispersions on the results are low (less than 10%). It can be observed, after 14 days, that samples obtained in the perpendicular coring direction of projection have a greater compressive strength than that obtained in the parallel coring direction. The difference in values is more than 10% and it can also be noticed that this evolution trend continues with time.

Another observation is that in the perpendicular coring direction, shotcrete has a compressive strength value equal to 45.2 MPa at 90 days, which represents a rise of more than 20% to that of 28 days, whereas the increase was only about 10% in the parallel direction. The anisotropic behaviour in compression is well shown. This also is very interesting for the mechanical properties of sprayed concrete in the long term. This anisotropy induced by the direction of projection can be explained as follows: during projection, a certain stratification is induced in the concrete. This stratification creates interfaces within the specimens where many defects concentrate. In the compression failure test, in a direction parallel to the projection, these defects play a major role and do not contribute to limiting lateral extensions. Local shears induced near the aggregates will be partially affected by these defects. On the other hand, during a test in a perpendicular direction, the compaction of the concrete linked to the dynamic projection of the material will induce a better mechanical behaviour: the specimen will then behave like a set of juxtaposed columns, made of a higher performance material. Since the stratification interfaces are not flat, lateral extensions will be limited and local shears will be better taken up.

The obtained values (at t = 90 days) have been compared with the ones measured by another apparatus (a triaxial cell only used with an axial loading, without confining pressure, see figure 6) in order to ensure that the measured values with the manual hydraulic press is similar and, thus, reliable. With the triaxial cell (named also hydraulic press), the test is carefully controlled in loading (constant loading rate), so fewer errors are occurred comparing to the manual pump of the ENERPAC® device, but it takes more time than a conventional test with a hydraulic press. As a result of this comparison, two relevant conclusions on the methodology used can be drawn:

1. In regards to the methodology of measurement, whether the hydraulic press or the triaxial cell, the difference in the values obtained for the compressive strength is less than 5%.
2. Dispersion from the mean value is of the same order of magnitude for both methods that is of about 10%. Some values were quite far from the mean value regardless of the methods used, therefore this is probably due to possible material heterogeneity and not to the methodology used to measure the compressive strength. The measurement accuracy with the hydraulic press seems therefore reliable.

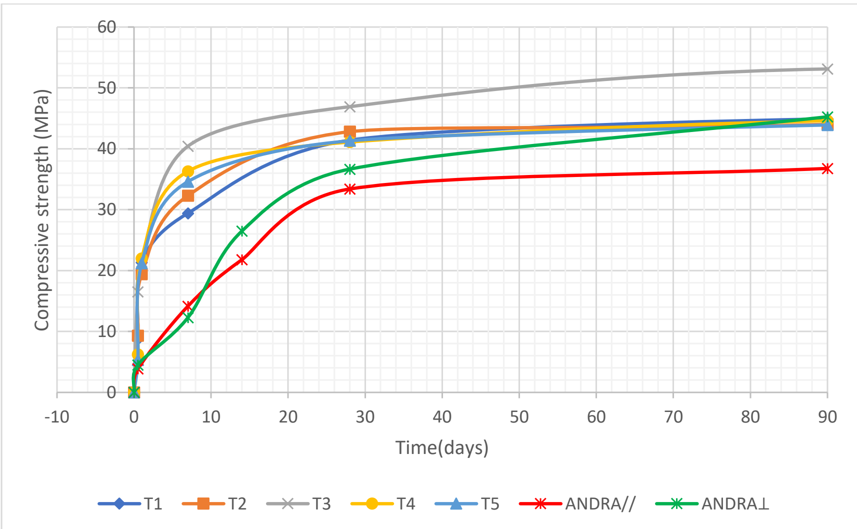

Figure 4: Evolution of the compressive strength of the Andra sprayed concrete in comparison with other sprayed concretes

In the figure 4, the tested shotcrete has been compared to other shotcretes data found in the literature [1]. T1 to T5 are in fact five different shotcretes with different composition mixture but that should give the same compressive strength at 28 days as the shotcrete of the present study. They are all composed with a dosage of 400 kg/m^3 of cement and a water/cement ratio of 0.41. Which differs for each shotcrete (T1 to T5) is the amount of aggregates, the types of fibers and the quantity of admixtures. The graphs (T1 to T5) shown in the figure 4 were obtained from the literature and samples tested were cored only in the parallel direction. From the figure above it can be observed that all the sprayed concretes have the same evolution trend with respect to time. There is a sharp rise in values up to 24 hours (50% of the value at 28 days) then a progression attenuated up to 90 days (see figure 4). However, the tested shotcretes represented by the red and green curves have an evolution of the compressive strength less important than the others. This can be explained by the differences between the formulations (water/cement ratio is greater in the present study, fiber quantity …) and in the projection setup.

3.2 Young's modulus

3.2.1 Experimental procedure

For the Young's modulus measurement, the tests were realized with a triaxial cell (figure 6) and each samples tested were equipped with four strain gauges, two in the longitudinal direction and two in the transversal direction (Poisson's ratio) as shown in figure 5. The Young's modulus is determined by submitting the cylindrical specimen to a uniaxial compression and measuring the deformation by means of two longitudinal strain gauges fixed opposite to each other. A series of reading are taken and then the stress-strain relationship is established. Regarding the experimental test procedure for the Young's modulus, each sample is submitting to 3 cycles of loading-unloading up to 10% of the compressive strength corresponding to the time given, then a loading-unloading cycle up to 30% of this compressive strength and finally the sample is loaded till failure. Afterwards the Young's modulus value is calculated from the series of reading taken from the unloading cycle up to 30% of the compressive strength corresponding to the time given.

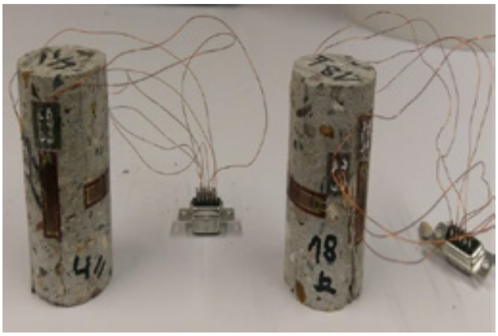

Figure 5: samples with 4 strain gauges

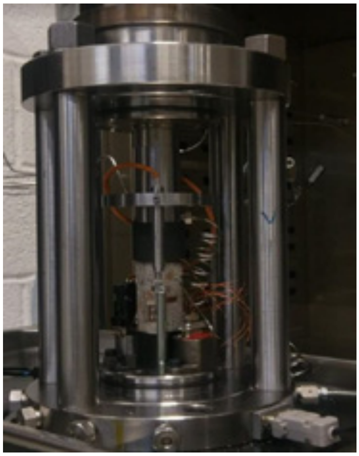

Figure 6: Triaxial cell

3.2.2 Tests results

Measuring the elastic modulus is a test that is rarely done for sprayed concrete. So there is not a lot of reference on the allowable values for this quantity. The knowledge of the evolution with respect to time of the Young's modulus is limited by the test methodology. The Young's modulus was measured using strain gauges and as a result, this methodology limit dispersion in the results obtained. However, it is still an unsuitable test procedure for shotcrete at young age, which will explain the absence of data at early age in the graphs below. For wet sprayed concrete, it is commonly accepted that the measured value for the Young's modulus is reliable only from 24 hours [3].

In this study the tested shotcrete samples have a mean Young's modulus value at 28 days equal to 25.3 GPa with a variation of 22.8 to 28.2 GPa in the parallel coring direction of projection and a value of 28.7 GPa with a variation of 27.0 to 30.0 GPa in the perpendicular coring direction as shown below in the figure 7. Generally speaking, the value obtained at 28 days gives us a good estimation of the Young's modulus value of the shotcrete in the long term. Dispersion on the results are weak that is less than 10% at 28 days and the averages were calculated on the basis of 3 specimens in each coring direction of projection and for each time sequences.

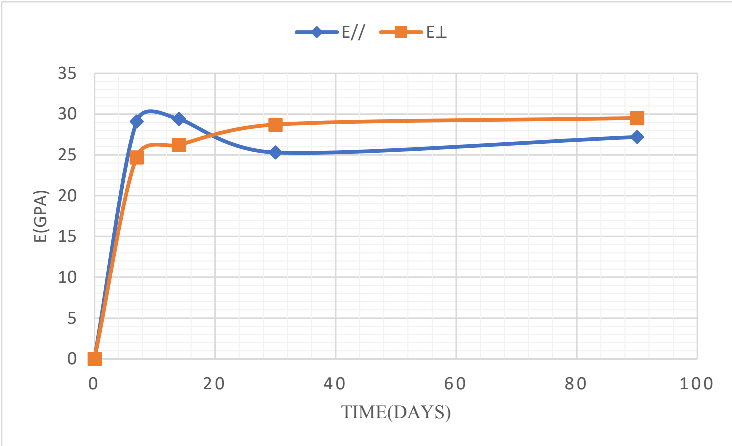

Figure 7: Evolution of the Young's modulus with time

According to the curves in figure 7, the Young's modulus increases after 28 days. Again for the Young's modulus, it is worth noting that samples cored perpendicular to the direction of projection have a Young's modulus equal to 28.7 GPa at 28 days which is an increase of more than 10% than those cored in the parallel direction. Since the difference in values between parallel and perpendicular coring is more than 10%, the effect of the direction is not negligible concerning the mechanical properties of shotcrete in the long term.

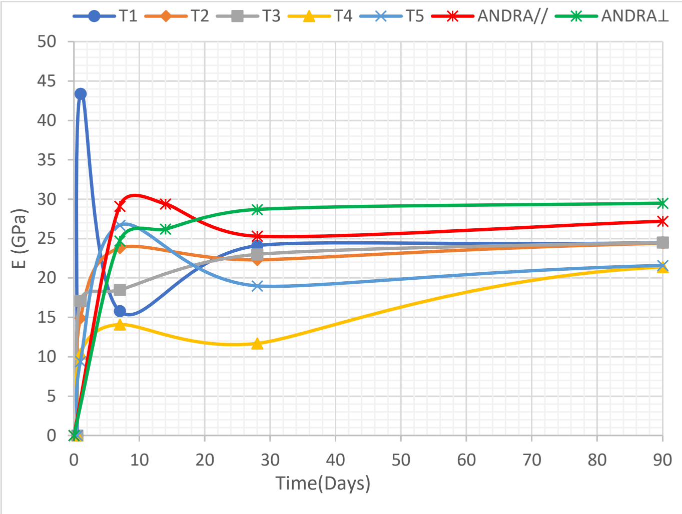

Figure 8: Evolution of the Young's modulus of Andra sprayed concrete in comparison with other sprayed concretes

In the figure 8, the Young's modulus values obtained from experimental tests are compared with other shotcretes data found in the literature [1]. T1 to T5 are the same shotcretes as above used for comparison in the study of compressive strength. The curves plotted in figure 8 show that the shotcrete tested, regardless of the direction of the projection, follow the same trend of evolution with respect to time as the other sprayed concretes. However, the tested shotcrete has greater Young's modulus values with respect to time than the other shotcretes. With regard to the expression of the Young's modulus based on the compressive strength at 28 days for sprayed concrete, it does not highlight a simple relationship between these two quantities as for a conventional concrete (the higher the strength, the higher the value of the modulus).

Another phenomenon is that the red curve (Andra / /) exhibits an increase of the modulus at 7 days and then a slight decrease of the modulus at 28 days. But this phenomenon occurs also in other shotcretes that have been compared (Figure 8). Finally, the evolution of the Young's modulus is gradually done till 28 days and then a progression attenuated up to 90 days for almost all shotcretes. The progression in time of the values of the Young's modulus (quite chaotic before 28 days) and the methodology for the test procedure (gluing strain gauges) tend to show that measuring a reliable modulus at early age is still not achieved. However, the test is very reliable for long term tests as seen above and compared to the tests and the results found in the literature [1].

3.3 Poisson's ratio

3.3.1 Experimental procedure

For the Poisson's ratio experiment, the tests were realized with the same procedure as for the Young's modulus experiment as shown in figures 5 and 6. Given that the samples were equipped with two strain gauges in both longitudinal and transversal directions, it allows determining the deformation in both directions and therefore the Poisson's ratio.

3.3.2 Tests results

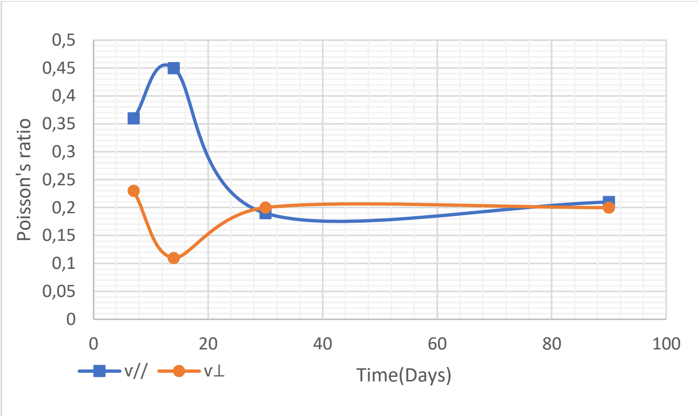

Figure 9: Evolution of the Poisson's ratio with respect to time

The measure of the Poisson's ratio is very rare in the literature that is done for the control of shotcrete. Thereby there is a lack of references on the allowable values for this quantity. In practice, mechanical calculations on such a material usually ignore the actual value of the Poisson's ratio of sprayed concrete. Calculations related to repairs of structures take into account a Poisson's ratio equal to 0.2 which is a value taken from cast concrete.

According to the experimental tests, the mean Poisson's ratio value measured for the tested shotcretes is equal to 0.2 regardless of the coring direction at 28 days as shown in figure 9. Here also, the methodology is adapted for long term test (from 7 days or more) and not for young age test. Between 7 and 14 days' intervals, in both coring directions, there are irregular values, but this phenomenon also occurs with the Young's modulus experiment. Generally speaking, the Poisson's ratio value at 28 days gives a good estimation of the value of the Poisson's ratio of shotcrete in the long term. Dispersion of the results is less than 10% at 28 days and the averages were calculated on the basis of 3 specimens in each coring direction. Following the curves (see figure 9), the values of the Poisson's ratio after 28 days do not seem undergoing great changes regardless of the coring direction. During the elastic phase, the presence of interfaces or defects does not play an important role in the evolution of elastic parameters after 28 days (10% deviation on the Young's modulus, none on the Poisson's ratio). This reflects the quality of the interfaces with regard to the mechanical behaviour of the material: it is therefore necessary to test the materials to destruction in order to observe differences in behaviour between the two directions of loading. Future studies will determine whether this conclusion extends to the delayed deformation of these concretes.

3.4 Ultrasonic measurements

3.4.1 Experimental procedure

The method of dynamic measurement is a non-destructive test that is frequently used to take measures without causing any damage to the tested samples. An important feature of non-destructive test is that it can be remade with the same sample, which allows us to monitor changes in the properties of the concrete with respect to time. Another interesting feature is that this method is suitable for very young age test (before 24 hours for example).

However, it is important to note that the use of the dynamic monitoring method has some drawbacks. It gives results that are underestimated in the presence of pores or cracks. And other factors that can influence the results given by the dynamic monitoring method are uncertainties created by the operator, the calibration, the contact condition at the surface of the concrete, the length of the path of the ultrasonic wave and the operating instructions (direct, indirect and semi-direct). Also known as the ultrasonic test, it is used to determine the velocity of propagation of longitudinal (in compression) waves through the concrete sample. The ultrasonic device displays the time that represents the passage of the ultrasonic wave through the concrete considered between transmitter and receiver (length of specimen). As a result, the velocity of the longitudinal wave of ultrasound through in the sample can be calculated. Then the dynamic modulus of elasticity (Ed) can be determined by the direct transmission of ultrasonic pulse which is given by the following equation [6-10]:

$$\boxed{Ed = \frac{(1+\mathrm{v})(1-2\mathrm{v})}{(1-\mathrm{v})}\gamma V^2;}$$

where E_d is the dynamic modulus of elasticity, ν the Poisson's ratio, V the ultrasonic longitudinal wave velocity and γ the density of concrete

3.4.2 Test results

The mean dynamic modulus values of the shotcrete tested at 28 days is equal to 36.4 GPa with a variation of 35.1 to 37.2 GPa in the parallel coring direction and a value of 37.1 GPa with a variation of 36.8 to 37.7 GPa in the perpendicular coring direction. The mean values were calculated on the basis of 3 specimens in each direction of projection. Note that with this method, dispersions on the results are very low that is less than 5% at 28 days but also for other sequences of time (see figure 10). The difference between the mean values of the dynamic modulus following the two coring directions is small.

However, the dynamic modulus values for samples coring in the perpendicular direction are higher than those from parallel direction. For the dynamic modulus like for the Young's modulus or the compressive strength, a same trend appears: samples cored in the perpendicular direction have greater mechanical properties values than for parallel direction.

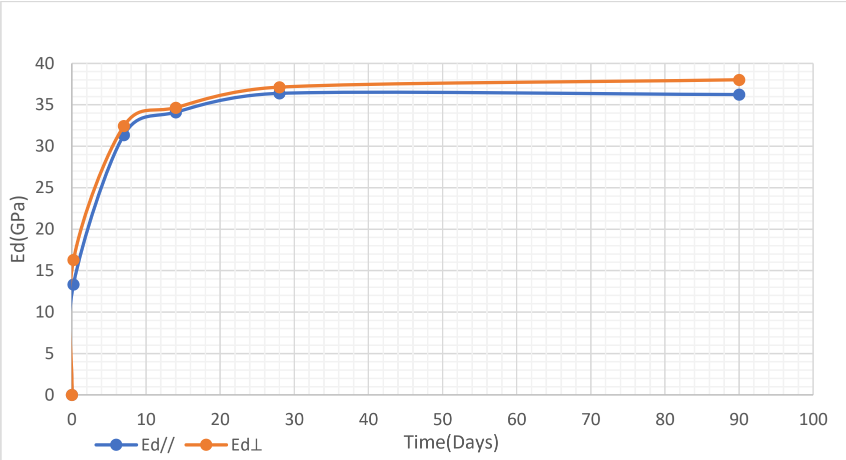

Figure 10: Evolution of the dynamic modulus with respect to time

Following figure 10, the evolution of the dynamic module is progressive up to about 14 days then a slower progression up to 90 days. The evolution trend for the dynamic modulus is the same regardless of the coring direction. It can be observed that the Ed for every specimen is greater than the Ec (elastic static modulus).

Nowadays in the literature, lots of correlations [8-10] relate the dynamic modulus (Ed) to the elastic modulus (Ec). According to Lydon and Balendron [11], there is a simple linear relationship that has been developed between the modulus of elasticity (Ec) and the dynamic modulus (Ed) for a concrete and it does not apply to concrete containing more than 500 kg/m^3 of cement. Given that the shotcrete used contains less than 500 kg/m^3 of cement, so the relationship below (eq. 1) is valid in such a case.

$$Ec = 0{,}83\ Ed \qquad \text{(Eq. 1)}$$

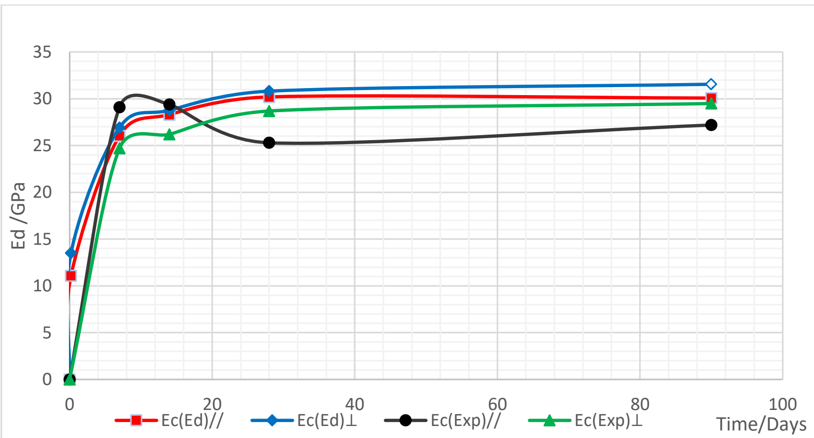

Figure 11: Evolution of the modulus of elasticity of the shotcrete tested with respect to time following two different methods: samples cored in the parallel direction with ultrasonic measure

(red curve) or strain gauges (black curve), samples cored in the perpendicular direction with ultrasonic measure (blue curve) or strain gauges (green curve).

Figure 11 shows a comparison between the evolution of the elastic modulus of the shotcrete tested obtained following the stress-strain loading method and the ultrasonic measurements method (corrected by the eq. 1). It can be observed that the results of the modulus of elasticity obtained by the stress-strain load method is very close to that obtained by the ultrasonic measurements method. So, it seems possible to find a good estimation of the modulus of elasticity from the dynamic modulus, even at early age. However, the elastic modulus calculated from the ultrasonic measurements test exceeds that calculated from the stress-strain load test. The difference between the dynamic modulus and the elastic modulus of the shotcrete tested is due to the fact that the heterogeneity of sprayed concrete affects the two moduli in different ways [12].

4. CONCLUSIONS

The main experimental results are summarized as follows:

a) From this study, it can be deduced that sample obtained from the perpendicular coring direction of projection has a compressive strength 10% higher than those from the parallel coring direction of projection with respect to time.

b) Even for the experimental results with the stress-strain load method, the Young's modulus for sample obtained from the perpendicular coring direction of projection is 10% higher than for the parallel coring direction at 28 days. The method used is suitable for long term test.

c) However, the value of the Poisson's ratio for the shotcrete tested can be considered to be equal to 0.2 at 28 days, regardless the coring direction of projection.

d) The ultrasonic measurements method allows using the dynamic modulus to obtain an approximation of the elastic modulus, even at early age.

Later on the evolutions of shrinkage and the creep (endogenous or coupled with desiccation) of this material in the short and long terms, as well as the determination of the thermo-hydro-mechanical behaviour of shotcrete depending on time will be studied [13-14]. Here also, the tests will be performed with samples cored in the parallel and perpendicular direction of projection. For a thorough understanding of shotcrete, other parameters such as the mode of implementation (characteristics of projection: wet or dry projections), type and percentage of fibers will also be taken in consideration, so that a numerical model can be developed to predict short and long term evolutions of the sprayed concrete used in the real underground disposal.

References

1. Geromey, S. "Evaluation des paramètres d'obtention de la qualité des bétons projetés utilisés dans des soutènements provisoires, des revêtements définitifs et des renforcements d'ouvrages". Thèse de doctorat de l'INSA de Lyon, 2003.

2. Armengaud, J. “Optimisation des propriétés des bétons projetés par voie sèche”. Thèse de doctorat de l’Université de Toulouse, 2016.
3. AFTES Recommendations on Fibre - Reinforced Sprayed Concrete Technology and Practice – Recommendations on tunnel technology
4. Larive, C. “Fonctionnement des bétons projetés fibrés” - Nouvelles specifications. Colloque Annuel de l’association ASQUAPRO, 2012.
5. Les huit fascicules d’ASQUAPRO – Guide de béton Projeté
6. Gadri, K. “Evalution du module d’élasticité à la compression à l’aide des techniques non destructives”. 22ème Congrès Français de Mécanique, August 2015
7. Bogas, J.A “Static and dynamic modulus of elasticity of structural lightweight and modified density concrete with and without nanosilica–characterization and normalization “. International Journal of Civil Engineering, January 2014
8. Antonaci, P. “Monitoring evolution of compressive damage in concrete with linear and nonlinear ultrasonic methods”. Cement and Concrete Research, February 2010.
9. Chavhan, P.P. “Correlation of Static and Dynamic modulus of Elasticity for different self-compacting concrete mixes”. International Journal on Recent and Innovation Trends on Computing and Communication, Vol. 3 Issue 7, July 2015
10. Mohammed, M.“The ratio between Static and Dynamic Modulus of Elasticity in Normal and High Strength Concrete”. Journal of Engineering and Develoment, Vol. 10 No. 2, June 2006
11. Lydon, and Balendran, “Some observations on the Elastic Properties of Plain Concrete”, Cement and Concrete Research, Vol. 16, No. 3, 1986
12. Neville, A. M., “Properties of Concrete”, Second Edition, Wiley, New York, and Longman, London, 1978.
13. Malmgren, et al. “Adhesion strength and shrinkage of shotcrete”. Tunnelling and Underground Space Technology, 20, 33–48, 2005.
14. Bryne, “Time dependent material properties of shotcrete for hard rock tunneling”. Thèse de doctorat du Royal Institut of Technology de Stockholm, Suède, 2014

QUALITY CONTROL OF FIBRE REINFORCED SPRAYED CONCRETE: NORWEGIAN REQUIREMENTS AND EXPERIENCES FROM LABORATORY STUDIES AND TUNNEL PROJECTS

Øyvind Bjøntegaard[1], Synnøve A. Myren[1] and Thomas Beck[2]
[1]Norwegian Public Roads Administration, Tunnel and concrete division, Norway
[2]Normet Norway AS
oyvind.bjontegaard@vegvesen.no, synnove.myren@vegvesen.no, thomas.beck@normet.com

SUMMARY

The paper discusses control and inspection of wet-sprayed fibre reinforced sprayed concrete according to today's Norwegian Concrete Association's Publication no. 7 "Sprayed concrete for rock support". On-site inspection results are presented, as well as laboratory test results on FRSC-panels studying the development of the energy absorption capacity over time, i.e. under hydration and the associated increase in compressive strength.

From the on-site data, it is evident that the fibre content and fibre distribution taken from fresh basic mixes are largely within the given tolerance limits. The energy absorption capacity from FRSC-panels may vary greatly from site to site, even though binder composition and fibre content can be more or less the same (whereas the type of aggregate is different). The series of laboratory tests showed that the energy absorption capacity can change significantly with time and strength level, especially this was shown for steel fibre. However, an adequate steel fibre dosage and fibre tensile strength can secure sufficient energy absorption capacity over longer times and significant increase in concrete compressive strength.

INTRODUCTION

In Norway the Norwegian Concrete Association's Publication no. 7 "Sprayed concrete for rock support" (NB7) has been the premise provider for production and execution of wet-sprayed fibre reinforced sprayed concrete (FRSC) since the early 1990-ies. NB7 has also been an "export article" worldwide in various mining and infrastructure projects.

The last edition of NB7 was in 2011 (NB7:2011) [1]. The former edition was from 2003 [2]. The paper discusses work done in connection with the last revision and the shift towards more intense control prior to start of each project and also that more inspection is now addressed earlier in the production process in the project.

The paper also presents site inspection results on fibre content on fresh basic mixes and on energy absorption capacity on sprayed panels. Results from a laboratory study is also presented showing aspects regarding the ability of the fibre to secure lasting toughness (energy absorption capacity) of the FRSC over longer times/curing ages. Regarding the latter, the state of knowledge on this issue is limited and information is lacking in the literature. Panel tests, measuring the toughness/the ability to stabilise and withstand rock deformations, is normally performed after 28 days of curing. The property is however important also early (safety for workers in a period when the rock deformations normally are at the highest) and at longer times (durability, long-term stability).

QUALITY CONTROL; BEFORE AND TO DAY

Before 2003, a 4-point loaded beam (residual flexural stress) was described in NB7 as the test method to verify the fibre action in FRSC. From 2003, NB7 opened also for the use of, at that time, the new panel test method (energy absorption). The practice was then a general declaration of a particular fibre and its effect on energy absorption and not documentation on the specific FRSC in the given project. Hence, at that time one single laboratory test showing satisfactory result more or less opened for general use of a fibre. Today's NB7:2011 requires both pre-documentation and quality control of energy absorption in each project.

When it comes to control of fibre content and fibre distribution the method before (NB7:2003, and previous editions) was to take out samples of newly sprayed concrete or drill cores from the hardened sprayed concrete lining. The sample volume was determined and then it was washed/crushed for the fibres to be extracted and quantified. The method involved generally small sample volumes and, consequently, the scatter was experienced to be high. In addition, the control was done at a late stage and any discrepancies gave rise to disagreements and disputes. From NB:2011 the control of fibre content and distribution is done on basic mix samples of larger volumes taken on arrival to the site; three 8 litres samples are collected from the concrete truck – one early, one in the middle and one late during emptying the truck. This control, prior to spraying, verify the fibre dosage and make probable a uniform distribution of fibres and sufficient toughness of the final sprayed concrete lining (provided normal rebound). Before project start, pre-documentation showing earlier results on fibre content in the basic mix and energy absorption capacity are required.

In other words, more of the quality control in projects involving sprayed concrete is now focused earlier in the process. NB7:2011 requires (for control frequencies, see NB7:2011 [1]):

- Pre-documentation of:
  - *energy absorption; for each given energy absorption class (E700, E1000). This then states the target fibre dosage for the FRSC to be used in the project.*
  - *fibre addition method and earlier results on fibre content and fibre distribution through concrete loads based on 8 litre basic mix samples. Serves as a check of the concrete supplier's ability to deliver evenly distributed fibres in the mix.*
  - compressive strength of basic mix (standard documentation).
- Regular inspection during the project:
  - mass ratio (mixing plant's control system + spent accerator)
  - compressive strength (cast, basic mix)
  - *fibre content/-distribution (basic mix)*
  - *energy absorption capacity (sprayed panels)*
  - compressive strength (drilled cores from final lining)
  - bond control, final lining
  - thickness control, final lining

The bullet points in italic represent the control tasks that became subjects to largest revision in NB7:2011. Fibre content/-distribution measurements on the basic mix was a new requirement. Pre-documentation of energy absorption capacity in every project was another. The test procedure for panel tests is now much more detailed formulated than before. NB7:2011 do not describe control of fibre content of drilled cores from the final lining. Today's control of fibre content/-distribution in the fresh basic mix is believed to be more sensible.

BRIEF SUMMARY OF PREVIOUS WORK AND FOLLOWING CONTENT

The following list gives an overview of the various investigations and considerations dealt with in connection with the revision of NB 7 and today's 2011-edition:

- The content and distribution of fibres through a concrete load
- Panel production method
- Panel test methodology: Effect of friction against the support fixture
- Panel test methodology: Panel test method comparison and variability
- Panel test methodology: Test and analysing procedure
- Effect of concrete parameters on energy abs. capacity (age/strength, fibre type and content)

Results have been reported in numerous Norwegian Public Roads Administration reports, and more summarizing overviews have been published in, for instance, [3, 4, 5, 6, 7, 8]. These tests comprised totally 52 individual test sets of round panels (continuous support) and 14 sets of square panels (continuous support). For the round panels the average coefficient of variation among the sets was 8.5% and for the square ones it was 12.1%.

The panel test method described in NB7:2011 equals to the EFNARC square panel test, EN 14488-5, but NB7 opens for both square and round panels (as they have shown to give equal results) and NB7 also describes the test procedure much more detailed (including correction for a 25% panel-support friction effect).

Lately, site inspection data have been collected on fibre content in basic mixes and on panel tests (energy absorption capacity) on sprayed concrete. In addition, all results from the investigation on the effect of age/strength on energy absorption energy have now been finalized and gathered (lower bullet point in the list above). In the discussions below, the following results have been brought together:

- **Site measurements on fibre content and –distribution**
- **Site measurements on energy absorption capacity of various FRSCs**
- **Laboratory test results on the effect of strength increase over time on the development of energy absorption capacity**

SITE DATA ON FIBRE CONTENT AND FIBRE DISTRIBUTION

Fibres are generally added to the basic ready-mix through the top opening of the concrete truck. Various methods are used to bring the fibres to the top; it can be manual, use of conveyer belt or air blown. Further mixing in the truck, its mixing efficiency and the transport length to the site will then decide the final degree of homogenization of fibres.

Fibre content and fibre distribution has from the release of NB7:2011 been controlled regularly on basic mixes on arrival of the truck to the tunnel site. Each control involves three measurements from a concrete truck; early, mid and late during emptying/pouring to the pump. By contribution from some contractors and concrete suppliers, we have been able to collect a respectable number of results from recent projects. The results add up to 213 controls on basic mixes with steel fibre and 5 controls on basic mixes with macro PP-fibre. The limited amount for the latter is due to the ban of macro PP-fibre in Norway from 2015, see [9]. The

213 mixes with steel fibre covers dosages from 19 to 55 kg/m^3 (both E700 and E1000). The PP-fibre dosages varies from 6 to 8 kg/m^3.

Before we look at the site data, the NB7-requirements for fibre content and fibre distribution should be clear:

- Fibre content (average of the three measurements): Not below 15% of intended dosage
- Fibre distribution (every single measurement): Not below 20% of intended dosage
- In addition, fibre control shall always be carried out on the same concrete truck delivering concrete for panel production. For such cases there are both minus and plus tolerances: ±15% for fibre content and ±20% for fibre distribution

The collected fibre control results for basic mixes with steel- and PP-fibre are presented in Figure 1 and Figure 2, respectively. The results are presented as % deviation to the agreed/intended fibre dosage. Both the minus and plus tolerances are indicated as dotted lines in the figures.

For the large amount of data for steel fibres it can be seen in Figure 1-a that only 4 of the (213 x 3 =) 639 single measurements fall below the generally valid lower tolerance. Moreover, for the upper tolerance also 4 single measurements fall outside. For the average fibre content in each truck, Figure 1-b, the results are also very satisfactory; only 2 results falls below and only 1 is above the tolerances. Hence, both the fibre distribution and the fibre content must be regarded generally as very satisfactory. Figure 1-c gives separate average results for early, mid and late single measurements, respectively, as well as the overall average of all single measurements. The overall picture is that the fibres are evenly distributed, but there is a trend that there is slightly more steel fibres in the mix in the beginning (early) of emptying the truck. This picture is somewhat different from what was reported before NB:2011 was released [5, 6]. The "overall average" shows that the concrete mixes on average appear to contain more fibres than the intended/agreed dosage. The reason for this not entirely clear, but is likely to be twofold: The concretes are intentionally added slightly more fibres than agreed (due to conservatism or due to practicalities such as using a given/rounded number of fibre bags), and/or the fibres are not entirely cleaned after being extracted from the fresh concrete mix.

From the results for the limited amount of mixes with PP-fibre, Figure 2, it can be seen that both the fibre distribution (Figure 2-a) and the fibre content (Figure 2-b) are well within the tolerances. Figure 2-c (and Figure 2-a) shows that there is a tendency of decreasing PP-fibre content in the mix during emptying the truck. This is similar trend as experience gained prior to the release of NB7:2011 [5, 6]. As for steel fibres, the "overall average" for PP-fibre also indicate that there is on average more fibres in the mixes than the agreed dosage, of reasons probably similar to steel fibre mixes as suggested above.

It is unclear whether the submitted results have been "adapted" in any way, for example if any disallowed results have not been included. However, we must rely on the general pattern shown here indicating good procedures for adding fibres and further mixing of the basic mix, giving good homogenization of fibres in the trucks.

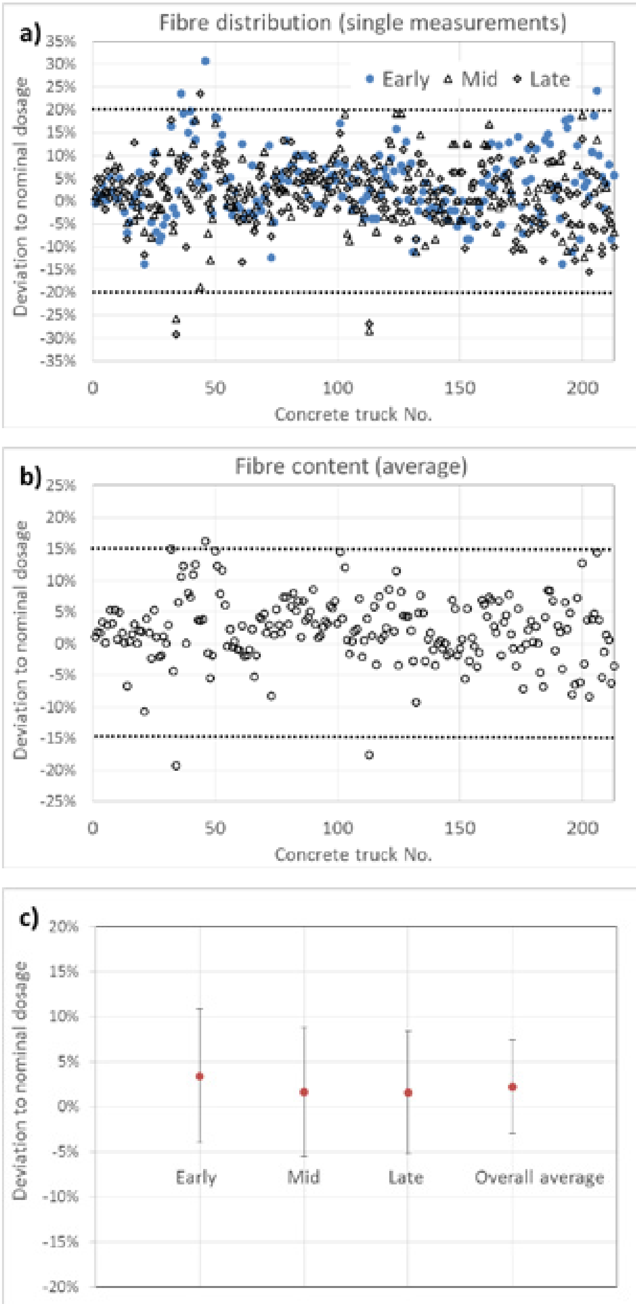

Figure 1: Steel fibre content measurements on sprayed concrete basic mixes taken from 213 concrete trucks on arrival to various tunnel sites; three measurements pr. truck. a) Single measurements from each truck, b) Average fibre content for each truck, c) Average of all measurements taken early, mid and late during loading, and overall average (incl. std.dev).

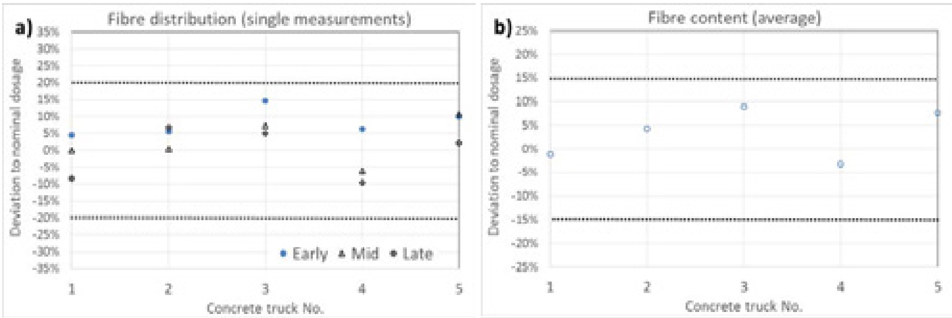

Figure 2: Macro polymer (PP) fibre content measurements from 5 trucks. See previous figure for figure text to a), b), c).

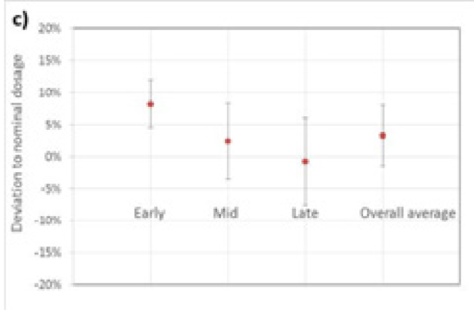

SITE DATA ON EFFECT OF FIBRE CONTENT ON ENERGY ABS. CAPACITY

When FRSC panels are produced, they are sprayed and stored for some days at the site, then transported to a certified laboratory and tested, normally after 28 days. The laboratory then makes a test report.

When it comes to sprayed FRSC panels only (not cast), we have received totally 32 panel test results from different sites of which 20 are with normal strength steel fibre and 12 with PP-fibre. To our knowledge all the FRSCs are made with a w/b of 0.45. Figure 3 shows the results where energy absorption capacity has been plotted vs. fibre content. FRSCs with steel fibres is shown in Figure 3-a and macro PP-fibres in Figure 3-b. The regression line with the best fit was linear, as indicated (still, the fit is not very good). The relation is not fair in many ways since many of the results are from different concretes made with different concrete constituents and fiber types. Anyhow, the figure shows (as expected) the trend that higher fibre dosage gives higher energy absorption capacity. The figure also shows, for these different concretes, that the energy absorption capacity may vary greatly for a given fibre dosage. The lesson to learn is that a relation between fibre dosage and energy absorption capacity for a given concrete in one project/site is not particular transferable to another project/site using another concrete/constituents, even if the fibre product is the same. Even though concrete compositions may be quite similar (cement type, w/b and fiber content and even fibre type), the type of aggregate will vary. The bond between fibre and concrete is likely to be influenced by a number of factors, including aggregate grading, -strength, -shape, etc. And, of course, the equipment used for concrete mixing, transport and execution also influence, as well as the personnel involved.

Each result in Figure 3 is the average of sets of three panels. The average coefficient of variation among the sets is quite the same for the steel fibre and the PP-fibre FRSCs. The average coefficient of variation among all 32 sets is 6.7%.

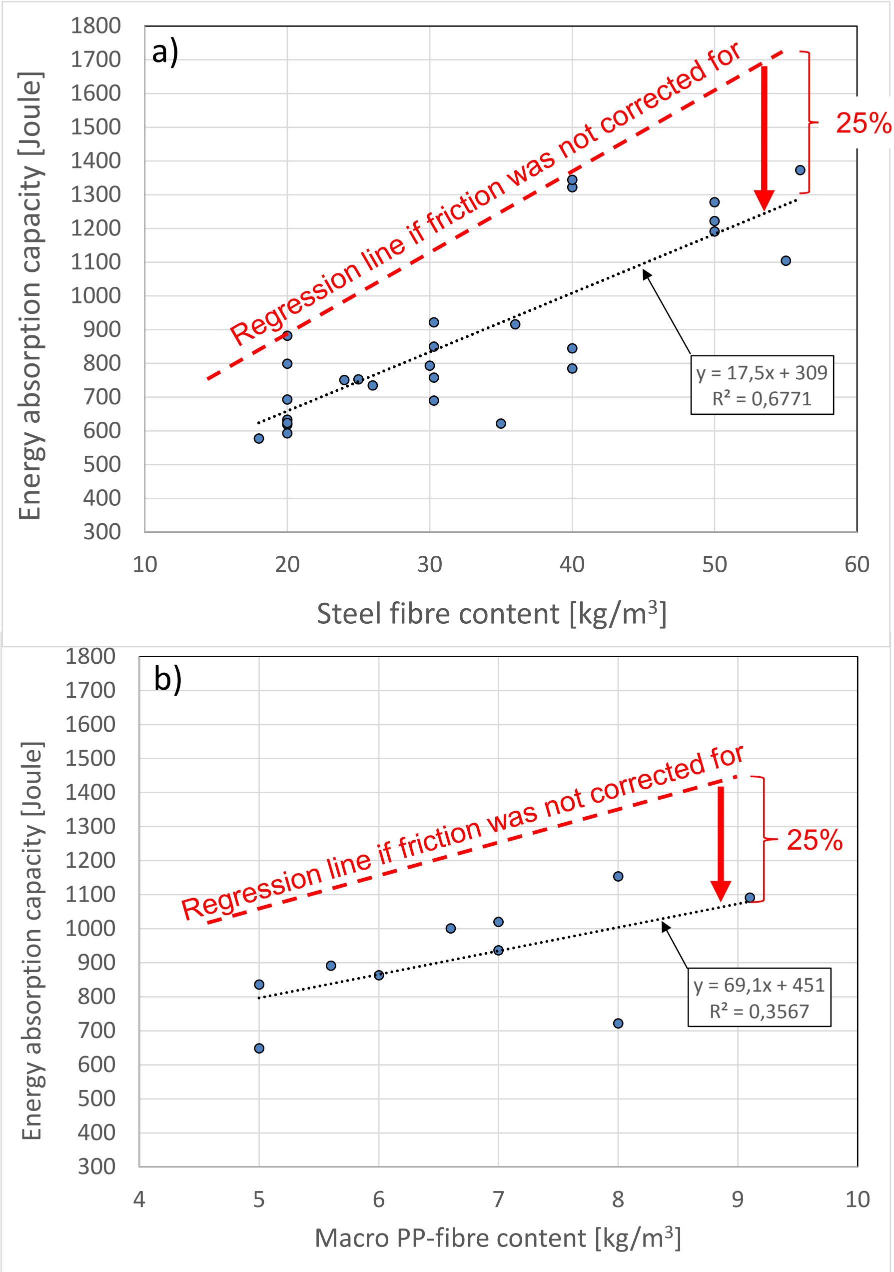

Figure 3: Energy absorption capacity vs. steel fibre content (a) and vs. macro PP-fibre content (b). All panels are sprayed on-site.

Figure 3 also show a “regression line if friction was not corrected for”. As mentioned earlier, the panel test procedure in NB7:2011 requires that the effect of friction between panel and support must be corrected for; this effect is found to constitute 25% of the energy uptake measured during each test. When final results are reported this correction is carried out. Therefore, if the same results were not corrected for friction, all results would be (1/0.75=1.33) 33% higher and the higher regression line (indicated) would then be the case. Previously, friction was not corrected for and the higher regression line is quite in line with the (low) fibre contents that were used previously to conform with E700 and E1000, respectively. After releasing NB7:2011, introducing the correction for friction, the fibre contents had to be increased to conform to the same E-classes.

EFFECT OF CONCRETE STRENGTH ON ENERGY ABSORPTION CAPACITY

Compressive strength and energy absorption capacity is normally determined at 28 days, while the ability of a sprayed concrete lining to work as rock support is dependent on these properties over the whole lifespan from very early (preliminary safety during tunneling) and over years (permanent support). Data is lacking in the literature on this issue. A laboratory study was therefore undertaken to determine the development of strength and energy absorption capacity over time. Table 1 gives a brief overview of concretes and fibre types.

For four of the concretes, with water-to-binder (w/b) ratio 0.45, compressive strength and panel tests were performed after 2, 4, 7, 30, 91 and 365 days (cured at 20 °C). The “steel fibre 2” is an exception as this series consists of three concretes with different w/b-ratios tested at one given test age, namely 49 days. Hence, in the “steel fibre 2” series different strengths were generated with the use of different w/b-ratios, and not with the use of the time component.

Table 1: Tested concretes; fibre types/dosage and characteristics

Fibre type in the concrete	w/b	Shape	Length / diameter	Tensile strength	Dosage
Steel fibre 1 *Normal strength*	0.45	End-hooked	35 mm / 0,55 mm	1250 MPa	35 kg/m^3
Steel fibre 2 *Normal strength*	0.37, 0.40 and 0.45 (test age: 49 days)	End-hooked	35 mm / 0,50 mm	1100 MPa	30 kg/m^3
Steel fibre 3 *High strength*	0.45	End-hooked	35 mm / 0,55 mm	2400 MPa	30 kg/m^3
PP-fibre 1	0.45	Embossed	54 mm / -	640 MPa	5 kg/m^3 6 kg/m^3

The results, given as energy absorption capacity vs. strength, are shown in Figure 4. “Steel fibre 2” is discussed separately, see later discussion below. For each curve the results with lowest strength levels is for test age 2 days, while highest strength levels is for the latest test age 365 days. It can be seen that the energy absorption capacity very early reaches significant levels (around 600-800 Joule). From around 7 days on (from around 45 MPa strength), the energy uptake of the concretes develops quite differently.

For the concrete with “steel fibre 1” (35 kg/m3) the energy absorption capacity declines significantly (17%) as the strength increases from 50 MPa (7 days) to 77 MPa (28 days). On further curing the decline continues with increasing strength and at 94 MPa strength (365 days) the capacity is only 55% of that at 7 days. This steel fibre (with normal tensile strength) could obviously not cope with such high strength levels, and fibres were observed to develop tensile failure in the cracks during the panel tests (perhaps a higher fibre dosage would have improved the performance). The energy absorption capacity is the energy uptake from zero to 25 mm central displacement during panel tests. It is notable that the reduced capacity over time discussed above is not present if the energy uptake was calculated only up to around 10 mm displacement, i.e. "steel fibre 1" performed well at smaller cracks.

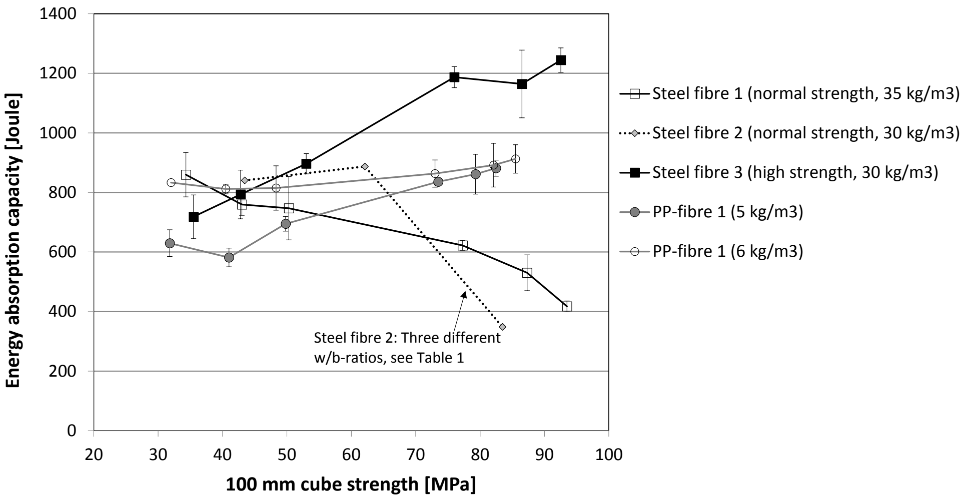

Figure 4: Energy absorption capacity vs. strength for various fibre types (standard deviation is indicated). For all concretes (except "Steel fibre 2") increasing strength is due increasing concrete age. Each result is the average of 3 panels

The concrete with the high tensile strength "steel fibre 3" (30 kg/m^3) shows completely opposite behavior as the energy absorption capacity increases continuously with time and strength. At the final strength level at 365 days (93 MPa), the capacity becomes very high (1200 Joule) which is around 40% higher than at 7 days (53 MPa). The high tensile strength of this fibre has obviously promoted bond failure in the cracks during loading of the panels, in contrast to the normal strength "steel fibre 1".

The two concretes with the macro "PP-fibre 1 (5 and 6 kg/m^3, respectively) show quite similar behavior, except in the early age where the one with the lowest fibre dosage has somewhat lower energy absorption capacity. Somewhere beyond 7 days (beyond 50 MPa), the two PP-fibre concretes more or less stabilize at energy absorption capacity levels of 850-900 Joule.

The three concretes (different w/b-ratios) with "steel fibre 2" display much the same feature as "steel fibre 1"; both are normal strength fibres. For "steel fibre 2" decreasing w/b-ratio systematically led to increased strength, as expected. It can be seen that there is a dramatic drop in the energy absorption capacity from the middle strength level (w/b=0.45, strength=62 MPa) to the high strength level (w/b=0.37, strength=83 MPa). For the latter it was observed after testing of the panels that the vast majority of the fibres were broken due to tensile failure.

Overall, the results show that the energy absorption capacity for FRSC can change significantly with time and strength level. Hence, the 28 days standard age for panel tests may not necessary give a representative energy absorption capacity. For normal strength steel fibres, a potential sensitivity to high strength levels was detected. However, an adequate steel fibre dosage and fibre tensile strength were shown to secure sufficient energy absorption capacity over longer times and over great increases in concrete compressive strength.

CONCLUSIONS

In NB7:2011 there is increased focus on pre-documentation and early control in the production process of FRSC.

Site data show satisfactory results for fibre content and fibre distribution of fresh basic mixes on arrival to the tunnel site.

Other data for panels sprayed at the tunnel site show that the energy absorption capacity may vary greatly from site to site even though the fibre content and the binder composition of the concrete is quite similar. The trend is, as expected, higher energy uptake on increased fibre dosage.

The laboratory programme on energy absorption capacity showed that normal strength steel fibres might give a potential sensitivity to high FRSC strength levels, which particularly can be the case at longer curing times. However, it was also shown that an adequate steel fibre dosage and fibre tensile strength could eliminate this sensitivity.

Looking on different national investigations, the coefficient of variation among sets of three parallel round panels lie around 7-9% and the standard variation range for COV is from around 3% to around 14%.

ACKNOWLEDGEMENT

The submission of site data from concrete suppliers and contractors is greatly acknowledged. Acknowledgements also go to the members of the Norwegian Sprayed Concrete Committee for their active contribution to panel tests and all other tests during and after the revision of NB7:2011.

REFERENCES

1. Sprayed concrete for rock support (2011) Norwegian Concrete Association's Publication no. 7 (NB 7), August 2011.
2. Sprayed concrete for rock support (2003) Norwegian Concrete Association's Publication no. 7 (NB 7), October 2003.
3. Bjøntegaard Ø. (2009) Energy absorption capacity for fibre reinforced sprayed concrete. Effect of friction in round and square panel tests with continuous support (Series 4).

Technology report no. 2534, Norwegian Public Roads Administration, Road Directorate. 2009-02-16, ISSN 1504-5005

4. Bjøntegaard Ø. (2010) Round and Square panels – effect of friction. Proc. of the Int. Conf. on Engineering Developments in Shotcrete, March 14.-17., 2010, Queenstown, New Zealand.
5. Bjøntegaard Ø. and Myren S.A. (2011) Fibre Reinforced Sprayed Concrete Panel Tests: Main results from a methodology study performed by the Norwegian sprayed concrete committee. In: Beck T., Woldmo O. and Engen S. (Ed.), 6th International Symposium on Sprayed Concrete, September 12.-15. 2011, Tromsø, Norway.
6. Bjøntegaard Ø. and Myren S.A. (2011) The accuracy of FRS concrete panel tests. Tunneling Journal, Oct/Nov 2011, pp. 44-50.
7. Bjøntegaard Ø., Myren S.A., Klemetsrud K. and Kompen R. (2014) Fibre reinforced sprayed concrete (FRSC): Energy absorption capacity from 2 days age to one year. Proc. of the 7th Int. Symp. on Sprayed Concrete – Modern Use of Wet Mix Sprayed Concrete for Underground Support, Sandefjord, Norway, 16. – 19. June 2014, pp. 88-97
8. Bjøntegaard Ø., Myren S.A. (2018) Fibre reinforced sprayed concrete panel test – Test procedure and influencing factors. Spritzbeton - Tagung 2018, 11.-12. January 2018, Alpbach, Tirol, Austria
9. Myren S.A., Hagelia P. and Bjøntegaard Ø. (2018) The ban of polymer fibre in FRSC in Norwegian road tunnels. In: Engen S., Beck T. and Myren S.A. (Ed.) 8th International Symposium on Sprayed Concrete – Modern Use of Wet Mix Sprayed Concrete for Underground Support, Trondheim, Norway, June 11-14

SUSTAINABILITY AND THE RESPONSIBLE DISPOSAL OF CONTAMINATED WASTE

8th International Symposium on Sprayed Concrete 2018.
11.-14. June Trondheim, Norway

Denis Crehan	Stein Eide	Des Vlietstra
General Manager EMEA	Area Manager Norden	Technical Consultant
dcrehan@elastoplastic.com	seide@elastoplastic.com	dvlietstra@elastoplastic.com

Elasto Plastic Concrete (EMEA) Ltd

Introduction

Macro synthetic fibre is by far the most sustainable solution for use as a reinforcement in concrete lined tunnels, offering a significantly lower carbon footprint, longer term durability and cost reductions compared to steel fibre. Due to the nature of sprayed concrete and its application there will always be a percentage of rebound which will include a small amount of fibre.

During the tunnel waste rock removal cycle, when waste rock is removed together with the concrete rebound, there will invariably be macro synthetic fibres and other contaminants such as the concrete itself, chemical admixtures, earplugs, detonator cords and a multitude of other non-organic waste material.

When this contaminated waste rock is irresponsibly disposed of into the environment, particularly into water environments, there will be negative environmental impact, the most obvious a contribution to plastic pollution, which is a major global concern. While some sources of plastics are extremely difficult to control, such as car tyre dust, ship paint and household laundry discharge, potential plastic pollution from projects such as tunnel construction can be solved with a properly administered environmental management plan.

Further, when designing any environmental plan, we must fully consider all potential risks. Tunnel discharge material contains a multitude of other contaminants that are less obvious but are more harmful, such as the ingredients of freshly sprayed concrete and associated chemicals which are highly alkaline and will therefore negatively affect the delicate biosphere in Fjords and oceans in particular.

This paper explores some of the solutions that can be employed to remove these contaminants so that the waste rock can be recycled or disposed of in a responsible manner, without contaminating the disposal area with undesirable materials and thereby removing the negative impact that these materials have on the environment. This allows the project to minimise its construction CO_2 emissions and benefit from the long term life cycle durability provided by macro synthetic fibre.

Keywords

Macro synthetic fibre reinforced concrete, shotcrete, plastic, environment, tunnels, responsible disposal.

Background

Macro synthetic fibre has been used in the Norwegian tunnel market for well over 10 years with thousands of metres of tunnels successfully completed. Significant research was undertaken by the Norwegian Roads Authority (NRA) in the mid 2000's to assess the performance characteristics of macro synthetic fibre compared to steel fibre [1]. This research showed that not only could equivalent performance be reached in panel tests but macro synthetic fibre (MSF) exhibited much higher durability characteristics. This research was also well supported by investigations undertaken in other countries [2] [3]. The NRA subsequently changed their concrete specifications to include macro synthetic fibre as an alternative to steel fibre for shotcrete reinforcement. Their extensive research showed that macro synthetic fibre was much more durable than steel fibre where shotcrete is subjected to corrosive environments such as in a subsea tunnel. The use of a non-corrosive fibre reinforcement eventually became mandatory in subsea tunnel construction.

For any tunnel construction project the disposal of tunnel excavated rock is always a high consideration and much thought is given to this prior to project commencement. The removal of waste rock can incur significant costs particularly where project sites are isolated and/or restricted by inner city truck movements. In Norway this is particularly so because of the lack of flat ground for fill sites and the cost involved in extra transport time for trucks traversing mountainous terrain to suitable disposal locations. Thus the predominant method for the disposal of waste rock in Norway, after appropriate environmental consideration and approval, has become to dump into nearby water bodies such as fjords or the ocean. In some cases this is a benefit as it allows for the extension of land for use as new industrial areas, harbours or similar applications.

Since the early 2000's, when macro synthetic fibre was able to meet the performance of steel fibre, suppliers of the product have always been open about the possibility of fibre floating in water sumps and collecting ponds. This was particularly the case in the mining industry where this type of reinforcement gained early acceptance in 2002. In many cases where projects used MSF it was a chance for them to review their pumping, dewatering facilities and waste management for the better by installing simple barriers to remove not only fibres but a whole array of contaminants from their waste water. This process stopped fibre and similar materials from becoming an environmental issue.

From the mid 2000's, MSF was the most widely used reinforcement in tunnelling projects in Norway, primarily due to its high durability and lower life cycle cost. As such, the possibility of MSF floating in tunnel pumping stations, batching plant wash out bays or any other water courses was well communicated to projects and batching plants by their suppliers.

On larger projects during this period tunnel sites implemented environmental practices (see Figure 1) to eliminate any contamination of waterways around infill sites and water dumping grounds.

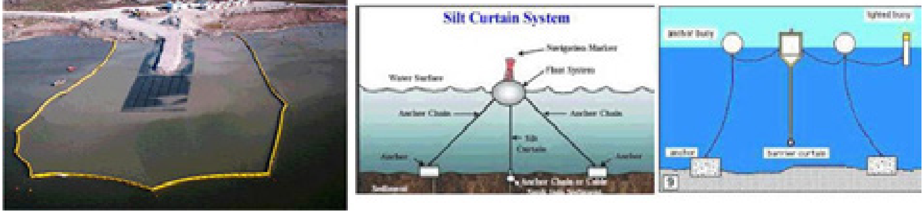

Figure 1: Examples of floating barriers to manage floating debris.

In 2015 the discovery of macro synthetic fibre floating on the ocean caused the NRA in a knee jerk response to restrict the use of MSF without due consideration of the real environmental impact of irresponsible dumping while also dramatically increasing the Co2 footprint of the projects by the reintroduction of steel fibre, reversing their environmentally responsible decision from a decade earlier.

Although simply removing the use of macro synthetic fibre would seem a resolution to the problem, it is merely turning a blind eye to the more serious problem of project sustainability and environmental responsibility. Over a project's life the use of steel fibre reinforced concrete substantially increases the project's carbon footprint and raw material volume. It is in fact more detrimental to the environment than using MSF with a properly adhered to waste management plan.

Shotcrete tunnel waste

On closer scrutiny of waste material from a tunnel, which comprises mainly of broken rock, there is also an element of bio chemicals (shotcrete rebound that contains cement, chemicals), and anything else that has been discarded on the tunnel floor. Although the quantities of these materials are small within the volume of the waste material, little thought has been given to their removal, presumably due to the cost, even though they all have a detrimental effect to the environment. We argue that all these contaminants should be removed before the waste rock is dumped. Table 1 below sets out the constituents for a typical 1.0 m^3 of concrete used for tunnel lining.

Table 1: Typical concrete mix and environmental impact of constituents

Constituent	kg/m^3	Carbon kg CO_2e/kg	Pollution potential	Percentage of total	Comment
Cement	400	2.5	High	86.7%	Reacts with water, impossible to clean. Can Negatively change water PH
Silica fume	30	2.5	Low	4.3%	Does not react with water, impossible to clean
Chemical additives	6	2.0	High	1.0%	Reacts with water, impossible to clean
Plastic fibre	5	2.5	Medium	0.9%	Floats, can be cleaned, can degrade to microplastics
(Steel fibre)	*(30)*	*(2.5)*	*(Low)*	*(4.3%)*	*Sinks, rusts, very difficult to clean*
Accelerator	40	2.0	High	7.0%	Reacts with water, impossible to clean. Can negatively change water PH
TOTAL	**451**				

Although the focus has been on macro synthetic fibre, the other individual constituents have far more potential to do significant harm to a water body. Each constituent has been assessed with a potential to pollute (High Medium Low) where a factor of HIGH indicates potential of high pollution and a constituent with LOW indicates a low pollutant risk level. High alkali constituents like cement which contains lime and is toxic to aquatic life [5] [6] and accelerator would have an extremely negative impact if they were to come into contact with local water bodies for example from dumping. Although we must consider that only a percentage (usually 5-7%) of the total concrete used becomes rebound and therefore available to contaminate, over the length of even a small tunnel project this can be significant as shown in Table 2.

Table 2: Potential dumped rebound for tunnel length

Shotcrete per lin. m	Tunnel length [lin. m]	Total Concrete [m^3]	Rebound [%]	Potentially Dumped rebound [m^3 / (t)]
5	5,000	25,000	5	1250 (2750)
5	10,000	50,000	5	2500 (5500)
5	15,000	75,000	5	3750 (8250)
5	20,000	100,000	5	5000 (11000)

Durability

The purpose of using macro synthetic fibre for concrete reinforcement in tunnelling applications, and even more so in subsea tunnels, is to increase the durability of the lining and so increase the life of the tunnel, which will be exposed to various corrosive environments, including leeching ground water, moisture and heavy salts [1].

One of the main shortcomings of concrete is its brittleness, i.e. its poor resistance to crack development and propagation due to its low tensile strength [7]. Randomly distributed fibres are introduced as reinforcement to bridge cracks and counteract the brittleness, thereby yielding a material with considerable toughness and strain capacity.[8] Fibres essentially, just like conventional rebars, lay dormant in concrete until a crack occurs at which point the fibres that bridge the crack will provide the concrete a post crack capacity, i.e. ductility (or toughness).

However, the crack will allow the fibre to come into contact with the corrosive environment and if made of steel, corrode it away, effectively rendering the fibre that is meant to be working useless. Recent research over a period of 17 years has found that steel fibre reinforced concrete exposed to an environment like in a European road tunnel that it is not realistic to expect a service life of 100 years [9].This severely compromises the tunnels integrity and negatively impacts the expected tunnels design life.

The ultimate result of this cycle is rehabilitation of the tunnel lining which is costly for the tax payer in monetary terms and also environmentally by using yet more material that increases the carbon footprint of the tunnel.

The European commission on climate action has set in place a low carbon economy road map that suggests by the year 2050 the EU should cut greenhouse gas emissions 80% below 1990 levels. The milestones to achieve this include 40% emissions cuts by 2030 and 60% by 2040, with all sectors required to contribute.

Using a conservative estimate of two rehabilitations over a 120 year design life, the carbon footprint of these works is outlined in Table 3 for 50 km of tunneling works with a Norwegian T8.5 profile showing a substantially greater carbon footprint for the steel fibre reinforced concrete lined tunnel.

Table 3: Carbon Footprint Comparison of FRS Tunnel Lining

Steel Fibre kg CO_2e [10]	Rehabilitation Concrete 2 x 25% (kg CO_2e) [13]	Rehabilitation Steel 2 x 25% (kg CO_2 e) [13]	Total CO_2 over 120 yrs[15] (kg CO_2e)
6,973,670	22,422,881	3,486,834	32,883,385

BarChip Fibre kg CO2e [11]	Rehabilitation Concrete	Rehabilitation Steel	Total BarChip (kg CO2e)	Total Carbon Saving (kg CO_2e)
1,414,022	Not Required	Not Required	1,414,022	31,469,363

A potential saving of **31,469,363 kg** of embodied carbon emission exists over 50 km of tunneling works simply by choosing macro synthetic fibre over steel fibre.

That is equivalent to;

- 6,647 passenger cars driven for 1 year.
- 9,987 tonnes of waste recycled instead of land filled.
- 4,647 homes electricity use for one year.
- 72,858 barrels of oil consumed.
- 815,565 tree seedlings grown for 10 years.
- 251 acres of forests preserved from conversion to cropland for one year. [13]

It is clear that macro synthetic fibre reinforced concrete is a much more sustainable reinforcement to use than steel fibre. It has a significantly lower carbon footprint and reduces the amount of raw material used over the life of a tunnel.

Dumping contaminated materials into water bodies is the most cost effective and convenient way of disposing of this material but individual materials cannot be cherry picked arbitrarily from a basket of materials as a token gesture, while leaving some of the most contaminating materials to be dumped into the water.

By working with owners, material suppliers, tunnelling contractors and environmental groups, it should be feasible to find a practical solution where harmful waste material is separated and dealt with in an appropriate manner.

In order to facilitate this discussion this paper presents a number of potential solutions to eliminate the dumping of these contaminants.

Practical solutions for preventing environmental contamination

Contaminated waste separation and stockpiling.

It is possible to implement a plan whereby after blasting at least 80% of the waste rock is removed from the tunnel prior to shotcreting works, for direct dumping where experience and common sense could increase the amount of initial removal to a higher percentage of 90 – 95% leaving a small amount of blasted rock across the base of the tunnel floor.

Once the shotcrete cycle is completed then the tunnel floor would be cleaned completely. This waste element would consist of rebounded shotcrete and other associated contaminants together with the remainder of the blast residue. This material should be stockpiled separately where it could be cleaned and/or sent to appropriate fill sites.

Where excavated tunnel masses are used in sea filling, masses can be cleaned by using a cofferdam where all tunnel masses are processed in a closed washing operation before loaded into open seawater.

Studies of the material could prove that after crushing it could be incorporated into road base for the tunnel and/or used as aggregate for any non-structural concrete works or precast elements where it could meet the appropriate standards for this type of application. Binding the contaminated waste into works would be a simple, economical yet environmentally friendly method of disposing this waste.

Waste material research

There are many instances where waste by-products have been successfully converted or used in applications to ensure that there is no environmental contamination. To this end waste concrete could be crushed and used for road fill, subbase or other similar applications.

Education

Education of the tunnel workforce to understand the importance of minimising rebound and optimising the waste rock removal process is imperative. "Buy in" from the tunnel crews is critical for them so they understand the reasons behind efficient waste rock removal, the location of contaminated waste rock stockpiles and how to reduce rebound in the shotcreting operation. Educational awareness programmes of littering, oil spills and other environmental hazards that could end up in the ocean or landfill along with the waste rock should also be put in place.

Filters and Screens

Where concrete may come into contact with free-flowing water or the ocean the appropriate on shore containment / bunding should be put in place along with the appropriate filters and screens to capture any liberated macro synthetic fibre from escaping into the environment. Where face pumps are used a face pump, such as the diaphragm pump (see Figure 3) that is also capable of pumping fibre should be utilised with the outlet water running through a large filter bag (see figure 3) to catch any fibre and other contaminants.

Figure 2: Diaphragm Pump

Figure 3: Filter bag set up

Conclusion

Tunnelling projects inevitably bring with them many technical and environmental challenges influenced by a number of factors including the design specification, excavation type, location, etc. These factors heavily influence how the project manages its environmental requirements across a range of tunnelling activities including the disposal of waste rock from a tunnel. The approach to this must be consistent across all contaminants not just those that can be seen.

It is imperative that the stakeholders work together to find a solution that truly benefits the environment. *Out of sight out of mind* is not good enough.

It is clear that removing macro synthetic fibre has made a short-term gain for the environment in preventing water contamination but has a much greater negative affect on the overall environment by significantly increasing the carbon footprint of the tunnel over its lifespan which could easily be solved by the implementation of relatively simple practical methods to stop contamination of the ocean by irresponsible disposal. Rising Co2 emissions are a major contributor to global warming with negative implications for the Ozone layer, melting polar ice caps, rising sea levels, famine and population displacement, this is arguably a much more serious threat to the global environment and this should be addressed by all stake holders in the Tunnelling Industry.

Elasto Plastic Concrete as an environmentally aware supplier of BarChip fibres has compiled a comprehensive Environmental Management Plan [14] which sets out measures and waste management concepts that seeks to protect the environment from possible environmental impacts resulting from the use of macro synthetic fibre in concrete applications. Elasto Plastic Concrete is willing to work together with all stakeholders to further develop environmentally friendly strategies incorporating BarChip Macro Synthetic Fibre for the longevity and environmental sustainability of the Norwegian Tunnelling Industry.

References

1. Per Hagelia, 2008. *Deterioration Mechanisms and Durability of Sprayed Concrete in Norwegian Tunnels*

2. ES Bernard, 2004. *Durability of cracked fibre reinforced shotcrete*

3. JP Kaufmann, 2014. *Durability performance of fibre reinforced shotcrete in aggressive environments*

4. Product Data Sheet - BarChip 54

5. Environment Bay of Plenty Regional Council *Concrete Information Sheet*

6. Neuwald, A. 2010. *Treating and Processing Concrete Process Water. National Precast Concrete Association*

7. Brandt, A. 2008. *Fibre reinforced cement based composites after over 40 years of development in building and civil engineering. Composite Structures.* **86**(1), p7.

8. Zhao, S.L., D. Sun, W. . 2015. *Deflection-crack mouth opening displacement relationship fpr concrete beams with and without fibres*. *Magazine of concrete research.* **67**(10), p8.

9. Nordstrom E, 2016. *Evaluation after 17 years with field exposures of cracked steel fibre steel fibre reinforced shotcrete*

10. EPC Mine Dewatering Management Procedures (2009) Elasto Plastic Concrete

11. ITATech *Guidance for Precast Fibre Reinforced Concrete Segmnets – Vol 1: Design Aspects* (2016)

12. Sinclair Knight Merz, 2013. "Elasto Plastic Concrete - BarChip 48 and 54 Carbon Footprints". Australia.

13. Greenhouse Gas Equivalencies Calculator, United States Environmental Protection Agency, https://www.epa.gov/energy/greenhouse-gas-equivalencies-calculator.

14. EPC Environmental Management Plan - Responsible Use of EPC Macro Synthetic Fibre Concrete Reinforcement (2017) Elasto Plastic Concrete

15. EPC Technical Note – Durability and long term performance of fibre reinforced concrete (2017)

Specifying and Testing Fibre Reinforced Spray Concrete: Advances and Challenges

Benoit de Rivaz
Bekaert Maccaferri Underground Solutions,
SkylinE40, Korte Keppestraat 23/02,
9320 Erembodegem – Aalst, Belgium
benoit.derivaz@bm-underground.com

ABSTRACT

The mechanisms through which FRSC(Fibre Reinforced Spray Concrete) controls deformations and absorbs energy are complex and involve the technicalities of both the spray concrete process and the fibre properties.

Toughness is generally the main criterion for FRSC as ground support. However, for the FRSC to have the highest strength and toughness, there must be an optimal design and combination of concrete strength, fibre anchoring and placement method.

Consequently, the choice of fibre type and content must correspond to the ground conditions of a specific area and the expected concrete mixture design. There is no unique design method broadly accepted for the design of FRSC for ground support. General guides exist, but there is no specific/complete design guide accepted for FRSC as ground support.

Multiple performance criteria: flexural strength, residual flexural strength after cracking, moment-normal force (M-N) behaviour, energy absorption (toughness).

This paper will underline, as mentioned in the European standard EN 14487-1 (ref 3) the different ways of specifying the ductility of FRSC in terms of residual strength and energy absorption capacity.

It also mentions that both ways are not exactly comparable:

- ⇨ The energy absorption value measured on a panel can be prescribed when - in case of rock bolting - emphasis is put on energy which has to be absorbed during the deformation of the rock. This is especially useful for primary sprayed concrete linings
- ⇨ The residual strength can be prescribed when the concrete characteristics are used in a structural design model.

This paper will presents the majors results on a research project undertaken this year at Laval and Bochum University.

- ⇨ To evaluate the energy absorption of fibre reinforced wet-mix spray concrete mixtures by testing specimens following two standards: the ASTM C1550 and the EN 14488-5.
- ⇨ To evaluate the residual strength of fibre reinforced wet mix spray concrete mixtures by testing the two standards: EN 14488-3 and the EFNARC three point bending test on square panel with notch.

Key words: Fibre Reinforced Spray Concrete (FRSC) Performance Testing

1. INTRODUCTION

Sprayed concrete technology has dramatically improved in terms of the use of advanced admixtures and application methods to give durable and high performance concrete.

With this improvement in sprayed concrete quality, tunnel linings were constructed using permanent steel fibre reinforced sprayed concrete instead of conventional in-situ concrete within the temporary sprayed concrete linings, lowering costs and significantly reducing the construction time, particularly in sections of complex geometry such as step plate junctions.

Currently modern sprayed concrete technology equips the tunnelling industry with a more economic tunnel lining system in the form of a single shell of permanent sprayed concrete. This technology provides a structural lining that is durable, watertight and can be surface finished to a degree that is similar to cast concrete.

The use of Fibre Reinforced Permanent Spray Concrete Lining (FRPSCL) allows to eliminate the traditional reinforcement in the final lining ~~precast segment production~~. Over the last few years, the use of this technology has increased.

One of the aspects that are boosting the use of FRC is the introduction of guidelines for the design of FRC. In 2013, the *fib* presented the fib Model Code 2010 (Ref 1) in which a specific part related to FRC is inserted. This document has sparked great interest in the tunnelling community and several documents consider fib Model Code 2010 as a reference.

The present paper would like to support the designer, contractors and clients in introducing FRSCL in future projects referring to the existing state of art in order to specify right performance and the right testing method.

This paper will underline, as mentioned in the European standard EN 14487-1, the different ways of specifying the ductility of fibre reinforced sprayed concrete in terms of residual strength and energy absorption capacity.

2. THE MATERIAL

Fibre Reinforced Concrete (FRC) is a composite material characterized by a cement matrix and discrete fibres (discontinuous). The matrix is either made of concrete or mortar. Fibres can be made of steel, polymers, carbon, glass or natural materials.
The properties of the composite depend on the characteristics of the constituting materials as well as on their dosage.

Other factors such as the geometry, the volume fraction and the mechanical properties of the fibres, the bond between fibre and concrete matrix, as well as the mechanical properties of the matrix, significantly affect the FRC properties.

The behaviour of fibre reinforced concrete is more than a simple superposition of the characteristics of the concrete matrix and the fibres; to analyse the behaviour of this <u>composite material</u>, also the interaction between both has to be taken into account, i.e. *the transfer of loads from the concrete matrix to the fibre system*

Therefore, for efficient load transfer, the following three conditions must be satisfied:

1. Sufficient <u>exchange surface</u> (number, length, diameter of fibres).
2. The <u>nature of the fibre-matrix interface</u> allows for proper load transfer.

3. The intrinsic mechanical properties (Young's modulus, anchorage and tensile strength) of the fibre allows the forces to be absorbed without breaking or excessively elongating the fibre.

In fact, in a hyper static mechanical system, the better the cracking is "controlled" as soon as it arises (small openings), the better will be the multi-cracking process and thus the more the structure will tend to show ductile behaviour.

According to ISO 13270 (Ref 2), '*Steel fibres are suitable reinforcement material for concrete because they possess a thermal expansion coefficient equal to that of concrete, their Young's Modulus is at least 5 times higher than that of concrete and the creep of regular carbon steel fibres can only occur above 370 °C.'*

Optimising the formulation of an FRC with a high fibre dosage does not pose any technical problems as such. This aspect is managed just as easily as the formulation of other cementitious materials.

The method named Baron-Lesage consists in finding the optimal granular skeleton (optimal sand-gravel ratio) that produces the best workability, for a given type and percentage of fibres. Theory and experience both show that the most workable SFRC is the most compact, i.e. the strongest and the most durable.
Practically, the method always uses an already optimised concrete, called the reference concrete, as basis.
Compared with this reference concrete, an optimised FRSC has:

- a greater sand-gravel ratio,
- More cement paste and/or superplasticiser.

Thus, the higher the fibre percentage, the greater the length-diameter ratio of the fibre and the length of the fibre, the greater the sand-gravel ratio, the greater the quantity of cement paste and/or percentage of superplasticiser will be.

2.1 Testing method and performance criteria

European standard EN 14487-1 mentions the different ways of specifying the ductility of fibre reinforced sprayed concrete in terms of residual strength and energy absorption capacity. It also mentions that both ways are not exactly comparable.

The energy absorption value measured on a panel can be prescribed when - in case of rock bolting - emphasis is put on energy which has to be absorbed during the deformation of the rock. This is especially useful for primary sprayed concrete linings (EN 14488-5: Testing sprayed concrete, part 5: Determination of energy absorption capacity of fibre reinforced slab specimens) (ref 4).

The residual strength can be prescribed when the concrete characteristics are used in a structural design model

2.2 Energy absorption

The plate test EN 14488-5 is designed to determine the absorbed energy from the load/deformation curve as a measure of toughness. The test is designed to model more realistically the biaxial bending that can occur in some applications, particularly in rock support. The central point load can also be considered to replicate a rock bolt anchorage. This test has proved to be of considerable benefit.

The square panel test is simulating at a laboratory scale the structural behavior of the system anchor bolt - sprayed concrete under flexural and shear load (Figure 1).

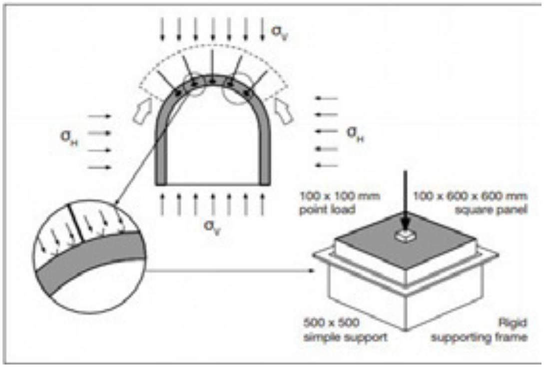

Figure 1. Sprayed concrete under flexural and shear load

No numerical material properties, such as post-crack strength values, can be determined from the square panel test due to an irregular crack pattern; however this has never been the intention of this test method; this method serves to quantify and illustrate the ductile behaviour of a steel fibre reinforced sprayed concrete tunnel lining.

The main performance criteria that can be applied for a reference concrete **C30/37**x are described in the EN 14 487. According the geological and geotechnical context. It must be determined for each project. However, Asquapro guideline (ref 5) provides the following indications:

Table 1. Specification for a classic concrete class C25/30 to C30/37 at 28 days

Application	**Minimum energy absorbing class**	**Energy absorption in J, for a 25 mm arrow**
Sprayed concrete acting as a protective skin, and for tough rocks / soils	E500	500
Sprayed concrete acting as a resistant skin, and for medium rocks / soils	E700	700

Beyond a C30/37, the energy values must be higher and the fracture ductility of concrete verified). Thus, for a C40/50 concrete, Asquapro proposes the following requirements (table 2):

Table 2. Specification for a concrete class C40/50

Application		**Minimum energy absorbing class**	**Energy absorption in J, for a 25 mm arrow**
Sprayed concrete acting as a protective skin, and for tough rocks / soils		E800	800
Sprayed concrete acting as a resistant skin, and for medium rocks / soils		E1000	1000

Restrictive specifications for reinforced sprayed concrete for underground support:

The minimum recommendation for sprayed concrete is an absorbed energy value greater than 500J. The following graph shows that such a value can be obtained when the concrete matrix is of good quality, but it does not ensure good post-crack stress absorption (sharp drop and limited post-peak absorption).

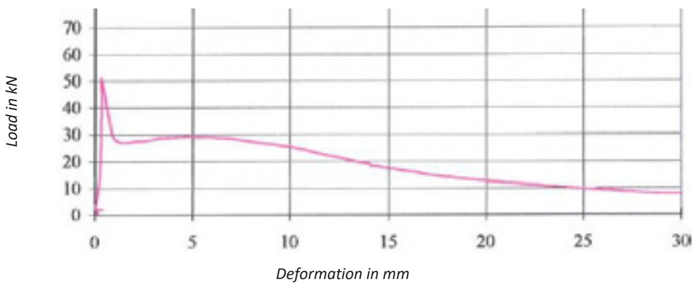

Figure 2. Unsatisfactory load-deflection curve in spite of 500J energy

However, a higher energy absorption value does not necessarily guarantee the appropriate behaviour for the substrate.

Consequently, Asquapro proposes to analyse each of the curves obtained according to the test in EN 14488-5 as follows (at least three curves per test):

1. The maximum load of the elastic zone ($F_{el\text{-}max}$) must correspond to a deflection value less than 2 mm.
2. The minimum load after cracking and up to a deflection equal to 5 mm must be greater than 70% of $F_{el\text{-}max}$.

Based on the study of a significant number of curves (conducted by test laboratory Sigma Béton), this 70% value seems appropriate to select quality concretes. It allows, for example, the concrete in figure 2 is to be rejected, in spite of its 500J energy.

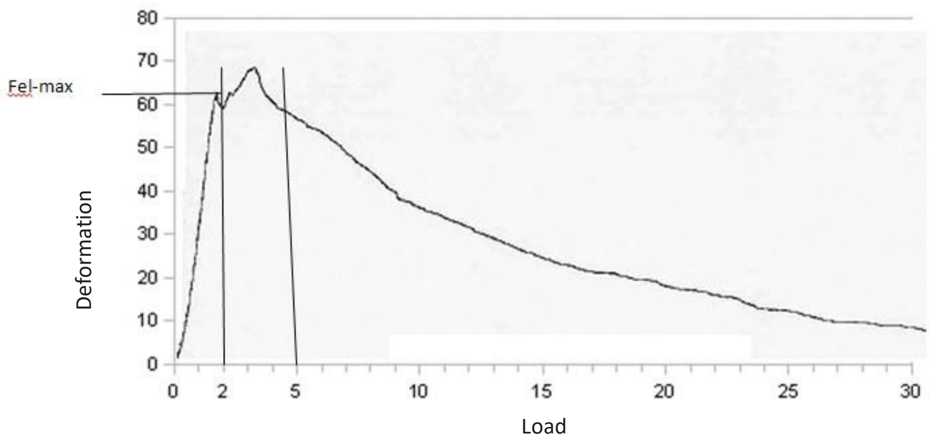

Figure 3. Typical energy absorption curves

Furthermore, Asquapro also proposes to specify the following points (some of these are included in the requirements of the standard but are not always observed in practice):

- ⇨ Prepare four slabs for the energy absorption capacity test (3 + 1 back-up) to obtain average values over at least three test runs.
- ⇨ Strictly observe the thickness of the slabs: 10 cm, +5 mm, -0. If their thickness exceeds 10.5 cm, the slabs are rejected.
- ⇨ The slabs must still be whole after the test.
- ⇨ In addition to the customary requirements, the test reports must include photos of the interior sides of each slab after testing, possibly after water spraying to clearly reveal the multicracking phenomenon.

Criterion for conformity: three tested slabs should not exhibit any value less than the specified energy.

2.3 Residual strength

For structural use, mechanical performance of FRC must be verified according to the Model Code 2010 requirements.

Typically, bending tests can be carried out to determine the load-deflection relationship of a beam under either a three point or four point loading. From this, the flexural tensile strength can be determined. Three point bending tests are usually performed in accordance with EN 14651.

The residual strength can be prescribed when the concrete characteristics are used in a structural design model.

For PSCL (Permanent Spray Concrete Lining) the residual strength will be the key material property to be determined.

2.3.1 EN 14651

With regard to the behaviour of FRC in tension, which is the most important aspect of FRC, various test methods are possible. Typically, bending tests can be carried out to determine the load-deflection relationship of a beam under either a three point or four point loading. From this, the flexural tensile strength can be determined. Three point bending tests are usually performed in accordance with EN 14651. Figure 4 shows the dimensions of the test beams.

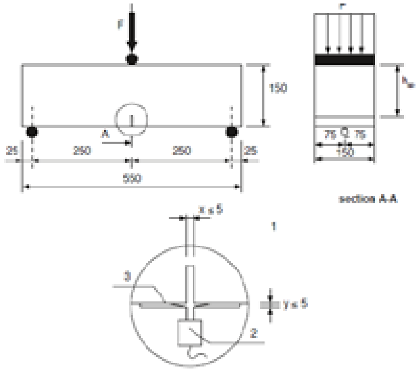

Figure 4. Dimensions of the test beams

The EN 14651 is a test developed specifically to characterize FRC and derive design parameters. EN 14651 is the reference standard for the European Union CE label for steel and polymer fibres and has been adopted by a number of fibre manufacturers and designers, primarily in Europe, Asia and Middle East.

The great advantage of this test is that it relates the strength to specific CMODs (Crack Mouth Opening Displacement) and the strength indices can be used directly in design for the appropriate Limit State. This test procedure has been adopted by fib Model Code 2010 and its implementation is relatively straightforward and independent of the type of fibre.

Since the use of EN 14651 for characterizing Fibre Reinforced Concrete was demonstrated effectiveness in the structural design (typically precast segment tunnel lining) with strain hardening materials in bending,

It has to be marked that the use of a three point bending configuration on notched specimen (EN 14651) is suitable for characterizing a FRC material since it reduces the structural effects on the tests.

Parameters, *fR,j* representing the residual flexural tensile strength, are evaluated from the F-CMOD relationship, as follows:

$$f_{R,j} = \frac{3F_j}{2bh_{sp}^2}$$

where:

fR,j [MPa] is the residual flexural tensile strength corresponding to CMOD = CMODj

Fj [N] is the load corresponding to CMOD = CMODj *l* [mm] is the span length;

b [mm] is the specimen width;

hsp [mm] is the distance between the notch tip and the top of the specimen (125 mm).

The residual strength indices which are of greater importance, according to fib Model Code 2010, are:

- Value f_{R1} (CMOD = O.5mm) is used for the verification of Service Limit State
- Value f_{R3} (CMOD = 2.5mm) is used for verification of the Ultimate Limit State

The RILEM (ref 6) and MC2010 design methods are based on notched beams because of the perceived benefits of notched samples. These are that the notch will provide a slower cracking process, thereby reducing the risk of a sudden drop in load. Also notch allows the test to be controlled on the basis of the rate of increase of CMOD and the rate of increase of deflection. Furthermore the test do not introduce structural effect. We focus on the FRC material properties.

With this issue in mind, it is essential that the design method and test methods are consistent. This shows that results from different tests cannot be compared directly in some cases and especially considering hardening post crack behaviour.

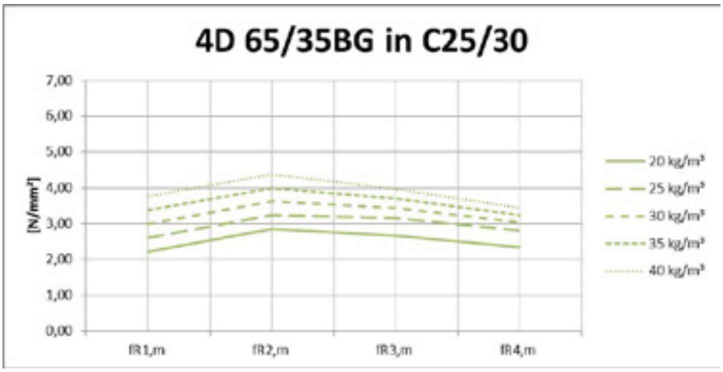

Figure 4. Typical curve on cast EN 14651 beams

Fibre reinforcement can substitute (also partially) conventional reinforcement at ultimate limit state if the following relationships are fulfilled:

- $f_{R1k}/f_{Lk} > 0.4$;
- $f_{R3k}/f_{R1k} > 0.5$

According to the project requirement minimum value of f_{r1} and f_{r3} should be specified.

We usually recommend the minimum performance class C35/45 3c according to fib Model Code 2010 for PSCL, means:

- Characteristic compressive strength f_{ck} 35 MPa

- Characteristic residual flexural tensile strength f_{R1k} > 3.0 MPa

2.3.2 Alternative test to EN 14651 : EFNARC (ref7) three point bending test on square panel with notch

A practical method to determine the tensile behaviour of SFRC for shotcrete applications is a three-point bending test on square panels. This test combines the output of the EN14651 (figure 5) with the advantages of the EN14488-5 test (the same moulds can be used and due to the larger cracked section, the scatter is lower).

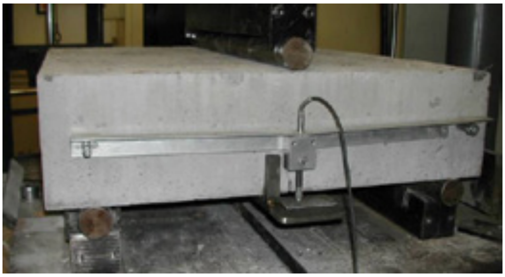

Figure 5. Three point bending test on square panel with notch

This test method is promoted by EFNARC for the following main reasons:

- The geometry and dimensions of the specimens, as well as the spray method adopted will ensure distribution of the fibres in the matrix, which is close as possible to that encountered in the real structure.
- The dimensions of the test specimen will be acceptable for handling within a laboratory (no excessive weights or dimensions).
- The test will be compatible, as far as the experimental means permit, with use in a large number of standard equipped laboratories (no unnecessary sophistication).
- The geometry will be the same as in the plate test for Energy Absorption
- The plate could be sprayed on the job site.
- No need to sawn a prism from a panel which influences the result
  The notch will provide a slower cracking process, thereby reducing the risk of a sudden fall
- By analogy with EN 14651, this test defines the residual flexural strength (f_{r1},f_{r3}) according to the updated international standard (fib Model Code 2010). The mechanical property obtained will serve as input for the dimensioning method.

The slab specimens need to be prepared according to the regulations of EN14488-1. A mould with inner dimensions 600 x 600 mm, and an inner thickness of 100 mm shall be positioned within 20° of the vertical (unless another orientation has been specified) and sprayed with the same equipment, operator, technique, layer thickness per pass and spraying distance as the actual work. Immediately after spraying, the thickness of the concrete specimens shall be trimmed to a 100_0^{+5} mm. It is very important to make sure that the spraying side of the specimen is perfectly flat, otherwise problems can be caused during testing.

The dimensions of the plates in a 3-point bending test on square panels are different than the dimensions of the beams in the EN14651 test. Because of this, the relation between the CMOD and the deflection is different as well.

Three definitions need to be taken into account (see also Figure 6):

- CMOD: crack mouth opening displacement: linear displacement measured at the bottom of the notch of the beam
- Deflection: linear displacement, measured by a transducer, between the bottom of the notch and the horizontal line which connects the points located in the middle of the beam, above the supports.
- CO: Crack opening: linear displacement measured at the top of the notch of the beam

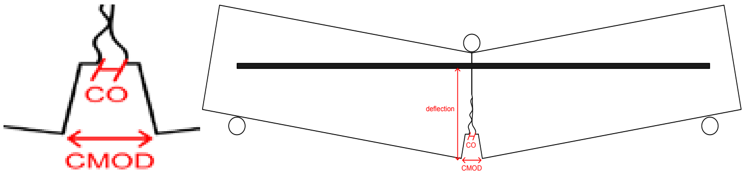

Figure 6. Definition of crack opening, CMOD and deflection

Table 3. Correlation table between CMOD, crack opening and deflection

What	EN14651			3-point bending test on plates		
	CMOD	Deflection	Crack opening	Crack opening	Deflection	CMOD
	mm	mm	mm	mm	mm	mm
Evaluation residual flexural strength	0.50	0.45	0.41	0.41	0.63	0.46
Evaluation residual flexural strength	1.50	1.36	1.23	1.23	1.89	1.36
Evaluation residual flexural strength	2.50	2.27	2.05	2.05	3.16	2.30
Evaluation residual flexural strength	3.50	3.18	2.86	2.86	4.42	3.22

This testing method has been investigated through an exhaustive RTT Program lead by Ruhr University for the CEN committee. Some key points of conclusion:

- Good Repeatability standard deviations and reproducibility standard deviations of EFNARC-panels in accordance with ISO 5725-2
- Very low standard deviation between-lab

Many test are currently conducted to better assess the correlation with EN 14651.

3. QUALITY CONTROL

A procedure for the control of Fibre Reinforced Concrete performance has to be defined in the design process.

Usually a quality control procedure considers two steps:

- initial qualification of the material (trials testing);
- tests during the spray concrete lining production (production testing).

Before starting the spray concrete lining, compressive and bending tests (EN14651 cut from spray panel or EFNARC three point bending test on square spray panel) have to be performed in order to control the fulfillment of the characteristic values defined in the design. In addition, tests can be suggested to be carried out in order to verify the fibre content or the fibre orientation.

In order to check the compressive properties of the concrete, the same procedure adopted for ordinary spray concrete should be followed.

For the definition of the tensile properties of the Fibre Reinforced Concrete, tests according to EN 14651 cut from spray panel or EFNARC three point bending test on square spray panel can be performed. The material should be classified according to fib Model Code 2010: characteristic values of the Fibre Reinforced Concrete residual strengths (f_{Lk}, f_{R1k} and f_{R3k}) have to be determined.

In this phase it is suggested to perform at least 9 specimen tests according to EN14651 or EFNARC three point bending at 28 days of curing.

The test results can be considered positive if:

- ⇨ the characteristic value of f_{R1k} is higher than the design one;
- ⇨ the ratio between f_{R3k} and f_{R1k} fulfills the design prescription; if a higher strength ratio is obtained the material can be accepted (if no specific prescriptions are present in the design);
- ⇨ the fulfillment of the fib Model Code 2010 prescription for substituting the traditional reinforcement with fiber is verified ($f_{R1k}/f_{Lk} > 0.4$ and $f_{R3k}/f_{R1k} > 0.5$).

With:

$$X_K = m_x \left\{ 1 - k_n V_x \right\}$$

In order to define the characteristic value from the tests results, the procedure suggested in Eurocode 2 (ref 8) can be used. The average value m_x and the coefficient of variation V_x are defined:

$$s_x = \sqrt{\frac{\sum (x_i - m_x)^2}{(n-1)}} \qquad V_x = \frac{s_x}{m_x}$$

The value of k_n is defined according to ISO 12491, with the use of a Student's distribution: with u0.05 fractile of the t- distribution for the probability 0.05.

Table 4. unknown V_x

n	k_n
3	3.37
4	2.63
5	2.34
6	2.18
8	2.01
9	1.96
10	1.92
12	1.87
15	1.82

Table 5. known V_x

n	k_n
3	1.89
4	1.83
5	1.80
6	1.77
8	1.74
9	1.73
10	1.72
12	1.71
15	1.70

4. CONCLUSION

Fibre reinforced spray concrete lining is a relevant material to be used for preliminary lining and for final lining.

All the relevant standard concerning the product, the testing, the design and quality control are today available to allow designers to specify the right performance. A good understanding of the material requires a complete information on the FRC material property. This is the reason why it is recommended to specify the Energy absorption and the residual strength in all cases. For structural use, mechanical performance of FRC must be verified according to the fib Model Code 2010 requirements.

A permanent sprayed concrete lining should be considered in the same way as any other permanent concrete structure. Hence, codes like Eurocode 2 (ref 8) and ACI 318 (ref 9), should be applied for the design and acceptance of the requirements for normal loading conditions in the long term.
Quality and safety can be achieved using the relevant product for the right use.

The use of the finished material should be considered along with the test and performance criteria:

- ⇨ post crack behavior,
- ⇨ match crack widths and deformation in the test to expectations in the project and durability requirements.

5. REFERENCES

Ref 1. *fib Model Code for Concrete Structures 2010 (2012), Final Complete Draft, fib* bulletins 65 and 66, March 2012-ISBN 978-2-88394-105-2 and April 2012-ISBN 978-2-88394-106-9.

Ref 2. ISO 13 270: *Steel fibres for concrete — Definitions and specifications.* (First edition 2013-01-15)

Ref 3. Test method for metallic fibre concrete – measuring the flexural tensile strength (limit of proportionality (LOP), residual)". EN14651:2005, April 3rd, 2005. To check with paper (EN14487-1)

Ref 4. Testing sprayed concrete – part 5: Determination of energy absorption capacity of fibre reinforced slab specimens". EN14488-5, February 27, 2006.

Ref 5. Asquapro. "Use of fibres in the reinforcement of sprayed concretes for tunnels temporary support".

Ref 6. RILEM TC 162-TDF (Oct2003): Steel fibre concrete

Ref 7. EFNARC. “Three point bending test on square panel with notch”.

Ref 8. Eurocode 2

Ref 9. ACI 318: Building Code Requirements for Reinforced Concrete

A NEW APPROACH FOR FIBRE REINFORCED SHOTCRETE UNDER DYNAMIC LOADING

Antoine Gagnon* and Marc Jolin
Laval University, 1065 ave de la médecine, Quebec City, Canada
*antoine.gagnon.5@ulaval.ca

Key Words: FRS, Design, Testing, Dynamic, Rockburst, ASTM C1550, EN 14488-5.

ABSTRACT

Fibre Reinforced Shotcrete (FRS) is used in underground support programs to protect workers and users from the movements of the ground by participating in the structural integrity of the excavation. This is particularly critical as mines reach deeper levels where seismic activities and high stresses may result in dynamic events such as rockbursts. Unfortunately, our current knowledge and understanding of FRS make it difficult to take advantage of its full potential under dynamic loads. Although engineers sometime avoid the use of shotcrete in such conditions, it appears that innovative high-toughness mixture designs could become high-performance alternatives to current systems. It is very difficult to simulate dynamic loads without having to go through complex, costly and often inaccurate test methods. To address this issue, a research program with emphasis on understanding current testing methods, developing new high-toughness FRS mix-designs and an innovative testing method using the pseudo-dynamic approach is undertaken. Ultimately, this will contribute to a better understanding of the behaviour of this ground support system; it will help develop FRS suited to dynamic loading and offer design tools for ground support engineers. In time, this will provide a safer underground environment for workers, provide access to previously difficult to reach areas and improve productivity in mine production cycles.

INTRODUCTION

Fibre Reinforced Shotcrete (FRS) has been used for many years in the tunneling and mining industry. This composite is used as part of ground support programs to help control the movements of the ground, therefore maintaining the structural integrity of the excavation. This is becoming critical as mines reach deeper levels where seismic activities and high stresses are the source of dynamic events such as rockbursts. These powerful events are known to be unpredictable; which makes them particularly dangerous. Unfortunately, our current knowledge and understanding of FRS make it difficult to take advantage of its full potential, especially under dynamic loads.

However, FRS and ground support programs are of great importance in underground activities as they control productivity through production cycles while protecting workers and equipment. Indeed, it is a construction method that can be deployed easily and rapidly. Therefore, it is crucial to address this issue and optimize the use of FRS in underground activities. This paper will focus on this general question while giving insights on the current projects undertaken at *Laval University* on FRS.

FIBRE REINFORCED SHOTCRETE

As shotcrete users we often forget the complexity of the spraying process and the unique material obtained. It seems important to recall that several parameters are involved in the process of spraying concrete making it a very unique construction technique. It becomes even more interesting when introducing fibres into this naturally brittle material, transforming it into a ductile composite.

In developing a discussion on FRS, we must consider the pneumatic spraying at high velocity, the specific rheology of the mixture, the properties of the concrete *and* the fibres, and the resulting combination. In fact, phenomena such as the rebound of shotcrete can significantly modify the performance of FRS, sometimes in a counterintuitive manner. For example, in dry-mix FRS, a higher compressive strength does not necessarily lead to a higher flexural toughness as a stiffer consistency increases the rebound phenomenon and reduce the dosage of fibres in place [1]. In this case, a higher toughness is reached when there is an optimal combination of concrete strength, fibre anchoring, concrete consistency and low rebound.

Design

When it comes to the design of FRS, there are many different approaches depending on the context and the ground conditions. Some ground support design methods are empirical and based on experience. The *Q-System* [2] is a great example as it has been widely used and some FRS performance values have been introduced into it [3, 4]. In this case, FRS thicknesses and energy absorptions have been associated with certain ground conditions to insure the integrity of the excavation. Unfortunately, these tools do not consider the *specific behaviour* of a FRS mixture. In fact, it is not possible to take into account, for example, that steel fibres may pick up more load at low crack opening than synthetic fibres or that, on the opposite, synthetic fibres often maintain a steady load capacity at larger deflexion. For simple situations where the ground conditions are predictable and the performance of FRS is average, these tools work generally well. However, with new material technologies (fibres and concrete) and more complex underground challenges like rockbursts, it is essential to analyse FRS thoroughly to better understand its behaviour under different ground conditions and therefore how to better use it.

Other design methods have shown to better integrate the specific properties and potential of FRS in the ground support system. For example, using the Moment-Normal force Integration Diagram (MNID) and specific Stress-Strain-Relationship (SSR) appears to better utilize the full potential of FRS [5-7]. Indeed, it makes it possible to take advantage of the elasto-plastic behaviour of FRS as the failure mode is a system failure rather than a cross-section failure [6]. This tunnel lining design method is well suited for arches and soft grounds, but does not necessarily apply to all underground conditions.

Modeling ground support systems makes it possible to integrate the true performance of FRS in the design method. However, from a material point of view, it seems like most methods do not focus enough on the potential of FRS. Also, numerical modeling of such complex environment and materials can become a tedious task. It has been shown that predictions are often fairly unreliable because of the sensibility of the models [8]. As big of a challenge it can be, creating simple and reliable design tools for FRS by combining empirical and analytical approaches is an important significant objective, and it is essential for the further development of the industry.

Testing

Another challenge related to the use of Fibre Reinforced Shotcrete is the characterization of its properties and the evaluation of its performance. There is actually a great variety of test methods that can be used to characterize FRS. However, these test methods are not necessarily comparable and do not report the same *material* or *structural* properties. Most common test methods are performed to evaluate properties such as compressive strength, flexural strength or energy absorption of FRS. Some of the most widely reported are:

- ASTM C1399 : Standard Test Method for Obtaining Average Residual-Strength of Fiber-Reinforced Concrete [9]
- ASTM C1550 : Standard Test Method for Flexural Toughness of Fiber Reinforced Concrete (Using Centrally Loaded Round Panel) [10]
- ASTM C1604 : Standard Test Method for Obtaining and Testing Drilled Cores of Shotcrete [11]
- ASTM C1609 : Standard Test Method for Flexural Performance of Fiber-Reinforced Concrete (Using Beam With Third-Point Loading) [12]
- EN 14488-3 : Flexural strengths (first peak, ultimate and residual) of fibre reinforced beam specimens [13]
- EN 14488-5 : Determination of energy absorption capacity of fibre reinforced slab specimens [14]
- EN 14651 : Test method for metallic fibered concrete - Measuring the flexural tensile strength (limit of proportionality (LOP), residual) [15]
- JSCE SF-4 : Method of test for Flexural strength and Flexural toughness of steel fiber reinforced concrete [16]

Due to the diversity of test methods and the variety of potential test results, the process of design and evaluation of FRS can be very complex. In fact, there is no universal method or guidelines an engineer can follow and it is not possible to compare FRS performance values from different test methods used in different design documents. Performing tests can give information such as crack opening or energy absorption, flexural or shear strength, overall behaviour or peak load [17]. It is therefore crucial to understand how to properly use the information provided when dealing with different loading conditions.

To illustrate this, a testing program was put together. In this case, the same wet-mix shotcrete mix-design was used in all experiments. Two different mixtures, one with a simple anchoring system steel fibre (A) and one with a with a more complex anchoring system and strain hardening steel fibres (B) at the same dosage (25 kg/m^3), were evaluated following the ASTM C1550 and the EN 14488-5 test methods (Fig. 1). In this example, test results showed different responses through different tests methods from the mixtures with different fibres.

Figure 1 : Setup for ASTM C1550 (left) and EN 14488-5 (right) test methods.

A factor of 2,9 was found between the energy absorption at a 40 mm deflection from the ASTM C1550 and the energy absorption at a 25 mm deflection from the EN 14488-5 for fibre A and a factor of 3,6 for fibre B (Fig. 2). A similar difference was observed for the values of peak load (Fig. 3). However, test results from previous studies showed differently. It would have been expected to see a factor of 2,5 between the energy absorption at a 40 mm deflection from the ASTM C1550 and the energy absorption at a 25 mm deflection from the EN 14488-5 [18]. It appears that more research is still needed.

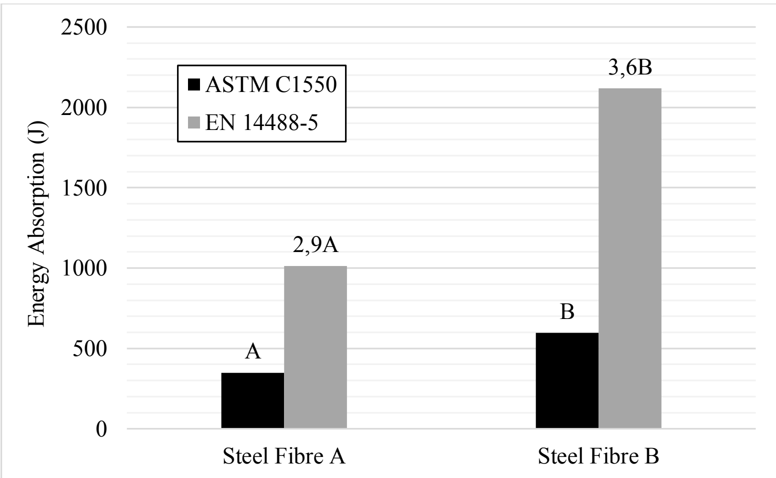

Figure 2 : Energy absorption of wet-mix shotcrete with fibres A and B measured with ASTM C1550 and EN 14488-5 test methods.

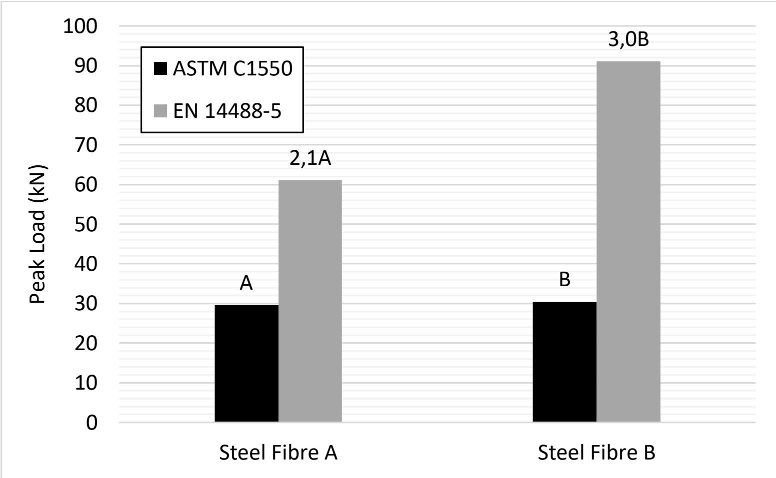

Figure 3 : Peak load of wet-mix shotcrete with fibres A and B measured with ASTM C1550 and EN 14488-5 test methods.

These results illustrate the fact that test methods, in general, do not reflect in the same way the changes in the behaviour and in the mechanical properties of FRS. In this case, fibre B can seem a lot better than fibre A with one test and more comparable with the other test. In fact, the square plate test (EN 14488-5) allows to better represent the potential of fibre B compared to the round determinate panel test (ASTM C1550). The round panel test mainly induces flexural stresses while the square panel test induces flexural and shear stresses. This is a simple example, yet an obvious reminder that more research and reflection is needed.

It is therefore difficult to compare results between test methods. It is even difficult to compare the potential of different FRS mixtures because the type of solicitation in one particular test may not be able to translate the potential of a mixture relative to another. This is why it is crucial to understand what information is given through one test method or the other and how to integrate it in the design process.

DYNAMIC LOADING

Dynamic events such as rockbursts are seen in underground areas with seismic activities and high stresses. As underground mines continue to reach greater depths, sometimes now several kilometres deep, these events have the potential of becoming more and more critical. Impact loads from released stresses and dynamic loads from seismic waves are two different aspects in terms of material testing and responses and both can provide interesting data. From a material engineer point of view, with the aim of optimizing the use of FRS, the focus on dynamic loading is more on the consequence of an event, rather than on the geomechanics mechanism.

Testing

On one hand, the speed of a rockburst event has been reported to be at a magnitude of approximately 1-10 m/s [19, 20]. On the other hand, the values of displacement rates in most test methods for FRS are quite far from these velocities; they are much slower, from a fraction to a few mm/min. This major difference (approx. 10^5) is particularly important as concrete is known to have stress-rate sensitivity [21]. Thus, the dynamic performances of FRS cannot be evaluated with conventional test methods which is why we believe FRS are not used to their full capacity nowadays.

The potential of FRS under dynamic loads has already been shown through complex mass drop experiments [22, 23]. Unfortunately, the available test methods are quite complex and hardly reproductible. There have not been any advances in the recent years regarding this subject. However, even more as it was in the past [24], it still seems important to keep working on dynamic test methods for FRS. In the aim of developing a new approach for testing FRS under dynamic loading, several possibilities are considered. The objective here is to reproduce the actual loading conditions with a relatively simple method.

For example, a method based on the Charpy impact test with a notched sample could be used to measure the toughness of FRS. This approach has already been used with fibre reinforced concrete in the past [25]. The geometry of the setup should be adapted to the requirements of shotcrete samples and the magnitude of the required energy should be designed according to the expected loads. Moreover, the use of explosives is also considered. This approach has recently been used to evaluate the performance of FRS subjected to explosion impacts in tunnels [26]. This is a more tedious method and definitely harder to universalize, but it would provide interesting information. These large-scale experiments are interesting because they demonstrate the residual behaviour of FRS. However, the data collection can be very complex and the interpretation of results is often very limited.

Finally, the principle of pseudo-dynamic testing is a new approach that could have potential for testing FRS under dynamic loading. This method has been used since the 1980s to measure the performance of structures under seismic loads [27]. It can replace complex and expensive large-scale dynamic tests by simulating dynamic loads. In an iterative loop, displacements are imposed on a structure, then its response is processed and new displacements are generated. The pseudo-dynamic analysis would be based on principles already used in the fields of structure and geomechanics while being adapted to the specificities of FRS as ground support [28, 29]. The geometry of the setup and the solicitation needs to be optimized in order to better measure and report actionable information needed by the designer. The setup needs to be realistic and replicable. A setup like the one used by Bernard [6] appears to be a great basis for such test (Fig. 3). Actuators could be controlled through the pseudo-dynamic software to simulate the dynamic event.

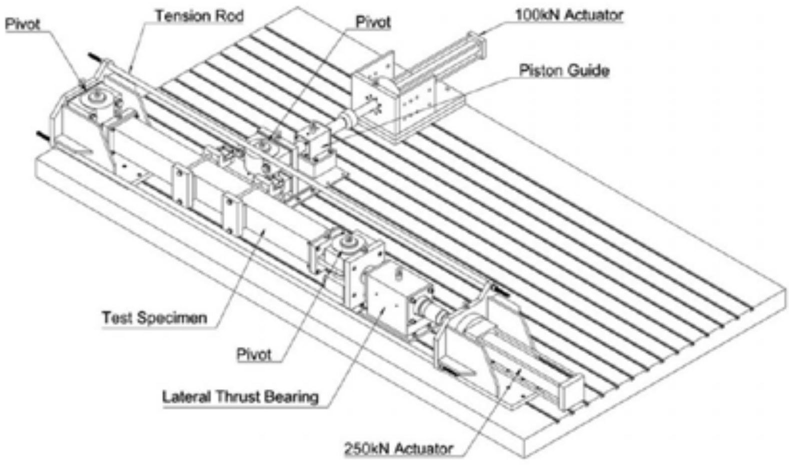

Figure 2 : Beam-column test setup used by Bernard (figure taken from [6])

Mix designs

It has sometimes been argued that shotcrete cannot be used to prevent violent underground events [20, 30]. However, it has been shown that FRS can absorb as much or even more energy than some traditional ground support systems [24, 31]. Combined with anchor bolts, FRS performs well in extreme conditions [8]; it can absorb more energy than steel mesh alone or in a shotcrete layer. Therefore, with the need for effective counter measures for dynamic events in deep underground areas, the development of new high-performance FRS mix designs is key for safety and further development in the industry.

The main challenge when developing such mixtures is mainly related to maintaining a certain degree of fluidity for pumping with a high dosage of fibres required to obtain a very high toughness and ductility. We are talking about dosages of more than 100 kg/m^3, values that have rarely been seen in the industry. Fortunately, some solutions have been raised in a recent project and motivate the development of new mix designs [26]. The fluidity issue can easily be resolved with the use air entraining admixtures: these admixtures make the concrete easier to pump without risking to significantly increase the air content in place as the compaction energy in the spraying process removes air bubbles in excess. In fact, this method has been known for several decades and is often used in wet-mix shotcrete [32-34].

In a new research project, new FRS mixtures will be designed and tested by targeting key parameters that can lead to a high ductility of the material and a high toughness of the structure. This can be done by optimizing the composite behaviour and the fibre anchoring in the shotcrete [21]. These new mixtures will contain different types of fibres (steel, synthetic, natural), different dosages, different geometries (thickness, length, hooks) and different concrete mixtures. The new FRS mix designs will be characterized and optimized. The main objective will remain to develop mixtures with high ductility and toughness.

CONCLUSION

As underground support becomes a great challenge in certain regions, it is crucial to improve our understanding of FRS and develop new technological approaches. In fact, FRS represent a powerful tool, especially in complex situations, as it can be deployed fast and easily. Therefore, it is important to understand how to utilize test results and design guidelines to better use the potential of FRS in ground support programs. Moreover, developing a new test method to simulate dynamic loads and high-toughness mixtures could also help engineers use the full potential of FRS in extreme underground conditions. The current projects undertaken at *Laval University* on FRS will focus on these interesting challenges.

ACKNOWLEDGMENTS

The authors would like to acknowledge the financial support of *Bekaert-Maccaferri Underground Solutions*, *King Shotcrete Solutions*, *Natural Sciences and Engineering Research Council of Canada (NSERC)*, *Fonds de Recherche du Québec – Nature et Technologies (FRQNT)*, *Programme de Bourses de Leadership et Développement Durable de l'Université Laval*, *Fondation Famille Choquette* and the *Transportation Association of Canada*. The technical support of Jean-Daniel Lemay, research engineer, René Malo, research technician, and Pierre-André Tremblay, research technician, is also acknowledged.

REFERENCES

1. Jolin, M., J.-D. Lemay, N. Ginouse, B. Bissonnette, and É. Blouin-Dallaire, *The Effect of Spraying on Fiber Content and Shotcrete Properties*, in *Shotcrete for Underground Support XII*. 2015: Singapore, Singapore.
2. Barton, N., R. Lien, and J. Lunde, *Engineering classification of rock masses for the design of tunnel support.* Rock mechanics, 1974. **6**(4): p. 189-236.
3. Palmstrom, A. and E. Broch, *Use and misuse of rock mass classification systems with particular reference to the Q-system.* Tunnelling and underground space technology, 2006. **21**(6): p. 575-593.
4. Papworth, F., *Design Guidelines for the Use of Fiber-Reinforced Shotcrete in Ground Support.* Shotcrete Magazine, 2002(Spring 2002): p. 16-21.
5. Nitschke, A., *Modeling of Load-Bearing Behavior of Fiber-Reinforced Concrete Tunnel Linings.* Shotcrete Magazine, 2017(Spring 2017): p. 28-34.
6. Nitschke, A. and E. Bernard, *Load-Bearing Capacity of Fiber-Reinforced Concrete Tunnel Linings Under Combined Moment-Normal Force Loading Conditions.* Rapid Excavation & Tunneling Conference 2017, 2017: p. 680-693.
7. Nitschke, A. and R. Winterberg. *Performance of macro synthetic fiber reinforced tunnel linings*. in *ITA-AITES World Tunnel Congress 2016, WTC 2016, April 22, 2016 - April 28, 2016*. 2016. San Francisco, CA, United states: Society for Mining, Metallurgy and Exploration.
8. Thomas, A., *Sprayed concrete lined tunnels*. 2008: CRC Press.

9. ASTM C1399-10, *ASTM C1399/C1399M-10 Standard Test Method for Obtaining Average Residual-Strength of Fiber-Reinforced Concrete.* ASTM International, 2010: p. 1-6.
10. ASTM C1550-12, *ASTM C1550-12a Standard Test Method for Flexural Toughness of Fiber Reinforced Concrete (Using Centrally Loaded Round Panel).* ASTM International, 2012: p. 1-13.
11. ASTM C1604-05, *ASTM C1604/C1604M-05 Standard Test Method for Obtaining and Testing Drilled Cores of Shotcrete.* ASTM International, 2005: p. 1-5.
12. ASTM C1609-12, *ASTM C1609/C1609M-12 Standard Test Method for Flexural Performance of Fiber-Reinforced Concrete (Using Beam With Third-Point Loading).* ASTM International, 2012: p. 1-9.
13. EN 14488-3, *EN 14488-3 Testing sprayed concrete - Part 3: Flexural strength (first peak, ultimate and residual) of fibre reinforced beam specimens.* European Committee For Standardization, 2006: p. 1-12.
14. EN 14488-5, *EN 14488-5 Testing sprayed concrete - Part 5: Determination of energy absorption capacity of fibre reinforced slab specimens.* European Committee For Standardization, 2006: p. 1-8.
15. EN 14651, *EN 14651 Test method for metallic fibered concrete - Measuring the flexural tensile strength (limit of proportionality (LOP), residual).* European Committee For Standardization, 2005: p. 1-17.
16. JSCE-SF4, *Method of Tests for Flexural Strength and Flexural Toughness of Steel Fiber Reinforced Concrete.* Concrete Library of The Japan Society of Civil Engineers (JSCE), 1984: p. 58-61.
17. Gagnon, A. and M. Jolin, *Specifying and Testing Fibre Reinforced Shotcrete: Advances and Challenges*, in *Shotcrete for Underground Support XIII*, E.C. International, Editor. 2017: Irsee, Allemagne. p. 1.
18. Bernard, E.S., *Correlations in the behaviour of fibre reinforced shotcrete beam and panel specimens.* Materials and Structures, 2002. **35**(3): p. 156-164.
19. Darling, P., *SME mining engineering handbook*. Vol. 3. 2011: SME.
20. Vandewalle, M., *Use of steel fibre reinforced shotcrete for the support of mine openings.* Journal of The South African Institute of Mining and Metallurgy, 1998. **98**(3): p. 113-120.
21. Bentur, A. and S. Mindess, *Fibre reinforced cementitious composites*. 2006: CRC Press.
22. Ortlepp, W. and T. Stacey, *Performance of tunnel support under large deformation static and dynamic loading.* Tunnelling and underground space technology, 1998. **13**(1): p. 15-21.
23. Stacey, T. and W. Ortlepp, *Tunnel surface support-capacities of various types of wire mesh and shotcrete under dynamic loading.* Journal of the Southern African Institute of Mining and Metallurgy, 2001. **101**(7): p. 337-342.
24. Stacey, T., *Energy-absorbing capacity of reinforced shotcrete, with reference to the containment of rockburst damage.* Journal of the Southern African Institute of Mining and Metallurgy, 1995. **95**(3): p. 137-140.
25. Barr, B. and A. Bouamrata, *Development of a repeated dropweight impact testing apparatus for studying fibre reinforced concrete materials.* Composites, 1988. **19**(6): p. 453-466.

26. Vollmann, G., M. Thewes, and E. Kleen, *Development of a highly ductile sprayed concrete as a counter-measure for explosion and fire impacts on underground structures.* International Tunneling Association, 2015: p. 1-10.
27. Donéa, J., P. Jones, G. Magonette, and G. Verzeletti, *The pseudo-dynamic test method for earthquake engineering: An overview.* Commission of the European Communities. EUR, 1990. **12846**.
28. Choudhury, D. and S. Nimbalkar, *Seismic passive resistance by pseudo-dynamic method.* Geotechnique, 2005. **55**(9): p. 699-702.
29. Choudhury, D. and S.S. Nimbalkar, *Pseudo-dynamic approach of seismic active earth pressure behind retaining wall.* Geotechnical & Geological Engineering, 2006. **24**(5): p. 1103.
30. Ortlepp, W. and T. Stacey, *Rockburst mechanisms in tunnels and shafts.* Tunnelling and Underground Space Technology, 1994. **9**(1): p. 59-65.
31. Morgan, D., R. Heere, N. McAskill, and C. Chan. *Comparative evaluation of system ductility of mesh and fibre reinforced shotcretes*. in *Shotcrete for Underground Support VIII*. 1999. ASCE.
32. Beaupré, D., *Rheology of high performance shotcrete*. 1994, University of British Columbia.
33. ACI 506R-16, *Guide to Shotcrete.* ACI Committee Report, 2016: p. 1-52.
34. Jolin, M. and D. Beaupré, *Understanding wet-mix shotcrete: mix design, specifications, and placement.* Shotcrete. Summer, 2003.

FROM LAB SCALE SPRAYING TO REAL SCALE SHOTCRETING AND BACK TO THE LAB

Isabel Galan[1], Maria Thumann[2], Lukas Briendl[3], Rudolf Röck[4], Florian Steindl[1], Joachim Juhart[3], Florian Mittermayr[3], Wolfgang Kusterle[2]

[1]Institute of Applied Geosciences, Graz University of Technology, Austria
[2]Faculty of Civil Engineering, Ostbayerische Technische Hochschule Regensburg, Germany
[3]Institute of Technology and testing of Building Materials, Graz University of Technology, Austria
[4]Institute of Construction and Materials Science, University of Innsbruck, Innsbruck, Austria
igalangarcia@tugraz.at

ABSTRACT

Before new mixes are sprayed in real scale applications, lab experiments have to be carried out to provide a basis for predicting a good performance in real scale. In many cases a further set of experiments after the real spraying is required to understand the correlations between the behavior in the lab and in real scale spraying. In this paper we present such a two-way process for two new wet mix designs, one with a very low tricalcium aluminate Portland cement and the other one with a CEM I with addition of ultrafine calcite. Calorimetry and shear modulus measurements were used in the lab to monitor hydration evolution. Compressive strength of non-sprayed prisms was measured after 6 hours, 24 hours and 28 days. At the real scale spraying tests compressive strength was measured at periodic intervals up to 24 hours and at 28 days. The hydration of the sprayed samples was stopped at 3, 6 and 24 hours and samples were scanned with X-ray for the identification of the phases present. The results presented are used to discuss the extent to which lab experiments can predict the behavior of mixes in real scale and how small changes in the raw materials and the mixes can lead to quite different results.

INTRODUCTION

For the preparation of real scale spraying tests, previous laboratory work is needed to guarantee maximum success of the trials. The type of tests and measurements needed to 'get ready' for the real scale depends mainly on the availability of spraying equipment, laboratory facilities, and previous personal experience.

Differences between hand-mixed and sprayed concrete relate to the compaction effect of spraying, the changes in morphology of the precipitated hydrates and possibly the differences in accelerator reactivity [1]. However, these differences are difficult to quantify as they rely on the rate at which the accelerator is mixed with the rest of the components (i.e. final homogeneity achieved), which is in turn dependent on personal skills and experience. Nevertheless, "hand-mixed" (non-sprayed) prisms are usually fabricated to evaluate the compressive strength evolution during the first day and after 28 days, giving these values a basis for comparison between mixes and a first proof of mechanical viability.

Proper compressive strength development is not the only prerequisite for a mix to be accepted as a candidate for real scale shotcreting. Other aspects such as workability, pumpability and sprayability are equally important and need to be taken into account. These two latter properties, however, can only be checked by spraying the corresponding mixes. For this purpose, some lab-scale spraying facilities have been developed in the last years. One example is the MiniShot device from Sika [2]: concrete made with the fine fraction of aggregates is sprayed on cells where the shear modulus (together with the temperature) is continuously monitored by means of ultrasound wave propagation measurements. Apart from proving if the sample is pumpable and sprayable (at this scale), the main advantage of this device is the correlation reported by the inventors between the shear modulus measured in the lab and the compressive strength of 'equivalent' real scale shotcrete [3,4].

As the evolution of the mechanical properties of shotcrete is directly related to the development of the hydrated cement phases during hydration, other analytical techniques like isothermal calorimetry and X-ray diffraction may also be helpful to follow the process in the first hours. The first one allows for the monitoring of the heat evolved during the hydration of the different phases (because cement hydration is an exothermic process) while the second one helps identifying the actual phases that are forming and reacting. Despite its importance, this field is still relatively new and very few studies have been published on the correlation between shotcrete microstructure and mechanical properties development [5,6].

Within the frame of the 'Advanced and sustainable sprayed concrete' (ASSpC) project, new mixes are being developed with the final aim of reducing the impact of shotcrete on the environment. This objective is envisaged in two ways: (i) by reducing the clinker content in the mixes, replacing it by mineral additions and fillers and (ii) by producing more durable products, which in turn reduce life-cycle costs, in particular those arising from maintenance and repair. Moreover, neither of these two goals should compromise the workability and the mechanical properties of the resulting shotcrete in any way.

In the present paper we have selected two mixes that were investigated in the lab and then sprayed in real scale: one with a very low tricalcium aluminate Portland CEM I cement, which should be considered as 'sulfate resistant', and the other one with a CEM I cement partially substituted by a limestone filler.

Apart from the characteristics of the mixes and their behavior, the suitability of the lab tests used for the prediction of real scale performance is analyzed. After the real scale trials, replicating mixes were sprayed again in the lab and the influence of the variables changed before and after the trials was assessed.

EXPERIMENTAL

Materials

Two types of cements were used for the mixes: CEM I 52.5R (from now on 'CEM I') and CEM I 52.5N SR0 (from now on 'CEM SR0'). The composition of the cements is shown in *Table 1*, together with the Blaine surface area. The d_{50} of the cements used for the lab tests was 7.1 and 8.0 μm for CEM I and CEM SR0, respectively.

Table 1. Composition of cements used as determined by XRD + Rietveld analysis, and Blaine surface area.

Phase %	**CEM I** Lab	**CEM I** Real scale	**CEM SR0** Lab	**CEM SR0** Real scale
Alite	55.0	52.2	58.2	58.2
Belite	13.1	10.8	12.6	16.9
Aluminate c	0.7	0.4	0.5	0.6
Aluminate o	10.8	10.7	1.2	2.0
Ferrite	7.4	7.1	12.3	11.9
Periclase	4.2	3.3	-	-
Anhydrite	3.8	2.2	3.4	3.9
Arcanite	2.0	2.1	0.4	-
Bassanite	1.7	3.0	0.5	2.0
Calcite	0.9	4.7	9.5	3.9
Gypsum	-	1.5	-	-
Portlandite	0.3	0.5	0.9	0.5
Dolomite	-	1.4	-	-
Quartz	-	0.2	-	-
Aphthitalite	-	-	0.5	0.2
Blaine (cm^2/g)	4308	4542	4193	4404

In the case of CEM I the main differences between the batches used in the lab and in the trials (both from the same producer) were (i) the calcite content, considerably higher in the real scale batch, and (ii) the sulfates: gypsum is only found in the real scale batch where also the bassanite content is higher, whereas the anhydrite content is lower than in the lab batch. These latter differences may be related to the temperature during the production of the cement and the dehydration of gypsum during the grinding and blending with the clinker.

In the CEM SR0 again a difference in the calcite content is observed, the lab batch being in this case the one with the higher percentage. In both cases the tricalcium aluminate is low, below 3%, but the ferrite content is very high, around 12%. The amount of bassanite is, like for CEM I, higher in the real scale batch than in the lab one.

An ultrafine limestone filler (96% calcite, 4% of dolomite and traces of quartz) with d_{50} of ~1 μm was mixed with the CEM I.

Four types of aggregates were used:

- Dolomitic aggregates for the real scale tests, both the fractions 0-4 and 4-8 mm: 97% dolomite, 1% calcite and 2% quartz.

- Limestone powder (Nekafill) for the MiniShot tests before the real scale trials: 92% calcite and 5% dolomite. This type of aggregate, with grain sizes smaller than 125 μm, allows for the MiniShot device to spray a micro-concrete (or "fines-based concrete"), the amount of aggregate having been calculated with the granulometric profiles of a reference concrete.
- For the MiniShot tests after the real scale trials, in order to reproduce the mixes as close as possible, the dolomitic aggregates used at the trials were sieved and the fine fraction, below 0.125 mm, was used.
- Calcitic aggregates with a grain fraction of 0-4 mm for the compressive strength mortar prisms.

Mixes and spraying

Sprayed and non-sprayed samples were prepared in the laboratory. For the non-sprayed ones, two types of mixtures were made: (i) cement and limestone powder aggregates (<0.125 mm) plus water and (ii) cement and calcitic aggregates (0-4 mm) plus water, retarder, superplasticizer and accelerator. The first samples were prepared for calorimetry measurements whereas with the second ones compressive strength tests were carried out. In both cases a Hobart mixer was used for the mixing of the ingredients. For the mortar prisms the following procedure was applied: water and SP were first mixed in a Hobart mixer; then the binder and aggregates were added and mixed for 90 seconds at about 150 rpm; the mix was then left for 10 minutes, after which the accelerator was added while mixing at 300 rpm for 15 seconds. The mix was then poured into the prism molds while vibrating for 15 seconds. The prisms were then covered and left for 6 h, after which they were demolded and stored at 99% RH and 20 °C for another 18 h. After the first 24 h, the prisms were stored under water at 20 °C until the 28th day [7].

For the sprayed samples, cement, water, aggregate, superplasticizer and retarder were previously mixed in a Hobart mixer and then pumped to the nozzle of the MiniShot device, where they were mixed with the accelerator and the air.

The composition of the MiniShot laboratory mixes is in *Table 2*. The superplasticizers used (SP1 and SP2) were in all cases based on polycarboxylate ether and the quantities, between 5 and 10 kg/m^3, were adjusted to achieve an adequate workability, similar in all cases. The alkali-free accelerator (A1) was based on aluminum sulfate and the quantities used varied between 65 and 80 kg/m^3. The temperature in the MiniShot lab was ~20 °C.

Table 2. MiniShot mixes sprayed before and after the real scale trials. LP: Limestone powder (<125 mm). D<125: fine fraction of aggregates used in real scale trials. SP (PCE): superplasticizer (based on polycarboxylate ether). A1: accelerator based on $Al_2(SO_4)_3$. The percentages of SP, retarder and accelerator refer to the binder mass.

	Cement (kg/m^3)	**Ultrafine limestone (kg/m^3)**	**Aggregate (kg/m^3)**	**Water (kg/m^3)**	**SP (PCE) (%)**	**Retarder (%)**	**Accelerator (%)**	**w/b**
Before	1155 CEM	-	353 LP	508	0.4 (SP1)	0.5	6/8 (A1)	0.44

	SR0							
After	1057 CEM SR0	-	442 D<125	513	0.7 (SP2)	-	7.6 (A1)	0.49
Before	1039 CEM I	55	352 LP	514	1.0 (SP1)	0.5	6/8 (A1)	0.47
After	1031 CEM I	53	440 D<125	499	0.8 (SP2)	-	7.5 (A1)	0.46

The mortar mixes used for the compressive strength prisms are in *Table 3*. Similarly to the MiniShot mixes the superplasticizer and accelerator used were based on polycarboxylate ether and aluminum sulfate, respectively. To produce 6 specimens (40x40x160 mm) two batches of 1200 grams of sand and 600 grams of binder were used.

Table 3. Mortar mixes for compressive strength prisms (non-sprayed).

CEM I (% of binder)	CEM SR0 (kg/m^3)	UFL (% of binder)	Aggregate 0-4 mm (% of solid)	SP (PCE) (% of binder)	Accelerator (% of binder)	w/b
95	-	5	66.7	1 (SP2)	6 (A2)	0.4
-	100	-	66.7	1 (SP2)	6 (A2)	0.5

The concrete mixes planned for the real scale tests with CEM SR0 and CEM I are presented in *Tables 4 and 5*, respectively. Together with the two real scale mixes, the 'equivalent concrete' sprayed in the lab with MiniShot before and after the trials is included for ease of comparison.

Table 4. Real scale shotcrete mix with CEM SR0 and equivalent concrete mixes sprayed with MiniShot before and after the trials.

	CEM SR0 (kg/m^3)	Aggregate (kg/m^3)	Water (kg/m^3)	SP (PCE) (%)	Retarder (%)	Accelerator (%)	w/b
Before (Mini Shot)	442	1686	208	0.3 (SP1)	0.5	6/8 (A1)	0.47
Real scale	406	1888	194/206*	1.0 (SP2)	-	8 (A1)	0.48/ 0.51*
After (Mini Shot)	400	1858	206	0.7 (SP2)	-	7.6 (A1)	0.52

*the amount of water planned for the real scale tests (194 kg/m^3) differed from the water content measured with microwave drying (206 kg/m^3).

Table 5. Real scale shotcrete mix with CEM I and equivalent concrete mixes sprayed with MiniShot before and after the trials. UFL: ultrafine limestone.

	CEM I (kg/m^3)	**UFL (kg/m^3)**	**Aggregate (kg/m^3)**	**Water (kg/m^3)**	**SP (PCE) (%)**	**Retarder (%)**	**Accelerator (%)**	**w/b**
Before (Mini Shot)	398	21	1686	209	1.0 (SP1)	0.5	6/8 (A1)	0.50
Real scale	391	20	1852	193/200*	1 (SP2)	-	8.2 (A1)	0.47/ 0.49*
After (Mini Shot)	388	20	1839	200	0.7 (SP2)	-	7.5 (A1)	0.49

* the amount of water planned for the real scale tests (193 kg/m^3) differed from the water content used (200 kg/m^3), which was calculated as the sum of the microwave drying content (195 kg/m^3) plus 5 kg/m^3 after-dosage.

The real scale shotcreting took place with the use of a Hittmayr equipment which had both the pump (CIFA Magnum MK24) and the manipulator mounted on a truck-mixer. The accelerator spraying was achieved by means of a peristaltic impeller and the spray performance was set at 20 m^3/h. Initially planned as 7% of binder mass, the actual accelerator dosage was then determined by weighting the accelerator tank with a hanging scale. A 17 m^3 compressor was used for the addition of the compressed air at the nozzle; the actual amount was measured with an air flow meter.

For each composition 3 m^3 of fresh concrete were sprayed: firstly, several panels (*Figure 1a*) were filled and then the rest was shot to the test tunnel (*Figure 1b*). The distance from the nozzle to the tunnel wall was 1.5 to 2 meters. Several specimens were drilled from the panels after 48 h and then stored in water for the 28 days compressive strength measurements. The ambient temperature during the real scale tests varied between 15 and 35 °C (although these temperature variations were much smaller while the concrete was fresh).

Figure 1. Real scale shotcreting: a) Spraying panels, b) Tunnel.

Characterization techniques

The mixes sprayed with the MiniShot device were characterized by means of continuous shear-modulus measurements as well as by isothermal calorimetry for the first 24 h. The equipment associated with the MiniShot consists of several cells whereby the amplitude attenuation of ultrasound waves is recorded and then converted to shear modulus values (*Figure 2*) [3]. From the same batch, samples were directly sprayed on the calorimeter containers and then placed inside the equipment (I-Cal 8000 Calmetrix) to start the measurement at 23 °C.

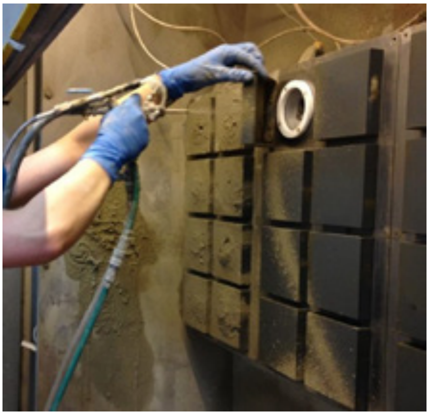

Figure 2. MiniShot device with ultrasound cells.

After spraying the samples, and after 3, 6 and 24 h samples were taken to perform XRD scans (Panalytical X'Pert Pro diffractometer, Cobalt radiation, time per step 100 s, step size 0.017). Before the measurements, the hydration was stopped in all samples by means of solvent exchange (with isopropanol) followed by drying at 35% relative humidity. In the case of the real scale trials, the samples extracted for XRD were gently ground and sieved and only the fraction below 0.125 mm was taken.

The compressive strength tests of the mortar prisms (40x40x160 mm) were carried out in an Amsler testing machine at the age of 6 h, 24 h and 28 days; for each measurement 4 prism halves were tested.

The on-site early strength of the real scale shotcrete was measured according to EN 14488-2 (i) from 0.2 to 1 MPa with a penetration needle (whereby the penetration resistance is converted to compressive strength), and (ii) from 2 to 16 MPa by means of a powder-activated Hilti gun, with which a bolt is driven into the young concrete and then pulled out again. The ratio of pull-out force to penetration depth is then converted in to compressive strength by means of calibration curves.

Finally, the 28 days strength of the drilled cores (100x100 mm) from the spraying panels was measured according to ONR 23303 in a testing machine with a maximum load of 300 Tones.

RESULTS AND DISCUSSION

Lab tests before the real scale trials

The instantaneous formation of significant amounts of ettringite due to the presence of the accelerator is the biggest difference between manually mixed samples (no accelerator) and sprayed samples (*Figure 3*). Despite the heat release in the very first minutes not having been recorded because of the external mixing, the difference in the first peak height of the calorimetry curves is noticeable. In the case of the CEM SR0 samples this difference is even greater due to the low aluminate content available (*Table 1* and *Figure 4a*) to dissolve and contribute to the formation of ettringite. The presence of superplasticizer and retarder lead to a longer dormant period (between the first and second peak in *Figure 3*) in the sprayed samples: the resulting shift in the kick-off of the silicate reaction is again more pronounced for the CEM SR0 samples (peak maximum reached after 6 and 11 h in manual and sprayed samples, respectively) (*Figure 3a*). In the CEM I + UFL samples the presence of the accelerator seems to also accelerate the silicate reaction, which does not start earlier but which happens faster (*Figure3b*): this may be a consequence of the dissolution of alite promoted by the low pH of the accelerator. Finally, once all the sulfate needed to form ettringite is consumed, transformation of ettringite into AFm phases (with a lower SO_3/Al_2O_3 ratio) takes place. This effect is only noticeable in sprayed CEM I + UFL systems (third maximum in *Figure 3b*), where hemi- and mono-carboaluminate phases start to form after 6-7 h, when tricalcium aluminate is still available (*Figure 4b*). In CEM SR0 systems anhydrite is still present after 6 h and transformation of ettringite to AFm does not take place in the first 24 h of hydration (*Figure 4a*).

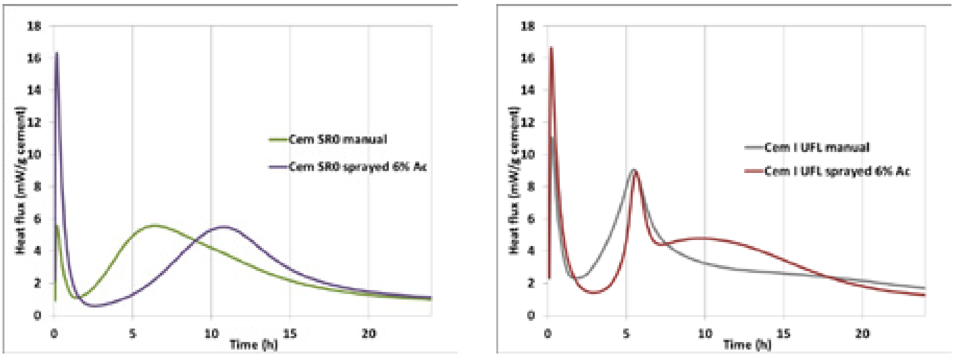

Figure 3. Calorimetry of hand mixed samples (with no SP, retarder and accelerator) and MiniShot sprayed samples with 6% $Al_2(SO_4)_3$ based accelerator (see Table 2) before the real scale trials: a) CEM SR0 and b) CEM I + ultrafine limestone.

Increasing the amount of accelerator in the sprayed mixes from 6 to 8% leads to an initial increase of the shear modulus, which then levels out with time and ends up reaching lower values after 24 h (*Figure 5*). This can be interpreted as an initial boost due to the greater ettringite network formation which is then counterbalanced by the less pronounced development of the C-S-H network, possibly related to space restrictions.

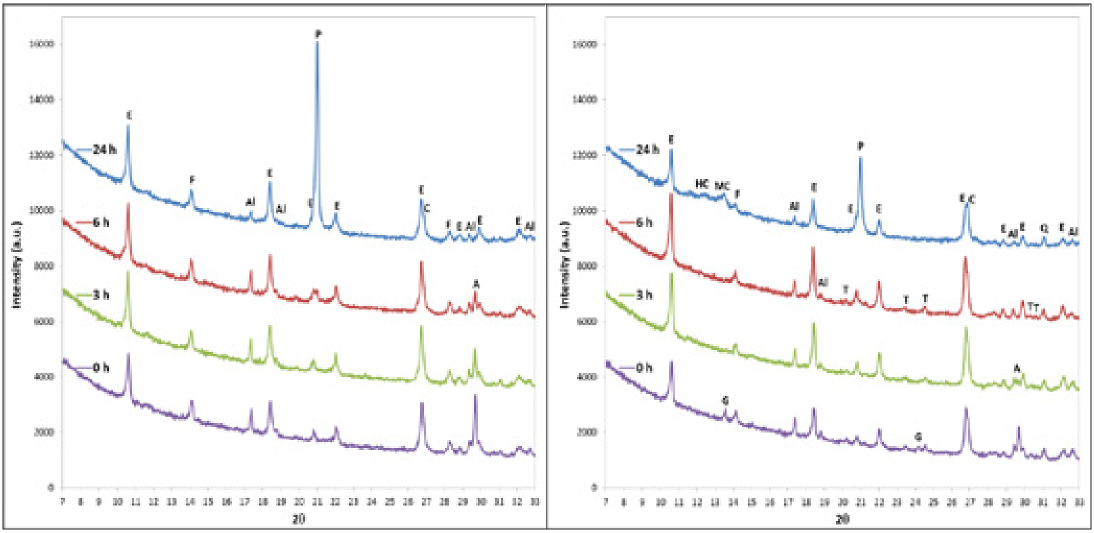

Figure 4. XRD of MiniShot sprayed mixes (with 6% accelerator) after spraying (0h), after 3 h, 6 h and 24 h: a) CEM SR0 and b) CEM I + ultrafine limestone. E: ettringite, F: ferrite, Al: alite, P: portlandite, C: calcite, A: anhydrite, HC: hemicarboaluminate, MC: monocarboaluminate, T: tricalcium aluminate, Q: quartz.

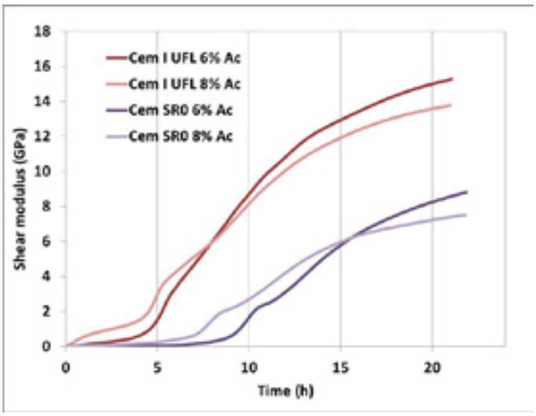

Figure 5. Shear modulus of MiniShot sprayed samples before the trials (see Table 2) with 6 and 8% accelerator.

In any case, after the first formation of ettringite, the further development of the microstructure (C-S-H), and the consequent mechanical properties, start at an earlier stage in the CEM I + UFL systems than in the CEM SR0 ones, leading to higher values of the shear modulus and to higher heat released, this being especially noticeable after 6-7 h (*Figure 6*). This behavior can be related to three aspects: (i) the different particle size of the cements (and the category 52.5R and 52.5 N): 7.1 and 8.0 µm for CEM I and CEM SR0, respectively; (ii) the presence of ultrafine limestone in the CEM I systems and the enhancement of the silicate hydration, and (iii) the different Al_2O_3/SO_3 ratio of the systems: while ettringite stops forming after about 6 h in the CEM I + UFL systems (due to sulfate depletion) and starts converting to AFm, it continues growing in the SR0 systems up to 24 h and does not convert to AFm (due to excess sulfate); this could cause space restrictions in the CEM SR0 systems.

This effect can also be appreciated in the evolution of the mortar prisms compressive strength (*Figure 7*), where the much higher 6 h values for CEM I + UFL are then leveled after 24 h, where both systems reach comparable strength. The fact that the silicate reaction takes place at a slower rate and at later stages in the CEM SR0 systems is also proven by the 28 days strength values, considerably higher than for CEM I + UFL specimens. This latter result may be related, at least partly, to the higher alite content in the SR0 cement.

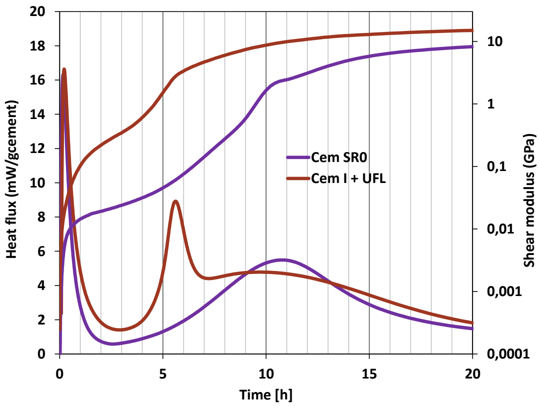

Figure 6. Shear modulus (log scale) and heat evolution for MiniShot sprayed samples with 6% accelerator before the trials.

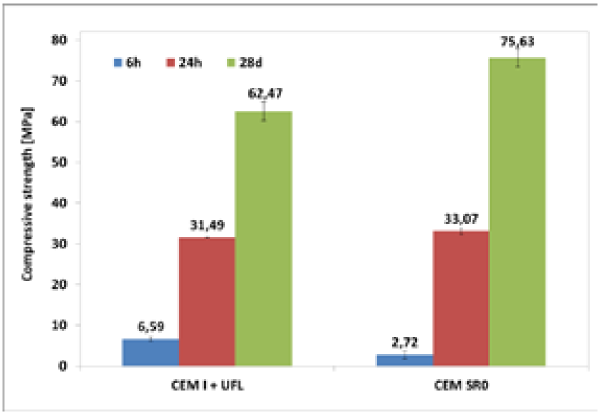

Figure 7. Compressive strength of accelerated (6%) mortar prisms.

Real scale trials

The evolution of the early strength of the shotcrete during the first 24 h (*Figure 8*) does not exactly match that of the shear modulus (*Figure 6*): during the first 6 h the differences between CEM SR0 and CEM I + UFL are notable in both cases; however, the difference in strength between both mixes is already leveled after about 11 h whereas the shear modulus values do not really converge in the first 24 h. Another difference between compressive strength and shear modulus development is the change in slope: in CEM I systems the steepest increase of the strength goes from the first to the 6th hour whereas the corresponding shear modulus shows a longer dormant period and the steepest increase between the 4th and 7th hour; in CEM SR0 systems a similar trend is observed, being the steepest period for the strength and the shear modulus 3-6th h and 6-10th h, respectively. These differences can be translated into an earlier silicate reaction in the real scale than in the lab.

The temperature difference between the lab test (~20 °C) and the real scale shotcreting (15-35 °C) played for sure a role, however with the current tests it is difficult to exactly determine how and to what extent it influenced the shotcrete strength. In general, higher temperature is supposed to enhance hydration at early ages, which would be the present case, but to also contribute to poorer curing leading to lower later age strength.
The acceleration of the reactions may also be related to the absence of retarder and the different SP used in the real scale tests.

The actual strength values of the shotcrete at 6 h, 24 h (*Figure 8*) and 28 days (CEM SR0: 55.6±1.5 MPa and CEM I: 41.1±1.9 MPa) are considerably lower than those of the 'equivalent' mortar (*Figure 7*). However, the development of strength with time follows a very similar trend in both cases: CEM I +UFL systems start earlier to gain strength but increase at a slower pace after one day than the SR0 systems, these latter reaching higher values after 28 days, again attributable partly to the higher alite (and belite) content. The differences in the values reached by the mortar prisms and the shotcrete can be explained by: (i) the possible layering and inhomogeneity in sprayed systems, and (ii) the different size and shape of the specimens used (40x40x160 mm prisms and 100x100 mm cylinders).

As for the differences in the phases formed, the XRD patterns of the real scale shotcrete (not shown here) indicate the earlier formation of AFm phases in the CEM I + UFL systems, at 6 h, than in the lab sprayed mixes. This is also proven by the earlier consumption of sulfate in the real scale samples. The explanation for this may lay in the differing contents of calcium sulfate phases in the cements (anhydrite, bassanite and gypsum) and their solubility and dissolution rate. The CEM I real scale batch contained more bassanite, which is the phase with the highest solubility and dissolution rate at 20 °C, and less anhydrite than the lab batch.

Despite the differences observed in the evolution of the shear modulus and the compressive strength of the shotcrete, the tests carried out before the real scale trials allowed for a valid prediction of the resulting good mechanical performance of the real scale shotcrete.

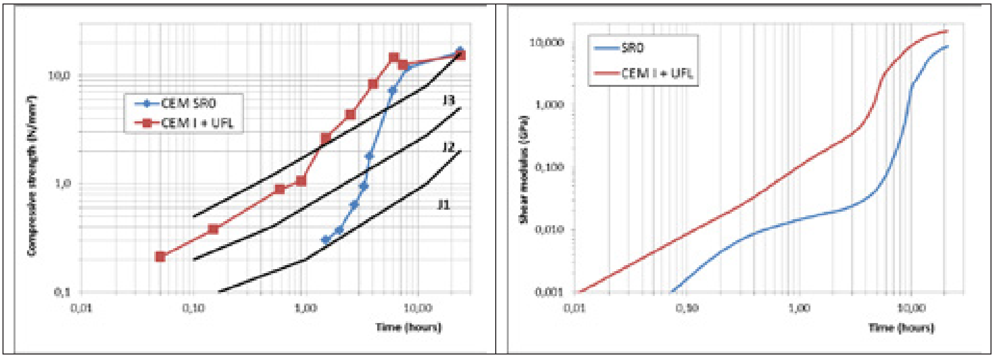

Figure 8. Early strength of real scale shotcrete plotted together with the three early strength classes J1, J2 and J3 established by the Austrian Guidelines for Sprayed Concrete [8]*: the measurements correspond to the square and diamond symbols. To help comparison the shear modulus curves measured before the real scale trials (corresponding to Figure 5) are also plotted here with the same logarithm scales on both axes.*

Lab tests after the real scale trials

Mixes with closer composition to the real scale shotcrete were hand-mixed and sprayed after the trials in the MiniShot lab. The main differences between the Minishot mixes before and after the real scale trials were (i) the superplasticizer, (ii) the percentage of accelerator, (iii) the cement, (iv) the absence of retarder after the trials, (v) the type of aggregate, and (vi) the w/c ratio, slightly lower for CEM I +UFL systems and higher for CEM SR0 mixes after the trials (*Tables 4 and 5*). The different evolution after the trials is more pronounced in SR0 mixes, especially in the silicate reaction, which takes place now at the same time as in the hand-mixed sample (cement plus water): in terms of speed the retardation effect of the SP is fully compensated by the accelerator (*Figure 9a*). In the CEM I + UFL mixes increasing the amount of accelerator from 6 to 7.5% does not have such an impact on the reaction rate, the silicate reaction being slightly delayed. This latter effect may be more related to the type of SP used. The type of CEM I used, specifically the changes in the calcium sulfate phases already stated, lead to a delay in the silicate reaction in the hand-mixed sample, where another event, probably related to the sulfate depletion, takes place at the beginning of the silicate reaction (*Figure 9b*).

The higher impact of the changes after the trials on the SR0 systems is also clear in the shear modulus evolution (*Figure 10*), which is now closer to the strength development of the real scale shotcrete than that of the mixes before the trials. The values reached after 24 hours are now higher for SR0 than for CEM I + UFL systems.

From all the variables changed at the real scale trials, the percentage of accelerator together with the composition of the cement, in particular the calcium sulfate phases, play the most important role in the development of mechanical properties. They control the amount of ettringite formed at the very early stages of hydration and also the starting of the silicate reactions and the rate; as they determine the evolution of the Al_2O_3/SO_3 ratio they also condition the transformation of ettringite into AFm phases.

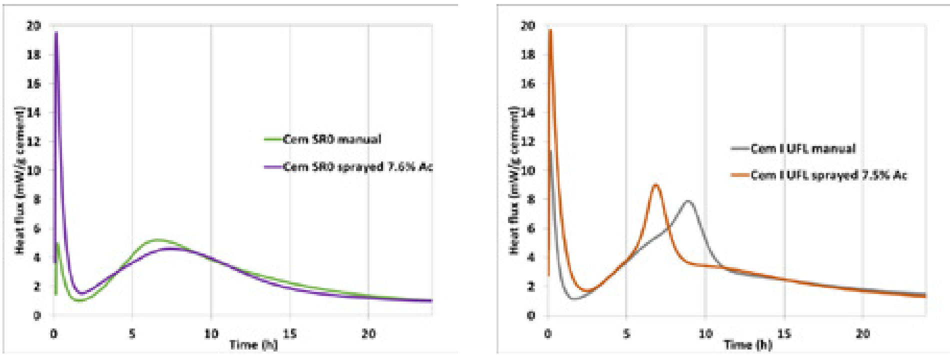

Figure 9. Calorimetry of hand mixed samples (with no SP, retarder and accelerator) and MiniShot sprayed samples with 7.6 and 7.5% $Al_2(SO_4)_3$ based accelerator (see Table 2) after the real scale trials: a) CEM SR0 and b) CEM I + ultrafine limestone.

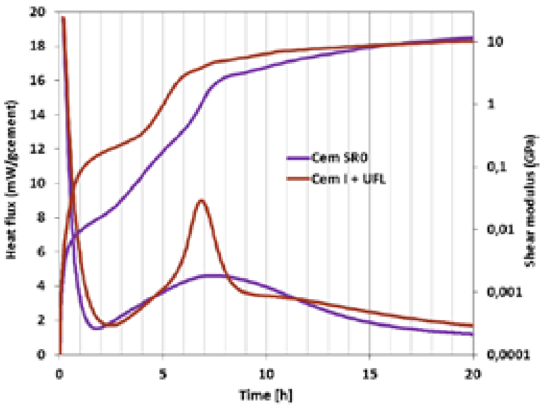

Figure 10. Shear modulus (log scale) and heat evolution for MiniShot sprayed samples (with 7.5 and 7.6% accelerator) after the trials.

CONCLUSIONS

The results presented here have shown that the MiniShot tests (with the shear modulus monitoring) together with the measurement of the compressive strength of equivalent mortar prisms could predict to a large extent the mechanical performance of the equivalent real scale shotcrete.

However, evitable and inevitable changes, like the accelerator dosage, the composition of the cement and, to a minor extent, the w/c and SP, contributed to the differences encountered in the lab tests and the real scale spraying strength progress.

The ratio Al_2O_3/SO_3 played a major role in the hydration process and the whole development of the mechanical properties.

Going back to the lab after the real scale spraying allowed to replicate the behavior of the mixes to a high degree: shear modulus and early strength correlate well. However, during the 'dormant period', between the first and the 3-4th hour, the strength increases much more steeply than the modulus. The temperature differences, between 10 and 15 °C, adjustments in water and SP content for the fines-based and the real scale shotcrete are possible causes of this different trend.

The two investigated mixes showed quite a different performance, the CEM I with ultrafine limestone addition increasing strength at a higher rate at early ages and the CEM SR0 developing earlier mechanical properties at a slower pace but reaching higher values at later stages. This behavior has been related to the different sulfate, aluminate and alite content, and the different sequence and rate of hydrated phases' formation.

Isothermal calorimetry and XRD analysis are not needed to predict mechanical behavior of shotcrete mixes but they have proven to give valuable information for understanding the hydration processes and the reasons behind the different mechanical performances and they could save time and resources when trying to identify problems and causes.

Acknowledgments

The authors gratefully acknowledge the funding by the industry partners, the Austrian Research Promotion Agency FFG (ASSpC Project-No. 856080) and the Austrian Building Technology Association ÖBV. SIKA Technology AG is also thankfully acknowledged for the support during the laboratory tests.

REFERENCES

[1] R.P. Salvador, S.H.P. Cavalaro, M. Cano, A.D. Figueiredo, Influence of spraying on the early hydration of accelerated cement pastes, Cem. Concr. Res. 88 (2016).

[2] B. Lindlar, L. Oblak, D. Lootens, C. Stenger, From tunnel to laboratory: scaling of shotcrete testing, in: X. et al. Beck (Ed.), 7th Int. Symp. Sprayed Concr., Sandefjord, 2014: pp. 282–286.

[3] L. Oblak, B. Lindlar, D. Lootens, Continuos monitoring of stength evolution of shotcrete, in: W. Kusterle (Ed.), Spritzbet. Tagung, 2012.

[4] B. Lindlar, C. Stenger, D. Lootens, Miniaturised laboratory spray method for shotcrete - New possibilities for the product development, mix design optimisation and quality control, in: W. Kusterle (Ed.), Spritzbet. Tagung, 2015.

[5] R.P. Salvador, S.H.P. Cavalaro, R. Monte, A.D.D. Figueiredo, Relation between chemical processes and mechanical properties of sprayed cementitious matrices containing accelerators, Cem. Concr. Compos. 79 (2017). doi:10.1016/j.cemconcomp.2017.02.002.

[6] A. Stauffacher, I. Galan, P. Juilland, M. Thumann, C. Stenger, A. Baldermann, F. Mittermayr, B. Lindlar, W. Kusterle, Influence of blast furnace slag and ultrafine limestone on early hydratoin of sprayed concrete, in: W. Kusterle (Ed.), Spritzbet. Tagung, 2018.

[7] J. Juhart, L. Briendl, F. Mittermayr, M. Thumann, R. Röck, W. Kusterle, Optimierte Eigenschaften von Spritzbeton durch kombinierte Zusatzstoffe, in: Spritzbet. Tagung, Alpbach, 2018.

[8] Österreichische Vereinigung für Beton und Bautechnik (ÖVBB), Richtlinie Spritzbeton, 2009.

Adhesion test with anchor bolts
Methodology for shotcrete adhesion tension on rock inside mining tunnels

Authors

Javier I, Guajardo
Mining civil engineer, Universidad de Santiago de Chile, Chile
javier.guajardoy@usach.cl

Juan A, Jarufe
Mining civil engineer, Universidad de Santiago de Chile, Chile
Juan.jarufe@usach.cl

Washington, Alegría
Hilti Chile, Chile
WashingtonElias.AlegriaFernandez@hilti.com

Sergio, García
Projects Vice President, CODELCO Chile, Chile
SGarc008@codelco.cl

Carmen P, Muñoz
Civil engineer, Universidad Andrés Bello, Chile
carmen.munoz@unab.cl

Abstract

The adhesion tension of shotcrete is a key factor of its supporting properties. Mainly, shotcrete failures as a reinforcement are caused by a low adhesion tension between substrate and shotcrete. The control of this parameter is a trial and error process which has historically hindered mining industries. Such reality is a consequence of the difficult application of current methodologies and the absence of a precise, fast and standardised procedure (at least in Chile). The validation of the proposed methodology was developed through force relations of adhesion tension between the in situ shotcrete core testing and test results following the current methodology through a laboratory. Also, the methodology application tried to induce a failure or breaking, mostly between shotcrete and substrate. Lastly, the study chief data source, besides laboratory applications, has its origin in the Underground Mining Project of Chuquicamata located in the northern of Chile.

Keywords

Shotcrete, Fortification, Adhesion, Mining tunel, Shotcrete

Introduction

It has been determined by researchers that shotcrete main failures take place by its lack of adhesion to rock substrate. Therefore, it is a key factor to consider during the support systems design [1]. Nowadays, there are various methodologies to measure adhesion tension of shotcrete, however, there is no trustworthy method to swiftly evaluate this parameter [2] (Australian Shotcrete Society, 2010).

At least 12.6% of mining accidents, according to evidence validated by the ChileanInstitute of Occupational Safety and Health and others organisations around the world, are related to rock fallings. Thus, shotcrete has an important role within any fortification system that seeks to prevent accidents [1].

Consequently, the main goal as to uphold an alternative in situ method to measure tension on shotcrete, with or without polymer fiber, over rock mass. The objective accomplishment will improve, for instance, the tunnels advance rate, shotcrete quality control as support element and excavation cycle. Such alternative and not regulated method of direct traction must be technically faster and more effective during its execution. Whitin this context, is determined the need of search a quality bolt, with the objective that this is not deformed in the tensile failure generating shearing in the contacts with the shotcrete, this led to the search of different providers, of which Hilti was selected as a standardized tool to aplly the methodology, based on its instrumental quality. The results were correlated with mining industry traditional methods for adhesion tension measurement.

Adhesion tension

Adhesion, according to the Australian Shotcrete Society (2010), is the feature that fixes the shotcrete to the rock substrate after its spraying. In other words, it refers to the bond strength between a shotcrete layer and adjacent rock substrate, specifically, in case of breaking. This parameter depends on many factors, among the most important are the mixing and operation conditions, cement paste quality, texture and grooving of aggregates, and substrate type, quality, and condition. The surface to be sprayed must be adequately clean and without considerable scraps in order to maximize adhesion development. It has been observed that a preliminary set up by water washing increase adhesion [2]. In Chile, there is no standard for adhesion tension between shotcrete and substrate trials, however, international methods, such as EFNARC or European Standard, are used[1].

Adhesion standards

Table 1 specifies the standards and measurement methodologies to adhesion endurance. In the absence of a standard international test, it is used as a reference the EFNARC method[2].

[1] It refers to Spanish standard UNE-EN-14888-4, 2008, EFNARC normative for adhesion tension measurement.
[2] European Federation of National Associations Representing of Concrete.

Table 1: Standards and methodologies for shotcrete adhesion tension, Australian Shotcrete Society, 2010			
Adhesion	Methods	Measurement parameter	Reference precondition
Initial Endurance	UNE-EN 1542 Swedish Standard 137243	Adhesion endurance (MPa) at 28 days	EFNARC (Table 2)

Table 2: Standards and methodologies for shotcrete adhesion tension, EFNARC, 1999, in MPa		
Adhesion Type	Minimal endurance of Adhesion to concrete	Minimal endurance of Adhesion to rock layer
Non-structural	0.5	0.1
Structural	1.0	0.5

Generally, the European standard methodology requires a field drilling with a core drilling machine (drilling equipment with diamond cylindrical bit) to get a core sample with a diameter between 50 and 100 millimeters and, according to UNE-EN 12504-1 [4], a length of over two times such measure. Then the core sample is transversely cut in such way that the contact area is near to half of the test tube with a length of 2 diameters. After this stage, the core is evaluate under the normative flatness. Later, it is fixed by an adhesive to two steel bases in order to apply the traction load on the superior base with a rupture equipment. And, by its relation with the core area, it is possible to know the adhesion tension.

The obtained data is evaluate depending on its rupture between two types, figure 1 shows a general diagram of the EFNARC test [5].

a) Tensile failure in linkage area
b) Indirect tensile failure in linkage area because the rupture strength overcomes the traction final value. Hence, the outcome exceeds the estimate.

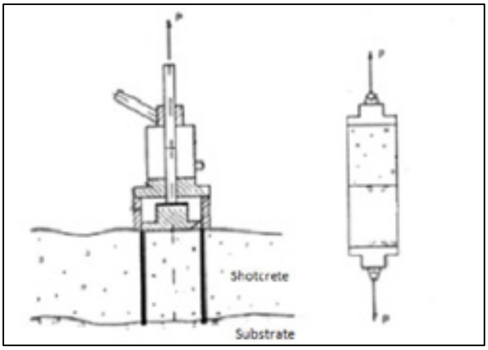

FIGURE 1: General diagram of the EFNARC test

In Situ Test of Adhesion Tension

The following methodology is designed to get in the field itself the magnitude of shotcrete adhesion tension.

The test comprehends three main stages: drilling, anchor installation and rupture. Distinctly, it is drilling in the interest area a shotcrete core between 50 and 100 mm that does not left the site. Later, it is installed an anchor in the core mid section that is pulled by a tensile failure equipment to induce an adhesion area breaking. Thus, the adhesion tension magnitude is obtained by the relation between the core area and the referred traction force (Figure 2).

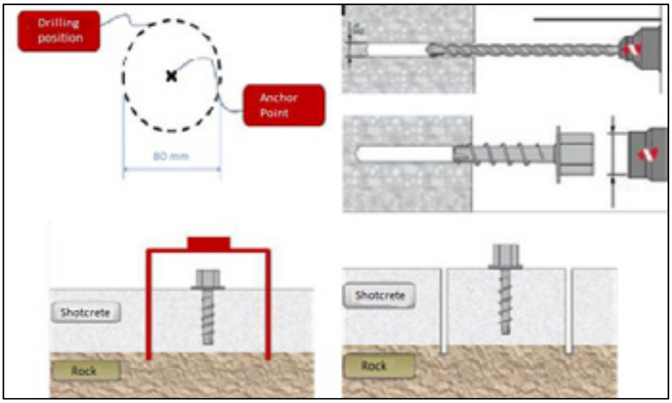

FIGURE 2: Methodology general diagram which details anchor preparation and setting in order to be extracted.

The methodology stands out for its simple execution, time reduction of results to one day and the possibility to select the type of breaking, such as shotcrete-rock, shotcrete-shotcrete, or for specific researching purposes (this study used the shotcrete-rock type).

Calculation of Adhesion Tension

Using a Hilti Anchor Tester a shotcrete cylinder fixed to the rock layer is extracted. At the time of adhesion failure the extraction force will be recorded (N) along with the extraction area in mm^2. The figure 3 illustrates the adhesion failure procedure to calculate the respective value. Once the magnitude of adhesion force is estimated (N[3]), the relation with core area will provide the adhesion tension in MPa. This method suppose that the applied load it is axially allocated in the shotcrete core area. The figure 4 shows field execution diagrams.

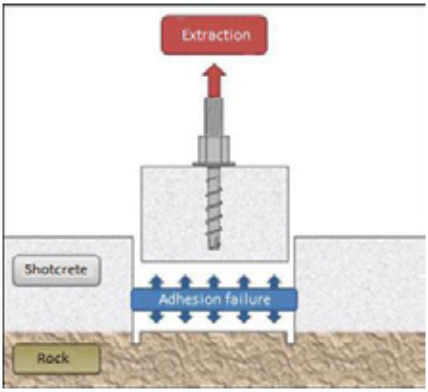

FIGURE 3: Shotcrete core extraction, profile view (6)

The following equation is used to calculate adhesion tension:

$$\sigma_a = \frac{F_a}{A}$$

[3] Newton, International System of Units, equivalent to 1 $\frac{kg*m}{s^2}$.

FIGURE 4: Field extraction of concrete core

Comparative Advantages

The alternative in situ methodology goal is to answer an actual challenge, swiftly giving outcomes and a field estimation of adhesion tension. This is a critical stage because once the core is extracted its properties undergo changes. The current mining picture look for a production increase, especially in the areas with a great demand of tunnels, within this context the proposed method advantages are:

- It is made in situ.
- Results in less than 24 hours.
- The traction test is mechanical (from this point it will be refer as AQ).
- There is no need to use adhesive, therefore, the measurement is faster [6] (Torres and other authors, 2017).
- There is no shotcrete failure conditions on its edges.
- It use similar equipment of others shotcrete tests.
- Bolt length variety for shotcrete thickness

Theoretical support

The theoretical validation of a balance of static forces is grounded in the Saint-Venant principle which states: "The tensile and traction limits of a lineal piece exclusively depend on forces" [7]. In other words, diverses traction systems which cause the same forces will create the same tensions and deformations.

When a force is applied on a structural element, the traction which appears in sufficiently distant points it not depends on the applied force. This phenomenon is illustrated by Figure 5 and it scientifically justifies the previous analysis [8].

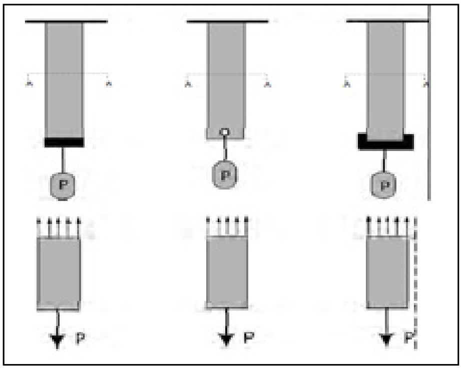

FIGURE 5: Principle of Saint Venant with different types of forces, Elaborated for this study purposes from Salazar Trujillo design, 2008.

Experimental Validation

Basic data statistics

Table 3 displays available information in the database to classify the adhesion tension values. This categorization will be used for comparison purposes between the tests under European normative for chemical anchoring and the alternative in situ method accordingly to several time terms.

Table 3: Database of Study Methodologies	
Item	Features
Location	It specifies the project physical site where the measurement was made, however, this parameter only will be for comparison purpose between the two tests.
Rock type	Each rock type is identified within a nomenclature system. It will be use only if it is strictly necessary.
Adhesion Tension	It is the adhesion tension magnitude expressed in MPa.
Failure type	It is the failure type at rupture A (1): shotcrete-rock; B (2) shotcrete-shotcrete; C (3) fragmentary rupture of shotcrete-rock.
Thickness	It shows the shotcrete thickness in cm.

Table 4 shows basic statistics of used data during the study, according to period and method, with a confidence of 95%. The approach with atypical data uses a box diagram regarding interquartile range and set its analysis limits according to table 4.

Table 4: Limits of anomalous data for adhesion tension					
Parameter	2012-2015 CAH (MPa)	2014-2016 EN (MPa)	2016 CAH (MPa)	2017 EN (MPa)	2017 CAH (MPa)
Inferior limit	0.25	0.15	0.25	0.16	0.25
Superior limit	1.75	1.27	2.25	1.06	2.25

The previous section set the basic statistics of Table 5 data, taking into account EN: European Normative and CAH: Chemical anchoring H.

Table 5: Basic statistics without anomalous data, in MPa					
Statistics	2012-2015 CAH	2014-2016 EN	2016 CAH	2017 EN	2017 CAH
Median	0.81	0.71	1.14	0.61	1.34
Mode	0.5	0.5	1.0	0.5	1.0
Standard deviation	0.34	0.18	0.39	0.16	0.35
Minimum	0.5	0.17	0.5	0.5	0.9
Maximum	1.5	1.13	2.0	1.0	2.0
Range	1.0	0.96	1.5	0.5	1.1

Table 5 illustrates the data erratic behavior in function of its range, nevertheless, the variation concentrates in the 0.5-1.5 MPa interval. A preliminary conclusion states that adhesion tension fluctuates in such range, hence, it concurs with the acceptable point of reference of 0.5 MPa.

A second analysis path will counterpose a test by direct traction (chemical anchoring) versus an in situ methodology by specific load. Each one of these values were acquired at a large scale mining project located in the northern of Chile. The trials covers the following failures types: A, shotcrete-rock; B shotcrete-shotcrete; and, C, partial rupture of shotcrete-rock. The shotcrete time was more than 28 days, meaning they were in a final stage. Moreover, the two variables analysis compares the adhesion tension of each value by European standards and in situ methodology. In the 18 sectors included in this study, although certain tendency is visible, there is no clear data correlation. Therefore, under such circumstances, it will be used others statistical elements for analysis, medians and standard deviation comparison, and individual parameter analysis of each one of the values.

The graphic 1 depicts through two parallel lines an analysis of each data value comprehending all tests with a 0.1 MPa tolerance margin. On the other hand, graphic 2 transforms those values of the same magnitude, using their average in order to avoid to use a same data twice. Thus, it will corroborate the previous data validation. For example, if three trials show a 1 MPa of chemical anchoring this will be replaced for one magnitude under the in situ method proper to the Chemical Anchore.

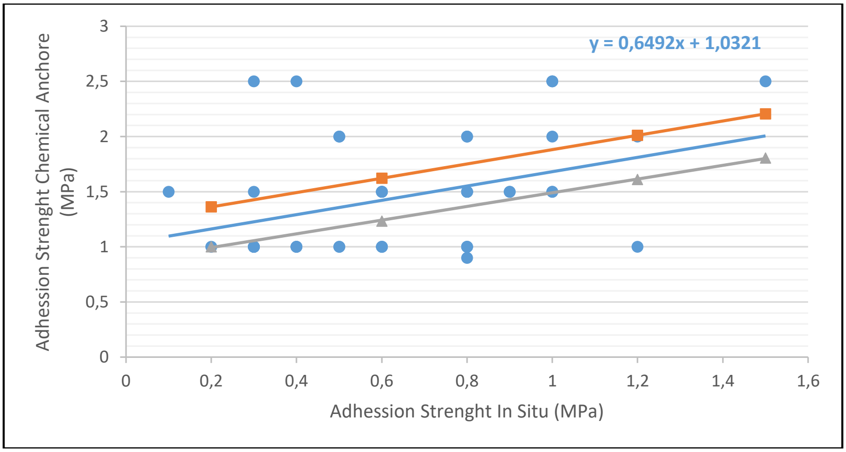

GRAPHIC 1: Two variables analysis of studied test sectors.

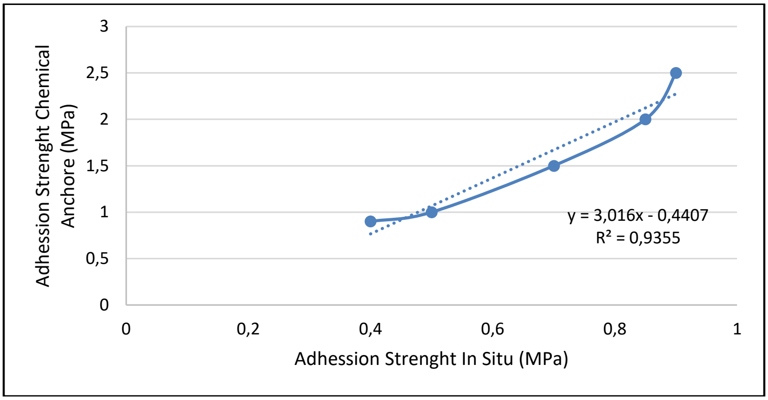

GRAPHIC 2: Two variables analysis of verified test

The data analysis stated a correlation coefficient between medians of 0.93, which validates the first conclusions, in case that both values will be perfectly correlated under a coefficient value of 1 [9].

The graphic 2 shows that medians of data groups are correlated. Such features define the relation between both adhesion tension methodologies (equation 2).

$$\text{Chemical Anchoring HY} \cong 2 * \text{In Situ Method (MPa)} \qquad (2)$$

The second equation take as references the information present in the graphic 1 and 2. Even though those data do not represent the same sectors, their comparison is grounded on the behavior of adhesion tension values and their closeness among data deviation.

The graphic 3 illustrates a medians comparison among the study five data groups which concludes at a 0.94. It also stated the formula behind such calculation.

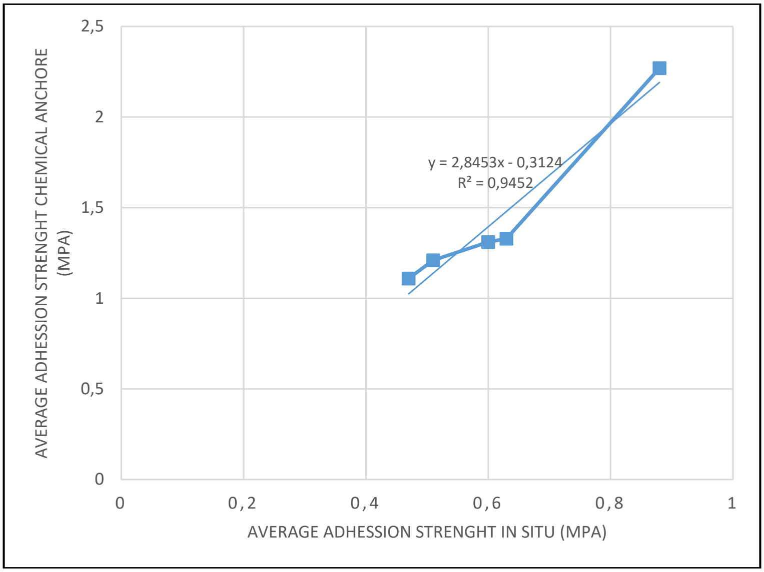

GRAPHIC 3: Comparison between adhesion tension medians.

It is important to explicit that adhesion tension was reported through its medians magnitudes because from a same area three samples were collected. The average of these samples will determine if such sector fulfills the study benchmark.

The in situ methodology gave additional value because it disclosed others effects. For instance, shotcrete permeability was uncovered during core drilling when water entered to the core. A second consequence refers to mixture weakness at the moment of anchor insertion because shotcrete suffers a surface fracture. Finally, the laminate presented application issues, features not referred under other methods.

Conclusions

The methodology can estimate values under the detection limit of 0.81 MPa. The performed tests had a 90% certainty, considering the real values as mode of tests of 0.8 MPa.

The results accuracy reaches a 47.7%, a parameter measured by a variation coefficient[4], a high magnitude for this methodology type.

---

[4] The variation coefficient is calculated as $CV = \frac{Sx}{X} * 100\%$,, namely the coefficient between standard deviation and data average (Zagal, and other authors, 2007).

The used equipment sensitivity concurs with European standard to measure adhesion tension.

Regarding the work range there is inconclusive background, nevertheless, the higher measured value by this methodology was 1.2 MPa.

The equipment of multinational company HILTI at recommended calibration assures a reliable performance level. Such instruments are wordly used in shotcrete tests application, for instance, at trials of early endurance.

Finally, it was not possible to identify a methodology sturdiness relation because the studied tests were not submitted to diverse experimental conditions to recognize the trial sensitivity under alterations.

On average, in order to data relation, the in situ methodology magnitude usually is half or a quarter of European standard methodology.

Concerning the two variables data analysis, it was possible to concentrate each of the collected data by direct traction tests, through chemical anchoring and in situ method. During this stage, it was noted the repetition pattern for a same magnitude, therefore they were given their average value to get a logical trend of data. It was procedure that gave a 0.88 correlation coefficient.

There is the possibility that the shotcrete core could modify its properties facing environmental factors proper of movement. In fact, a 40% of shotcrete cores fail because of transfer or during a test stage, for the above, the proposed method granted the adhesion tension results three time faster that the European standard and in a more effective way.

Bibliography

1. Seymour, B., and other authors. 2011.*A shotcrete adhesion test system for mining applications.* Washington, DC : NIOSH, 2011. Technical Report
2. Australian Shotcrete Society. 2010.*Shotcreting in Australia: Recommended Practice.* 2nd Edition. Penrith : Australian Shotcrete Society, 2010.
3. UNE-EN 12504-1:2009. Ensayos de hormigón en estructuras. Parte 1: Testigos. Extracción, examen y ensayo a compresión.
4. European Specification for Sprayed Concrete. 1999.*Guidelines for Specifiers and Contractors.* Surrey : EFNARC, 1999
5. Torres, Luis and Alegría, Washington. 2017.*Ensayo de Adherencia Hilti: Shotcrete-Roca.* Santiago : HILTI, 2017. Informe Técnico.
6. Miquel Canet, Juan. 2012.*Resistencia de Materiales y Estructuras.* Barcelona : CIMNE, 2012
7. Salazar Trujillo, Jorge Eduardo. 2007.*Resistencia de Materiales Básica para Estudiantes de Ingeniería.* Manizales : Centro de Publicaciones Universidad Nacional de Colombia, 2007

8. Zagal, Erick and Sadwawka, Angélica. 2007.*Implementación del Sistema para la Validación de los Métodos de Análisis y Mediciones de Laboratorio en Suelos y Lodos*. Chillán : Universidad de Concepción, 2007. Technical report.
9. Instituto del Cemento y del hormigón de Chile, 2015, Guía Chilena de Hormigón Proyectado Shotcrete, Second Edition ICH:2015

8th INTERNATIONAL SYMPOSIUM ON SPRAYED CONCRETE – Modern Use of Wet Mix Sprayed Concrete for Underground Support
– Trondheim, Norway, 11. – 14. June 2018

DURABILITY OF SPRAYED CONCRETE FOR ROCK SUPPORT A TALE FROM THE TUNNELS

Per Hagelia
Tunnel and Concrete Division, Norwegian Public Roads Administration, Norway
per.hagelia@vegvesen.no

SUMMARY

Modern steel fiber reinforced sprayed concrete used for rock support is generally regarded as a durable construction material. However, long-term durability data are scarce. The main durability challenge in Norway is related to sulfate attack in the Alum Shale environment and a combined microbial and abiotic attack in the subsea environments. In previous studies, we found that Alum Shale still represents a concern and that biofilm accumulations in subsea tunnels had caused localised loss of cross section and severe steel fiber corrosion after few years in service. This paper discusses the effects of four categories of ground waters, hydrogeology and mix design (w/b-ratios 0.40-0.50) at concrete ages up to about 25 years. Sprayed concretes thinner than 80 mm suffered some degradations in aggressive environments, being accentuated in areas characterised by a poor and permeable adhesion zone. Cement paste degradation and steel fiber corrosion were mainly unimportant in cases where sprayed concrete layers are thicker than 100 mm. It is significant that reactions causing cement paste degradations are mainly independent of fiber type. A minimum thickness of 100 mm, w/b-ratios = 0.40 and low capillary porosities (< 20 %) is regarded as sufficient for long lifetime in aggressive grounds.

INTRODUCTION

Durability is the ability of a material or structure
to withstand its design life without significant deterioration.
Yunus Ballim

Durability of sprayed concrete used for rock support in tunnels represents an important research topic. The Norwegian road authorities are responsible for over a thousand tunnels, including more than thirty subsea tunnels and yet others in aggressive sulfide bearing ground. Several more subsea tunnels are currently under construction and others are at the planning stage. Rock reinforcement in Norwegian tunnels always comprise fiber reinforced sprayed concrete and rock bolts. In the most unstable rock masses reinforced sprayed concrete ribs are employed, whilst cast concrete linings are rare. The engineering classification for rock masses and the design of rock support is based on the Q-system invented by Barton and co-workers at the Norwegian geotechnical institute (NGI) [1,2].

However, the Norwegian Public Roads Administration (NPRA) has specified a more conservative design, involving a thicker sprayed concrete than NGI's Q-chart. There has been a development regarding minimum thickness of sprayed concrete, from initially 50 mm (e.g.

the Q-system) through 60 mm and 80 mm, irrespective of environmental load [3,4,5]. Recently NPRA has specified a 100 mm minimum thickness for aggressive subsea environments [6]. This is due to the need to cope with potential durability problems in the long run [5]. In particular, NPRA has specified a 100 years design lifetime for the rock reinforcement since 2005-2010. Regarding fiber type, there has also been a significant amendment in the code of practice over the years. Already in 1997 fiber corrosion due to chloride penetration was regarded as a durability challenge notably in thin sprays [3]. In 2007, NPRA specified polymer fibers of non-corrosive materials "where large rock deformations and/or where a highly corrosive exposure may be expected (i.e. in salt water sections in subsea tunnels)". At the same time, the contractor was allowed to be free to choose between steel or polymer fibers in any environment (cf. [5]).

This new regulation caused a rather quick shift from steel fiber reinforcement to extensive use of polypropylene (PP-) fibers in both subsea tunnels and freshwater tunnels. However, due to rather significant rebound during spraying operations, it was discovered that macro-PP-fibers were released into the water environment, ultimately polluting the sea. Hence, due to the severity of the problem and in light of global contamination of the sea by plastic materials, the Norwegian Environment Agency demanded restrictions on runoff of PP-fibers. In reality, the NPRA was not able to meet with these requirements, since no available technology has yet been able to cope with this problem in an appropriate way in a rainy country. Faced up with this situation the NPRA in 2015 introduced a general ban on macro-PP-fibers in all tunnel work and return to steel fiber reinforcement in all sprayed concrete used for rock support (cf. [7]). This was possible also from a durability point of view, because accumulated evidence from long term monitoring of several subsea tunnels clearly suggested that durability would not be at stake provided the minimum thickness of steel fiber reinforced sprayed concrete for rock support was increased to 100 mm. Such an increased thickness would be favourable for the preservation of long-term integrity of the cement paste matrix, however, being *independent* of the fiber type used [8]. Steel fiber corrosion is a consequential damage of cement paste degradation.

There is a great interest in durability data in the international community; however, few long-term studies have been undertaken. The International Tunnelling and Underground Space Association (ITA) has requested durability data from long-term exposure of sprayed concrete, however, stating that the evaluation of durability of sprayed concrete linings in underground works "turned out to be an extremely complex subject". The ITA Working Group 12 focused much on strategies for future work and recommended the use of *four main durability aspects* pertaining to data collection and interpretation [9]:

1. *Complete information about the exposure situation* (i.e. chemical- and mechanical loads based on ground water chemistry and rock mass characterisation, respectively).
2. *All necessary sprayed concrete material information to be able to quantify exposure resistance parameters* (documentation of the mixes used, spray thicknesses, presence of structural inhomogeneities etc.).
3. *Duration of exposures*, if necessary, split on the local set of processes (time elapsed since a defined diagnosed deterioration process has influenced the spray, involving mechanical loads and deformations, freeze/thaw cycles, vibrations, impacts and abrasive action, chemical attack from ground water and other liquids along with aggressive components in the atmosphere).
4. *Design basis and lifetime expectancy* compared to specifications and work execution (the balance between requirement and design, f. ex. permanent linings require more than preliminary).

Presently, an international state of the art report regarding sprayed concrete durability is still missing. However, a great number of data has accumulated through tunnel investigations and research efforts promoted by the Norwegian Public Roads Administration. Our data represent:

1. Tunnel exposure environments, involving freshwater, sulfate bearing ground waters and subsea ground waters under variable water loads and rock mechanical conditions. The selected tunnels were representative regarding traffic conditions.
2. Variable "resistance" parameters such as concrete mix design and thicknesses.
3. Duration of exposures varying from about 2 to 25 years for well-defined degradation mechanisms, being treated separately.
4. Design basis as permanent linings with lifetime expectancy corresponding to 100 years.

Regarding lifetime expectancy, a 50 years' service life was apparently the design basis for tunnels constructed up to at least 2000 and perhaps even later. However, in any case an empirical study of durability development of representative sprayed concretes should in any case provide important constraints on optimal concrete mixes and structural design for 100 years' service life.

Objectives of this paper

A detailed and comprehensive summary report regarding durability of sprayed concrete was prepared as part of the R&D program Durable Structures [8]. The report summarises results from previous investigations [3,4,10,11,12,13,14,15,16,17,18,19] along with recent results on sprayed concrete durability from Mannvit within the umbrella of Durable Structures [20]. The objectives of the present paper were to:

- Give an outline of environmental loads acting on sprayed concrete for rock support
- Present results from "Durable structures" with a main focus on the evidence behind NPRA's recent specification of a minimum spray thickness of 100 mm exposed to aggressive subsea environments
- Discuss the durability development in view of spray thickness, steel fiber corrosion, adhesion, concrete mixes and fiber types (e.g. steel and PP-fibers) based on evidence from several exposure environments

ENVIRONMENTAL LOADS ACTING ON SPRAYED CONCRETE

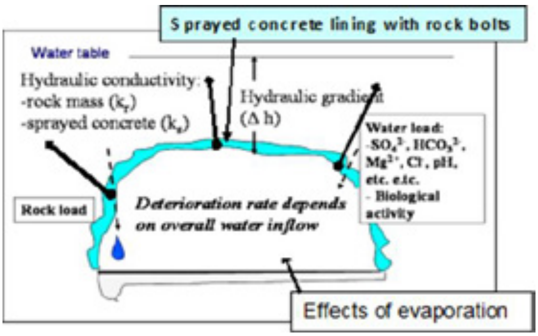

Figure 1. The main environmental loads acting on sprayed concrete used for rock support in tunnels.

The environmental loads acting on sprayed concrete used for rock support are complex and differ in many respects from the loads acting on concrete bridges and other cast concrete structures above ground. This is mainly because tunnel concrete is in direct contact with the surrounding rock mass, representing an inhomogeneous and uneven substrate reflecting different rock mass properties (crack frequencies etc.), hydrogeological conditions and different chemical environments. Quite frequently, the overall exposure conditions vary over short distances. The principal exposure conditions, which may influence the durability development, are (Figure 1):

- Hydrogeological conditions and water pressure
- Rock mass stability and mechanical load
- Mineral composition and possible aggressives within the rock mass
- Chemical composition of the ground water
- Conditions within the tunnel space, including tunnel fumes, de-icing salts and the possibility of draught and increased aggressiveness of water due to evaporation

In most tunnels leakage waters affect sprayed concrete both from the adhesion zone to rock mass as well as from the outer surface. In tunnels with an inner lining, the sprayed concrete for rock support is screened from the potential effects of tunnel fumes and evaporating waters, whilst otherwise conditions within tunnel space may have an impact on the durability development.

The Exposure Classes in NS EN 206, including the national annexes, is a useful tool for characterising the ambient chemical environment and potential for steel corrosion. However, the standard does not refer to the possible effects of hydrogeological environment and rock mass properties. Moreover, influence from biodegradation and increased aggressiveness due to evaporating waters is not mentioned. This has been discussed further in [16]. In the present paper, we refer to chemical exposure classes and corrosion classes as based on water chemical analysis and other tunnel data. All data are available in the summary report from the R&D project Durable Structures [8].

RESULTS FROM THE R & D PROJECT "DURABLE STRUCTURES"

Sampling and methods

The investigated tunnel objects were chosen according to the following main criteria:

- The tunnels should encompass typical variations with respect to hydrogeology, ground water chemistry, conditions in tunnel space and rock mass conditions, hence representing "all" exposure conditions in Norwegian tunnels.
- The sprayed concretes should be regarded as "modern", e.g. made by the wet-method technology under a modern quality regime and good workmanship
- Reliable documentation regarding concrete mix design "as built" should be available, representing material properties typical of modern wet-sprayed concrete
- The sprayed concrete ages should represent a longest possible time span
- The degradation mechanisms should be representative and relevant regarding potential for a reduced bearing capacity
- Some tunnels should have been investigated in previous durability projects
- The tunnels should represent a relevant variation regarding degradations

At an early stage, NPRA concluded that sprayed concretes from before 1983 should be regarded as obsolete technology and were not included in this study. Our detailed investigations were focusing on nineteen objects, which met the above criteria. The concretes studied were ranging from 2 to 27 years old, yet with some differences within each main exposure category.

Due to budget constraints, it is in reality impossible to obtain statistics representative of all sprayed concrete. Instead, our selected tunnel locations represented well-documented typical variations. All investigated tunnels were screened over most of their length, whilst few locations were chosen for detailed sampling, hence representing typical potential durability problems encountered. Several locations have been investigated more than once over the years. Dry tunnel sections (albeit with some humidity) were characterised by insignificant degradations, being suggestive of high durability and long service life. They are underrepresented in our data. In this paper we investigate the overall design requirements due to effects of well-defined environmental loads, whilst the establishment of total costs related to affected and not affected concretes is a separate problem for the tunnel managers to take care of. Our investigations comprised the following laboratory methods:

- Standard concrete tests (compressive strength, fiber contents, porosity measurements, chloride contents, carbonation depth)
- Structural analysis with emphasis on polarising microscopy of thin sections from concrete cores, also assisted by Scanning electron microscopy (SEM) and microchemical analysis
- Mineral identification of small friable samples representing precipitates, biofilms and biominerals by X-ray diffraction (XRD)
- Chemical analysis of leakage waters collected from different settings (rock water, waters interacting heavily with sprayed concrete etc.), from the concrete sampling sites or as close to them as possible

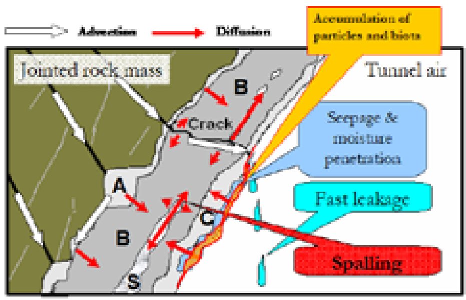

Figure 2. Schematic cross section through water bearing rock mass and sprayed concrete. Zone A = degradation adjacent to rock mass, B = sound internal concrete, C = outer degraded concrete, S = spalling zone. Spalling might as well take place along the rock/concrete interface.

Concrete cores, spall samples and friable material were collected, representing the entire cross section of the sprayed concrete layer, the adhesion zone and mostly some of the rock behind. The sampling strategy was chosen in order to cover both degrading concretes and sound concrete in accordance with the general "anatomy" of attack as defined by zonation (Zones A, B, C and S, see Figure 2). Microscopy (including SEM) and XRD were very useful techniques for establishing the state of cement paste degradations and the degree of steel fiber corrosion in each zone, yet as seen in light of mesoscale observations. The degree of degradation (A, C and S) varied at the expense of sound concrete (B), representing a measure of the total state of degradations. Also the permeability and eventual deposits on the adhesion zone were characterised. The results were finally seen in light of variable hydrogeological conditions, water chemical exposure conditions, concrete mixes, spray thicknesses, adhesion and other concrete properties.

Table 1 gives a summary of deterioration mechanisms found in Norwegian sprayed concrete for rock support, their potential effects and associated typical environments. Alkali aggregate reactions and other aggregate related degradations do apparently not occur, mainly due to good practice of aggregate screening.

Table 1: Deterioration mechanisms encountered in Norwegian sprayed concrete for rock support. S = steel fiber, P = polypropylene fiber, C-S-H = calcium silicate hydrate (continued overleaf).

Type of degradation	**Potential effects on cement paste**	**Potential effects on fiber reinforcement**	**Exposure environment and agents**
Ordinary surface carbonation	Degradation of portlandite & C-S-H in surface region. Low permeability. pH ~ 8-9	S: Corrosion as consequential damage P: No effect	Atmospheric CO_2 All environments
Internal carbonation: Popcorn calcite deposition (PCD). Related to decalcification. Trough solution process	Internal degradation of portlandite & C-S-H Formation of calcite spots in Ca- poor silica gel. Loss of strength. Increased permeability pH ~ 8-9	S: Corrosion as consequential damage P: No effect	Dissolved HCO_3^- in ground water penetrating into concrete in many environments. Depending on water pressure
Decalcification by through solution process	Ca -leaching from portlandite & C-S-H. Loss of strength Increased permeability pH ~ 8-12	S: Corrosion as consequential damage P: No effect	Dissolved carbonic acid or ordinary fresh ground water with HCO_3^- penetrating into concrete. Depending on water pressure
Chloride penetration. Through solution process	Slight loss of strength. pH ~ < 10 to > 13	S: Corrosion as consequential damage P: No effect	1) Subsea environments. Depending on water pressure. Brackish to seawater-like ground waters 2) De-icing salts
Thaumasite sulfate attack (TSA). Through solution process, frequently related to decalcification and PCD	Degradation of portlandite & C-S-H. Loss of strength Increased permeability pH ~ 8-12.	S: Corrosion as consequential damage when PCD is present P: No effect	Dissolved sulfate and bicarbonate in ground water penetrating into concrete. Alum shale & subsea environments. Depending on water pressure
Acid attack (commonly H_2SO_4) Trough solution process	Fast degradation of portlandite & C-S-H, significant strength reduction and much increased permeability pH < 2 to 5	S: Corrosion as consequential damage P: Not studied. Likely minor effects	Related to sulfide oxidation and dissolution of certain sulfates. Alum shale and sulfide bearing gneiss, notably after drawdown of ground water table

Type of degradation	Potential effects on cement paste	Potential effects on fiber reinforcement	Exposure environment and agents
Magnesium penetration Trough solution process	Mg replacement of Ca in C-S-H and formation of $Mg(OH)_2$ Loss of strength. Increased permeability pH ~10	S: Corrosion as consequential damage P: No effect	Subsea tunnels notably at high water pressure in rock mass with high hydraulic conductivity
Biofilm with Mn & Fe bacteria combined with ingress of aggressive ions from saline ground water NB: Not all biofilms cause damage.	Degradation of portlandite & C-S-H, formation of Mn-Fe biominerals, ± TSA, PCD & Mg-attack. Loss of strength and outer mass loss. High permeability. pH ~5.5-7.5	S: Severe corrosion P: Not documented in Norway (see [21] for detrimental effects of photosynthetic microbes and algae)	Some subsea environments. Other environments yet to be investigated
Mechanical loads	Macro and micro cracking. Increased permeability beyond level expected by w/b-ratio of concrete mix	S: Corrosion as consequential damage P: No effect under ordinary loads	Instable rock mass: mainly where designed rock reinforcement is insufficient
Frost action (regarded as of minor importance [4])	Macro and micro cracking, mainly observed in old «unmodern» thin sprayed concrete	S: Corrosion as consequential damage P: No effect	Freeze-thaw cycles. Frost Index

The freshwater environment (XC2-XC4, XD1-XD3, X0)

The great majority of Norwegian tunnels are exposed to ion-poor fresh ground waters. *The degradation mechanisms were ordinary surface carbonation and occasional effects of de-icing salts.* Long-term data representing conditions at 5 to 26 years were collected from nine tunnels, some of which were freshwater sections in subsea tunnels. Spray thicknesses varied from 39 mm to 180 mm. 39 concrete cores were extracted and 25 thin sections were prepared for microscopy.

Sprayed concrete mixes in the selected tunnels varied. Cements were rapid setting and standard Portland cements, yet also including one case with a standard fly ash cement, using either water glass or alkali free setting accelerators. The w/b- ratios were ranging from 0.41 to 0.49, with binder contents from about 450 to 570 eq.kg/m^3. The silica fume contents varied from 1% to 14 % by cement weight, commonly around 5 %. The steel fiber contents were ranging from 19 to 46 kg/m^3 with compressive strengths 27 to 75 MPa.

Exposure conditions. The bedrock was predominated by various granitic gneisses, amphibolite, pegmatite, phyllite and syenite: all of which were without problematic minerals. Water loads in terms of flow rates were mostly small. Rock mass ratings in terms of Q-values were not available. Fifteen water samples were analysed, typically showing low ion contents and pH ranging from around 7 to 8 (occasionally even higher).

Effects of degradations. Surface carbonation due to atmospheric CO_2 was generally not deep and affected a maximum of 20 mm in a sample after 15 years of exposure to tunnel fumes (Figures 3 and 4). In contrast, carbonation of sprayed concrete behind inner concrete linings reached only 1-1.5 mm after 13 years in service. There were no sign of degradations taking place from the adhesion zone, although the adhesion zone varied from permeable to non-permeable. A single case showed internal carbonation (PCD) affecting 2.5 mm adjacent to a water permeable contact zone in 15 years old sprayed concrete with w/b = 0.47. Apparently, the carbonation depths dropped towards increasing w/b-ratios in exposed concretes. This seems at odds with mainstream results, but may reflect a higher degree of hydration at higher w/c-ratios, which should result in a denser cement paste. We frequently see residual clinkers in sprayed concretes with w/b-ratios < 0.45. Figure 4 demonstrates that the highest capillary porosity correlated with deeper carbonation in concretes exposed to tunnel fumes, which assists to the above contention. Yet samples devoid of micro cracks tend to have less deep carbonation.

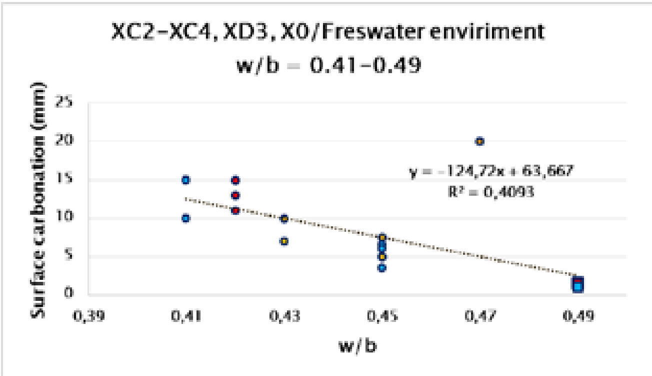

Figure 3. Surface carbonation depth apparently decreased with increasing water/binder ratios (v/b). Symbol colours: red = many micro cracks, beige = intermediate micro cracks & blue = few or no micro cracks as seen in thin sections.

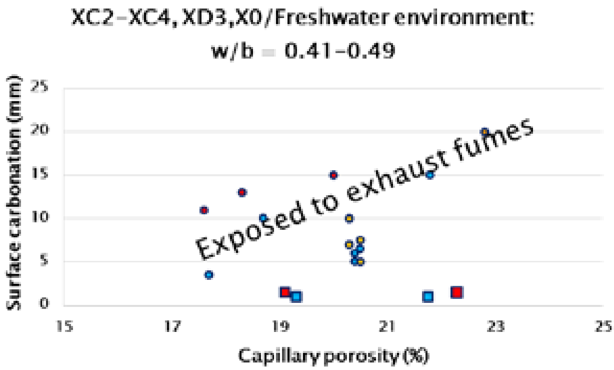

Figure 4. Exhaust fumes had caused a relatively deeper surface carbonation (circles) compared to non-exposed (squares) behind inner linings. Symbols as in Figure 3.

De-icing salts may potentially influence sprayed concrete. However, our few chloride profiles from exposed concrete suggest that effects of de-icing salts are absent or might reach concentration higher than 0.1 % of concrete weight in the outermost 10 mm.

Steel fiber corrosion. There was no sign of steel fiber corrosion in these concrete cores with their intact cement paste matrix. Fiber corrosion was marginally developed within the portions affected by surface carbonation, showing no sign of significant weakening of the fibers up to 27 years in service.

Age and accumulated traffic loads. Due to the complexity of exposure conditions and mix design etc., it was not possible to establish a clear aging effect, such as increasing degree of carbonation year by year. We also tested for the effect of accumulated traffic loads by multiplying age with annual traffic loads (vehicles per day), without finding any correlation.

In conclusion, concrete durability in the freshwater environment was by no means alarming, suggesting no problem with concrete thicknesses of minimum 80 mm using concrete mixes based on CEM 1 with w/b-ratios of 0.41 to 0.49. Regarding sprayed concrete, being screened from traffic loads in the freshwater environment, it has been suggested that 100 years' service life seems realistic [22].

Mildly acidic environment (XC2, XD0, XA1)

Sprayed concrete in this environment was studied in a service tunnel leading down to a hydro-power plant. *The degradation mechanism involved surface carbonation and effects of sulfur attack with occasional surface deposition of Na-sulfate (thenardite).* Samples from the tunnel were collected at concrete ages 13 and 16 years, being 9 concrete cores and some precipitates. The spray thicknesses varied from 20 mm to 110 mm. 13 thin sections were prepared and studied in in collaboration with BRE-Garston, UK [13].

The sprayed concrete mix was based on a 1984 Portland cement with 20 % fly ash (MP20) using water glass as setting accelerator. The w/b-ratio was about 0.50 and the cement contents were assumed to be somewhat higher than 450 eq./kg/m^3. The concrete was fiber free and strength and other standard concrete tests were not performed.

Exposure conditions. The bedrock in the area is characterised by presence of a sulfide bearing black shale of eocambrian age (less aggressive than Alum shale). Water chemistry in four samples showed elevated sulfate concentrations (102-112 mg/L) and pH = 5.66- 6.06, reflecting some contribution from sulfide oxidation. The water load was generally small at the time of sampling, with most surfaces being rather moist. However, there was clear evidence of earlier somewhat heavy water loads, as seen from calcite and thenardite deposits on the concrete surfaces. Rock mass rating data were not available.

Effects of degradations. Surface carbonation was not deep, ranging from 1 to 13 mm. Adhesion to the rock mass behind varied from very good without precipitates to somewhat weak and permeable with calcite and ettringite deposits. Thaumasite sulfate attack occurred in a very thin 20 mm thick spray affecting 7.5 mm adjacent to the contact with rock mass, whilst all of the thicker sprays were mainly unaffected.

The effects of mildly acidic tunnel environment on more modern sprayed concrete should be further investigated in road tunnels crossing through eocambrian black shale.

Alum shale environment (XC2-XC4, XD0-XD3, XSA)

Sprayed concrete in Alum shale environment was studied in two road tunnels and one road cut within the city of Oslo. *The degradation mechanisms associated with Alum shale are thaumasite sulfate attack (TSA), leaching and internal carbonation (Popcorn calcite deposition, PCD) with effects of sulfuric acid.* Samples were collected at concrete ages ranging from about 2 to 22 years and inspection of the sprayed concrete in the road cut even at age 27 years. The spray thicknesses varied from about 30 mm to 375 mm, most commonly between 50 and 130 mm. Altogether 23 concrete cores were extracted along with three spalls and loose debris material and precipitates. 46 thin sections were examined by polarising microscopy and/or SEM and loose material were analysed by XRD, first in a collaboration with BRE-Garston, UK (summarised in [12,13]) and later on as part of Durable Structures (Mannvit [20]).

The sprayed concrete mixes were based on Sulfate Resisting Portland Cements (SRPC) with added silica fume ranging from 5-10 % by cement weight. Water glass was used except for alkali free accelerator in one of the tunnels. The w/b-ratios varied from 0.40 to 0.50, with cement contents about 500-530 eq./kg/m^3. All concretes had steel fiber reinforcement. Compressive strengths varied from about 30 to 46 MPa in concretes exposed for 16 to 22 years. There was usually a certain extent of visible cracks through thin concrete, whilst thicker layers appeared to be mainly devoid of cracks.

Exposure conditions. Alum shale is a black shale of Cambrian to Ordovician age, which historically has caused great problems regarding extensive sulfate attack, steel corrosion and ground heave. This is due to abundant sulfide minerals (pyrite and minor monoclinic pyrrhotite), which upon oxidation liberated high concentrations of sulfate and under certain circumstances sulfuric acid. This also leads to dissolution of calcite and enhanced bicarbonate concentrations. Analysis of several water samples showed sulfate concentrations ranging from 300 to 2000 mg/L with pH ~ 7. However, we have also discovered weathering minerals such as jarosite and ferric hydroxide at the adhesion zone, which reflects much lower local pH (2-3). Q-values were about 0.1 to 1.

The effects of degradations. Surface carbonation varied from almost zero to about 4.5 mm depth, with no clear relationship to concrete age, w/b-ratio and micro cracks (most of the examined concretes had few or no micro cracks). <u>Deterioration reactions responding to Alun shale ground water are two-fold</u>: 1) variable degree of Ca-leaching, internal carbonation (PCD) and TSA in the zones adjacent to the contact with Alum shale and 2) localised sulfuric acid attack on the adhesion zone, leading to weakening and spalling along the interface. Where adhesion to the shale is very good, often underneath quite thick sprayed concrete, there was almost no sign of degradation due to TSA after 22 years of exposure [23], whilst sprayed concrete with open and permeable contact zones frequently showed extensive degradations at younger ages (Figure 5). Deterioration due to TSA, Ca-leaching and PCD also tended to increase with increasing w/b-ratio, although being more influenced by the adhesion properties. The most degraded sprayed concretes documented in Figure 5 were over 100 mm thick, with w/b = 0.50 and highly permeable adhesion zones, some of which carried sulfuric acid. Also sulfate laden ground water on very tight adhesion zones had caused significant transformation of the cement paste.

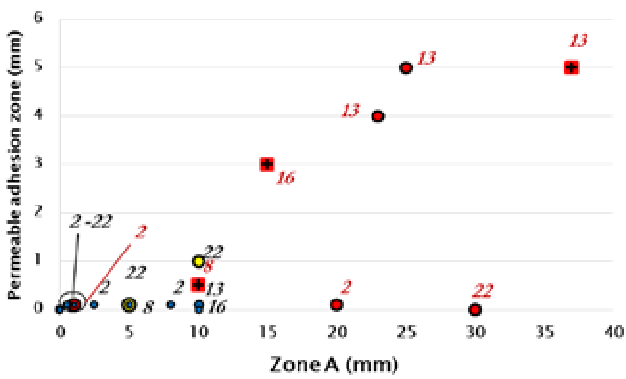

Figure 5. Effect of permeable adhesion zone (width in mm) on deterioration of concrete adjacent to Alum shale (Zone A). Red squares with cross = influence of sulfuric acid, red circles = influenced by sulfate laden ground water, yellow = slightly permeable adhesion zone, blue = none-permeable adhesion zone. Numbers refer to concrete age at time of sampling.

Age versus degradation. Our long term monitoring within single locations *does* show increasing degradation over time, yet at different paces. The different paces are largely governed by the initial thicknesses of the spray (see Figure 6) along with variable access to sulfate and acid laden waters, being channelized along the adhesion zone.

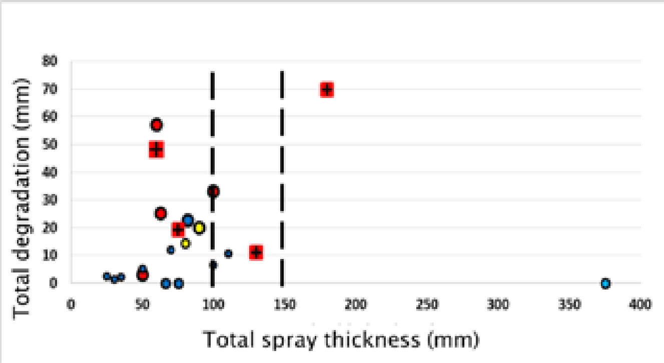

Figure 6. Effect of total deterioration plotted versus total spray thickness. A minimum 100 mm thick spray should be sufficient for long service life unless the adhesion zone is severely affected by sulfuric acid. The line at 150 mm represents the thickness required in typical Alum shale rock mass with Q-values between 0.4 and 1.0. Same symbols as in Figure 5.

Steel fiber corrosion. Steel fiber corrosion was severe and completely destructive where internal carbonation and TSA was extensive, e.g. powderised concrete related to spalling [12]. Otherwise, marginal to destructive fiber corrosion was found in most concrete with effects of PCD, yet being rather insignificant in association with surface carbonation [8].

Capillary porosity measurements of some selected cores (16 and 22 years old), with variable degradation across the entire sprayed concrete layer, showed that samples with capillary porosity less than 18 % were not significantly deteriorated adjacent to Alum shale, whilst when > 20 %, the transformation (e.g. in Zone A) reached 14 mm even in concrete with w/b = 0.40.

It may be concluded that sprayed concrete with w/b-ratio = 0.40, low capillary porosity in the order of 18 % and a minimum spray thickness of 100 mm will resist aggressives derived from Alum shale for a long time. There is still an uncertainty related to the long-term effect of acidification. Although thicker sprays certainly represents a lower oxygen permeability than a thin spray, both with respect to bulk past O_2-diffusion and fewer cross cutting cracks, the effects need to be further monitored. As yet, we have not studied the effects of very low pH-waters. However, systematic pre-grouting can certainly inhibit drawdown of the ground water table, which otherwise can severely increase the acidification potential in Alum shale [24].

Subsea environment (XC2-XC4, XS3, XD1-XD3, XA2-XA3)

Sprayed concrete in subsea tunnel sections characterised by saline ground water loads was investigated in six subsea road tunnels. *The degradation mechanism were governed by composite abiotic attack due to ion-rich saline ground waters and variable effects of Mn-Fe-rich biofilm. This involved penetration of chloride, magnesium, sulfate and bicarbonate; leading to breakdown of portlandite, magnesium substitution of C-S-H, leaching of the cement paste with internal carbonation (Popcorn calcite deposition) and thaumasite sulfate attack. Variable acidification within and underneath Mn-Fe biofilms caused variable weakening and material loss on the outer surface region.*

Samples were collected at concrete ages ranging from 5 to 26 years, some of which are based on [3]. The spray thicknesses varied from about 35 mm to 200 mm. Altogether 56 concrete cores were extracted along with four spalls and many loose debris materials and precipitates. 132 thin sections were examined by polarising microscopy and/or SEM, whilst minerals in debris and precipitates were identified by XRD (details given in [8,17].

The sprayed concrete mixes were mainly based on rapid setting Portland cements and standard Portland cements with added silica fume ranging from 1 to 14 % by cement weight. Water glass or alkali free accelerators were used. The w/b-ratios varied from 0.40 to 0.47, with cement contents about 510 to 580 eq./kg/m^3. All concretes had steel fiber reinforcement. Compressive strengths varied from about 30 to 63 MPa in concretes exposed for 5 to 22 years. There was usually a certain extent of visible cracks through thin concrete, whilst thicker layers appeared to be mainly devoid of cracks.

Exposure conditions. Subsea saline ground waters are ion-rich, ranging from brackish to mainly sea-water like salinities. Yet, the waters are chemically modified due to some interaction with the rock mass. Analysis of about 40 water samples showed sulfate, Cl and Mg concentrations about 500 to 3300 mg/L; 5000 to 50 000 mg/L and 570 to 1420 mg/L, respectively. The highest concentrations were due to evaporation within the tunnel space. The pH was commonly slightly alkaline (7.5 to 8). However, pH in some biofilms were 5,5-6,5 to neutral, reflecting temporal changes at some individual sites (see [8,17]), whilst pH = 7-7.5 was typical of less or non-aggressive biofilms. There was some indication that degradations were small where the sprayed concrete thicknesses were designed in light of Q-values according to Statens vegvesen's procedures (e.g. [6]).

Effects of degradations. Surface carbonation varied from about zero to 25 mm in sprayed concrete exposed to tunnel fumes, whilst being significantly less deep in unexposed concrete behind inner linings (0-4 mm). There was an apparent tendency for deeper carbonation related to accumulated traffic (age x vehicles per day), whilst no clear effect related to w/b-ratio could be found. The effects of abiotic attack, mainly acting within concrete adjacent to the adhesion zone and localised biofilm attacks resulted in focused weakening and local loss of material. The degree of weakening and loss was most effective where both abiotic and biological activity operated simultaneously (see [17]).

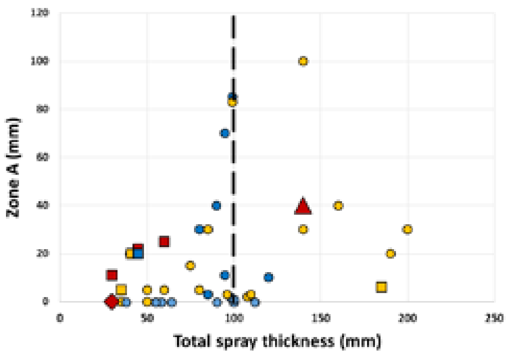

Figure 7. Degradations in Zone A with symbols for abiotic attack: Circles = no degradation or very diffuse effect of Mg ingress and internal carbonation (no structural effects). Squares = domains with leaching, internal carbonation, TSA and Mg ingress (some weakening of the paste). Triangle = effects of acid from the contact zone with structural weakening (very rare case where biofilm, acted from behind the spray. *Adhesion zone characteristics*: Red = with influence of mild acid, orange = precipitation of brucite and calcite (no acid), blue = no precipitation.

Figure 7 shows the effects of degradation acting from the adhesion zone. With the exception of a single case structural weakening is mainly restricted to concrete less than 75 mm thick. The remaining degradations involving variably weak diffuse transformation due to Mg ingress and internal carbonation have so far not resulted in structural weakening. Figure 8 shows the influence of total thickness on deterioration from the outer surface, including examples of biofilm attack, excluding minor effects from ordinary surface carbonation.

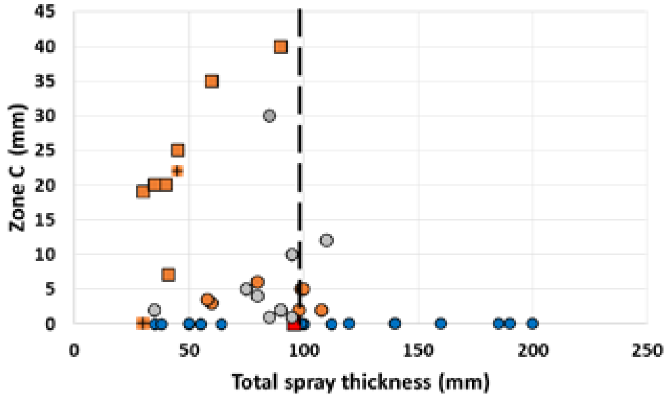

Figure 8. Degradation within Zone C due to biofilm. Orange squares = effects of thick biofilm with mild acids including some material loss of 1-25 mm (w/b = 0.41) (crosses with spalling), orange circles = thin biofilm with neutral pH, red square = non-degrading biofilm with neutral pH (concrete with w/b = 0.40), grey circles = Magnesium and PCD (mainly diffuse without structural consequences), blue circles = completely intact concrete.

The most significant degradations were associated with thick mildly acidic biofilms on concrete thinner than 100 mm. The thinner concretes were characterised by leaching of calcium and other elements into the local water on the surface, and there was a simultaneous diffusion across the sprayed concrete. Calcium and other leachable elements are nutrition's for biofilms. Since thinner concretes are more prone to fast diffusion through the bulk paste, the apparent absence of biofilm on thicker concrete may reflect less favourable growth conditions. The evidence from Zones A and C clearly suggests that degradations in the cement pastes were unimportant in subsea sprayed concrete layers thicker than 100 mm. *The deterioration mechanisms in question are essentially independent on the type of fiber used, whilst their action may also assist in steel fiber corrosion.* In some biofilms steel was involved in acid forming reactions [14,17], whilst some biofilms apparently did not form acids [8, 20]. The role of biofilms are currently under investigation at Chalmers- Gothenburg, including identification of microorganisms by DNA techniques [25].

Steel fiber corrosion. It can be demonstrated that also steel fiber corrosion was a function of sprayed concrete thickness and that significant corrosion has not occurred in sprays thicker than about 100 mm. Obviously this reflects the various degradations including internal carbonation, which do not sustain stability of steel in the long run. *Figure 9 shows the effect of steel fiber corrosion in two different ways.* The y-axis represents a rating of corrosion in cross section, as weighted by influence in each zone (Zones A, B, C of Figure 2). The individual coloured points show the worst case of corrosion in each single core. The red point (high local corrosion) at total thickness about 140 mm represents a very unusual case, where biofilm had penetrated into the adhesion zone. All data taken together shows that concretes thicker than 100 mm have few signs of corrosion after about 25 years in service. Moreover, capillary porosities < 18-20 % seems to largely have prevented diffusion of saline waters and corrosion [8].

Chloride profiles showed elevated and sometimes deep diffusion, with Cl contents commonly ranging from 0.3 to 0.5 % sometimes even 1 to 1.4 %. Yet the steel fibers are still intact while in contact with chloride laden paste. This has also been reported by Holm [18,19] and Mannvit [20]. This "paradox" may, however, be explained by lack of significant influence

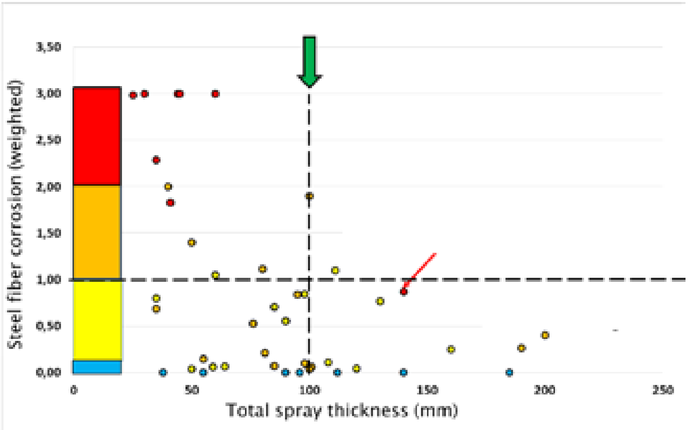

Figure 9. Thickness versus steel fiber corrosion rated by weighting of influence across the thickness. Each point is also coloured showing the worst case in each zone. Red = severe to fully destructive (rating 3), orange = marginally destructive (rating 2) yellow = insignificant to marginal corrosion only visible in microscope (rating 1), blue = no corrosion (rating 0).

by oxygen, i.e. this cathode is not established at bulk scale [8]. Instead, we observe that steel fibers in subsea concrete remain uncorroded until after core extraction, whilst they rather quickly start to show surface corrosion after core extraction when in contact with air, even when first washed in distilled water. In contrast, steel fibers in sprayed concrete from the freshwater environment remain essentially intact [8, 15, 17, 20]. In addition, it has recently been established that steel fiber reinforcement in concrete may slow down degradations by chloride penetration due to mechanical effect [26]. However, cracked sprayed concrete exposed to chloride over 17 years have shown important steel fiber corrosion with loss of strength and are not expected to yield a service life of 100 years [27].

FINAL REMARKS

The above documentation, obtained during the tenure of the R&D program "Durable Structures (2012-2015), provided new evidence regarding design of durable sprayed concrete subjected to aggressive environmental loads. We admit that our durability data still represents only 25 % of the designed lifetime and there are still remaining uncertainties regarding the ultimate service life of many of the studied concretes with w/b-ratios around 0.45 or higher. However, the use of steadily better concrete mixes in new projects, presently specified with w/b-ratios = 0.40, in combination with minimum 100 mm thickness in subsea tunnel sections seems to represent a very durable design also for steel fiber reinforced concrete.

Future research should still focus on ways to make adhesion of sprayed concrete even better in order to reduce the influence of aggressive ground waters in the subsea environment as well as in Alum shale.

Acknowledgements

The author is indebted to Reidar Kompen (NPRA) for sharing his extensive experience over two decades. Jan Viggo Holm (†) of Norconsult, Gísli Gudmundsson, Atli Karl Ingmarsson, and Guðjón Helgi Eggertson at Mannvit are thanked for tunnel investigations. Børge Wigum and Thorbjörg Hólmgeirsdóttir were responsible for the Mannvit reports. Technical assistance by Per Sydsæther, Knut Kjuul, Øystein Lahaug, Bente McGonnel, Ferhat Tasmin Kahn, Per Geir Sigurssen (NPRA), Sveinbjörn Svenbörnsson, Sigurjón Árnason (Mannvit) and Salah Akhavan (University of Oslo), is gratefully acknowledged. Finally, I thank Synnøve A. Myren and Alf T. Kveen at Tunnel and Concrete Division (NPRA) for comments and discussions, and for their good management of the R&D program on sprayed concrete durability within "Durable Structures".

REFERENCES

1. Barton, N., Lien, R. & Lunde, J., (1974): Engineering classification for rock masses and for the design of tunnel support. *Rock Mechanics* 6, pp. 189-236.
2. Barton, N. and Grimstad, E. (2004): The Q-system following thirty years of development and application in tunnelling projects. Rock Engineering – Theory and Practice, Proceedings of ISRM Regional Symposium EUROCK 2004, Salzburg, Austria, pp. 15-18.
3. Davik, K.I. (1997): Proper use of sprayed concrete in tunnels. Parts A, B, C, D, E and Final report. Statens vegvesen. (In Norwegian).
4. Davik, K.I. (1998): Proper use of sprayed concrete in tunnels. Nordic Road and Transport Research 1998-1, 16-17.
5. Kompen, R. (2008): Specifications for sprayed concrete. EN 14487 for sprayed concrete generally, Norwegian Concrete Association Publication 7 for rock support and NPRA Specifications for Road Tunnels. In: K Berg, C Hauck, R Kompen (Eds.), 5th International Symposium on Sprayed Concrete – Modern Use of Wet Mix Sprayed Concrete for Underground Support. Lillehammer, pp. 256-261.
6. Norwegian Public Roads Administrations (2015): Manual 761, General Specifications 1 – Standard specification texts for road contracts. Principal specifications 1-7.
7. Myren. S.A., Hagelia, P. & Bjøntegaard, Ø. (2018): The band of polymer fiber in FRSC in Norwegian road tunnels. In: S. Engen, Th. Beck & S.A. Myren (Eds.), 8th International Symposium on Sprayed Concrete – Modern Use of Wet Mix Sprayed Concrete for Underground Support. Trondheim (this volume).
8. Hagelia, P. (2018): Summary of durability development of sprayed concrete used for rock support in different tunnel environments. R & D Program Durable Structures. Statens vegvesen report nr 566 (In Norwegian).
9. Franzén, T., Garshol, K.F. and Tomisawa, N. (2001): ITA/AITES Accredited Material. Sprayed concrete for final linings: ITA working group report. Tunnelling and Underground Space Technology 16, p 295-309.
10. Skjølsvold, O. & Jensen, V. (1990): Examination of sprayed concrete in subsea road tunnels SINTEF-FCB, Rapport STF65 F90058, 81p.(in Norwegian)
11. Hagelia, P. and Grønhaug, A. (2000): Thaumasite – infection causing concrete deterioration. Våre Veier Nr. 9, 54-55 (in Norwegian).

12. Hagelia, P., Sibbick, R.G., Crammond, N.J., Grønhaug, A. and Larsen, C.K. (2001): Thaumasite and subsequent secondary calcite deposition in sprayed concrete in contact with sulfate bearing Alum Shale, Oslo, Norway. 8th Euroseminar on Microscopy Applied to Building Materials, Athens, Greece, p 131-138.
13. Hagelia, P., Sibbick, R.G., Crammond, N.J.and Larsen, C.K. (2003): Thaumasite and secondary calcite in some Norwegian concretes. Cement and Concrete Composites 25, 1131-1140.
14. Hagelia, P. (2007): Sprayed concrete deterioration influenced by saline ground water and Mn-Fe biomineralisation in subsea tunnels, In: B., Jamtveit (Ed.), Mechanical Effects on Reactive Systems, the 20th Kongsberg Seminar, Physics of Geological Processes (PGP) – University of Oslo, 2007, pp. 26 (abstract/invited talk).
15. Hagelia, P. (2008): Deterioration mechanisms and durability of sprayed concrete in Norwegian tunnels, In: K. Berg, C. Hauck, R. Kompen (Eds.), 5th International Symposium on Sprayed Concrete – Modern Use of Wet Mix Sprayed Concrete for Underground Support. Lillehammer, 2008, pp. 180-197.
16. Hagelia, P. (2008): Does the EN 206-1 Exposure Classification Apply to Tunnel Concrete? Nordic Exposure Sites – Input to revision of EN 206-1, Workshop Proceedings from a Nordic Miniseminar, Hirtshals, pp. 241-263.
17. Hagelia, P. (2011): Deterioration mechanisms and durability of sprayed concrete for rock support in tunnels. PhD-thesis, TU-Delft, the Netherlands.
18. Holm, J.V. (2011a): Modern road tunnels – Sprayed concrete in the Freifjord tunnel. Sprayed concrete, Norconsult, report No 5013053 (in Norwegian).
19. Holm, J.V. (2011b): Modern road tunnels – Sprayed concrete in the Oslofjord tunnel. Norconsult, two reports No 5013053 (in Norwegian).
20. Mannvit (2016): Durability investigation of sprayed concrete in seven tunnels. R & D program Durable structures 2012-2015. Statens vegvesen report nr. 475 (in Norwegian)
21. Hughes, P. (2012): A new mechanism for accelerated degradation of synthetic fiber reinforced marine concrete. Concrete, Vol 46, No 9. pp 18-20, September 2012
22. Fjose, A. (2015): Degradation of sprayed concrete in E39 Hopstunnelen and Nesttuntunnelen. Master thesis, NTNU Trondheim, 244 pp (in Norwegian).
23. Gulland, J. (2015): Sprayed concrete tested by destructive and non-destructive methods Master thesis, NTNU Trondheim, 138 pp (in Norwegian).
24. Bastiansen, R., Moum. J. & Rosenqvist, I.Th. (1957): Contribution to high-light certain construction problems associated with Alum shale in Oslo. Norwegian Geotechnical Institute, Publication No. 22, Oslo, 69 pp (In Norwegian with English summary).
25. Karačić S, Hagelia P, Persson F and Wilen B-M (2016): Microbial attack on subsea sprayed concrete. RILEM Conference on Microorganisms-Cementitious Materials Interaction, 63-75, RILEM Publications SARL.
26. Berrocal CG (2017): Corrosion of Steel Bars in Fibre Reinforced Concrete: Corrosion mechanisms and structural performance. PhD-thesis. Chalmers University of Technology, Gothenburg.
27. Nordström E (2016): Evaluation after 17 years field exposure of cracked steel fiber reinforced sprayed concrete. BeFo Report 152 Stockholm (In Swedish with English summary).

UTILIZATION OF MODERN IOT SYSTEMS IN SPRAYED CONCRETE PROCESSES

Marius Hauki
Normet International Ltd, Switzerland
marius.hauki@normet.com

Thomas Beck
Normet Norway AS

ABSTRACT

Sprayed concrete process has always had variations in many parameters related to fresh concrete properties, pumping process, spraying process, temperatures and so on. Modern spraying robots may be equipped with IoT systems which are able to log data and save these data for wireless transmission to a secure data store accessible in the Internet cloud. The data can be either an average value for one concrete load or work-shift, or it can be broken down to time series data. This data, when seen together, presents an interesting opportunity to utilize the information in a more systematic way to get information about the spraying process and equipment.

Normet has developed an IoT tool for collecting and analyzing sprayed concrete related data from all modern Normet sprayers. It is possible to use the IoT tool to get information about the spraying process and equipment. The contractors or mines who own the spraying robots with this option enabled, will have the opportunity to have information on a more detailed and systematic level than before. Normet as an equipment manufacturer will have the possibility to improve the equipment and do remote technical support and diagnosis more effectively.

This paper and presentation will give some examples of how a modern IoT system for sprayed concrete processes works and some examples how data from such a system can be used in order to understand and improve the spraying process and equipment.

INTRODUCTION

The sprayed concrete process quality is a combination/interaction of:

- Fresh concrete and its properties
- Accelerator
- Mechanical equipment (spraying robot)
- Practical operation/execution done by the nozzle man

The spraying process is unfortunately not always strait forward and predictable and is not always working as expected. The main problems and challenges is often related to:

- Early strength development (and too high consumption of accelerator)
- Poorly adhesion between sprayed concrete and rock surface

Some typical daily challenges can be (examples):

1. Concrete mix design issues (cement type, water/binder-ratio, aggregates)
2. Concrete properties issues (slump, temperature, fiber distribution)
3. Accelerator (type, temperature, consumption (kg/m^3 or liters/m^3)
4. Concrete pumping (stable or variating pumping pressure, filling degree on cylinders)
5. Spraying process (mix of accelerator into concrete, "cooperation" of concrete and accelerator pump and air compressor)
6. Surroundings (temperature in tunnel/mine, both air and rock surface, thickness, water leakages, ventilation with cool air)

The above list is not exhaustive; however the above shows some parameters which are regarded important for a good final product. The focus and main goal can often be very different and the goals depend on the project. In order to understand the process fully, it should be possible to compare and have a good over-view of the process. And then it is necessary to be able to observe many parameters in parallel and on a common time base. It is also necessary to have data from the process over a certain time, not only when the process is not working optimally but from times when the process were not working optimally for comparison purposes.

When collecting data from a process, it can be done manually or by an automated IT-system. The challenges with manually collected data are that different operators do measure parameters differently and may forget to write them down. Manually recorded data also need to be plotted in a suitable spreadsheet or graph in order to understand the process and observe possible changes. This takes time and manual effort and due to limited time and resources it is not always done so important information is lost. An IoT system which automatically logs and transmits data from shotcrete process via WLAN (wireless network) is a new way of securing a lot of information about the spraying process. Such information can later be fed into traditional time domain analysis systems and artificial intelligence systems for further analysis.

WORKING PRINCIPLES OF A MODERN IOT SYSTEM FOR SPRAYED CONCRETE APPLICATIONS

Introduction

IoT is a shortcut for Internet of Things. Internet of Things means that devices (“things”) instead of PCs and laptops with people behind the keyboard are being connected and communicate via the Internet. In recent years significant developments in using modern and standardized networking technology has been realized and IoT in mining and tunneling becomes more widespread [1]. Mining and tunneling machines can now be connected to the Internet and communicate from machine to machine in an automatic way. The data can be stored and the data can be built and queried for analysis. The computer involved for data logging is typically not a PC or laptop, it is often an embedded, low cost and self-contained unit. IoT used for remote monitoring purposes is also called Telemetry. Telemetry systems have been utilized in other industries than mining and tunneling for significant time already.

In tunneling and mining, IoT is typically implemented on the same computer as runs the automation system on a specific machine. However some domain specific challenges exist. One challenge is connectivity. Since there is no regular 3G/4G network and seldom wireless networking available at the face, the data needs to be stored until a wireless network connection is available. Another challenge is often access to the public Internet: from mine and tunneling sites in remote locations, Internet access can be challenging. A third challenge is security and privacy: customer process data and personal data must be kept secure at all times. New regulations such as the GDPR (Global Data Protection Regulation) must be followed if the company carrying out IoT activities on any personal data is based within the EU regardless if the data is logged on a site outside EU [2]. (Personal data is any data where the user of the equipment can be directly or indirectly identified). These issues must be handled to enable successful utilization of IoT in a tunneling and mining environment.

A modern IoT system for tunneling and mining typically consists of several sensors on the machine chassis, engine, booms and process units. Sensor data is normally stored as a sensor readout value and a time as a pair. A large number of value plus time pairs are sent with a regular time interval between when the data values are recorded as telegrams. The IoT system also typically includes a data logging computer with tailored software for data logging, a means for data transmission to a location on the Internet, a means of secure and central data storage and a means of data analysis and visualization.

Data analysis is typically carried out by predefined automated analysis tools or by external tools such as Excel or more advanced tools. The data visualization can be carried out on a laptop, on a tablet or mobile phone. Different reports can typically be generated to PDF, Excel etc.

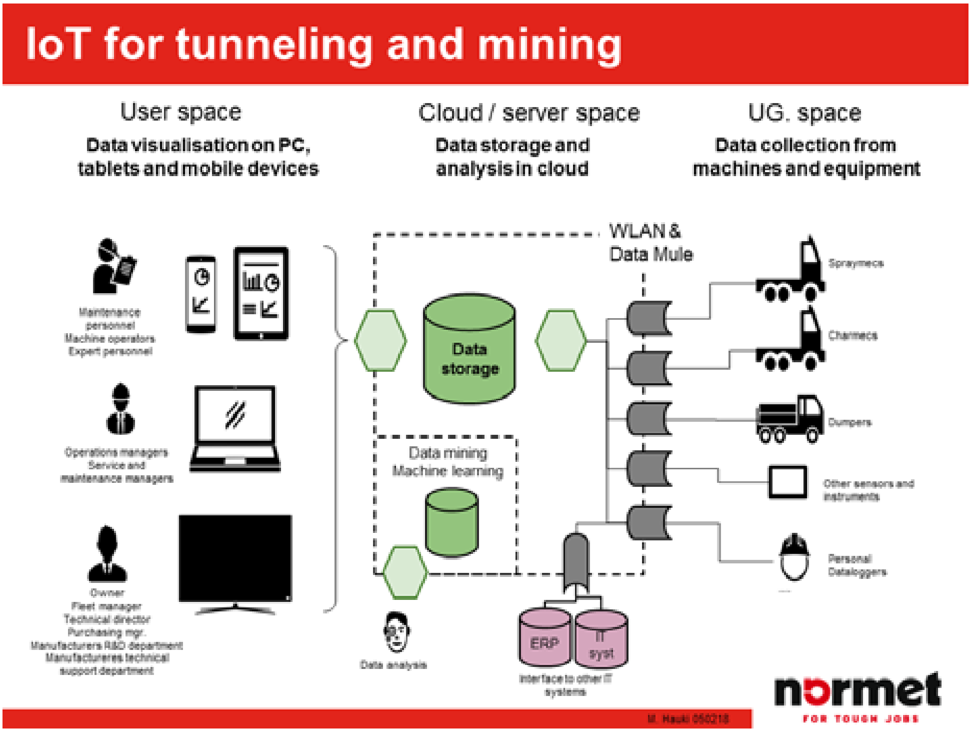

Figure 1. Overview of a typical IoT system for tunneling and mining

The above figure shows the block diagram of one example of a modern IoT system for mining and tunneling equipment. Data flow is from right to left and all data is sent on industry standard network connections. There is a central data storage system, where all data is stored securely. This can be a cloud server (a machine or virtual machine not in the client's data center, but in a hired space accessible via Internet). There can be several visualization systems that for example show data in a web browser and in a dedicated application. There can also be data exchanges with more advanced systems such as artificial intelligence systems and machine learning systems. Finally, data exchange with more traditional Enterprise Resource Planning and production systems can be done easily since there is data stored in a centralized location.

Relevant data channels on a modern concrete spraying machine

On a modern tunneling / mining machine there are numerous sensors. The main groups of sensors are engine, fuel and energy consumption, hydraulics, electric and charging system on electrical vehicles and drivetrain.

Then there are process specific sensors like filling state of chemical tanks, sprayed concrete parameters, bucket load in terms of a dumper vehicle etc.

In this paper, the focus is on utilization of IoT for sprayed concrete applications and therefore the coverage of data channels in this chapter below is limited to the sensors of most relevance to sprayed concrete equipment. Data from sensors is often noted as a "signal". In this context it means that there is a recording of a numeric value or state on a time basis.

Temperature of concrete in degrees C

The concrete temperature as delivered from the batching plant and concrete truck is measured. The concrete temperature is important for the early strength development and quality of the sprayed concrete application. This temperature is typically measured every 10 second or every 2 minutes.

Ambient temperature in degrees C

Even if ambient temperature is probably less important than concrete temperature, the ambient temperature is also measured. The air temperature can give an indication of if spraying is carried out close to the entrance to the tunnel / mine under winter conditions and the ambient temperature is lower than expected.

Temperature of the additive in degrees C

The additive temperature is measured. The temperature of the additive should be within certain limits. Any temperature deviations outside normal range of the additive can affect the spraying process.

Additive dosage setting in %

The additive dosage setting is recorded. This is the setting that the operator dials in on the remote control. Immediately if the operator changes this setting, the new setting state and the time of the change is recorded. The correct additive dosing is important for quality.

Concrete pump speed in RPM or m^3/hour

The concrete pump speed is recorded by measuring the number of piston strokes per time interval. The concrete pump cylinders are normally not filled completely and the degree of filling is dependent of the concrete slump. However, by using a calibration factor, the volume in m^3/hour can be calculated by multiplying piston strokes by the number of cylinders and by a calibration factor that has to be set by the operator. This is output as a signal and is an important for diagnosis purposes.

Filling degree of concrete pump, calibration factor in %

Since there is no automatic measurement of slump, there needs to be manually entered a cylinder filling degree calibration factor. This is for example done by the operator. By comparing the delivered concrete volume per batch to the reported pumped volume from the machine automation system a calibration factor can be calculated. When this calibration factor is correctly entered, the reported pumped volume given to the IoT system should be the same as the delivered concrete volume. Since the dosing of accelerator is typically calculated from the amount of concrete measured by the control system, this calibration factor is often important. If this calibration factor is incorrect, the dosing of accelerator may be incorrect as well. Monitoring the change over time of this calibration factor can give important information and clues to root causes of eventual problems.

Concrete pump hydraulic pressure in BAR

The concrete pump hydraulic pressure is recorded as well. This pressure is typically higher if the slump of the concrete if low and the pressure is typically lower if the slump of the concrete is high. Correct consistency of the concrete and therefore slump in the correct range is important. Several quality related parameters including mixing is affected by slump. The concrete pump hydraulic pressure signal can give important clues to root causes of process problems.

Accelerator density, calibration factor in g/l

The accelerator density is a parameter that should be given by the manufacturer. This is important for the dosing system. If this setting is incorrect, the dosing system will dose incorrectly, likely affecting quality. While this density data is recorded, it is probably not needed to have a very dense data set of this parameter. However, it can give important clues to if and when the calibration factor has been altered or set incorrectly and to be able to do corrections.

The usage of concrete per shift in m^3

In addition the sprayed concrete volume *per shift* is recorded. This is probably not directly related to the quality of the spraying process, however it is an important productivity measure. It can be used for comparison purposes and for calculating and planning concrete demand by feeding this information back to the batching plant.

The usage of additive per shift in l

Furthermore the usage of additive per shift is recorded. This data is important when seen in relation to the usage of concrete per shift. If the ratio of additive to concrete is incorrect in average, this can give a clue towards incorrect operation of the equipment and how to solve related issues.

USE CASES FOR IOT IN SPRAYED CONCRETE

When a problem occurs in a sprayed concrete process, the service personnel from the machine manufacturer, the chemical suppliers and the specialist personnel on the site would typically become involved. These specialists will often have to rely on mainly verbal information from the operators. Typically such information is given some time after the issue occurred (days or even weeks). Often the needed information about actual temperatures, actual additive settings, actual concrete slump etc. is not systematically recorded and subjective opinions may be given. This opens up a multitude of possibilities for error. Diagnosis may be incorrect or inaccurate and it may take more time that necessary before a resolution is found.

The purpose of a data logging and an IoT system is not to replace specialists or verbally given information. This will still be needed in the foreseeable future. Automated and systematic ways of accurately recording relevant data channels can be seen as an *additional tool* in the arsenal of the shotcrete fleet owner and operator. Its purpose is to *augment* the information given by personnel on site and to help the overall understanding of the issues that may occur. The authors believe that this is one of the major strengths of using an IoT system in sprayed concrete applications.

In this chapter some case examples where an IoT system may be used with benefits are discussed.

Case example 1: concrete temperature outside ideal range

For example in Norway, it is normal to order concrete with a temperature of minimum 20 °C. This is done to ensure a good reaction between cement and accelerator, in order to develop good early strength in sprayed concrete.

There are number of cases where temperature of fresh concrete has been delivered far below the specified minimum temperature, especially during the winter season due to use of too cold ingredients in the mix or due to cooling during transport. Not everyone is controlling the temperature of the fresh concrete received. Sometimes the temperature is in fact measured manually, but it is forgotten to be written down in any report. Operators also often do measure temperature with different equipment (laser pointer and thermo-couple), and operators do measure at different stages (in the very first concrete coming out of truck and after some hundred liters). This may introduce errors and inconsistencies in data making comparisons difficult.

Temperature of fresh concrete is a very important factor and quite easy to measure. Still it is forgotten or measured differently. There is often a lack of data or variation in the data. If temperature is measured automatically on the spraying machine and stored in the data storage by the IoT system, the operators and owners of the equipment will always have historical data on temperature and can precisely state when changes in temperature have occurred.

If suddenly the early strength of sprayed concrete is improper, it will take only a small effort to find out if the fresh concrete temperature has dropped and if this can be the main reason by looking at the data from the IoT system. This data can typically be viewed on a PC or tablet or even mobile phone.

Case example 2: concrete slump issues
Pumping speed is another important factor, and it can indicate indirectly the flow of the concrete. Slump of the fresh concrete is relatively easy to measure, but is not done very often in practice. It is well known that a high slump concrete with greater flow will fill the volume of the pump's cylinders more. The time it takes to pump and empty a truck containing 8 m^3 concrete will vary dependent on the slump. If slump changes from 180 mm to 220 mm from one load to another, the effective flow will be increased (if everything else is kept constant). This occurs even though the pumping set-point is set to the same by the operator at for example a 20 m^3/h. Unless the operator is entering into the computer on the spraying machine that the concrete filling degree has changed, the actual volume per pump stroke will be incorrect.

In the nozzle, the concrete is exposed to very high air pressure and mixed with a mix of compressed air and accelerator. This process happens in very short time (less than a second). A difference of pumping speed of 4 m^3/h can be important in order to achieve a good mixing process. Too fast pumping can lead to less effective mixing of accelerator into concrete and again lead to reduced early strength in sprayed concrete. If the operator thinks that he pumps at a certain rate, but the change in slump causes him to actually pump at a different rate than he thinks, the mixing process can be affected.

A quite variating pumping speed can also be a clear signal of unstable slump in fresh concrete.

If pump speed is logged by an IoT system, it can therefore help to debug both concrete slump outside normal range or outside expected range and to detect variations in concrete slump within the same delivery.

Case example 3: accelerator dosage
Accelerator dosage is also a parameter which is closely linked to pumping speed of concrete. The accelerator dosage pump is running at a certain speed based on the theoretical flow of concrete through the nozzle. Unwanted variation in the fresh concrete slump can therefore indirectly lead to quite big variations in effective accelerator dosage.

The accelerator pump is running at a certain number of liters/min. If the system is "calibrated" on a concrete with slump 180 mm, but the slump is suddenly becoming 220 mm, the concrete flow through the nozzle will increase and accelerator dosage will decrease. In the opposite way, if concrete becomes less flow-able and has a slump of 140 – 160 mm, it is still possible to pump. The time it takes to empty on concrete batch takes longer time and accelerator pump will feed more accelerator into this load of concrete. This concrete will be slightly over-dosed, which is not good for the economy and can in worst case lead to "burning" in the nozzle, and un-wanted maintenance stops and delayed spraying process. This type of issues can more easily be diagnosed by an IoT system.

Summary of case examples

The advantages of having good quality systematically recorded data from the spraying process are fairly obvious. The advantages of an IoT-system can be summarized as follows:

1. An IoT-system may remove the factor of personal and subjective impact on measurement.
2. The ability to look at data collected over time and observe several parallel-processes at the same time with an IoT system is assumed to be beneficial.
3. Since the data is always saved automatically and is always available later, the operator does not have to remember the measured values, does not have to remember to write it down in a systematic way and to re-enter the information in Excel sheets or similar.
4. Facts can be looked up later, when they are needed.

SOME APPROACHES TO PRESENTATION OF DATA

An *easy to understand presentation of data* from the IoT system is considered very important. The reason for this is that even if high quality data is available, that doesn't help if the data is not used because it is not understood. In the mining and tunneling industry it is also regarded as important to consider the audience. Typical users of an IoT system are not IT experts. The presentation and way to operate the system must be easy to use and easy to understand, tailored to this specific industry. IT terminology must be avoided if there are risks of misunderstandings or placing barriers to use.

There are several approaches to data presentation. Some shows a very specific process oriented picture. Other shows a "dashboard" view over the whole fleet. The third class uses graphs on a traditional time scale to show objective data. In the latter example it would be up to the user to draw any conclusions from this data.

In this chapter some approaches to data presentation from an IoT system will be presented. (These are examples and future implementations of IoT systems may look different).

Parameter dashboard

The below example shows a process oriented dashboard view of a spraying process. The normal ranges are shown inside black squares. The actual averaged measurement is shown as a cross inside a circle. If the value is inside the normal range, the circle is green. If the value is outside the normal range, the circle is red. The date and time range is seen and can be selected by clicking on the screen.

Batch1: in the first concrete batch, the operator (as usual) wants to spray as fast as possible. He sprays at almost 25 m^3/h. While it looks like he is within the correct pump speed range, it may in fact not be the case. The IoT system shows that he sprays too fast because the concrete delivered has lower slump than anticipated. The pump pressure then as a result of this becomes high and outside the ideal range. The red circle and cross clearly shows this condition in the parameter dashboard.

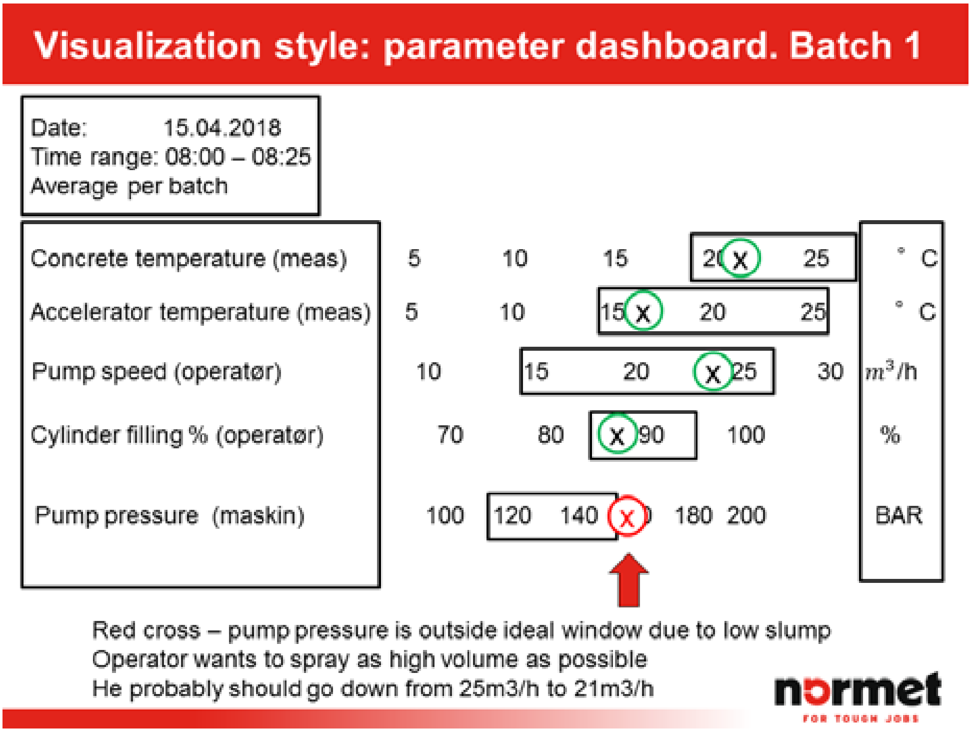

Figure 2. Parameter dashboard showing key parameters of the spraying process (batch 1)

Batch2: in the second concrete batch, the operator did reduce the pump speed down to 21 m^3/h. Now the pump pressure was reduced and was within the normal range. The circle and cross on the pump pressure now is green and shows the pressure is within normal range. With this information it is easy to compare different batches and to use this for diagnosis for different parameters as well as for training purposes.

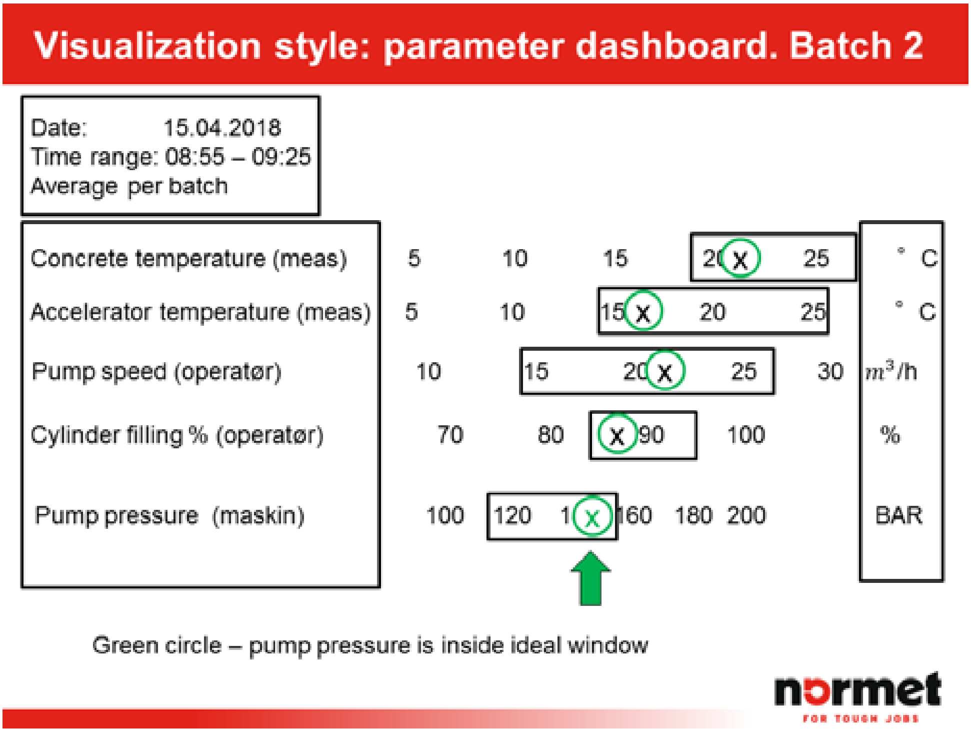

Figure 3. Parameter dashboard showing key parameters of the spraying process (batch 2)

Comparison view

Often there is a need to compare one batch to the other or to compare a batch with a problem to a known good batch even without explicitly knowing "what we are looking for" in terms of the parameters. Then a comparison view can be used. This typically shows two time periods and parameters from each time period side by side. A manual comparison can be done.

The below examples shows two examples of periods recorded on the same day. The IoT system is used to compare pump pressure and pump speed as well as concrete temperature and accelerator dosage. The batch at left starting at 11:00 has a higher slump and the pump pressure is quite low. However when we look at the batch at the right starting at 11:40, the pressure increases to around 145 BAR combined with a pump speed that was set down to around 15.5-18 m^3/h as a consequence of lower slump. By comparing these two batches, it is possible to see if a slump problem or change has occurred and the batching plant can be notified if necessary. It is also possible to see the operators adjustments.

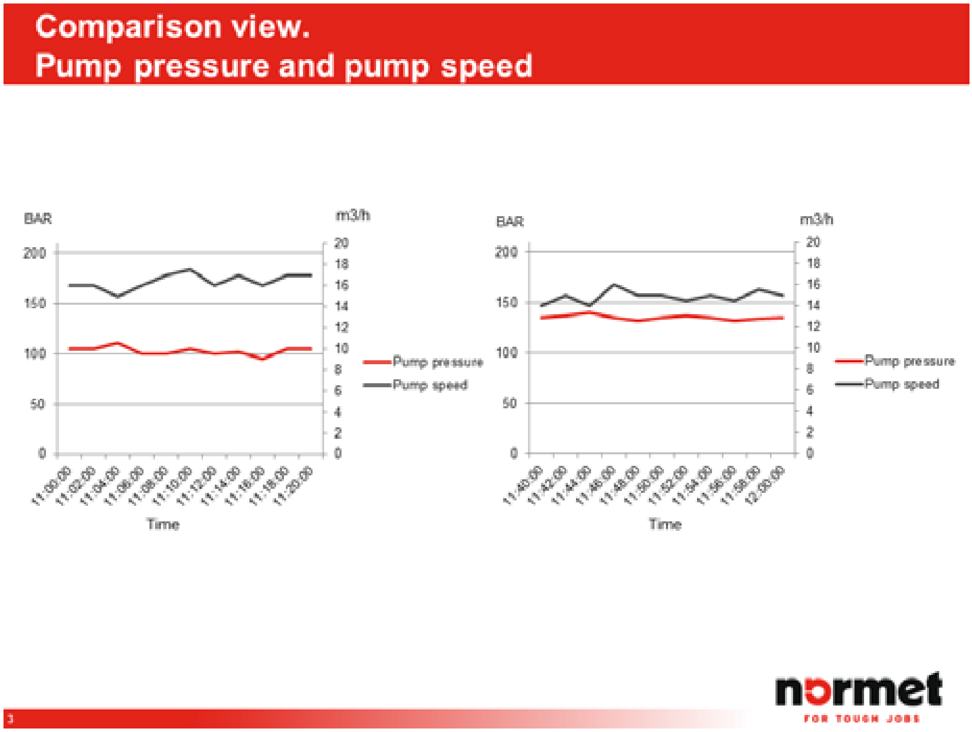

Figure 4. Comparison view showing side by side comparison of pump pressure and pump speed

In the next example it is also shown two periods recorded on the same day. The IoT system is now used to compare concrete temperature and the accelerator dosage settings. The batch at left starting at 11:00 had a fairly warm concrete at around 24°C and a setting of around 5,5% of additive was selected by the operator. In the batch starting at 11:40 the concrete temperature was delivered lower at around 16°C (outside the considered normal range). The operator determines from experience and observation that the concrete can’t be applied in as thick layer as in the previous spraying session. He adjusted the additive dosage to 7%. This seems to be correct, given the low concrete temperature. Had however the operator not adjusted the additive dosage in this situation, the quality of spraying may have been negatively affected. An IoT system would record this and it would be possible to suggest improvements and to give the batching plant updated feedback about the concrete temperature issue.

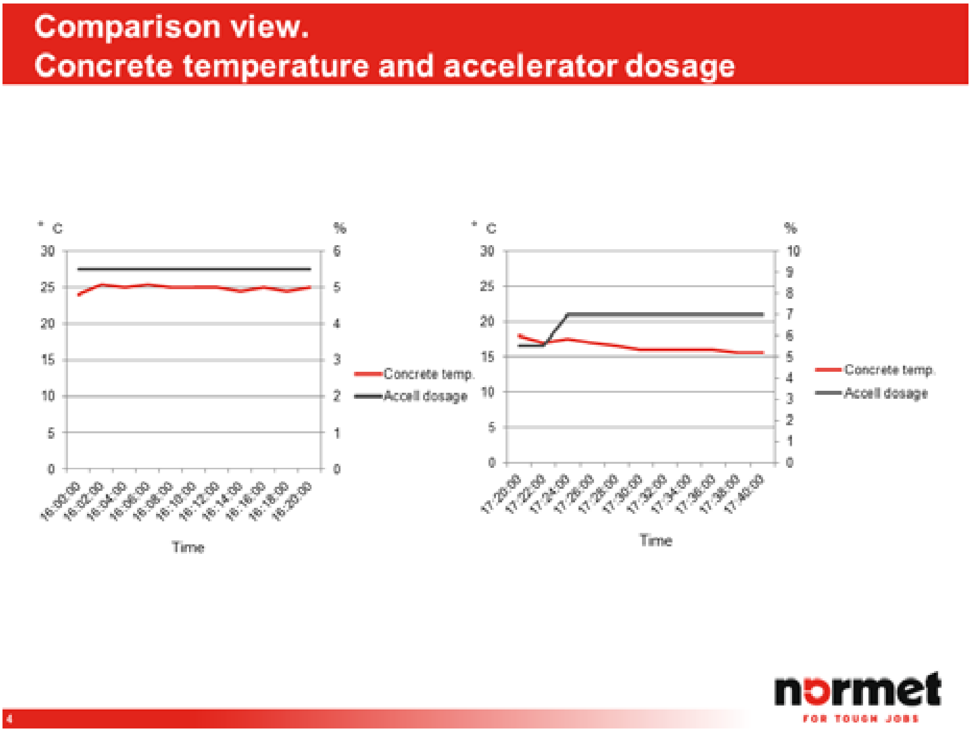

Figure 5. Comparison view showing side by side comparison of concrete temperature and accelerator dosage

Time series graphs

Often there is the need for studying signals from several sensors on a time scale. This can probably considered the "classic" approach to data visualization in an IoT system. Having access to overlay several signals and to vary the time scale, a trained IoT operator with domain specific knowledge about the sprayed concrete process can analyze many problems and issues by visual inspection. The example below shows how the concrete pump speed varies and how the operator is adjusting the additive setting. Many other signals can also be shown: engine, drivetrain, braking system, running hours, fuel consumption etc. From this for example the shift cycle on the site can be determined and a trained eye can in addition tell much about the spraying process a quick glance at the data.

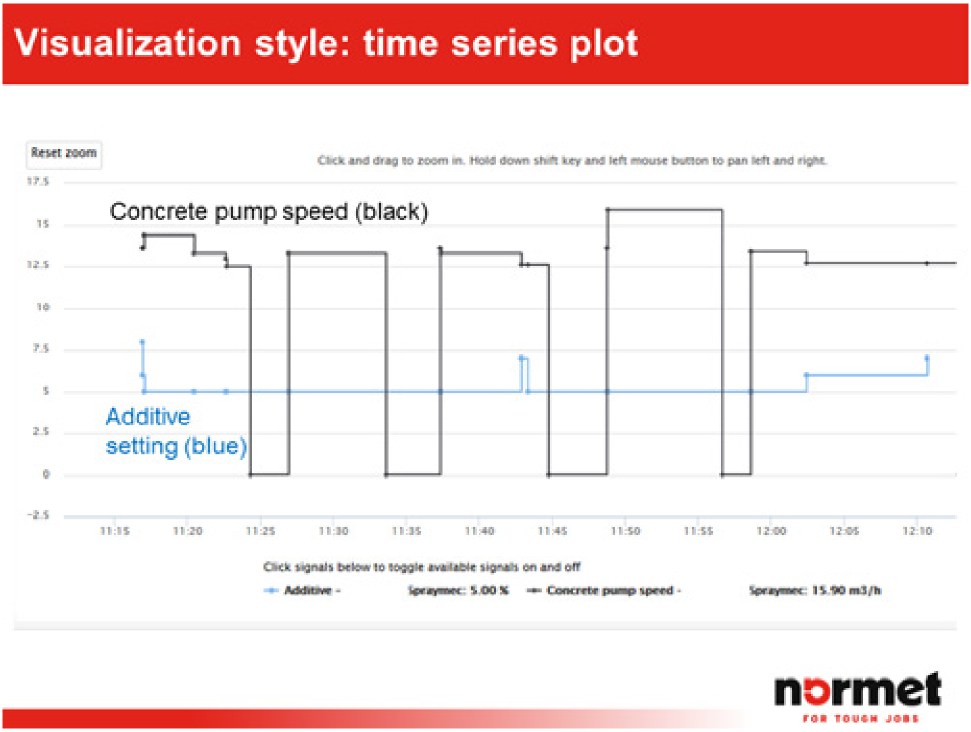

Figure 6. Classic time series graph where several signals can be overlaid on the same time scale

Fleet overview

For mine and tunnel site maintenance personnel and management a more overall and general view is typically offered. In the fleet overview, the whole fleet of a site can be seen provided the fleet has IoT capabilities. Data such as spraying performance over the last shift in m^3, how long time it is to next service interval on engine and power pack, if are there any error codes etc. There is also the possibility to see serial numbers of the machine and other data. Digital service records and previous diagnostic comments by service personnel could also be visible here.

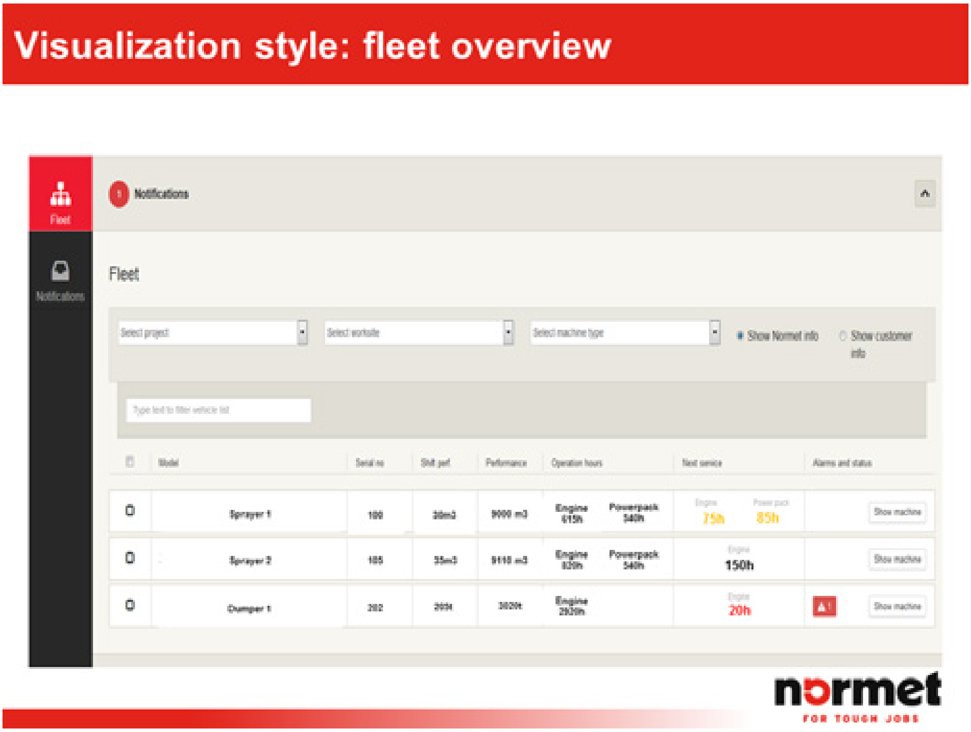

Figure 7. Fleet overview that gives most important information at a glance

Warnings and error codes

On modern equipment for spraying there is a computer controlled control system that receives error and diagnostic codes from engine, power pack, braking system, filters, compressor system, electrical system, sensors, pumps, valves and so on. Traditionally there has sometimes been the need to send service personnel to the site to diagnose error codes if the meaning of error codes is not understood by the existing personnel on site. With access to data from an IoT system, the manufacturer can from their HQ (or even R&D department if needed) access all error codes and diagnose most problems. Alarms may also be cleared and comments may be entered so other maintenance personnel can see the history and what have been done in the past. One example of benefit is that experts from the manufacturer of the machine can help diagnose problems remotely via Internet immediately. This saves travel time and travel costs for both client and for the manufacturer as well as having environmentally positive effects. Personnel at the manufacturer gaining experience from remote diagnosis of a whole worldwide fleet via an IoT system may build a wider experience base to base their recommendations and diagnosis on. Such personnel are typically employees with long field service experience in the past to build upon.

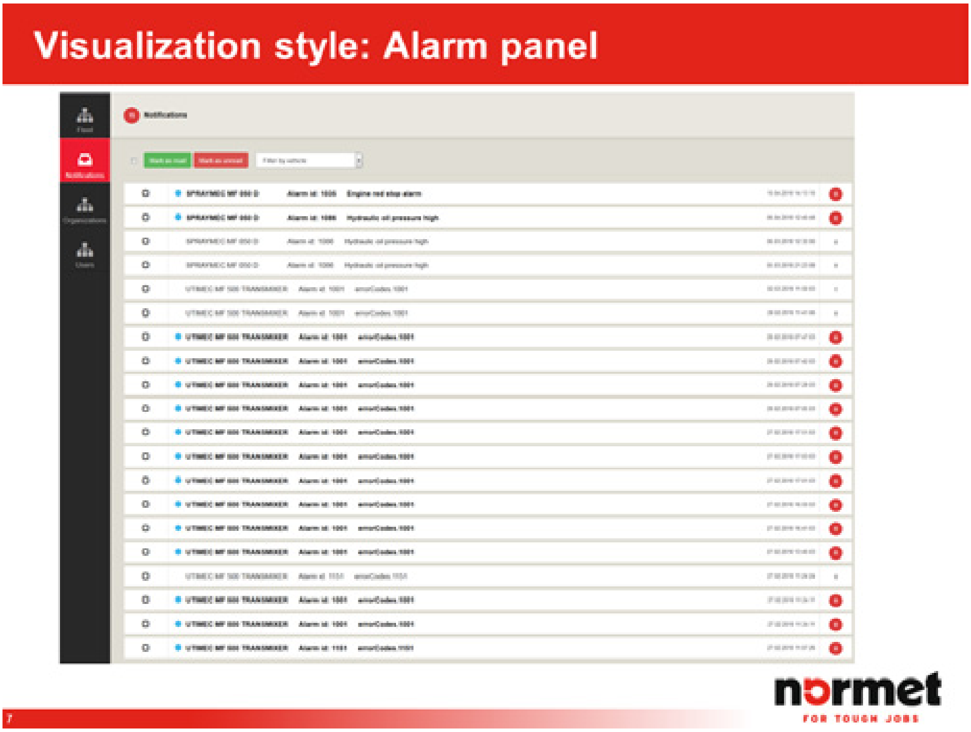

Figure 8. Alarm panel that gives an overview of all alarm codes of the whole fleet

Export to Excel and to other tools

Not always can the standard IoT visualization tools give the specific data presentation or analysis the situation requires. In modern IoT systems there is the possibility to export time series data to Excel and direct to file. Then specially tailored analyses can be carried out. Export to machine learning / artificial intelligence software, Tableau, “R” and even tailor-made Python or C++ programs can also be done via application program interfaces (API).

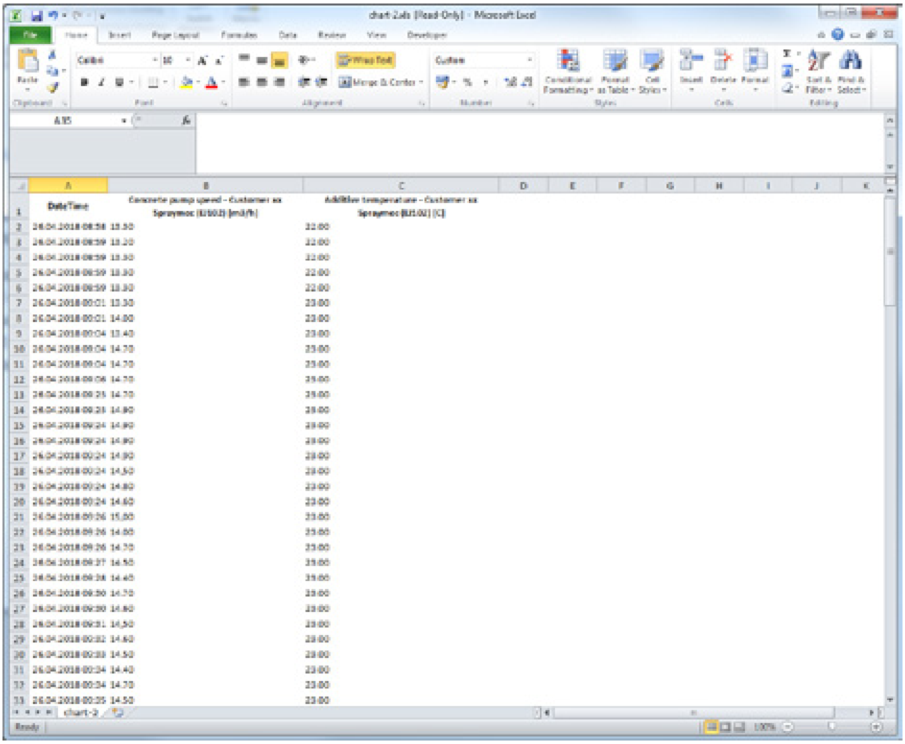

Figure 9. Export to external program. In this case Microsoft Excel

CONCLUSION

The sprayed concrete process consists of many sub-processes. When some (inevitable) spraying process problems occur from time to time, it is often challenging to detect and understand where the problem is and the underlying root cause of the problem. Getting access to larger amount of data which have been collected systematically, objectively and automatically over a long time period can be represent significant improvement. It can be easier to understand the actual sprayed concrete process parameters and the root cause of any problems. Process improvement and optimizations can also likely be done more systematically. By using a modern IoT system designed for tunneling and mining to collect data from spraying equipment and transmit relevant data over WLAN / Internet and presenting the data in a suitable way accessible on a PC or mobile phone, the contractor and mine owner can now utilize a new powerful tool in his toolbox.

REFERENCES

1. Sharma, A, Smarma, S, Gupta S, "IoT in mining: a review", JEECS Vol 6(2), 2017, pp 1-8.

2. REGULATION (EU) 2016/679 OF THE EUROPEAN PARLIAMENT AND OF THE COUNCIL of 27 April 2016 on the protection of natural persons with regard to the processing of personal data and on the free movement of such data

A 20 YEAR HISTORY OF STRESS AND STRAIN IN A SHOTCRETE PRIMARY LINING

Benoît D Jones
Inbye Engineering, United Kingdom
bjones@inbye.co.uk

What happens to tunnels in the long-term? Does the ground load increase to the in situ value or does it reach an equilibrium at a lower value? What is that lower value? Is there load sharing between a primary and secondary lining? Designers mainly have to guess the answers to these questions because there are so few data. This results in significant overdesign of tunnel linings. The lack of data is partly due to the difficulties of measuring stresses in tunnel linings, partly due to the planning and commitment required to continue to monitor tunnels for long periods of time after handover to the client, and partly due to a bizarre lack of interest on the part of the tunnelling industry in a subject that should be of critical interest. This paper will present a summary of nearly 20 years of monitoring stresses and strains in the Heathrow Terminal 4 Station Concourse Tunnel primary lining. It will compare these measurements to other measurements made in the literature and come to some conclusions about how we have been getting things wrong and how we should design tunnels in the future.

INTRODUCTION

Tunnel lining design is inherently conservative, in that characteristic values of ground strength parameters and characteristic values of the tunnel lining materials are used, along with partial factors on the tunnel lining materials and on the 'actions or the effects of actions' (i.e. the loads in the tunnel lining). This should make failure very unlikely, which is a good thing. However, the initial prediction we make, that is then factored, is clouded in more uncertainty than we care to admit.

The design of tunnel linings is based on trying to predict the stresses that will be present in the structure throughout its life, from construction to the design life of 120 years. We usually attempt to predict these lining stresses using analytical solutions or numerical models. A methodology often followed when modelling in 2D is to vary the amount of relaxation allowed prior to lining installation until the ground movements approximately match the expected ground movements. This could be called a 'semi-empirical approach', in that it is based partly on a calibration to the expected reality and is partly deduction from theory and geotechnical laboratory tests. However, Jones (2012) showed that very similar ground movements could be obtained using different constitutive models for the ground, while giving very different values of lining stresses. This is shown in Figure 1, where different constitutive models give very different values of lining stress at the same value of ground deformation. For example, to achieve a target volume loss of 1%, the lining stress could be anywhere between 24% and 60% of full overburden pressure[1], depending on the constitutive model used.

[1] 'Full overburden pressure' is the initial in situ vertical total stress at the axis level of the tunnel.

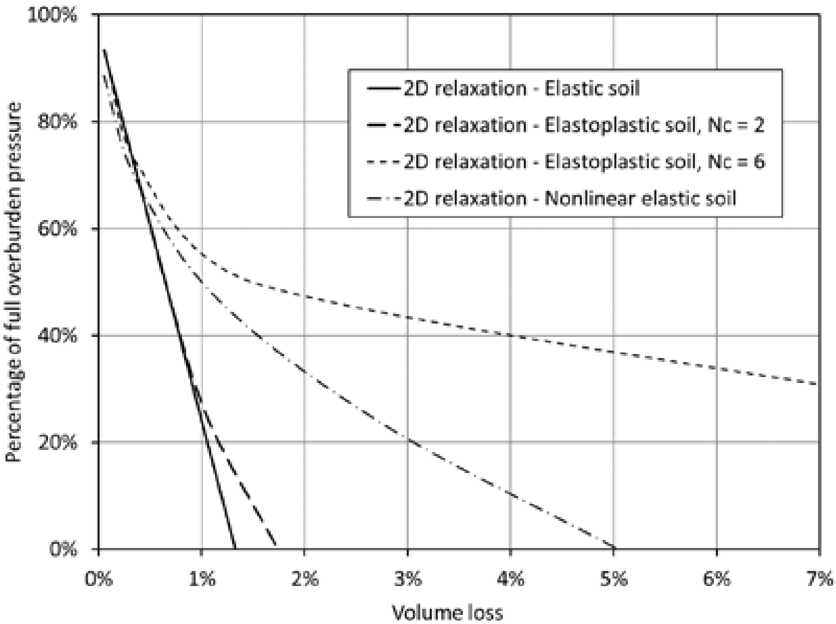

Figure 1: Relationship between lining stress (expressed as percentage of full overburden pressure) and ground deformation (expressed as volume loss), from Jones (2012).

Another area of uncertainty is the role of groundwater in low permeability soils that can be said to exhibit 'undrained' behaviour in the short-term followed by 'drained' behaviour in the long-term. During excavation, the ground around the tunnel is unloaded in the radial direction, but in low permeability soils the pore water cannot move quickly enough during this timeframe and so changes of mean total stress are experienced by the soil as changes in pore pressure. These excess pore pressures (note they are 'excess' to some long-term hydrostatic equilibrium or steady state flow, not excess to the initial in situ pore pressure) will dissipate over time, causing changes in the effective stress (the 'grain-to-grain' stresses in the soil) and volume changes in the soil (swelling or shrinkage). In addition, shear stresses in the soil may cause contraction or dilation, depending on how overconsolidated the soil is. Overconsolidated stiff clays tend to dilate when sheared (generating negative excess pore pressures), and normally consolidated or lightly consolidated soft clays tend to contract when sheared (generating positive excess pore pressures).

It used to be assumed that in the long-term the initial in situ stresses in the ground would come to act on the tunnel lining hydrostatically, and this seemed to be supported by stress measurements in tunnels by Skempton (1943), which showed full overburden pressure acting on the tunnel lining only 2 weeks after construction, and stress measurements made in tunnels up to 50 years after construction by Ward & Chaplin (1965) and Ward & Thomas (1965), from which they concluded that the full overburden pressure would always eventually come to act on the tunnel lining. However, since then stress measurements by Belshaw & Palmer (1978), Bonapace (1997), Barratt et al. (1994), Muir Wood (1969) and Bowers & Redgers (1996) have shown that lining stresses rarely exceed 70% of the full overburden pressure in the medium- or long-term. The measurements that correspond to stiff overconsolidated clays are shown in Figure 2.

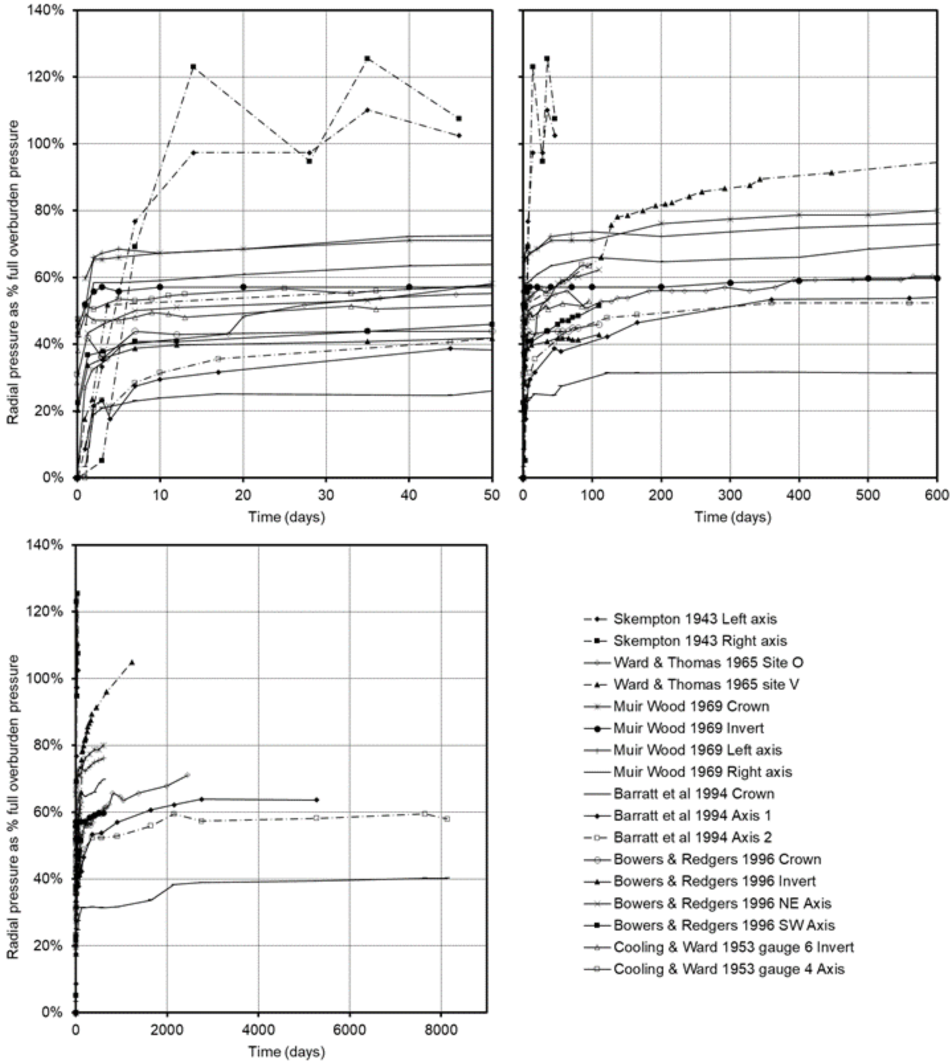

Figure 2: Historic stress measurements in segmental tunnel linings in stiff clay, shown on 3 timescales – the first 50 days, the first 600 days, and 9000 days (note a log-time chart was deliberately not used as it gives a false impression of how stresses change in the long-term).

Another area of uncertainty is not just the final long-term value of stress in the tunnel lining, but the period of time over which this develops. Long-term measurements of load in the Jubilee Line tunnels at Regent's Park in London over 19.5 years by Barratt et al. (1994) showed a gradual increase in load over time, though the majority of the increase occurred in the first 3-4 years (Figure 2). They found similar increases in load in an Oxford sewer in overconsolidated clay. Similarly, measurements by Bonapace (1997) showed radial stresses increasing from a mean of 250 kPa at 3 months to a mean of 350 kPa at 12 months. In contrast, long-term stress measurements in the Heathrow Cargo tunnel in London Clay by Muir Wood (1969 – see Figure 2) showed a less than 10% increase in the load between 2 days and 600 days. Similar measurements in an instrumented ring by Bowers & Redgers (1996 – Figure 2) over 100 days showed a less than 30% increase in load.

Jones (2005) discussed the possible reasons for these very different behaviours. It may be that the degree of unloading of the ground is critical to the subsequent behaviour, i.e. that if there are large ground deformations during construction then the short-term load will be lower but there will be a gradual increase over the long-term as excess pore pressures dissipate, and if the ground deformations during construction are kept very small then the short-term load may be higher but there will be very little increase in the long-term. Another complicating factor is whether the tunnel lining acts as a drain or is impermeable and what effect this has on the long-term pore pressure distribution.

In summary, there are many unanswered questions remaining about how loads come onto tunnel linings in the short and long-term that have a negative impact on design. This is particularly true of sprayed concrete linings, for which there are very few data. This paper will present selected results from a detailed case study of stresses and strains in a shotcrete primary lining in London Clay over almost 20 years and will seek to answer some of these questions.

INTRODUCTION TO THE CASE STUDY

The main tunnels at Heathrow Express Terminal 4 station were constructed between May 1994 and November 1996. In order to confirm the adequacy of design, particularly of the sprayed concrete primary lining, a considerable array of instrumentation was installed and monitored during construction. In previous papers the movements ahead of the advancing concourse tunnel (van der Berg et al., 2003), and the in-tunnel displacements and surface settlements (Clayton et al., 2006) were presented. An earlier paper by Clayton et al. (2002) studied the performance of pressure cells in sprayed concrete linings, focussing mainly on laboratory tests and numerical modelling to improve understanding of cell action factor, temperature sensitivity and installation effects, but did not present a complete set of field data. The radial pressure cell data up to 8 years were previously published in Jones (2005).

The layout, geology, construction sequence and construction details of the concourse and platform tunnels were described in van der Berg et al. (2003) and Clayton et al. (2006), but important details will be replicated here. The layout of the Heathrow Express Terminal 4 station is shown in Figure 3. It consists of two platform tunnels with a central concourse tunnel at the north-eastern end. These tunnels are connected by a series of cross-passages and connected to the north and south ventilation tunnels at each end. The concourse tunnel was constructed after the platform tunnels but before the crosspassages. The downline ventilation tunnel, which connects the north ventilation tunnel to the downline platform tunnel, underpassed the concourse tunnel while the concourse tunnel was itself being constructed.

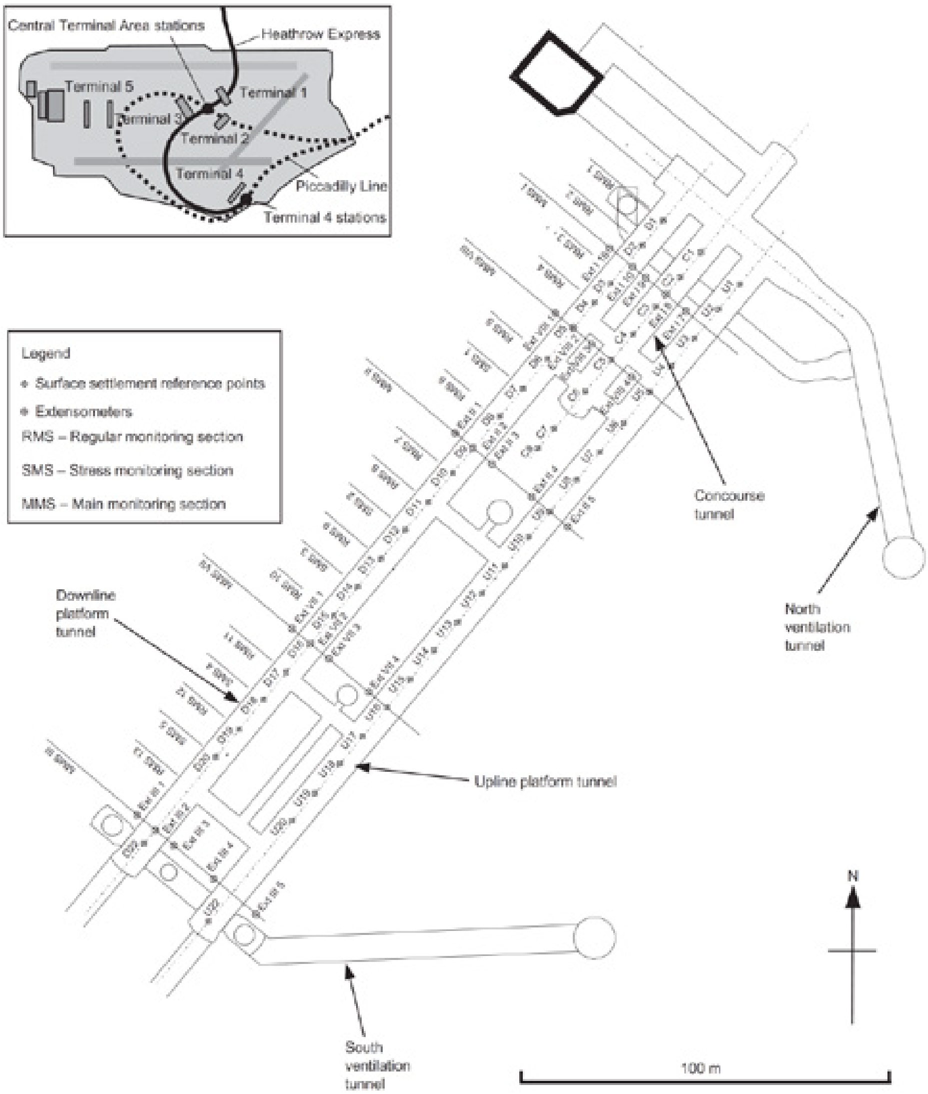

Figure 3: Plan of tunnels at Heathrow Express Terminal 4 station, showing location of concourse tunnel and layout of monitoring points and instruments (from van der Berg et al., 2003).

The platform tunnels were over 220 m long with a cross-sectional area of 62 m^2, and the concourse tunnel was 64 m long with a cross-sectional area of 49 m^2. A typical cross-section of the concourse and platform tunnels is shown in Figure 4, which also shows the surface level and geological strata. The concourse tunnel axis is at a depth of approximately 17.2 m below ground level and the tunnel is entirely within the London Clay. Piezometers across the site and at different depths indicated a piezometric level in the Terrace Gravels at approximately ground level with a hydrostatic distribution from there down to the basal beds of the London Clay, well below the tunnel horizon (van der Berg et al., 2003). The centreline spacing between the concourse tunnel and the platform tunnels was 13.5 m.

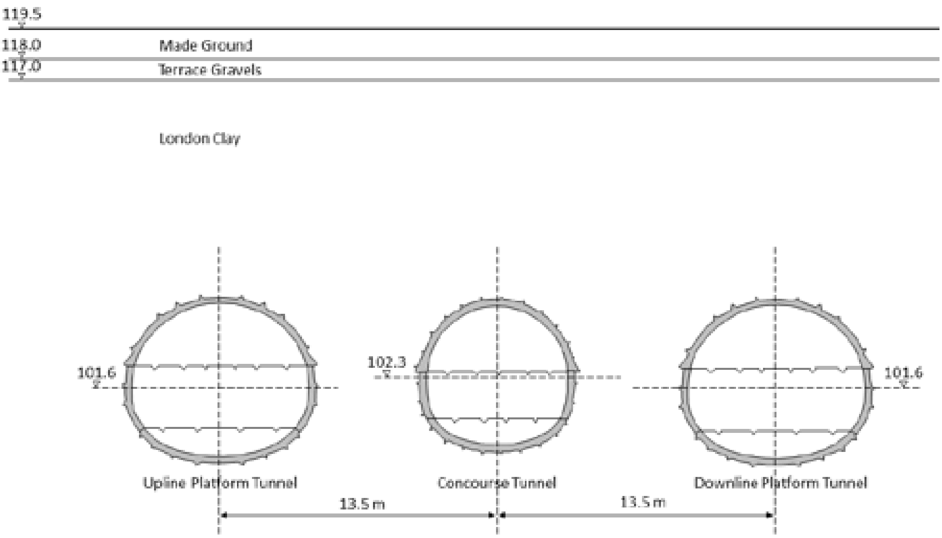

Figure 4: Cross-section of concourse and platform tunnels at MMS I or MMS VIII, looking south. Levels are in m above tunnel datum, which was set 100 m below Ordnance Datum.

The construction sequence for the concourse tunnel used a top heading, bench, top heading, bench, double-invert sequence. The invert was closed a maximum five rounds from the face. The construction sequence is schematically illustrated in Figure 5. The advance length varied from 0.8 m to 1.2 m depending on ground conditions and design requirements, including the proximity of sensitive structures. The primary support for the concourse tunnel consisted of 350 mm of shotcrete, reinforced with two layers of welded wire mesh (8 mm diameter at 150 mm centres) and full-section lattice girders 'Type 110 ROM E3'. The exposed ground was supported by a 50–100 mm shotcrete sealing layer applied immediately after each advance. The 350 mm total thickness included the sealing layer.

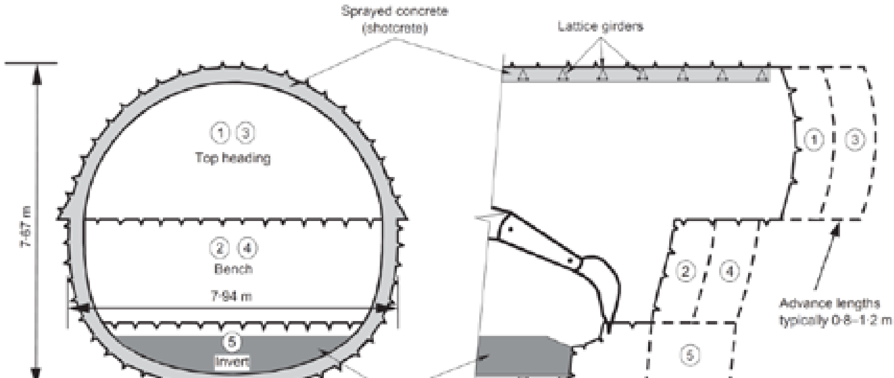

Figure 5: Concourse tunnel construction sequence (from van der Berg et al., 2003).

The typical construction procedure was as follows. Excavation was carried out using a track-mounted excavator. Areas where the radial pressure cells were to be placed were prepared and covered with timber (van der Berg et al., 1998). The nozzleman then applied a sealing layer of shotcrete, typically between 50 mm and 100 mm thick, on all the exposed London Clay surfaces, including the face. Following the application of the sealing layer, the radial pressure cells were installed against the ground on a bed of weak mortar. Then the lattice girder and first layer of mesh were installed. The first layer of shotcrete was then applied. The tangential pressure cells were then secured in their positions in the centre of the lining thickness with their longest dimension (200 mm) in the longitudinal tunnel direction and 100 mm dimension in the radial orientation. A second layer of shotcrete was then applied. Then the second layer of mesh was fixed and finally, a third layer of shotcrete was applied. Some excavated material was used to fill the invert of the tunnel, which served as a working platform and access when excavating the top heading and bench. Strain gauges were welded to approximately 500 mm long 8 mm diameter reinforcement bars and the bars were then fixed to either the outer or the inner layer of mesh in the tangential orientation.

This paper will focus on the long-term readings from pressure cells and strain gauges installed in Main Monitoring Section I (MMS I) and Main Monitoring Section VIII (MMS VIII) of the concourse tunnel. The locations of these sections were shown in Figure 3. At each section, 12 tangential pressure cells and 12 radial pressure cells were installed. The locations are shown in Figure 6.

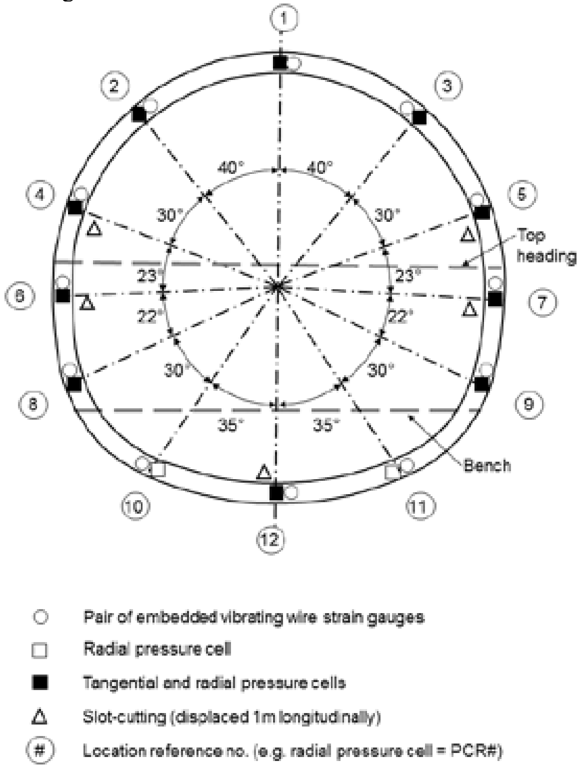

Figure 6: Section schematically showing locations of pressure cells and strain gauges embedded in the sprayed concrete primary lining at MMS I and MMS VIII.

RESULTS FROM RADIAL PRESSURE CELLS

Selected results from the MMS I and MMS VIII radial pressure cells will be presented. The readings are compared to the in situ stress normal to the lining calculated at the positions of the radial pressure cells, based on a bulk unit weight for the Made Ground, Terrace Gravel and London Clay of 19.5 kN/m^3 and a coefficient of earth pressure at rest (K_0) of 1.5 (Powell et al., 1997).

MMS I radial stresses

Figure 7 shows the average of all the radial pressure cells in MMS I as a percentage of the average in situ radial stresses. Also shown are the average temperatures measured by the thermistors attached to the pressure cells. Casting the invert section of the secondary lining caused a transient increase in temperature and an increase in radial pressure at the invert. Underpassing by the downline vent tunnel, only 5 m below the concourse tunnel, caused decreases in radial pressure, particularly at the bench and invert. Shortly afterwards the radial pressure cells in the crown stopped functioning, probably caused by damage to the cables when the upper part of the secondary lining was cast.

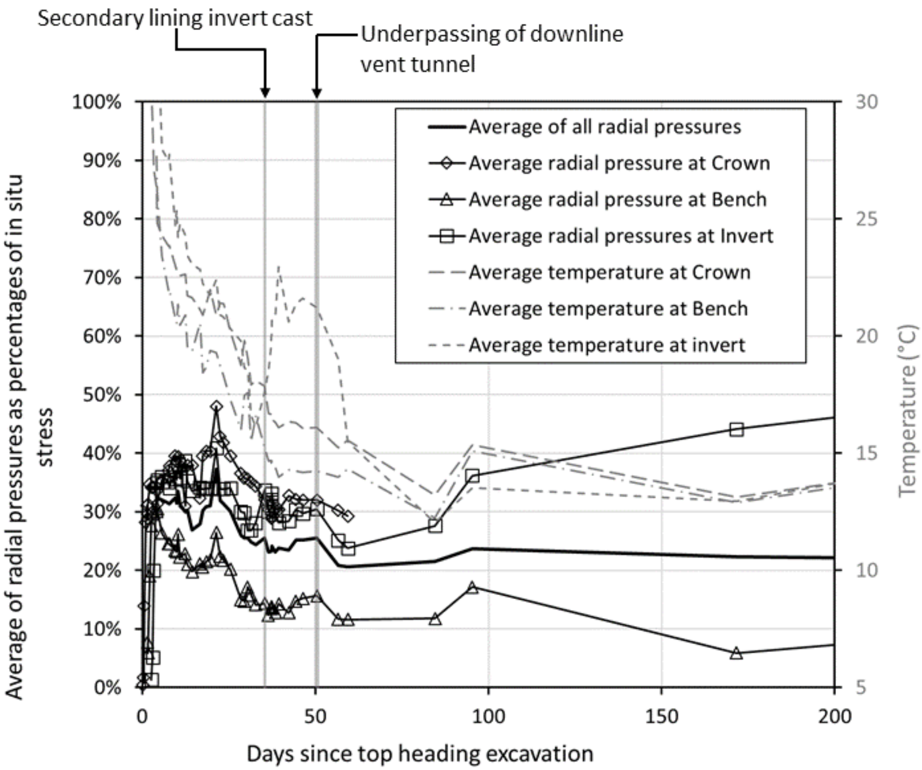

Figure 7: MMS I - average of radial pressures as percentages of in situ radial stresses at Crown (PCR1-5), Bench (PCR6-9) and Invert (PCR10-12), and average temperatures, from invert closure to 200 days.

It is important to remember that this was not a greenfield situation, and the radial pressures were influenced by the adjacent north vent tunnel enlargement, downline vent tunnel and the platform tunnels, as well as at times by compensation grouting. However, the long-term trends may still provide valid insights into the behaviour of sprayed concrete tunnels. The MMS I radial pressures over 18.6 years are shown in Figure 8. The two most recent readings of average radial pressures in the crown were from position 3 only. The radial cell at position 3 had not responded for many years and so these values should be treated with some caution.

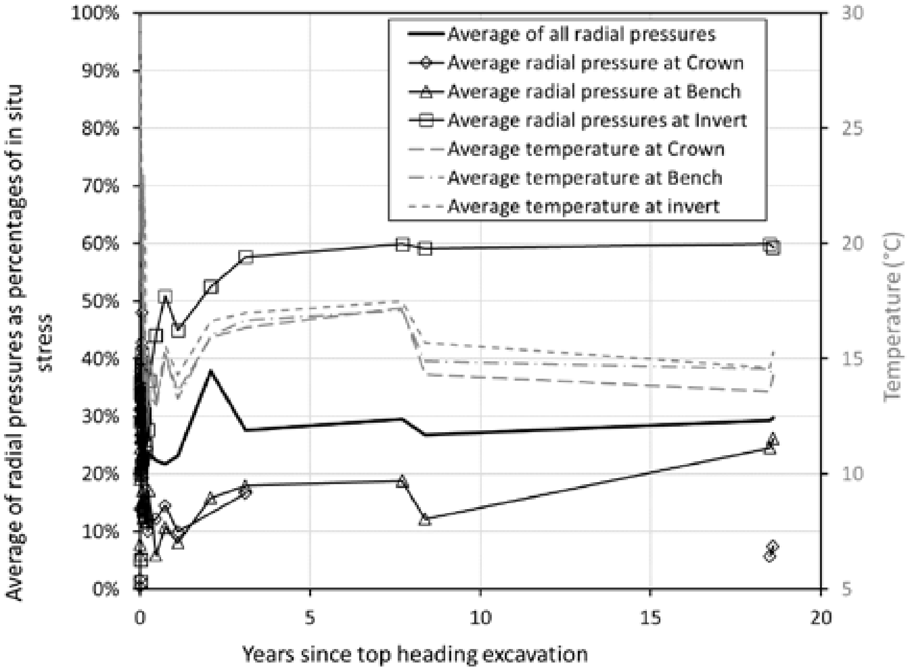

Figure 8: MMS I - average of radial pressures as percentages of in situ radial stresses at Crown (PCR1-5), Bench (PCR6-9) and Invert (PCR10-12), and average temperatures, from invert closure to 18.6 years.

The fluctuation of average radial pressure between readings at 2.1 and 3.1 years is because readings could not be obtained from all the pressure cells each time and so the average was affected. Apart from this blip, we can see a strong dependence of radial pressure on temperature, which is particularly noticeable between the readings at 7.7 and 8.4 years. This has been estimated to be of the order of 7 kPa/°C and is due to thermal expansion and contraction of the tunnel lining, increasing and decreasing the radial pressure between the ground and the lining. This was referred to by Jones (2005) as ‘ground reaction temperature sensitivity’, to differentiate it from other kinds of temperature sensitivity that affect radial and tangential pressure cells. Therefore, a tunnel lining does not have a single state of long-term equilibrium, but an equilibrium that changes as the temperature in the tunnel varies.

MMS VIII radial stresses

The survivability of the MMS VIII radial pressure cells was much better than for MMS I, and so there is more detail available in the results. The readings over the first 100 days are shown in Figure 9. Again, casting the invert section of the secondary lining caused an increase in temperature and radial pressure at the invert. The increase in radial pressure was partly caused by temperature and partly caused by added weight.

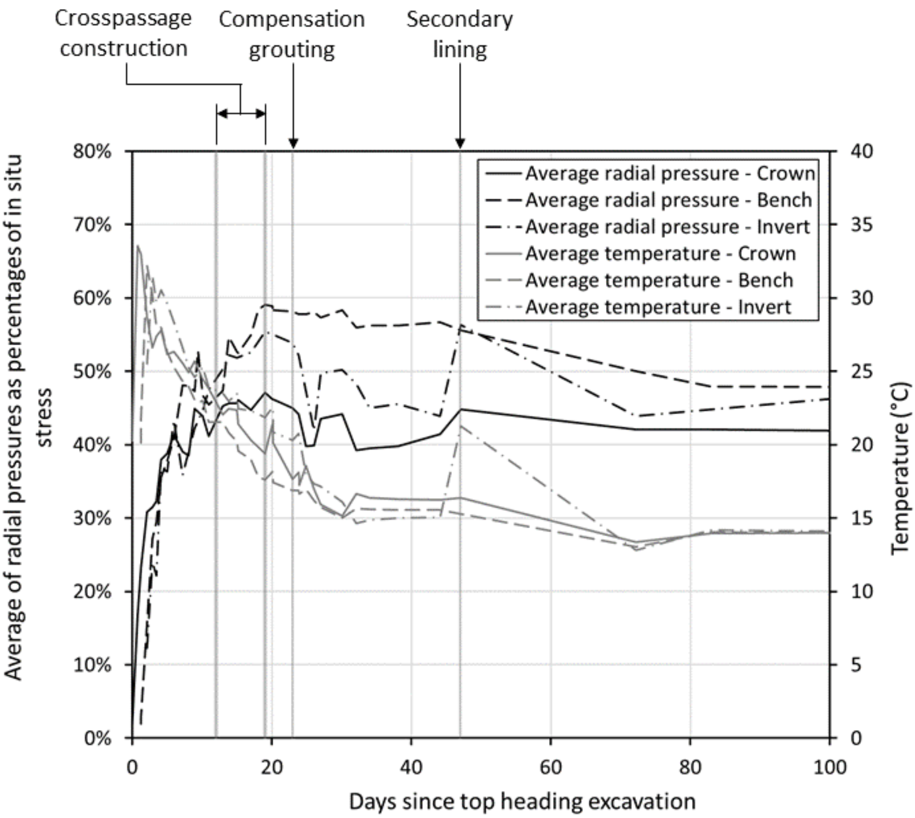

Figure 9: MMS VIII – average of radial pressures as percentages of in situ radial stresses at Crown (PCR1-5), Bench (PCR6-9) and Invert (PCR10-12), and corresponding average temperatures.

Figure 10 shows the long-term trends of average radial pressures at the crown, bench and invert at MMS VIII. Although there was a gradually slowing increase of radial pressures, radial pressures over this timescale were dominated by temperature effects, with a magnitude of around 7 kPa/°C. There will be no final equilibrium value of radial pressure, as it will constantly be changing as temperature changes. However, the measured radial pressures were between 40 % and 77 % of the in situ radial stress at 18.6 years, with an average of 59 %, at an average temperature of 14.2°C.

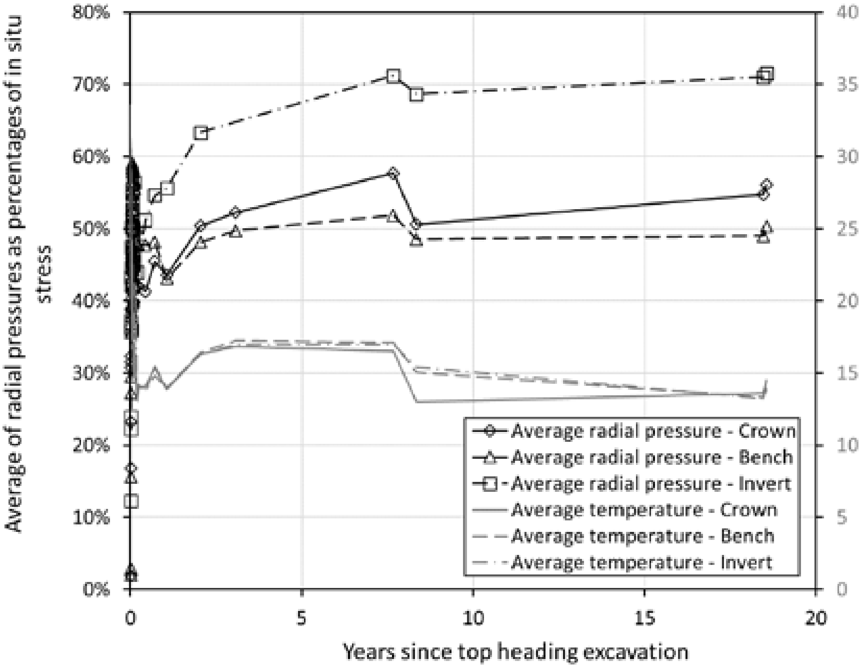

Figure 10: MMS VIII - average of radial pressures as percentages of in situ radial stresses, and average temperatures, at Crown, Bench and Invert, from construction to 18.6 years.

The invert radial pressures in Figure 10 are higher than at the crown and bench, and this was also true in MMS I (Figure 8). The vertical pressure acting on the invert should be in equilibrium with the vertical pressure on the crown plus the weight of the tunnel lining plus any shear stress on the sides of the tunnel, so it is reasonable for the invert radial pressures to be higher than the crown radial pressures. The reason why the bench radial pressures appear to be lower is that pressures are presented in the graphs as a percentage of the in situ total stress at the location and orientation of the pressure cells. The horizontal in situ total stress is higher than the vertical because K_0 has been taken as equal to 1.5. It is known from large numbers of lining measurements by Wright (2013) , that after tunnel excavation in London Clay horizontal stresses acting on a tunnel lining are always lower than vertical stresses, and the in situ K_0 does not reassert itself.

COMPARISON WITH TANGENTIAL PRESSURE CELLS AND STRAIN GAUGES

There is insufficient space in this paper to present even the radial pressure cell results in full, let alone the tangential pressure cell and strain gauge results, which require significantly more interpretation. These will be published in detail elsewhere. However, some comparisons will be made to highlight or confirm certain aspects.

What happens in the long-term after construction activities have ceased?

The radial pressure cells indicate that there is little or no increase in radial pressure acting on the tunnel lining in the long-term. This is corroborated by the tangential pressure cells, which show negligible changes in the stress state of the primary lining in the long-term that cannot be attributed to ground reaction temperature sensitivity.

It is also corroborated by the 48 strain gauges, which showed a very small increase in strain over the first 3 years, followed by a very slight decrease in strain over the subsequent 15-16 years. An example is shown in Figure 11. It should be noted that strain gauges will not notice changes in temperature, as their coefficient of thermal expansion is very similar to that of concrete, so they do not register the effect of ground reaction temperature sensitivity.

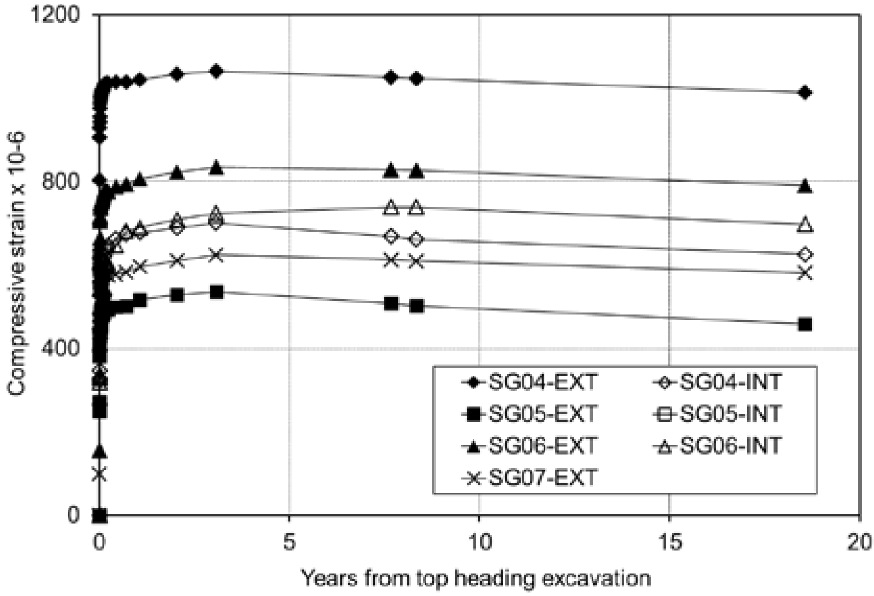

Figure 11: Extrados (-EXT) and intrados (-INT) strain gauges at positions 4-7 in MMS VIII.

One possible explanation for the slight increase in compressive strain between 1 and 3 years is a slight increase in radial pressure during this period and ongoing compressive creep of the lining. It seems unlikely that much shrinkage would occur after installation of the waterproof membrane and after the lining is already 1 year old. The subsequent slight decrease in the longer term may be due to water penetration, which will be discussed in the following section.

Is the groundwater pressure acting on the secondary lining in the long-term?

In the original design for this tunnel, the primary lining was assumed to be permeable and temporary, and so a sheet waterproof membrane was installed, followed by a secondary lining to support the water pressure and the ground loads. Unfortunately, no instrumentation was installed in the secondary lining, so it is difficult to know what its stress state actually is.

In the short-term, ground and water loads are applied to the outside of the primary lining. Then the waterproof membrane and secondary lining are installed, and there are 2 possible scenarios:

- If the primary lining is watertight, the situation will remain unchanged. Any further increments in ground or water load after secondary lining installation may be shared with the secondary lining, but this would need to be a significant increment to overcome the differential shrinkage and any compliance in the geotextile fleece and waterproof membrane. In fact, the increment of stress needed to make contact with the secondary lining is so large (perhaps > 10 MPa) that it is theoretically impossible for a tunnel at this depth.

- If the primary lining is permeable, groundwater will penetrate to the back of the waterproof membrane, flowing around the outside of it and applying a hydrostatic pressure. This water pressure can only be supported by the secondary lining.

Given the results of long-term structural monitoring of the primary lining, we know it has not substantially degraded or experienced structural failure. Therefore, there are only two possibilities: either water has penetrated to the back of the waterproof membrane, or it has not. The ground loads are still supported by the primary lining, but the water load may be supported by either the primary or the secondary lining.

Radial pressure cells measure *total* stresses, so if the primary lining were saturated and the water pressure was acting on the secondary lining, then they would not notice any change. This is illustrated in Figure 12.

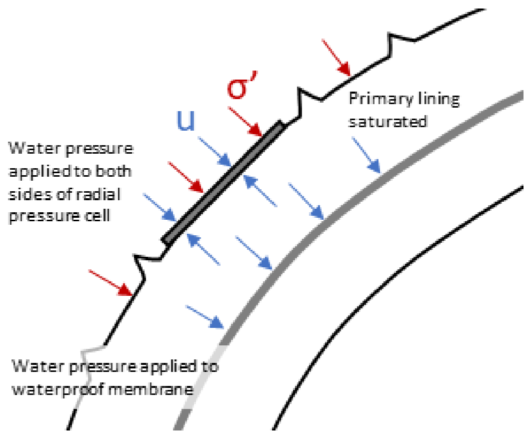

Figure 12: Effect of primary lining saturation on radial pressure cell

If the water did penetrate the primary lining to act on the waterproof membrane, then this would result in a reduction in tangential compressive stress in the primary lining as the water pressure on its extrados and intrados balanced out. But if the primary lining were saturated, then the water pressure would still be applied to the tangential pressure cells and they would not register a change in stress state.

What would happen to the strain gauges measuring tangential strains in the primary lining? Unloading of the concrete as water pressure is applied to both the extrados and the intrados should result in a reduction in compressive strain as the primary lining stress is based only on the applied radial effective stress from the ground. This may be the cause of the gradual reduction in compressive strain between 3.1 and 18.6 years as shown in Figure 11, which was on average 44 x 10^{-6} for MMS I and 34 x 10^{-6} for MMS VIII. This reduction may have other causes (e.g. chemical changes in the concrete causing swelling) but given the lack of response of the pressure cells, the most likely explanation is penetration of water.

It is impossible to say for sure in this case whether the water load is being taken by the primary or the secondary lining, but it seems likely that water has penetrated, and the water pressure is acting on the secondary lining. It is recommended that instrumentation is installed in a secondary lining (or perhaps piezometers installed behind the waterproof membrane) of future tunnels to investigate this.

Is there sharing of ground load between the primary and secondary linings?

Load sharing of ground load between the primary and secondary linings can be partial (scenario 1), complete transfer of all loads to the secondary lining (scenario 2), or no transfer to the secondary lining (scenario 3). This is illustrated in Figure 13.

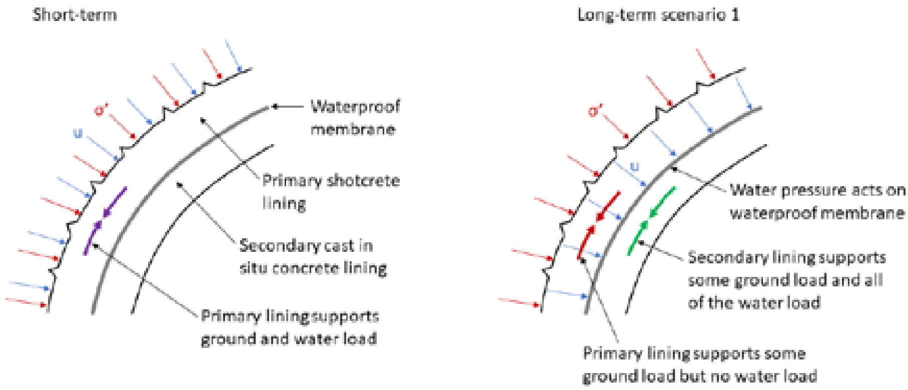

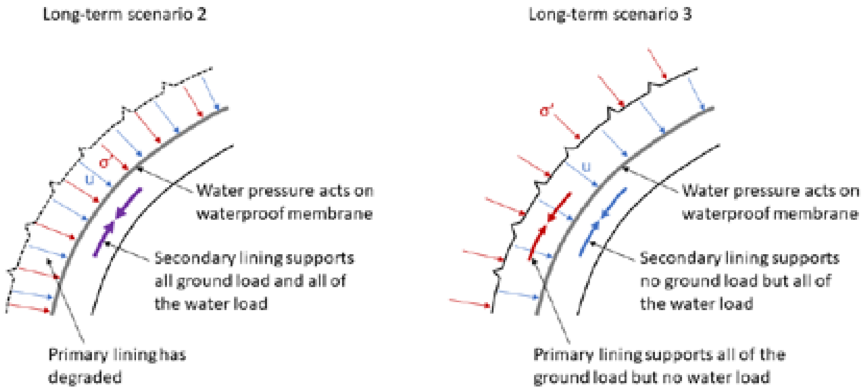

Figure 13: Different scenarios for transfer of ground and water loads to primary and secondary linings

As discussed previously, partial load sharing (scenario 1) is unlikely, as for this case study it would require failure of the primary lining, in which case one would assume most if not all the load would be transferred (scenario 2). The current situation in the Heathrow Terminal 4 concourse tunnel is probably where the water load is applied to the secondary lining, but the ground loads are supported by the primary lining (scenario 3), though it is possible that the short-term situation where both ground and water loads are applied to the primary lining is still active.

CONCLUSIONS

Long-term structural monitoring of the Terminal 4 Station concourse tunnel indicates that ground loads on shotcrete primary linings will stabilise at a value well below full overburden pressure, as has been found by several other previous studies on tunnels in London Clay. The reasons why some tunnels experience loads up to full overburden pressure are not well-understood but could be due to the amount of ground deformation allowed during construction, and whether the tunnel lining is impermeable or acts as a drain on the ground around the tunnel.

The reasons why some tunnels achieve their long-term stable load within a few weeks or months of construction, but some take up to 3-4 years or more are also not well understood. This may be to do with how long it takes for pore pressures to reach equilibrium or a steady state.

Tunnels do not have a single long-term state of equilibrium. As temperature in the tunnel increases and decreases, the tunnel lining expands and contracts against the ground, increasing and decreasing the radial pressure at the ground-lining interface. This has been termed ‘ground reaction temperature sensitivity’. In some cases, for instance for London Underground tunnels where during tunnel operation the temperature in the lining and the surrounding ground gradually increases over many years, one may expect a gradual long-term increase in lining stress as a result.

If the groundwater has permeated through the primary lining and the water pressure is acting hydrostatically on the outside of the waterproof membrane, this will not be registered by radial or tangential pressure cells because they measure total stresses.

It is likely that for this case study, by about 3 years after construction the groundwater had permeated through the primary lining and the secondary lining is now supporting the groundwater load. On the other hand, it is very unlikely that the secondary lining is not supporting any of the ground load (the effective stress).

Stresses and strains in tunnel linings are very rarely measured. To improve design predictions for future tunnels, and to better understand the tunnels we have already built, we need this kind of data.

REFERENCES

Barratt, D. A., O'Reilly, M. P. & Temporal, J. (1994). Long-term measurements of loads on tunnel linings in overconsolidated clay. In *Proc. Tunnelling '94*, pp.469-481. London: IMM.

Belshaw, D. J. & Palmer, J. H. L. (1978). Results of a program of instrumentation involving a precast segmented concrete-lined tunnel in clay. *Can. Geotech. J.* **15**, 573-583.

Bonapace, P. (1997). Evaluation of stress measurements in NATM tunnels at the Jubilee Line Extension Project. In *Proc. of Tunnels for People* (eds. Golser, Hinkel & Schubert), pp.325-330. Rotterdam: Balkema.

Bowers, K. H. & Redgers, J. D. (1996). Discussion: Observations of lining load in a London Clay tunnel. In *Proc. Int. Symp. on Geotechnical Aspects of Underground Construction in Soft Ground* (eds. Mair & Taylor), London, UK. Rotterdam: Balkema.

Clayton, C. R. I., van der Berg, J. P., Heymann, G., Bica, A. V. D. & Hope, V. S. (2002). The performance of pressure cells for sprayed concrete tunnel linings. *Géotechique* **52**, No.2, 107-115.

Clayton, C. R. I., van der Berg, J. P. & Thomas, A. H. (2006). Monitoring and displacements at Heathrow Express Terminal 4 station tunnels. *Géotechnique* **56**, No.5, 323-334.

Jones, B. D. (2005). Measurements of ground pressure on sprayed concrete tunnels using radial pressure cells. *Proc. Underground Construction 2005*, London, UK. London: Brintex.

Jones, B. D. (2012). A loaded question. *Tunnelling Journal*, April-May issue, 26-28.

Muir Wood, A. M. (1969). Written contribution, plenary session 4. In *Proc. 7th Int. Conf. on Soil Mechanics and Foundation Engineering*, Vol.3, Mexico, pp.363-365.

Skempton, A.W. (1943). Discussion of Groves, G.L., Tunnel linings with special reference to a new form of reinforced concrete lining. Journal of the Institution of Civil Engineers, Vol.20, No.5, March, 53-56.

van der Berg, J. P., Clayton, C. R. I. & Hope, V. S. (1998). An evaluation of the role of monitoring during the construction of shallow NATM tunnels in urban areas. *Proc. North American Tunnelling '98* (ed. L. Ozdemir), Newport Beach, California, USA, pp.251-257.

van der Berg, J. P., Clayton, C. R. I. & Powell, D. B. (2003). Displacements ahead of an advancing NATM tunnel in the London clay. *Géotechnique* **53**, No.9, 767-784.

Ward, W. H. & Chaplin, T. K. (1965). Existing stresses in several old London Underground tunnels. In *Proc. 4th Int. Conf. on Soil Mechanics and Foundation Engineering*, Montreal, Vol.2, pp.432-436.

Ward, W. H. & Thomas, H. S. H. (1965). The development of earth loading and deformation in tunnel linings in London Clay. In *Proc. 6th Int. Conf. on Soil Mechanics and Foundation Engineering*, Toronto, Vol.2, pp.432-436.

Wright, P. J. (2013). Validation of soil parameters for deep tube tunnel assessment. *Proc. ICE Geotechnical Engrg* **166**, No.1, 18-30.

TamCrete SSL (Structural Spray-on Liner)

Odd-Bjørn Kleven Normet Group, Switzerland

For Underground Rock support, mesh and bolts was for decades the ultimate (and only) option for Rock Support. Introduction of Sprayed concrete, for the last about 35 years by the wet method, took the Rock Support to a new level. Sprayed Concrete has to a large extent replaced mesh, via its main benefits of "preventing" the rock from starting to move; safe application by Robotic application; no personnel exposed under unsecured rock, and the speed of application. Rock bolting is still needed to perform a proper Rock Support in poor ground conditions.

Introduction

For many years, there has been an on-going development of Thin Spray-on Liners (TSL), based on "requests"/wishes from the Mining market, without any real breakthrough. The SSL (Structural Spray-on Liner), is a slightly different concept as it is a more rigid material, but still a relatively thin shell, sprayed on to a thickness of 5 – 10 mm. The material gains 70 – 80% of its final mechanical strength within 3 – 5 minutes, making it suitable for immediate support.

This paper will give an overview of our experience from different sites such as rehabilitation work in room and pillar mining or as final permanent shell in hard rock conditions. The paper will also discuss the usage concepts for:

- immediate active strata support
- alternative to mesh
- rock burst zones
- shaft sinking
- immediate sealant against weathering
- final conclusion

The paper will show results from field and lab tests, discuss the limitations and give an outlook on future development.

1. Immediate active strata support.

In both tunnelling and mining, thin coatings of concrete (4-5 cm thickness) are used as temporary rock support.

But while the final concrete lining of 20-30 cm acts via the arch effect, a thin liner acts via bond to substrate and point loads against its tensile-, shear and flexural strength. To assess the functionality of thin linings their tensile strength and bond strength is more important than compressive strength and this needs to be evaluated.

For sprayed concrete, especially in an early stage, the direct tensile strength is not measured and will be very low. Many engineers estimate the tensile strength by rule of thumb to be about 10% of the compressive strength.

In the literature there are different correlations where e.g. the British Code of Practice BS 8007:1987 offers the following formula:

$F_{tensile} = 0.12\,F_{compression}^{0.7}$

(see also “Properties of Concrete” A.M. Neville, Fourth Edition ISBN 0-582-23070-05)

Following the above basis, J1, J2 and J3 of the Austrian Guidelines will give:

Concrete Age (Hours)		Compressive Strength (N/mm²)			Tensile Strength MPa				
		J1	J2	J3	J1	J2	J3	SSL	Concrete
6min	0.10		0.200	0.500	0.000	0.039	0.074		
10min	0.17	0.100	0.240	0.670	0.024	0.044	0.091	1	
30min	0.50	0.155	0.350	1.200	0.033	0.058	0.136		
	1.00	0.205	0.520	1.760	0.040	0.076	0.178	1	
	2.00	0.315	0.775	2.600	0.053	0.100	0.234		
	3.00	0.405	1.000	3.250	0.064	0.120	0.274		
	6.00	0.635	1.470	4.750	0.087	0.157	0.357		
	9.00	0.830	1.850	5.970	0.105	0.185	0.419		
	12.00	1.000	2.200	7.000	0.120	0.208	0.469		
	24.00	2.000	4.500	15.500	0.195	0.344	0.817		
7d	168.00							2	2.000
28d	672.00								4.000

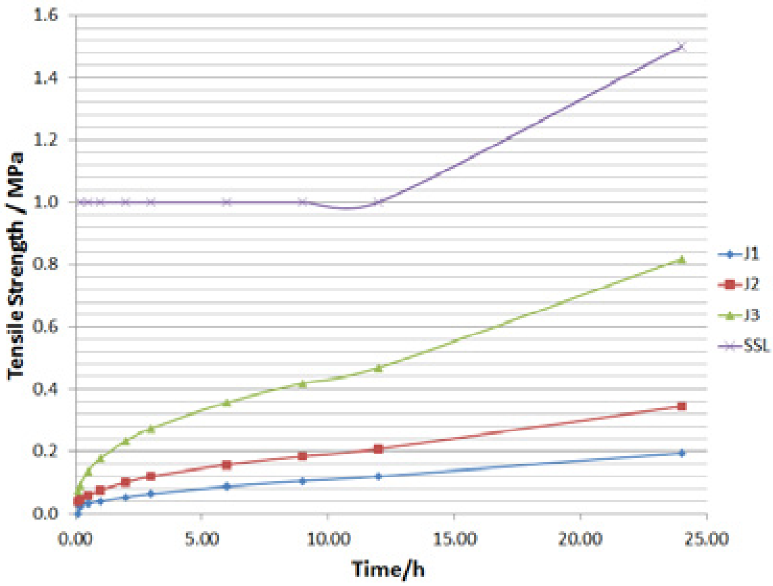

Failure mode of thin linings, flexural strength

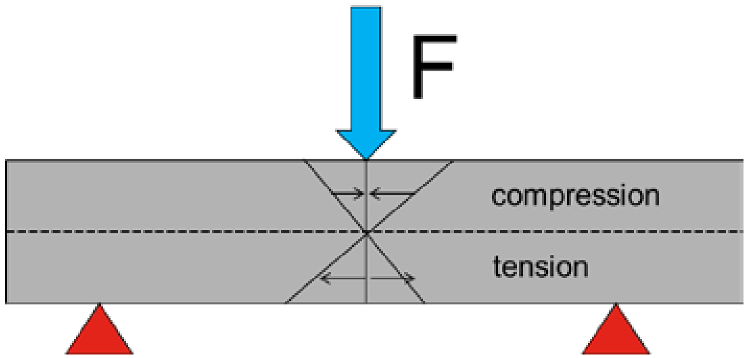

SSL as Rock support

Conclusion

The rapid curing of SSL gives a tensile strength after 10 minutes that sprayed concrete cannot gain within 24 h. The supporting effect is therefore practically immediate.

A comparison can only be made when the curing of sprayed concrete is known. SSL can achieve up to 10 times higher performance than the existing system.

2. Alternative to mesh

Mesh is used under a wide variety of rock conditions and more investigations are needed to identify when SSL may be an alternative. However, it is proven that an SSL product can replace mesh to a large extent, and further development of SSL with fibres will further improve its ability to replace mesh in many cases.

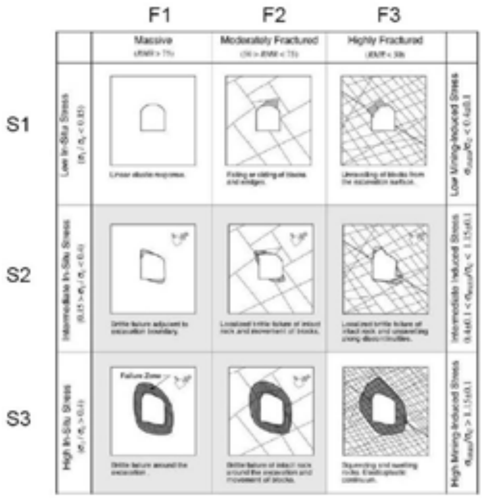

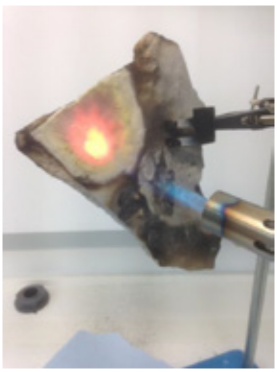

SSL Exposure to 1400°C

- 2.5 h no spalling
- 1 cm carbonization inside the SSL

Benefits of using SSL compared to mesh are:

- Fast (and possibly robotic) application. No need for personnel under unsupported ground
- Logistic of support material (just a fraction of the material weight needed per m^2)
- Product having a very high fire resistance (no toxic gases)
- Fast and easy to repair, if or when needed

Conclusion

Can replace mesh under various circumstances, but more investigations and documentation are needed to identify the best usage of SSL. Possible further development of the product is also expected to widen the range of rock conditions that may be controlled by SSL.

3. Rock burst zones

SSL, with its technical properties has shown benefits in Rock burst zones, by reducing failure in rock strata during a seismic event.

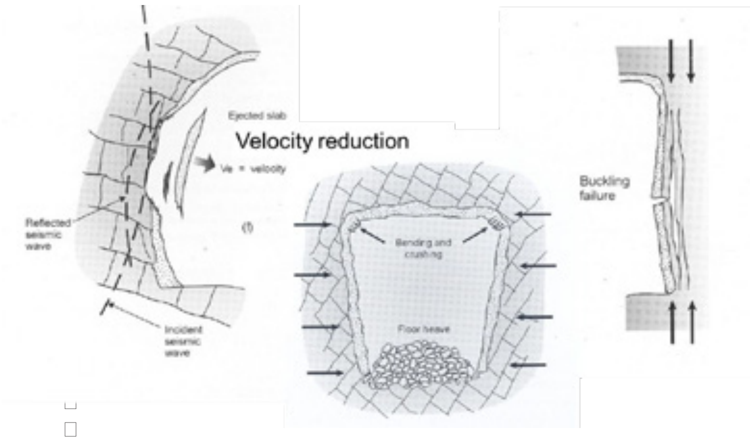

10.0 MPa	Compressive	in 2 hours
1.0 MPa	Tensile	in 2 hour
6.8 MPa	Flexural strength	in 2 hours

Conclusion

The technical performance has shown improvements and benefits in Rock burst zones, and there are strong reasons to believe that in connection with dynamic bolts it can reduce damages and improve significantly the safety factor in rock burst areas both in mining and tunnelling. In this area as well, further investigations and documentation are needed. Since rock burst is a dynamic release of high stresses, the best approach to damage control will typically be by a system offering high failure energy. SSL with extra high ductility and tensile resistance can probably be offered by combining the polymer product with suitable fibre material.

4. Shaft sinking

SSL has been successfully used in shaft sinking, both in mining and in tunnelling. The main benefits compared to sprayed concrete are:

- Light equipment
- Low consumption of product (due to very thin layer application)
- Low or hardly any rebound
- Ease of application, also within very small cross sections
- Increased shaft sinking progress due to ease and speed of SSL application as well as no waiting time for strength development.

TamCrete SSL treatment of weak rock zone in shaft D2, Raise bored shaft by Dragages in Hong Kong.
Presented at **Hong Kong Tunnelling Society**

5. Immediate sealant for anti-weathering

Since SSL is polymer based, it can be used as sealant against the influence of air and humidity. Many mines and tunnel sites want to stop the oxidation and swelling of ground. Typically, the ground is in solid hard rock condition after the blast, but may decompose into soft, sand-like material with time (air slaking).

Immediate sealants. No 100% coverage required.

- 99% coverage leads to 100 times slower decomposition
- 95% coverage leads to 20 times slower decomposition.
- 90% coverage leads to 10 times slower decomposition.

Conclusion

The faster the sealant acts, the better so fast setting times are beneficial. In hard rock a rigid product is preferable, like TamCrete SSL. In soft ground a thin flexible coating might be a better choice and both TamCrete SSL and TamSeal 800 will work. If waterproofing is the main purpose, TamSeal 800 is the best choice.

6. **Ilmala Water supply tunnel Helsinki, Finland**

For the Ilmala water supply tunnel some tests were requested by the designers and owners of the tunnel.

Following tests were requested:

- Adherence (Bond strength)
- Block Bearing capacity (practical)
- Penetration into cracks and joints
- Compressive strength
- Flexural strength

Apart from the Block bearing capacity, all tests were carried out with satisfying results. Block bearing capacity tests failed because of rock conditions in test area (very fractured rock), and the test plan was changed to test with the use of concrete panels, instead of in rock.

Photos from SSL being applied at Ilmala water supply tunnel rehabilitation

7. Final conclusion

The Structural Support Liner (SSL) offers benefits in many rock support situations and conditions as described above and in addition, the ease of application, low materials consumption and hardly any rebound, offers important advantages in TBM tunnels, especially in the L1 area. Research and practical experience shows already that SSL offers many advantages in various conditions and the potential for further improvements may be considered highly interesting.

8. References

Kothe T, Jakas P, 2017, *TamCrete SSL tests for HSY Ilmala Tunnel Final test report*

British Standards BS EN ISO, *Pull-off tests for adhesion*

British Standards BS EN 1015-11, *Methods of test for mortar for masonry. Determination of flexural and compressive strength of hardened mortar*

“CORRELATION BETWEEN TRIALS OF POLYMER FIBERS SHOTCRETE (SRF): FIBER CONTENT IN FRESH MIXTURE, ENERGY ABSORPTION AND BARCELONA TEST”

Carlos A., Madrid
Consortium Acciona Ossa, Calama, Chile
carlos.madrid@gmail.com

Sergio E., García
Vicepresidencia de Proyectos, CODELCO Chile, Chile
SGarc008@codelco.cl

Flavio B., Rodriguez
ACCIONA, Santiago, Chile
flavio.rodriguez@acciona.com

Claudio F., Parada
Elasto Plastic Concrete, Santiago, Chile
CParada@elastoplastic.com

ABSTRAC

The double-punch Barcelona Test [11], is a method for concrete with fibre. There is no record of any Barcelona Test review neither real scale comparison with others energy absorption trials in fortifications of mining and tunnels. The development of this study and application to Chuquicamata Underground Mine Project is unique in Chile and South America.

Carmona (et al 2015) proposed a similar intention, but this study used elements molded inside a laboratory. Instead, the present study was conducted using real scale samples of Shotcrete used in fortification works of minning tunnels.

The valid correlation between the tests of Energy Absorption on Square Panel (Efnarc o UNE [8]) and the Barcelona Test has its precedent for both cases in the fibre content trial on fresh mixture [9].

Chuquicamata Underground Mine Project (PMChS) is a structural and strategic operation for Codelco's future (its main business is copper exploitation). It's the change from world´s greatest open pit mine to a huge underground plan of action. This will explote the resources under the present deposit. This will give crucial safeness improvements, savings in test cost and quality control effectiveness in the remaining kilometer to develop inside the PMChS.

Keywords: Energy absorption, Concrete reinforced with fiber, Barcelona Test, Double-punch test of fiber-reinforced concrete, Shotcrete, Shotcrete Reinforced with fiber, Quality Control, Quality assurance.

CORRELATION BETWEEN TRIALS OF POLYMER FIBERS SHOTCRETE (SRF): FIBER CONTENT IN FRESH MIXTURE, ENERGY ABSORPTION AND BARCELONA TEST

INTRODUCTION

The double-punch Barcelona Test [11], is a method for concrete with fibre since July 2010. Its identification code, UNE EN 83515 Concrete with fibre, define it as a trial aimed to calculate its resistance to cracking, toughness and residual strength to traction (Barcelona Test [5]).

Although Shotcrete is used in fortifications of mining and civil tunnels, there is no record of any Barcelona Test review neither comparison with others energy absorption trials. Except for the academic researchings promoted by the laboratory of the Universidad Técnica Federico Santa María (Valparaíso, Chile).

Chuquicamata Underground Mine Project (PMChS) is a structural and strategic operation for Codelco's future (its main business is copper exploitation). It's the change from world´s greatest open pit mine to a huge underground plan of action. This will explote the resources under the present deposit. The PMChS is located in Chile's north (Figure 1), involving a serie of mining contract and underground works for the construction of mining galleries, caves, production tunnels and ore transport.

Figure 1. Geographic Location PMCh

The study was carried out under the contract of "Development of tunnels for main ventilation infrastructure", Acciona - Ossa Consortium (Figure 2). It considered areas where the shotcrete was sprayed directly on rock mass, therefore, in absence of steel mesh, steel framework or any kind of fortification. Each rock type, shotcrete thickness applied and fibre content were clearly identified.

The application of this study and its correlation within the Chuquicamata Underground Project will be pioneered in mining infrastructure and civil underground construction.

Figure 2. Access to the main ventilation tunnels

DESCRIPTION

The measurement of energy absorption in underground mining projects (Square Panel according to UNE-EN 14488- 5 normative, henceforth ABS), bring together operative and technical difficulties. Among them are the caused by panels weight, samples deterioration for other equipments and blast damages. Also, it was observed during the samples gathering others errors and omissions related with background information of samples manipulation and preparation, defective and unregistered panels, absence of evaluation criteria to panel discard and dispersion control, flexion measurement mistakes and high variability of results. These difficulties linked to quality control, demand an optimization and improvement of methodoly to evaluate the quality of Shotcrete with fibre.

The Barcelona Test trials (BCN) have already proved to be appropriate for the characterization and control of the reinforced concrete with fibre.

The manufacturing, transport and sprayed process of Shotcrete with fibre demand an exhaustive control. Hence, the authors estimate the viability of a study which link the trials with a new control method of performance. Consequently, in case of obtain a reliable result that proves the expected relationship, it will be possible to consider in a serie of benefits and improvements for the double-punch named BCN

This study was carried out in one of the contracts, which has proved to be an ideal controlled scenario during the last years. Thus, the execution of a Barcelona Test will increase the frequency of energy absorption trials, reduce the extraction risk, transport, manipulation and samples preparation.

The Table 1 summarizes the mix composition used by the contract since the samples gathering. This dosification has been used from the project beginning. And, the performance and the characteristic of the mixture have remained stable with the additives that are described.

Table 1. Mixture Design

Material	Quantity (kg/m3)	Observations
Cement	450 kg	Cemento Polpaico P400 UNE-EN 197-1:2000, CEM IV / A - AR ASTM C150, tipo II NCh 148.Of68: Portland Puzolánico Alta

		Resistencia
Water	208 kg.	
Sand	1.480 kg.	T.Max 8-10mm
Additive 1	4,36kg	Sika Viscocrete, Superplasticizer Additive UNE EN 934 T3. 1/3.2 ASTM C494 type F Nch 2182 Of95, type F
Additive 2	2,34kg	Sika Plastocrete, Additive Plasticizer Retarder UNE EN 934-5 T.2 ASTM C494 type D Nch 2182 Of95, type D
Additive 3	31,5 – 40,5kg (7-9% rpc)	Sika Sigunit AFA , Additive Setting Accelerator without alkaline UNE EN 934-5 T.2 Nch 148 Of168 / Nch 151 of 68 / Nch 152 Of71
Fiber	4 kg: CS1, CS2 y CS3 5 kg: CS4 y CS5	EN 14888-2, Class II. ASTM C-1116: Type III EPC-Barchip 54, with a length of 54 mm, a tensile strength of 640 MPa, a specific gravity of 9.1 kN / m3 and a Young's modulus of 10 GPa.
W/C	0,46	Average of all samples (w/c :water-to-cement-ratio)
Slum	22 - 24 cm.	Average of all samples
Energy Absortion.	>700 Joules: CS1, CS2, CS3 >1.000 Joules: CS4 y CS5	Project Requirements.

ANALYSIS OF RESULTS

The samples were gathering from each Shotcrete spraying in order to measurement energy absorption of the panel, fibre counting, besides samples of an additional panel to core extraction for the BCN. The samples total was 15. Once obtained, the samples were extrated from the tunnel for 24 hours and cured with wet burlap. After 20 days the energy absorption panels were cut and polished. At this time the cores were extracted following the spraying course for the BCN.

Each trials were performed between 40 and 50 days after Shotcrete spraying because the Chuquicamata Project (near Calama in Chile's north) is situated at 1530 kilometers from Valparaíso, were the BCN laboratory is established.

Insomuch as the fibre content and interference of this study on the contractor company, the counting was carried out during the unload of mixture in the spraying equipment. The data collected were close to the 95% of the value loaded in the plant. It considered the analysis with just 5kg/m of fibre.

The BCN tests were made at the constant speed of 0,5 mm/min. The circumferential dilation was measured with a strain gauge, fixed in a chain ends and set to the half of height of the specimen. The square trials were made in hydraulic system with 100 kN limit. The deflection was calculate with a 50 mm diameter needle, placed on the central lower face of the sample (Figure 3). After testing the 45 samples with the Barcelona test, the coefficient of variation between the samples was less than 10%.

Figure 3. Example Barcelona Test and Efnarc Test

The Table 1 summarizes the collected values with fibre doses of 4 kg/m3 and 5 kg/m3.

Table 1. Results promedios

Fiber doses	Values	Energy Absorption	Barcelona Test
4 kg/m3	Average	1027 J	279 J
5 Kg/m3	Average	986 J	270 J

Maintaining the same methodology and analytical sequence exposed by Carmona (et al 2016), two equivalents. The more advisable was the "nonlinear" because their relationship coefficient is r2 = 0,9976. Given by the expression (1) and illustrated by graph (Figure 3), where X axis represents the values expressed in Joules of BCN test, and Y axis, the values of the ABS test:

$$E_{ABS}(J) = 0{,}7191\ E_{BCN}{}^{1{,}2938}(J) \qquad (1)$$

Where:

EABS = Energy Absorption (Joule), Square panel test.

EBCN = Energy Absorption (Joule), Barcelona test.

Figure 3. Graph dose correlation with 5kg/m3

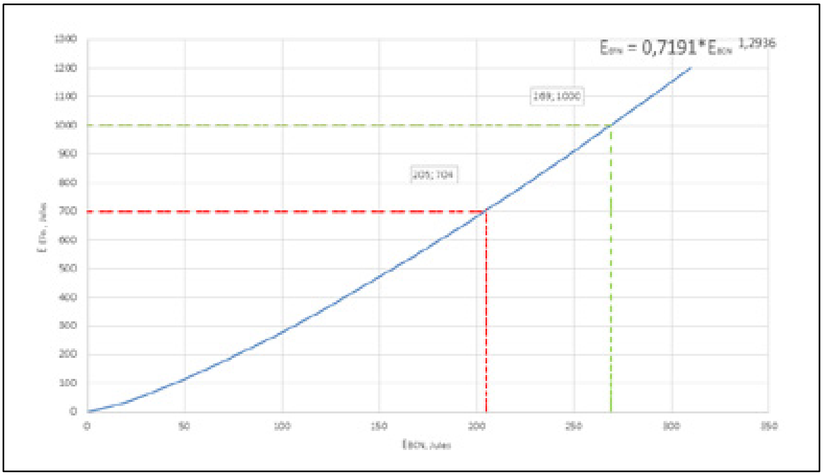

The expression (1) allows to use BCN test instead of ABS for the quality control of Shotcrete with fibre at 5kg/m3 dosage, in the PMChS main ventilation tunnels.

CONCLUSION

The equivalence stated by Carmona (et al. 2016) guides similar relationships under operative condition proper to each project and contract. Therefore, each project can made its own relationship valid for its operative conditions only and no extended to others scenarios.

The study made possible a "nonlinear" expression between energy dissipation de BCN (with a deformation limit of 6mm) able to absorb energy of the ABS (with a 25 mm deflection), with a very high determination coefficient, similar to Carmona's (et al. 2016)

Up to date, the study has gathered 2300 samples of absorption panels from the ventilation contract started at mid 2013. Undoubtedly, the samples with cores for BCN trials are a huge technical advantage for procedural safeness during sampling, core extraction, manipulation and samples treatment.

From the declared relationship, the fibre dosage still requires an optimization depending on fibre type and spraying equipment. However, it is a matter of another study.

It is mandatory a complementary study, linked to cores extracted from the substratum, compared with ABS and BCN, because the fibre quantity left on the substratum is relevant to fortification system behavior compared to a panel fibre quantityl.

Acknowledgements

To the Executive of the Chuquicamata Underground Project, Mr. Germán Flores, and to the Executive of Strategic Planning, Mr. Francisco Carrasco for their support in this kind of iniciatives and constant interest in quality management. To the Consortium Acciona Ossa Executive Mr. Jesús Ortego C. for his disposition to the study execution. To the Acciona Executive David Jimenez G. for his constant interest for efficiency.

REFERENCES

1. Carmona S., Molins, C. et. al 2016, Use of Barcelona test for controlling fiber Reinforced shotcrete in tunnelling
2. Molins, C.; Aguado, A.; Saludes, S., et. al 2009, Double punch test to control the energy dissipation in tension of FRC (Barcelona test). Mater Struct 2009, 42, 415–425.
3. Blanco, A. et al. 2014. Constitutive model for fibre reinforced concrete based on the Barcelona test. "Cement & concrete composites", 01 Octubre 2014, vol. 53, p. 327-340.
4. Cavalaro, S.H.P., López, R., Torrents, J.M. et al. Mater Struct (2015) Improved assessment of fibre content and orientation with inductive method in SFRC, 48: 1859. doi:10.1617/s11527-014-0279-6
5. Double Punch Test to evaluate indirect tensile strength of Fiber Reinforced Concrete: Barcelona Test, ISBN: 978-607-02-6283-8, diciembre 2013
6. AIRE, C.; CARMONA, S.; AGUADO, A.; MOLINS, C. Double-punch test of fiber-reinforced concrete: effect of specimen origin and size. ACI Mater J 2015, 112 (2), 199-208.
7. AENOR, UNE-EN 14488-1 : 2006 Testing sprayed concrete - Part 1: Sampling fresh and hardened concrete
8. AENOR, UNE-EN 14488-5 : 2007 Testing sprayed concrete - Part 5: Determination of energy absorption capacity of fibre reinforced slab specimens
9. AENOR, UNE-EN 14488-7 : 2007 Testing sprayed concrete - Part 7: Fibre content of fibre reinforced concrete
10. AENOR, UNE-EN 14889-2 : 2008 Fibres for concrete - Part 2: Polymer fibres - Definitions, specifications and conformity
11. AENOR, UNE-EN 83515 : 2010 Fibre reinforced concrete. Determination of cracking strength, ductility and residual tensile strength. Barcelona test.
12. EFNARC, European Specifications for spreyed concrete, 1996

ULTRA FAST RAPID HARDENING SPRAYED CONCRETE

Peter Mills, Steve Tadolini & Alun Thomas
Minova, USA & Denmark
alun.thomas4@minovaglobal.com

Summary

Early age strength has always been a big concern for tunnellers using sprayed concrete, particularly when spraying thick layers in soft ground. The industry has seen a series of developments in the use of accelerators to achieve this with ordinary Portland cements (OPC). Accelerators have always been accompanied by concerns over their impact on the long term strength and in some cases durability. The latest alkali-free accelerators overcame this but at the expense of the early age strength. Tekcrete Fast® is an innovation which overcomes these challenges – achieving both extremely high early strengths (41 MPa after 3 hours) and very durable concrete in the long term. Tekcrete Fast® also has good flexural strengths, thanks to the PVA fibres. Based on calcium sulfoaluminate cements rather than OPC, this could radically change sprayed concrete in tunnelling, improving safety and durability as well as potentially enhancing sustainability as a result of using thinner linings. Tekcrete Fast® is already being used in the mining sector and repair projects in civil engineering.

1. INTRODUCTION

The goal of a high early age strength has been at the heart of the development of sprayed concrete, especially in underground applications where the concrete can be loaded almost immediately. Generally this has been achieved by adding accelerators to Portland Cement (OPC) based concrete mixes but it remains a challenge, given the competing influences on the mix design [1]. Special "spray cements" were developed based on Portland Cement clinker with an optimised gypsum content to reduce the need for accelerators (e.g. [2] and [3]). However, these were not adopted widely in part because they required the use of oven dried aggregate for the highest early age strengths. The subject of Ultra high strength fibre reinforced concrete is also now gaining interest in the area of segmental linings as a means producing thinner linings.

This paper presents an innovative, high strength sprayed concrete, based on calcium sulfoaluminate cements. The main properties are described and the results of both laboratory and full scale tests are outlined.

2. BACKGROUND

Tekcrete Fast® was originally developed for the rapid stabilization of shock damaged structures, for example, due to earthquakes or explosions. As such it falls outside the purview of normal construction and mining practices because of the critical time issue and the nature of the damaged structure. The stabilization of damaged structures requires materials and equipment that can be rapidly deployed to place materials that have very rapid strength development. These materials need to be placed from a distance to provide some degree of safety to the rescue workers. In addition, the materials must be able to adhere to structural surfaces that have not been specially prepared and conditioned and which may also be highly fractured, dusty, wet, hot, or extremely cold.

The technology for the rapid delivery of large volumes of cementitious materials to vertical or even overhead surfaces is well-established. Pneumatic delivery (shotcreting / spraying concrete) has been used in construction for more than 100 years. Sprayed concrete is often used for rock support both on the surface and underground. In the course of the rapid development of this technique, a range of technologies, cements and additives have been developed. Sprayed concrete is also sometimes used for the repair of structures, such as bridges and buildings. In parallel one can find numerous rapid setting cements for use in the repair of structures on a small or large scale. However, few of these products are specifically marketed for use in sprayed concrete applications. The majority of rapid-setting cements are based on, or at least contain, Portland cement as the principle component. Other components are added that to help provide early strength, such as high alumina cement (HAC), organic polymers, chemical accelerators (which can also be added during concrete batching), and calcium sulfate hemihydrate (e.g., gypsum plaster) [4]. Cementitious mortars prepared with some of these cements can achieve compressive strengths of 6.8–13.8 MPa (1,000–2,000 psi) within 1 hour. However, Portland cement mortar and concrete typically require many weeks of proper curing to reach significant proportions of their ultimate strengths. In addition, high early strengths require the use of large proportions of Portland Cement in the concrete mix, which can lead to high heat evolution, excessive shrinkage of the material, and cracking. The cost also increases substantially with increasing cement content.

Alternatives to Portland Cement are also capable of rapid strength development. These include the well-known calcium sulfate hemihydrate and calcium sulfoaluminate (CSA) cements. Unlike Portland Cement, these rapid-setting cements can gain 75–80% of their strength within 1 day, which means less cement can be used in the mix to achieve comparable early strength. Additionally, CSA cement and calcium sulfate hemihydrates can be fabricated, for the most part, from Coal Combustion By-product (CCBs). These CCBs include fluidized bed combustion spent bed materials and forced air oxidation flue gas desulfurization by-products (i.e., synthetic gypsum), which potentially represents both a cost advantage, as well as an environmental advantage [5].

3. DEVELOPMENT OF TEKCRETE FAST®

As mentioned earlier, the primary considerations of this project were the rate of strength development (compressive and tensile), short-term dimensional stability (i.e. low shrinkage), and bonding strength to the damaged surfaces. Other considerations include heat generation, ease of use, stiffness of the set material, and cost. CSA cements were of interest in this application mainly because they gain strength very rapidly. They also require lower energy to produce, with significantly lower CO_2 emissions than Portland cement. CSA-based sprayed concrete mixes can be formulated so that they have lower cement content than Portland-based mixes, a higher water-to-cement ratio, lower viscosity, but still achieve very high early strength. This is due to the nature of the principal cementitious hydration product: ettringite. These properties are difficult to achieve with Portland cement-based rapid-setting materials. In addition, the large water-to-cement ratio of CSA cement mixes, coupled with the low heat hydration of plaster cement, offers a capacity to manipulate the heat of reaction of these materials within a wide band of strength and set parameters. Heat generation is critical in the rapid placement of masses of highly reactive cementitious materials. These cements also offer the potential of lower overall costs.

Unlike Portland cement, which gains its strength primarily from the hydration of the calcium silicates "alite" (Ca_3SiO_5) and "belite" (Ca_2SiO_4), calcium sulfoaluminate (CSA) cements contain Klein's compound, which hydrates in the presence of calcium sulfate (e.g., gypsum) to form a cementitious phase called ettringite [6]:

$$Ca_4Al_6O_{12}SO_4 + 2CaSO_4{\bullet}2H_2O + 34H_2O \rightarrow Ca_6Al_2(SO_4)_3(OH)_{12}{\bullet}26H_2O + 4\,Al(OH)_3$$

Klein's compound + Gypsum + water → Ettringite + Aluminium hydroxide

A compound similar to ettringite called "monosulfate" can also form under sulfate-deficient conditions. Belite is often present in CSA cement, but its hydration is slow and only contributes to long-term strength ([7] & [8]). Because of the rapid rate of formation of ettringite, CSA cements gain strength very quickly. If enough lime ($Ca(OH)_2$) and calcium sulfate is present in the system, additional ettringite can also be formed through the reaction with the aluminium hydroxide, a product of the Klein's compound. However, if the system contains excess lime, the cement can induce destructive expansion [6]. CSA cement actually represents a series with a broad range of compositions, from nearly pure Klein's compound to Klein's compound with belite, calcium ferroaluminate, or ($Ca_4(Al_2Fe_2)O_{10}$), free lime (CaO), calcium sulfate ($CaSO_4$), and other minor phases (e.g. $Ca_{12}Al_{14}O_{33}$). Three types of CSA cements were studied and tested during this project to determine which of the three types would meet project requirements.

4. PROPERTIES OF TEKCRETE FAST®

4.1 Testing programme

Once the CSA-based materials to be used in the sprayed concrete were developed and tested, they were used to produce mortars and concretes. After an initial round of screening, specimens prepared from selected mixes were tested for strength and shrinkage. When determining what tests to use to evaluate the chosen mixes, it was important to keep in mind that the sprayed-concrete material must provide structural strength within one hour and bond sufficiently to any substrate or surface under any conditions long enough to provide the necessary assistance to rescue workers.

A testing programme was developed based on standards that determine bond strength between different concretes and it included the following:

- compression and stability testing of ASTM standard cubes, cylinders, bars, and cores
- flexural strength beam testing
- tensile testing
- rapid freezing and thawing testing
- resistance to carbonation testing
- variations of heat production based on cement thickness
- calorimetry measurements for reaction time of CSA cement phases
- slant-shear testing
- pull-off testing
- time-of-set

These methods are all included in the ASTM International Specifications: C192, C109, C78, C293, and C666.

After years of research, Tekcrete Fast® was developed. Worldwide patents have been filed jointly by the University of Kentucky and Minova USA, Inc., and awarded [9]. This is an inherently durable mix since the chemical formulation avoids the risk of delayed ettringite formation, mentioned earlier. Hence Tekcrete Fast® is resistant to sulphate attack since the main product of hydration is ettringite. Tekcrete Fast® can be used in conventional, dry-process shotcrete equipment as a one-bag system. These features are ideal for use by emergency situations because there is usually little time to prepare the surface to be sprayed and simple, easily mobilized equipment is needed. This concrete can also to be used to repair tunnels, bridges, roadways, overpasses and runways in more normal situations where time is constrained or high strength is needed.

4.2 Compressive strength

Tab. 1 shows the average compressive strength for Tekcrete Fast® [10].

Tab. 1: Average compressive strength for Tekcrete Fast®.

Compressive strength, MPa (psi)						
15 min	30 min	1 hour	3 hour	1 day	7 days	28 days
17.2	24.1	31.0	41.4	55.2	62.1	75.8
(2,500)	(3,500)	(4,500)	(6,000)	(8,000)	(9,000)	(11,000)

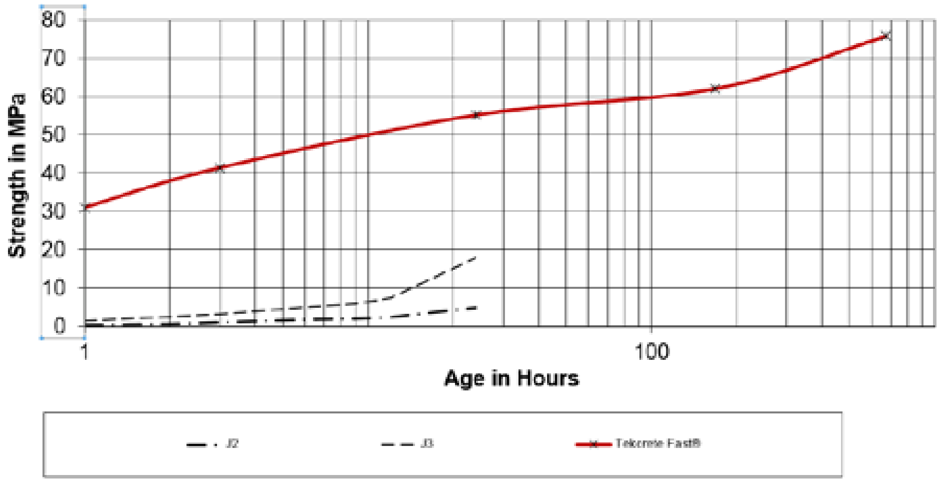

Figure 1 Compressive strength gain vs age compared to the J curves

4.3 Flexural strength

Tekcrete Fast® contains polyvinyl alcohol fibres to give it some tensile strength. Tab. 2 shows the average flexural strength for Tekcrete Fast® [10].

Tab. 2: Average flexural strength for Tekcrete Fast®.

Peak Flexural strength, MPa (psi)		
3 hours	1 day	7 days
8.3	9.7	11.7
(1,200)	(1,400)	(1,700)

Square panels were also tested in accordance with EN 14488-5 at 28 days. The energy absorption was recorded as 300 Joules after 10 mm of displacement (see Figure 2). There may be scope to optimize the fibre time to bring this energy absorption up to higher levels – e.g. such as the 700 Joules normally required in the Q system for tunnel rock support.

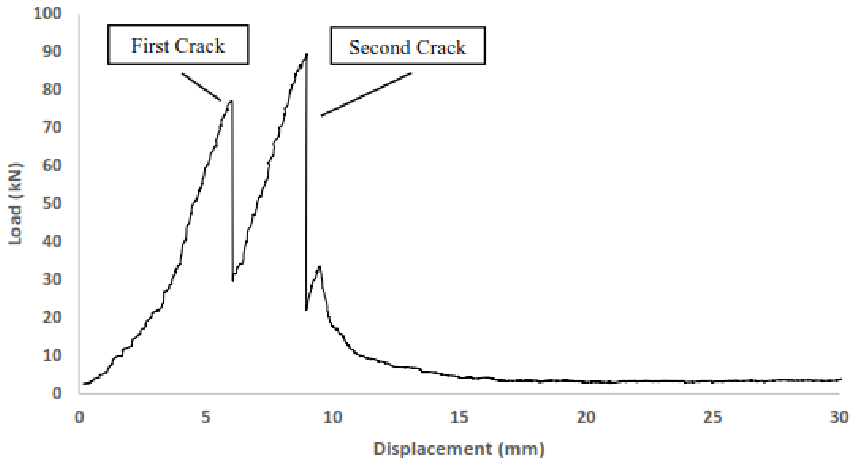

Figure 2 Load-displacement curve from a panel test

4.4 Adhesion

Tekcrete Fast® has the ability to adhere to any structural surface, whether it is fractured, wet, hot, or cold. Dust is no problem either because the nozzleman will spray the surface with water before spraying the Tekcrete Fast®, quickly removing any dust accumulation. Tests according to ASTM C1583 "Tensile Strength of Concrete Surfaces and the Bond Strength or Tensile Strength of Concrete Repair and Overlay Materials by Direct Tension (Pull-off Method)" were used to determine the near surface tensile strength. In this case, the surface is unprepared to evaluate the bond strength on an unprepared surface—free from any adhesives or additional preparatory processes.

Tekcrete Fast® was sprayed on a cured concrete sample and allowed to cure for 7 days. A core drill with a diamond core barrel, nominally 50 mm (2 inch) diameter and at least 25 mm (1 inch) thick, drilled through the material. A tensile loading device was attached, and a uniform loading device was used to extract the sample and measure the load with a calibrated gauge. The average direct bond test for 10 samples after 7 days of cure was 2.9 MPa (420 psi). These results are extremely high for applied materials on unprepared or cleaned surfaces. The observation, shown in Figure 3, was that the material adhered to the surface so well that the concrete was actually failing, not the interface of the Tekcrete Fast®. This adhesion discovery prompted the experimentation of applying the product directly on unprepared rock and coal surfaces.

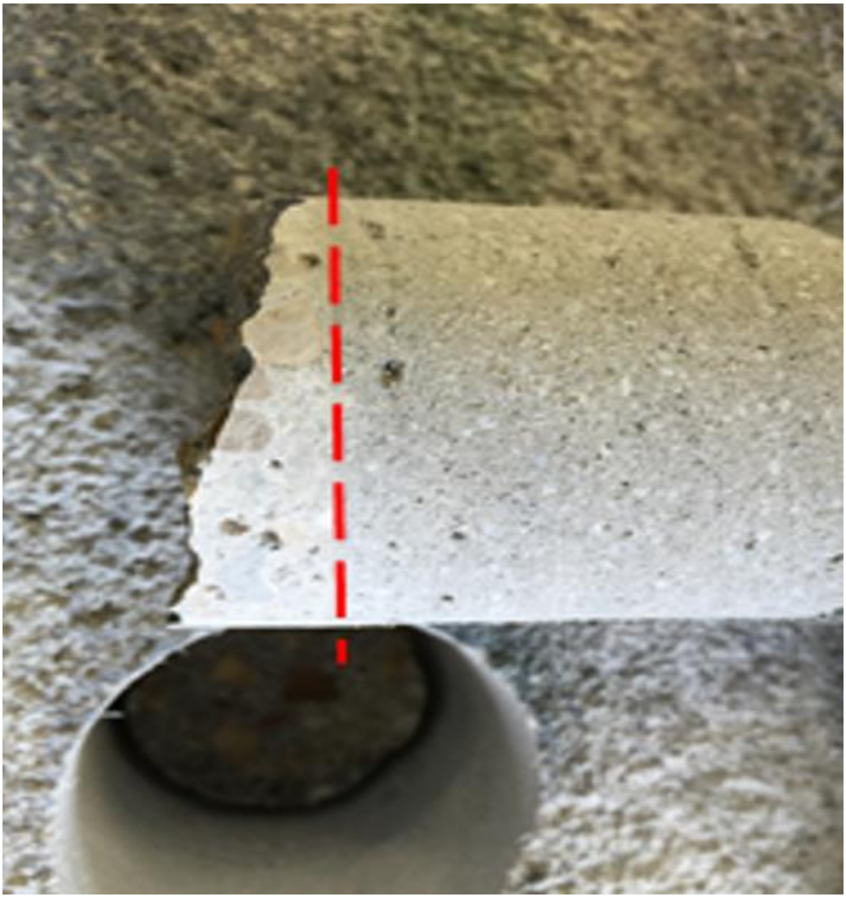

Figure 3 Sample from adhesion test showing failure in the substrate, not Tekcrete Fast®

4.5 Rapid Chloride Permeability

In the context of repair, a key concern is the durability of the repaired section. One of the main risks for a reinforced concrete structure is the corrosion of the reinforcing steel, leading to spalling and a loss of load bearing capacity. This concern does not exist in the context of ground support as Tekcrete Fast® contains non-corroding PVA fibres.

A critical parameter for any repair material is the ability to resist chloride penetration. Chloride migration through concrete, even in high water-to-cement ratio concrete, is a very slow process. Therefore, test methods have been developed to accelerate this migration. Electrical current applied to a concrete specimen increases the acceleration rate at which chlorides migrate into concrete. The measurements in Coulombs (the integral of current vs time plot) that pass through a sample are compared to results from a traditional ponding test, indicating that a good correlation exists.

The test method used is described in detail in ASTM C1202-12, "Standard Test Method for Electrical Indication of Concrete's Ability to Resist Chloride Ion Penetration". This method determines the electrical conductance of concrete to provide a rapid indication of its resistance to chloride ions. The results showed that, after 28 days, 176 Coulombs passed through the specimen when a non-industry standard spray nozzle was used. When the samples were prepared using a high-pressure nozzle, the 28-day measurements indicated a reading of 20 Coulombs. As detailed in the ASTM standard, a reading between 100 and 1,000 Coulombs is considered "very low". When considering the high-pressure nozzle application, a reading as low as 20 Coulombs is classified as "negligible".

Clearly, the Tekcrete Fast® can provide a surface that is highly impenetrable to these destructive, highly corrosive ions and could also serve as a protective barrier for traditional concrete materials used in highly corrosive environments.

5. FULL SCALE TRIAL

Disaster City Demonstration – College City, Texas, USA

In November 2014, a demonstration of Tekcrete Fast® took place at the Disaster City® training facility located in College Station, Texas, USA. The purpose of the testing program was to demonstrate, with the University of Texas A&M Civil Engineering High-Bay Structural & Materials Testing Laboratory, the repair of damaged or wrecked, reinforced concrete vertical beams. The simulations replicated damage done to structure from catastrophic events such as an explosion or earthquake. The demonstration was to show that Tekcrete Fast® and the dry-mix application system can help rescue workers to stabilize a structure, so they can get in and out quickly and safely.

The reinforced concrete vertical beams were intentionally formed with a missing section, and a purposefully damaged beam was placed into the ground. These beams were repaired with Tekcrete Fast®. All concrete beams used in the demonstration had been poured several months in advance of the demonstration to make sure that they were fully cured and at full strength. The beams had a column cross-section that was 300 mm x 300 mm (12 inches x 12 inches), with the length of the damaged area on two of the four columns approximately 450 mm (18 inches) long. The third column was damaged a day or two before the demonstration by bending it until it cracked. The fourth column was left whole and used as a control beam during testing. Once spraying was finished, the repaired beams were immediately removed from the ground and taken directly to the Texas A&M Civil Engineering lab for compressive strength testing. The entire process for this demonstration, including repairing the beams, getting the beams out of the ground, and transferring them over to the laboratory for testing took less than five hours. With less than five hours of curing time for the Tekcrete Fast®, the beams tested were shown to fail outside of the repaired section; the original concrete failed, but the section repaired with Tekcrete Fast® did not. Figure 4 shows the beams being formed for the application of the material. The failure plane (Figure 5) occurred in the mature concrete, which had a strength of about 31 MPa (4,500 psi) compared with a strength of the 5 hour old Tekcrete Fast® of approximately 40 MPa (5,800 psi).

Figure 4 Columns with defects prior to spraying

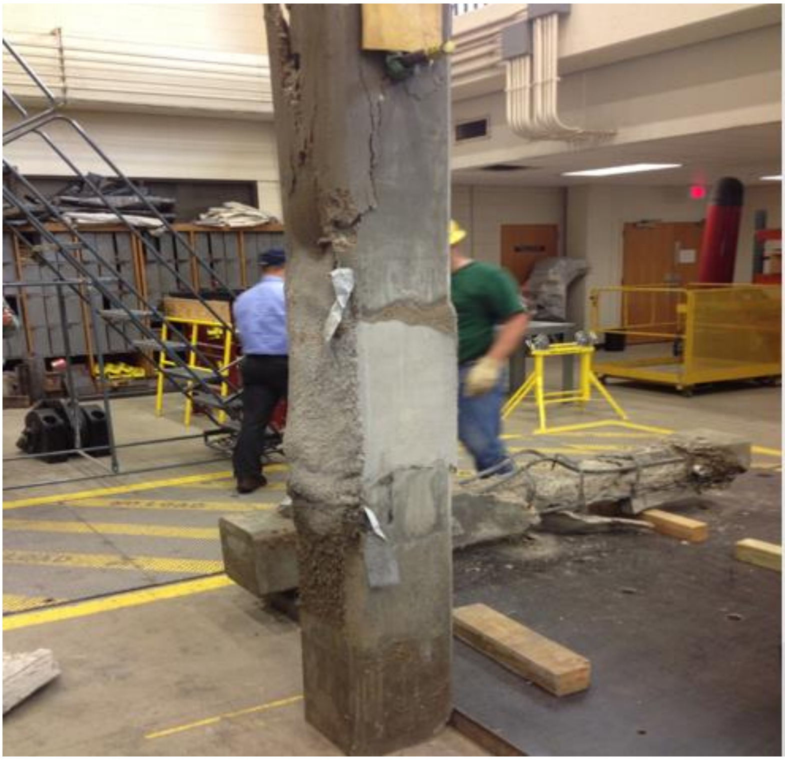

Figure 5 Tested column showing failure outside the repaired area

6. CONCLUSIONS

Early age strength is an important requirement in emergency cases such as stabilising damaged buildings but also in more normal cases such as ground support for mining and tunnelling. Tekcrete Fast® is a pre-bagged, dry mix fibre reinforced sprayed concrete with exceptional adhesion, even to imperfect surfaces, and a very rapid gain in both compressive and flexural strengths. Tekcrete Fast® also has a low permeability to chlorides makes it an excellent candidate for use in corrosive environments and for longer term repairs.

Tekcrete Fast® has been designed with ease of application in mind. The logistics are simplified by using a small pump, providing compressed air, and a low volume of water to mix and appl y the material directly from the nozzle. Full scale test results indicate that the material can work in extreme conditions and is stronger than the original concrete. This makes bridge and tunnel repairs quick and permanent. In mining applications, the material has been used with extremely positive results for repair of existing, damaged support and roof stabilization. It is particularly useful in areas where access has to be limited to reduce the impact on mining operations such as coal mine belt lines.

Based on calcium sulfoaluminate cements rather than OPC, Tekcrete Fast®, could also radically change sprayed concrete in tunnelling, improving safety and durability as well as potentially enhancing sustainability as a result of using thinner linings.

7. ACKNOWLEDGEMENTS

The authors would like to thank the partners in the development of Tekcrete Fast®, most notably the University of Kentucky.

References

1. Thomas, A. H. (2009) "Sprayed concrete tunnel tunnels". Taylor and Francis, Abingdon UK ISBN: 9780415368643 - www.taylorandfrancis.co.uk.
2. Brux, G. (1994) "Spritzbeton im Tunnelbau – Tendenzen und Entwicklungen" Tunnel 3/94, pp 42 – 48.
3. Kusterle, W. (1992) "Qualitatsverbesserungen beim Spritzbeton durch technologische Massnahmen, durch den Einsatz neuer Materialien und auf Grund der Erfassung von Spritzbetoneigenschaften", Habilationsschrift, Vol. 1 & 2, University of Innsbruck
4. Lea, F. M. (1970). The Chemistry of Cement and Concrete. 3rd ed. London: Edward Arnold Publishers, pp. 727
5. Jewell, R. B., Rathbone, R. F., Duvallet, T. Y, Robl, T. L., & Mahboub, K. C. (2015). "Fabrication and testing of low-energy calcium sulfoaluminate-belite cements that utilize circulating fluidized bed combustion by-products." Coal Combustion and Gasification Products 7: 9–18.
6. Mehta, P. K. (1973). "Mechanism of expansion associated with ettringite formation." Cement and Concrete Research 3(1): 1–6.
7. Glasser, F. P. and Zhang, L. (2001). "High-performance cement matrices based on calcium sulfoaluminate-belite compositions." Cement and Concrete Research 31(12): 1881–1886.
8. Torre A.F. dl, Aranda M.A. G., Aza Moya A. H. d, Aza Pendas S. d & Pena Castro M. dP (2005) "Belite Portland Clinkers. Synthesis and Mineralogical Analysis", Bulletin of the Spanish Society of Ceramics and Glass, Vol. 44, No. 3, 2005, pp. 185-91.
9. Mills, P. (2016). Cementitious Compositions. United States Patent US9284226 B2. https://www.google.com/patents/US9284226
10. Oberlink, A., Robl, T., Jewell, B., Duvallet, T. Mills, P., and Jones, R. (2016). "Rapidly deployable shotcrete system for the structural stabilization of shock damaged structures." In: Proceedings of the 9th International Concrete Conference. Dundee, Scotland: University of Dundee.

SPRAYED CONCRETE WITHOUT PORTLAND CEMENT

Roar Myrdal
Normet International Ltd, Switzerland
roar.myrdal@normet.com
Sammy Tong
Normet Taiwan Co. Ltd, Taiwan

ABSTRACT

Alkali activated binders – often referred to as geopolymers – have been studied extensively over the last years and have emerged as alternatives to Portland cement binders. The alkali activated binders are considered eco-friendly and durable. However, they normally require thermal curing to gain acceptable strength. Further, due to the high alkalinity and caustic nature of the binders (containing a blend of alkali silicate and highly concentrated alkali hydroxide), precautions must be taken when handling these materials on site. Both the thermal curing requirement and the handling risk exclude these interesting binders to be used in sprayed concrete.
The ultimate goal of the present study is to develop a fly ash binder for sprayed concrete. This binder does not contain the caustic alkali hydroxide (only the alkali silicate), which makes the binder substantially less caustic. To achieve acceptable setting times and early age strength at ambient temperature, an accelerator has been developed. Set times in the same range as for normal Portland cement based binders have been measured and early age compressive strengths similar to 'normal' sprayed concrete have been obtained. Simple laboratory tests indicated that these binder are extremely resistant to fire and chemical attack. A grout made of silica flour, fly ash and sodium silicate set fast and developed high early age strength when sprayed at ambient temperature.

BACKGROUND AND SCOPE OF RESEARCH

The binder in sprayed concrete, as in almost all concretes, is based on Portland clinker, i.e. either pure Ordinary Portland Cement (OPC), or Portland clinker blended with pozzolanic materials. To some extent also Calcium Aluminate Cement (CAC) and Calcium SulphoAluminate (CSA) cement are used as binders for spray applied mortars and grouts [1]. In all these binders calcium plays a key role in the chemistry involved in the chemical reaction (hydration reaction) which leads to the formation of calcium silicate and calcium aluminate hydrates. This chemistry can be described as 'calcium chemistry'.

Over the last two to three decades another type of binder has been investigated heavily, not for sprayed concrete, but for ordinary concrete, preferably precast concrete, namely alkali activated aluminosilicates, often referred to as geopolymers [2, 3]. These binders are considered 'green' and durable [4, 5]. Their resistances to fire [6] and chemical attack [7] are reported to be much better than for OPC binders. However, the engineering properties are challenging since in most applications thermal curing is needed to gain acceptable early age strength [8]. Therefore, geopolymer concrete is typically used in precast industry. In order for these binders to be utilised in sprayed concrete, setting time and strength gain at ambient temperatures need to be improved. If this could be accomplished, such binders would be an interesting option for sprayed concrete, and possibly for other applications like sprayable fire protective layers in tunnels.

Challenges linked alkali activated binders

These binders are inorganic aluminosilicate polymeric compounds formed by the chemical reaction between a pulverised amorphous aluminosilicate (typically industrial bi-product like fly ash) and a concentrated liquid solution of alkali hydroxide and alkali silicate [2]. There are two main challenges linked to alkali activated fly ash grouts, mortars and concretes:

1) The need of thermal curing to obtain acceptable early age strength [8, 9]
2) Handling of very caustic materials (pH≥14) [10, 11]

One way to overcome these challenges is to introduce a calcium source (typically slag, or OPC) to achieve setting time and compressive strength values comparable to those of OPC [12, 13]. When introducing a calcium source, also the caustic problem can be eliminated by removing the alkali hydroxide from the liquid part. Such binders has been termed 'User-friendly geopolymer cement' that cures at room temperature: Sodium silicate solution + blast furnace slag + fly ash [11].

The unwanted side effect of this 'user-friendly' approach is that adding calcium to a fly ash/sodium silicate mix will lead to the formation of calcium silicate/aluminate hydrate gels, similar to those found in hydrated OPC. This again will have a negative impact on the durability of such binders since these gels are not resistant to fire and chemical attach the same way the 'pure' geopolymers are. Therefore, durable alkali activated binders, using neither calcium compounds nor caustic alkali hydroxides, would be highly welcomed.

This paper summarises the first attempts to develop accelerating admixtures for a fly ash/sodium silicate binder cured at ambient temperature using neither alkali hydroxides nor any source of calcium. Previous research on admixtures for highly alkaline/caustic geopolymer binders has shown that some organic compounds may have accelerating properties on such binders [14]. In the present study only non-caustic binders are considered.

Results from initial laboratory testing of such binder and a simple spray trial of a grout using this binder are presented. Next step would be to take this further and see if a sprayable concrete can be designed.

EXPERIMENTAL INVESTIGATIONS

Initial laboratory tests

A simple paste was made of fly ash, sodium silicate and water. Table 1 shows the chemical composition of the fly ash and Table 2 shows the mix design (pH~11).

Table 1. Chemical composition of fly ash used in paste mix (% by weight)

SiO_2	Al_2O_3	Fe_2O_3	CaO	TiO_2	MgO	K_2O	Na_2O	SO_3	LOI*
45-51	27-32	7-11	1-5	0.8-1.1	1-4	1-5	0.8-1.7	0.3-1.3	5-7

* LOI = Loss on ignition

Table 2. Paste mix design

Material	(% by weight)
Fly ash	64.5
Sodium silicate, SiO_2:Na_2O molar ratio 3.25, 38% solution	25.8
Water	9.7
Total	100.0

Mixing and casting of paste samples were done at room temperature (20°C). First, the fly ash was added into a high speed shear mixer. Then the sodium silicate and the water were added and the blend was mixed for approx. 2 minutes at medium speed until a fluid paste was obtained to which an accelerator was added. The accelerator can be characterised as a non-aqueous, non-hazardous, clear liquid formulated by blending organic compounds found among polyols and esters. The blend was then mixed for another 30 seconds. Once the mixing was completed, the paste were taken out for setting time measurements (Vicat apparatus in accordance with test method EN 480-2), and the remaining paste was cast into 40x40x160 mm steel moulds, covered with plastic sheets, and cured in air at 20°C. The specimens were demoulded when strength allowed, and then left to cure at 20°C under plastic sheets until compressive strength measurements were carried out at 1 hour, 4 hours and 24 hours (after casting).

Well cured (28 days) 40x40x40 mm cubes were tested for chemical resistance by submerging the cubes in a 10% sulphuric acid solution for two days at 20°C. Similar cubes were exposed to an extremely high temperature caused by a propane torch. The heat exposure lasted about 2 minutes.

Spray trial

A simple grout was made of silica flour (finely ground crystalline silica), fly ash, sodium silicate and water. Table 3 shows the chemical composition of the silica flour and the fly ash, and Table 4 shows the mix design (pH~11). The fly ash and the sodium silicate solution were not from the same sources as for the initial laboratory tests, and have therefore not identical composition characteristics.

Table 3. Chemical composition of fly ash and silica flour used in grout mix (% by weight)

Material	SiO_2	Al_2O_3	Fe_2O_3	CaO	TiO_2	MgO	K_2O	Na_2O	SO_3	LOI*
Fly ash	48.03	21.85	11.54	9.96	-	3.48	1.11	1.09	1.69	0.46
Silica flour	>99.5	<0.4	<0.02	-	-	-	-	-	-	-

* LOI = Loss on ignition

Table 4. Grout mix design

Material	(% by weight)
Silica flour	34.3
Fly ash	34.3
Sodium silicate, SiO_2:Na_2O molar ratio 3.71, 46% solution	24.5
Water	6.9
Total	100.0

Mixing and spraying of grout were done at ambient temperature (~25°C). The fly ash and silica flour were first mixed with the liquid part (sodium silicate and water) in the mixing unit of an electrical driven spray machine (Normet SSL 15, Figure 1) until a thick paint like grout was obtained. This grout was then sprayed onto a vertical well cured sprayed concrete substrate. An accelerator dosing pump unit along with compressed air was used to mix in the accelerator at the spray nozzle. Dosage of accelerator was in the range of 5.5-6.0% by weight of fly ash. Slump or flow were not measured. Approximate setting time was observed by simply scratching the surface during spraying. Cubes (100x100x100 mm) for compressive strength measurement were prepared by spraying into steel moulds during the spray trial. Early age compressive strength was measured 2 hours and 4 hours after spraying.

4-5 hours after spraying, the cured grout was exposed to fire by using a propane torch (Figure 2) that was pointed directly onto to the grout surface for 1 minute. Similar test was also made with a plain concrete surface (age 28 days). The flame touching the surface had a temperature of at least 1300°C.

Figure 1. Normet SSL 15 used for the spray trial.

Figure 2. Propane torch.

RESULTS AND DISCUSSION

Setting and strength development of fly ash paste

Table 5 shows the setting times and early age compressive strength of the fly ash paste, with and without the accelerator, at ambient temperature (accelerator dosage in % by weight of fly ash). The initial and final setting times of the reference was more than 1 day and 4 days respectively. The results clearly show that these long setting times can be significantly shortened by adding an accelerator to the mix. The setting times obtained with the accelerator are close to typical values found when alkali-free accelerators are used in OPC based sprayed concrete.

Table 5. Setting times and early age compressive strength (MPa) of fly ash paste at 20°C*

Material	Initial set	Final set	1h strength	4h strength	24h strength
Reference	~30h	>100h	-	-	-
4 % Accel.	3m10s	5m48s	1.5	1.8	2.2
6 % Accel	1m32s	4m0s	1.5	2.6	2.7

* m=minutes, s=seconds, h=hours

It is also seen (Table 5) that the accelerator was able to speed up early age compressive strength development the first few hours after casting. However, the 24 hours strength was very low. The later strength development (not shown in Table 5) was also very slow. The reference grout was too soft to be measured after 24 hours curing. After 28 days the reference strength was approximately 3 MPa. The accelerated samples was only slightly higher. The results clearly show that this binder is not able to meet strength requirements set for normal sprayed concrete. However, this new binder/accelerator combination opens the possibility of developing a non-caustic, fly ash based sprayed material without using Portland cement or any additional calcium material in the binder.

The resistance of fly ash paste against acid and fire

Figure 3 shows two 40x40x40 mm cubes (plain OPC paste on the left and the fly ash paste on the right) after two days in a 10% sulphuric acid solution [15]. This shows that the chemical resistance of the fly ash paste outperforms the OPC when exposed to an acidic solution. The OPC sample clearly disintegrated, whilst the fly ash paste did not show any sign of deterioration.

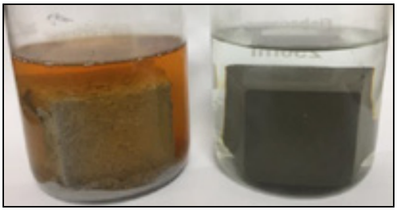

Figure 3. Well cured (28 days) 40x40x40 mm cubes after two days in a 10% sulphuric acid at 20°C. Left: OPC paste. Right: Fly ash/sodium silicate paste with 6% accelerator [15].

The severe deterioration of OPC in acid is caused by the solubility of high calcium constituents in the binder – calcium hydroxide and calcium silicate/aluminate hydrates [16, 17]. The fly ash paste does not contain these constituents, and are therefore more resistant to acidic attack. It is well known that the sulphuric acid resistance of fly ash based geopolymer concrete is significantly better than that of Portland cement concrete [18].

Figure 4 shows the effect of fire exposure [15]. The fire – caused by a propane torch – made the fly ash paste glow with no sign of spalling or damage. When cooled down after the exposure, only a dark spot remained. A similar exposure of an OPC sample resulted in a clearly audible crackle sound, and the sample suffered from violent spalling after just a few seconds. Cured OPC is known for displaying this kind of explosive spalling when exposed to fire [19].

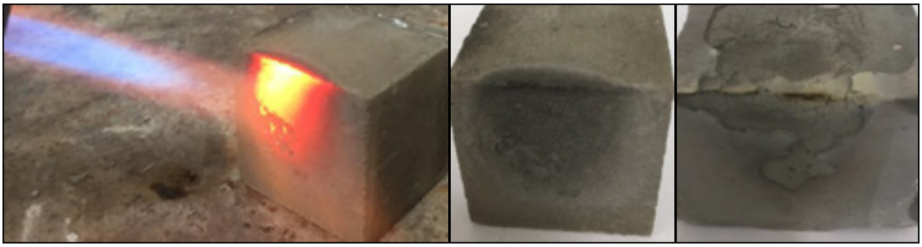

Figure 4. Well cured (28 days) 40x40x40 mm cubes exposed to a propane torch (≥1300°C). Left: Fly ash/sodium silicate paste (6% accelerator). Middle: Same as left after cooled down. Right: Propane torch exposed OPC after cooled down [15].

Properties of sprayed fly ash grout

The fly ash grout set almost instantly (less than 60 seconds set time) during spraying at an accelerator dosage of 6% (by weight of fly ash). The rebound was insignificant and the accelerator worked very well. However, during spraying it was noticed that if the accelerator was overdosed the spray mix formed hard lumps before it hit the wall with the risk of forming voids and dropping. An accelerator dosage of 5.5% seemed optimal. During the trial it was sprayed with a thickness up to approx. 25 mm (Figure 5). However, the instant setting behaviour indicates that much thicker layers could be sprayed. Figure 6 shows a sprayed steel mould (100 mm thickness) for later compressive strength measurements on cubes.

Figure 5. Sprayed fly ash grout

Figure 6. Spraying into 100x100x100 mm mould

Table 6 shows the early age compressive strength of the sprayed grout. These strength values are very close to those measured on the samples of pure fly ash paste mixed in the laboratory (Table 5). Unfortunately, strength values at 24 hours and onwards were not measured in this trial. Still, this trial demonstrated, beyond doubt, that it is possible to spray a simple fly ash/sodium silicate grout and obtain fast setting and high early age strength if a suitable accelerator is used.

Table 6. Early age compressive strength of sprayed fly ash grout at 25°C*

Age	2 hours	4 hours
Compressive strength (MPa)	1.8	2.5

* Measured on 100x100x100 mm cubes (6% accelerator dosage)

Figure 7 shows the the effect of fire exposure (1 minute propane torch, ≥1300°) on a the same grout area shown in Figure 5. At the time of fire exposure the grout had cured for a period of only 4-5 hours. No sign of damage was observed on the grout surface. Right after the fire exposure the grout surface was white hot (Figure 7A). After cooled down to ambient temperature the same spot went dark (Figure 7B). Similar test performed on a well cured concrete slab (28 days old) resulted in an explosive behaviour just after a few seconds with broken particles shooting out.

Geopolymer mortars (high pH) have been suggested to be used as fire resistant materials, e.g. for tunnel linings [20]. The results documented in the present study suggests that low pH ('User friendly') fly ash/sodium silicate grouts cured at ambient temperature might also have this attribute.

No doubt, the fire resistance of fly ash/sodium silicate grout – probably mortar and concrete as well – calls for the development of various application areas. Besides, this material has a fairly low pH value of about 11, which is significantly less basic/caustic than OPC concrete (pH~13) and concentrated alkali hydroxide based geopolymers (pH~14), the latter sometimes referred to as 'User hostile' materials [11].

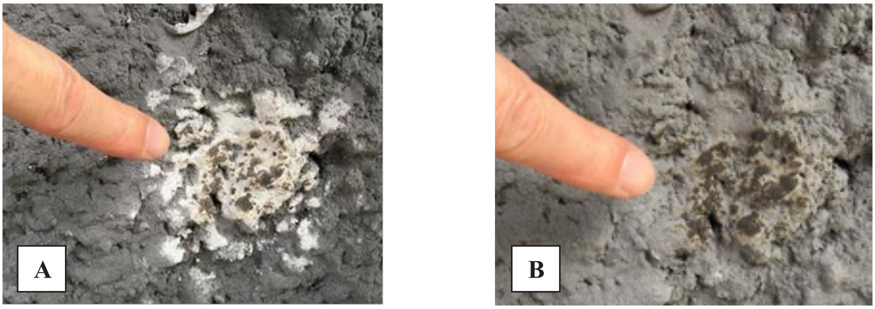

Figure 7. Effect of propane torch on a 4-5 hours old fly ash grout after 1 min fire exposure (≥1300°).
A: Immediately after heat exposure (white hot/glowing)
B: After cooled down to ambient temperature (dark spots)

CONCLUSIONS

The following conclusions can be drawn from this study on a simple fly ash/sodium silicate binder:

- A fly ash/sodium silicate binder without highly caustic hydroxides or additional calcium materials can set and cure at ambient temperature if a proper accelerator is added to the mix.
- The reference (without the accelerator) does not set within the first 24 hours after mixing, while the accelerated version sets in approx. 1 minute at ambient temperature.
- Early age compressive strength in the range of 1-2 MPa after 2 hours can be obtained when fly ash/sodium silicate grouts are sprayed at ambient temperature with 6% accelerator dosage.
- The long term strength of the fly ash/sodium silicate grout cured at ambient temperature was low.
- The chemical resistance against sulphuric acid attack and the fire resistance of this fly ash/sodium silicate binder are very good.

REFERENCES

1. Lemay, J-D., Jolin, M., Gagné, R., "Ultra Rapid Strength Development in Dry-Mix Shotcrete for Ultra Rapid Support in Challenging Mining Conditions", Shotcrete Magazine, Vol 16, No 4, American Shotcrete Association, 2014, pp 14-19.
2. Provis, J.L., "Geopolymers and other alkali activated materials: why, how, and what?", Materials and Structures, Volume 47, 2014, pp 11-25.
3. Shi, C., Jiménez, A.F., Palomo, A., "New cements for the 21st century: The pursuit of an alternative to Portland cement", Cement and Concrete Research, Volume 41, 2011, pp 750-763.

4. Komnitsas, K.A., “Potential of geopolymer technology towards green buildings and sustainable cities”, Procedia Engineering, Volume 21, 2011, pp 1023-1032.
5. Duxson, P., Provis, J.L., Lukey, G.C., van Deventer, J.S.J., “The role of inorganic polymer technology in the development of ‘green concrete’”, Cement and Concrete Research, Volume 37, 2007, pp 1590-1597.
6. Dao, D.V., Forth, J.P., “Investigation of the behaviour of geopolymer mortar after heating to elevated temperatures”, Proceedings 3rd International Conference on Sustainable Construction Materials and Technologies, Kyoto, Japan (http://claisse.info/Proceedings.htm), 2013, 9 p.
7. Al Bakri, M.M., Mohammed, H., Kamarudin, H., Niza, I.K., Zarina, Y., “Review on fly ash-based geopolymer concrete without Portland cement”, Journal of Engineering and Technology Research Volume 3(1), 2011, pp 1-4.
8. Ken, P.W., Ramli, M., Ban, C.C., “An overview on the influence of various factors on the properties of geopolymer concrete derived from industrial by-products”, Construction and Building Materials, Volume 77, 2015, pp 370-395.
9. Hardjito, D., Wallah, S.E., Sumajouw, D.M.J., Rangan, B.V., “On the Development of Fly-Ash Based Geopolymer Concrete”, ACI Materials Journal, November-December 2004, pp 467-472.
10. Davidovits, J. “Application of Ca-based geopolymer with blast furnace slag, a review”, Proceedings 2nd International Slag Valorisation Symposium, 18-20 April 2011, Leuven, Belgium (Eds. P.T. Jones et al), 2011, pp 33-49.
11. Davidovits, J. “Geopolymer Cement, a review”, Institute Geopolymere, Saint-Quentin, France, 2013, 11 p.
12. Somna, K., Jaturapitakkul, C., Kajitvichyanukul, P., Chindaprasirt, P., “Effect of GGBFS on setting, workability and early strength properties of fly ash geopolymer concrete cured in ambient condition”, Fuel, Volume 90, 2011, pp 2118-2124.
13. Nath, P., Sarker, P.K., “Use of OPC to improve setting and early strength properties of low calcium fly ash geopolymer concrete cured at room temperature”, Cement & Concrete Composites, Volume 55, 2015, pp 205-2014.
14. Myrdal, R., Griffith, R., “Admixtures for Geopolymer Concrete: The Performance of Accelerating Admixtures”, 2nd International Congress on Durability of Concrete, New Delhi, India, 4-6 December 2014, Conference Proceedings, Paper No. 24, 11p.
15. Myrdal, R., Galloway, D., “Accelerating Admixture for Fly Ash / Sodium Silicate Binders Cured at Ambient Temperature”. Proceedings 2nd Concrete Innovation Conference, Tromsö, Norway, 7-8 March 2017, Paper No. 59, 8 p.
16. Fernández-Jiménez, A., Palomo, A., “Chemical durability of geopolymers”, in Provis, J. L., van Deventer, J.S.J. (Eds.), Geopolymers - Structure, Processing, Properties and Industrial Applications, Woodhead Publishing Limited, Oxford, Cambridge, 2009, pp 167-193.
17. Bakharev, T., “Resistance of geopolymer materials to acid attack”, Cement and Concrete Research, Volume 35, 2005, pp 658-670.
18. Al Bakri, M.M., Mohammed, H., Kamarudin, H., Niza, I.K., Zarina, Y., “Review on fly ash-based geopolymer concrete without Portland cement”, Journal of Engineering and Technology Research Volume 3(1), 2011, pp 1-4.
19. Khoury, G.A., “Effect of fire on concrete and concrete structures”, Progress in Structural Engineering and Materials, Volume 2, 2000, pp 429-447.
20. Dao, D.V., Forth, J.P., “Investigation of the behaviour of geopolymer mortar after heating to elevated temperatures”, Proceedings 3rd International Conference on Sustainable Construction Materials and Technologies, 2013, Kyoto, Japan (http://claisse.info/Proceedings.htm), 9 p.

THE BAN OF POLYMER FIBRE IN FRSC IN NORWEGIAN ROAD TUNNELS

Synnøve A. Myren, Per Hagelia and Øyvind Bjøntegaard
Norwegian Public Roads Administration, Tunnel and concrete division, Norway
synnove.myren@vegvesen.no, per.hagelia@vegvesen.no and
oyvind.bjontegaard@vegvesen.no

SUMMARY

As of November 2015, macro polypropylene fibre (polymer fibre) is prohibited in Norwegian road tunnels, and steel fibre is currently the only alternative for fibre reinforcement of sprayed concrete. This was new in the Norwegian Public Roads Administrations latest edition of Manual R761 General Specifications 1 Standard specification text for road contracts, principal specifications 1-7. Earlier editions of R761 placed both fibre types on equal terms in land tunnels, while only polymer fibre was allowed in subsea tunnel sections. The prohibition of polymer fibre is of environmental considerations, and this paper gives a further account of the challenges involved. In addition, we explain the reasons why our regulations could change almost overnight, and what the future might bring regarding fibre reinforcement of sprayed concrete.

INTRODUCTION

The Norwegian Environment Agency assumes that approximately 75 % of all marine litter is plastic [1], other assumptions vary from 60 to 90 %. In contrast to organic waste, plastic has a life in the environment that can vary from hundred and up to thousands of years. This explains the large amount of plastic in the oceans despite the fact that "only" 10 % of yearly generated litter is plastic. Plastic waste comes from many sources; from individuals, from industry and landfills, from fishing, offshore and shipping, from toothpaste and cosmetics, and others.

The total amount of marine litter, and then plastic in the ocean, is impossible to quantify, but World Economic Forum [2] states that the best research so far estimates that there are over 150 million tonnes of plastic in the ocean. We find plastic everywhere in the ocean; on the beaches, on the surface of the ocean, on the bottom, and everywhere in between. It is especially the amount of plastic on the deepest sea beds that are hard to quantify. Plastic in the ocean comes in all sizes, but all of it will eventually be broken down to micro plastic (< 5 mm). Plastic can also attract environmental poisons, which then could be spread over large distances.

Earlier, marine litter was considered only an aesthetic problem, polluting our beaches, but we now know the consequences are potentially huge. The less severe effects are economical, e.g. expenses due to cleaning beaches, less attractive tourist destinations and anglers getting their equipment destroyed. More serious are plastic found in the stomach of seabirds, fishes and sea animals, and it is likely to believe that in the longer term it can effect human health as well. If we continue our use and misuse of plastic, by 2050 there will be more plastic in the ocean than fish (by weight) [2].

POLYMER FIBRE GONE ADRIFT

From the increasing number of subsea tunnel projects, where tunnel muck was approved by the environmental authorities for filling in the sea or deposited in the sea, emerged the challenge of synthetic material (mostly macro polymer fibres, but also firing lines) accompanying the muck deposited in the sea. The Ryfast project estimated that 0.7-1 kg polymer fibres per meter tunnel could follow the tunnel muck. This gives a great potential of fibres going adrift, e.g. one of the most widely used polymer fibre in Norway has 37 000 fibres/kg. An attempt to reduce the amount of fibres that are transported out by gathering rebound from the tunnel floor and measures with silt curtain/boom to contain fibres in the sea was not at all sufficient. Sadly, the consequence was that large amounts of fibres had gone adrift locally and polluted the ocean and the beaches. It all culminated in the autumn of 2014: While drifting the submerged tunnels in the Ryfast project at the west coast of Norway, The Green Warriors of Norway and the Rogaland division of Friends of the Earth Norway reported the Norwegian Public Roads Administration (NPRA) to the police for environmental offences. The NPRA, as the owner of the project, was fined 450.000 NOK (approximately 50.00 EUR). In addition, the NPRA and the contractor had to clean up.

Figure 1: Clean-up of plastic litter from tunnel muck deposited in the sea. Photographer: Øyvind Ellingsen

The NPRA does not wish to contribute to pollution. In any case, Norwegian Law supersedes the NPRA specifications, and something had to be done. Using heavy polymer fibres that do no float could be less problematic provided the tunnel muck is plastered (immobilised). However, there is a great uncertainty about the effects of such immobilisation and the proportion of polymer fibres that, nonetheless, will come into contact with various organisms in the sea. Steel fibres, however, is not spread by wind and water, and in time will break down into rust, which has no known harmful effects on the aquatic environment.

Eventually, the result was a change in type of fibre being used, both at the Ryfast project and in general.

CHANGE IN REQUIREMENTS

In 2007 a requirement to use synthetic fibres of non-corrosive material in areas where a highly corrosive environment could be expected (such as in subsea tunnels) was introduced in Manual R761 [3]. This requirement was mainly a result of a concern for corrosion of steel fibres due to saltwater intrusion. Later observations of biofilm that could cause degradation of steel fibre-reinforced sprayed concrete in particularly exposed areas of subsea tunnels supported this choice. The objective was to reduce the risk of deterioration, over the lifespan of the tunnel, of the rock support due to reduced load-bearing thickness caused by biofilm and/or corrosion of fibres due to saltwater. Elsewhere the fibre type was optional.

In the last revised edition of Manual R761 [4], the NPRA made changes to the requirements for steel fibres in sprayed concrete for rock support. The requirement in specification "33.4 Support with sprayed concrete" now states that fibres shall be in accordance with NS-EN 14889-1 Fibres for Concrete, Part 1: Steel Fibres [5]. This means that only steel fibres shall be used in sprayed concrete for rock support in road tunnel projects.

The change in requirements was accordingly due to environmental considerations, not technical.

TECHNICAL QUALITY

So, how about the durability of the rock support now? Various surveys regarding durability of sprayed concrete as rock support has been carried out over the last 25 years. The R&D programme "Durable structures (2012-2015)" looked into earlier research and also conducted own investigations. The sprayed concrete in several tunnels with different environmental conditions (fresh water environment, mildly acidic environments, alum shale environments and subsea environments) were sampled and examined in detail. All findings were then compiled. The results indicated that the long-term durability of sprayed concrete with steel fibres could be ensured by introducing stricter requirements for durability class in areas with saltwater (M40). Implied is also a stricter requirement for the identification of saline environments during the geological mapping. Further analyses of the data also show, irrespective of fibre type, that 100 mm minimum (average) thickness of the sprayed concrete lining is necessary to give an expected service life of 100 years in saline environments (bad rock types may require higher thickness due to load-bearing concerns). Durability of sprayed concrete is further discussed in [6], and all findings from "Durable structures" is reported in [7].

FIBRE TYPES IN THE FUTURE

Although steel fibre is the only fibre allowed in Norwegian tunnels currently, this could change. In the future, other fibre types proven to be non-harmful for the environment (and technical satisfactory) could be relevant. A possible use of polymer fibres in the future depends on developing a method to collect the fibres, avoiding them to spread in the nature, and especially in the ocean. By the time being there is no such method secure enough. Regarding other fibre types, not comprised by European standards, three primary matters must be documented. Firstly, there must be no negative effect on the environment, and meet given environmental demands; secondly, the fibre must have no negative effect on the durability of the sprayed concrete; and finally, the fibre must be proven to have the intended long-term technical effect when used as fibre reinforcement in sprayed concrete for rock support.

REFERENCES

1. Standal, E. et al: *Knowledge on marine litter in Norway 2014*, Norwegian Environment Agency, Oslo, 2014 (in Norwegian, summary in English)
2. The Ellen MacArthur Foundation: *The New Plastics Economy Rethinking the future of plastics*, World Economic Forum, 2016
3. Norwegian Public Roads Administrations Manual 761 General Specifications 1 – *Standard specification texts for road contracts principal specifications 1-7*, 2007
4. Norwegian Public Roads Administrations Manual 761 General Specifications 1 – *Standard specification texts for road contracts principal specifications 1-7*, 2015
5. NS-EN 14889-1 Fibres for Concrete, Part 1: *Steel Fibres. Definitions, specifications and conformity,* 2006
6. Hagelia, P.: *Durability of sprayed concrete used for rock support – A tale from the tunnels*, In: Engen, S., Beck. T. and Myren, S.A. (Ed.), 8th International Symposium on Sprayed Concrete – Modern Use of Wet Mix Sprayed Concrete Underground Support, Trondheim, 2018
7. Hagelia, P. (2018). *Summary of durability development of sprayed concrete used for rock support in different tunnel environments,* R&D Program Durable Structures, Statens vegvesen report no 566 (in Norwegian).

SHOTCRETE QUALITY CONTROL FOR THE NEW M5 TUNNEL, SYDNEY AUSTRALIA

David A.F. Oliveira[1], Brodie W. Aitchison[1], Adam Gowans[2], Grant Andersen[2]
[1]Aurecon-Jacobs Joint Venture, Australia and
[2]CPB-Dragados-Samsung Joint Venture, Australia
david.oliveira@jacobs.com

ABSTRACT

This paper presents some of the lessons learnt and challenges observed during quality control for the shotcrete of the New M5 tunnel currently under construction in Sydney, Australia. High levels of within-batch variability created significant difficulty in interpreting and applying the results confidently. To reduce the risk of rejection, the results were interpreted taking into consideration how the adopted design methodology addresses uncertainty which is also discussed in the paper.

INTRODUCTION

Quality management is an essential component in any construction project, and typically involves both Quality Assurance (QA) and Quality Control (QC). Quality Assurance refers to planned systematic actions that aim at achieving a final product that perform as intended. It typically starts with a project specification, design, construction drawings, and preparation of contract documents. Quality Control, on the other hand, targets measurements and controls of the physical characteristics of the materials and processes by means of testing and inspections to achieve predefined quality standards and/or performance criteria. This paper presents some of the lessons learnt and challenges observed during quality control for the shotcrete of the New M5 tunnel currently under construction in Sydney, Australia.

The New M5 is one of three stages of a larger infrastructure project known as WestConnex. The WestConnex project is a 33-kilometre underground motorway currently being constructed in Sydney's Inner West (Figure 1). The New M5 comprises of approximately 10-kilometres of dual underground motorway from Kingsgrove to St Peters. The tunnels are essentially two-lane tunnels future proofed for three-lanes, except between Arncliffe and St Peters where the excavation increases to four-lane tunnels allowing for a future connection with a tunnel currently being planned under the name of F6 motorway.

Figure 1 WestConnex motorway

The tunnels spans vary from approximately 13 m for the two-lane tunnels to approximately 20 m for the four-lane tunnels with some local enlargements for jet fans, breakdown bays, longitudinal egress passages etc. The largest tunnel roof spans occur at two Y-junction caverns located at Arncliffe and St Peters with approximately 30 m width.

TUNNEL SUPPORT AND SHOTCRETE REQUIREMENTS

The majority of the New M5 tunnel is excavated through a Triassic age formation known as Hawkesbury Sandstone. This “soft” and horizontally bedded sedimentary rock has average compressive strengths between 20 MPa and 30 MPa and often fresh to slightly weathered only. These characteristics provide favourable tunnelling conditions due to the overall good quality rock mass with Q-values generally between 22.5 and 150.

The ground support in these conditions generally consists of a pattern of permanent double corrosion protected rock bolts and thin layers of shotcrete. Rock bolts provide the main ground support by the reinforcing the rock mass and the shotcrete is designed mainly to support potential rock wedges that may form between bolts. Therefore, in good ground conditions the shotcrete thickness typically varies between 50 mm and 125 mm and is checked against four main failure mechanisms (adhesion, direct shear, flexural and punching shear) using closed form design methods ([1], [2]). Other failure mechanisms such as compressive and tensile failures are typically checked through tunnel scale numerical modelling. Designing such thin layers typically impose significant reliance on a good shotcrete adhesion with flexural failure mainly considered for design redundancy particularly for long term performance in moderately weathered rock where adhesion may be lost.

The exception exists in areas of shallow tunnelling where poorer ground conditions or surface settlement criteria may require more robust and thicker structural linings and a combined axial-flexural behaviour becomes predominant. In these situations, the shotcrete design philosophy changes from that described above, and the shotcrete is designed to contribute to the overall tunnel stability rather than supporting small rock wedges forming between rock bolts.

Although in theory two sets of performance requirements could be specified for the two types of ground support described above, without always knowing in advance where the different support types are required to be installed along the tunnel alignment, the common practice is to specify a single shotcrete performance criterion. During the design phase of the New M5 Tunnel the minimum shotcrete performance criteria was developed and used in the design of ground support (Table 1).

Table 1 Minimum structural performance requirements for permanent shotcrete

Parameter	Test method		Requirement
Compressive strength (28 days)	Cast samples - AS 1012.9		40 MPa
	Cored samples - AS 1012.14		
Residual flexural strength (CMOD4)	EN 14651 (Beams)		3 MPa
Toughness	ASTM C1550 (RDPs)	5 mm	60 joules
		40 mm	280 Joules
Adhesion to rock substrate (28 days)	AS 1012.24		0.5 MPa
Maximum shrinkage (56 days)	AS 1012.13		800 $\mu\varepsilon$

SHOTCRETE MIX AND FIELD TRIALS PRIOR TO FULL PRODUCTION

The shotcrete mix was designed with a total cementitious content of 430 kg/m^3 which consisted of 32% supplementary cementitious materials (SCMs). The SCMs comprised of 25%fly ash and 7% of silica fume. The maximum water/cementitious content ratio was set at 0.45. Other admixtures included a high range water-reducing superplasticizer (Tytro WR172) and a hydration stabiliser (Tytro HC270). An initial steel fibre count of 35 kg/m^3 (Dramix 3D RC 65/35BG) was adopted as part of the preproduction trials. The use of alkali-free set accelerators was specified with an allowable range of 3% to 8% such that the dosage chosen during application did not decrease in strength of any shotcrete type at an age of 28 days by more than 25% when compared with the base shotcrete mix without any accelerators.

The results of the preproduction field trials on the proposed final mix confirmed a cored 28-day compressive strength of 56 MPa, residual flexural strength of 3.6 MPa, 5 mm toughness of approximately 100 Joules, 40 mm toughness of 450 Joules, and 56 days shrinkage of 630 $\mu\varepsilon$.

PRODUCTION TEST RESULTS

Despite the shotcrete performance being confirmed in the preproduction field trials, production test results indicated a potential high percentage of non-conformances than what would be expected, i.e. typically 5% or less of the test results. The population of the test results for a period of approximately 1 year into tunnel construction is presented in the following sections for the different performance criteria. All test results are shown as the average of a minimum of 3 specimens. Normal distribution fits are also presented to assess the relative variability of the results. Characteristic design values are also estimated in accordance with AS 5100 [3] corresponding to a strength that is exceeded by 95% of the between-batch results. However, the values were estimated based on the actual test result values rather than the normal distribution fit as not always the normal distribution provided the best-fit to the data.

Compressive strength

The compressive strength results are presented in Figure 2 with statistical distributions for the cored samples given in Figure 3.

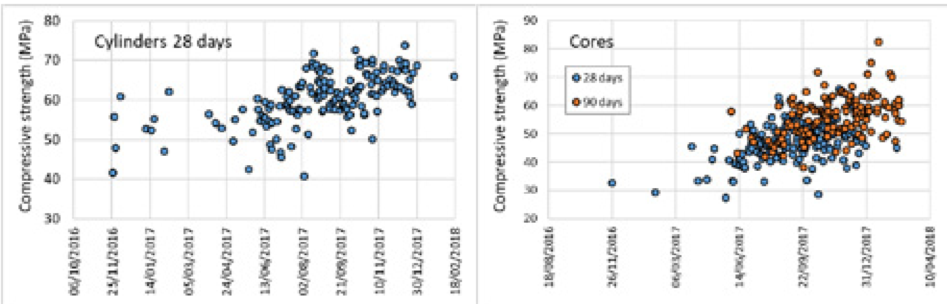

Figure 2 Compressive strength results – cylinder and cored samples from sprayed panels.

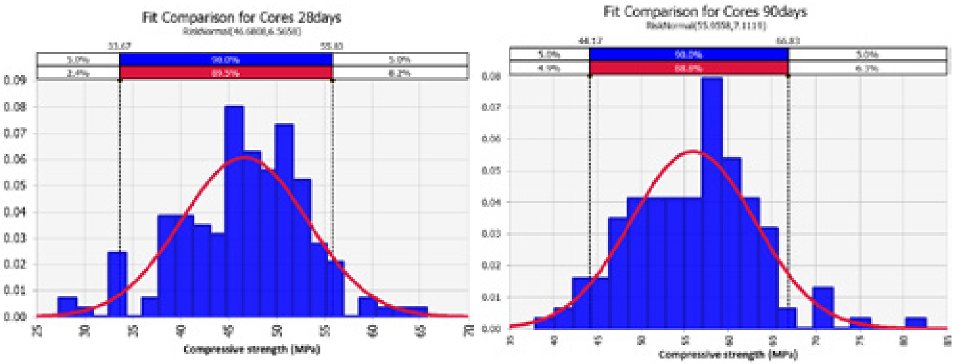

Figure 3 Normal distribution for cored samples compressive strength results at 28 days and 90 days.

The difference in results between cylinders and cores at 28 days is evident in Figure 2. While all cylinder results achieve the 40 MPa, several cored samples sit below the strength requirement. This is likely a combination of the spraying process which introduces variability and the inclusion of accelerator at the time of application which is not included in the cast samples.

The cored sample results at 28 days indicate a mean value of approximately 46.7 MPa, with a between-batch coefficient of variation CoV = 14% and a characteristic design value of approximately 33.7 MPa. On the other hand, the 90-day cored sample results indicate a mean value of approximately 56 MPa with a between-batch CoV = 13% and an estimated characteristic design value of approximately 44.2 MPa. This indicates an increase of about 20-30% past 28 days which is deemed associated with the effect of the fly-ash content (25%) causing a delay in strength gain.

Residual flexural strength – CMOD4 beams - EN 14651

The EN 14651 residual flexural strength results are presented in Figure 4 with statistical distributions given in Figure 5. Experience gained in Stage 1b of the WestConnex project indicated that the mix being used could potentially yield low values of residual flexural strength. As a result, a decision was made early in the New M5 Project to start the shotcrete production with a slightly higher steel fibre count of 40 kg/m^3 reducing at later stage to 35 kg/m^3 as production test results were confirmed for the project.

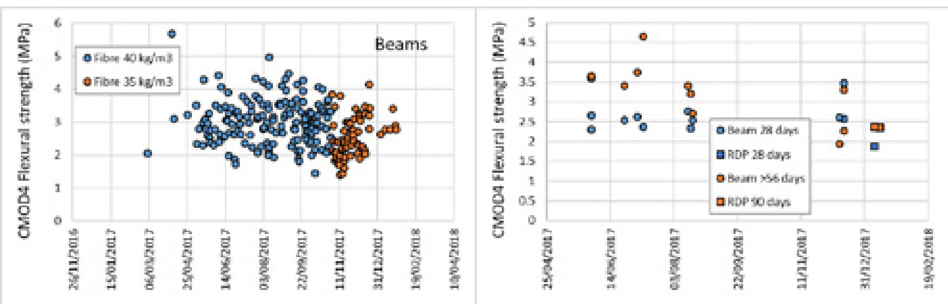

Figure 4 Residual flexural strength – CMOD4 beams.

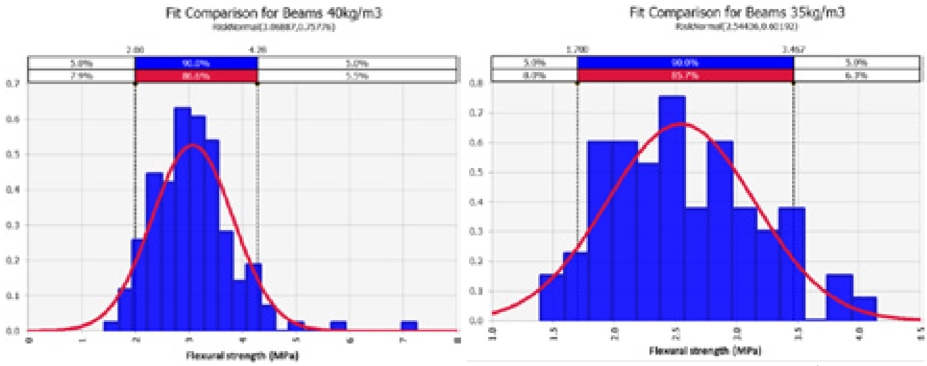

Figure 5 Normal distribution for residual flexural strength CMOD4 results at 28 days for 40 kg/m³ and 35 kg/m³.

The 40 kg/m³ fibre dosage results indicate a mean value of approximately 3.1 MPa with a between-batch CoV = 25% and characteristic design value of 2 MPa. The 35 kg/m3 fibre dosage results indicate a mean value of approximately 2.5 MPa with between-batch CoV = 24% and characteristic design value of approximately 1.7 MPa. The mean within-batch CoV of the beams were observed to be approximately 15% for all test results. These CoV values, both between-batch and within-batch, are somewhat consistent with past experience in Australia [4].

Based on the delayed strength gain observed in the cored samples compressive strength that was inferred to be associated with the fly-ash content, the project team considered it appropriate to investigate performance of both beams and RDPs at 90 days' which is currently underway. Early test result data indicates some potential gain in flexural strength of approximately 20-30% (Figure 4) although further testing is required to achieve a reasonable statistical representation.

Flexural Toughness – Round Determinate Panels - ASTM C1550

The ASTM C1550 RDP toughness results are presented in Figure 6 with statistical distributions shown in Figure 7 and Figure 8. The 40 kg/m³ fibre dosage results indicate mean values of approximately 91.3 Joules and 419.7 Joules with between-bacth CoVs of approximately 16% and 14% with characteristic design values of 72 Joules and 320 Joules for the 5 mm and 40 mm toughness respectively. The 35 kg/m³ fibre dosage results indicate mean values of approximately 88.2 Joules and 354.6 Joules with between-batch CoVs of approximately 16% and 15% with characteristic design values of 67 Joules and 256 Joules for the 5 mm and 40 mm toughness respectively. The mean within-batch CoV of the RDPs were observed to be approximately 10-11% for all test results.

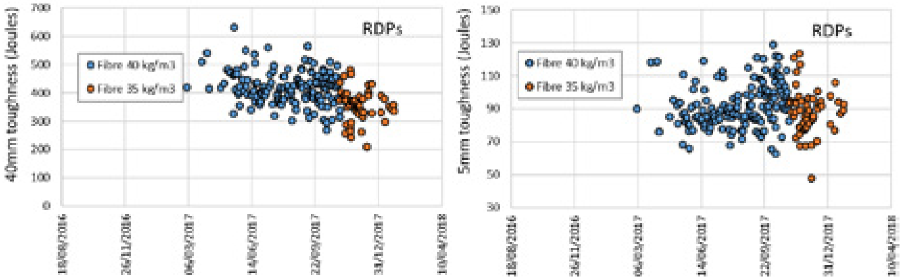

Figure 6 RDP toughness.

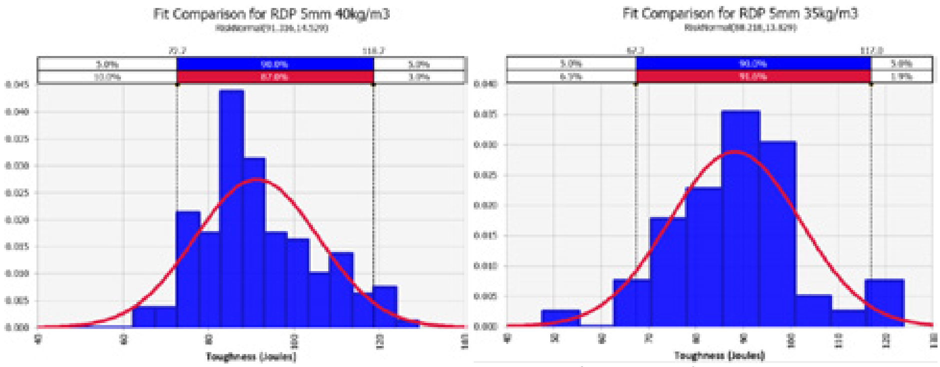

Figure 7 Normal distribution for 5 mm toughness results for 40 kg/m^3 and 35 kg/m^3.

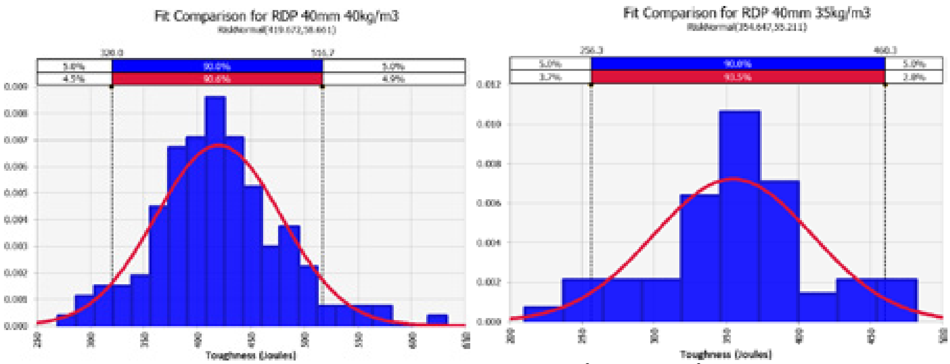

Figure 8 Normal distribution for40 mm toughness results for 40 kg/m^3 and 35 kg/m^3.

Adhesion

The adhesion test results are presented in Figure 9. The results indicate a mean value of approximately 0.75 MPa with a CoV = 31% and an estimated characteristic design value of approximately 0.375 MPa.

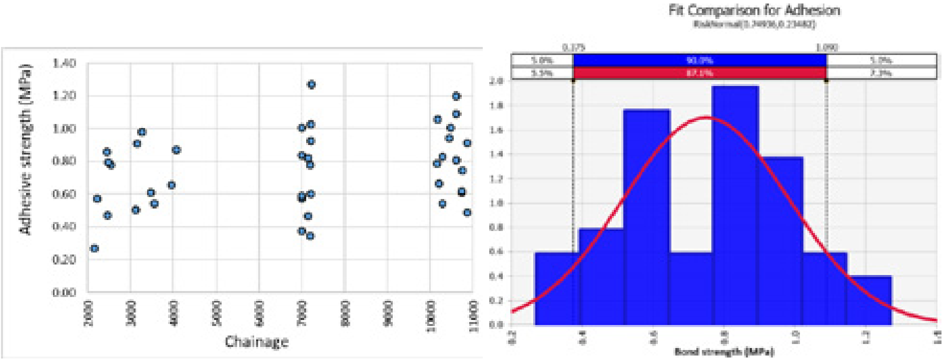

Figure 9 Adhesion test results.

ASSESSMENT OF NON-CONFORMING RESULTS

Although all test results achieve mean values that fully satisfy the minimum performance criteria set in Table 1, the typical between-batch CoV in excess of 13% observed in the sprayed samples generally significantly reduces the characteristic design values which fall under the minimum performance requirements adopted in the tunnel support design. As a result, if the raw test data is considered in isolation, the immediate conclusion would be that the production shotcrete would be non-conforming despite the successful preproduction field trials (generally based on a limited number of samples). For example, the core samples at 28 days achieved a characteristic design strength of approximately 34 MPa whereas the requirement was set at 40 MPa. The EN14651 residual flexural strength at CMOD4, achieved a characteristic design strength of between 1.7-2 MPa whereas the requirement was set at 3 MPa.

However, the assessment of the test results should consider the design methodology adopted. The New M5 Tunnel followed the Australian Standard AS 5100 [3] where design is carried out in terms of Limit States. Safety against an Ultimate Limit State (ULS), i.e. collapse, is achieved by factoring up loads estimated to act on the structure and by applying reduction factors on material strength. In accordance with AS 5100.5 [3], clause 1.4.3.11, the material strength, is defined as a characteristic value that is exceeded by 95% assessed by **standard tests**. In Australian Standards for ULS design, load factor of $L_f = 1.5$ is generally applicable, combined with a capacity reduction factor $\phi_s = 0.6$ applied on fibre reinforced shotcrete without conventional reinforcement. The combined effect results in an equivalent factor of safety FoS = 2.5 which is essentially based on characteristic values assessed from **standard tests**.

The definition of **standard tests** typically implies cast samples, e.g. cylinders, where construction effects are generally ignored, thus with a higher level of uncertainty. For example, Petersons [5] compared the concrete strength obtained from standard test specimens and the strength of samples taken from the actual structures (cores) for 112 building sites in Switzerland. He identified that the actual concrete strength in the structure generally only reached 65 to 75% of the standard tests results. To achieve safety, material reduction factors or global factors of safety have therefore been specified to compensate for the difference in strength between the material in the structure and that in the standard test specimens.

The American Concrete Institute document ACI 318M [6] follows similar reasoning in its clause R26.12.4. It states that concrete in an area represented by core tests shall be considered structurally adequate, without detailed analysis required, if (1) the average of three cores is equal to at least 85% of the characteristic compressive strength and (2) no single core is less than 75% of the characteristic compressive strength. An 85% average of the characteristic compressive strength is equivalent to multiplying the average raw data by approximately 1.18. In fact, the ACI 318M [6] states that it is not realistic to expect the average core strength to be equal to the characteristic compressive strength based on standard samples because of differences in size of specimen, conditions of obtaining the specimens, degree of consolidation and curing conditions.

Based on the above discussion, it is reasonable that similar consideration is applied to test results from compression tests on shotcrete cores and tests on sprayed beams and RDPs. This is particularly valid considering that, in tunnel construction, sprayed samples are prepared in the same way and in the same environment as the final structure, thus, including several construction effects that do not exist in standard samples. This is further reinforced by the larger apparent CoV observed between-batches than within-batches for RDPs and beams emphasizing the impact of construction effects. In fact, the latest version of AS 5100 [3], clause A6.4.2 already recognises that the strength of the concrete may be estimated as 1.15 times the average strength of cores and beams which is equivalent to compare the raw test data to the 87% of the performance requirement.

As a result, if the AS 5100 capacity reduction factor of 0.6 is to be maintained, the characteristic compressive strength of the cores of approximately 34 MPa is to be compared with 34.8 MPa (i.e. 87% of 40 MPa) which could therefore be deemed acceptable particularly considering the 90-day results. Similar comparison could be made with the beam test results, i.e. the characteristic strength of 1.7-2 MPa could be compared to 2.6 MPa (i.e. 87% of 3 MPa) which would still be non-conforming. However, considering the satisfactory performance of the RDPs in terms of toughness, further discussion on the beam test results is warranted which is presented in the following section.

With respect to the lower adhesion characteristic strength, it should be noted, that most of the average values below 0.5 MPa are affected by samples with significantly lower strength than the others and where failure occurred significantly through the substrate (Figure 10), i.e. rock rather than the bond interface, indicating that adhesion would in fact be higher. If these samples are removed from the average, the characteristic value satisfies the design requirement of 0.5 MPa.

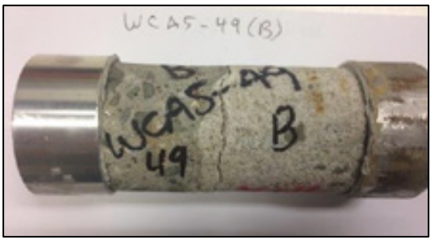

Figure 10 Sample failure through substrate.

EN 14651 (Beams) and ASTM C1550 (RDPs) results

As discussed by Bernard [4], notched beams have only recently started to be used for Quality Control within Australia. There is therefore a deficit of experience and knowledge regarding this test method and the characteristics of results typically obtained.

The most well-known characteristic of the beam tests to contractors and designers is the degree of variability exhibited in the post-crack performance parameters. As presented above, the test results indicated between-batch CoVs of 24-25% in comparison to the RDPs with a more reasonable between-batch CoV = 14-16%.

It is known that the number of fibres crossing a crack contributes to the degree of variability in post-crack residual strength estimates. Therefore, such high variation is often attributed to the small cross-sectional area of the EN14651 beams which are also inferred to cause inadequate crack propagation from the small fracture area. Although the presence of the notch is claimed to reduce variability in crack width, supposedly leading to reduced variability in residual strength, larger coefficient of variation is consistently observed in tests results. According to Bernard [4], EN14651 also fails to include limitations on the magnitude of friction in the supporting rollers. High friction has been shown to substantially influence the apparent post-crack performance of simply-supported beams and can be responsible for large variations in performance between laboratories. For this reason, rollers conforming with ASTM C1812/C1812M (which limits the coefficient of friction) should be used.

Such a higher level of within-batch variability creates significant difficulty in interpreting and applying the results confidently. To reduce the risk of rejection it would be necessary to test large numbers of beams for each batch, which is cumbersome and expensive. Alternative solutions have therefore been sought and more recently, the post-crack performance of round panels has been expressed in terms of flexural strength at first peak and residual flexural strength in the post-crack range [4]. The residual strength of round panels can be estimated by several means, but one accepted method incorporates yield line theory to estimate moments within a panel after which elastic engineering bending theory is used to estimate the flexural stress. This is essentially the same approach that is used to estimate flexural strength in both EN14651 beams and ASTM C1609/C1609M beams. The method is presented in [4].

Bernard [4] demonstrated a good correlation between EN 14651 parameter CMOD4 and residual strengths at 10 mm deflection in ASTM C1550 (Figure 11a) for varying mixes with different target residual strengths. Such a good correlation could not be observed in the New M5 Tunnel results as only one mix is tested with varying residual flexural strength being the result of high between-batch variability (Figure 11b). However, the lower CoV allows for an improved characteristic residual flexural strength when estimated from the ASTM C1550 RDPs (Figure 12). It should be noted that a smaller population was adopted as preliminary investigation which is currently being extended. Nevertheless, a characteristic residual flexural strength of approximately 2.25 MPa was considered acceptable particularly considering the potential increase in strength past 28 days currently being investigated. This value was then selected as the new characteristic residual strength. The new design value is used to re-analyse any installed ground support that relies more significantly on flexural capacity and has non-conforming beam test results that show uncorrected/raw values below 2.6 MPa (i.e. 87% of 3 MPa). It should be noted, however, that when applied in a structural analysis with the conventional AS 5100 strength reduction factor $\phi_s = 0.6$, the new characteristic residual strength of 2.25 MPa is then be multiplied by 1.15 which coincidently results in a value of 2.6 MPa. Although identical, the latter has no relationship with the performance requirement of 2.6 MPa based on 87% of the original 3 MPa.

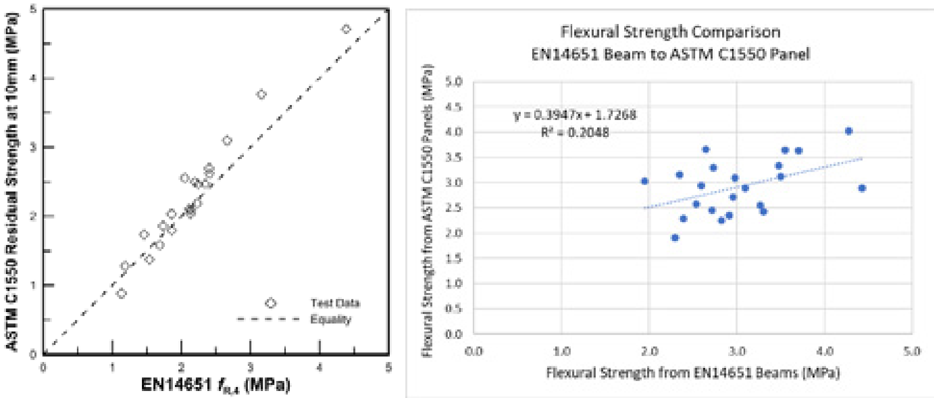

Figure 11 Correlation between EN 14651 parameter CMOD4 and residual strength at 10 mm deflection in ASTM C1550: (a) after Bernard [4] including both steel and macro synthetic. (b) New M5 test results.

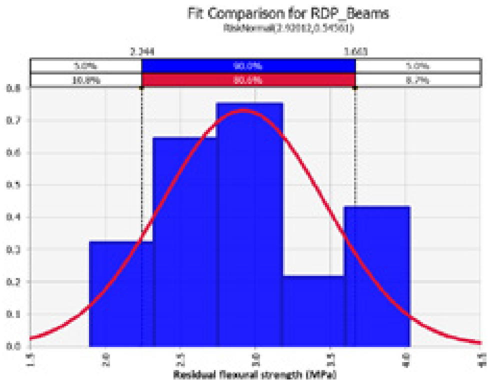

Figure 12 Normal distribution for residual strength estimated from ASTM C1550 RDPs.

Ground support specific acceptance criteria

Based on the observed variabilities, it was also important to recognise that, although the design specified a single shotcrete performance requirement for the project against primary permanent support, the actual performance requirement is dependent on the ground support type and associated failure mechanisms. For example, on the NewM5 Tunnel Project, certain sandstone supports associated with good quality fresh to slightly weathered sandstone primarily relies on shotcrete adhesion to rock and compressive strength for fire purposes and M&E support with a lower reliance on residual flexural strength. On the other hand, other supports associated with moderately weathered and/or poorer rock classes more significantly on residual flexural and compressive strength with a lower reliance on adhesion to rock. Therefore, support specific acceptance criteria was then specified for each support type and added to the shotcrete specification to minimise unnecessary rejection and non-conformance reports.

CONCLUSIONS

The results of the shotcrete testing carried out as Quality Control for the New M5 tunnel project were presented. High levels of population variability, i.e. between-batches, created significant difficulties in interpreting and applying the results confidently. To reduce the risk of unnecessary rejection, the test results were interpreted taking into consideration how the adopted design methodology addresses uncertainty.

Corrections or adjustments are proposed to analyse the results of a population of sprayed samples which already take into consideration some of the construction effects. This is particularly relevant when the design codes are based on characteristic strengths that are defined from statistical analysis on standard tests, thus with material reduction factors that would likely double penalise the design. When assessing the results of cored samples and sprayed beams and RDPs, a value of approximately 85-87% of the design value is considered reasonable as acceptance criteria without the need for detailed structural assessments. In addition, when a characteristic design value is back-analysed from cored samples, sprayed beams or RDPs, it is also considered reasonable to apply a correction factor of 1.15-1.18 if conventional material reduction factors based on characteristic values from standard testing is to be used.

The paper also presented the use of yield line theory to estimate residual flexural strength from ASTM C1550 RDPs which provided an alternative solution to reduce the high variability observed in the EN 14651 beam test results.

REFERENCES

[1] Barrett, S. V. L. and McCreath, D. R. (1995), "Shotcrete Support design in Blocky Ground: Towards A Deterministic Approach", Tunnelling and Underground Space Technology, Volume 10, Number 1, pp. 79-89(11)

[2] Christine Y., Oliveira, D. and Asche, H. (2017). Shotcrete support design in blocky ground: Revisited. In: 16th Australasian Tunnelling Conference, 30 October – 1 November 2017.

[3] Australian Standard AS 5100 – 2017 Bridge Design.

[4] Bernard, E. S. (2017). Correlations in the Performance of Fibre Reinforced Concrete Assessed using Round Panels and the EN14651 Beam Test. In: 16th Australasian Tunnelling Conference, 30 October – 1 November 2017.

[5] Petersons, N. (1964). Strength of concrete in finished structures and its effect on safety. In: IABSE congress report/Rapport du congrès AIPC /IVBH Kongressbericht.

[6] ACI 318M-14 (2015). Building code requirements for structural concrete (ACI 318M-14) and commentary (ACI 318RM-14).

MiniBars^{TM} – A new durable composite mineral macro fiber for shotcrete, meeting the energy absorption criteria for the industry.

Sindre Sandbakk
Dr. Techn. Olav Olsen AS, Trondheim, Norway.

Leonard William Miller and Per Cato Standal
ReforceTech AS, Røyken, Norway.

ABSTRACT: The new innovative macro fiber MiniBars™, is a stable and inert composite mineral macro-fiber meeting the requirements for durability and no alkaline silica reaction ASR. The MiniBars™ specific gravity is similar to that of concrete and will ensures that it will mix homogenously into the concrete, and (ARS) will not float. MiniBars™, made of Alkaline Resistant-Glass or Basalt, are a durable alternative for shotcrete reinforcement in tunnels. Recently, an experimental program has been carried out to quantify the necessary fiber amount to reach E700 and E1000 per the Norwegian Concrete Association's Publication No 7.

1 INTRODUCTION

MiniBars^{TM} developed and produced by ReforceTech AS are a macro mineral fiber made of Alkaline Resistant Glass- or Basalt fibers.
ReforceTech developed the MiniBar^{TM} in Norway starting in 2010. Using the ReforceTech patented production process the MiniBar^{TM} has evolved through 3 Generations with each iteration offering a more competitive solution in terms of cost per MPa in flexural tensile strength. The production process developed in Norway is a wet layup process capable of higher speeds than the typical pulltrusion process. This enables production costs to be lower and more competitive. The MiniBar^{TM} is made from 2 main raw materials, the fiber (Alkaline Resistant (AR) Glass or Basalt Fiber) and a vinyl ester resin from Polynt(Dion 9100 family). The process involves wrapping two strands under tension to create the unique helix shaped geometry. This has been proven to significantly increase the pull-out resistance from concrete and thus increase the average residual tensile strength of concrete when tested in accordance to EN 14651 (2005)
The MiniBars^{TM} have the unique features of length and helix pitch that can be tailored for specific applications to achieve the specified performance. The journey to secure certificates has led to both the AR Glass and Basalt Fiber versions receiving DIBt German National Approvals for Structural (DIBt 2016a) and Non Structural applications (DIBt 2016b) .
The testing regime to secure national approval in Germany included extensive testing for harmless in concrete, effectiveness on plastic shrinkage and structural effectiveness. Extended testing included durability testing, creep testing, and alkali silica reaction (ASR) testing for the Basalt Fiber MiniBars^{TM} (IBAC 2015) and CemFIL MiniBars™ (SINTEF 2017). The DIBt German National Approval has led to the U mark (IBAC RWTH Aachen 2016) and plant audit (IBAC RWTH Aachen

2015) in accordance to EN 14889-2 (2006). The U mark is the first step to get CE marking. The process to finalize the CE marking is ongoing with DIBt leading the European Technical Approval (ETA) process through the remaining EU countries.
The physical and mechanical properties of MiniBars™ as a reinforcement for concrete has some profound advantages. The most obvious include non-corroding which means the wasteful cover layers associated with steel reinforcements can be reduced or eliminated. The second is the is the density which is very close to that of the concrete meaning the MiniBar™ does not float or sink. This results in a favorable fiber distribution in the mixed concrete. This has been demonstrated in various shotcrete trials where the outcome is the MiniBar™ can meet the NB 7 (2011) energy absorption criteria. The environmental aspects have been documented and demonstrated in many applications. The combination of the CO_2 footprint of the MiniBars™ and reduction of the amount of concrete lead to reductions CO_2 in all applications.

2 MINIBAR PROPERTIES

MiniBars™ are made of either Alkali Resistant Glass fiber or Basalt fiber. A picture of the two types of MiniBars are shown in Figure 1.

Figure 1 AR Glass MiniBars™ (left) and Basalt MiniBars™ (right)

The density of the MiniBar™ is 2100 kg/m^3. The MiniBars are available in lengths of 12 mm, 24 mm, 30 mm 42 mm 48 mm and 54 mm. The Diameter for Generation 3 is nominally 0.65 mm. The pitch length is specified to 17 mm although recent shotcrete testing has shown that for larger CMOD/displacements a relaxed helix pitch can increase energy absorption at larger displacements. The concrete grade and type of application plus the desired performance in concrete tensile strength determines the length and the dosage required. This is based on generalized or project specific concrete characterization tests according to EN 14651 and recently NB 7 round panel tests.
The MiniBars™ consist of 1100 discrete fibers with 1000 fibers in the main thread and 100 fibers in the helix thread. The basalt or AR glass fibers are coated with a sizing compatible with Vinyl Ester resin. This specific sizing assists in the bonding of the fibers to the vinyl ester resin. The cured resin impregnating the fibers creates the FRP (Fiber Reinforced Polymer) composite MiniBar™. The 1100 fibers bonded together creating the MiniBar™ working in the concrete to transform the concrete to a ductile material.
The composite MiniBars™ have a tensile strength of >1000 MPa and Elastic Modulus of 44 GPa when tested in single fiber testing conditions, see Figure 2.

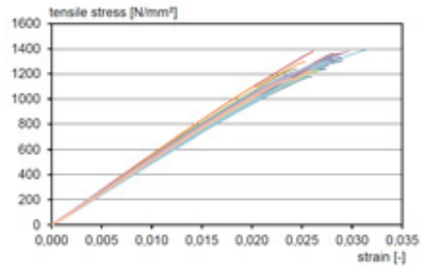

Figure 2 Stress vs. strain relationship of the Basalt Fiber MiniBar™

The high strength and the density give the fiber the advantages of both steel fibers (strength) and plastic fibers (fiber count per kg). It should be stressed that it is the fibers behavior in concrete that determine the performance of the concrete. Engineers are often quick to point out that steel has a higher modulus for example; however, the higher fiber count and geometry and bonding mechanisms offset this. The EN 14651 curves or round panels tests used to characterize the fiber reinforced concrete are the ultimate engineering input. In this case, the tensile strength and the bonding mechanisms are being balanced to ensure the fiber does not rupture and resists pull out. One important difference to steel fibers and plastic fibers as the figure 2 above illustrates is that the MiniBar being purely elastic is contributing to prevent crack growth immediately due to behaving purely elastic. This means the crack widths can be maintained at low levels for water tightness for example and thus slow down or prevent mechanisms related to concrete degradation.

3 MINIBAR™ REINFORCED CONCRETE

The development, testing and certification process has demonstrated that MiniBars™ can be effective in both crack control and structural applications as noted by the two DBIt approvals referenced above.

The MiniBars™ were tested according to a plan devised by IBAC at Aachen University with the following test regime.

1. Preliminary screening phase, testing of fiber breakage during mixing, performance of beams in bending, pull out and creep pull out at 60 °C, and performance of beams after accelerated ageing. Once IBAC was satisfied with the above test results, an application was made to DIBt for the certification process to begin and to the DIBt committees proposed testing regime.
2. The second phase included tests to measure MiniBar™ conformity, harmless in concrete, and effect on early shrinkage. These tests led to certification of the MiniBars™ being harmless in concrete
3. The third phase was specific to demonstrating the static effectiveness leading to the structural performance certification. Testing included bending tests on beams of different concrete grades, and dosages of MiniBars™ from 0.25 % to 4 % VF. Creep tests on beams, fiber tensile creep at different temperatures (-20 °C to + 60 °C).
4. The fourth and final phase was the fire resistance according to DIN 4102 where the MiniBar™ reinforced concrete (3VF%) achieved the highest rating, A1 nonflammable. The AR glass MiniBars™ received the DIBt certificate upon completion of this test.
5. The Basalt MiniBar™ was subjected to an added 5th phase particular to durability pertaining to concerns about alkali silica reactions and is dealt with later in this paper.

The resulting outcome from the three plus years of testing was the German National Approvals (DIBt 2016a and DIBt 2016b)

4 MINIBAR BONDING MECHANISMS

There are four bonding mechanisms:

1. Length
2. Helix
3. Fiber roughness
4. Fiber diameter

4.1 *Fiber length*

Similar to the bond length of reinforcing bars, the MiniBar™ length is tailored to maximize the bond length friction while preventing fiber rupture if the MiniBar™ is too long. The effects of concrete grade from C25 to C100 plus are documented allowing ReforceTech to recommend a fiber length for the grade of concrete. In general, longer fibers leads to higher residual strengths. Furthermore, as the grade of concrete is increased the effectiveness in the concrete increases meaning the fibers can be shorter. Typical fiber length for C25/30 is 54 mm and 42 mm, for C50/60 is 42 mm, and for high strength concrete (C100 plus) 24 mm to 30 mm.

4.2 *Helix*

The helix height and pitch length are critical to the average residual strength performance as the 1100 fibers must move relative to each other when being pulled out of the helix shaped hole in the cured concrete thus absorbing energy and resisting pullout and cracking.

The pitch length is typically 17 mm as was optimized in testing at NTNU for the standard EN14651 performance. illustrates the effect of helix in a typical EN14651 test.

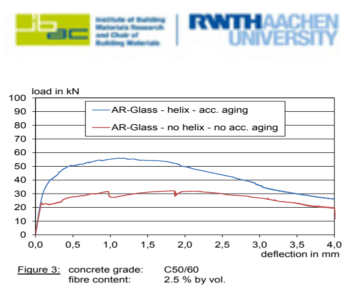

Figure 4 Effects of Helix

The recent shotcrete trials with much larger displacement/crack openings saw an improvement in energy absorption with slightly longer pitch lengths for longer fibers. Higher pitch height leads to higher average residual strength. Higher dosage leads to more fibers and more fibers across a crack lead to higher average residual strength

4.3 *Fiber roughness*

The rough surface is important in the initial static bond and resists the initial crack development. Since the MiniBar™ is purely elastic, this means the static bond increases the pre-crack strength. For the post crack strength or residual strength the helix is the main contributor to resistance of the MiniBar being pulled out.

4.4 *Fiber diameter*

The nominal fiber diameter is 0.65 mm for the Generation 3 MiniBar™, thus allowing the shrinking concrete to grip the MiniBar.

5 DURABILITY

Durability as a topic for MiniBars™ development is a complex field. During the certification process with IBAC and DIBt there were numerous tests performed with compelling results, but the consensus on which test was to be the standard was the aged beam tests.

Durability testing for the AR MiniBar™ was conducted in accordance to IBAC accelerated ageing of beams test, which determines if there is a degradation in EN 14651 beam strength after exposure at high temperature, moisture content and time. The AR glass is known to be alkaline resistant with previous ETA approvals and CE mark and over 40 years of experience globally and thus easily received the DIBt approval (DIBt 2016a)

The raw material Basalt however, does not have a similar previous DIBt approval or CE marking thus is was subjected to a tougher and wider regime to assess the ASR (Alkali Silica Reaction). This is related to ASR experiences with well-documented bridges in the 1960s. This is similar to the questions posed in Norway due to experiences from the 1980s resulting in two publications from the Norwegian Concrete Association, namely NB 21 (2008) and NB 32 (2005).

ReforceTech's early work focused on testing and approving the Basalt MiniBar™ and thus it was subjected to a more rigorous testing regime.

There were three methods to which the MiniBars™ was subjected to testing. This included SIC testing of the raw fibers to assess the durability of the raw materials under alkaline exposure. The second test was the accelerated aged beam testing and finally for Basalt ASR prism testing. Testing in 2017 at SINTEF exposed samples from the Konsberg shotcrete trials to 80C for 14 days in accordance with NB 21 per the mortar test to see if there was any sign of ASR or degradation to the AR CemFil MiniBars. No signs of deterioration or ASR products could be found at the MiniBars or surrounding the MiniBars even at in the highest dosage. See SEM photo.

The development of the MiniBar™ had the normal product development cycles of success and failures. This has led to the development of a better resin and attention to the degree of cure of the resin, and improved sizing.

It has led to the focus on the structural integrity and fiber resin ratio of the MiniBar™ to improve the elasticity in mixing and the tensile strength in beam testing. This resulted in a MiniBar™ that is impervious to the both the chemical and physical attack from the concrete during curing and ageing and the subsequent approvals from DIBt.

As a footnote the same materials are commonly also as human dental implants and are approved by the FDA for such thus illustrating the durability and inertness of the AR glass/Vinyl Ester FRP.

5.1 *Durability of the Raw Material under Alkaline Exposure*

Initial testing was focused on the SIC test (EN 14659 2005) where ReforceTech were able to work with the raw material suppliers to specify the best sizing. This resulted in the Basalt Fiber having equivalent results as the AR glasses tested. This test was used to select the best possible raw materials for the production and certification of the MiniBars™.

5.2 *Durability of the MiniBars™ and Concrete in beams exposed to accelerated ageing*

The IBAC approach is to test the MiniBars™ in accelerated ageing beam tests, which was aged, in high temperature and moisture for 1 month. Then examined for signs of degradation. The American approach in testing with International Code Council (ICC) according to AC32 (2003), which is a similar approach, but measuring the beams over 4, 8, 16, 32 and 52 week intervals and limiting the performance drop to 15%. In both the German and American cases, the researcher is looking for a drop in ARS between a control beam (unaged) and the aged beams.

The mechanisms of the durability are complicated and more than chemical attack in nature as the matrix and fibers are proven resistant to the chemicals as measured in SIC testing.

The development of the Basalt MiniBar™ due to the general lack of previous experience with basalt fibers and negative experience with basalt aggregate and ASR issues has been a significant challenge in terms of gaining acceptance and certification. However, with improvements in the MiniBar™ production process, sizing and resin properties significant gains have been made and the results are now approaching that of the AR glass MiniBars™.

For the certifications, the DIBt committee settled on the IBAC accelerated beam tests as the acceptance test for the AR Glass iniBars™ as it tested the durability of the MiniBar™ in the concrete.

5.3 *Durability of the Concrete reinforced with MiniBars™*

The AR glass MiniBar™ has the advantage of 40 years of experience and knowledge related to the 16% zirconia additions to the glass mineralogy, thus the AR MiniBar™ has not had the same hurdles to overcome in the German National Approval certification process. Owens Corning products have been certified in Germany and AR Glass with 16% Zirconia is a known and accepted product and is clearly differentiated from normal glass and glass fibers which are alkali silica reactive.

The experience with Alkali Reactive Aggregates as noted in the earlier reference to NB 21 and NB 32 is similar to the concerns noted with the DIBt committee and the Basalt MiniBarsTM. The NB 21 and NB 32 are primarily focused on aggregates, which may have the specific forms of reactive silica. DIBt requested testing by Verein Deutscher Zementwerke e.V. (VDZ the German Cement Works Association) to assess the ASR of MiniBar™ reinforced concrete. As testing progressed it was very clear the Basalt MiniBar™ was passing the test. This lead the DIBt committee to extend the duration of the test from 168 days to 224 days. The findings concluded that there was no ASR reaction from the Basalt MiniBars™ (VDZ 2015). The graph in Figure 5 shows the growth of the prism over time do to ASR. It is related to the concrete and not the MiniBars™.

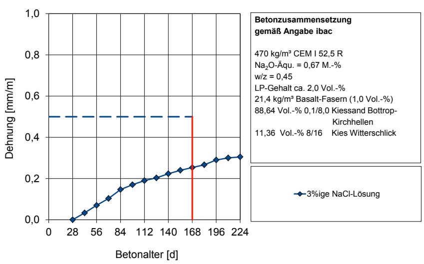

Bild 2 Dehnung des Betons im 60 °C-Betonversuch mit Alkalizufuhr von außen, Betonzusammensetzung gemäß Angabe des Instituts für Bauforschung (ibac)

Figure 5 Growth of prisms over time

The photo in Figure 6 illustrates no ASR around the Basalt MiniBars™.

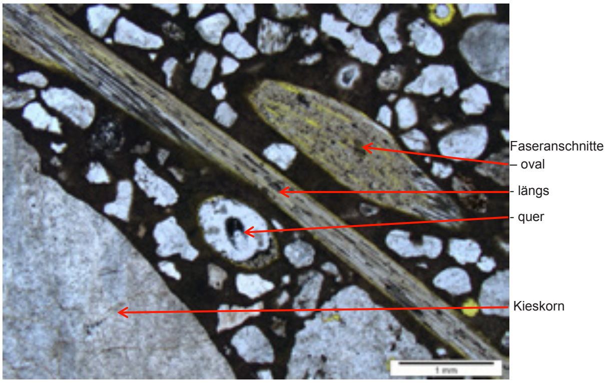

Bild A3 Anschnitte von Faserbündeln in der Betonmatrix (polarisiertes Licht)

Figure 6 No sign of ASR around the Basalt MiniBar^{TM}

The testing at SINTEF also concluded the same that there was no deterioration nor ASR products around the AR Cem-FIL MiniBars™.

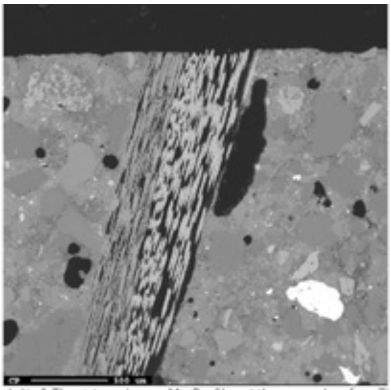

Photo No 6. Sample No 1. The picture shows a MiniBar fibre at the exposed surface. There is no sign of deterioration of the single fibres.

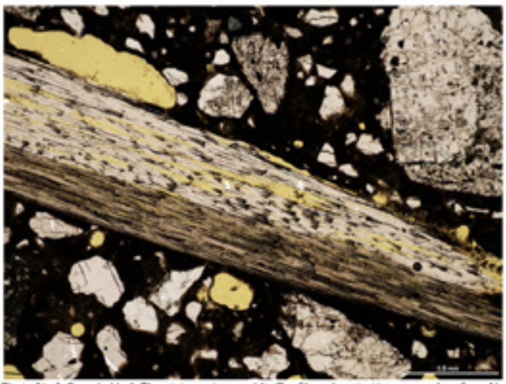

Photo No 1. Sample No 1. The picture shows a MiniBar fibre close to the exposed surface. No deterioration of the fibre could be observed. The voids between the single fibres are partly filled with epoxy (yellow).

6 FIELD TESTING AT KONGSBERG

Due to durability criteria for tunnels, the AR Glass MiniBar™ was selected. Field trials were conducted on two occasions using dosages of 5 kg/m^3 up to 25 kg/m^3. The mixing was performed by blowing the MiniBars™ into the back of the concrete truck at the batching site.

The truck was driven to the site and the concrete poured into the shotcrete truck and sprayed using normal practices. Videos of this and other experiences are available on the ReforceTech YouTube channel.

Samples were taken in accordance to NB 7 to measure the fiber content at three points during each sampling. The fiber content showed remarkably low values of variation. This is due to the density of the MiniBars™.

The fiber counting was facilitated using a Cesium Formate Brine solution allowing the MiniBars™ to float in a liquid with a specific gravity of 2.3. The average coefficient of variation was 5% over 5 samples.

The rebound was determined to be normal and in line with other fibers, but was not examined. The fibers were not observed to be broken or damaged while fiber counting was ongoing or in field observations in the trials from rebound MiniBars™ on the ground.

6.1 *May 2016*

Three series of three panels were made to determine the energy absorption capacity. The fiber dosage in the three series was 5 kg/m^3, 10 kg/m^3 and 15 kg/m^3. The fibers were 60 mm long, and had a helix pitch length of 17 mm.

The absorbed energy according to NB 7 was 229 J, 394 J and 620 J for 5 kg/m^3, 10 kg/m^3 and 15 kg/m^3, respectively. Nominally, the NB 7 results and EN 14488-5 results would give about the same results, but in NB 7 there is a reduction factor of 0.75 to account for the effect of friction at the support.

A typical load vs. deflection curve is shown in Figure 7 (SINTEF 2016a).

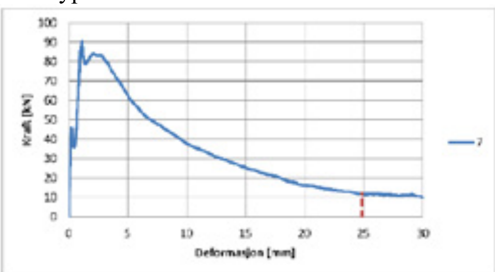

Figure 7 Load vs. deflection, 15 kg/m^3, 17 mm helix, 60 mm length

As can be seen from Figure 7, the capacity “collapsed” after cracking. This was because the fibers’ bond to the concrete was too good, and the fibers simply broke instead of being pulled out. The knowledge gained from the may resulted in a new field test at the same location in September.

6.2 *September 2016*

In September, six series of three panels were made to optimize the fiber geometry and to demonstrate that MiniBars™ is able to reach E1000 according to NB 7. The fiber variation, and energy results (SINTEF 2016b) are shown in Table 1.

Table 1.Fiber variation

Parameter	Dosage [kg/m^3]	Length [mm]	Pitch length [mm]	Energy [J]
Series 4	25	50	32	1072
Series 5	15	50	32	719
Series 6	25	43	32	1054
Series 7	15	50	27	714
Series 8	15	43	27	633
Series 9	25	43	27	1061

The tests performed at Kongsberg clearly demonstrates that it is possible to reach E700 with 15 kg/m^3 MiniBars^{TM}, and E1000 with 25 kg/m^3 MiniBars^{TM}. Further, when comparing the load vs. deflection curve for one panel from series 5 with similar curve for one panel from series 7 (i.e. Figure 7 and Figure 8), it is seen that the increase in absorbed energy is caused by increased load capacity at larger deflections. This is an important effect. For all fiber types, it is possible to increase the capacity to absorb energy simply by increasing the fiber dosage, while for MiniBars^{TM} it is also possible to adjust the geometry. Further, the authors' conviction is that the optimal fiber geometry is not yet found, and that it is still possible to adjust the fiber to reduce the necessary dosage for E1000.

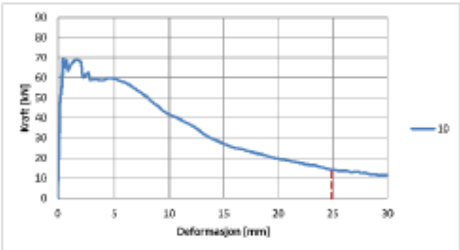

Figure 8 Load vs. deflection, 15 kg/m^3, 27 mm helix, 50 mm length

With regard to Figure 7 and Figure 8, by further optimizing the fiber geometry, it should be possible to adjust the load vs. deflection curve even more. Increasing the load capacity by an average of 5 kN from 15 to 25 mm deflection will result in 50 J higher energy absorption capacity.

6.3 *Shotcrete MiniBar^{TM} optimization*

One of the purposes of the field testing was to optimize the MiniBar^{TM} in order to achieve the most effective energy absorption as E/kg fiber. As previously mentioned, the round panel testing subjects the MiniBar^{sTM} to much larger pull out lengths compared to beam testing. The EN 14651 procedure gives crack widths in the range from 0 mm to 4.0 mm, while the NB 7 procedure gives crack widths up to typically 20 mm (Sandbakk 2011). In early testing, the helix pitch was tested at 17 and 24 mm and at MiniBar^{TM} lengths of 35 and 55. The longer MiniBar^{TM} and pitch length was determined to absorb more energy. Subsequent testing also played with 32 mm pitch lengths and 60 mm lengths. The length was found to be too long and the bond too good! So the final shotcrete MiniBar^{TM} is designed to be 50 mm long and with a 32 mm pitch length. It is available in either AR Glass or Basalt Fiber versions.

At the dosage of 25 kg/m3, the MiniBar^{TM} was able to achieve 1061 J according to the specification in NB 7, which equals 1415 J according to EN 14488-5. By use of the correlation factor of 2.5 by Bernard (2002), the capacity to absorb energy according to ASTM C 1550 should be about 565 J.

7 OTHER APPLICATIONS

Today, MiniBars™ are being used in many applications. The typical application sees benefits in reducing the amount of concrete used due to the cover layer, time savings, and reduction in logistics costs. In each case, there can be a savings of CO_2 primarily based on the comparison of steel versus MiniBars™ used to meet the specifications through engineering, but also when the reduction in the amount of concrete is also factored in. ReforceTech has many applications including the following.

1 Facade-panels, where the outer layers are produced at 50% of previous thickness lowering material costs, production costs, shipping costs and making the buildings roomier.
2 Slab on ground, where the concrete can be thinner, have smaller crack widths preventing water and radon gas ingress and lowering costs by allowing larger crack/joint free areas.
3 Inner walls, where the replacement of wire welded mesh saves time and costs.
4 Screeds, where the screed can be thinner and have a better crack free finish.
5 Rafts, where the crack widths can prevent water ingress and radon gas ingress thus protecting the reinforcement and lengthen the building life.
6 Floating infrastructure, where the corrosion free attributes have and can enable unique applications such as fish farms barges.
7 Utility poles, where the combination of MiniBars™ and BasBars™ (bars made of basalt) create a non-conductive reinforcement.
8 Pavements, where the MiniBar™ can replace wire welded mesh and reduce the cracking and destruction of the concrete related to the MiniBars™ being close to the surface.
9 Tunnel elements, where the segment can be produced thinner, allowing thinner bore TBMs and savings in removal of the excavated rock.
10 Shotcrete, where the MiniBars can be used to permit thinner layers and still meet the loading criteria and allowing savings in material costs, construction time and CO_2 emissions.

8 CONCLUSION

MiniBars™ have been subjected to extensive investigations to be approved for use in structural and/or non-structural applications. The investigations have been primarily focused on durability and possible degradation of both the fiber and the concrete. No such signs are found, meaning that concrete reinforced with MiniBars™ is durable, even in areas where the concrete is cracked!
The field testing at Kongsberg, and the following NB 7 testing at SINTEF, demonstrates that there are no difficulties in mixing, pumping and spraying MiniBar™ reinforced concrete in energy class E700 and E1000. The new innovative macro fiber MiniBars™, is a stable and inert composite mineral macrofiber meeting the requirements for durability and no ARS reaction. The MiniBars™ specific gravity is similar to that of concrete and ensures that it will mix homogenously into the concrete.

ACKNOWLEDGEMENTS

The authors wants to thank Veidekke, Normet and the Norwegian Public Road Administration for help and guidance and for allowing us to perform the field test at Kongsberg.

REFERENCES

1. DIBt 2016a. *AR Glass MiniBars fur die Verwendung in Beton.* Zulassungsnummer Z-3.72-2098. Deutches Institut für Bautechnik (DIBt). 7 p. (In German)
2. DIBt 2016b *Basalt MiniBars für die Verwendung in Beton.* Zulassungsnummer Z-3.79-2126. Deutches Institut für Bautechnik (DIBt). 7 p. (In german)

3. IBAC 2015 *Report M2012*. Consist of several internal reports regarding approval of AR MiniBars™.
4. SINTEF 3039-167 Test Report, Testing of Shotcrete with AR CemFIL MiniBar Fibers. Evaluation of Alkali Resistance Project no. 102003039-167 6 p.
5. NB 7 2011. *Sprayed Concrete for Rock Support*. Norwegian Concrete Association, Publication no. 7. 108 p.
6. NB 21 2008. *Durable concrete with Alkali Reactive Aggregates*. Norwegian Concrete Association, Publication no. 21. 44 p.
7. NB 32 2005 *Alkali Aggregate Reaction in Concrete. Test Methods and Requirements to Laboratories*. Norwegian Concrete Association, Publication no. 32. 48 p.
8. Owens Corning 2016. *AR Glass Fibers and Alkali-Silica Reactions*. Letter from Gèrard Tardy, Product Engineer in Owens Corning. 1 p.
9. VDZ 2015. *AKR-Performance-Prüfung eines Faserbetons für die Feuchtigkeitsklasse WA*. VDZ, Technical report P-2015/0380; A-2015/2113. 16 p. (in german)
10. SINTEF 2016a. *Test Report. Testing shotcrete according to NB7:2011*. Project no. 102013956. 14 p. (in norwegian)
11. SINTEF 2016b. *Test Report. Testing shotcrete according to NB7:2011*. Project no. 102014634. 17 p. (in norwegian)
12. AC32 2003 *Acceptance criteria for concrete with synthetic fibers*. ICC Evaluation service, INC.
13. EN 14649 2005. *Precast concrete products – Test method for strength retention of glass fibres in cement and concrete (SIC TEST).)*. European Standard, European Committee for Standardization, CEN, 40 p.
14. EN 14651 2005. *Test method for metallic fibre concrete. Measuring the flexural tensile strength (limit of proportionality (LOP), residual)*. European Standard, European Committee for Standardization, CEN, 20 p.
15. EN 14889-2 2006. *Fibers for concrete. Part 2. Polymer fibers. Definitions, specifications and conformity*. European Standard, European Committee for Standardization, CEN, 32 p.
16. Bernard 2002 *Correlation in the behavior of fibre reinforced shotcrete beams and panel specimens*. Stefan Bernard. Material and Structure, Vol 35, pp 156-164.

MODELLING ASPECTS TO PREDICT FAILURE OF A BOLT-ANCHORED FIBRE REINFORCED SHOTCRETE LINING

Andreas Sjölander
KTH Royal Institute of Technology, Stockholm, Sweden
andreas.sjolander@byv.kth.se

Rikard Hellgren
KTH Royal Institute of Technology and WSP Group Stockholm, Sweden
rikard.hellgren@byv.kth.se

Anders Ansell
KTH Royal Institute of Technology, Stockholm, Sweden
anders.ansell@byv.kth.se

ABSTRACT

Tunnels in hard and jointed rock are normally excavated with an arch shape to enable the rock to carry itself. The arch effect depends on the stability of individual blocks and too high or too low horizontal stresses could cause blocks to be pushed out or to fall down. To prevent this, systematic rock bolting in combination with fibre reinforced sprayed concrete (FRSC) is commonly used to support the rock. To understand the failure mechanism of the lining when subjected to the load from one block is therefore important for the design. In this paper, the three main failure mechanisms for a rock support shotcrete lining has been identified as failure in the fibre reinforced concrete, bond failure between shotcrete and rock or failure of rock bolts. For each of the failure modes, a short review of numerical methods is presented followed by a selection of a preferred modelling approach. The selected methods are then verified against experimental results from the literature. The selected methods all shows good agreements with tests and demonstrates the ability to simulate each failure mode one by one.

INTRODUCTION

Tunnels in hard rock are normally excavated with an arch shape to enable the rock to carry itself. For a jointed rock mass, the stability of the tunnel will depend on individual blocks [1]. Low or high horizontal stresses could cause individual blocks to either fall out or be pushed out from the arch. To secure the tunnel, systematic rock bolting is commonly used in combination with fibre reinforced sprayed concrete (FRSC). Rock bolts are used to secure single blocks and in some cases also ensure a structural connection between shotcrete and rock. Sprayed concrete is applied with high air pressure which enables the material to fill out small voids on the surface of the rock and to penetrate and fill out joints [2] which stabilize individual blocks from rotation. The primary use of shotcrete is to support blocks that fit between the rock bolts but also to prevent deterioration of the rock mass [3]. The bond strength developed between the concrete and the rock is able to transfer stresses from small blocks to the surrounding rock mass. Sprayed concrete can therefore, in some cases, be used as the only rock support.

The design of rock support is complicated and empirical methods, such as the Q-method developed by Barton et al. [4], are widely used. The reason to this is the difficulty to determine the geometry and the loads that act on the support. However, numerical analysis is a great tool to understand how variation in material strength and thickness of the concrete affects the load capacity of the support.

For numerical analysis, the rock support should be regarded as a composite structure of rock, FRSC and rock bolts. One load case normally considered in numerical analysis is the load from a single block between the rock bolts. This load case is described in the standards for road and railway tunnels in Sweden [5] and potential failure mechanisms caused by the block are discussed in e.g. [6, 7]. It is assumed that the final failure mode is governed by the bond strength. If bond is sufficient, shear failure might occur and if bond fails, a flexural failure can occur in the lining. Analytical solutions for the capacity of the lining are presented for the mentioned failure modes in [6, 7]. However, it is difficult to account for effects caused by the irregular rock surfaces and the varying thickness of the shotcrete in the analytical solutions. Such effects are discussed in [8] and it was shown by Sjölander et al. [9] that both of these factors have a significant effect on the load capacity. Nilsson [10], showed that the placement of the bolts with respect to the uneven rock surface affects the load capacity of the lining. Malmgren and Nordlund [11] studied the interaction between shotcrete and rock and how various parameters such as the bond strength and surface roughness influence failure in the concrete and the interface of the lining.

In this paper the failure mechanisms of a bolted FRSC lining subjected to a quasi-static load from one block is reviewed through analysis of previous experimental results. A numerical model for each of the important individual failure mechanisms of the lining, i.e. cracking of the fibre reinforced concrete, bond failure between shotcrete and rock as well as pull-out failure of rock bolts is presented. Each of the failure mechanisms are complicated and have previously been thoroughly studied within their respectively field. This paper presents a short review of numerical methods for each of the failure modes followed by a presentation of the preferred modelling approach. The selected methods are verified against experimental results from the literature.

FAILURE OF A SHOTCRETE LINING

To investigate the failure mechanisms and the structural capacity for a bolted FRSC lining, large scale experimental series was performed by Holmgren [12, 13] and Fernandes-Delgado et al. [14]. Several influencing factors such as; the thickness of the concrete, location of rock bolts and the addition of reinforcement were investigated. The setup included three blocks that were covered with one layer of sprayed concrete (30 to 140 mm). A displacement controlled hydraulic jack was used to push the center block through the lining. The setups are shown in Figure 1, in a) with the rig vertical and the blocks fixed to the ground by a steel rig and in b) with the rig horizontal and steel rods used to tie the fixed block to the ground. Furthermore, the distance between the movable block and the rock bolts were varied for the setup in Figure 1b).

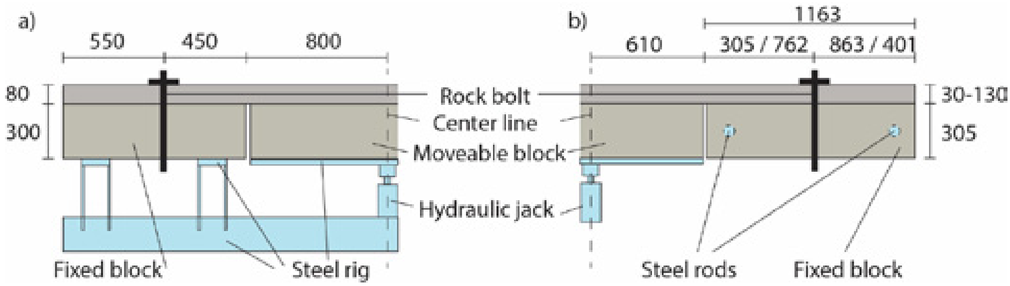

Figure 1 Setup for testing of bolt-anchored sprayed concrete lining by a) Holmgren [12] and by b) Fernandes-Delgado et al. [14]. All measurements in mm.

According to Holmgren [12], the primary failure mechanism is bond failure, characterized by a drop in external force as shown in Figure 2 a). For unbolted and unreinforced lining, the load drops approximately to one third of the failure load and can then not be further increased. Thereafter the bond failure propagates until a flexural failure, occurs in the concrete. Fernandes-Delgado et al. [14] also reported that bond failure is the primary failure mechanism for linings with a thickness between 50 to 130 mm. The moving block induces mainly tensile stresses at the interface and bond failure will therefore be governed by Mode-I opening, i.e. tensile separation. For reinforced and bolted linings, the load can be increased after the initial drop and the magnitude is governed by the amount of reinforcement and the structural connection between the bolt and the reinforcement [12].

In Figure 2a), results from Holmgren [12] are presented where A2 to A4 represents increased structural connection between bolt and reinforcement while the difference between A4 and A5 is an increased amount of reinforcement. Bond failure was decisive for the structural capacity of the lining it was therefore not possible to increase the load any further than the initial peak load. Test performed by Holmgren [13] with large amount of fibres (1.5 to 2.0 % of volume) in combination with rock bolts and steel washer plates showed similar behavior to previous test with reinforcement [12]. In the study by Fernandes-Delgado et al. [14], the entire area of the fixed block was in some cases covered with tape to decrease the bond strength. In Figure 2b), test S3 and S5 had high bond strength and no rock bolts while test S4 and S6 had low bond strength and rock bolts placed at a distance of 91 cm from the edge of the moving block. The results indicates that a higher failure load is achieved for linings with good bond strength and that the failure load is unaffected by the thickness of the concrete.

Both studies [12, 14] conclude that bond stresses are transferred over a narrow band and that the length of debonding, i.e. separation between the interfaces, is partly related to the thickness of the shotcrete when no rock bolts are used. When rock bolts with steel plates are used, debonding is arrested at the location of the plates. The location of the rock bolts with respect to the moving block is therefore important for the failure mode of the lining. Fernandes- Delgado et al. [14] assumed that bond stresses are triangularly distributed while Holmgren [12] assumed a uniform stress distribution. With a uniform stress distribution and bond strength, the width of the band was by Holmgren calculated to be approximately 30 mm [12]. The same width was calculated in numerical studies by Banton et al. [15] and a uniform stress distribution is commonly accepted for how bond stresses are transferred between blocks, see e.g. Barret and McCreath [6] and the Swedish design guidelines for tunnels [7].

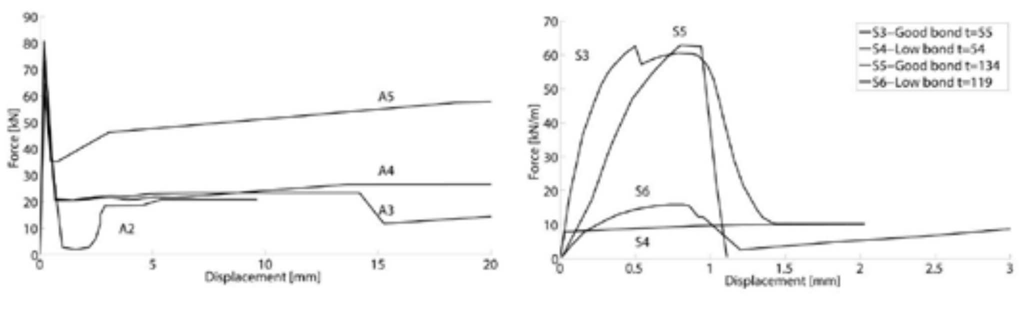

Figure 2 Test results for a bolted FRSC lining showing the influence of an increased structural connection between reinforcement and bolt (A2-A4) and amount of reinforcement (A4-A5) from [12]in left figure while the influence of thickness (t) and bond strength from [14] is shown in right figure.

FAILURE OF FIBRE REINFORCED CONCRETE

Research regarding fibre reinforced sprayed concrete for rock support in tunnels begun in the 1970's [16] and is today the dominating support methods for rock tunnels in Sweden and Norway [17]. Structural, or macro, fibres have commonly a length of 25 to 60 mm and a diameter of 0.3 to 3.0 mm [18] and are added to increase the ductility of the concrete. Extensive testing of the structural behaviour of fibre reinforced concrete (FRC) have been performed by Barros and co-workers [19, 20] as well as Banthia and co-workers [21, 22]. Results have shown that the contribution from fibres to the mechanical properties of concrete is negligible before cracking. After cracking, fibres are able to bridge and transfer stresses across the crack which results in an increased ductility compared to unreinforced concrete. The post-cracking response depends on the number and orientation of fibres as well their geometry and anchorage in the concrete. A scatter in test results is expected due to the random mixing of fibres in the concrete, as seen in Figure 3a). The main failure and energy consumption mechanism for tensile failure is sliding and pull-out of fibres [23]. The pull-out force for individual fibres was investigated by Soetens et al. [24]. The results indicates that the ultimate pull-out force is unaffected by the embedded length of a fibre in the concrete matrix but the ductility increases with an increased embedded length, see Figure 3b). The pull-out forces is also affected by the strength and diameter of the fiber as well as strength of the concrete [25, 26]

Due to the random orientation of fibres and how it affects the failure behaviour, modelling of FRC is complex and many different approaches can be found in the literature. Modelling of individual fibres is uncommon due to the large amount of fibres which makes the model computationally heavy. A computational efficient model was presented by Soetens and Matthys [25] in which fibres were modelled as cable elements but only activated if they crossed a cracked concrete element. The stress-strain curve for the fibres was based on pull-out tests of individual fibres and Monte Carlo simulations were used to distribute them in a finite element model [25]. Luccioni et al. [26] used information regarding the pull-out force of individual fibres to create a composite model of plain concrete and fibres. The fibres were not modelled explicit but their contribution was described depending on the assumed volume fraction of fibres and concrete.

The benefit of models based on the constitutive relations of individual fibres is that once these are established, the influence of volume, orientation and distribution of fibres could be investigated numerically [26]. However, if the distribution of fibres is unknown, more simple models exist that yields the same results. FRC can be modelled as a homogenous material and the effect of fibres is then accounted for by defining a relation between stress and crack opening $\sigma(w)$. For such models, the non-linear behaviour is commonly modelled using plasticity theory or continuum damage mechanics (CDM) [27].

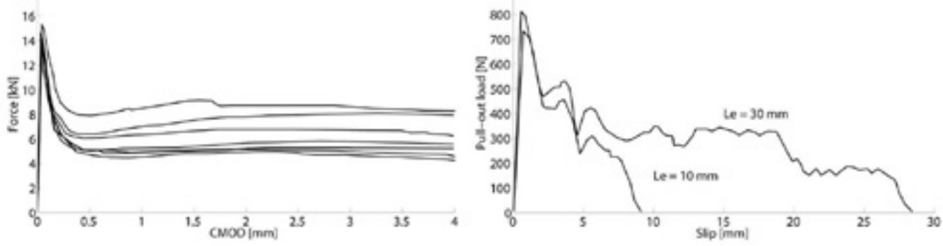

Figure 3 Test results for fibre reinforced concrete. Left figure shows the scatter in force-displacement for notched beams [28] and right figure shows force-slip curves for pull-out of individual fibres [24].

Numerical model for FRSC

Models based on CDM are straight forward to implement and normally more computational efficient compared to plasticity model [27, 29]. A CDM is therefore used here and its main principle is that cracking can be described as a reduction of the load bearing area [30]. An isotropic damage model was used for Mode-I failure based on the work by Oliver et al. [29]. The implementation of the governing equations and extensive testing of the capability to describe cracking of plain concrete is presented by Gasch [27]. Stresses are calculated according to Eq. (1) where E is Young's modulus of the undamaged material and ω is the damage parameter ranging from zero for undamaged material to one for fully damaged material.

$$\sigma_{\mathrm{i}} = (1-\omega)E\varepsilon_{\mathrm{i}} \tag{1}$$

To evaluate when failure occurs, an equivalent strain$\varepsilon_{\mathrm{eq}}$ based on Rankine's theory was used. This states that failure occurs once one of the maximum principal stresses in any direction reaches the failure stress.

$$\varepsilon_{\mathrm{eq}} = \frac{1}{E}\max\langle\sigma_{\mathrm{i}}\rangle\ ;\ i = 1,2,3 \tag{2}$$

Only positive (tensile) stresses were used to evaluate $\varepsilon_{\mathrm{eq}}$ and compressive damage was not considered in the model. To ensure that damage is irrecoverable, a history-dependent variable κ was introduced to keep track of the maximum tensile strain in each element.

$$\kappa = \max\left(\varepsilon_{\mathrm{eq}}, \kappa_{\mathrm{old}}\right) \tag{3}$$

A damage criterion $f(\varepsilon_{\mathrm{eq}}, \kappa)$ was defined based on strains according to Eq. (4) and a Kuhn-Tucker condition was used to control the growth of damage as specified in Eq. (5). This states that damage can only increase when the current state of strain $\varepsilon_{\mathrm{eq}}$ is larger than the history dependent strain κ.

$$f\left(\varepsilon_{\mathrm{eq}}, \kappa\right) = \varepsilon_{\mathrm{eq}} - \kappa \leq 0 \tag{4}$$

$$f \leq 0\ ;\ \kappa' \geq 0\ ;\ \kappa' f = 0 \tag{5}$$

Once damage occurs, stresses are described as a function of the crack opening w. The $\sigma(w)$ function is based on the cohesive crack model (CCM) from Hillerborg et al. [31]. The basic concept of the CCM is that a fracture process zone exists in front of the crack tip and that the stress at the tip is equal to the tensile strength. Behind the crack tip, stresses are a function of the crack width up to critical width in which the stresses have reached zero. In the literature, several shapes are found for the $\sigma(w)$ function. A perfect plastic or a bi-linear hardening or softening curve is suggested in Model Code [32]. Several researchers use a tri-linear $\sigma(w)$ function which is able to capture both the initial softening and the subsequent hardening that could occur, see e.g. Yoo et al. [22] and Sotens and Matthys [25]. To decrease mesh dependency, crack widths are converted to strains based on the crack band width h_{f}. In this paper, h_{f} have been set equal to the characteristic element length, this is a common assumption [27, 33].

$$w_{\mathrm{i}} = (\kappa - \varepsilon_0)h_{\mathrm{f}} \text{ for } \varepsilon_0 < \kappa \tag{6}$$

As the post-cracking response for FRC depends on the amount and distribution of fibres the response can either be strain-softening, characterized by an initial drop in force at cracking before the fibres are activated, see Figure 3a), or strain-hardening where the force instead can be increased post cracking. The model presented here describes the effect of strain-softening which is the expected response of FRSC with the amount and type of fibres used in Sweden [8]. A combined damage function representative for plain and reinforced concrete was developed and is presented in terms of strain according to Eq. (7) and (9). At crack initiation ε_0, damage is governed by the softening of plain concrete. Softening is described with an exponential function as in Eq. (7). The slope of the softening curve is controlled by ε_{f} which is based on the fracture energy G_{f} and tensile strength σ_{t} of the concrete as described in Eq. (8).

$$\sigma(\kappa) = \sigma_{\mathrm{t}} \exp\left(-\frac{\kappa - \varepsilon_0}{\varepsilon_f}\right) \text{ for } \varepsilon_0 \leq \kappa \tag{7}$$

$$\varepsilon_{\mathrm{f}} = \frac{\varepsilon_0}{2} + \frac{G_{\mathrm{f}}}{\sigma_{\mathrm{t}}} \tag{8}$$

At the crack width ε_1, fibres are activated and softening is governed by the response of the fibres. This is described with two identical defined linear functions of which the first on is presented in Eq. (9).

$$\sigma_1(\kappa) = \sigma_{\mathrm{f1}} - k_1 \kappa \text{ for } \varepsilon_1 \leq \kappa < \varepsilon_2 \tag{9}$$

The slope of the linear $\sigma(\kappa)$ curve is defined by $k = \Delta\sigma/\Delta\varepsilon$ and defined for the total strain κ. A schematic $\sigma(w)$ function is shown in Figure 4a) where σ_{f1} is the stress at the intersection with the stress axis. The stress σ_{f1} has a fixed value and can be seen as a fictitious stress used to define the $\sigma(w)$ function for the total strain. The exponential and linear damage function $\omega(\kappa)$ is derived by setting Eq. (2) equal to Eq. (8) and Eq. (10), respectively.

$$\omega(\kappa) = 1 - \frac{\varepsilon_0}{\kappa} \exp\left(-\frac{\kappa - \varepsilon_0}{\varepsilon_f}\right) \text{ for } \varepsilon_0 \leq \kappa < \varepsilon_1 \tag{10}$$

$$\omega_1(\kappa) = 1 - \frac{\sigma_{\mathrm{f1}} - k_1 \kappa}{E\kappa} \text{ for } \varepsilon_1 \leq \kappa \leq \varepsilon_2 \tag{11}$$

Verification of numerical model for FRSC

Buratti et al. [28] tested a notched beam of fibre reinforced concrete in three-point bending. These results were used to verify the presented model. For the simulation, a 2D model with a free triangular mesh with a size of 8-10 mm was used. To define the material model, G_{f} and σ_{t} for the concrete is needed as well as the crack widths w_{i} and stress ratios $\alpha_{\mathrm{i}} = \sigma(w_{\mathrm{i}})/\sigma_{\mathrm{t}}$, at the intersecting points see Figure 4a). The material data were chosen to reproduce the experimental results and are presented in Table 1. The scatter in results was captured by varying w_1, w_2 and α_1 within the given intervals. It should be noted that the $\sigma(w)$ function is not a constitutive law and several solutions, i.e. different shapes of the $\sigma(w)$ could be used to match the experimental results. A comparison of simulated result (solid) and experimental results (dashed) from [28] are plotted in Figure 4b).

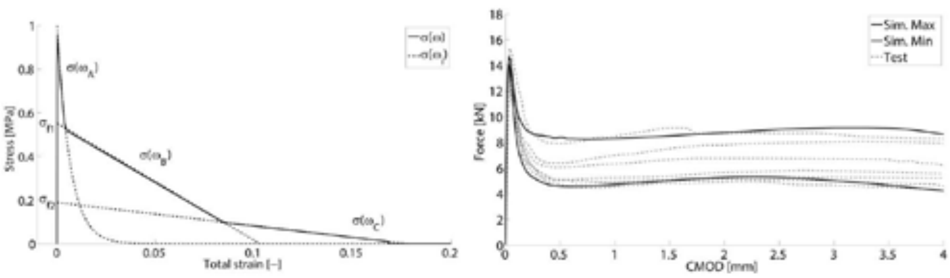

Figure 4 Schematic relation between stress-strain for the individual (dashed) and resulting (solid) $\sigma(\omega)$function in left figure and comparison between numerical (solid) and experimental (dashed) results from [28] in right figure.

Table 1 Material parameters used for damage model

σ_t [MPa]	G_f [J/m²]	w_1 [mm]	w_2 [mm]	w_3 [mm]	α_1 [-]	α_2 [-]
3.2	100	0.045-0.065	1.75-2.5	5.0	0.18-0.3	0.01

BOND FAILURE

Bond failure is important for the performance for various structures and categorizes as Mode-I (tensile/opening), Mode-II (sliding/shear) or Mixed-Mode. Krounis et al. [34] studied Mode-II failure in the interface between rock and concrete subjected to a compressive stress and shear displacement. Results indicate that this failure mode can be modelled with an elasto-perfectly plastic model, see Figure 5a). Tensile failure, i.e. Mode-I cracks, are the predominated cause of failure in concrete structure. These cracks normally propagate along the interface between cement paste and aggregate. Studies of bond strength and softening behaviour between cement paste and different rock types have therefore been focused on Mode-I failure, see e.g. Tschegg et al. [35, 36], Alexander et al. [37], Dong et al. [38, 39]. In Figure 5b), Force-CMOD (crack mount opening displacement) curves for Mode-I failure from Dong et al. [38] are shown. The force is normalized against the maximum force for each test and the results indicate that the interface is stiff and that failure is quasi-brittle. Dong et al. [38] suggest that Mode-I failure can be modelled with a bi-linear or exponential function.

Two common methods to model contact between structural components are the augmented Lagrange method and the penalty method. In both models, contact between two surfaces is modelled using a stiff spring that resolves the contact stresses [40]. The primary difference between the two models is that the penalty method changes the stiffness of the involved degrees of freedom (DOF) while the augmented Lagrange method adds DOF to solve the contact problem [41].

Numerical model for bond failure

An isotropic damage parameter ω_{b} and a cohesive crack model $\sigma(u)$ were used in this paper to describe the non-linear behaviour of the interface. These are the same principles as was used for FRSC and was used for the same reasons. Contact was modelled with the penalty method and zero thickness elements were used at the interface as presented by Camnaho et. al [42]. In this model, stresses at the interface are evaluated according to Eq. (12)

$$\sigma_{\mathrm{i}} = K_{\mathrm{i}} u_{\mathrm{i}} (1 - \omega_{\mathrm{b}}) \tag{12}$$

Where, K_{i} is the stiffness of the spring added to each element in contact and u_{i} is the displacement (gap-distance) of the interface. As can be seen in Eq. (12), displacement of the spring, i.e. interface, must occur for stresses to develop. A small penetration of the surface is required for compressive stresses to develop. The compressive stiffness, K_{Ic} has no physical meaning but prohibits penetration and thereby decreases the physical error with an increased stiffness. The stiffness could be a cause for numerical problems [41] and the initial stiffness should at least be equal to:

$$K_{\mathrm{Ic}} = \frac{E_{\min}}{h_{\min}} \tag{13}$$

Here, $E_{\min}$ and $h_{\min}$ is the minimum Young's modulus respectively element length of the two materials at the interface. Thus, the minimum stiffness of the interface is equal to the minimum axial stiffness of the elements in contact. To evaluate tensile stresses, the penalty stiffness K_{It} is

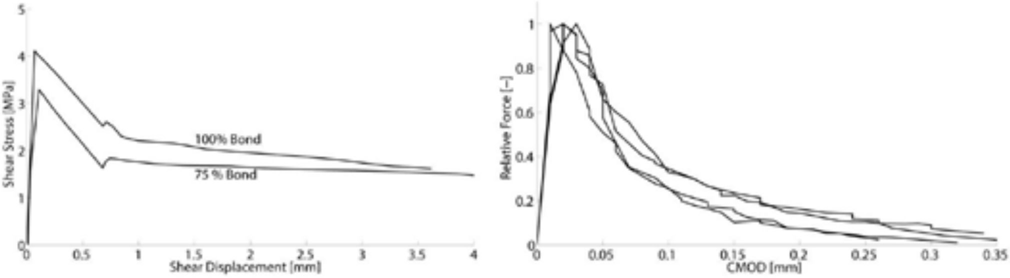

Figure 5 Test of bond failure where left figure shows Mode-II failure with interaction of compressive stress and variation in bond area from [34] and right figure shows normalized curves for Mode-I failure from [38].

calculated according to Eq. (12) with the displacement at failure initiation u_{I0} and the tensile bond strength σ_{It} known from experiments. The relation between σ_{I} and u_{I} is linear up until σ_{It} is reached. Thereafter, an exponential $\sigma_{\mathrm{I}}(u_{\mathrm{I}})$ function according to Eq. (14) was used.

$$\sigma_{\mathrm{I}}(u_{\mathrm{I}}) = \sigma_{\mathrm{It}}\exp(-\frac{u_{\mathrm{I}} - u_{\mathrm{I0}}}{u_{\mathrm{If}}}) \tag{14}$$

Here, u_{I0} is the displacement at initiation of failure and u_{If} controls the slope of the softening curve. The damage function in Mode-I was derived by setting Eq. (12) and Eq. (14) equal to each other.

$$\omega_{\mathrm{b}}(u_{\mathrm{I}}) = 1 - \frac{u_{\mathrm{I0}}}{u_{\mathrm{I}}}\exp\left(-\frac{u_{\mathrm{I}} - u_{\mathrm{I0}}}{u_{\mathrm{If}}}\right) \tag{15}$$

The displacement u_{If} is calculated based on fracture energy as:

$$u_{\mathrm{If}} = \frac{u_{I0}}{2} + \frac{G_{\mathrm{If}}}{\sigma_{\mathrm{I}}} \tag{16}$$

The used bond model is valid for Mode-I failure. The reason for this choice is that failure is expected to be governed by Mode-I. Furthermore, accurate test data to for Mode-II, i.e. σ_{II}, $\sigma_{\mathrm{II}}(u_{\mathrm{II}})$, G_{IIf} and K_{II}, as well as Mixed-Mode failure with a relevant combination of tensile and shear stresses at the interface are difficult to find. However, the model can be extended to account for Mode-II and Mixed-Mode failure by, the Mixed-Mode displacements u_{m} as proposed by Camanho et al. [42]:

$$u_{\mathrm{m}} = \sqrt{u_{\mathrm{I}}^2 + u_{\mathrm{II}}^2} \tag{17}$$

The corresponding Mixed-Mode failure criterion can be based on a power law of the ratio between released fracture energy G_{i} and total fracture energy G_{if} [42] as:

$$\left(\frac{G_{\mathrm{I}}}{G_{\mathrm{If}}}\right)^{\eta} + \left(\frac{G_{\mathrm{II}}}{G_{\mathrm{IIf}}}\right)^{\eta} = 1 \tag{18}$$

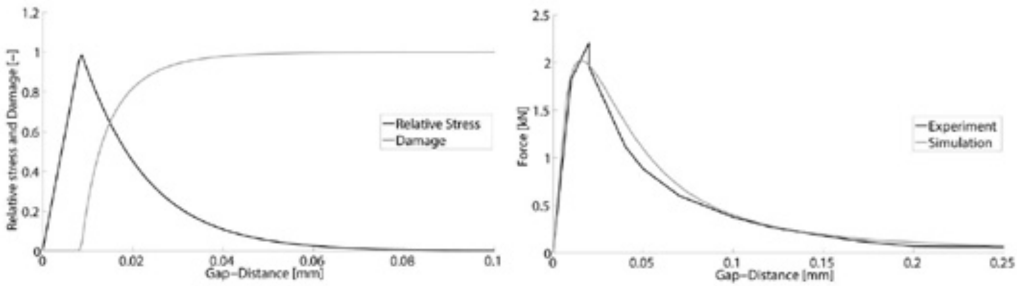

Figure 6 Left figure shows relation between relative stress and evolution of damage as a function of gap distance between interfaces and right figures shows comparison between experimental [39] and numerical results with the presented model.

Verification of numerical model for bond failure

Dong et al. [39] performed 3-point bending test with a composite beam with dimensions 500*100*100 mm^3 to evaluate tensile strength and fracture energy of the interface between concrete and rock. Half of the beam was a rock block and the other half concrete. After hardening, a notch was cut in the center of the interface. For the simulation, a 2D model was created with a free triangular mesh. The ratio between mesh sizes at the interface was one and the mesh size was 30 mm and the material data is presented in Table 2. In Figure 6a), the relation between stress and Mode-I opening is presented for the numerical model. Stresses were normalized against the failure stress. In Figure 6b), simulated results are compared with experimental results from [39].

Table 2 Material data for mode-I bond failure

K_{It} [GPa/m]	σ_{If} [MPa]	G_{I} [J/m^2]
250	1.9	20

INTERACTION BETWEEN SHOTCRETE AND ROCK BOLTS

Rock bolts are used to secure single rock blocks and to ensure a structural connection between the shotcrete and the rock. Three types of conventional rock bolts exists, fully-grouted rebar bolts, frictional bolts and expansion bolts [43]. Rock bolts can either be pre-tensioned or passive un-tensioned. Two kinds of movement occur in a rock joints; opening in the normal direction (perpendicular to the joint plane) and shear displacement in the plane. Rock bolts are used to decrease the deformation of the joint and are therefore subjected to both normal and shear forces. When rock bolts are installed, grout is used to fill the void between bolt and rock to ensure a structural connection. The behavior of the bolts is therefore governed by a complex interaction of contact pressure between shotcrete and washer as well as bond/friction between the material interfaces between bolt, grout and rock. For rock bolts loaded in the normal (axial) direction, three main failure modes exist; cone failure, tensile failure in the steel or bond failure in one of the three interfaces (concrete-bolt, grout-bolt and grout-rock). According to Guan et al. [44], the most common failure mode during pull-out tests is failure at the bolt–grout interface. For passive rock bolts loaded in the shear plane, a pure failure mechanism is not present. Such bolts will bend and deform in an S-shape [45]. The normal and bending forces as well as the failure of the bolt depends on the interaction between steel, rock and grout. The contribution of the bolt to the shear capacity of a joint exceeds the pure shear capacity of the steel material [REF??] due to an added frictional force at the joint interface.

Two basic approaches are used when analyzing rock bolt by numerical methods; explicit [46, 47, 48], and implicit [49, 50, 51] methods. In the explicit method, the rock bolt is modeled as an own part while in the implicit method, the contributions from rock bolts are smeared over the rock mass and added to the constitutive laws of the rock or joint. In general, the implicit method is used for more complicated engineering problems where it is unpractical or unmanageable to model each rock-bolt. In contrary, the explicit method allows a more detailed study of the rock bolts behavior. As the position of the rock bolts affects the structural behavior of a bolted FRSC lining, the implicit method is inappropriate for a detailed analysis. In explicit models [52], either a detailed analysis of the bar, rock and grout or a simplified approach is used. For the detailed analysis, nonlinear material behavior and interactions between interfaces are modelled. These types of analysis are therefore computational heavy and are in most cases limited to the simulation of a single bolt. In the simplified approach, the bolt is modeled with a truss or beam element and the attachment is modeled with springs. The choice between truss or beam depends on if the bolt is assumed to contribute only by axial forces or with axial forces and bending. Two types of spring models are used for the attachment; non-linear spring adopted in structural engineering characterized by a non-linear force-displacement relationship [32] or the spring-slider approach adopted in rock mechanics [44], where the spring determines the stiffness and the slider the failure load.

Numerical model for rock bolts

As the focus of this paper is on simulating the behavior of shotcrete, a priority for the selection of rock bolt model was to reduce the computational effort for the rock bolt part. An explicit model was therefore used where the bolt is represented with a beam element and the attachment to the rock with springs. For the axial behavior, the principle of bond stress-slip relationship from fib Model Code [32] was used. Here, the anchorage of rebars in concrete are modeled with a bond stress-slip $\tau(s)$ relationship consisting of four parts according to Eqs. (19-22) where τ is the bond stress and s the slip displacement. The input for the model is the maximal bond stress τ_{m}, the residual bond stress τ_{r}, the tree slip displacements $s_1 - s_3$ and the parameter α which determines the shape of the initial part of the curve.

$$\tau(s) = \tau_m \left(\frac{s}{s_1}\right)^{\alpha} \text{ for } s \leq s_1 \tag{19}$$

$$\tau(s) = \tau_{\mathrm{m}} \text{ for } s_1 < s \leq s_2 \tag{20}$$

$$\tau(s) = \tau_{\mathrm{m}} - (\tau_{\mathrm{m}} - \tau_{\mathrm{r}}) \left(\frac{s - s_2}{s_3 - s_2}\right) \text{for } s_2 < s \leq s_3 \tag{21}$$

$$\tau(s) = \tau_{\mathrm{r}} \text{ for } s_3 < s \tag{22}$$

The recommended values for a pull-out failure in well-confined concrete are presented in Table 3. The maximal bond stress is assumed to be related to the concretes compressive strength and the quality of the bond. This stress-slip relation can be implemented in a FE-model as non-linear springs with a force-slip relationship. The relationship for each axial spring is obtained by multiplying the stress with the element length h and the circumference of the bolt πd according to:

$$F(s) = \tau(s)\pi d h \tag{23}$$

Verification of numerical model for rock bolts

Chen [53] performed pull, shear and mixed mode displacement tests on bolt specimens. From their test series, the pull test (90° displacement angle) with conventional reinforcement was used for comparing the model. In this test, two concrete blocks of high strength concrete (compressive strength 110 MPa) with the dimensions 950*950*950 mm^3 were used to represent the rock. A 33 mm

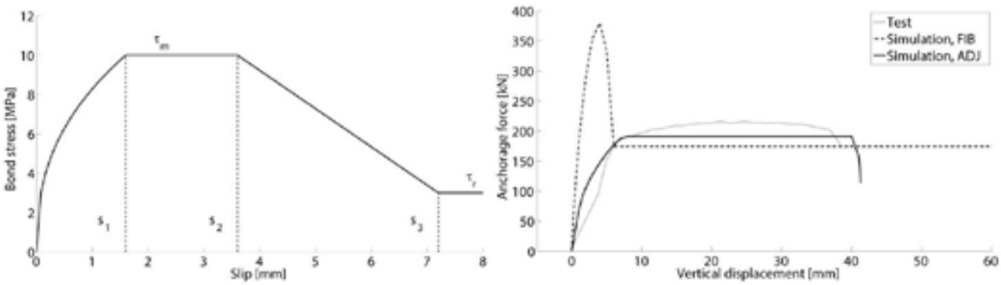

Figure 7 Left figures shows schematically the relation between bond stress and slip for the numerical model and right figure shows comparison between experimental results [53] and numerical simulations for the fib model (dotted) and adjusted model (solid)

diameter hole was drilled through the blocks. Thereafter a bolt with the diameter 20 mm was placed in the hole and filled with grout with a compressive strength of 60 MPa. The bolt was loaded until failure in the axial direction by displacing one of the block while keeping the other in a fixed position. The experiment was simulated in 3D using beam elements for the bolt and solid elements for the rock with an average element size of 0.1 m. The bolt was attached to the moving concrete block by tying the translational degrees of freedoms to the concrete. For the fixed part, one spring in each direction was used to simulate the connection. In the axial direction, a non-linear spring was used with the described force-slip relationship. In the two shear directions, linear spring was used to represent the elastic behavior of the grout under small shearing displacements. A comparison between simulated results and experimental results from [53] is plotted in Figure 7. When using values recommended by fib [32], the stiffness as well as the strength of the attachment is overestimated. Instead, the input to the model was adjusted to achieve a better agreement with the experiment. The adjusted values presented in Table 3 gives a smaller maximal load and greater displacements compared to the fib model.

Table 3 Bond stress–slip relationship

Model	τ_{max} [MPa]	α [-]	s_1 [mm]	s_2 [mm]	s_3 [mm]
Fib	$1.25\sqrt{\frac{f_{cm}}{MPa}}$	0.4	1.6	3.6	c
Adj	3	0.4	6.0	35	36

This shows that the anchorage for a grouted rock bolt is weaker and softer than the anchorage of a bolt embedded in concrete. There are several possible explanations for this. Rock bolts are installed in drilled holes and grout is then used to fill the void between the bolt and rock. The bolt can therefore slip along two interfaces, between bolt and grout or between grout and rock. A bolt embedded in concrete, such as the one used for the calibration of the fib model, can only slide along one interface. The reason to why the interface between the bolt and concrete is stiffer could be that a more uniform bond is achieved along the interface when the bolts are placed before casting of the concrete. Another reason could be that mechanical interlocking between the ribbons of the bolt and the concrete increases the stiffness.

CONCLUSIONS

In this paper, the three important failure mechanisms of a bolted FRSC lining were identified through analysis of experimental results. The results from Holmgren [12, 13] and Fernandez-Delgado [14] showed that tensile bond failure is the primary failure mechanism for a lining when the thickness of the concrete is between 50 to 130 mm. For all tested cases, the peak load was determined by the primary failure mechanism and the bond between sprayed concrete and rock is therefore the decisive parameter for the structural capacity of a lining. When rock bolts in combination with steel plates are used, bond failure will be arrested at the location of the steel plates [12]. The ultimate failure mechanism is in such case flexural cracking of the concrete, i.e. a Mode-I crack. Both tensile bond failure and tensile cracking of the FRSC must therefore be included in a numerical model of bolted lining. To capture to complete failure behaviour of a bolted lining, the interaction between the rock bolts and steel plates with the sprayed concrete must be included since the steel plates will arrest the bond failure.

A short review of different numerical models for each of the individual failure mechanisms was then presented. Each one has been studied thoroughly by other researchers and many different techniques to model each failure mechanism exist. The models can be divided into two different types; simple or detailed. The simple type aims at describing the structural response caused by the failure mechanism. For FRSC, such models are presented by e.g. Yoo et al. [22] and Sjölander [8] and are able to describe the structural response such as the peak load and the softening caused by cracking in the concrete. These models are unable to predict the true failure mechanism, i.e. if failure is caused by sliding or rupture of the fibres. To capture such effects, detailed models such at the one presented by Soetens and Matthys [25] must be used. Their model is based on the constitutive laws for a single fibre and individual fibres are modeled explicit. The tradeoff for such a model is of course that it is more computational heavy compared to the more simple models. The focus in this paper was to present a numerical model that can be used to simulate failure and predict the structural capacity of a bolted FRSC lining. Therefore, the numerical model for each of the failure mechanism were chosen based on that it should be computational efficient and easy to implement in a FE software. All of the selected models are of the simple kind and showed good agreement with experimental results.

The numerical model presented in this paper is able to describe each of the failure mechanisms of a bolted FRSC lining. The next step in this research project is to combine the numerical models for the individual failure mechanisms to simulate failure of a lining. The complete model will be validated against experimental results and used to study how the structural capacity of the lining is affected by important in-situ factors such as varying thickness of the concrete and an irregular rock surface.

ACKNOWLEDGEMENT

The financial support for this research project has been given by BeFo, Rock Engineering Research Foundation and their support is greatly appreciated.

Bibliography

[1] A. Palmström and H. Stille, Rock engineering, London: Thomas Telford Limited, 2010.

[2] S. Austin and P. Robins, Sprayed Concrete: Properties, Design and Application, Whittles Publishing, 1995.

[3] A. Thomas, Sprayed Concrete Lined Tunnels, Oxford, London: Taylor & Francis, 2009.

[4] N. Barton, R. Lien and J. Lund, "Engineering classification of rock masses for the design of tunnel support," *Rock Mechanics,* no. 6, pp. 189-236, 1974.

[5] Trafikverket, Krav Tunnelbyggande, Borlänge: Trafikverket, 2016.

[6] S. V. L. Barrett and D. R. McCreath, "Shotcrete support design in blocky ground: Towards a deterministic approach," *Tunnels and Deep Space,* vol. 10, no. 1, pp. 79-89, 1995.

[7] U. Lindfors, R. Swindell, L. Rosengren, M. Holmberg and J. Sjöberg, "Projektering av bergkonstruktioner," Trafikverket, Stockholm, 2015.

[8] A. Sjölander, "Analyses of shotcrete stress states due to varying thickness and irregular rock surfaces," KTH Royal Institute of Technology, Stockholm, 2017.

[9] A. Sjölander, W. Bjureland and A. Ansell, "On failure probability in thin shotcrete shells," in *World Tunnel Congress 2017*, Bergen, 2017.

[10] U. Nilsson, Structural behaviour of fibre reinforced sprayed concrete anchored in rock, Stockholm: KTH Royal Institute of Technology, 2003.

[11] L. Malmgren and E. Nordlund, "Interaction of shotcrete with rock and rock bolts - A numerical study," *International Journal of Rock Mechanics & Mining Sciences,* vol. 45, no. 4, pp. 538-553, 2008.

[12] J. Holmgren, Punch-loaded shotcrete linings on hard rock, Stockholm: Swedish Rock Mechanics Research Foundation -BeFo, 1979.

[13] J. Holmgren, "Bolt-Anchored, Steel-Fibre-Reinforced Shotcrete Linings," *Tunneling and Underground Space Technology,* vol. 2, no. 3, pp. 319-333, 1987.

[14] G. Fernandez-Delgado, J. Mahar and E. Cording, "Shotcrete: Structural Testing of Thin Liners," University of Illinois, Urbana, USA, 1975.

[15] C. Banton, M. S. Diederichs, D. J. Hutchinson and S. Espley, Mechanisms of shotcrete roof support, London, England: Taylor & Francis Group, 2004.

[16] T. Franzén, "Shotcrete for underground support: a state-of-the-art report with focus on steel-fibre reinforcement," *Tunneling and Underground Space Technology,* vol. 7, no. 4, pp. 383-391, 1992.

[17] J. Holmgren, "Shotcrete research and practice in Sweden - development over 35 years," in *Shotcrete: Elements of a system*, Queenstown, New Zealand, 2010.

[18] N. Banthia, M. Azzabi and M. Pigeon, "Restrained shrinkage cracking in fibre-reinforced cementitious composites," *Materials and Structures,* vol. 26, pp. 405-413, 1993.

[19] J. A. O. Barros and J. Sena Cruz, "Fracture energy of steel fibre-reinforced concrete," *Mechanics of Composite Materials and Structures,* vol. 8, pp. 29-45, 2001.

[20] J. A. O. Barros, V. M. C. F. Cunha, A. F. Riberio and J. A. B. Antunes, "Post-cracking behaviour of steel fibre reinforced concrete," *Materials and Structures,* vol. 38, pp. 47-56, 2005.

[21] N. Banthia and J. Sheng, "Fracture toughness of micro-fiber reinforced cement composites," *Cement & Concrete Composites,* vol. 18, pp. 251-269, 1996.

[22] D.-Y. Yoo, Y.-S. Yoon and N. Banthia, "Predicting the post-cracking behaviour of normal- and high-strength steel-fibre-reinforced concrete beams," *Construction and Building Materials,* pp. 477-485, 2015.

[23] N. Banthia, "Steel fibre-reinforced concrete at sub-zero temperatures: from micromechanics to macromechanics," *Journal of Materials Science Letters,* vol. 11, pp. 1219-1222, 1992.

[24] T. Soetens, A. Van Gysel, S. Matthys and L. Taerwe, "A semi-analytical model to predict the pull-out behaviour of inclined hooked-end steel fibres," *Construction and Building Materials,* vol. 43, pp. 253-265, 2013.

[25] T. Soetens and S. Matthys, "Different methods to model the post-cracking behaviour of hooked-end steel fibre reinforced concrete," *Construction and Building Materials,* vol. 73, pp. 458-471, 2014.

[26] B. Luccioni, G. Ruano, F. Isla, R. Zerbino and G. Giaccio, "A simple approach to model SFRC," *Construction and Building Materials,* vol. 37, pp. 111-124, 2012.

[27] T. Gasch, Concrete as a multi-physical material with applications to hydro power facilities, Stockholm, Sweden: KTH Royal Institute of Technology, 2016.

[28] N. Buratti, C. Mazzotti and M. Savoia, "Post-cracking behaviour of steel and macro-synthetic fibre-reinforced concretes," *Construction and Building Materials,* vol. 25, no. 5, pp. 2713-2722, 2011.

[29] J. Oliver, M. Cervera, S. Oller and J. Lubliner, "Isotropic damage models and smeared crack analysis of concrete," in *Computer Adided Analysis and Design of Concrete Strucutres*, Zell am See, Austria, 1990.

[30] L. Kachanov, "Time of rupture process under creep conditions," *Izvestilia Akademii Nauk SSSR,* vol. 8, pp. 26-31, 1958.

[31] A. Hillerborg, M. Modéer and P. Petersson, "Analysis of crack formation and crack growth in concrete by means of fracture mechanics and finite elements," *Cement and Concrete Research,* vol. 6, no. 6, pp. 773-781, 1976.

[32] Fib, Model Code for concrete structures 2010, Lausanne: Wilhelm Ernst & Son, 2013.

[33] R. Schütz, D. Potts and L. Zdravkovic, "Advanced constitutive modelling of shotcrete: Model formulation and calibration," *Computers and Geotechnics,* vol. 38, no. 6, pp. 834-845, 2011.

[34] A. Krounis, F. Johansson and S. Larsson, "Shear Strength of Partially Bonded Concrete–Rock Interfaces for Application in Dam Stability Analyses," *Rock Mechanics and Rock Engineering,* vol. 49, no. 7, p. 2711–2722 , 2016.

[35] E. Tschegg, H. M. Rotter, P. E. Roelfstra, U. Bourgund and P. Jussel, "Fracture Mechanical Behavior of Aggregate–Cement Matrix Interfaces," *Journal of Materials in Civil Engineering,* vol. 7, no. 4, pp. 199-203, 1995.

[36] E. K. Tschegg and S. E. Stanzl, "Adhesive power measurements of bonds between old and new concrete," *Journal of Materials Science,* vol. 26, no. 19, pp. 5189-5194, 1991.

[37] M. G. Alexander, S. Mindess, S. Diamond and L. Qu, "Properties of paste-rock interfaces and their influence on composite behaviour," *Materials and Structures,* vol. 28, no. 9, pp. 497-506, 1995.

[38] W. Dong, Z. Wu and X. Zhou, "Fracture Mechanisms of Rock-Concrete Interface : Experimental and Numerical," *Journal of Engineering Mechanics,* vol. 142, no. 7, pp. 1-11, 2016.

[39] W. Dong, D. Yang, X. Zhou, G. Kastiukas and B. Zhang, "Experimental and numerical investigations on fracture process zone of rock-concrete interface," *Fatigue and Fracture of Engineering Materials and Structures,* vol. 40, no. 5, pp. 820-835, 2017.

[40] Comsol, *Comsol Multiphysics version 5.2a,* Stockholm, Sweden: Comsol AB, 2016.

[41] R. D. Cook, D. S. Malkus, M. E. Plesha and R. J. Witt, Concepts and applications of finite element analysis, Madison, USA: John Wiley & Sons, 2002.

[42] P. Camanho, C. Davila and M. F. de Moura, "Mixed-Mode Decohesion Finite Elements in for the Simulation Composite of Delamination Materials," *Journal of Composite Materials,* vol. 37, no. 16, pp. 1415-1438, 2003.

[43] C. Li, G. Stjern and A. Myrvang, "A review on the performence of conventional and energy-absorbing rockbolts," *Journal of Rock Mechanics and Geotechnical Engineering,* vol. 6, no. 4, pp. 315-327, 2014.

[44] Z. Guan, Y. Jiang, Y. Tanabasi and H. Huang, "Reinforcement mechanics of passive bolts in conventional tunnelling," *International Journal of Rock Mechanics and Mining Science,* vol. 44, no. 4, pp. 625-636, 2007.

[45] G. Grasselli, "3D behaviour of bolted rock joints: experimental and numerical study," *International Journal of Rock Mechanics and Mining Science,* vol. 42, no. 1, pp. 13-24, 2005.

[46] S.-H. Chen, S. Qiang, S.-F. Chen and P. Egger, "Composite element model of the fully grouted rock bolt," *Rock Mechanics and Rock Engineering,* vol. 37, no. 3, pp. 193-212, 2004.

[47] H. Jalalifar and N. Aziz, "Experimental and 3D numerical simulation of reinforced shear joints," *Rock Mechanics and Rock Engineergin,* vol. 43, no. 1, pp. 95-103, 2010.

[48] K. Spang and P. Egger, "Action of fully-grouted bolts in jointed rock and factors of influence," *Rock Mechanics and Rock Engineergin,* vol. 23, pp. 201-229, 1990.

[49] S.-H. Chen, Z.-M. Yang, W.-M. Wang and I. Shahrour, "Study on rock bolt reinforcement for a gravity dam foundation," *Rock Mechanics and Rock Engineering,* vol. 45, no. 1, pp. 75-87, 2012.

[50] S.-H. Chen and P. Egger, "Three dimensional elasto-viscoplastic finite element analysis of reinforced rock masses and its application," *International Journal of Analytical and Numerical Methods for Geomechanics,* vol. 23, no. 1, pp. 61-78, 1999.

[51] H. Stille, M. Holmberg and G. Nord, "Support of weak rock with grouted bolts and shotcrete," *International Journal of Rock Mechanics and Mining Science,* vol. 26, no. 1, pp. 99-113, 1989.

[52] N. Bahrani and J. Hadjigeorgiou, "Explicit reinforcement models for fully-grouted rebar rock bolts," *Journal of Rock Mechanics and Geotechnical Engineering,* vol. 9, no. 2, pp. 267-280, 2017.

[53] Y. Chen, "Experimental study and stress analysis of rock bolt anchorage performance.," *Journal of Rock Mechanics and Geotechnical Engineering,* vol. 6, no. 5, pp. 428-437, 2014.

[54] K. G. Holter, "Loads on sprayed waterproof tunnel linnings in jointed hard rock: A study based on Norwegian cases," *Rock Mechanics and Rock Engineering,* vol. 47, pp. 1003-1020, 2014.

[55] E. Hoek and E. T. Brown, Underground excavation in rock, London, England: The institution of Mining and Metallurgy, 1980.

[56] L. E. Bryne, A. Ansell and J. Holmgren, "Laboratory testing of early age bond strength of shotcrete on hard rock," *Tunnelling and Underground Space Technology,* vol. 41, no. 1, pp. 113-119, 2014.

[57] V. Andjelkovic, N. Pavlovic, Z. Lazarevic and V. Nedovic, "Modelling of shear characteristics at the concrete-rock mass interface," *International Journal of Rock Mechanics and Mining Sciences,* vol. 76, pp. 222-236, 2015.

[58] V. Slowik, J. M. C. Kishen and V. E. Saouma, "Mixed mode fracture of cementitious bimaterial interfaces; Part I: Experimental results," *Engineering Fracture Mechanics,* vol. 60, no. 1, pp. 83-94, 1998.

[59] J. Červenka, J. C. Kishen and V. E. Saouma, "Mixed mode fracture of cementitious bimaterial interfaces:; Part II: numerical simulation," *Engineering Fracture Mechanics,* vol. 60, no. 1, pp. 95-107, 1998.

THE DESIGN PHILOSOPHY FOR PERMANENT SPRAYED CONCRETE LININGS

Alun Thomas & Ross Dimmock
Minova, Denmark & Normet, UK
alun.thomas4@minovaglobal.com & Ross.Dimmock@Normet.com

Summary

Permanent sprayed concrete linings (PSCL) have existed in various forms for decades but the technology has recently taken significant strides forwards with adoption on several major projects in the UK, most notably, Crossrail. This paper will review the key elements of the design philosophies that underpin current applications of PSCL in soft ground conditions. Achieving this transition required the combination of a set of interrelated technological advances, such as the use of laser survey to control profile for excavation and spraying, omission of lattice girders and mesh, fibre reinforcement, permanent sprayed concrete and spray applied waterproofing membranes. By reviewing the design assumptions and methods, it is possible to map out the path for future significant improvements in PSCL.

1. INTRODUCTION

Despite a long history of using permanent sprayed concrete linings (PSCL) in tunnels, especially in rock tunnels, this technique is still relatively rarely applied in soft ground. Adoption of PSCL is also very variable geographically with the concept largely embraced in some countries and flatly rejected in others. Even on pioneering projects, there has been concern that PSCL in its current form does not offer the most economic option. There is clearly scope for more innovation and improvement before the full benefits have yet to be realised [1].

This paper reviews the development of design concepts for permanent sprayed concrete linings (PSCL) and proposes a new design concept for fully Composite Shell Linings which could represent a very cost-effective and more sustainable option. This paper is based on an earlier one by the authors [2].

2. DEVELOPMENT OF PERMANENT SPRAYED CONCRETE LININGS

The early development of NATM / SCL tunnelling in the form of the double shell approach of temporary primary linings and cast insitu permanent secondary linings has been described by others (e.g. [3] and [4]). It has been recognized for a long time that, as the quality of sprayed concrete has improved, the traditional double shell lining is potentially overly conservative and wasteful. It has been noted that measurements for real tunnels have shown that the secondary linings are often not carrying the loads that would be expected, based on the assumption that the primary lining has disintegrated [5]. At the same time, the good durability of sprayed concrete has been demonstrated on many projects [4].

A range of options now exist (some in practice and some still only on the drawing board) for SCL tunnels in soft ground, stretching from Double Shell Linings (DSL) to Single Shell Linings (SSL) – see Fig.1 [6]). While permanent SSL was used successfully at Heathrow Terminal 5 [7], its success relied on the generally impermeable nature of the London Clay and the fact that these were non-public tunnels. The “Holy Grail” remains the creation of a permanent SSL with a waterproofing layer on the extrados, since a truly impermeable sprayed concrete lining is not possible because of all the joints and potential imperfections. This has been explored but as yet a viable version has not been implemented [6].

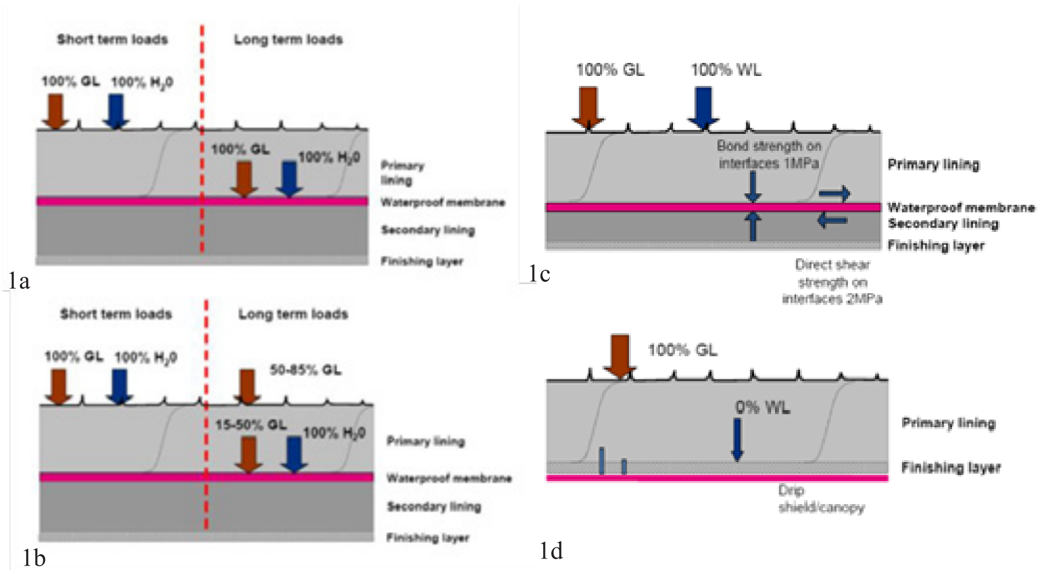

Fig.1 SCL design options current considered in the tunnelling industry
1a: Typical Double Shell lining (DSL) 1b: Typical Composite Shell Lining – (CSL with partial composite with no shear or adhesive bond). 1c: Fully Composite Shell Lining (CSL) 1d: Typical Single Shell Lining (SSL)   GL = ground load; WL or H20 = water load

A significant leap forward was made on the Crossrail project by harnessing a series of technological and conceptual advances into a coherent design concept for PSCL for both public and non-public tunnels [1].

Fig.2 shows the components of this design. The design can be characterized as a “partially composite shell” lining since, at that time, the designers felt that there was insufficient test data and project experience on the performance of the bond to the membrane to adopt a “fully composite shell” design approach [6]. While this design was adopted by all of the contractors on Crossrail (without major changes during the Value Engineering period) and it was successfully built, the design has been criticized as overly conservative and even a retrograde step because of the large thicknesses of expensive fibre reinforced sprayed concrete [8]. While the overall thickness may not have been reduced, it should be remembered that the new design reduced the steel reinforcement dramatically and reduced overall construction time. With the benefit of hindsight, some have questioned whether or not cast insitu secondary linings with sheet membranes would have been better [9]. As will be explained later, two key design decisions - namely, the assumptions of zero bond at the membrane and that the water pressure acts on the outer face of the membrane - lie behind the limitations of this design concept and solutions are proposed to overcome them and increase the potential for a better design approach.

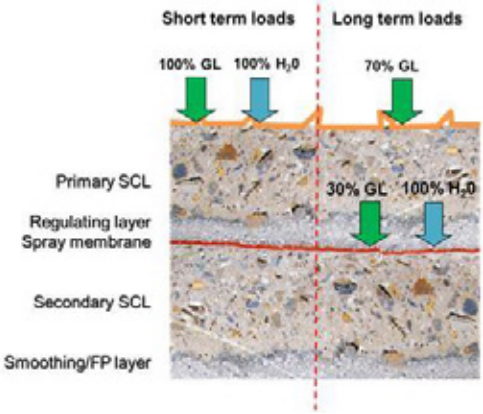

Fig.2 Fibre reinforced PSCL for Crossrail with design load assumptions

3. COMPOSITE LININGS

The Composite Shell Lining (CSL) approach is only relevant to cases where there is an increase in loads over time or where there is an integral waterproofing layer is needed. Otherwise there would be no reason to increase the primary lining. Much of the discussion of CSL has centred on the application in London Clay where the heavily over-consolidated clay initially exhibits undrained behaviour and then drained behaviour in the longer term. This results in an increase in water loads and to a lesser extent ground loads too. However, these sorts of ground conditions are not just seen in London. Furthermore, it is not uncommon for loads on a lining to increase with time in other ground conditions. This could be due to an increase in water pressure, following the re-establishment of the initial pore pressures which were lowered during construction. Also this could arise from creep or swelling, albeit this is rarer. Some load could also be transferred to the secondary lining by other means such as creep in the primary lining. However, these loads are probably very small (e.g. [5] and mitigated by other effects such as creep and shrinkage in the secondary lining.

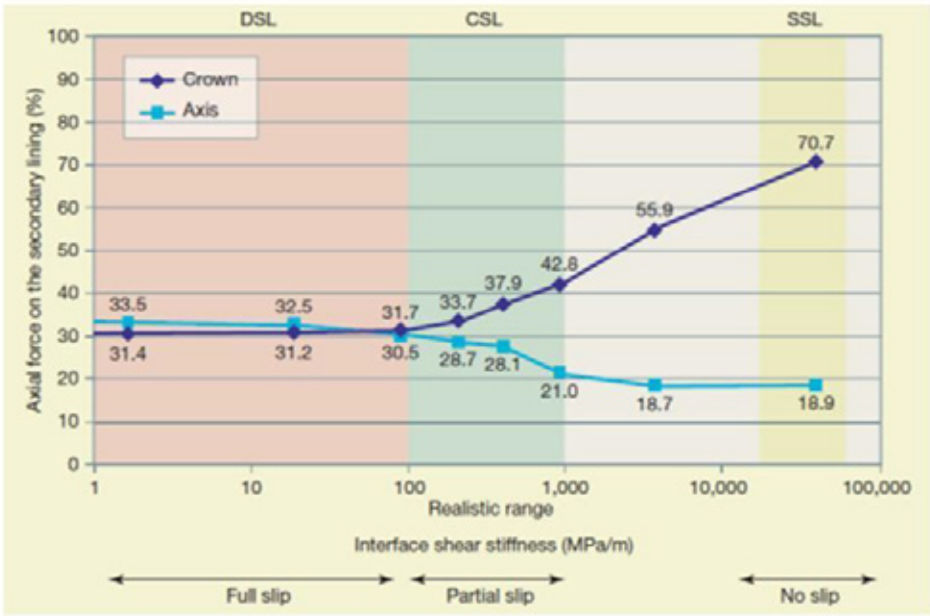

Fig.3 The hoop load in a secondary lining vs the shear stiffness of the interface with the primary lining [10]

Several studies have been made into the structural behaviour of composite linings - either made up of multiple layers of concrete or including a spray applied waterproofing membrane (e.g. [6], [11] and [12]). Considering the likely range of shear stiffnesses for typical membranes, they have concluded that a CSL would function as a partially bonded structure – see Fig.3.

It has been suggested that the assumption of zero bond (and water pressure applied to the secondary lining) is not necessarily conservative [12]. This is because the two rings of concrete tend to move in concert and so both end up with significant bending moments in them while the axial force is shared. At these levels of loading, the linings have less bending capacity at lower axial forces. Hence, there is an increased risk of overstressing in bending, albeit, if one models the resultant cracking, the overstressing would be redistributed. These studies imply that simply making a decision to include a structurally effective bond at the membrane will not lead immediately to a major reduction in the overall lining thickness. It has been suggested that this might be a 50 mm reduction from a total thickness of 700 mm (i.e. 7%) [6]. This small benefit may be offset by the increased costs of this more demanding method; a comment that has also been made in relation to the choice between DSL and CSL.

Recent studies have examined the effect of varying the thickness of the secondary lining [11]. Naturally, increasing the overall lining thickness leads to a stiffer lining which attracts more load. However, for the typical range of shear stiffnesses of membranes, the increase in the lining stiffness is modest [13]. Others found that thinner secondary linings were not overloaded in their test case (except in the invert) whereas thicker secondary linings could experience overloading in bending in the crown [11]. The high bending moments for all secondary linings in the invert appear to be a quirk of the Crossrail design which featured a thickened invert slab.

Looking at this from a different angle, another good reason to minimize the use of a secondary lining is the fact that it can be quite difficult to transfer the load into the secondary lining [6], with the exception of the case of traditional double shell linings with a sheet membrane.

4. DESIGN CONCEPT

This section outlines a new potential design concept for permanent sprayed concrete linings in soft ground with comments on each aspect. The ideal characteristics of the design are listed below and illustrated in **Feil! Fant ikke referansekilden.**. Each one is examined in turn in the following sections and real case compared with the ideal one.

1. No temporary material; all parts of the lining are permanent
2. Water pressure acts at the extrados of the tunnel
3. Non-zero bond at the interface between the waterproofing membrane and concrete
4. As few construction steps as possible
5. No delamination

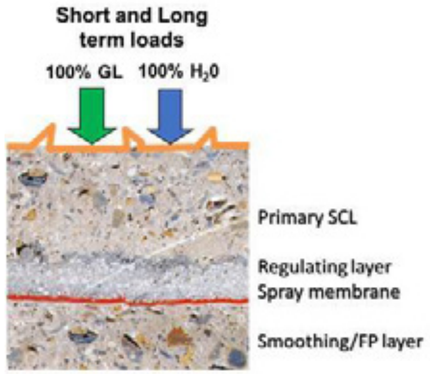

Fig.4 New design concept for PSCL (FP = Fire protection)

4.1 Permanent lining

Of course, the ideal situation involves minimal waste. Permanent sprayed concrete is a proven technology. However, many recent designs have assumed that the very first layer of sprayed concrete – sometimes called a “sealing layer” – is temporary. This is sometimes described as a sacrificial layer on the basis that this layer will help protect the primary lining from aggressive groundwater, in the same way as the cover layer protects steel bars in conventional cast concrete. Another reason for regarding this initial layer as temporary is a concern over the quality of the concrete sprayed onto the ground which may have loose ground bound into it or may be weakened by ground water. However, if there are no steel bars in the lining, there is no need for a cover layer. Groundwater is rarely so aggressive that it might impair the durability of the concrete itself.

It is proposed that 50 mm is ample for a sealing layer in typical soft ground conditions [3] and this should be considered as a non-structural layer in the longterm for the reasons above. Alternatively, Thin Support Liners (TSLs) could also be used as a sealing layer but, for ease of construction, it is often better to use the same concrete mix and equipment set-ups as for the primary lining.

4.2 Water pressure

This is the critical aspect in the design of PSCL tunnels with spray applied waterproofing membranes. In the case of a tunnel in ground conditions like London Clay, where there is no water pressure in the short-term but a significant water pressure acts in the longterm, the choices of where this water pressure acts and its magnitude have a huge impact on the thickness of the secondary lining. For example, if the full water pressure acts on the external face of an unbonded waterproofing membrane, then the secondary lining must carry all of this load. Typically this would lead to a 300 mm thick secondary for a shallow 10m diameter tunnel.

One view is that over the long term the concrete will become saturated and the full pore pressure will act in the primary lining, assuming that there is no leakage through the lining. While the concrete itself can be produced with very low permeability [4], the lining itself is harder to make watertight [14].

Another view is that the primary lining is made with high performance concrete which has a low permeability. While there may be isolated cracks, water is not able to penetrate behind the membrane because it is bonded. Hence the water pressure acts on the extrados of the primary lining.

Several studies ([15] & [16]) have investigated the saturation of the concrete either side of a spray applied membrane. Paraphrasing the conclusions of Holter's extensive research, one could consider the membrane like a Gore-Tex jacket. In other words, the membrane keeps out liquid water but it can "breathe" and permit water vapour to pass through the barrier. The result of this is a reduction in the saturation and presumably the pore pressure too on the external face of the membrane. The water is lost at the intrados of the secondary into the air by evaporation. The volumes transmitted were back-calculated in two cases from measurements of concrete and membrane properties and the degree of saturation with a numerical model [14]. In both cases, these were much lower than the ITA recommended limit for dry storerooms of 0.02 l/m2 per day, although in practice some damp patches were reported [16].

In a similar way, the design of dams have in some cases relied on the benefit of leakage which reduces the pore pressure within the dam. In the context of a single shell permanent sprayed tunnel lining (without a waterproofing membrane), a reduced value of pore pressure of 85% of the external pressure has been proposed to account for this [17]. This is similar in value to the reduction in Degree of Capillary Saturation (DCS) observed at the extrados of the membranes in 3 real tunnels [16]. It is worth noting that while these were all drained tunnels in rock, the lining thicknesses were similar to those in soft ground tunnels (150 to 350 mm) and the DCS was close to 100% at the rock-primary lining interface, which would seem to imply the full water pressure in the ground around the tunnel acted there. Since these were drained tunnels, this water pressure in the ground around is lower than the insitu hydrostatic pressure.

Add a section on wet crack phenomenon?

Tab. 1: Interface strengths in different modes of loading for mature ages (i.e. 28 day or older) from various authors

	Compression	***Tension***	***Shear***	***Reference***
	MN/m2	MN/m2	MN/m2	
Thin membrane - smoothed or regulated surface	30.0	0.7	2.1	[18] – "dry samples" (RH= 60%)
Thin membrane - as sprayed surface	11.0	0.7	2.0	[18]– "dry samples" (RH= 60%)
Thick membrane - smoothed or regulated surface	10.0	0.7	2.0	[18]– "dry samples" (RH= 60%)
Thick membrane - as sprayed surface	8.0	0.7	1.7	[18]– "dry samples" (RH= 60%)
Dry samples (M1)	-	1.1 – 1.6	0.75	[16]
Moist samples (M1)	-	0.3 – 1.15	-	[16]
Thin membrane – as sprayed surface – various TSLs and membranes*	-	0.64 – 0.89	-	[6]
Medium to Strong TSLs	-	0.5 – 4.5	1 - 7	[19]

** TSL = Thin Skin Liner; from a study of spraying membranes onto freshly sprayed concrete*

While one could construct an argument based on this concept and the experimental evidence to support the use of a reduced pore pressure acting on the external face of the membrane, the benefit may be marginal compared to the effort required to gain acceptance.

While this reduction in load is helpful, a much greater benefit can be gained from assuming that the membrane is bonded to the primary. Then, whether the water pressure is assumed to act on the extrados of the primary lining or the water pressure is acting on the external face of the membrane the structural effect is the same. The latter case of the water pressure pushing on the extrados of the membrane is analogous in structural terms to a uniformly distributed load (UDL) pulling a beam (the primary lining) downwards. The structural effect on the beam is the same as irrespective of whether the UDL acts on the top or bottom face of the beam, provided that the beam does not delaminate – i.e. the membrane remains bonded to the primary lining..

Feil! Fant ikke referansekilden.lists typical interface properties. Some results from Thin Support Liners (TSLs) have been included here for comparison since they are similar products, although they are not intended to act as water barriers. Considering a typical metro tunnel at a depth of 30m, one would expect a maximum water pressure of 300 kPa, which can be compared to bond strengths in direct tension of 600 kPa or more. Hence, there is a global factor of safety of about 2 against delamination of the membrane. If there is any secondary lining inside, this will also help to resist the water pressure, increasing the factor of safety further.

In other words, in design calculations, one can effectively consider the water pressure as acting on the extrados of the primary lining. Extending this concept further, if the primary lining is carrying the water load and the tensile bond keeps the membrane glued to the primary lining, the secondary lining is redundant from a structural point of view and can be omitted [1]. In reality, there are several good reasons for retaining a thin secondary lining, as will be discussed later.

4.3 Bonded spray applied waterproofing membranes

As explained in the previous section, it has been proven that there is a bond in both direct tension and shear in the short and long term ([16] & [18]) – see **Feil! Fant ikke referansekilden.**. The magnitude of the bond may depend on the water content of the membrane [15]. Some researchers have argued that the membrane will generally be dry [18] but this is questionable and data from real tunnels suggests otherwise [16]. While recognising that each of the different products on the market today exhibits a level of different performance, there is a growing confidence in this behaviour which opens the door to embracing composite lining action in designs.

Various authors have begun to investigate this ([6], [11] & [12]). The results have yielded some contradictory findings in the context of the typical PSCL application with the membrane sandwiched in between two layers of concrete with similar thicknesses. The balance of the loads shifts between the layers and the two layers interact in terms of deformations to a greater or lesser extent, depending on the degree of bonding. The “fully bonded” case can even be more adverse for the secondary, if it is bent a lot while much of the axial load lies in the primary, since the bending capacity is lower at low axial loads.

The benefit of the bond in direct tension has already been discussed. This would permit the complete omission of a secondary lining (for structural purposes). Despite the evidence, some have shied away from taking this step, preferring a “belt and braces” approach to resisting water pressures. With the current pressure to deliver value for money, all components in a lining system should have a defined engineering function, rather than being added through uncritical application of precedent practice.

Considering the bond in shear, while one can use some simplified calculations (e.g. after [17]) to compare the likely shear stresses at the interface and prove that the bond is adequate, this is arguably a moot point, if the secondary lining has no structural function. Likewise, the fact, that the bond inevitably will result in some load transfer to a non-structural secondary lining, is irrelevant because overstressing and cracking of this layer will simply shed the load back into the structural layer – the primary layer. There is limited data on the longterm shear strength of the membranes and it has been suggested that creep in the longterm

At this juncture, it is worth reflecting on the role of the secondary layer, now that it has been demonstrated that it serves no structural purpose. There are several possible purposes.

- A fire protection layer for the waterproofing layer and the primary lining
- To carry fixing loads (e.g. for signs, cable trays or cladding)

- An aesthetic finish

4.4 Fire protection

A fire protection layer of sprayed concrete with micro polypropylene (PP) fibres could be designed to insulate the membrane and primary lining. This requires detailed consideration in each case. However, one could make some general comments based on typical results. Firstly, the layer should be at least 50 mm as there is usually some spalling, even in this layer. While the fire design for each tunnel requires its own detailed study and possibly testing, considering Fig.5 as a conservative estimate of fire tests, one could choose a thickness of about 75 mm to keep the temperature of the primary layer below 250 °C for a 120 minute fire, in accordance with the Eurocode. This temperature would reduce the strength of the concrete but the loads would probably still remain within the capacity of the primary lining. For more significant hydrocarbon fires, thicker fire protection layers might be needed.

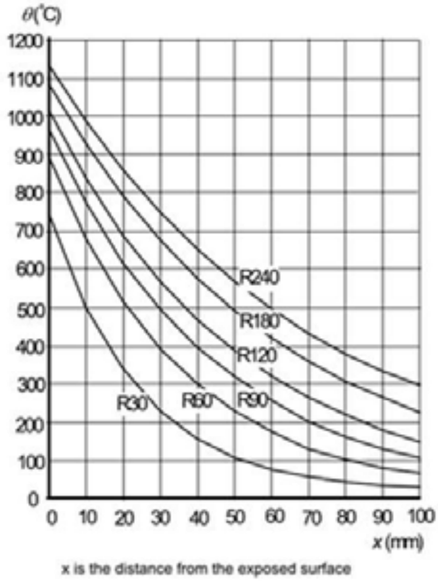

Fig.5 Temperature profiles for slabs (height h = 200) for R60 - R240 [20]

Spray applied waterproofing membranes are polymeric compounds which decompose when exposed to high temperatures. Typically, at 250°C, half of bonds in an EVA polymer decompose within 2 hours but the membrane is still functioning. The risk of the membrane reaching these elevated temperatures and the consequences of its decomposition should be considered as part of the global structure fire study.

In terms of the risk of fire posed by the membrane itself, spray applied waterproofing membranes are typically classed as "non-ignitable" (Class E when fire tested against BS EN ISO 11925-2, single-flame source test). This is the minimum requirement recommended by ITAtech. Some are classed as "self-extinguishing" in terms of Flammability (in accordance with DIN 4102-B2). Minova's Tekflex DS-W has also been tested according to a standard used in mines, "EN ISO 340 Conveyor belts – Laboratory scale flammability characteristics – Requirements and test method" and it has does not ignite under a direct flame.

In typical cases, the worst case design fire would probably result in some spalling of the fire protection layer, the general loss of its strength and the decomposition of the membrane. After such a fire, a tunnel would inevitably require repair to damaged sections of the membrane and fire protection. This is relatively straightforward using high pressure water milling and then re-spraying both components. The primary lining (and ground) will be impermeable enough to permit this repair. Depending on the design fire, it may be possible to use a fire protection layer to avoid any decomposition of the membrane.

4.5 Fixing loads

A secondary lining thickness of about 75 mm would be adequate for most fixings. Typical fixing bolts are embedded around 40 - 50 mm into the lining. There may be some practical difficulties in carrying large fixing loads and a risk of puncturing the membrane while drilling anchors. Special measures may be required such as inserts into the primary that are sprayed over with the membrane or local thickening of the secondary lining. This has been done successfully already on projects such as the A3 Hindhead and Crossrail projects in the UK.

4.6 Aesthetics

Since this secondary no-longer has a structural function, the mix of the concrete can be optimised to suit the surface finish needed. In many cases, an as-sprayed finish is deemed acceptable for non-public areas such as highway tunnels (Fig.6 a – Hindhead Road Tunnel, UK where the sidewall are cast insitu and the crown is sprayed concrete, as with the majority of road tunnels in Norway), As sprayed finishes for rail, metro and service tunnels are also suitable and functional. For example, numerous metro stations in Sweden and Finland detail as-sprayed concrete finishes for public spaces (see Figure 6 b).

Fig.6 (a) A3 Hindhead Road Tunnel - as-sprayed finish in the crown and cast insitu concrete sidewalls (b) Architectural finish with sprayed concrete in the Stockholm Metro

For other metro and rail projects, the need for higher reflectance, the use of advertising and a system to discretely cover the multitude of service cables lends itself to cladding systems are needed, as shown in

Fig.7. The choice of finish and cladding will depend on the client's requirements and preferences.

Fig.7 HRH Queen Elizabeth II inspecting cladding system of PSCL on Crossrail

4.7 Minimizing construction steps

Tab. 2 sets out the different layers in a lining according to this new design concept and compares them with the Crossrail design. Not only are the layers thinner but also there are fewer steps. This speeds up and simplifies construction, which also reduces cost. The performance of spray applied waterproofing membranes is heavily dependent on the preparation of the substrate. Attempting to minimize this step and layer further often turns out to be a false economy.

Tab. 2: Layers and proposed thicknesses for a typical soft ground 10m SCL tunnel (New concept and Crossrail)

	Layers for PSCL	**New concept**	**Crossrail**
1	Sealing layer	50	75
2	Primary layer	325	325
3	Regulating layer	40	40
4	Membrane	4	4
5	Secondary layer	0	300
6	Fire protection layer	75	50
	Total	494	794
	Saving Potential ~ 40%	62%	100%

A more subtle benefit of this approach is that the roles of the different layers have been simplified. The trend recently has been to place ever greater demands on sprayed concrete as a “multifunctional” material. Typically permanent sprayed concrete must be pumped and sprayed easily, gain early age strength rapidly, transform into a dense, high strength material with low permeability and maintain these characteristics for a design life of more than 100 years. Considering the new CSL approach here, the primary layer must fulfil many of the above but it does not have to be impermeable. Any reduction in the overall thickness of the sealing layer and the primary layer will improve safety as spraying thick layers can be dangerous [21]. The secondary layer is no-longer structural and it is much thinner so it only needs micro PP fibres and the early age strength demands are lower.

Substrate surface preparation is an essential step for a successful application of a spray applied waterproofing membranes. Paradoxically the waterproofing membrane can only be applied in dry conditions as running water will wash it off during spraying and excessive humidity will prevent the complete curing of the membrane. Also a regulating layer is required to create a relatively smooth surface. This minimizes the quantity of spray applied waterproofing membranes needed and the risk of pinhole defects.

Normally the required level of dryness is achieved by a combination of the temporary drainage during construction and channelling any active leaks through pipes which are injected with chemical grouts, such as Minova's CarboPUR, after the membrane has cured. The smoothness is achieved using a fine-grained, pre-bagged dry mix sprayed mortar like Minova's Minotor-C.

An alternative to solve both issues in one step would be to use Minova's innovative FT-30 sprayed mortar. This rapid hardening mortar forms a permeable skeleton as soon as it is sprayed which resists wash-out and slowly cures to form an impermeable, albeit brittle regulating layer. Depending on the quantity of water inflow, this can take up 2 or 3 weeks. Then the membrane (which is flexible) can be sprayed over it. Concentrated inflows have to be treated with channelling and post-grouted as mentioned earlier. This process can simplify the substrate preparation and permit the use of spray applied membranes in wetter conditions than normal.

4.8 No delamination

While this is an ever-present risk, there are well-established quality control measures to ensure that each pass of sprayed concrete is applied to a clean, dry, suitably strong substrate to maximise the bond. Applying these measures should result in bond strengths (in direct tension) of more than 1.0 MPa [4]. As discussed earlier, the strengths are much larger than the likely loads in shear and direct tension. Hence, delamination is not considered to be a general problem. Where it has occurred in sprayed concrete linings, this has usually been traced back to failures in quality control, in substrate preparation and/or during spraying, leading to errors such as overdosing accelerator, inadequate curing or application of very thin layers.

Traditionally, on tunnelling projects such as the Heathrow Express in the UK, steel fibre reinforced PSCL were over-sprayed with 20-25 mm pre-manufactured spray mortars using the dry spray process. Whilst some would consider this being a retrograde step in terms of dust generation, rebound and low productivity outputs, the key advantage of this approach was the ability to spray thin layers with very low water cement (w/c) ratios of between 0.28 and 0.32, producing a very fine surface finish and very low, if negligible thermal and drying shrinkage, resulting in very durable, bonded layers. On more recent projects, this smoothing layer has increased to 50mm to cover sprayed secondary lining protruding steel fibres, and has also been used as a fire protection layer with the inclusion typically of 1 kg/m^3 microfilament polypropylene (PP) fibres. These layers have been applied in many projects, using a wet-mix approach, and the considerations in Tab.3 for future projects should be evaluated and adopted to ensure successful application and serviceability.

20-50 mm thick wet-mix applied sprayed concrete layers designed for smoothing for aesthetic needs and/or fire protection do have a tendency to dry-out quickly when subject to relatively high temperatures in the working tunnel and also being exposed to the significant ventilation, which is needed to ensure the tunnel operatives are in a dust free environment. Added to this, wet-mix smoothing layers often achieve their better finish by operatives using higher set accelerator doses, this of course exacerbates the thermal and drying shrinkage effects, and risk of cracking and potentially de-bonding.

Tab.3: Requirements for Sprayed Fire Protection and Smoothing Layers

Criteria	Requirements
Substrate strength	Perform adhesive bond strengths using resin applied steel pull-off dollies. Adhesive strength of substrate should be greater than 1MPa.
Substrate Preparation	Jet washing to remove dust and deleterious materials. Require both pressure *and* volume to remove materials. Spraying air and water out of spraying robot nozzle is normally not sufficient in all cases.
w/c	Use superplasticisers to achieve preferable less than 0.4 and closer to 0.38 wherever possible.
Grading	Smooth aggregate gradings from 0-4mm
Air content of mix	Use defoaming admixtures if micro pp fibres entrain excessive air
Accelerator	Do not overdose. Keep below 8%. Pre-test cement – accelerator to ensure good spraying performance.
Micro pp fibres	Use minimum required to achieve fire protection performance. Check air entrainment effects in lab test mixes.
Spraying	Maintain the correct distance to enable compaction and smooth finish – Avoid being too close or too distant. Use correct nozzle type and operate auto nozzle oscillator to avoid “ridged” or “lumpy” sprayed finishes
Curing	Evaluate relative humidity in tunnel and implement correct curing regime. Consider internal curing/bond improvers such as TamCem iCure, or externally applied curing membranes
Trials	Do pre-construction tests to evaluate performance of substrate, mix and spraying processes

The 75mm smoothing and fire protection layer inside the spray applied waterproofing membrane proposed here is inherently more robust in the context of the risk of delamination. These are also common thicknesses for tunnel linings constructed in hard rock environments. Nevertheless, the criteria set in Tab.3 are valid.

Finally, it is worth noting that the typical spray applied waterproofing membranes exhibit good crack-bridging properties so that they can span across any cracks up to 3 to 4mm in the primary lining whether pre-existing when the membrane is sprayed, or cracks that develop during the service life of the structure. The crack-bridging capacity does decrease with falling temperatures [16]. However, performance is still adequate at the low temperatures (-5 °C) that a membrane might be exposed to. Special measures can be applied in very exposed areas such as portals in cold climates.

5. CONCLUSIONS

Having reviewed the current design practice for PSCL tunnels and evidence from research, a refinement of the design concept has been proposed for a composite shell lining, which could further improve the cost effectiveness and sustainability of PSCL tunnels. This new concept is shown in **Feil! Fant ikke referansekilden.** and consists of a minimal secondary lining, mainly as a fire protection layer for the spray applied waterproofing membrane. The tensile bond of the membrane to the primary lining means that the primary lining carries all ground and water loads in the short and longterm. In the case of a typical tunnel in soft ground, this new concept could result in a 40% saving in the overall lining thickness. The tunnel lining is one of the worst culprits in the carbon footprint of a tunnel. Reducing lining thickness will improve this greatly, perhaps by as much as 20%. This also means a 10% reduction in the excavated volume of the tunnel which would reduce settlement by the same amount. The construction time will be shortened too, which is often seen as the greatest cost driver in any construction project.

Further improvements could be made in the design of composite linings by the nonlinear modelling of the sprayed concrete. Typically designers still assume that this behaves linear elastically in their calculation models.

While the preceding discussion has focused on soft ground applications of PSCL, this design concept can also be applied to both drained and undrained rock tunnels. All that differs in rock tunnels is the thickness of the primary lining which is much thinner and often incorporates the sealing layer.

References

1. Dimmock, R. 2011. "SCL in the UK". Tunnelling Journal, Dec 2010/Jan 2011, pp 20-23.
2. Thomas, A.H. & Dimmock, R.H. ″The design philosophy for permanent sprayed concrete linings″. Proceedings of the World Tunnel Congress 2017 – Bergen, Norway.
3. Dimmock, R. & Lackner, J. 1997. "A Unique NATM solution for the London Underground". Proceedings of the "Tunnelling in Difficult Conditions" international conference, ITC, Basel, Switzerland. October 1997, pp 261-272.
4. Thomas, A.H. 2009. "Sprayed concrete lined tunnels". Taylor and Francis, Abingdon UK ISBN: 9780415368643 - www.taylorandfrancis.co.uk.
5. Golser, J. & Kienberger, G. 1997. "Permanente Tunnelauskleidung in Spritzbeton - Beanspruchung und Sicherheitsfragen", Felsbau, 1997, Issue 6, pp 416 – 421.
6. Thomas, A.H. & Pickett, A.P. 2012. "Composite Shell Linings". Spritzbeton Tagung, Alpbach. pp 1 – 17.
7. Hilar, M., Thomas, A.H. & Falkner, L. 2005. "The Latest Innovation in Sprayed Concrete Lining - the LaserShell Method". Tunel – Magazine of the Czech Tunnelling Committee and the Slovak Tunnelling Committee ITA/AITES, 2005, Vol 4, pp. 11-19.
8. Dimmock, R. & Bowers, K. 2015. BTS Debate Presentation "This house believes further development of SCL for complex urban tunnels is the best way forward for our industry". ICE, London, December 2015.

9. Batty, E., Bond, N., Kentish, E., Skarda, A. & Webber, S. 2016. "Comparison Between Sprayed and Cast In Situ Concrete Secondary Linings at Bond Street and Farringdon Stations". Proceedings of the World Tunnel Congress 2016, San Francisco, USA.
10. Thomas, A. H. & Pickett, A P. 2011. "The design of composite sprayed linings. Modern use of wet mix sprayed concrete for underground support". Tromsö, Norway 2011.
11. Su, J. & Bloodworth, A.G. 2016a. "Utilizing composite action to achieve lining thickness efficiency for Sprayed Concrete Lined (SCL) tunnels". Proceedings of the World Tunnel Congress 2016, San Francisco, USA.
12. Su, J. & Uhrin, M, 2016. "Interactions in sprayed waterproof membranes". Tunnelling Journal, Oct/Nov 2016, pp 20 - 27
13. Jager, J. 2016. "Structural design of composite shell linings". Proceedings of the World Tunnel Congress 2016, San Francisco, USA.
14. Holter, K.G. & Geving, S. 2016. "Moisture Transport Through Sprayed Concrete Tunnel Linings". Rock Mechanics and Rock Engineering, January 2016, Volume 49, Issue 1, pp 243–272
15. Holter K.G., Nilsen B., Langas C. & Tandberg M. K. 2014 "Testing of sprayed waterproofing membranes for single shell sprayed concrete tunnel linings in hard rock". Proceedings of the World Tunnel Congress 2014 – Tunnels for a better Life. Foz do Iguaçu, Brazil.
16. Holter, K.G. 2015. "Properties of waterproof sprayed concrete tunnel linings Thesis (PhD)", Norwegian University of Science and Technology, 197 p.
17. Kupfer, H, & Kupfer, H. 1990. "Statical behaviour and bond performance of the layers of a single permanent shotcrete tunnel lining". Proc. 3rd Conference on Shotcrete Technology. lnnsbruck-Igls: Institut fiir Baustofflehre und Materialpriifung, Universität Innsbruck, pp 11 – 18.
18. Su, J. & Bloodworth, A.G. 2016b. "Interface parameters of composite sprayed concrete linings in soft ground with spray-applied waterproofing". Tunnelling and Underground Space Technology, 59. pp. 170-182.
19. Yilmaz, H. 2009. "Comparison of mechanical properties of shotcrete and Thin Spray-on Liner (TSL) ", ITA, SAIMM and SANCOT: Shotcrete for Africa, 2009.
20. BS/EN 1992-1-2:2004. "Eurocode 2: Design of concrete structures Part 1-2: General rules — Structural fire design", BSI 2004.
21. Smith, K. 2016. "Where next for SCL?" Tunnelling Journal, Sep 2016, pp 28 – 33.

8th INTERNATIONAL SYMPOSIUM ON SPRAYED CONCRETE – Modern Use of Wet Mix Sprayed Concrete for Underground Support
– Trondheim, Norway, 11. – 14. June 2018

PUMPABILITY OF WET MIX SPRAYED CONCRETE WITH REDUCED CLINKER CONTENT

Maria Thumann
OTH, University of Applied Sciences Regensburg
maria1.thumann@oth-regensburg.de

Wolfgang Kusterle
OTH, University of Applied Sciences Regensburg
wolfgang.kusterle@oth-regensburg.de

ABSTRACT

The research project „Advanced and Sustainable Shotcrete - ASSpC" aims at the improvement of sprayed concrete mix design regarding durability and sustainability. One possible improvement is to replace part of the clinker content in the binder with different supplementary cementitious materials. It is crucial that new mix designs fulfil the basic technical requirements on site concerning workability and early age development, too. One central issue of the project is to investigate which parameters influence the pumpability of sprayed concrete. Several test methods are used to determine the stability, tendency to segregation, bleeding and of course the consistency of concrete. An essential test method is a concrete sliding pipe rheometer (Sliper). This rheometer determines the pumping characteristics of concrete in the laboratory and on construction site. In comparison to other rheometers, the Sliper evaluates the rheological characteristics of the thin layer of paste which is lubricating the wall of the conveying pipe. The paper presents the tests procedures in detail as well as first results from lab-tests and from site-tests with different advanced shotcrete mix-designs.

INTRODUCTION

Nowadays tunnel constructions have achieved a high standard of safety and quality, but there is still a need for optimisation. The construction has to be able to withstand the environmental conditions for the (expected) service lifetime. The maintenance of tunnels is very costly and time consuming and causes disruptions to traffic. The durability has to be improved to minimize the tunnel maintenance work. The research project „Advanced and Sustainable Shotcrete - ASSpC" aims at the improvement of sprayed concrete mix design regarding durability and sustainability. The processes of chemical attacks (sulfate attack, formation of thaumasite) and of the leaching of calcium hydroxide (precipitation of calcite in the drainage system) are investigated. The aim is to gain a deeper understanding how to improve the sprayed concrete mix design. One possibility is to replace part of the cement in the binder with supplementary cementitious materials (SCM) and/or to decrease the water content. The modification of the mix-design influences the workability and the early-strength development of the sprayed concrete. The paper presents results from lab tests focussed on the workability of sprayed concrete with reduced clinker content as well as theoretical principles of pumpability.

WORKABILITY OF WET MIX SPRAYED CONCRETE

Workability is a physical property of concrete [1], but it can't be described with only one single parameter or measured with one single test method. Some attempts to describe workability include the following parameters and characteristics [2]: viscosity, yield stress, mobility, internal friction, pumpability, stability, cohesion, segregation, bleeding, compactability, finishability etc.
Pumpability plays an important role for wet mix sprayed concrete. The material has to be conveyed through the pipe without changing its properties and mix proportion. The concrete has to be flowable and stable even under pressure. But there is no standardized test procedure to measure pumpability. Models describing the conveying process of concrete in a pipe are explained in the following section.

Pumpability

When concrete is pumped through a pipe a thin layer of paste is lubricating the wall of the pipe (see Figure 1). The interaction of the lubricating layer and the pipe wall is of great importance for pumpability. The shear of the layer allows the slipping of the concrete and leads to a reduction in the required pumping pressure. The composition and thickness of the lubricating layer and its rheological properties influence the pumping process [3,4]. The lubricating layer consists of binder, (additions), (admixtures), water, fine aggregates and air.

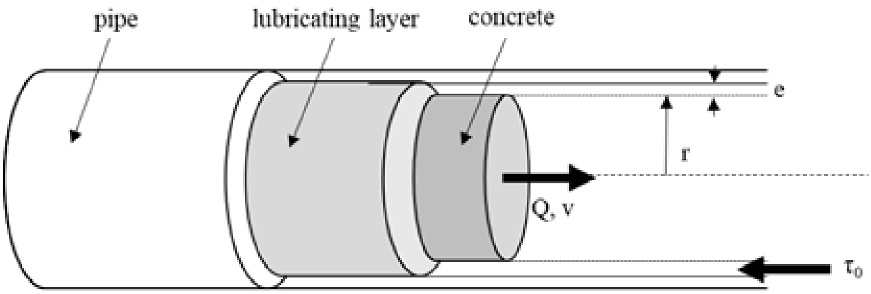

Figure 1: Plug flow of concrete in a pipe according to [5]

In the remaining part of the pipe the concrete is pumped as a plug. For further information concerning the pumping process is referred to [5–10].

Test methods

The workability of wet mix sprayed concrete is usually determined by the spread flow table or the slump test. Several publications and investigations show that results based on these conventional test methods only are not reliable for the pumpability of modern concretes [5,11–13]. Slump test or spread flow table can be used to measure in a simple way the consistency of concrete on site but not to predict pumpability. "Conventional" concrete consists of water, cement and aggregates. The water content (or the paste volume) modifies the consistency. The use of additions and admixtures, e.g. superplasticizer (SP), changes the rheological properties of concrete essentially.

Stability

The stability of concrete is important to avoid blockages in the conveying pipe. Blockages can occur when the paste separates from the aggregate skeleton because of a high pressure in the pipe [14]. The segregation is often contributed to mix-design with an inadequate particle size distribution or a high water/cement ratio [6]. The lubricating layer is missing and the friction at the pipe wall increases. Consequently the conveying process will be blocked [13].

The stability of concrete under pressure can be measured by the filter pressing test (see Figure 2).

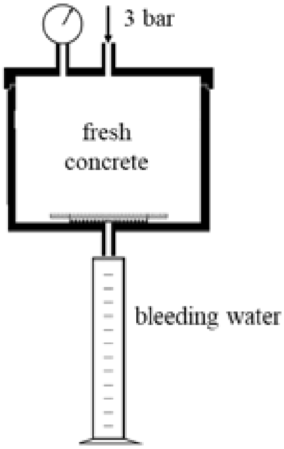

Figure 2: Filter pressing test according to [15]

This test method is usually used for concrete with a spread of more than 560 mm. The concrete is filled and compacted in a vessel and a pressure of three bar is applied. At the bottom of the vessel is a small hole covered by geotextile, so that water can flow out. After 15 minutes and 60 minutes the amount of bleeding water is measured.

$$bleeding\ [kg/m^3] = \frac{mass\ of\ bleeding\ water\ [ml] \cdot 1000}{volume\ of\ the\ vessel\ [cm^3]} \tag{1}$$

Sliding pipe rheometer „Sliper“

The sliding pipe rheometer “Sliper” [16] is used to determine the pumping capacity of a concrete in the laboratory and on construction site. The Sliper consists of a pipe and a guided piston which is standing on the ground floor (Figure 3). A pressure sensor is integrated onto the piston. If the pipe is sliding downwards, the pressure in the pipe is measured and the speed of the pipe is recorded. The measurement data are sent wireless to a common smart phone. Rheological parameters as well as the supposed pump pressure may be estimated.

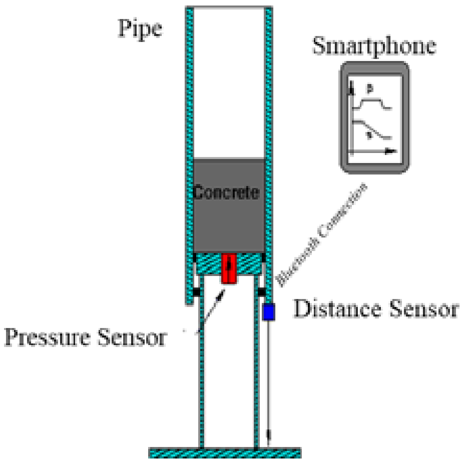

Figure 3: Sliding pipe rheometer (Sliper) [16]

The result shows the estimated pumping pressure (p) in correlation to the flow rate (Q). The value "a" and "b" characterize the graph. The value "a" correlates to the yield stress and the value "b" correlates to the viscosity of the lubricating layer [5]. The values are used to differentiate from the yield stress and the viscosity as rheological parameters of the concrete. The Sliper measures the rheological behaviour of the lubricating layer but not of the concrete itself.

EXPERIMENTAL PROGRAMME – LAB TESTS

Mix-design

The basis for testing different mix design is a reference mix with a w/c-ratio of 0.5, cement content of 420 kg/m³ and aggregates with a maximum grain size of 8 mm (see Table 1). It represents a mix design, which is typically used on site in central Europe. The consistency of the mixture is adjusted with a superplasticizer (SP) to achieve a flow table spread of 60 cm.

Table 1: Mix design "reference"

		density [kg/dm³]	**mass** [kg/m³]	**volume** [dm³/m³]
binder	CEM I 52.5 N SR0	3.2	428	131
water		1.0	214	214
aggregates		2.7	1655	625
air				30
total			2316	1000

In the lab, seven different grain fractions of quartz are used to avoid scattering of the grain size distribution.

Test series "volume of paste"

The volume of paste influences the thickness of the lubricating layer and consequently the pumpability. The pumpability of mixtures with different volumes of paste was measured by the Sliper. The maximum size of aggregates, which will be part of the lubricating layer, is under discussion. For the following test series, the volume of paste includes the volume of binder, water, aggregates < 0.125 mm and air. The volume of paste was reduced from 419 dm³/m³ (reference) to 388 dm³/m³ (PV_r) (see Table 2). The w/c was kept constant.

Table 2: Mix design (volumes), test series "volume of paste" (PV = paste volume, r = reduced volume, A = air voids)

		reference	**PV_r**	**PV_r_A**
binder	[dm³/m³]	131	118	118
water	[dm³/m³]	214	192	192
aggregates < 0.125	[dm³/m³]	37	40	40
air void content (measured)	[dm³/m³]	36	38	76
total paste volume	[dm³/m³]	419	388	426

Figure 4 shows the estimated pumping pressure (p) in correlation to the flow rate (Q) measured by the Sliper. The values of pressure relate to the testing equipment, not to the real shotcrete pump.

The results show clearly that the reduction of paste volume leads to a higher estimated pumping pressure.

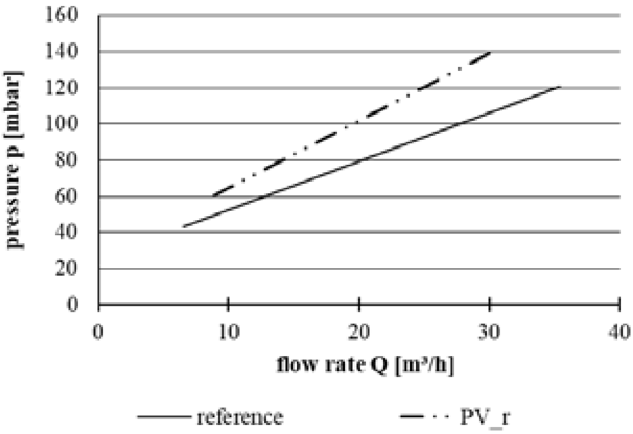

Figure 4: p-Q Chart determined by Sliper, test series "volume of paste"

(Comment: Mixtures with a paste volume of 359 dm^3/m^3 only blocked the rheometer. The paste content was too low to create an adequate thickness of the lubricating layer.)
As already mentioned, the paste content is expressed as the sum of the volume of air, water, binder and fines of the aggregates. The volume of paste can be increased through the addition of air entraining admixtures (see Table 2). Subsequently the estimated pumping pressure determined with the Sliper decreased (see Figure 5).

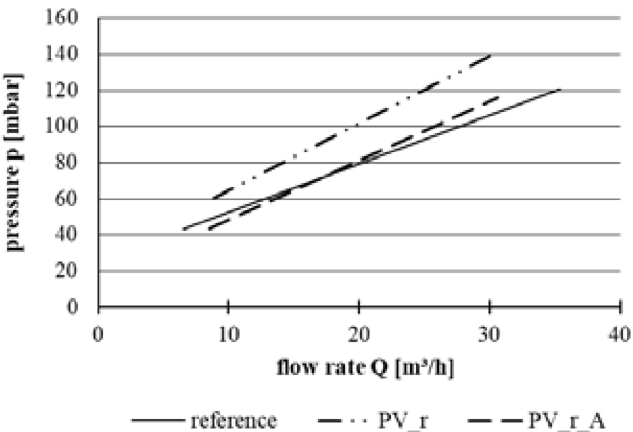

Figure 5: p-Q Chart determined by Sliper, test series «volume of paste – air content»

But you have to consider that a real concrete pump applies a much higher pressure to the concrete than the Sliper. The air might be compressed and might not influence the lubricating layer [6]. Other experiences report on a quite beneficial effect of an enhanced air content [17].

Test series “grading curves”

The paste of the lubricating layer consists of water, binder, air and fines of the aggregates [13,18]. If the grading of the fines changes, the pumpability will be influenced. In the lab the grading of fine aggregates was varied systematically (see Figure 6).

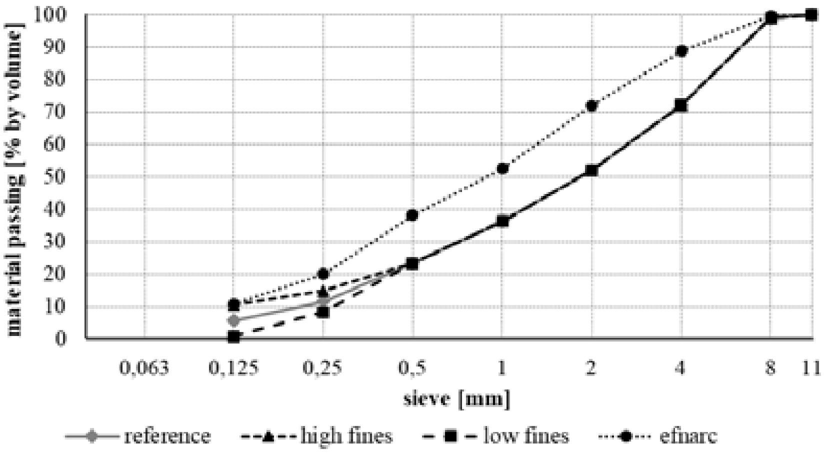

Figure 6: Grading curves with different content of fines

The consistency was adjusted with a superplasticizer to achieve a flow table spread of about 60 cm. Figure 7 shows the results measured by the Sliper. The higher the content of fines the higher the estimated pumping pressure.

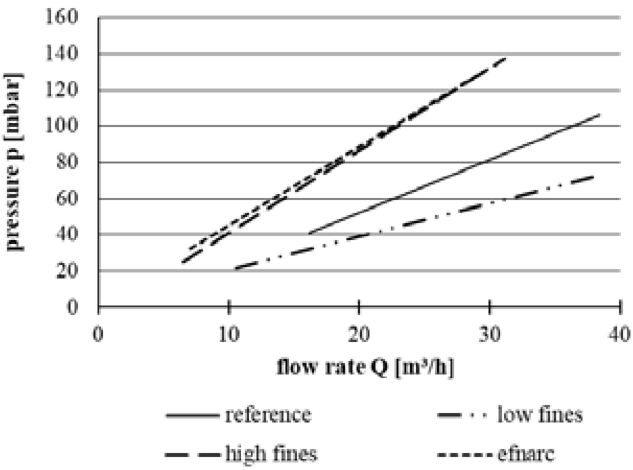

Figure 7: p-Q Chart determined by Sliper, test series «grading curve»

It is noteworthy that the results of mixtures “low fines” and “efnarc” are almost the same even if the grading is different. But the amount of fines below 0.125 mm is equal and consequently the volume of paste (see Table 3).

Table 3: Volume of paste of mix-design with different grading curves

		reference	low fines	high fines	efnarc
binder	[dm^3/m^3]	131	131	131	131
water	[dm^3/m^3]	214	214	214	214
aggregates < 0.125	[dm^3/m^3]	37	6	62	62
air void content (theoretical)	[dm^3/m^3]	36	30	30	30
total paste volume	[dm^3/m^3]	419	382	438	438

It was already mentioned that an increase of the paste volume can decrease the estimated pumping pressure. In this series (Table 3) the water content was not adjusted to the higher amount of fines, but kept constant. The resulting stiffer rheological properties of the lubricating layer influenced the estimated pumping pressure significantly.

Test series "Rheological characteristics of the paste"

The rheological characteristics of the paste are of great importance for pumpability, especially the rheological characteristics of the lubricating layer. Lab test with different w/c-ratios are a good option to investigate the influences of the rheological properties. The theoretical paste volume was kept constant for mix-designs of the following two test series. In the first series no superplasticizer was added, and the flow table spread varied between 28 and 41 cm. In the second series the consistency of all mixtures was adjusted with a superplasticizer (SP) to achieve a flow table spread of almost 60 cm (see Figure 8).

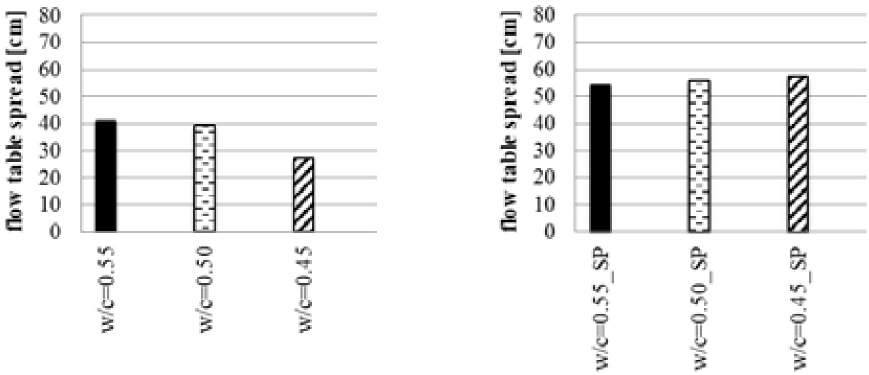

Figure 8: Flow table spread, test series "w/c-ratio" (left) and "w/c-ratio_SP" (right)

The results of the Sliper show that the estimated pumping pressure is lower with increasing water cement ratio (see Figure 9). This is valid for both test series.

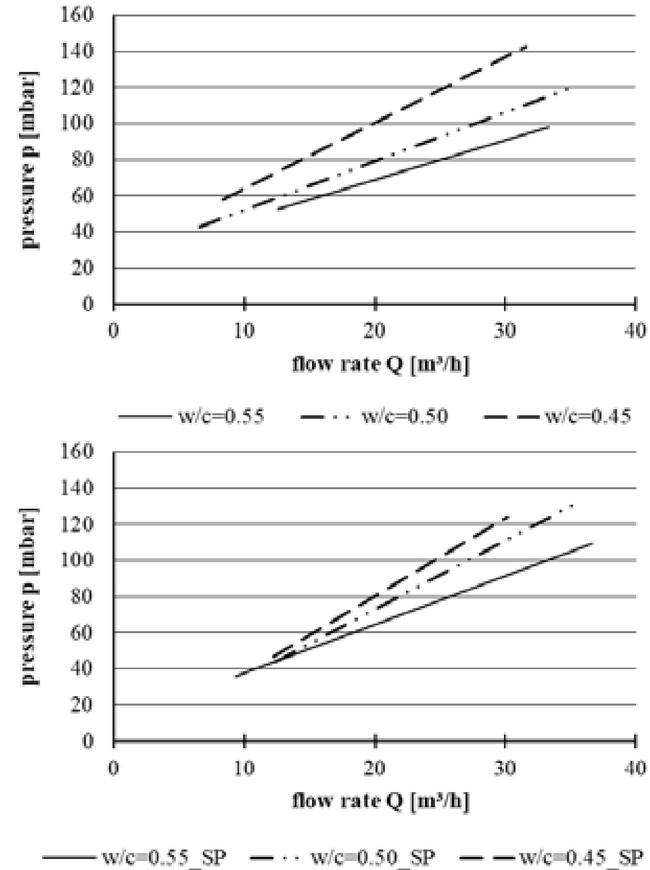

Figure 9: p-Q Chart determined by Sliper, test series “w/c-ratio” (above) and “w/c-ratio_SP” (below)

In addition to the Sliper the V-funnel flow time was determined. The results of the test series with and without superplasticizer are completely different. For the series “w/c-ratio” it was not possible to measure the V-funnel flow time according to DIN EN 12350-9 [19] because the concrete blocked the V-funnel (see Figure 10)

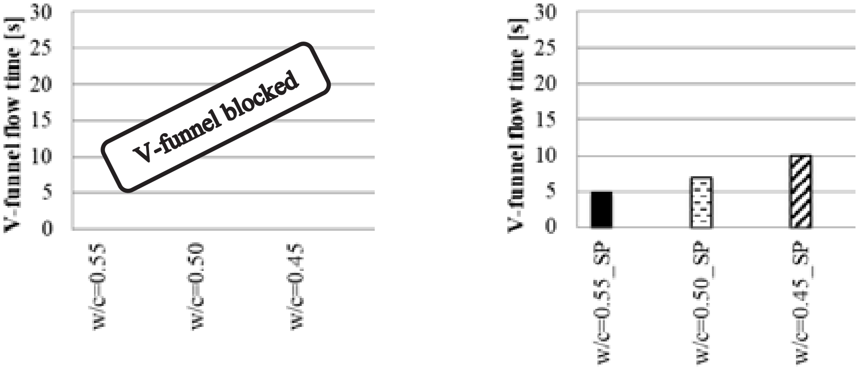

Figure 10: V-funnel flow time, test series “w/c-ratio“ (left) and “w/c-ratio_SP“ (right)

The results of the Sliper show that the estimated pumping pressure of mix-design with and without superplasticizer is almost the same even if results of V-funnel flow time and spread flow table are completely different. The rheological characteristics of the lubricating layer and of the concrete are different.
The influence of the rheological characteristics of the paste was further investigated. Part of cement was substituted with SCM (10 M.-% metakaolin, 30 M.-% und 50 M.-% slag). The paste volume (cement, addition, water, fines < 0.125 and air) was kept constant. The substitution of clinker with slag has no influence to the estimated pumping pressure compared to the reference mix (see Figure 11). The substitution with only 10°M.-% of metakaolin increases the estimated pumping pressure significantly.

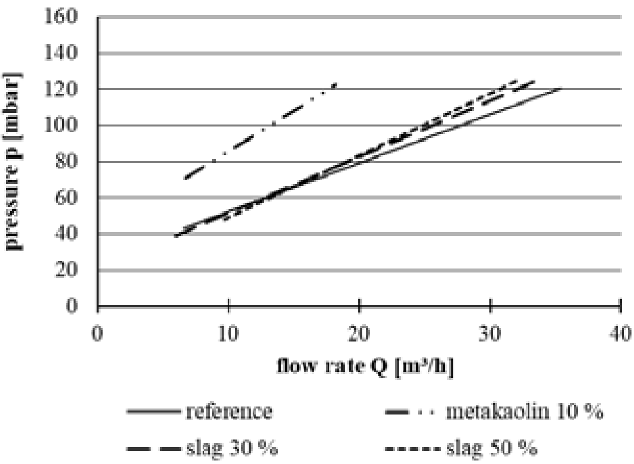

Figure 11: p-Q Chart determined by Sliper, test series "SCM"

The results are of course not valid for all types of SCMs, because it depends on the quality and the fineness of materials (see Figure 12).

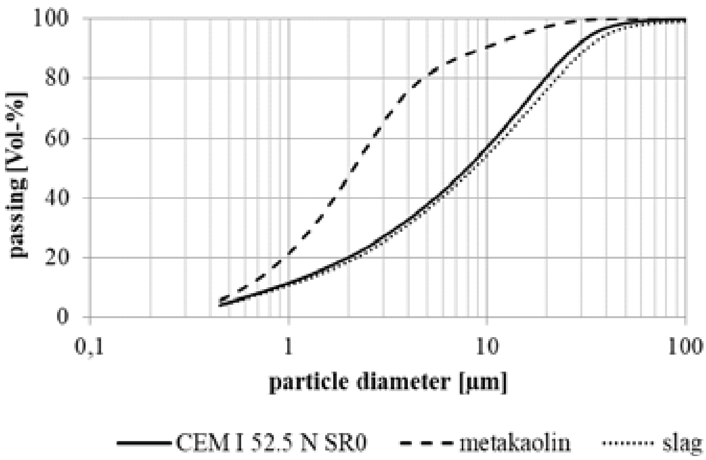

Figure 12: Particle size distribution of CEM I 52.5 N SR0, metakaolin and slag

Generally, the results of the estimated pumping pressure determined by the Sliper show that the rheological properties of the lubricating layer influence the pumpability.

Correlation of test methods

Several publications describe that the spread flow table and the pumpability do not correlate for concretes (especially when admixtures and additions are used). The results of lab tests determined by the "Sliper" confirm this observation. The following graphs show that the spread flow table and the value "a" do not correlate as well as the V-funnel flow time and the value "b".

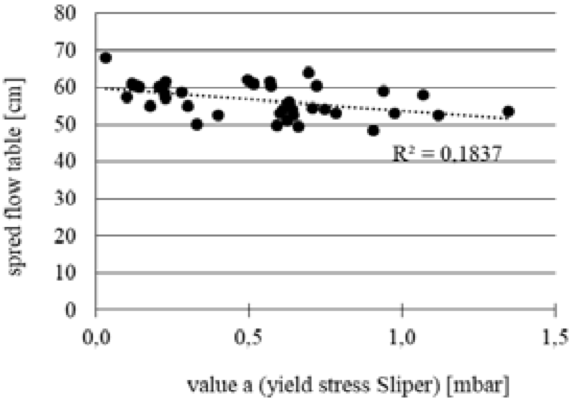

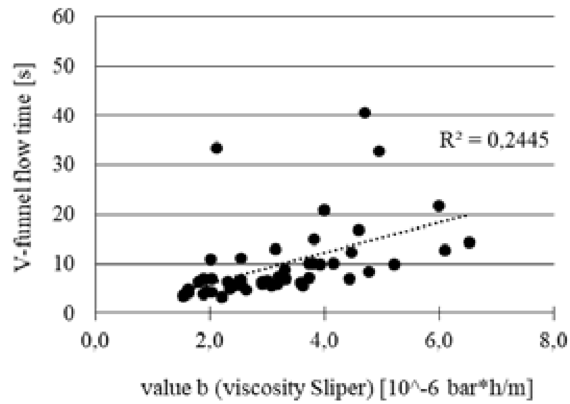

Figure 13: Correlation of V-funnel flow time and value b (viscosity parameter determined by Sliper) and correlation of spread flow table and value a (yield stress parameter determined by Sliper)

The Sliper determines the rheological characteristics of the lubricating layer, which is important for the pumpability. The spread flow table and the V-funnel flow time measure the properties of the concrete.

Stability

The stability of the mixtures was determined by the filter pressing test (according to [15]). In addition to the rheological properties of the lubricating layer, the stability is important for

pumpability. The concrete has to be stable even under pressure. Otherwise, the paste separates from the aggregate skeleton in the pipe and blockages can occur. Results of mixtures with different w/c-ratio showed that the higher the w/c-ratio, the lower the estimated pumping pressure (see Figure 14 left).
However, it must be considered, that a high w/c-ratio causes high bleeding rates (see Figure 14 right).

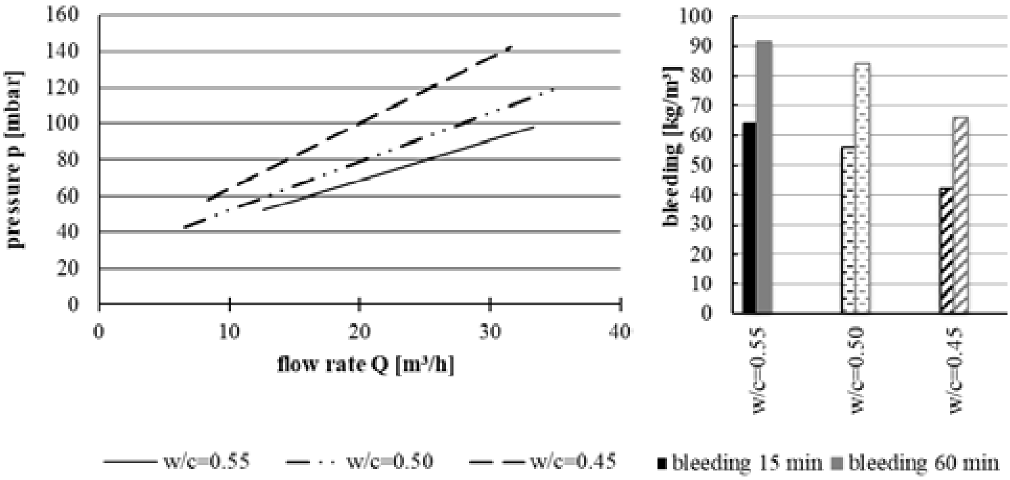

Figure 14: p-Q Chart determined by Sliper and bleeding rate, test series “w/c-ratio“

It is not possible to determine high bleeding rates by the Sliper. Therefore, the combination of the filter pressing test and the Sliper seems to be a good possibility to estimate pumpability.

SUMMARY AND OUTLOOK

Using concrete-base mix design with new binders and low water content may increase durability and sustainability of sprayed concrete. However, the borderline of good pumpability and sprayability may be reached too. Standard workability tests deliver too little information and judge the entire concrete mass only. The composition and thickness of the small layer of paste lubricating the pipe wall are the key influence on pumping properties. It is shown that a combination of a sliding pipe rheometer and a filter pressing device may deliver the required information for good pumpability. Paste rheology and paste volume seem to be the decisive factors for the mix. As the sliding pipe rheometer measures under low pumping pressure, questions regarding influence of high pressure on lubricating layer still must be investigated in detail.

REFERENCES

[1] A.M. Neville, Properties of concrete, 5th ed., Pearson, Harlow, England, 2011.
[2] P. Bartos, Fresh Concrete - Properties and Tests, Elsevier Science Publishers B.V., Amsterdam, 1992.
[3] E. Secrieru, V. Mechtcherine, Zur Prüfung der Pumpbarkeit von Beton, Beton 1+2 (2016) 18–23.
[4] E. Secrieru, F. Shirin, C. Schröfl, V. Mechtcherine, Study on concrete pumpability combining different laboratory tools and linkage to rheology, Construction and Building Materials 114 (2017).

[5] K. Kasten, Gleitrohr-Rheometer. Ein Verfahren zur Bestimmung der Fließeigenschaften von Dickstoffen in Rohrleitungen. Dissertation, Dresden, 2009.
[6] M. Jolin, D. Burns, B. Bissonette, F. Gagnon, L.-S. Bolduc, Understanding the Pumpability of Concrete, in: Engineering Converences International (Ed.), Proceedings Shotcrete for Underground Support XI, 2009.
[7] V. Mechtcherine, N.N. Venkatesh, K. Kasten, Testing pumpability of concrete using Sliding Pipe Rheometer, Construction and Building Materials 53 (2014) 312–323.
[8] E. Secrieru, V. Mechtcherine, S. Palzer, Rheological and Tribological Characterization of Concrete in the Context of Estimating its Pumpability, in: K.H. Khayat (Ed.), 8th International RILEM Symposium on Self-Compacting Concrete, 2016.
[9] D. Kaplan, F. de Larrad, T. Sedran, Design of Concrete Pumping Circuit, ACI Materials Journal Volume 102 (2005) 110–1117.
[10] S. Jacobsen, M. Hâvard, S. Foon Lee, L. Haugan, Pumping of concrete and mortar - State of the art. COIN Project report 5 -2008, 2008.
[11] M. Reinhold, Methoden zur zielsicheren Vorhersage der Pumpbarkeit von Betonen mit nicht idealer Gesteinskörnungs-Sieblinie, BetonWerk International 1 (2014) 56–59.
[12] E. Secrieru, M. Butler, V. Mechtcherine, Prüfen der Pumpbarkeit von Beton - Vom Labor in die Praxis, Bautechnik 91 (2014) 797–811.
[13] T.T. Ngo, Relationship between concrete composition and boundary layer composition to optimise concrete pumpability, European Journal of Environmental and Civil Engineering 16 (2012) 157–177.
[14] Browne, R.: Bamforth, P., Tests to Establish Concrete Pumpability, ACI Journal 74 (1977) 193–203.
[15] Österreichische Vereinigung für Beton- und Bautechnik, Merkblatt Weiche Betone, Wien, 2009, accessed 10 March 2016.
[16] Schleibinger, Sliper, http://www.schleibinger.com/cmsimple/en/?Rheometers%26nbsp%3B:.recent_news:SLIPER_%96_Determining_the_pumping_capacity_of_concrete.
[17] D. Beaupré, Rheology of High Performance Shotcrete. PhD Thesis, Vancouver, 1994.
[18] K.E. v. Eckardstein, Pumpbeton und Betonpumpen, Herne, 1983.
[19] DIN Deutsches Institut für Normung, DIN EN 12350-9: Testing fresh concrete – Part 9: Self-compacting concrete –V-funnel test (German version), Beuth Verlag GmbH, Berlin, 2010.

ACKNOWLEDGEMENT

We want to thank the FFG (Austrian Research Foundation) for funding part of this research.

Applications of Cellular Sprayed Concrete at Tunnel Portals

Kyong-Ku Yun[1,*] Seung-Yeon Han[2], Kyeo-Re LEE[2] and Yong-Gon KIM[3]

Abstract

An economic method for architectural and structural wall was developed with a cellular sprayed concrete, which was applied at tunnel portal for a very regional symbol. The cellular sprayed concrete could be used to improve the performance of shotcrete material, to maximize the construction advantages of shotcrete and further harmonize with the surrounding environment. The cellular sprayed concrete is a very economic feasibility by manufacturing a high-performance cellular shotcrete using an ordinary ready-mixed concrete and concrete pump car. It is produced by incorporating cellular and mineral admixtures in the process of remixing and dispersing the mineral admixture in an ordinary ready-mixed concrete at a job site.

The cellular sprayed concrete was applied at tunnel portals which highlight nature-friendly scenery since it is a construction method that comprehends natural rock shapes and colors, by carving various natural rock patterns on the placed high-performance shotcrete before it hardens. After curing for a certain period of time, an acid stain is sprayed on the surface to develop a color by neutralization reaction.

KEY WORDS: tunnel portal, shotcrete, cellular sprayed concrete, silica fume, stain

---

[1]Director, Center for Regional Construction Technology Dept. of Civil Eng, Kangwon National Univ. 1 Kangdae-gil, Chuncheon, 200-701, S. Korea. Corresponding Author: kkyun@kangwon.ac.kr,
[2]Ph.D Student, Dept. of Civil Eng. Kangwon National Univ. 1 Kangdae-gil, Chuncheon, 200-701, S. Korea.
[3]CEO, DaeSang E&C Company, Wonju, S. Korea.

1. Introduction

Since the construction of the first expressway in the 1970s, the total length of expressways in Korea has increased to 4,437 km, of which 872 km are aligned with 1,055 tunnels. Currently, the local inhabitants are demanding on a much higher standard of living. Besides the improvement of transportation quality, environmental protection and ecological conservation must be taken into account increasingly, thereby the beauty of tunnel portal should be achieved. They has asked a very regionally-symbolic tunnel portal at their tunnel because it could be utilized to advertise their cities to the thousands of drivers every day [Han, 2014].

Cellular sprayed concrete is a very economic and simple methods for producing a high-performance shotcrete, by incorporating a large amount of cellular, adding and dispersing silica fume and other mineral admixtures into an ordinary ready-mixed concrete at a job site. Because it is constructed without accelerators, it secures a certain time for carving the surface and high strength and high durability. This method could be used to construct by top-down or bottom-up manner. It is a technique that maximizes economic efficiency by manufacturing high-performance cellular sprayed concrete using an ordinary ready-mixed concrete and remixing it into a high performance concrete at a jobsite. It has an excellent application in slope surface stabilization as well as in maintenance since it is possible to prevent weathering of the exposed rock cut surface by applying cellular concrete. In addition, it includes a symbolic and natural rock scene [Yun, etc, 2016].

The tunnel portals were constructed using a cellular sprayed concrete technology with carving and texturing for the surface and acid staining for coloring, which were resulted in an artificial rock. These tunnel portals were designed according to the demand of the local inhabitants, representing the regional characteristics [Yun, etc, 2106]. The inhabitants were very satisfied to the beautiful and symbolic their own tunnel portals. All these were possible with a cellular sprayed concrete technologies of various uses such as well adaption for curved and irregular surface, different surface finishes possibility, excellent physical properties and fast and economical process.

2. Cellular Sprayed Concrete

A very new concept of cellular sprayed concrete was developed, which is produced by incorporating cellular and mineral admixtures in the process of remixing and dispersing the mineral admixture in an ordinary ready-mixed concrete at a job site. High strength and high durability are secured by adding and dispersing the mineral admixtures. Adding a cellular forms by 20 to 30 percent by volume transfers a stiff concrete into a slurry concrete by ball bearing effect of cellular inside of concrete, and add silica fume then this could be dispersed in the slurry concrete. Then this should be pumped and sprayed at the end of nozzle by high air pressure which dispel out the air in the remixed concrete, resulted in high performance sprayed concrete having a proper slump [Lee, 2013]. Therefore, the production cost and construction can be reduced thereby maximizing the economic feasibility since the high-performance cellular sprayed shotcrete is produced only with the cost of silica fume itself by adding and dispersing it in the ready-mixed concrete on a job site without the need for production, transportation, and storage which are required when special blended cement is used [Yu, etc, 2017].

The processes of cellular sprayed concrete are as follows: ① bring an ordinary ready-mixed concrete having a low slump in a truck to a job site. ② add a preformed cellular by 20 to 30 % by volume into a truck, then the stiff concrete would be resulted in a slurry one having a very high slump. ③ add silica fume, remix and disperse it. The silica fume would be easily dispersed at the slurry concrete, however, the concrete contains lots of air inside of concrete. ④ supply the air bubbled concrete to a concrete pump car which is attached by a nozzle at the end, and spray the air bubbled concrete with a high air pressure. This resulted in repelling out the air in concrete with a low-slump high-performance concrete [Yum, etc, 2017]. Figure 1 illustrates the concept of cellular sprayed concrete.

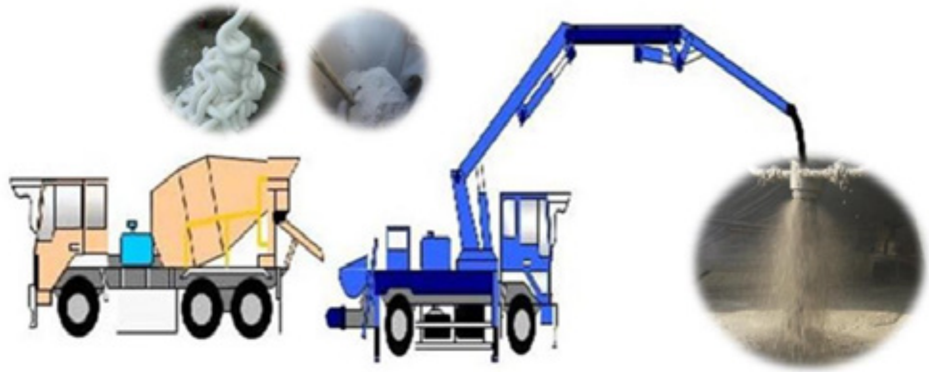

Figure 1. Concept of cellular sprayed concrete

3. Mixture Design and Test Methods

The materials were developed to ensure structural performance and high-performance quality as well as better color expression. The cellular sprayed concrete was adopted for economic applications. Table 1 shows an ordinary and high performance concrete mixtures. The slumps were measured to be 80mm in the ordinary ready-mixed concrete, 190mm after adding cellular and silica fume, and 10mm after spraying. The final targeted air content was between 3 to 6% after spraying.

A cellular sprayed concrete was developed for the improved pumpability and less rebound without using accelerator by adjusting the air content having an above 10% before shooting and 3 to 6% after shooting, targeting a high compressive strength of above 35MPa at 28 days and high durability with a relative freeze-thaw index of 80%. In addition, after spraying the concrete, various natural rock patterns are sculpted before the concrete hardens and an acid stain is sprayed on the concrete surface after curing for a certain period of time. The cellular sprayed concrete was developed to have a water-tightness not to be water permeable.

In this experiment, slump test was conducted to determine the workability of the fresh concrete; air content was measured before adding foam, after adding foam and after spraying. In addition, compressive strength test of the hardened concrete was performed on the 28 and 56 days. Table 2 shows the test methods conducted at this research, including rapid chloride permeability, surface scaling resistance and freeze-thaw resistance.

Table 1: Concrete mixture designs

Type	W/B	S/a (%)	Unit content (kg/m^3)						
			water	cement	S.F.	sand	gravel	AE	Cellular
OPC	0.42	65	164	390	-	1,146	619	3.9	-
Cellular sprayed concrete	0.43	65	164	390	30	1,146	619	3.9	220

Table 2: Concrete test methods

Category	Standard	Schedule
Slump test	KS F 2402	After Mix / Air Slurry in Mix / After Sprayed
Air content test	KS F 2421	After Mix / Air Slurry in Mix / After Sprayed
Compressive strength	KS F 2405	Age 28, 56 Days
RCPT test	KS F 2711	Age 28 days
Surface scaling	ASTM C 672	Age 28 days
Freeze-thaw	ASTM C 666	Age 28 days

4. TEST RESULTS

The high-performance cellular sprayed concrete should have the required strength and durability since it is applied to the tunnel portals. Three specimens for each test were prepared on site for strength and durability tests. The test results are as follows:

The change in air content and slump was measured, compared and analyzed in accordance to the required criteria. Due to the air ball bearing effect, a higher slump was measured as the incorporated amount of cellular increased. However, the slump measured after spraying has reduced to less than 5cm. There was high air content in the variables before spraying but it reduced to a constant air content of 2~5% after sprayed. The slump and air content test performed on the fresh concrete gave a result that satisfied the targeted values. The targeted slump before shooting was between 70 to 130mm, and it was measured to be 110mm. The targeted air content after shooting was between 3 to 6 percent, and it was measured to be 4.6 percent. Thus, both of slump and air content were satisfied.

Compressive strength and flexural strength were measured only on the 28 day. The compressive strength was measured to be 45.3MPa which is higher than the targeted criteria of 35MPa. The flexural strength was measured to be 5.3MPa which is, also, higher than the targeted criteria of 5.0MP.

Durability was evaluated through three kinds of test: rapid chloride permeability test, freeze-thaw test and surface scaling test. Rapid chloride ion penetration resistance test was performed on 28 days old core specimen by taking the upper and lower face of the cut surface in order to prevent the neutralization reaction when the chemical reaction coloring agent neutralizes the concrete surface. It was performed at 28 days for core specimen according to KS F 2711. As a result, the relative dynamic modulus after freezing and thawing for 300 cycles was 87%, which is higher than the standard high durability performance, 80%. This shows that it have a very excellent freeze-thaw resistance.

The freeze-thaw resistance test was conducted by ASTM C 666 type A, which is a method of freezing and thawing in water, and the relative dynamic modulus was measured in every 30 cycles by repeating a total of 300 cycles, 1 cycle taking 4 hours. The relative dynamic modulus after 300 cycles of freezing and thawing was 87% which is higher than the criteria of high durability performance, 80%.

The surface scaling resistance test was performed by repeating freezing and thawing for 50days in a condition that the concrete surface was saturated with 4% calcium chloride solution; the amount of peeling and the state of aggregate exposure on the surface was measured and observed. As a result, the surface scaling resistance was evaluated as excellent ranked as grade 1 in ASTM C 672 standard and measured below 0.1kg/m^2 in SS 13 72 44 standard.

The strength and durability test results confirmed that the quality standards were met in all tests and it was recognized as an excellent structure that maintains the landscape for long-term without harming it.

5. APPLICATION AT TUNNEL PORTALS

5.1 Preparation

The rebar's were placed and tied according to the shop drawing for the tunnel portals, and then a high-performance concrete were shoot using a modified concrete pump car and cellular sprayed concrete. The shortening of construction period could be obtained by adopting the cellular sprayed concrete because it could provide a quite massive quantity of concrete using a ready-mixed concrete and concrete pump car, which could be done by the top-down or bottom-up manner with high-performance cellular sprayed concrete without formworks. This may results in shortening of construction period.

It uses a very common ready-mixed concrete truck and pump car with a nozzle. The additional required equipment are a foam generator, a nozzle, and air compressor. It is very efficient way of production for high-performance concrete by minimizing a special equipment required. This method enables top-down or bottom-up construction of tunnel portal with high-performance cellular sprayed concrete without formwork as shown in the Figure 2.

5.2 Spraying, carving and coloring natural patterns

Spraying, carving and coloring natural rock patterns is an eco-friendly technology that harmonizes with the surrounding landscape. The cellular sprayed concrete was produced at the job site by adding a cellular, silica fume and other mineral admixture into the ready-mixed concrete truck, than sprayed against the prepared tunnel portal. This is an optimized technique for slopes because it uses a pump car attached by a nozzle at the end of pump car. The additional required equipment are foam generator, a concrete spraying device, and air compressor. It is very efficient production methods for a high-performance cellular sprayed concrete.

This method was adopted to tunnel portals. It was designed according to the demand of the local inhabitants, representing the regional symbolic characteristics. The inhabitants were very happy to the beautiful and symbolic their own tunnel portals. Spraying, carving and coloring the regionally-symbolic tunnel portal are done as shown in Figure 3, 4 and 5, respectively.

Figure 2. Construction of tunnel portal using cellular sprayed concrete

Figure 3. Spraying at tunnel portal

Figure 4. Carving the regional symbol at tunnel portal

Figure 5. Coloring the regional symbol at tunnel portal

6. CONCLUSIONS

The results are as followings:

(1) The strength and durability test results confirmed that the quality standards were met in all tests and it was recognized as an excellent structure that maintains the landscape for long-term without harming it.

(2) Cellular sprayed concrete is a very simple and economic method to produce a high-performance sprayed concrete by adding cellular and silica fume in an ordinary stiff ready-mixed concrete. This was applied at a tunnel portal, and then a high-performance concrete were shoot using a modified concrete pump car and cellular sprayed concrete.

(3) The high production rate of high-performance cellular sprayed concrete were possible at the first lift shooting by an optimized technique; it uses a concrete pump car having a nozzle at the end of pump car together with air compressor and foam generator. After shooting the second lift, carving natural rock patterns and coloring were made.

(4) This technique is an eco-friendly technology that harmonizes with the surrounding landscape by comprehending natural rock shapes and colors the placed high-performance shotcrete before it hardens without using accelerators. This method was adopted to tunnel portals. It was designed according to the demand of the local inhabitants, representing the regional symbolic characteristics. The inhabitants were very happy to the beautiful and symbolic their own tunnel portals.

REFERENCES

ASTM C 672(2015), Standard Test Method for Scaling Resistance of Concrete Surfaces Exposed to Deicing Chemicals

ASTM C 666(2015), Standard Test Method for Resistance of Concrete to Rapid Freezing and Thawing

Han, S-Y. (2014), Dispersion of Silica Fume by Air Slurry and its Effect on Mechanical Properties at Ready Mixed Concrete, Kangwon National University.

KS F 2042(2007), Method of test for slump of concrete

KS F 2021(2016), Method of test for air content of fresh concrete by pressure method

KS F 2405(2010), Standard test method for compressive strength of concrete

KS F 2408(2016), Method of test for flexural strength of concrete

KS F 2711(2002), Testing method for electrical indication of concrete's ability to resist chloride ion penetration

KS F 2456(2013), Standard test method for resistance of concrete to rapid freezing and thawing

Lee, K-R. (2013), Durability Assessment for Crushed Sand Wet-mix Shotcrete mixed with Mineral Admixtures, Kangwon National University.

Yun, K.K, Kim, D.A., Namkung, K.,(2016), Dispersibility of Silica Fume in Cellular sprayed concrete for Simple and Economical Two-Lift Concrete Pavement, ICCP, San Antonio, USA

Yun, K.K, Jo, J.W, Han, S.Y., Lee, K.R., (2016), Variation of Water-Cement Ratio at Cellular Sprayed Concrete for Two-Lift Concrete Pavement, ICCP, San Antonio, USA

Yun, K.K, Namkung, K., Han, S.Y., Lee, K.R., (2017), Field Application of a Very-simple and Economic Two-Lift Concrete Pavement by only OPC Supply, ASCP 4th Concrete pavement conference, Australia.

THE IMPORTANCE OF RHEOLOGY ON SHOTCRETE PERFORMANCE

Ezgi Yurdakul, PhD; GCP Applied Technologies, Cambridge MA, USA
Klaus-Alexander Rieder, Sc.D.; GCP Applied Technologies, Cambridge MA, USA

ABSTRACT

In shotcrete mixes, slump measurements are commonly used to determine the suitability of the mixes for pumping and spraying. While high slump mixes that are flowable are desired for pumpability, engineers often specify low slump mixes to reduce sagging and rebound rate. Although the results of the slump test used to be a good indicator of the workability of the mixes containing water only, slump is no longer a reliable indicator of the overall suitability of a mix for shotcreting considering it is almost impossible to come across a mix that contains no admixture in today's modern construction. Therefore, the aim of this paper is to demonstrate the limitations of the slump test and present the importance of rheological characteristics for shotcreting. Field trials were conducted on mixes having various rheology control agents to compare against a plain mix. The relationship between rheological parameters and slump, rebound, cohesion, and build-up thickness are discussed.

Test results show that the rheological behavior of shotcrete is too complex to be oversimplified with one test but rather requires a delicate balance between flowability, cohesiveness, and viscosity. Considering different phases of shotcreting require conflicting rheological properties, it is ideal to maintain the highest possible fluidity (lowest yield strength) while providing the desired viscosity and cohesiveness to satisfy all needs.

INTRODUCTION

Shotcrete is no different than concrete as a material; however, the application method being pneumatic results in demanding complex rheological behavior from shotcrete compared to the conventional concrete. To better explain this complexity, it would be convenient to consider shotcreting process under the following two stages: 1) pumping and 2) spraying. Although these two stages momentarily take place one after another without allowing any changes to the rheology of shotcrete, it is important to note that each individual stage requires completely conflicting rheological properties. For pumpability, it is desired to have a mix with low viscosity and high flowability (usually associated with high slump). However, for sprayability, high viscosity and low flowability mixes (often named as stiff and sticky mixes with low slump and high cohesiveness) are desired [1]. Despite the importance of rheology on the overall performance of shotcrete, there is no standardized test method or an equipment that can evaluate the required rheological parameters (e.g. cohesion, stickiness, thixotropy) together by taking into an account of their interactions with each other. Instead, the industry often relies on the slump test to predict the pumpability (pump's pressure gauge is used as an indicator), and sprayability (tested by measuring rebound rate, build-up thickness, and material amount sloughing off from the vertical or overhead receiving surface) [2].

Limitations of the slump test

Slump is a simple test method that measures the yield stress (ease of flow) of concrete. While the results of this test method used to be a good indicator of the workability of the mixes containing only water, considering it is almost impossible to come across a mix not containing any admixtures in today's modern construction, slump is not a reliable indicator of the overall quality or suitability of a mix for shotcreting anymore since there is no direct correlation between slump and the mix' thixotropic properties. Furthermore, it is now possible to have two mixes with the exact same slump values but with completely different rheological properties as a result of the advancements in chemical admixture technology. Therefore, the guidance provided from the slump test results are actually limited despite the common misconception where slump test results are expected can be used to judge the sprayability, placeability, finishability, and rebound rate.

To better demonstrate the reason why slump cannot be used to predict the rebound rate, it is important to understand the basics mechanisms causing rebound. During the spraying process, rebound occurs as a result of the larger aggregate particles segregating from the mix after hitting the receiving surface at high velocities and subsequently bouncing off. Considering a high volume of rebound material consists of mainly aggregate particles, paste quality and aggregate gradation play a more important role for rebound reduction than the amount of cementitious materials as long as a sufficient quantity of paste is available that will fill the voids between the aggregates. In other words, the quality of paste is more important than the quantity of paste for evaluating the rebound characteristics. The quality of the paste is affected by the mix' rheological characteristics such as i) stickiness (adhesion to substrate surface that allow large build-up thickness), ii) cohesiveness (adhesion to itself to resist against the segregation of the mix which is critical for shotcrete as it is prone to segregation under pressure), and iii) viscosity (essential to resist against sagging on vertical walls). Therefore, instead of solely relying on the slump which only informs the users about the ease of flow and thus one of the good indicators for the pumpability, those three rheological parameters should be evaluated in order to reduce the rebound rate. Until a sufficiently thick paste layer accumulates on the substrate creating a "sticky" viscoplastic surface, rebound of these materials is inevitable especially at very early stages of spraying (e.g. first layer of spraying) where the concrete is sprayed onto hard walls or rock surface. When a layer of mortar adheres to the substrate which absorbs the kinetic energy of the aggregates providing a cushion, the rebound rate becomes lower in the subsequent layers. Therefore, although it is not feasible to completely eliminate rebound, it is possible to reduce the rebound rate by changing the mix' rheological characteristics. The ideal mixture for a given project should draw a delicate balance between these rheological characteristics as they not only affect the rebound but also influence all aspects of shotcrete quality including compaction, consolidation, and encasement.

Factors affecting rheology

The following mix components affect the rheological behavior of shotcrete [3]:

- Type, shape, gradation, porosity, texture, and amount of aggregates
- Type and amount of cementitious materials (silica fume, fly ash, etc.)
- Mix proportions (water-to-cementitious materials ratio, paste-to-aggregate ratio, etc.)

- Type and amount of admixtures (rheology control agents, superplasticizers, air-entraining agents, accelerators)
- Type and amount of fibers

EXPERIMENTAL PROGRAM

Mix design

Mix components	Amount used
ASTM C150/C150-M Type I ordinary portland cement, lb/yd³ (kg/m³)	712.5 (422.7)
Water, lb/yd³ (kg/m³)	146.5 (86.9)
Water-to-cementitious materials ratio (w/cm)	0.43
3/8" (9.5 mm) aggregate, lb/yd³ (kg/m³)	840 (498)
Fine aggregate, lb/yd³ (kg/m³)	1970 (1169)
Sand-to-total aggregate ratio, %	70.1
High-range water-reducing agent, oz/cwt (ml/kg)	3-9 (195-585) Dose varied to achieve similar slump in all mixes
Rheology control agent, oz/cwt (ml/kg)	7-13 (455-850) Dose varied depending on the type used

Test matrix

Tested property	Equipment/Standard used
Slump	ASTM C143
Slump flow	ASTM C1611
Yield stress, peak torque, plastic viscosity, and dynamic viscosity	ICAR rheometer
Rebound	JSCE-F 563-2005
Build-up thickness	-

ICAR Rheometer

The rheology of shotcrete was measured with a rheometer which helped determining the resistance of concrete to shear flow at various shear rates. Concrete rheology measurements are typically expressed in terms of the Bingham model, which is a function of:

- Yield stress: the minimum stress to initiate or maintain flow
- Plastic viscosity: the resistance to flow once yield stress is exceeded

In this experiment, ICAR rheometer was used (Figure 1). It was developed based on wide-gap, coaxial cylinders design where vane (h: 5 in. [125 mm], and diameter: 5 in. [125 mm]) acts as inner cylinder [4].

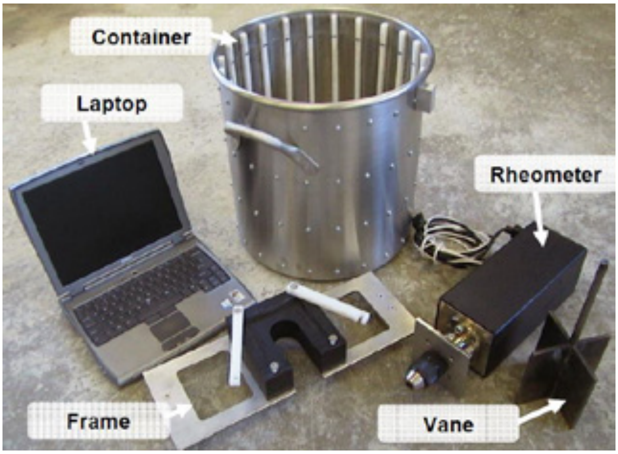

Figure 1. ICAR rheometer set up

TEST RESULTS

The correlation between rebound and slump/slump flow

Shotcrete tends to present material loss due to rebound since compressed air is pneumatically applied [1]. Although, a certain percentage of rebound is inevitable and even necessary since paste is needed to create a sticky surface for subsequent shotcrete material to become compacted into the surface, it is desirable to keep the rebound to a minimum [5]. To reduce rebound, a "sticky" mix is desirable as it will exhibit a lower tendency to fall off the wall. However, there is no test method that can measure stickiness. Furthermore, as seen in Figures 2(a) and 2(b), there is no correlation between slump/slump flow and rebound.

For instance, two mixes with the same mix design but different rheology control admixtures to have the exact same rebound performance despite one having significantly higher slump flow (e.g. mixes having 16 in. (406 mm) and 24 in. (610 mm) slump flow achieved the same rebound rate of 7%). It is also possible to see the impact of rheology control agents compared to the plain mix where for a given slump of 9.5 inches (241 mm), the rebound rate is reduced from 24% to 4% with the addition of rheology control agents.

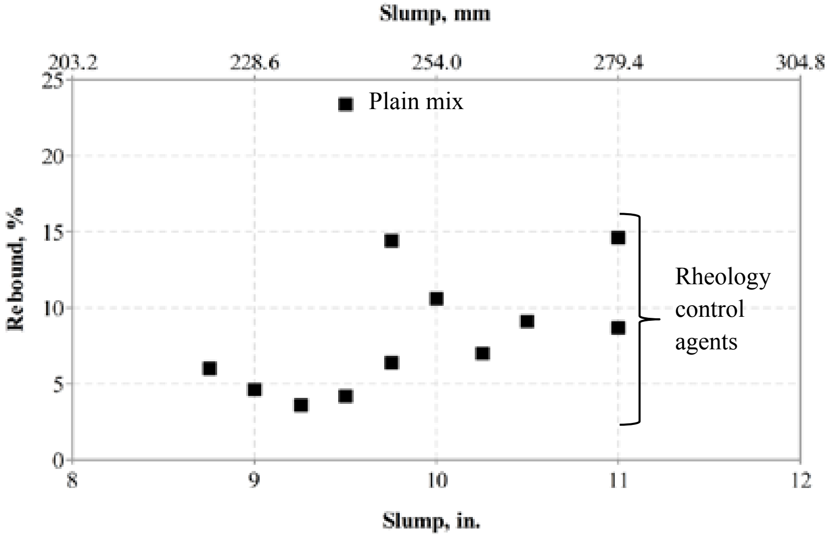

Figure 2(a). The relationship between rebound and slump

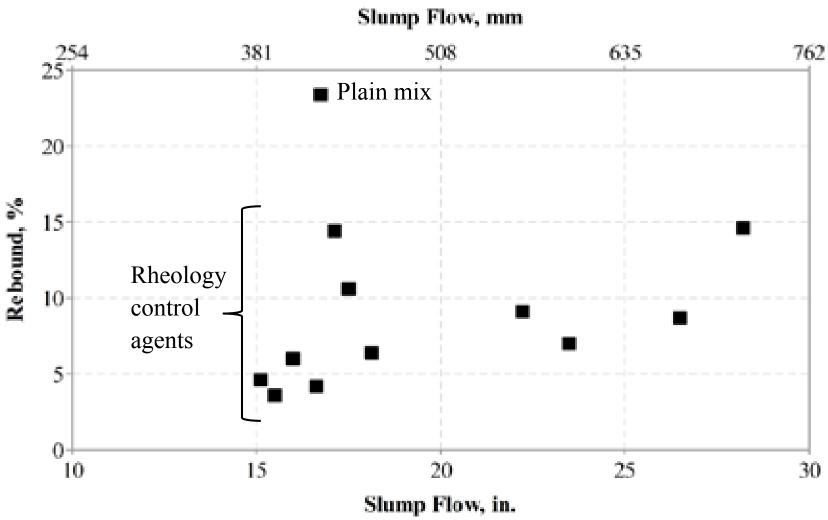

Figure 2(b). The relationship between rebound and slump flow

The relationship between plastic viscosity and slump/slump flow

Figures 3(a) and 3(b) show the relationship between plastic viscosity and slump/flow, respectively. As expected, no correlation was found between viscosity and slump due to slump representing the yield stress value that is independent of the viscosity. However, it is important to note that highly flowable mixes (high slump mixes) are prone to sagging if they do not possess a certain degree of viscosity which helps material to remain on the applied surface and resist the effect of gravity. Therefore, mix components should be selected to provide adequate viscosity and yield strength that could minimize sagging while having a minimal impact on pump pressure..

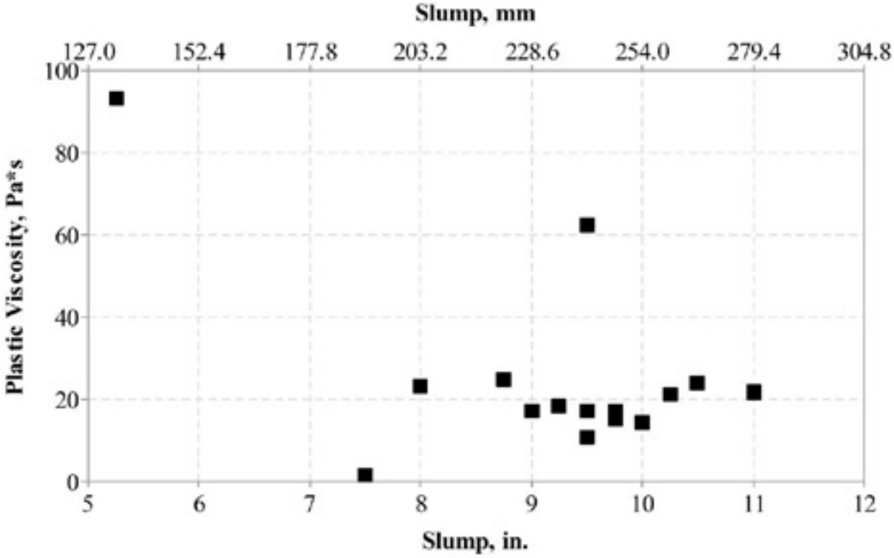

Figure 3(a). The relationship between plastic viscosity and slump

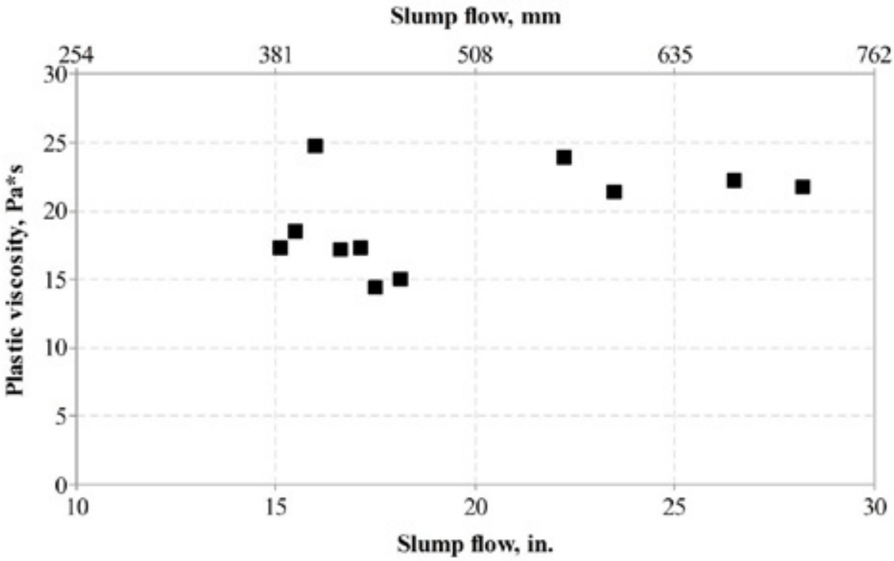

Figure 3(b). The relationship between plastic viscosity and slump flow

The relationship between yield stress and slump flow

Figure 4 shows the strong correlation between yield stress and slump flow. As the slump flow increases, the yield stress decreases due to increased fluidity of the mix requiring lower stress to initiate flow.

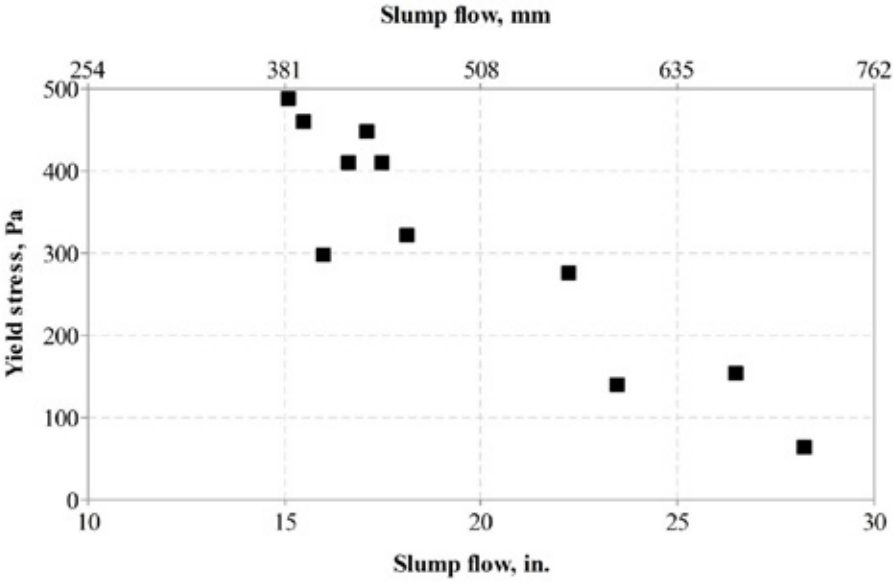

Figure 4. The relationship between yield stress and slump flow

The relationship between plastic viscosity and rebound

As shown in Figure 5, for a given viscosity, the rebound rate varied from 5% to 15% which shows that plastic viscosity has no impact on rebound rate. This finding aligns with the literature where Beaupré also found no correlation between rebound and viscosity [3].

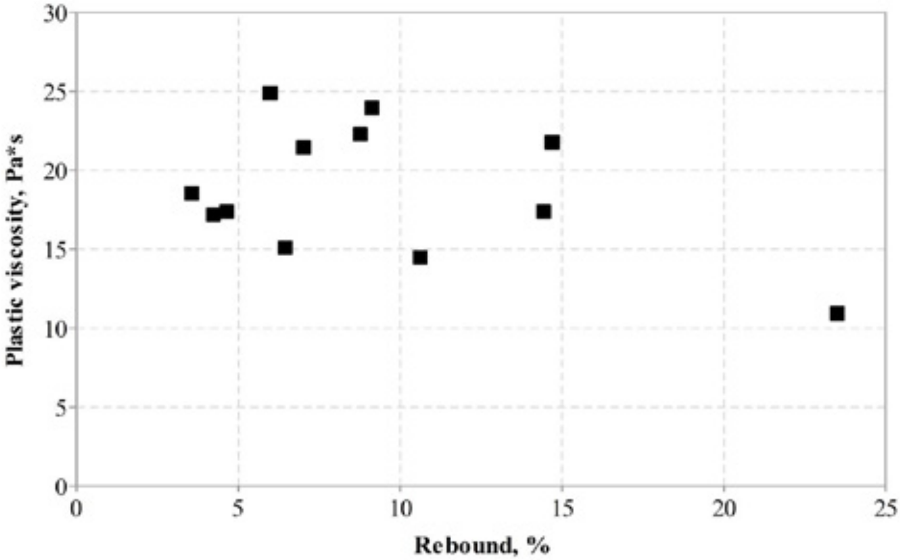

Figure 5. The relationship between plastic viscosity and cohesion

The relationship between peak torque and slump flow

As expected, there is a strong correlation between the peak torque and slump flow (Figure 6). When the slump flow increases, the torque required to rotate the vane decreases due to increased fluidity/flowability.

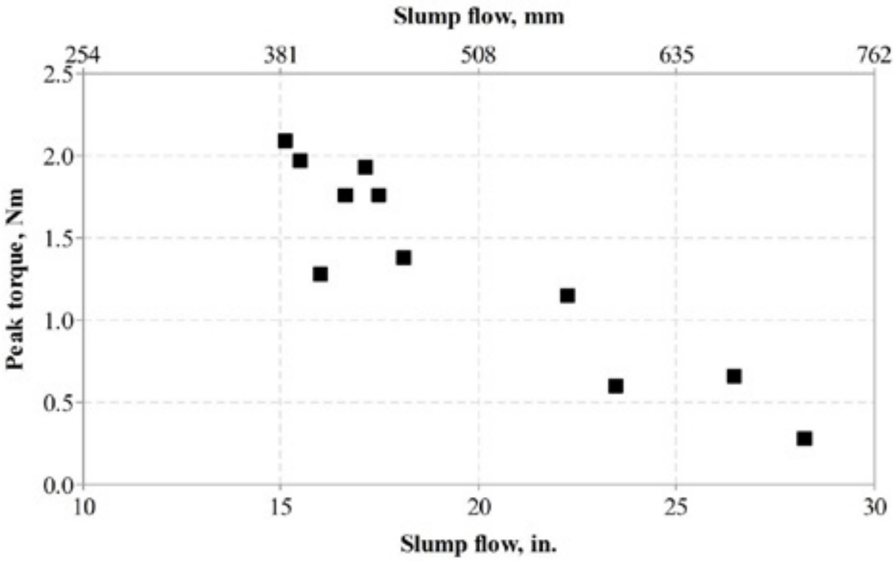

Figure 6. The correlation between peak torque and slump flow

The relationship between static and dynamic yield stress

Concrete exhibits different rheology when at rest than when flowing. Static yield stress is used to evaluate the minimum shear stress required to initiate flow from rest. On the other hand, dynamic yield stress is used to assess the minimum shear stress requires to maintain flow after breakdown of thixotropic structure. Based on this, when Figure 7 is evaluated, it is seen that the plain mix exhibits the highest static and dynamic yield stress which in turn indicates that there is more shear stress (higher pump pressure) needed to flow the plain mix; thereby it is expected to have the lowest pumpability. On the other hand, the impact of the rheology control agents were significant as they reduced the shear stress required to initiate and maintain flow; hence improved the pumpability.

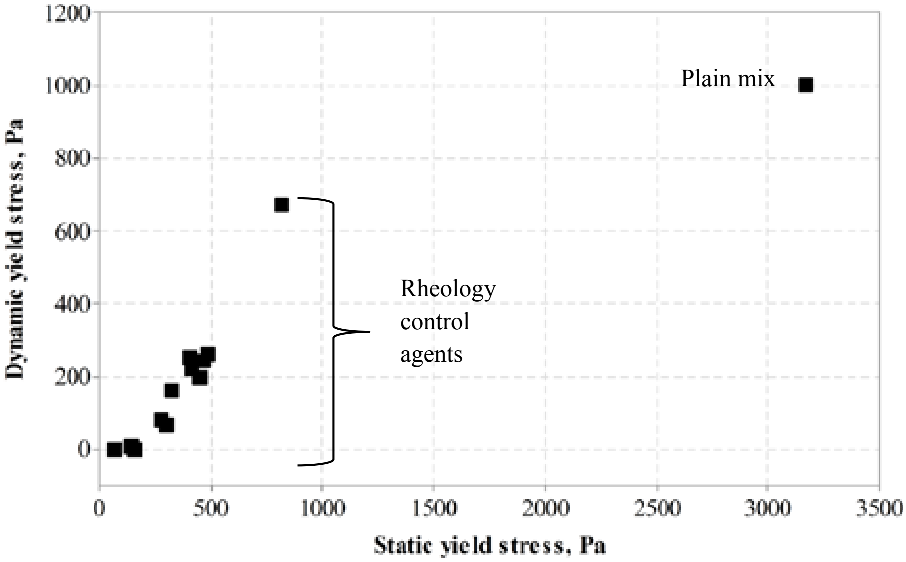

Figure 7. The correlation between dynamic and static yield stress

CONCLUSIONS

There are many factors contributing to the quality of shotcreting. Slump is only one parameter, and the rheological behavior of shotcrete is too complex to be oversimplified with one test but rather requires a delicate balance between flowability, cohesiveness, viscosity, and "stickiness". Considering different phases of shotcreting require conflicting rheological properties, it is ideal to maintain the highest possible fluidity (lowest yield strength) while providing the desired viscosity, cohesiveness, and "stickiness" to satisfy all needs.

REFERENCES

1) Jolin, M., Burns, D., Bissonnette, B., Gagnon, F., and Bolduc, L.S., 2009, "Understanding the pumpability of concrete," *Proceedings of Shotcrete of Underground support XI*, Switzerland.
2) Pfeuffer, M., and Kusterle, W. (2001). "Rheology and rebound behavior of dry-mix shotcrete." Cement and Concrete Research, Vol. 31, pp. 1619-1625.
3) Beaupré, D. (1994). "Rheology of high performance shotcrete", Ph.D. Thesis, The University of British Columbia, 250 pages.
4) Koehler, E.P., and Fowler, D.W. (2007). "ICAR mixture proportioning procedure for SCC" International Center for Aggregates Research, Austin, TX.
5) Jonsson, B., Nonat, A., Labbez, C., Cabane, B, and Wennerstrom, H., 2005, "Controlling the cohesion of cement paste," Langmuir, American Chemical Society, 21, pp. 9211–9221.

Monitoring and behaviour of an instrumented thick sprayed concrete lining excavated in the Callovo Oxfordian Claystone at the Meuse Haute-Marne Underground Research Laboratory (URL) - Andra, France

Jad Zghondi, Gilles Armand

Andra (French National Radioactive Waste Management Agency), Meuse/Haute-Marne Underground Research Laboratory, 55290 Bure, France
Jad.zghondi@andra.fr

ABSTRACT

One of the main concerns of the ongoing Andra's Meuse/Haute-Marne URL (Underground Research Laboratory) technological and demonstration research program is the development of construction methods and lining optimization on the Callovo-Oxfordian claystone layer at 490 m depth. The analysis of the hydromecanical behaviour of the rock and lining is an important design input for Cigéo, the French reversible deep geological disposal of high-level and intermediate-level long-lived radioactive waste.
One of the URL experiments called "BPE", consist on projecting a 4 layers wet-mix sprayed concrete while excavating a drift parallel to the major horizontal stress (σH), in a way to oppose as quickly as possible a rigid lining to the rock convergence. Rock and lining are monitored with 138 sensors installed before, during and after excavation. Vibrating wires, and pressure cells, flat jacks are embedded in the sprayed concrete. Laboratory testing and numerical modelling were conducted. The results highlights the interaction between the rock and the lining up to the current date (4 years), and the importance of the understanding of the early age behaviour of the sprayed concrete, especially with a quick loading, to better model and predict stress/strain evolution of the sprayed concrete layer.

1. INTRODUCTION

The French reversible deep geological disposal of high level (HLW) and intermediate level long live waste (IL-LLW) Cigéo, will be located on the eastern boundary of the Paris Basin, at the fringe of the Meuse and Haute-Marne departments. Andra, the agency in charge of radioactive waste in France, locally started in 2000 (with the shaft sinking operations) the construction of Meuse/Haute-Marne URL (Underground Research Laboratory), in the framework of its general research program (Delay et al, 2007) aimed at proving the feasibility of a reversible deep geological disposal of radioactive waste (HLW, IL-LLW). The URL drifts are used to study the Callovo-Oxfordian claystone layer, the host rock formation, (COx) between 420 m and 550 m depth.

The main objective of the first research phase (2000 to 2005) was to characterize the confining properties of the clay through *in-situ* hydrogeological tests, chemical measurements and diffusion experiments and to demonstrate that the construction and operation of a geological repository would not introduce pathways for radionuclides migration.

The ongoing research program (started in 2006) following the "Technology Readiness Level" (TRL) scale is more dedicated to technology improvements and demonstration issues of the different disposal underground components (drifts, seals, disposal cells and vaults), even if characterization and monitoring activities are still ongoing.

Geomechanical analysis confirmed an anisotropic stress state at the level of the URL, (Wileveau et al., 2007). The major horizontal stress (σH) is oriented at NE150°. The vertical stress (σv) is nearly equal to the horizontal minor stress (σh). The ratio σH/σh is close to 1.3. Armand et al (2013) described the excavation induced fractures network observed around drift at the main level of the URL and show that the fracture pattern and extent depend on the drift orientation. The excavation induced fractures network is more developed at roof and ceiling for drifts parallel to σh and at the wall for the ones parallel to σH. Anisotropic convergences are observed in all drifts (Armand et al 2013). However, this anisotropy is smaller for the drift parallel to the major horizontal stress than observed in the drift perpendicular to the minor horizontal stress. Highest convergence is observed where the extent of induced fractures is larger. That's why, disposal cells (HLW, IL-LLW) in Cigéo are oriented along the major horizontal stress σH.

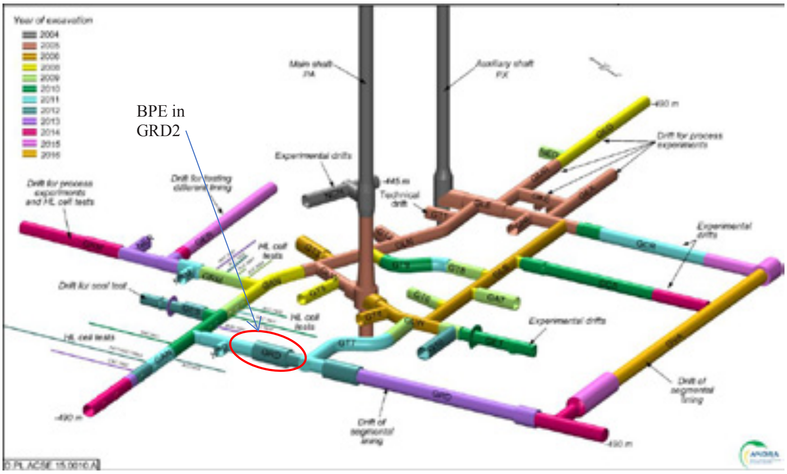

Figure 1: Meuse Haute-Marne URL drift network

2. MEUSE/HAUTE-MARNE URL CONTRIBUTION TO CIGEO DRIFT DESIGN

Cigéo basic design outlines several types of drifts (access drift, IL-LLW disposal vaults, technical drifts…), excavation methods (TCM or TBM), lining type (primary & final support or precast segments) or requirements.
The MHM URL offers the possibility to understand for different experiments cases the hydromechanical behaviour of the COx and the linings, their interaction, and evolution in time (Armandet al., 2013).

Table 1. Characteristics of the different experimental drifts dedicated to hydro-mechanical (HM) behaviour.

Drift		Diameter (m)	Length (m)	Direction Vs σH	Start	finish	Excavation technic	Primary support: Yieldable wedges	Primary support: Shotcrete	Final concrete support: Site-cast concrete (C30/35 MPa)	Final concrete support: Site-cast concrete (C60/75 MPa)	Final concrete support: Pre-cast lining elements	Structure measure point
GCS		5,2	64,3	∥	mai-10	oct.-10	Road header	X	X(21 cm)				74
GCR	zone 1	5,4	64,3	∥	janv.-11	mars-12		X	X(21 cm)		X (30cm)		464
	zone 2							X	X(21 cm)	X			
	zone 3								X(21 cm)		X (30cm)		
BPE		6,3	15	∥	févr.-12	mars-13			X (45cm)				156
GRD4	zone 1	6,27	66	∥	mai-13	nov.-13	TBM					X + "classical grout"	739
	zone 2											X + "comp grout"	
GER	GER2	5,4	83	⊥	janv.-15	juil.-16	Road header	X	X(21 cm)				778
	GER3							X	X(21 cm)		X (30cm)		
	GER4								X(21 cm)				
GVA2	zone 1	6,27	119	⊥	janv.-17	Dec-17	TBM					X + "classical grout"	1353
	zone 2											X + "comp grout"	
	zone 3											X + "comp lining"	

A step by step approach is carried out, based on comparison of HM behavior of parallel drifts excavated/supported by different construction methods and structure stiffnesses (Armand et al., 2015). These various configurations (table 1) give insight of the influence of various construction methods on the excavation damaged zone (EDZ), on the progressive loading of the structural support, which are key issues to design and select the most suited excavation methods and lining for the appropriate Cigéo structure. *In-situ* experimental strategy for the study of drift behaviour is based on the following activities (Armand et al., 2015):

- Observing real behavior of drift under different conditions (depth, size, geometry, ventilation, temperature…). Each drift excavation in the URL is a rock mechanics experiment in itself,
- Sequencing of drift construction to highlight the role of support/excavation method on the HM behavior (support loading, EDZ…) starting with "flexible" support up to “rigid” support,
- Comparing the different behavior (Figure 2) of drifts excavated with different methods,
- Applying “mine by experiments” (instrumented boreholes in-place before the excavation) to study the HM behavior (at short and long terms).

BPE (Béton Projeté Epais) experiment as shown in red circle in figure 1, aimed to apply with respect to the scale and conditions of the Meuse/Haute-Marne URL, within a short time a 45 cm thick layer of sprayed concrete, in a way to oppose as soon as possible a stiff lining to the COx convergence.

3. BPE DRIFT FEATURE

3.1 Construction description

GRD2 drift dedicated to BPE experiment is parallel to the major horizontal stress. It is a 15 m long circular drift, excavated with a road header machine, with an excavation diameter of 6.3 m (figure 2).

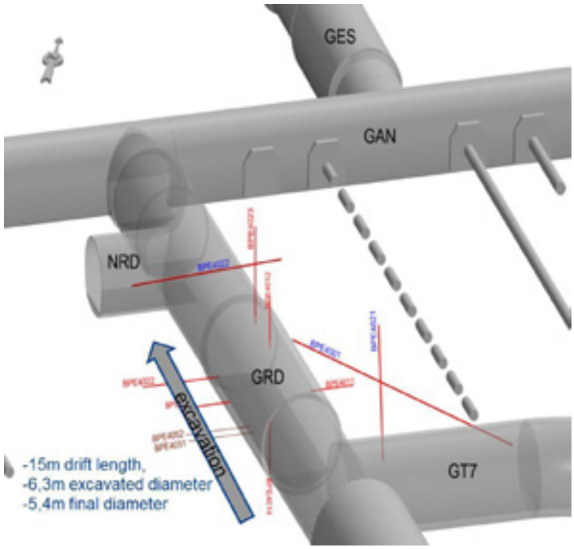

Figure 2: BPE experiment in GRD drift

Excavation sequence (figure 3) was realized with a 1 m excavation span. After each excavation, an average of 11 cm layer of wet mixed fiber reinforced shotcrete was applied on the vault of the last 4 excavation, and 45cm on the counter vault. The vault final thickness was reached after 2 weeks' time, after proceeding with the three following step of excavation.

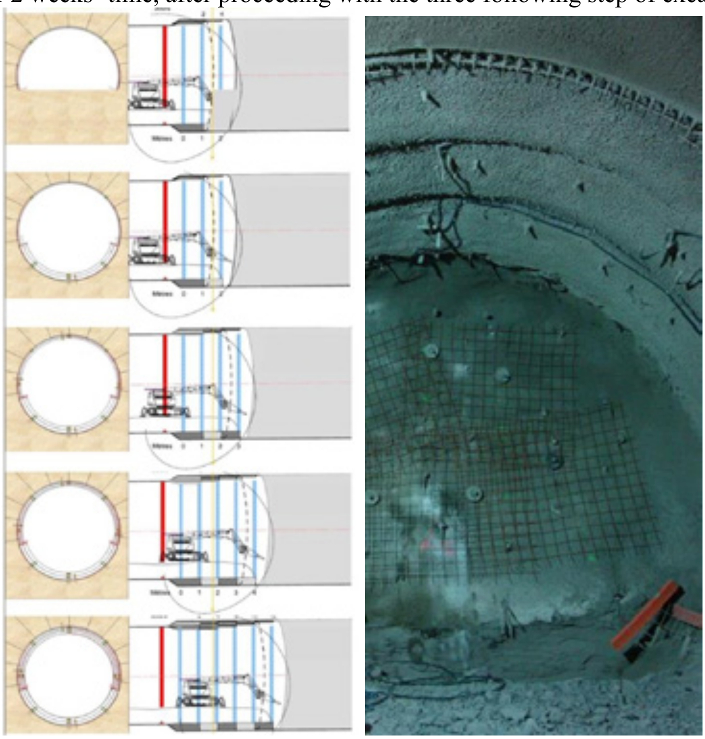

Figure 3: BPE excavation and instrumentation sequence

3.2 BPE instrumentation description

To understand the interaction between the rock mass and the sprayed concrete lining and to evaluate the loading on the lining, several measurement wires were used (Figure 4).
The hydro mechanical behavior of the rock is followed before, during and after excavation. Boreholes were instrumented to follow deformation and water pressure, taking in consideration the feedback from the previous excavation drift at the underground laboratory (Armand et al., 2013).

- Before excavation: three instrumented boreholes were installed around the drift, equipped with water pressures and deformation measurements.
- While excavating, shotcrete was instrumented with embedded vibrating wires for deformation measurements, and total pressure cells. Three dimensional laser scans were performed in a way to estimate shotcrete layers thicknesses, sensors position and short term deformations. Measurement of displacement and convergence of the excavated section have also been realized.
- After excavation: three dimensional scanners, convergence as well as flat jacks measurements are carried.

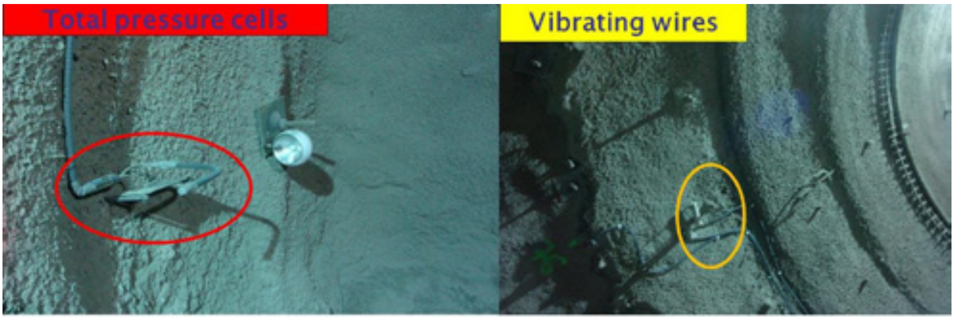

Figure 4: BPE lining instrumentation

Five sprayed concrete sections have been monitored:
- 2 sections with 16 total pressure cells each,
- 2 sections with 21 vibrating wires each,
- 1 section of 3 measures of flat jack to follow orthoradial stresses.

As shown on the Figure 5, pressure cells and vibrating wires were distributed on the 4 sprayed concrete layers, and positioned in a way to follow mainly the orthoradial behaviour. Orthoradial stress are the stresses which will develop the more under the loading of the ring that why the monitoring is gathering on orthoradial stresses (extrados and intrados) .
The 16 orthoradial sensors in both cell pressure sections and vibrating wires have the same position (figure 5).

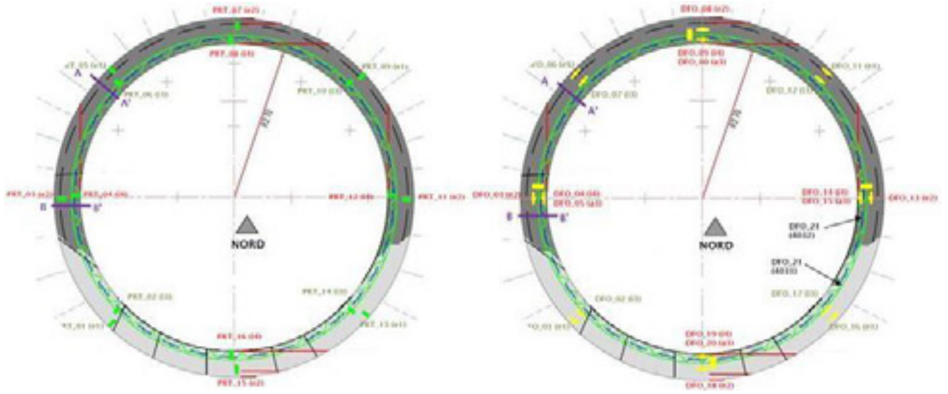

Figure 5: BPE cell pressure section (16 cells in green), and vibrating wires (21 vibrating wires in yellow)

Two embedded vibrating wires were mechanically disconnected from the ring structure. The aim of their measure is to be able to correct a part of the strains due to shrinkage and temperature fluctuation.

The results presented on this paper concern lining monitoring.

4. SPRAYED CONCRETE

A wet-mix sprayed concrete formulation was manually sprayed. It should be noted that this formulation is not designed to answer Cigéo's specifications, but it answer only the strength criteria needed for experimental use at the URL.
The targeted performance is to have a minimum compressive strength of 40 MPa (28 days), with an S2 slump class.

Mixture composition : CEM 1 cement (GUNIDOR 30 PMES) 400 kg/m^3, with a water dosage 40% of cement weight, with polypropylene fibers (6 kg/m^3), accelerator (MEYCO SA 167) 6% of cement weight, and stabilizer admixture (DELVO) 0.05% of the cement weight, and granularity 0/8mm (recommended by AFTES).

4.1 Sprayed concrete testing

- Formulation validation before and during construction (compressive strength, and workability tests),
- A laboratory testing program; characterization of the elastic modulus, creep, shrinkage, and hydromechanical behavior of the interface between two layers of shotcrete. Tests were run in LMDC Toulouse laboratory, on cores drilled at early (48h) or after 28 days in:
  - o the drift structure,
  - o test panels (1x1x0.15m), and a test wall (figure 6)
- Hydromechanical behavior of the interface between two layers of shotcrete (not presented in this paper) : testing wall (figure 6) taking into account the sequence of the structure drift : 4 layers, 45 cm final thickness, and 3 days of time laps between two layers, campaign test done in LaMcube laboratory (University of Lille).

Figure6: BPE Sampling of sprayed concrete cores

4.2 Main results

Table 2 present the mechanical results obtained; compressive strength (NF EN 12504-1 and NF EN 12390-6), modulus (Rilem-CP8) over time, and porosity (Rilem-TC 107-CSP) after 28 days was measured around 19,5%.

Table 2. Mechanical tests results (Lmdc Toulouse).

BPE	7 days	14 days	28 days
R_c (MPa)	30.9 (37.1 - 24.5)	36.1 (36.6 - 48.5)	50.0 (41.8 – 53.6)
R_f (MPa) 3 values	2.9	3.4 (0.7)	3.6 (1.0)
E_i (MPa) 2 values	20671 (2541)	24546 (3705)	25472 (3602)

Autogeneous and drying shrinkage (figure 7) were measured on different cores, and showed:

- Evolution in time up to 140 days
- A loss of weight up to 2.6% concerning drying core

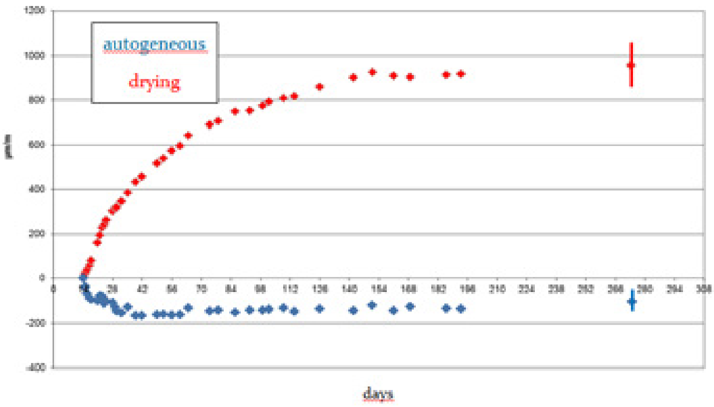

Figure7: BPE monitoring autogeneous and drying (20°C, 50%H.R.) shrinkage (LMDC Toulouse laboratory)

Creep tests were conducted as soon as possible 14 days (panel projection, transportation, cutting, then drilling cores perpendicular to spraying direction).That's why autogeneous conditions are not well fulfill after such a delay, and can be probably not unreliable.

A first 7 MPa loading stress was applied; a value equivalent to the higher total stress measured with the cell pressure sensors in the sprayed concrete layer at early drift age. Later on an unloading followed by a new loading up to 15 MPa loading was conducted. Figure 8 shows the strain evolution as a function of time:

- A great creep potential whether in both loading phase (1800 µε in drying mode under 7MPa, and 800 µε under 15 MPa). For instance, 1800 µε under the first loading in drying mode are an enormous creep value comparing to other cementitious mixtures (mortar, concrete or grout).
- Instantaneous unloading deformation is only up to 18% of drying creep.
- Creep strains for the first loading step are similar to the shrinkage ones for the over the same period.

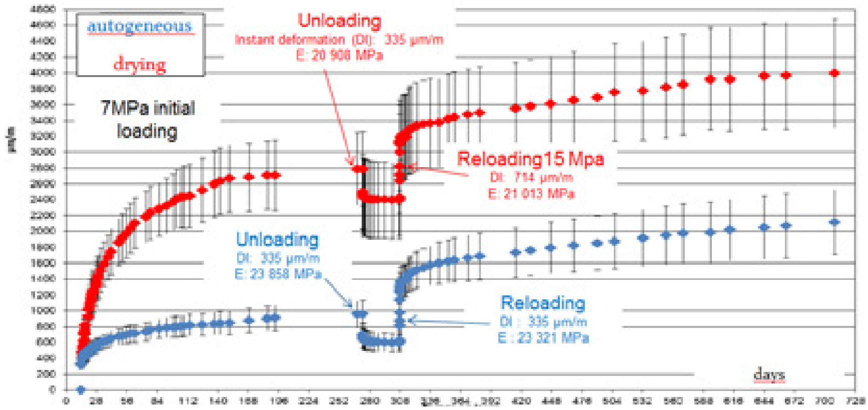

Figure8: Total creep strains for autogenous and drying conditions, with 2 loading phase, 7 and 15 MPa (LMDC Toulouse).

5. HOST ROCK MECHANICAL BEHAVIOR ANALYSIS

The analysis of the rock behavior confirms what is observed on drifts in the same direction (Armand et al. 2013). Even though the drift direction is parallel to the major stress, the excavation work induces anisotropic fractures network around the drifts due to the semi-brittle behavior of the rock (even if cross section initial stresses are nearly isotropic). The fracture network induces an anisotropic convergence more marked on the horizontal direction.

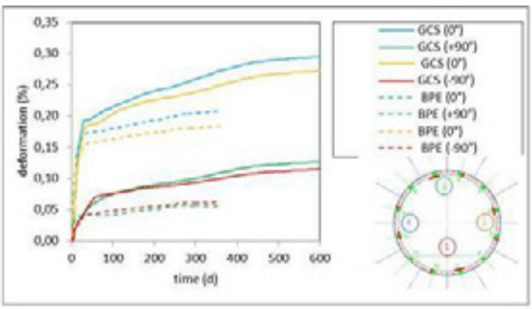

Figure 9: Rock convergence, BPE experiment Vs a parallel drift GCS (more flexible lining)

Figure 9 shows the influence of the stiffness of the lining on the rock convergence. In fact for the two parallel drifts with a same construction sequence, only the lining differs. The BPE lining is more rigid then the GCS one (with *perfect elastoplastic wedge in the shotcrete lining)*. In the two cases, horizontal convergences are larger than the vertical ones. The high stiffness of the BPE lining allows lower convergence after the shotcrete setting time.

6. LINING MECHANICAL BEHAVIOR ANALYSIS

6.1 Monitoring analysis

Figure 10 and 13 present the strains and stresses evolution (1st year, and 4 years) on two instrumented section of the lining circumference. The results show:

- A quick loading of the lining. Some strain exceeded 2000 με in the vault and counter vault before even the end of the 4th sprayed layer emplacement.
- Orthoradial deformations and stress are more concentrated at the vault and counter vault (figure 11).
- Strains evolution continue over time, confirming the rock creep behavior evolution
- Stresses measured in cell pressure sensors seem to increase less after final lining thickness was reached, even though the excavation continues. Flat jacks installed after 30 days show better evolution with time (figure 13b).
- Intrados and extrados strains and stresses are not symetric like expected as the ring is anisotropically sollicitated. Concentration of orthoradial compression in the intrados and extrados of the vault and counter vault are well marked.

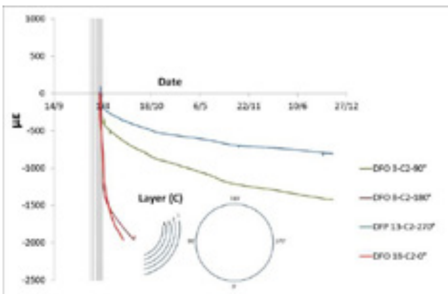

(a)

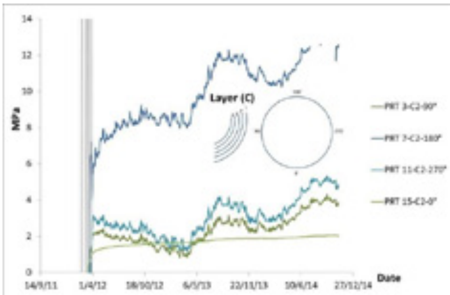

(b)

Figure 10 (a) Vibrating wires strains (embedded in the second layer) evolution in time (BPE4031). (b) Orthoradial stresses measured with total pressure cell (embedded in the second layer) evolution (BPE4041)

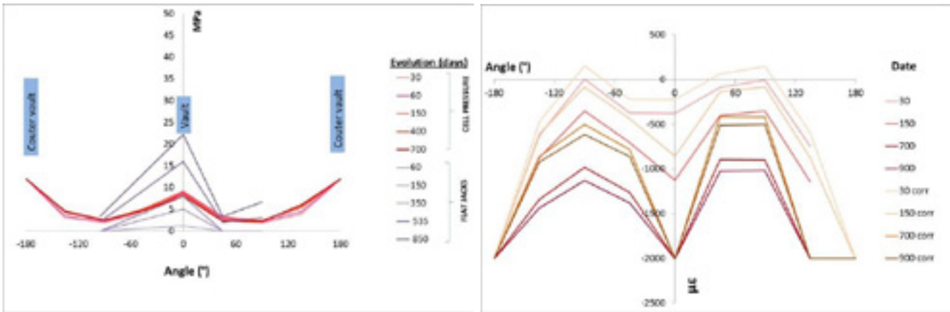

(a) (b)

Figure 11 (a) Evolution of the orthoradial stresses (MPa) as function of the angle location (0° is the vault) at different time (in days) and (b) initial/corrected strains (shrinkage and temperature effect) on the intrados (3rd and final sprayed layer) of the lining.

6.2 Modelling analysis

Difficulty to find the appropriate early age behavior law concerning loaded sprayed concrete is presented on that paragraph. That's why not all the modelling procedure and phases are detailed.

A parametric modelling program was done by Ineris, the important key points of that study:

- 2D calculation taking in account the rock behavior (behavior law Andra/Ineris, Souley et al, 2011)
- The as-built construction sequence, geometry and characteristics was respected
- Only behaviour law of the sprayed concrete was modified: modulus variation (Figure 12), behaviour law (elastic and Mohr Coulomb),…)

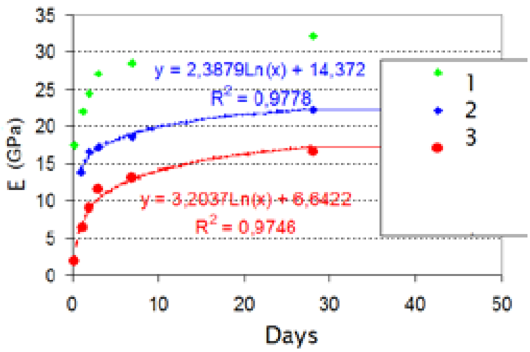

Figure 12 the three sprayed concrete Young modulus evolution case studies (1 following AFTES recommendation, 2,3 lower modulus to take into account creep effect on the shotcrete)

Below the results concerning Young modulus, three cases were studied (figure 12).

First case study (figure 12 curve 1) take in account the AFTES recommendations; using early age compression results, later the mechanical behavior was modified (reducing Young modulus) in order to take it account some creep effect (figure 12 curve 2 and 3).
Those assumptions conducted to a better prediction of the results but were not sufficient in order to catch the creep behavior at early age. Figure 13, with a Young modulus represented by number 2 on figure 12, shows the most fitted study case:

- stresses measures were always higher than calculation, even if difference is more acceptable using flat jack measurements.
- Strains long-term slope time behaviour seems to be acceptable. It is more related to the creep behaviour well generated by the INERIS/Andra COx behaviour law.

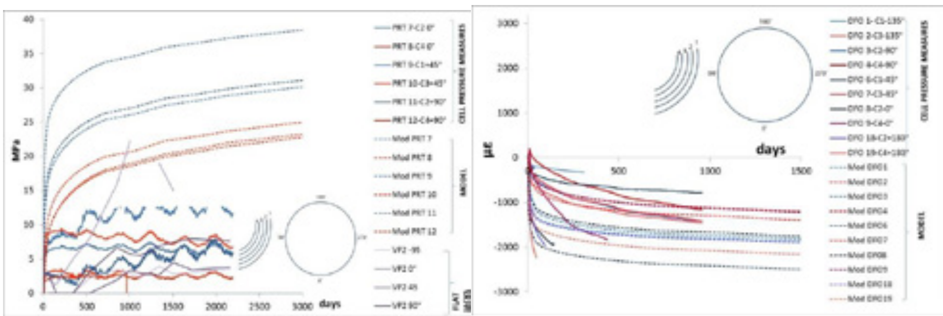

(a) **(b)**

Figure 13 (a) Vibrating wires strains (microdef) evolution in time Vs 2D calculation result.(b) Orhtoradial cell pressure stresses (MPa) evolution Vs 2D calculation result.

Classical approaches used in design calculation do not take into account the sprayed concrete creep, leading to overestimate stresses and underestimate strains in the designed sprayed concrete lining. In order to better predict the measured strains and stresses in the sprayed concrete layers more complex behaviour has to be taken into account.

7. CONCLUSION

Both creep measures on cored samples, as well as BPE monitoring results, highlight under loading effect the enormous creep potential effect in early age of the sprayed concrete. In fact, a quick spraying of a thick shotcrete lining creates a support of the drift which counter-acts the convergence of the rock. This leads to a quick early loading of the sprayed concrete layer. Early age loading as measured mobilizes an important creep potential. That creep potential releases more strains and decreases the stresses evolution.
The early age creep and its evolution depending on confinement is difficult to represent with a simple evolution of Young's modulus as a function of time as it is done for long term creep classical approach. A more accurate modelling approach to better represent the early age behaviour of shotcrete would benefit the optimization of lining thickness.
For all those reasons, Andra with LaMcube Lille are cooperating on a PHD study bases on an experimental and behaviour law development program, concerning instant and delayed mechanical behaviour of sprayed concrete.

8. ACKNOWLEDGEMENTS

- The authors acknowledge P.Nicot, (Lmdc Toulouse Laboratory) and N. Burlion, (LaMcube laboratory , University of Lille) for performing lab tests and for the discussion over the sprayed concrete behavior at early age and
- M.Souley, (INERIS) for the modelling of BPE experiment and Andra colleagues (H Djizanne,…) for discussion and review of the paper. All those contributions were an important insight to understand the overall behavior of the in situ BPE experiment.

REFERENCES

Armand, G., Plas, F., Bosgiraud, J.-M., 2015. “The contribution of Andra’s Underground laboratory to selection and developpement of excavation techniques for the underground structures of Cigéo radioactive repository project”. Tunnels et espace souterrain , n° 250, p.251-268 ;

Armand, G., Noiret, A., Zghondi, J.& Seyedi, D.M. 2013, Short- and long-term behaviors of drifts in the Callovo-Oxfordian claystone at the Meuse/Haute-Marne Underground Research Laboratory, Journal of Rock Mechanics and Geotechnical Engineering 5, pp 221–230

Armand, G., Noiret, A., Cruchaudet, M. & Conil, N., 2011, Mine by experiment performed in the Callovo-Oxfordian claystone at the Meuse Haute Marne Underground Research Laboratory (France), ISRM 12th International Congress on Rock Mechanics, 9-13 October 2011, Beijin.

Delay, J., Vinsot, A., Krieguer, J.M., Rebours H. and Armand, G. 2007. “Making of the underground scientific experimental programme at the Meuse/Haute Marne URL, North Eastern France”. Phys. & Chem. of the Earth, 32, 2-18 ;

Souley M., Armand G. Su K., Ghoreychi M. (2011) “Modeling the viscoplastic and damage behavior in deep argillaceous rocks”. Phys. Chem. Earth, Vol. 36, 1949–1959

Wileveau, Y., Cornet, F.H., Desroches, J. & Bluemling, P. 2007. “Complete in situ stress determination in an argillite sedimentary formation”. Physics and Chemistry of the Earth, vol. 36, 1949-1959.

ISBN: 978-82-8208-060-6